ISSN: 0439-5689

HORMIGÓN y ACERO

REVISTA CUATRIMESTRAL DE ACHE ASOCIACIÓN ESPAÑOLA DE INGENIERÍA ESTRUCTURAL

Enero - abril 2026 I Volumen 77 - Número 308

www.hormigonyacero.com

FOTO DE PORTADA: HUGO CORRES y ANTONIO MARÍ, fotografiados por Gonzalo Ruiz.

HORMIGÓN y ACERO

Enero - abril 2026 I Volumen 77 - Número 308

REVISTA CUATRIMESTRAL DE LA ASOCIACIÓN ESPAÑOLA DE INGENIERÍA ESTRUCTURAL

El Consejo Editorial de la revista tiene como misión la definición de la política editorial (estilo de la revista, redacción, normas de presentación de originales, diseño, creación y orientación de las distintas secciones). **El Comité de Redacción** se constituye como un comité permanente del Consejo Editorial y se encarga de dirigir y supervisar la gestión diaria de la revista, controlar la selección de contribuciones y tomar las decisiones sobre los contenidos que han de conformar cada número de la revista. La función del **Consejo Asesor Científico** es la de velar por el prestigio científico y técnico de la revista, promoviendo e impulsando su difusión internacional.

Una descripción más amplia puede consultarse en *www.hormigonyacero.com*

ÍNDICES Y SERVICIOS DE INFORMACIÓN: *Hormigon y Acero esta indexada en las bases de datos siguientes: Emerging Sources Citation Index/Web of Science Core Collection (ESCI/WoS) - Journal Citation Reports (JCR) – Scopus - Pascal – InDICEs-CSIC – Dialnet-Sumaris – Catalogo Latindex 2.0 – ScienceDirect.*

ISSN 0439-5689
Publicación cuatrimestral (3 números al año)
www.hormigonyacero.com

Protección de datos: CINTER DIVULGACIÓN TÉCNICA, S.L. declara cumplir lo dispuesto por la Ley orgánica 15/1999, de 13 de diciembre, de Protección de Datos de Carácter Personal.

Suscripciones y atención al cliente

CINTER DIVULGACIÓN TÉCNICA

CINTER DIVULGACIÓN TÉCNICA, S.L.
C/Doctor Santero, 7 , 28039 Madrid (España)
Teléfono: 913191200
Correo electrónico: cinter@cinter.es

Impresa en España por Gráficas Muriel
Diseño gráfico y maquetación: MGráfico
Depósito legal: M-853-1958

HORMIGÓN y ACERO

Disponible en **www.hormigonyacero.com**

SUMARIO | CONTENTS

ENERO - ABRIL 2026 I Volumen 77 - Número 308
January - April 2026 I Volume 77 - Issue 308

REVISIÓN HISTÓRICA Y HUMANÍSTICA | *HISTORICAL AND HUMANISTIC REVIEW*

Publicado por Cinter Divulgación Técnica S.L.
E.T.S.I. de Caminos, Canales y Puertos. Laboratorio de Estructuras. Avda. del Profesor Aranguren, s/n. 28040 Madrid
Tel.: (+34) 91 067 41 64 - www.e-ache.com

MIEMBROS PATROCINADORES DE LA ASOCIACIÓN ESPAÑOLA DE INGENIERÍA ESTRUCTURAL (ACHE)

Según los Estatutos de la Asociación existen dos tipos de miembros, uno para personas jurídicas y otro para personas físicas. De entre los primeros, y por la importancia que tienen para la Asociación por su contribución económica, destacan los miembros Patrocinadores y los Protectores. Hasta la fecha de cierre del presente número de la Revista, figuran inscritos como **Miembros Patrocinadores** los que a continuación se indican, citados por orden alfabético:

ACCIONA INFRAESTRUCTURAS
Avda. de Europa, 18
28108 ALCOBENDAS (MADRID)

ALLPLAN Systems

ARENAS & ASOCIADOS, INGENIERÍA DE DISEÑO, S.L.P.
C/ Marqués de la Ensenada, 11 - 3º
39009 SANTANDER

C/ Jordi Girona 31 - 2º, Edifici Til·lers
08034 - BARCELONA

AZUL CONSTRUCCIÓN REPAIR, S.A.
Pq. Comercial San Jerónimo, Calle A,
Nave 11. 41015 SEVILLA

CALIDAD SIDERÚRGICA
C/ Orense, 58 - 10º
28006 MADRID

CARLOS FERNANDEZ CASADO, S.L.
OFICINA DE PROYECTOS
C/ Orense, 10
28020 MADRID

CEDEX (Laboratorio Central)
C/ Alfonso XII, 3
28014 MADRID

CONSEJO GENERAL COLEGIOS ARQUITECTOS TÉCNICOS
Paseo de la Castellana, 155 - 1º
28046 MADRID

CYPE INGENIEROS, S.A.
Avda. Eusebio Sempere, 5 - Bajo
03003 ALICANTE

DRAGADOS, S.A.
Avda. Camino de Santiago, 50
28050 MADRID

EDARTEC CONSULTORES
C/ Manufactura, 4 - Planta 2 - Mod. 3
41297 MAIRENA DE ALJARAFE (SEVILLA)

E.T.S. INGENIEROS DE CAMINOS - DPTO. MECÁNICA
Ciudad Universitaria, s/n
28040 MADRID

FCC CONSTRUCCIÓN, S.A.
Avda. Camino de Santiago 40
28050 MADRID

FHECOR ingenieros consultores S.A.
C/Barquillo, 23. 1º izq.
28004 MADRID

FLORENTINO REGALADO INGENIERÍA & ARQUITECTURA S.L.P.
C/ Granja de Rocamora, 18
03015 ALICANTE

GRUPO MECÁNICA ESTRUCTURAL S.L
C/ Amílcar González Díaz, 18
38550 ARAFO (SANTA CRUZ DE TENERIFE)

HILTI ESPAÑOLA, S.A.
Avda. Fuente de la Mora, 2 - Edificio I
28050 MADRID

INSTITUTO EDUARDO TORROJA
C/ Serrano Galvache, 4
28033 MADRID

IECA
C/ José Abascal, 53 - 2º
28003 MADRID

MAMMOET
P.I. Los Frailes. Ctra Alcalá de Henares a Daganzo,
km 9. P 101-106, 28814 DAGANZO (MADRID)

MEKANO4 INNOVATIVE SOLUTIONS
P.I. Can Nadal, Carrer Can Nadal, s/n, Nave 1-A, 08185
Lliçà de Vall, Barcelona

OVE ARUP & PARTNERS, S.A.
C/ Alfonso XI, 12
28014 Madrid

PUENTES Y CALZADAS, GRUPO DE EMPRESAS, S.A.
Ctra. de la Estación, s/n
15888 SIGÜEIRO-OROSO (A CORUÑA)

SORIGUÉ ACSA
Calle de la Pirotecnia. 28052.
Madrid

MEMBER OF BASQUE RESEARCH
& TECHNOLOGY ALLIANCE

TYLin Spain, S.L.

MIEMBROS PROTECTORES DE LA ASOCIACIÓN ESPAÑOLA DE INGENIERÍA ESTRUCTURAL (ACHE)

Según los Estatutos de la Asociación existen dos tipos de miembros, uno para personas jurídicas y otro para personas físicas. De entre los primeros, y por la importancia que tienen para la Asociación por su contribución económica, destacan los miembros Patrocinadores y los Protectores. Hasta la fecha de cierre del presente número de la Revista, figuran inscritos como **Miembros Protectores** los que a continuación se indican, citados por orden alfabético:

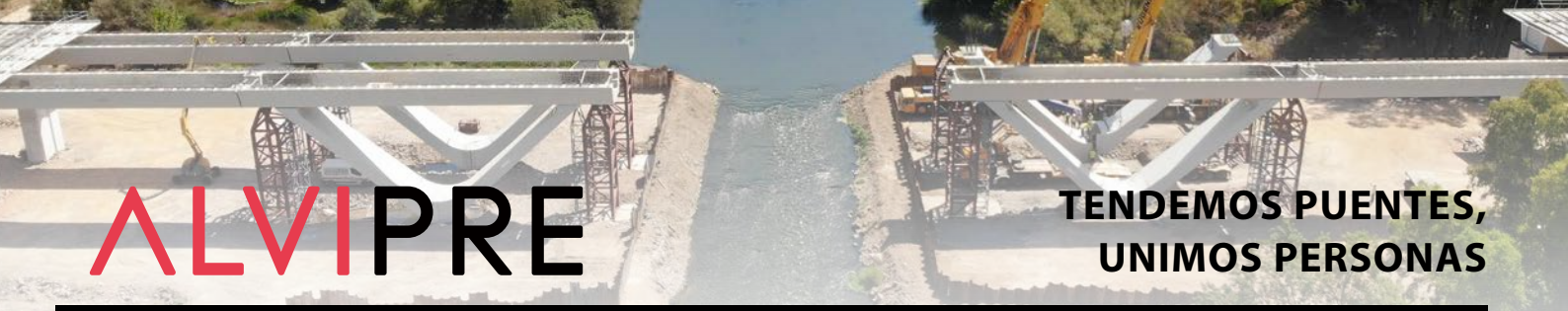

ALVIPRE

TENDEMOS PUENTES, UNIMOS PERSONAS

Construimos todo tipo de puentes, siendo las grandes piezas de obra civil, vigas para estructuras lineales, pilas, pasarelas peatonales y puentes hiperestáticos nuestro máximo exponente.

VIGAS


Vigas de fondo curvo adosadas


Vigas de fondo curvo


Vigas rectas adosadas


Vigas acarteladas de fondo variable recto

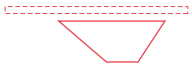
Vigas con muñón


Vigas parabólicas

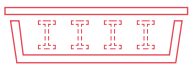
Vigas losa


Artesas

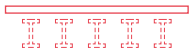
Doble T

PASARELAS


Pasarela viga cajón


Pasarela vientre pez


Pasarela arco


Pasarela fondo curvo

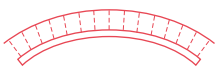
Pasarela parabólica


Pasarela recta

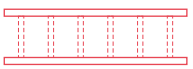
Pasarelas peatonales

ACUEDUCTOS

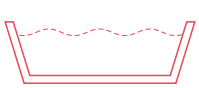

CONSTRUYAMOS juntos hoy, los **PUENTES** del mañana

PUENTES

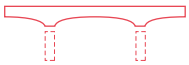

Puente de grandes luces
L > 60m

Puente con jabalcones longitudinales

Puentes pórtico

Arcos prefabricados

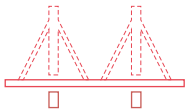

Puentes atirantados

PLACAS

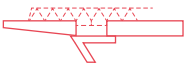

Prelosas de celosía para puentes monoviga y multiviga

Losas estándar y curvas, placas de encofrado perdido para puentes monoviga y multiviga

Losas especiales para ampliaciones y renovaciones de puentes preexistentes, para puentes de estructura metálica, o con nervios inferiores vistos

Losas para ampliaciones de calzada en voladizo

CANTO CONSTANTE

Puente con trazado recto en planta, canto constante y multiviga

Puente con trazado recto en planta, canto constante y monoviga

Puente recto o curvo en planta con jabalcones laterales

Puente con trazado recto en planta, canto constante y vigas adosadas

Puente con trazado curvo en planta, canto constante

CANTO VARIABLE

Puente con trazado recto o curvo en planta, canto variable parabolicamente

Puente con trazado recto o curvo en planta, canto variable con acartelamiento recto.

SOLUCIONES PERSONALIZADAS

De la pantalla del ordenador a la obra, pasando por la fábrica



ALVIPRE

Mejoramos las propuestas que nos llegan, gracias a una **OFICINA TÉCNICA** especializada y muy experimentada. Esto nos permite anticiparnos a los problemas de una manera ejecutiva y solvente.

El MONTAJE, nuestra diferenciación

Finalizamos nuestro trabajo a medida con el montaje de todos los elementos que fabricamos.
De esta forma, ofrecemos un valor añadido para nuestros clientes,
reduciendo tiempos de ejecución en obra, y optimizando los rendimientos tradicionales,
gracias a la experiencia atesorada por equipos de montaje especializados y propios.

CARTA DEL DIRECTOR

El número 308 de la revista *Hormigón y Acero* se publica en reconocimiento a los profesores Hugo Corres (Universidad Politécnica de Madrid) y Antonio Marí (Universitat Politècnica de Catalunya) con motivo de su jubilación. Ambos han desarrollado trayectorias académicas y profesionales de relevancia en el ámbito de la ingeniería estructural, contribuyendo al avance del conocimiento en el campo de las estructuras, así como a la formación de numerosas generaciones de ingenieros e investigadores.

Los 21 artículos (13 en inglés y 8 en español) que integran este número abordan distintos aspectos de las estructuras, han sido elaborados por compañeros, colaboradores y antiguos alumnos de diferentes países, y reflejan la diversidad de temas y enfoques que han caracterizado las trayectorias de ambos profesores.

Este número ha sido coordinado como editores asociados por Julio Sánchez, subdirector de esta revista y director técnico de Fhecor Ingenieros, y por lo profesores Jesús María Bairán y Noemí Duarte de la Universidat Politècnica de Catalunya, quienes en la carta de los editores asociados resaltan la trayectoria profesional de los dos profesores.

Con este número, *Hormigón y Acero* continúa una tradición iniciada en la etapa anterior de la revista, bajo la dirección del profesor Gonzalo Ruiz, consistente en dedicar números especiales en reconocimiento a personas que han desempeñado un papel relevante en el ámbito de la ingeniería estructural con ocasión de alguna efeméride profesional o personal.

Esta iniciativa se inició en 2018 con el número publicado en reconocimiento a la profesora de investigación Carmen Andrade, experta internacional en el campo de la durabilidad de las estructuras, y desde entonces, ha permitido reconocer la trayectoria y las aportaciones de investigadores y profesionales que han contribuido de forma destacada al progreso de nuestra disciplina. Así, en 2019 se continuó con un número en reconocimiento al profesor Javier Manterola, catedrático en la Universidad Politécnica de Madrid y gran proyectista de puentes de relevancia internacional; y en el año 2021, se publicó otro número en reconocimiento a Luis Ortega Basogoiti quien fue director de la revista e ingeniero de gran trayectoria profesional en el campo del estudio e intervención en las estructuras existentes.

La revista indexada *Hormigón y Acero* publica artículos revisados por pares sobre ingeniería estructural, en el campo de las obras civiles y de la arquitectura, en los idiomas inglés o español. Por ello, se invita encarecidamente a los autores interesados en difundir sus trabajos científicos y técnicos que consideren esta revista para sus publicaciones, siendo gratuita tanto la publicación como el acceso a todos los artículos en la web www.hormigonyacero.com.

LETTER FROM THE DIRECTOR

Issue 308 of *Hormigón y Acero* is published in honour of professors Hugo Corres (Universidad Politécnica de Madrid) and Antonio Marí (Universitat Politècnica de Catalunya) on the occasion of their retirement. Throughout their distinguished academic and professional careers, both have made significant contributions to the field of structural engineering, advancing knowledge on structural behaviour and educating several generations of engineers and researchers.

The 21 papers (13 in English and 8 in Spanish) included in this issue address different topics in structural engineering. They have been authored by colleagues, collaborators and former students from different countries, reflecting the diversity of research topics and perspectives that have characterised the professional trajectories of both professors.

This special issue has been coordinated by the Associate Editors Julio Sánchez, Deputy Director of the journal and Technical Director of Fhecor Ingenieros, together with professors Jesús María Bairán and Noemí Duarte from the Universitat Politècnica de Catalunya. In their letter, the Associate Editors highlight the academic and professional contributions of professors Corres and Marí.

With this issue, *Hormigón y Acero* continues a tradition initiated during the previous editorial period of the journal under the direction of professor Gonzalo Ruiz, consisting of dedicating special issues honouring individuals who have played a significant role in the development of structural engineering, often on the occasion of an important professional or personal milestones.

This initiative began in 2018 with a special issue in honour of Carmen Andrade, research professor and internationally recognised expert in the durability of structures. It continued in 2019 with an issue in honour of Javier Manterola, professor at Universidad Politécnica de Madrid and a renowned international designer of recognised bridges. Later, in 2021, another issue in honour of Luis Ortega Basagoiti, former director of the journal and an engineer with a distinguished career in the assessment and intervention of existing structures.

Hormigón y Acero is an indexed journal that publishes peer-reviewed articles in structural engineering, covering topics related to civil engineering works and architecture. Manuscripts are accepted in English or Spanish. Authors interested in disseminating their scientific and technical work are warmly invited to consider the journal for publication. Both publication and access are free of charge, and all articles are available at www.hormigonyacero.com.

Jesús Rodríguez
DIRECTOR DE *HORMIGÓN Y ACERO*
DIRECTOR OF *HORMIGÓN Y ACERO*

CARTA DEL EDITOR ASOCIADO

Dos trayectorias paralelas al servicio del hormigón estructural

Con este número monográfico la revista *Hormigón y Acero* quiere reconocer la contribución que dos profesores, recientemente jubilados, han realizado a la modernización y actualización de la normativa y la reglamentación de nuestro país: Antonio Marí Bernat y Hugo Corres Peiretti, cuyas trayectorias, a lo largo de más de cuatro décadas, han discurrido como dos líneas paralelas en favor del desarrollo de conocimiento del hormigón estructural en España.

Formados como ingenieros de caminos, canales y puertos en la segunda mitad de los años setenta y doctores en 1981 y 1980, respectivamente. Ambos iniciaron tempranamente una intensa labor académica e investigadora centrada en el análisis del comportamiento mecánico del hormigón armado y pretensado, contribuyendo a su integración bajo el concepto unificador de hormigón estructural, superando así la antigua dicotomía entre ambas tecnologías.

Alcanzaron la cátedra a finales de los años ochenta y comienzos de los noventa, consolidándose como referentes de una generación que transformó la concepción del hormigón estructural en España. Compartían la convicción de que esta disciplina debía apoyarse en modelos mecánicos sólidos, criterios de seguridad rigurosamente fundamentados y una normativa coherente con el estado más avanzado del conocimiento.

Desde la Universidad Politécnica de Cataluña y la Universidad Politécnica de Madrid, respectivamente, fueron decisivos en la creación de dos escuelas basadas en el rigor científico y la coherencia entre teoría y práctica. Su participación en la Comisión Permanente del Hormigón y en organismos nacionales (ATEP, GEHO y ACHE) e internacionales (CEB, FIP, fib y los comités de los Eurocódigos) contribuyó decisivamente a esa visión común. Esta convergencia culminó en la Instrucción EHE (1998) y, posteriormente, en la EHE-08, de las que fueron ponentes principales y motores conceptuales. Ambas no supusieron una mera actualización normativa, sino la síntesis de décadas de investigación, docencia y práctica profesional. Tras casi un cuarto de siglo de vigencia, respaldaron también la transición hacia los Eurocódigos Estructurales, hoy implantados de forma creciente en la ingeniería española, favoreciendo la integración de la normativa europea en el marco reglamentario nacional.

Este monográfico rinde, así, homenaje a estos dos profesores que formaron varias promociones de ingenieros y sabiendo compaginar su labor académica con una obra intelectual y profesional. La cuidadosa retroalimentación de ambas dimensiones permitió fraguar conocimientos tanto rigurosas como prácticos que marcaron de manera indeleble la evolución de la ingeniería estructural en España.

A través de las aportaciones de los diferentes autores, el presente número reúne artículos que abarcan tres dimensiones esenciales de la disciplina de la ingeniería estructural, donde el lector podrá encontrar artículos sobre investigaciones y estudios de carácter científico, trabajos sobre innovación en diseño y técnicas constructivas, así como el análisis de la visión histórico-humanista del hormigón estructural. Asimismo, el hecho de que ambos sean figuras internacionalmente reconocidas queda patente en la diversidad de los especialistas, tanto internacionales como nacionales, que han contribuido a dar a este número de la revista una enriquecedora pluralidad de enfoques y una marcada proyección internacional.

Para nosotros es un gran honor presentar al lector este número conmemorativo que aporta contribuciones de gran calidad en tres pilares fundamentales de la ingeniería civil.

Jesús Miguel Bairán García
Noemí Duarte Gómez
Julio Sánchez Delgado

EDITORES ASOCIADOS DE *HORMIGÓN Y ACERO*

HORMIGÓN y ACERO

ASSOCIATE EDITOR'S LETTER

Two Parallel Paths in the Service of Structural Concrete

With this special issue, *Hormigón y Acero* acknowledges the contribution made by two recently retired professors to the modernization and updating of Spanish structural regulations and codes: Antonio Marí Bernat and Hugo Corres Peiretti. Over more than four decades, their path ran parallel, fostering the development of knowledge in the field of structural concrete in Spain.

Both were educated as civil engineers in the second half of the 1970s and obtained their PhDs in 1981 and 1980, respectively. From an early stage, they embarked on an intense academic and research career focused on the analysis of the mechanical behaviour of reinforced and prestressed concrete, contributing decisively to their integration under the unifying concept of structural concrete, thus overcoming the former dichotomy between the two technologies.

They attained full professorships in the late 1980s and early 1990s, becoming leading figures of a generation that transformed the understanding of structural concrete in Spain. They shared the conviction that this discipline should be grounded in sound mechanical models, rigorously justified safety criteria, and regulations consistent with the most advanced state of knowledge.

From the Universitat Politècnica de Catalunya and the Universidad Politécnica de Madrid, respectively, they played a decisive role in the creation of two schools characterized by scientific rigor and coherence between theory and practice. Their participation in the Permanent Commission on Concrete and in national (ATEP, GEHO, ACHE) and international associations (CEB, FIP, fib, and Eurocode committees) was instrumental in shaping this shared vision. This convergence culminated in the Spanish Code for Design of Concrete Structures EHE (1998), and later in EHE-08 (2008 edition), for which they served as principal rapporteurs and conceptual driving forces. These documents were not a mere code update, but the synthesis of decades of research, teaching, and professional practice. After nearly a quarter of a century of application, they also supported the transition to the Structural Eurocodes, now increasingly implemented in Spanish engineering practice, thus promoting the integration of European standards into the national regulatory framework.

This special issue therefore pays tribute to two professors who educated several generations of engineers and who successfully combined their academic work with an intellectual and professional endeavour. The careful interplay between these two dimensions allowed them to forge rigorous and practical knowledge that shaped the evolution of structural engineering in Spain.

Through the contributions of the various authors, this issue brings together articles that spans three essential dimensions of the discipline of structural engineering, where the reader will be able to find contributions on scientific research, innovations in design and construction techniques, as well as analysis of humanistic and historical perspective of structural concrete and engineering. Moreover, the fact that both honourees are internationally recognized figures is reflected in the diversity of specialists—both international and national—who have contributed to this issue, providing a rich plurality of approaches and a strong international outlook.

For us, it is a great honour to present this commemorative issue to the reader, which offers high-quality contributions in three fundamental pillars of civil engineering.

Jesús Miguel Bairán García
Noemí Duarte Gómez
Julio Sánchez Delgado

ASSOCIATE EDITORS OF *HORMIGÓN Y ACERO*


Montreal, CANADÁ

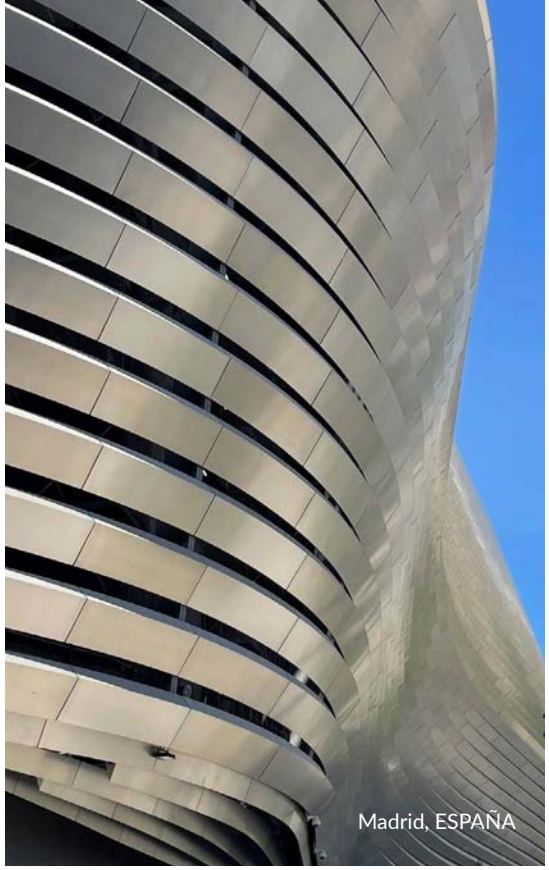
Madrid, ESPAÑA


Cadarache, FRANCIA

a world of structures fhecor

fhecor north america · fhecor deutschland · grupo fhecor ogup · fhecor consultants canada · fhecor italia · fhs · fundación fhecor


SH99, Texas, EE.UU.


Buriano, ITALIA


Santiago, CHILE


Bechem, GHANA

Disponible en **www.hormigonyacero.com**
https://doi.org/10.33586/hya.2025.4130

Comparison of Code Approaches for the SLS Design of GFRP Reinforced Concrete Flexural Members

Comparación de enfoques normativos para el diseño en el estado límite de servicio de elementos de hormigón armado con barras embebidas de GFRP.

Lluís Torres[a], Cristina Barris[a,*], Eva Oller[b], Marta Baena[a]

[a] *Department of Mechanical Engineering and Industrial Construction, Universitat de Girona*
[b] *Department of Civil and Environmental Engineering, Universitat Politècnica de Catalunya*

Recibido el 12 de mayo de 2025; revisado el 23 de junio de 2025, aceptado el 15 de septiembre de 2025

ABSTRACT

When Fibre Reinforced Polymer (FRP) bars are used as embedded reinforcement in concrete structures, serviceability behaviour often governs the design due to the lower modulus of elasticity of FRPs compared to conventional steel. While many design principles for steel-reinforced concrete remain applicable, the distinct mechanical and bond properties of FRPs require special consideration. In recent years, several international codes and guidelines have been updated or newly issued to address FRP reinforcement.

This paper presents a comparative analysis of the main aspects and provisions for serviceability limit state (SLS) design of Glass FRP (GFRP) reinforced concrete flexural members included in Eurocode 2 (2023), fib Model Code 2020 and ACI440.11-22. Stress limitation, crack width and deflections are carefully reviewed, and a design example is included, where the effects of different assumptions and limitations among codes are analysed and discussed.

KEYWORDS: Embedded FRP reinforcement, flexural members, design codes, serviceability .

RESUMEN

El comportamiento en servicio suele determinar el diseño de las estructuras de hormigón con armadura embebida de polímeros reforzados con fibras (FRP) debido a su menor módulo de elasticidad en comparación con el acero convencional. Si bien muchos principios de diseño para el hormigón armado con barras de acero siguen siendo aplicables, las características mecánicas y de adherencia de los FRPs requieren una consideración especial. En los últimos años, se han actualizado o publicado diversos códigos y guías de diseño internacionales para el refuerzo con armaduras de FRP.

Este artículo presenta un análisis comparativo de los principales aspectos y disposiciones para el diseño en estado límite de servicio (ELS) de elementos a flexión de hormigón armados con barras de polímeros reforzados con fibras de vidrio (GFRP), incluidos en el Eurocódigo 2 (2023), el Código Modelo fib 2020 y ACI440.11-22. Se revisan en detalle la limitación de tensiones, el ancho de fisura y la flecha, y se incluye un ejemplo de diseño donde se analizan y discuten los efectos de los diferentes enfoques y limitaciones entre códigos.

PALABRAS CLAVE: Armadura de FRP embebida, elementos a flexión, códigos de diseño, comportamiento en servicio.

* Persona de contacto / *Corresponding author*:
Correo-e / *e-mail*: cristina.barris@udg.edu (Cristina Barris)

How to cite this article: Torres, L., Barris, C., Oller, E., & Baena, M. (2026). Comparison of code approaches for the SLS design of GFRP reinforced concrete flexural members. *Hormigón y Acero*. 77(308):13-26. https://doi.org/10.33586/hya.2025.4130

1. INTRODUCTION

Fibre reinforced polymer (FRP) bars have emerged as an alternative to conventional reinforcement in reinforced concrete structures (RC) exposed to environments likely to cause corrosion in steel reinforcement. Likewise, FRP reinforcement has demonstrated its suitability for applications requiring magnetic neutrality, or good cuttability, as for example for diaphragm walls [1-3]. Among the several types of fibres used in manufacturing the FRPs, the glass-FRP (GFRP) reinforcement has been the most used as embedded reinforcement for RC, due to the good combination of properties and cost.

Although design recommendations for FRP reinforcement were already introduced in the 1990s in Japan [4,5], it has been in the last years when a major development of codes and guidelines has been carried out. Among them, the American Concrete Institute recently published the ACI440.11-22 code for structural concrete reinforced with GFRP [6], after the publication of some previous documents in the form of guidelines [3,7]. Likewise, the fib Model Code 2020 [8] has also incorporated provisions for FRP RC design, after having introduced the FRP reinforcement in the previous fib Model Code 2010 [9]. And even more recently, the FRP RC has been introduced in the new Eurocode 2 (EN 1992-1-1:2023) in the informative Annex R [10]. In addition to these documents, there are also codes and recommendations available in other countries as for example Italy, Canada, France or Japan [11-15].

These codes and guidelines are generally based on the same principles as for conventional steel RC, although they present some modifications to accommodate the specific properties of FRPs. It is worth to mention their linear elastic behaviour up to failure, high tensile strength combined with low modulus of elasticity [16-19], and reduction of resistant capacity under sustained stresses (creep rupture) [2,3]. Additionally, there might be high variability of mechanical properties and surface treatment among the available products, due to current lack of general standardization. The existing codes for FRP RC tend to follow similar procedures to those stablished in the corresponding code of the promoting entity for steel RC. This leads to some differences among them that mainly affect design framework, calculation models, material properties to be used, and limit values of the relevant parameters to be controlled in the design. Consequently, despite that the concepts are similar, partial or global results of the design process may present differences.

This paper presents and compares the main aspects and provisions for serviceability limit state (SLS) design of GFRP RC flexural members included in current recent codes. Three of them have been selected due to their relevance at the international level: Eurocode 2 (EC2) [10], fib Model Code 2020 (MC2020) [8] and ACI440.11-22 (ACI440.11) [6]. A detailed presentation of the design methodology for control of stresses, crack width and deflections is carried out, including a design example in which the partial and global results of the design process are presented and discussed.

2. FRP MECHANICAL PROPERTIES FOR DESIGN

As mentioned, FRP reinforcement presents some significant differences with respect to conventional steel reinforcement. Differently from steel, FRP shows a linear elastic stress-strain behaviour up to failure. In general, the tensile strength of available products is higher than that of steel reinforcement, however, their modulus of elasticity is lower (mainly for GFRP). Consequently, these materials may present high deformability with strong incidence on the serviceability behaviour of the structure [20]. Another relevant difference is that FRP materials subjected to sustained stresses, jointly with the influence of the exposure environment, may fail due to creep rupture with a lower strength than that of the short-term value [2,3,6,8].

Material properties to be considered in design are generally defined in codes where guidance is given to obtain the corresponding values either analytically or experimentally. In terms of strength, the tensile creep rupture strength at 100 years in the relevant exposure environment is the parameter taken as a reference in both EC2 (f_{ftk},100a) and MC2020 (f_{fk},100a), while the long-term limit for sustained stresses in ACI440.11 was based on a service life of 114 years [21].

According to EC2, the tensile design strength, f_{ftd}, is obtained from the long-term strength, f_{ftk},100a, divided by a material partial factor γ_{FRP} (1.5 for ULS persistent and transient and 1.0 for SLS):

$$f_{ftd} = \frac{f_{ftk,100a}}{\gamma_{FRP}} \tag{1}$$

EC2 allows directly obtaining the long-term strength for any specific rebar from experimental tests. In that sense, the European Assessment Document EAD 260023-00-0301 for carbon, glass, basalt and aramid FRP bars as reinforcement of structural elements [22] provides procedures based on ISO 10406-1 [23] to assess the influence of sustained loads on the performance of FRP bars commonly used as tensile reinforcement in RC structures.

In absence of data from tests, $f_{ftk,100a}$ can be conservatively evaluated by multiplying the characteristic short-term strength, f_{ftk0}, by several reducing factors:

$$f_{ftk,100a} = C_t \cdot C_c \cdot C_e \cdot f_{ftk0} \tag{2}$$

where C_t considers the temperature effects (1.0 for indoor and underground environments, 0.8 for outdoor members if heating through solar radiation cannot be excluded), C_c represents the effect of sustained load on the strength under short-term load (0.35 for GFRP reinforcement and 0.8 for CFRP reinforcement), and C_e accounts for the effect of ageing (taken as 0.7). The use of these coefficients may provide substantially low values of $f_{ftk,100a}$, as can be seen for example for a case of ULS (γ_{FRP} = 1.5) with outdoor exposure (C_t = 0.8), and GFRP reinforcement (C_c = 0.35) in which f_{ftd} would attain a value of $0.13f_{tk0}$. Additionally, according to EC2 the FRP reinforcement must have a modulus of elasticity $E_{fR} \geq$ 40000 MPa and a ratio of $f_{ftk,100a} / E_{fR} \geq 0.005$.

A schematic representation of the stress-strain behaviour and relevant parameters is shown in Figure 1.

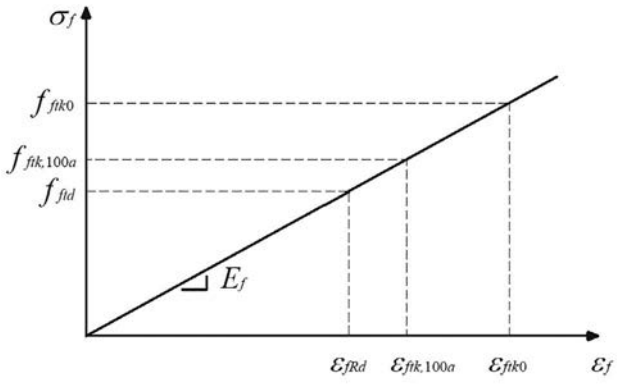

Figure 1. FRP stress-strain behaviour [10].

In MC2020 a different value is defined for the tensile design strength of FRP reinforcement to be used in ULS verifications:

$$f_{fd} = min\left\{\eta \frac{f_{fk}}{\gamma_f}; \frac{f_{ftk,100a}}{\gamma_f} \frac{\gamma_G \cdot G + \gamma_Q \cdot Q}{G + \psi_2 \cdot Q}\right\} \quad (3)$$

in which the term corresponding to the long-term strength (i.e. creep rupture) is increased according to the ratio between the design factored load and the quasi-permanent load. Additionally, the design value of the stress limit for FRP creep rupture under SLS is given by:

$$\sigma_{f,creep,Rd} = \frac{\eta_e \cdot f_{ftk,100a}}{\gamma_f} \quad (4)$$

where $f_{fk,100a}$ is the characteristic value of creep rupture strength; η_{eis} an environmental factor (a typical value of 0.85 is proposed); $\gamma_G \cdot G + \gamma_Q \cdot Q$ and $G + \psi_2 \cdot Q$ are the ULS and quasi-permanent combinations, respectively; and γ_f is a material partial factor equal to 1.3 for ULS and 1.0 for SLS.

On the other hand, in ACI440.11 the design tensile strength, ffu, is defined by:

$$f_{fu} = C_E \cdot f_{fu}^* \quad (5)$$

where f_{fu}^* is the guaranteed tensile strength and CE is an environmental reduction factor taken as 0.85. In this case, the limit value for sustained stresses in GFRP bars is $0.30 f_{fu}$ [6,21].

3. STRESS LIMITATION AND EFFECT OF CREEP RUPTURE ON DESIGN

Stresses of FRP RC flexural members are limited in a similar way as for conventional steel RC members. When using FRP reinforcement, the major differences arise from the linear behaviour up to failure and the consideration of its lower strength under sustained stresses (creep rupture), previously mentioned. Although the limits in the different codes and guidelines are based on the same principles, their values, as well as procedures and results, may differ from each other.

Concrete compression stresses in EC2 and MC2020 are similarly limited to $0.6 f_{ck}$ to avoid longitudinal cracking under the characteristic combination for certain exposure classes. Mention is done about possible effects of non-linear creep of concrete for high stresses under quasi-permanent loads.

For conventional steel RC, codes propose stress limitations under SLS conditions while in ULS the stress is limited by the design strength, based on the yield strength. Similarly, both types of limitation are applied to FRP RC design, although the way in which creep rupture is considered may represent a relevant difference. In the codes analysed in this work the effect of creep rupture is included in SLS design in ACI440.11, while EC2 and MC2020 additionally incorporate it in the ULS calculations. Therefore, the comparison of design among codes would not make sense without including the ULS for bending in EC2 and MC2020.

Stresses under SLS combinations of actions are calculated following the usual assumptions of fully cracked section and linear behaviour of materials:

$$\sigma_f = \frac{\alpha \cdot M \cdot (d - x)}{I_{cr}} \quad (6)$$

where $\alpha = E_f / E_c$ is the ratio between moduli of elasticity of FRP reinforcement and concrete, M is the flexural moment under the relevant combination of actions, d is the effective depth, x is the neutral axis depth and I_{cr} is the moment of inertia of the transformed cracked section.

In EC2, the limitation for SLS reinforcement stresses follows a similar framework as for steel with a limit equal to the design tensile strength, f_{ftd}, under the quasi-permanent combination to avoid excessive crack width and to $0.8 f_{ftd}$ under the characteristic combination of actions to avoid failure at SLS.

In MC2020, the stresses under the quasi-permanent combination should not exceed the stress limit for FRP creep rupture, $\sigma_{f,creep,\ Rd}$.

In the case of ACI440.11, the stress caused by the sustained loads (assimilable to the concept of quasi-permanent loads) should be lower than $f_{fs,sus\ max} = 0.30 f_{fu}$.

The inclusion of the creep rupture tensile strength in the ULS calculations in some codes [8,10] may have a relevant impact on the design. Although the basis of design for FRP RC bending members are the same as for steel RC, the linear elastic behaviour up to failure introduces some changes in the conventional procedures. Bending failure may be due either to concrete crushing (compression-controlled) or tensile FRP rupture (tension-controlled), and both types of failures are accepted by existing provisions. Due to their low modulus of elasticity GFRP RC beams will have large deflections at rupture, mainly for tension-controlled sections [6]. The equations governing both types of failure are slightly different; therefore, for the calculations, it will be necessary to check which is the expected failure mode. Essentially, in compression-controlled sections, the FRP stress at failure will be lower than its design strength. In contrast, for tension-controlled sections, the FRP will attain its design strength, while the concrete will not reach its ultimate strain. A summary of the procedures and equations for the three codes compared in this work can be found in Appendix B. Figure 2 presents

a non-dimensional design chart following EC2 or MC2020 procedures in which it is seen a unique curve for concrete failure and different curves for FRP rupture, depending on the reinforcement design strain. The intersection point indicates the change in model of failure. Details about the design procedure for bending FRP RC elements can be found in [24].

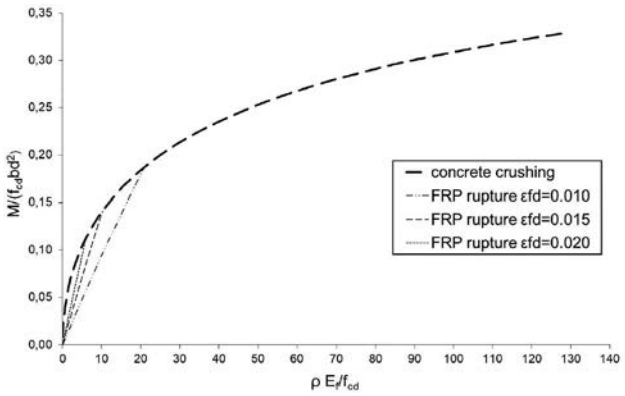

Figure 2. Design chart for flexural capacity of FRP RC members.

4. CRACK CONTROL

Because of its low tensile strength, concrete usually cracks under the tensile stresses due to bending forces. The main reasons to limit crack width are due to its incidence on the appearance, durability or functionality of the structure. Regarding the FRP reinforcement, most recommendations take into account the non-corrosive properties of FRP and propose a relaxation of usual crack limits in absence of appearance or functionality restrictions (e.g. water tightness).

The approaches for crack control in codes for FRP RC are similar to those for steel RC, with slight modifications to account for the FRP characteristics.

Crack control in the last versions of EC2 and MC2020 is based on the same procedure, although equations may apparently look different when compared. For convenience in the exposition of the conceptual basis, the equations and notation from MC2020 are summarized in the following.

In order to meet the requirements for crack control, the crack width must satisfy the condition:

$$w_{cal} \leq w_{lim} \tag{7}$$

where wcal is the design (or calculated) crack width and w_{lim} is the nominal limit considered at the concrete surface. It is emphasized that due to the highly probabilistic nature of cracking, calculated values are intended for comparison with nominal limits, and the actual measured crack widths can differ from these nominal calculated values [8].

It is considered that the procedures for steel may be applied for FRP reinforcement, provided that the corresponding material properties are used.

The crack width calculations are based on the behaviour of a prismatic RC tensile element with a simplified load-strain law with constant tension-stiffening effect after a horizontal line for the crack formation stage (Figure 3).

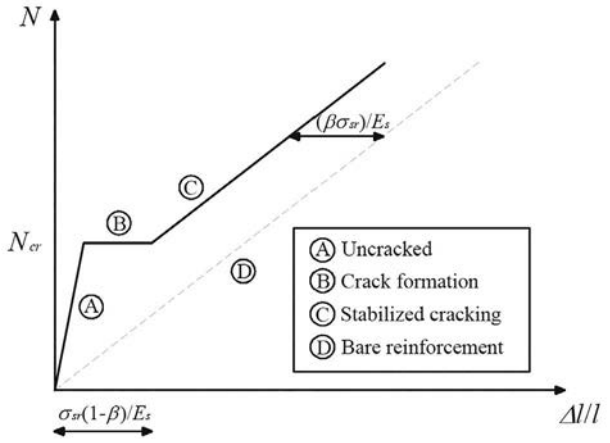

Figure 3. Load-strain model for crack control (adapted from [8]).

The calculated crack width is estimated as the product of the maximum crack spacing, $s_{r,max}$, and the difference of mean strains of FRP reinforcement and concrete ($\varepsilon_{fm} - \varepsilon_{cm}$):

$$w_{cal} = k_{l/r} \cdot s_{r,max} \cdot (\varepsilon_{fm} - \varepsilon_{cm}) \tag{8}$$

$$k_{l/r} = \frac{h-x}{d-x} \tag{9}$$

where $k_{l/r}$ accounts for the increased crack width at the concrete surface due to curvature in bending, being h the total depth of the section, d the effective depth and x the neutral axis depth of the fully cracked section.

The maximum crack spacing can be obtained by:

$$s_{r,max} = \beta_w \left(k_1 \cdot c + k_{\phi/\rho} \cdot k_{f1} \cdot k_b \frac{f_{ctm}}{\tau_{bmf}} \frac{\phi}{\rho_{f,ef}}\right) \tag{10}$$

being β_w a factor to obtain maximum crack spacing from mean crack spacing (1.7 for stabilized cracking and 2.0 for crack formation stage); k_c a parameter to consider influence of concrete cover; c is the clear cover; $k_{\phi/\rho}$ quantifies the influence of the mean bond strength τ_{bmf} (assumed as 0.25); k_{f1} accounts for stress distribution before cracking (pure tension, bending); k_b accounts for poor bond conditions (1.2) or good bond conditions (0.9); f_{ctm} is the mean tensile strength of concrete; ϕ is the bar diameter; and $\rho_{f,ef}$ is the effective reinforcement ratio (in a defined effective concrete area in tension surrounding the bars, $A_{c,ef}$). By default, this procedure assumes a bond effect between FRP and concrete similar to that of steel reinforcement, although the equation contains parameters to consider the influence of bond.

The mean strain difference for elements subjected to direct load may be calculated as:

$$\varepsilon_{fm} - \varepsilon_{cm} = \frac{\sigma_f - \beta_{TS}\,\sigma_{fr,ef}}{E_f} \geq \frac{\phi_f}{E_f}(1-\beta_{TS}) \tag{11}$$

with

$$\varepsilon_{fm} - \varepsilon_{cm} = \frac{f_{ctm}}{\rho_{f,ef}}(1+\alpha_e \cdot \rho_{f,ef}) \tag{12}$$

where σ_f is the reinforcement stress in the cracked section; E_f is the modulus of elasticity of FRP reinforcement; α_{eis} the modular ratio E_f/E_c; and β_{TS} is 0.6 for crack formation stage and short-term loading in stabilized cracking, and 0.4 for long-term loading in stabilized cracking.

According to EC2, the limiting value of crack width under the quasi-permanent combination is 0.4 mm for appearance requirements. In absence of appearance conditions, fasteners, punctual wheel pressure, lap splice or freeze thaw, this limit may be relaxed to values up to 0.7 mm. The same limitations apply in MC2020.

Control of cracking in ACI440.11 is carried out by limiting the longitudinal reinforcement spacing using a procedure developed in [25] based on modifications of [26]. Instead of obtaining a calculated value of crack width to be compared with a limiting value, the equations have been arranged by introducing a crack width limit of 0.7 mm, to explicitly obtain a maximum allowed value of reinforcement spacing, having at the same time to satisfy a maximum reinforcement stress:

$$s \le \frac{0.36\,E_f}{f_{fs}\cdot k_b\cdot \beta_{cr}} - 2.5\cdot c_c \ge 0.65\,\frac{E_f}{f_{fs}\cdot k_b} \tag{13}$$

$$f_{fs} \le \frac{0.36\cdot E_f}{d_c\cdot k_b\cdot \beta_{cr}} \tag{14}$$

where c_c is the least distance from bar surface to tension face; d_c is the concrete cover to centre of bar; f_{fs} is the tensile stress at service loads; β_{cr} is the ratio of the distance from neutral axis to extreme tensioned fibre to the distance from neutral axis to centroid of reinforcement; and k_b is a bond factor taken as 1.2 for GFRP. In specific situations where a smaller crack width value is judged to be appropriate, the coefficients 0.81 and 0.36 can be adjusted linearly.

5. DEFLECTION CONTROL

Excessive deflections of RC flexural members may derive in problems of appearance, integrity of non-structural elements or loss of functionality of the structure or equipment. To avoid the aforementioned problems, deflections are limited generally to a fraction of the member span. Since these effects are independent of the type of reinforcement, the same limits as for steel RC apply for FRP RC members.

Because of the many factors that influence deflections, the actual values can differ significantly from those calculated. Uncertainties in assessing the actual material properties, loading history, construction procedures, assessment of member forces, and environmental conditions may have a strong influence on deflections. In that sense, calculated deflections (as for the case of crack width) should be taken as reference values intended for comparison with specified limits [8,27,28].

The relatively low modulus of elasticity of FRP reinforcement (mainly for GFRP), makes them susceptible to experience large deflections. However, the same basis and subsequent formulation for assessing the flexural deformations of steel RC members applies also for FRP reinforcement as experimentally proven. For short-term deflections, the main aspect to take into account is the change in the modulus of elasticity. Since long-term deformations depend on the sectional area of concrete creeping and shrinking (i.e. the neutral axis depth), a reinforcement with different stiffness may lead to a different ratio between short and long-term deflections (lower if the modulus of elasticity is lower) [29]. In that sense, methods based on general procedures [8,10], where the main properties can be introduced, may be directly applied. On the other hand, simplified methods for steel RC based on multiplicative coefficients may need some adjustment [30-32].

Calculation of deflections for FRP RC members in EC2 follows the general procedure in the main body of the code for steel RC. Deformation of cracked members is obtained as an interpolation of sectional deformations in uncracked and fully cracked states:

$$a = (1-\zeta)\cdot a + \zeta\cdot a_{II} \tag{15}$$

where a is the deformation parameter considered (strain, curvature or rotation; as a simplification, it may also be taken as deflection) and subscripts I and II account for uncracked and fully cracked states; and ζ is a distribution coefficient (allowing for tension-stiffening effect) given by:

$$\zeta = 1-\beta_T\left(\frac{\sigma_{fr}}{\sigma_f}\right)^2 \ge 0 \tag{16}$$

with ζ=0 for uncracked sections; β_t equal to 1.0 for single short-term loading or 0.5 sustained/repeated loading; σ_{fis} the highest tensile reinforcement stress having occurred; σ_{fr} is the reinforcement stress under the cracking conditions. In case of flexure σ_{fr}/σ_f may be replaced by the ratio of corresponding bending moments M_{cr}/M.

The effective tensile strength of the concrete, $f_{ct,eff}$, may be taken as the mean axial tensile strength, f_{ctm}, or the mean flexural tensile strength, $f_{ct\,fl}$.

Long-term deflections due to creep are calculated using transformed sections through the effective modulus of elasticity of concrete, $E_{c,eff}$:

$$E_{c,eff} = \frac{1.05\cdot E_{cm}}{1+\varphi} \tag{17}$$

where E_{cm} is the secant modulus of elasticity of concrete; and φ is the concrete creep coefficient.

Shrinkage deflections can be calculated from sectional curvatures given by:

$$\left(\frac{1}{d}\right)_{\varepsilon_{cm}} = \varepsilon_{cm}\,\frac{E_f}{E_{c,eff}}\,\frac{S_i}{I_i} \tag{18}$$

being ε_{cs} the shrinkage strain; S_i the first moment of the reinforcement about the centroid of the long-term transformed cross-section for the uncracked ($i = I$) or fully cracked ($i = II$) conditions; and I_i the second moment about the centroid of the long-term transformed cross-section for the states I and II.

For a rigorous calculation, deflections can be assessed from double integration of averaged sectional curvatures along the member. Since the deflection is very sensitive to the curvature of the determinant section, a more simplified procedure

consists in the interpolation of member deflections in states *I* and *II*. This simplification is equivalent to use an effective moment of inertia for the flexural element, deduced by introducing curvatures ($(1/r)=M/(E\cdot I)$) in Eq. (15) [9,33,34]:

$$I_{ef}=\frac{I_I\cdot I_{II}}{\zeta\cdot I_I(1-\zeta)\cdot I_{II}} \tag{19}$$

that replacing ζ from Eq. (16) may be rearranged to [18,35]:

$$I_{ef}=\frac{I_{II}}{1-\beta_t\cdot\left(M_{cr}/M\right)^2\left(1-I_{II}/I_I\right)} \tag{20}$$

Figure 4 shows a typical representation of the sectional moment-curvature behaviour.

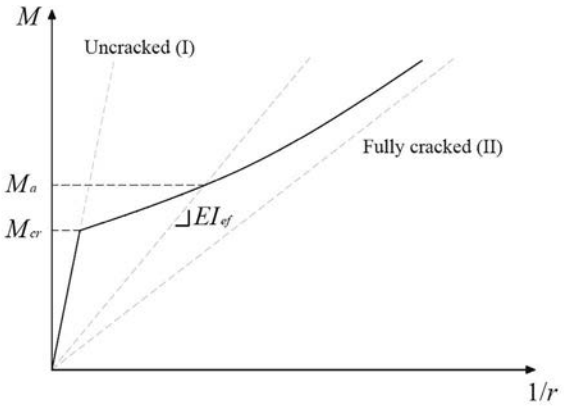

Figure 4. Moment-curvature and Ief.

According to the Eurocodes [36], the total long-term deflection under the quasi-permanent combination is limited to *L*/250, which has been the criterion to deduce the proposed span-to-depth ratios to comply with deflection limitations in EC2.

MC2020 introduces three levels of approximation to calculate deflections due to bending, which are based on the same principles and general methodologies exposed in previous versions of fib Model Code [9,37] and Eurocode 2 [38]. A general method (LoA III) and a simplified method for RC structures (LoA II) are applicable to FRP RC members.

LoA III refers to methodologies based on nonlinear numerical analysis of reinforced and prestressed concrete structures accounting for the most relevant aspects influencing their actual behaviour: cracking, time-dependent properties, load history, construction sequence, deterioration or retrofitting, among others [28,39-50]. MC2020 explicitly includes as an option for a general approach, the procedure already mentioned for EC2 (Figure 4, Eqs. (15-18)) to obtain averaged sectional deformations from interpolation between the uncracked and cracked states and consequent integration along the member [45,47]. In this case, the bending moments can be approximated by linear analysis and subsequent redistribution if needed. It also has been implemented in general models for nonlinear serviceability analysis of beams and frames [51]. Other methodologies for accounting of cracking and tension-stiffening, such as those based on modified constitutive models for concrete or steel, would also be included among the nonlinear procedures [52-55].

The simplified method LoA II is derived from LoA III and is appropriate for RC flexural members either simply supported or continuous with or without side cantilevers, and fixed-end cantilevers. It allows usual sections shapes (rectangular, T, I) and variable reinforcement layout along the member. No explicit integration of curvatures is needed; cracking, tension-stiffening, creep and shrinkage of concrete are considered [8,28].

The instantaneous deflections are calculated interpolating deflections in the uncracked (the gross section may be used) and fully cracked states (with averaged tensile and compressive reinforcement ratios along the member) by using Eq. (15) and adopting a secant modulus of elasticity of concrete $E_c=0.9E_{ci}$. The distribution factor in Eq. (16) is modified to:

$$\zeta=k_e\left[1-\beta\left(\frac{M_{cr}}{M_a}\right)^2\right] \tag{21}$$

where M_{cr} is calculated with f_{ctm}; M_a is obtained from the characteristic combination; and k_e accounts for the uncracked parts of the beam on the global member stiffness, an effect that may be relevant for low reinforcement ratios and high concrete strength (i.e. relatively high ratio M_{cr}/M_a). For simply supported and continuous beams: $k_e=1$ for $M_{cr}/M_a\leq 0.5$, and $k_e=2\cdot(1-M_{cr}/M_a)$ for $0.5<M_{cr}/M_a\leq 1$; while for cantilevers: $k_e=1-(M_{cr}/M_a)^2$ for $0.5<M_{cr}/M_a\leq 1$.

The time-dependent deflection is computed as the sum of creep and shrinkage deflections. For cracked sections, creep deflection will be assessed by applying a multiplicative factor to the previously calculated instantaneous deflection due to quasi-permanent loads. The factor is deduced considering a cracked section where the effect of creep causes a redistribution of compressive concrete stresses, while the stress in the tensile reinforcement is assumed constant, which is very close to experimental behaviour [45,56,57]. A detailed deduction can be found in [28]. Equilibrium and compatibility equations lead to:

$$a_\varphi=a_{i,qp}(t_0)\frac{x_0}{d}\frac{0.8\cdot k_t\cdot\varphi}{1+12\cdot\alpha\cdot\rho'_m} \tag{22}$$

where $a_{i,qp}$ is the instantaneous deflection due to quasi-permanent load; x_0 is the instantaneous neutral axis depth computed with the averaged tensile ($\rho_m=\Sigma(\rho_i\cdot l_i)/\Sigma l_i$) and compressive ($\rho'_m=\Sigma(\rho'_i\cdot l_i)/\Sigma l_i$) reinforcement ratios along the member; φ is the creep coefficient; α is the modular ratio E_f/E_c; and $k_t=0.3+100\rho_m\leq 1$ is a correction factor to account for the uncracked parts of the beam calibrated through LoA III method [44].

The shrinkage deflection is calculated by integration of curvatures due to shrinkage, accounting for free shrinkage strain, effective depth, element length and boundary conditions. For a cracked member:

$$a_{cs}=a_{cs}\,k_t\,\psi_{cs}\frac{l^2}{8} \tag{23}$$

being φ_{cs} a reference curvature given by:

$$\psi_{cs}=\frac{\varepsilon_{cs}}{d}\frac{1}{1+12\cdot\alpha\cdot\rho'_m} \tag{24}$$

where ε_{cs} is the shrinkage strain and k_s an integration factor that may be taken as 1 for simply supported beams, 0.7 for

end spans of continuous beams and 0.85 for interior spans.

MC2020 suggests limiting total deflections to L/250 under the quasi-permanent combination for appearance requirements and general utility of the structure.

The ACI 440.11 code for GFRP RC structures follows the framework of ACI 318-19 for steel RC [58]. Current equations for deflection calculation in ACI formulate an effective moment of inertia [18], Ie, equivalent to a weighted average of flexibility based on the concept indicated in Eqs. (19) and (20) [32,59].

The effective moment of inertia to calculate immediate deflections in GFRP RC cracked members is obtained from:

$$I_{ef} = \frac{I_{II}}{1 - \gamma \cdot \left(M_{cr}/M\right)^2 \left(1 - I_{cr}/I_g\right)} \quad \text{for } M_a \geq M_{r,cr} \tag{25}$$

where $M_{r,cr}$ is a reduced cracking moment to account for restraints and reduced tensile strength that is set to $0.8M_{cr}$ for GFRP members (instead of $0.67M_{cr}$ used for steel RC) [58,60]; M_{cr} is calculated using the gross moment of inertia, I_g, and the modulus of rupture of concrete, f_r; and γ accounts for the variation of stiffness over the member length due to the bending moment diagram [60], whose value for uniformly distributed load is given by:

$$\gamma = 1.72 - 0.72 \left(\frac{0.8M_{cr}}{M_a}\right) \tag{26}$$

It is worth noting that the use of the factor $\beta = 0.5$, for sustained or repeated loading in EC2 and Model Code equations, causing a shift in the deformation response, would be equivalent to the effect of a reduced cracking moment of $\sqrt{0.5}\ M_{cr} = 0.71M_{cr}$ (for $M \geq M_{cr}$), in between those used in ACI for steel and FRP reinforcement [32].

For slabs and continuous beams, the effective moment of inertia may be taken as a weighted average of the critical positive and negative moment sections.

The time-dependent deflections are assessed by multiplying the short-term deflections due to sustained loads with a reduced factor $\lambda_\Delta = 0.6\xi$, where ξ is taken from ACI 318-19 for steel RC [58]. The method is practical and easy to use in design, although it does not explicitly consider the moduli of elasticity, sectional stiffness, creep coefficient or shrinkage strain, which may present different values and have relevant influence on the time-dependent-to-immediate deflection ratios [29,30,61].

In ACI440.11, the immediate deflection due to live load of floors not supporting elements likely to be damaged is limited to $L/360$, while the increment of deflection after installation of the non-structural elements is limited to $L/240$. When the floor supports elements likely to be damaged, the increment of deflections after installing those elements is $L/480$.

6. COMPARISON – DESIGN EXAMPLE

This section presents an illustrative example of design of a simply supported reinforced concrete beam of a building for service and administrative uses subjected to a marine environment, with the aim of comparing the procedures of the different codes when designing the longitudinal GFRP reinforcement to accomplish the different serviceability limit states.

The geometry of the beam, with a rectangular cross-section of 300 × 470 mm and a span length of 4.5 m, is shown in Figure 5. The effective depth is taken as 415 mm, accomplishing the different cover requirements for all considered codes. The reinforcement rebars are distributed in one layer.

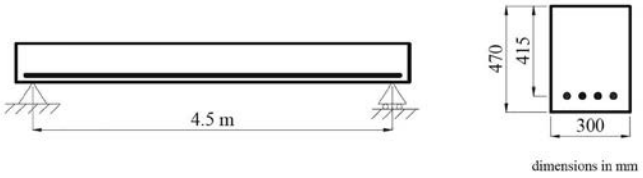

Figure 5. Geometry of the studied beam.

The loads acting on the structure consist of a uniformly distributed permanent (dead) load of g = 16 kN/m (including self-weight), and a variable load (live) q = 10 kN/m, resulting in a characteristic (service) load $g + q$ = 26 kN/m. The combination factor for quasi-permanent (sustained) loads is ψ_2 = 0.3. Table 1 shows the maximum bending moment at midspan for the different load combinations that should be considered for design at Ultimate Limit State (ULS) and Serviceability Limit State (SLS). It is assumed that a pre-cracking load corresponding to the characteristic load is applied at 28 days to globally represent effects on cracking level of construction loads.

Material mechanical properties are summarized in Tables 2 and 3. The characteristic concrete compressive strength is f_{ck} = 35 N/mm², assuming a weighted creep coefficient to take into account loading history of φ = 1.60 [8,52] and a shrinkage strain of ε_{cs} = 0.000450. For the sake of simplicity, the specified concrete strength, f_c', in ACI has been assumed equal to the characteristic strength, f_{ck}, in EC2 and MC2020. Concrete material properties have been calculated according to the different codes (see Appendix A). As can be seen, there are some differences in the nominal values of the moduli of elasticity, which is due to the definition of each code (secant, tangent). As for the tensile strengths, EC2 uses the mean axial tensile strength, fctm, for crack control calculations, while for deflection control

TABLE 1.
Maximum bending moment at midspan for the different load combinations.

Combination	ULS	SLS characteristic (service)	SLS quasi-permanent (sustained)
EC2/MC2020	M_{Ed} = 92.6 kN·m	M_k = 65.8 kN·m	M_{qp} = 48.1 kN·m
ACI440.11	M_u = 89.1 kN·m	M_s = 65.8 kN·m	M_{sus} = 48.1 kN·m

both mean axial tensile strength and flexural strength, $f_{ctm,fl}$, can be considered according to the designer's criteria. In this example, both values were used for comparative purposes. For the case of MC2020, fctm is used for both crack and deflection control. Definitions of fctm from these codes are just slightly different. Finally, the tensile strength value according to ACI (modulus of rupture) is in that case similar to the flexural tensile strength according to EC2.

The GFRP characteristic tensile strength is f_{ftk0} = 1000 N/mm² and the modulus of elasticity is E_f = 60000 N/mm². The value of characteristic tensile f_{ftk0} strength was assumed equal to the guaranteed tensile strength in ACI, f^*_{fu}. The long-term strength (100 years) is assumed to be provided by the manufacturer from creep rupture tests according to ISO 10406-1 and is taken as $f_{ftk,100a}$ = 480 N/mm². If the manufacturer has not performed the tests to characterize the long-term strength, then $f_{ftk,100a}$ can be conservatively evaluated using Eq. (2). Depending on the environmental conditions (indoor or outdoor), this value is obtained as 245 N/mm² or 196 N/mm², respectively. As observed, the absence of tests may lead to significantly lower values.

Tables 4 to 6 show the minimum area of reinforcement needed to accomplish the requirements for the aforementioned design aspects in relation to the different provisions under study (EC2, MC2020 and ACI440.11). In addition, the disposed number of rebars assuming a diameter of 16 mm, is given in each Table.

In this example, deflections have been calculated by means of the common simplified procedure of interpolation of member deflections in uncracked and fully cracked states. The use of f_{ctm} or $f_{ctm,fl}$ for calculating M_{cr} has been traditionally based on the consideration of the existence or not of residual tensile stresses that may cause a reduction of cracking moment [38]. According to EC2 (Table 4), if the long-term strength of the FRP rebars ($f_{ftk,100a}$) is obtained from tests, the more restrictive criteria is deflection control when using f_{ctm} to obtain the cracking moment (755 mm²), while using $f_{ctm,fl}$ would require a slightly lower reinforcement area (711 mm²). This way, if $f_{ctm,fl}$ is used the more restrictive value would be that given by the effect of creep rupture of FRP rebars on the flexural capacity (730 mm²). In any case, the obtained results are not very different and lead to the same number of FRP rebars (4Θ16). It is worth noting that the absence of creep rupture tests, and therefore the assessment of the long-term strength from Eq. (2) with $f_{ftk,100a}$ = 245 MPa, would have given the largest FRP area as a requirement for flexural capacity, with a value of 1425 mm² (88.7% higher). Consequently, when applying the EC2 provisions the importance of characterizing the long-term strength through experiments should be highlighted.

SLS of deflection also controls design according to MC2020 (Table 5). Both LoAII and LoAIII were considered. For the LoAIII approach, the option indicated in MC2020 based on integration along the member of averaged sectional curvatures between the uncracked and cracked states and consequent has been used here. Its application to the example gives a minimum longitudinal reinforcement area of 665 mm² for LoAII, while a similar slightly lower value of 648 mm² is obtained from LoAII. In comparison with the EC2 procedure, it is seen that the effect of creep rupture on flexural capacity provisions is not as relevant in this case. Using the same value of the long-term strength obtained from tests (i.e. 480 MPa) the design tensile strength, f_{fd}, according to Eq. (3) would be 711 MPa, that represents a noticeable increase over the value f_{ftd} = 320 MPa applied for EC2. Consequently, the area needed for this requirement is 330 mm², which is 43.8 % of 730 mm² for EC2.

TABLE 2.
Material properties according to EC2 and MC2020.

	GFRP bars			Concrete		
	f_{ftk0} (N/mm²)	$f_{ftk,100a}$ (N/mm²) (indoor)	f_{ftd} [3] (N/mm²)	f_{ctm} (N/mm²)	$f_{ctm,fl}$ (N/mm²)	E_c (N/mm²)
EC2	1000	480[1] 245[2]	320 163	3.21	3.63	33282[4]
MC2020	1000	480[1]	711	3.30	-	34962[5]

(1) Data from tests developed by suppliers.
(2) Indoor value from EC2 (Annex R) in absence of tests (see Sect. 2).
(3) See Sect. 2.
(4) Secant modulus.
(5) Tangent modulus.

TABLE 3.
Material properties according to ACI440.11

	GFRP bars			Concrete	
	f_{fu}^* (N/mm²)	f_{fu} (N/mm²)	$f_{fs,sus\ max}$ (N/mm²)	f_r (N/mm²)	E_c (N/mm²)
ACI440	1000	850	255	3.67	27806[1]

(1) Secant modulus.

According to ACI440.11 (Table 6), the total area of reinforcement required for SLS deflections is 763 mm², which in this case is very close to the value obtained from EC2 and not very different to those from MC2020. The case of floors not supporting elements likely to be damaged has been considered, and as exposed in Sect. 5, the immediate deflection due to live load has been limited to $L/360$, and the increment of deflection after installation of the non-structural elements to $L/240$, being the last one the most restrictive for the required area of reinforcement.

In relation to the cracking verification, the default value in EC2 for maximum crack width is 0.4 mm, due to appearance conditions. In absence of these conditions the value can be increased up to 0.7, which for comparison purposes has been used in this section for the calculations since it is the default value in ACI440.11 (although the code also allows more restricted values according to the designer's criteria). As indicated in the table footnotes, for crack width calculations a diameter must be previously assumed, in that case 16 mm. Based on these assumptions, the requirements for crack control from the three codes have resulted in lower reinforcement areas than those previously discussed. When cracking is verified following EC2 and MC2020, the bottom reinforcement is located in good casting conditions and k_b = 0.9. The required area for both EC2 and MC2020 is the same (590 mm²), because both formulations are similar. When designing according to ACI440.11, crack control requires a higher amount of longitudinal reinforcement (744 mm²) compared to EC2 and MC2020, although it has not been the conditioning criteria.

In case of limiting the crack width to 0.4 mm, EC2 and MC2020 provisions would have resulted in 857 mm² that corresponds to 5Θ16. For this limitation, ACI440 provisions would have led to 1076 mm², corresponding to 6Θ16, which could not be allocated in one layer. Thus, a rebar diameter of 19 mm would be more convenient, requiring in this case a reinforcement area of 1115 mm2 (4Θ19).

For the FRP stress limitation condition related to creep rupture under SLS, and according to EC2, the verification of stresses for the characteristic combination of actions is more restrictive than that of the quasi-permanent combination of actions. In the first case, the stresses in the reinforcement for the characteristic combination are compared to 80% of the design value of the long-term strength, and in the verification of the quasi-permanent stresses, the comparison is with the design value of the long-term strength. In the last case, the effective properties of the cross-section have been used. As indicated in Table 4, the required area for SLS stress limitation in case of using the long-term strength from tests in EC2 would be 428 mm². In absence of tests, use of long-term strength from Eq. (2) would require 850 mm².

MC2020 only considers the verification of stresses under sustained conditions. Therefore, the quasi-permanent combinations of actions is used. The sustained stress should be lower than the design value of the stress limit for creep rupture which in that case is equal to the long-term strength of the FRP affected by a factor of 0.85 as seen in Eq. (4). The application of these combinations and limitations globally leads to a required area is 298 mm² (70% of that in EC2).

As for ACI440.11, the verification of creep rupture through the limitation of stresses is only carried out under SLS. Unlike EC2 and MC2020, the code does not mention the option to use values obtained from tests. For that verification, the stress is calculated for the sustained loading combination and the limit is fixed to $0.30f_{fu}$. This leads to a required area of 474 mm².

Anyway, for the case of this example, the requirement of stresses under SLS would not be the governing factor for any of the three codes.

Table 7 summarizes the required reinforcement area, the number of rebars considering a 16 mm diameter, and the limiting condition for design for the three codes. It is seen that SLS deflection governs in all cases if in EC2 the long-term strength is characterized through tests and fctm is used for deflection calculations. In case of using $f_{ctm,\,fl}$ for deflections in EC2, creep rupture for flexural capacity would govern for this code. Although there are some slight differences among codes, in all cases 4Θ16 are needed to globally comply with every requirement. When the long-term strength due to creep rupture in EC2 is not obtained from tests, but assessed through Eq. (2), the reinforcement area would increase up to 1425 mm², to comply with the requirements of flexural capacity.

The final results in terms of number of rebars required by the different codes in this example are the same and mainly due to deflection control. However, when comparing the different limit states analysed it is seen that there might be larger differences in the verification of cracking and stresses. For the case of stresses the calculation models do not provide significant differences and the divergences are mainly due to the combination of actions and prescribed limits. For the case of cracking, some differences may arise from the calculation models (EC2 and MC2020 versus ACI) as well as from the limitations inherent to each model. It is shown that limiting crack width to 0.4 mm instead of 0.7 mm may cause a significant increment of reinforcement area.

Moreover, it is seen that the value and provisions to account for the long-term design strength due to creep rupture may lead to significant variations in the required reinforcement area. Obtention of this strength through tests, mainly for EC2, seems to be of major importance since the proposed equation may result in very conservative values. Consideration of creep rupture only in SLS or also in ULS may also have relevant incidence. In that context, a more in-depth study on reliability, based on experimental data from commercially available rebars, would be needed to help harmonize the treatment of creep rupture across different design codes.

Finally, it should be emphasized that this is only an illustrative example with the objective to allow comparison and discussion of the main requirements in FRP RC flexural design. These results and conclusions should not be taken as broadly representative, given the number of variables involved in the flexural design of FRP RC and the high variability of properties that may be found among the available products. In that sense, a wide parametric study would be necessary to arrive at more general conclusions.

Table 4.
GFRP reinforcement areas in mm² needed to comply with EC2 provisions

EC2	Cracking(1)	Deflection		FRP stresses (SLS)		FRP stresses (ULS) *Flexural capacity*
		f_{ctm}	$f_{ctm,fl}$	*quasi-perm.*	*charact.*	
Strictly required (mm²)	590(2)	755	711	252	428	730(3)
Disposed	3Θ16 (603)	4Θ16 (804)	4Θ16 (804)	2Θ16 (402)	3Θ16 (402)	4Θ16 (804)

(1) Crack width limit of 0.7 mm is assumed, in absence of appearance conditions. A diameter must be assumed for crack control calculations, being in that case Θ16.
(2) Minimum required area which does not correspond to an integer number of bars of Θ16.
(3) Tension-controlled failure (FRP rupture).

TABLE 5.
GFRP reinforcement areas in mm² needed to comply with MC2020 provisions

MC2020	Cracking(1)	Deflection		FRP stresses (SLS)	FRP stresses (ULS)
		LoAIII	*LoAII*		
Strictly required (mm²)	590(2)	648	665	298	330(3)
Disposed	3Θ16 (603)	4Θ16 (804)	4Θ16 (804)	2Θ16 (402)	2Θ16 (402)

(1) The cracking model in MC2020 is similar to that in EC2. The same values are obtained, and the same comments apply.
(2) Minimum required area which does not correspond to an integer number of bars of Θ16.
(3) Tension-controlled failure (FRP rupture).

TABLE 6.
GFRP reinforcement areas in mm² needed to comply with ACI440 provisions

ACI440.11	Cracking(1)	Deflection		FRP stresses (SLS)	FRP stresses (ULS) *Flexural capacity*
		Δ_{inc}	$\Delta_{i,L}$		
Strictly required (mm²)	744(2)	702	763	474	495(3)
Disposed	4Θ16 (603)	4Θ16 (804	4Θ16 (804)	3Θ16 (603)	3Θ16 (603)

(1) Crack width limit of 0.7 mm is assumed, as default value in the code, in absence of additional requirements. A diameter must be assumed for crack control calculations, being in that case 16
(2) Minimum required area which does not correspond to an integer number of bars of Θ16.
(3) Tension-controlled failure (FRP rupture).

TABLE 7.
Required GFRP reinforcement areas in mm² needed to comply with all provisions

FRP area (mm²)	EC2	MC2020	ACI440.11	
Strictly required	755(1)	730(2)	665	763
Disposed	4Θ16	4Θ16	4Θ16	4Θ16
Condition	Deflection	Flex. capacity	Deflection	Deflection

(1) Long-term strength characterized through tests and f_{ctm} for deflection control.
(2) Long-term strength characterized through tests and $f_{ctm,fl}$ for deflection control.

7. CONCLUSIONS

A comparative analysis of existing standards (EC2, MC2020 and ACI440.11) for the design of GFRP RC flexural members has been included in this paper, focusing on the main aspects and provisions for serviceability limit state (SLS). These three standards were selected due to their relevance at international level. From the performed study the following conclusions can be drawn:

- In general, the design of FRP RC flexural elements follows principles similar to those of steel RC elements, but there are some particularities derived from the linear-elastic behaviour and from the possible creep rupture under sustained loads.
- Stress limitations are applied in all reviewed codes, but with varying allowable stress values. ACI440.11 only addresses creep rupture effects at the serviceability level, while EC2 and MC2020 additionally incorporate it in the ULS calculations.

- The models for crack control are the same in EC2 and MC2020, but different from ACI. For all studied standards, the crack width might be relaxed to values up to 0.7 mm, in the absence of more restrictive conditions such as appearance or water tightness.
- The simplified procedures for deflection calculation of the three codes are based on averaged curvatures leading to an effective moment of inertia in the case of ACI440.11 and allow considering the influence of the uncracked parts of the member. While EC2 and LoA II of MC2020 interpolate between uncracked and fully cracked states, incorporating effects like tension-stiffening, creep, and shrinkage, ACI 440.11 uses a multiplicative factor for long-term deflections.
- The inclusion of creep rupture effects in the ULS verification besides SLS has relevant consequences in the particular case of EC2. In that sense, it is of major importance to assess the long-term strength of the reinforcement through tests, since the proposed equation may lead to very conservative results.
- For the example presented in this paper, SLS deflection governs in all cases. However, for EC2, creep rupture for flexural capacity would govern if fctm, fl is used to calculate the cracking moment when checking deflections. For cracking, it is seen that limiting crack width to 0.4 mm instead of 0.7 mm may cause a significant increment of reinforcement area. For SLS stresses the divergences are mainly due to the combination of actions and prescribed limits.
- Given the numerous variables involved, a wide parametric analysis is required to reach generalized conclusions.

Acknowledgements

This article is dedicated to Professor Antonio Marí, with whom we have had the privilege to collaborate over a long time in the field of serviceability behaviour of concrete structures. His extensive knowledge, commitment to excellence and leadership have been a reference and source of inspiration for us. We also extend this dedication to Professor Hugo Corres, for his valuable contributions to the field of structural concrete.

We would also like to acknowledge the financial support provided by projects CPP2022-009555 and PCI2023-143361 funded by MICIU/AEI/10.13039/501100011033, European Union-NextGenerationEU/PRTR and by ERDF/EU.

References

[1] L.C. Bank, Composites for Construction: Structural Design with FRP Materials, Wiley, 2007.

[2] fib T.G. 9.3, Bulletin 40. FRP reinforcement in RC structures, Lausanne, Switzerland, 2007.

[3] ACI Committee 440, Guide for the Design and Construction of Structural Concrete Reinforced with Fiber Reinforced Polymer (FRP Bars) (ACI440.1R-15), American Concrete Institute, Farmington Hills, Michigan, USA, 2015.

[4] JSCE, Application of Continuous Fiber Reinforcing Materials to Concrete Structures, Concrete Library, No. 72, 1992, published in Japanese.

[5] K. Pilakoutas, M. Guadagnini, K. Neocleous, L. Taerwe, Design guidelines for FRP reinforced concrete structures, in: Proceedings of the 3rd International Conference Advanced Composites in Construction (ACIC2019), Bath, 2007.

[6] ACI Committee 440, Building Code Requirements for Structural Concrete Reinforced with Glass Fiber-Reinforced Polymer (GFRP) Bars (ACI440.11-22), American Concrete Institute, Farmington Hills, Michigan, USA, 2022.

[7] ACI Committee 440, Guide for the Design and Construction of Structural Concrete Reinforced with FRP Bars, (ACI440.1R-06), American Concrete Institute, Farmington Hills, Michigan, USA, 2006.

[8] fib, fib Model Code for Concrete Structures 2020 v1.2, International Federation for Structural Concrete, Lausanne, Switzerland, 2024.

[9] fib, fib Model Code for Concrete Structures 2010, International Federation for Structural Concrete, Lausanne, Switzerland, 2013.

[10] CEN, Eurocode 2: Design of concrete structures — Part 1-1: General rules — Rules for buildings, bridges and civil engineering structures (EN 1992-1-1:2023), European Committee for Standardization, Brussels, Belgium, 2023.

[11] CNR, Guide for the design and Construction of Concrete Structures Reinforced with Fiber-Reinforced Polymer Bars (CNR-DT 203/2006), Italian National Research Council, Italy, 2007.

[12] CSA, Design and construction of building components with fibre-reinforced polymers (CAN/CSA-S806-12 R17), Canadian Standards Association, Mississauga, Ontario, Canada, 2012.

[13] CSA, Canadian Highway Bridge Design Code (CSA-S6:19), Canadian Standards Association, Mississauga, Ontario, Canada, 2019.

[14] AFGC, Utilisation d'armatures composites (à fibres longues et à matrice orga-nique) pour le béton armé, Association Française de Génie Civil, France, 2021.

[15] JSCE, Recommendation for Design and Construction of Concrete Structures Using Continuous Fiber Reinforcing Materials, Concrete Engineering Series 23, Japan Society of Civil Engineers, Japan, 1997.

[16] A. Nanni, Flexural behaviour and design of RC members using FRP reinforcement, ASCE Journal of Structural Engineering 119 (11) (1993) 3344-59. https://doi.org/10.1061/(ASCE)0733-9445(1993)119:11(3344).

[17] S. Matthys, L. Taerwe, Concrete slabs reinforced with FRP grids. I: One-way bending, ASCE Journal of Composites for Construction 4 (3) (2000) 145-153. https://doi.org/10.1061/(ASCE)1090-0268(2000)4:3(145).

[18] P. Bischoff, Revaluation of deflection prediction for concrete beams reinforced with steel and fiber reinforced polymer bars, ASCE Journal of Structural Engineering 131 (5) (2005) 752-76. https://doi.org/10.1061/(ASCE)0733-9445(2005)131:5(752).

[19] C. Barris, L. Torres, M. Baena, K. Pilakoutas, M. Guadagnini, Serviceability limit state of FRP RC beams, Advances in Structural Engineering 15 (4) (2012) 653-63. https://doi.org/10.1260/1369-4332.15.4.653.

[20] C. Barris, L. Torres, C. Miàs, I. Vilanova, Design of FRP reinforced concrete beams for serviceability requirements. Journal of Civil Engineering and Management 18 (6) (2012) 843 - 857. https://doi.org/10.3846/13923730.2012.720934.

[21] B. Benmokrane, V. Brown, K. Mohamed, A. Nanni, M. Rossini, C. Shield, Creep rupture limit for GFRP bars subjected to sustained loads, ASCE Journal of Composites for Construction 23 (6) (2019) 06019001. https://doi.org/10.1061/(ASCE)CC.1943-5614.0000971.

[22] EAD 260023-00-0301, Carbon, glass, basalt and aramid fibre reinforced polymer bars as reinforcement of structural elements. 2019, EOTA, OJ Publication: Decision (EU) 2024/1944.

[23] ISO/TC 71/SC 6 Non-traditional reinforcing materials for concrete structures, ISO 10406-1. Fibre-reinforced polymer (FRP) reinforcement of concrete - Test methods - Part 1: FRP bars and grids, 2015.

[24] L. Torres, K. Neocleous, K. Pilakoutas, Design procedure and simplified equations for the flexural capacity of concrete members reinforced with fibre-reinforced polymer bars, fib Structural Concrete 13 (2) (2012) 119 – 129. https://doi.org/10.1002/suco.201100045.

[25] C.E. Ospina, C.E. Bakis, Indirect flexural crack control of concrete beams and one-way slabs reinforced with FRP bars, in: T. Triantafillou (Eds.), 8th International Symposium on Fiber Reinforced Polymer Reinforcement for Concrete Structures (FRPRCS-8), University of Patras, 2007.

[26] R. J. Frosch, Another look at cracking and crack control in reinforced concrete, ACI Structural Journal 96 (3) (1999) 437-442. https://doi.org/10.14359/679.

[27] P. Bischoff, Computing deflections using ACI CODE-318-19 and beyond, Part 1, Concrete International 47 (2) (2025) 47-50.

[28] fib Bulletin 114, Serviceability Limit State of Concrete Structures - Background Document of fib MC2020, International Federation for Structural Concrete, fib. Lausanne, Switzerland, 2024.

[29] C. Miàs, L. Torres, A. Turon, C. Barris, Experimental study of immediate and time-dependent deflections of GFRP reinforced concrete beams, Composite Structures 96 (2013) 279–285. https://doi.org/10.1016/j.compstruct.2012.08.052.

[30] L. Torres, C. Miàs, A. Turon, M. Baena, A rational method to predict long-term deflections of FRP reinforced concrete members, Engineering Structures 40 (2012) 230–239. https://doi.org/10.1016/j.engstruct.2012.02.021.

[31] V. Brown, Sustained load deflections in GFRP reinforced concrete beams. In: Proceedings of the 3rd International Symposium on Non-Metallic (FRP) Reinforcement for Concrete Structures (FRPRCS-3) V. 2, pp. 495-502, Japan Concrete Institute, Japan,1997.

[32] P. Bischoff, L. Torres, Rational approach for computing long-term deflection of reinforced concrete. ACI Structural Journal 118 (2) (2021) 215-224. https://doi.org/10.14359/51728192.

[33] G. L. Balázs et al., Design for SLS according to fib Model Code 2010, fib Structural Concrete, 14 (2) (2013) 99-123. https://doi.org/10.1002/suco.201200060.

[34] T. Hall, A. Ghali, Long-term deflection prediction of concrete members reinforced with glass fibre reinforced polymer bars, Canadian Journal of Civil Engineering 27 (5) (2000) 890–8. https://doi.org/10.1139/l00-009.

[35] I.G. Gilbert, G. Ranzi, Time-Dependent Behaviour of Concrete Structures, CRC Press, London, UK, 2011.

[36] CEN, Eurocode – Basis of structural and geotechnical design – Part1: New structures (prEN 1990-1:2023), European Committee for Standardization, Brussels, Belgium, 2023.

[37] Comité Euro-International du Béton (CEB), CEB-FIP Model Code 1990 (MC-90), Thomas Telford, London, UK 1993.

[38] CEN, Eurocode 2, Design of Concrete Structures - Part 1-1: General Rules and Rules for Buildings, European Standard EN 1992-1-1 (2004), European Committee for Standardization, Brussels, Belgium, 2004.

[39] A. C. Scordelis, Computer models for nonlinear analysis of reinforced and prestressed concrete structures, PCI Journal 29 (6) (1984) 116-135. https://doi.org/10.15554/pcij.11011984.116.135.

[40] A. Marí, Nonlinear geometric, material and time dependent analysis of three dimensional reinforced and prestressed concrete frames, Department of Civil Engineering, University of California, Berkeley, California, 1984.

[41] CEB Design Manual Cracking and Deformations, CEB Bulletin d'Information N.158, Lausanne, 1984.

[42] Y.J. Kang, A.C. Scordelis, Non-linear segmental analysis of reinforced and prestressed concrete bridges. In: Proceedings of the 3rd International Conference on Short and Medium Span Bridges, pp. 229–240, Canadian Society for Civil Engineering, Montreal, Canada, 1990.

[43] P. Cruz, A. Marí, P. Roca, Nonlinear time-dependent analysis of segmentally constructed structures, ASCE Journal of Structural Engineering 124 (3) (1998) 278-287. https://doi.org/10.1061/(ASCE)0733-9445(1998)124:3(278).

[44] A. Marí, Numerical simulation of the segmental construction of three dimensional concrete frames, Engineering Structures 22 (6) (2000) 585-596. https://doi.org/10.1016/S0141-0296(99)00009-7.

[45] fib Bulletin 92, Serviceability Limit State of Concrete Structures, International Federation for Structural Concrete, fib. Lausanne, Switzer¬land, 2019.

[46] M.M. Elbadry, A. Ghali, Analysis of time-dependent effects in concrete structures using conventional linear computer programs, Canadian Journal of Civil Engineering 28 (2001) 190-200. https://doi.org/10.1139/l00-093.

[47] A. Ghali, R. Favre, M. Elbadry, Concrete structures. Stresses and deformation, third ed., London, UK, CRC Press, 2002.

[48] A. Marí, M. Valdés, Long-term behaviour of continuous precast concrete girder bridges model, ASCE Journal of Bridge Engineering 5 (1) (2000) 22-30. https://doi.org/10.1061/(ASCE)1084-0702(2000)5:1(22).

[49] A. Marí, J.M. Bairán, E. Oller, Assessment of the efficiency of strengthening solutions in concrete structures by means of non-linear step by step analysis models, Hormigón y Acero 72 (294/295) (2021) 59-75. https://doi.org/10.33586/hya.2021.3043.

[50] A. Marí, J.M. Bairán, E. Oller, N. Duarte, Modeling serviceability performance and ultimate capacity of corroded reinforced and prestressed concrete structures, fib Structural Concrete 23 (1) (2022) 6-15. https://doi.org/10.1002/suco.202100159.

[51] A. Ghali, M. Elbadry, User's manual and computer program CPF: Cracked plane frames in prestressed concrete, Research Report No. CE85-2, Department of Civil Engineering, University of Calgary, Calgary, AB, Canada, 1985.

[52] A. Scanlon, D.W. Murray, Time-dependent reinforced concrete slab deflections, ASCE Journal of the Structural Division 100 (9) (1974) 1911-1924. https://doi.org/10.1061/JSDEAG.0003881.

[53] R. I. Gilbert, R.F. Warner, Tension stiffening in reinforced concrete slabs, ASCE Journal of the Structural Division 104 (12) (1978) 1885-1900. https://doi.org/10.1061/JSDEAG.0005054.

[54] G. Kaklauskas, J Ghaboussi, Stress-strain relations for cracked tensile concrete from RC beam tests, ASCE Journal of Structural Engineering 127 (1) (2001) 64-73. https://doi.org/10.1061/(ASCE)0733-9445(2001)127:1(64).

[55] L. Torres, F. López-Almansa, L.M. Bozzo, Tension-stiffening model for cracked flexural concrete members, ASCE Journal of Structural Engineering 130 (8) (2004) 1242– 1251. https://doi.org/10.1061/(ASCE)0733-9445(2004)130:8(1242).

[56] A. Marí, J.M. Bairán, N. Duarte, Long-term deflections in cracked reinforced concrete flexural members, Engineering Structures 32 (3) (2010) 829-842. https://doi.org/10.1016/j.engstruct.2009.12.009.

[57] A. Marí, L. Torres, E. Oller, C. Barris, Performance-based slenderness limits for deformations and crack control of reinforced concrete flexural membres, Engineering Structures 187 (2019) 267-79. https://doi.org/10.1016/j.engstruct.2019.02.045.

[58] ACI 318-19, Building Code Requirements for Struc¬tural Concrete (ACI 318-19) and Commentary (ACI 318R-19), American Concrete Institute, ACI Committee 318, Farmington Hills, Michigan, USA, 2019.

[59] P. Bischoff, Comparison of existing approaches for computing deflections of reinforced concrete, ACI Structural Journal 117 (1) (2020) 231-240. https:/doi.org/ 10.14359/51718072

[60] P. Bischoff, S.P. Gross, Equivalent moment of inertia based on integration of curvature, ASCE Journal of Composites for Construction 15 (3) (2011) 263–273. https://doi.org/10.1061/(ASCE)CC.1943-5614.0000164.

[61] S. Walkup, E. Musselman, S. Gross, Effect of service load levels on long-term deflection multiplier, ACI Structural Journal 116 (2) (2019) 89-100. https://doi.org/ 10.14359/51711137.

APPENDIX A: Concrete mechanical properties in codes

A1. EC2 (2023)

$$f_{ctm} = 0.3 \cdot f_{ck}^{2/3} \qquad \text{for } f_{ck} \leq 50 \text{ MPa} \tag{A1}$$

$$f_{ctm,fl} = \max\left\{(1.6 - h/1000)\, f_{ctm};\, f_{ctm}\right\} \tag{A2}$$

$$f_{cd} = \eta_{cc}\, k_{tc}\, f_{ck} / \gamma_C \tag{A3}$$

with $\gamma_C = 1{,}5$ for persistent and transient situations, and

$$\eta_{cc} = (40/f_{ck})^{1/3} \leq 1.0 \tag{A4}$$

$$k_{tc} = 1.0 \qquad \text{for } t_{ref} \leq 28 \text{ days} \tag{A5}$$

$$Ecm = k_E\, (f_{ck} + 8)^{1/3} \tag{A6}$$

with $k_E = 9500$ for quartzite aggregates.

$$E_{c,eff} = 1.05 \cdot E_{cm} \Big/ \left(1 + \varphi(t,t_0)\right) \tag{A7}$$

where f_{ck} = characteristic compressive strength; f_{ctm} = mean axial tensile strength; $f_{ctm,fl}$ = mean flexural tensile strength; h = total depth of the section; f_{cd} = design compressive strength; γ_C = partial factor for concrete; E_{cm} = secant modulus of elasticity of concrete; $E_{c,eff}$ = effective modulus of elasticity accounting for creep deformations; $\varphi(t,t_0)$ = creep coefficient at the age of loading.

A2. MC2020

$$f_{ctm} = 1.8 \cdot l_n(f_{ck}) - 3{,}1 \tag{A8}$$

$$f_{ctm,\,fl} = f_{ctm}\,(1+0.06 \cdot h^{0,7}) \Big/ 0{,}06 \cdot h^{0,7} \tag{A9}$$

$$f_{cd} = \alpha_{cc} \cdot \eta_{fc} \cdot f_{ck} \Big/ \gamma_C \tag{A10}$$

with $\gamma_C = 1.5$ for persistent and transient situations, $\alpha_{cc} = 1.0$ for new structures and

$$\eta_{fc} = (40/f_{ck})^{1/3} \leq 1.0 \tag{A11}$$

$$E_{ci} = E_{c0} \cdot \alpha_E \left((f_{ck}+8) \Big/ 10 \right)^{1/3} \tag{A12}$$

with $\alpha_E = 1.0$ for quartzite aggregates and $E_{c0} = 21500$.

$$E_{c,ef} = E_{ci} \Big/ \left(1 + \varphi(t,t_0)\right) \tag{A13}$$

where E_{ci} = tangent modulus of elasticity and the rest of symbols are the same as those defined for EC2 (2023).

ACI 440.11-22

$$f_r = 0.62 \cdot f_c' \tag{A14}$$

$$E_c = 4730 \sqrt{f_c'} \tag{A15}$$

where f_r = modulus of rupture (flexural tensile strength); f_c'= specified compressive strength; E_c = secant modulus of elasticity.

APPENDIX B: Summary of procedures for the ULS of bending with FRP reinforcement

B.1. Types of failure

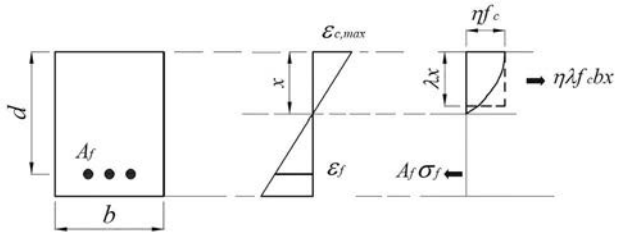

Figure B1. Sectional strains, stresses and parameters.

There are two possible modes of failure: a) concrete failure (compression-controlled) and b) FRP failure (tension-controlled). The balanced condition can be defined as that in which failure is attained simultaneously for both materials:

$$\varepsilon_{c,max} = \varepsilon_{cu} \qquad \varepsilon_f = \varepsilon_{fd} = f_{fd} \Big/ E_f$$

where ε_c is the concrete strain; ε_{cu} is the ultimate compressive concrete strain; ε_f is the reinforcement strain; f_{fd} is the FRP design tensile strength already defined for each code in Sect. 2 (named ffu in ACI440.11); and E_f is the modulus of elasticity of FRP.

The balanced reinforcement ratio, ρ_{fb}, can be obtained from equilibrium and compatibility equations:

$$\rho_{fb} = \eta \cdot \lambda \frac{f_{cd}}{f_{fd} E_f} \frac{E_f \cdot \varepsilon_{cu}}{E_f \cdot \varepsilon_{cu} + f_{cd}} \tag{B1}$$

and therefore
$\rho_f > \rho_{fb}$ concrete failure; $\rho_f \leq \rho_{fb}$ FRP failure
where λ, η are parameters defining the equivalent rectangular stress block of concrete, and f_{cd} is the concrete design strength for each code.

B.2. Eurocode 2 (2023)/fib Model Code 2020

The design bending moment M_{Ed} must be lower than the moment capacity M_{Rd}

$$M_{Ed} \leq M_{Rd}$$

where, for a combination case of simple bending with one variable action

$$M_{Ed} = 1.5 \cdot M_q + 1.35 \cdot M_g \quad \text{(B2)}$$

being M_q and M_g the bending moments due to variable loads and permanent loads, respectively.

The concrete design strength is $f_{cd} = f_{ck}/\gamma_c$, where f_{ck} is the characteristic design strength, while the material partial factor for concrete is $\gamma_c = 1.5$.

Although theoretically the parameters of the rectangular stress block depend on the maximum concrete strain attained, assumption of $\eta = 1$, $\lambda = 0.8$ for both concrete and tension failure leads to simplification in calculations with accurate enough values.

B.2.1. Compression-controlled failure

$$\rho_f > \rho_{fb} \quad ; \quad \varepsilon_{c,max} = \varepsilon_{cu} = 0.0035 \quad ; \quad \varepsilon_f = \sigma_f/E_f < \varepsilon_{fd}$$

from equilibrium of forces and compatibility of deformations:

$$\sigma_f = \left(\sqrt{\frac{(E_f \cdot \varepsilon_{cu})^2}{4} + \frac{0.8 f_{cd}}{\rho_f} E_f \cdot \varepsilon_{cu}} - 0.5 \cdot E_f \cdot \varepsilon_{cu} \right) \leq f_{fd} \quad \text{(B3)}$$

and the moment capacity is:

$$M_{Rd} = \rho_f \cdot \sigma_f \left(1 - 0.5 \frac{\rho_f \cdot \sigma_f}{f_{cd}}\right) b \cdot d^2 \quad \text{(B4)}$$

where σ_f is the actual reinforcement stress.

B.2.2. Tension-controlled failure

$$\rho_f \leq \rho_f{}^b \qquad \varepsilon_{c,max} < \varepsilon_{cu} = 0.0035 \qquad \varepsilon_f = \sigma_f/E_f < \varepsilon_{fd} = f_{fd}/E_f$$

the moment capacity is:

$$M_{Rd} = \rho_f \cdot f_{fd} \left(1 - 0.5 \frac{\rho_f \cdot f_{fd}}{f_{cd}}\right) b \cdot d^2 \quad \text{(B5)}$$

B.3. ACI440.11-22

The factored bending moment M_u must be lower than the design flexural strength, defined as the nominal flexural strength, M_n, multiplied by a strength reduction factor ϕ.

$$M_u \leq \phi \cdot M_n$$

where

$$M_u = 1.6 \cdot M_q + 1.2 \cdot M_g \quad \text{(B6)}$$

No material partial factors are used; f_{cd} in Figure B.1 must be the specified concrete strength f_c'.

The strength reduction factor depends on the FRP reinforcement strain, with values of 0.65 for a compression-controlled section and 0.55 for a tension-controlled section. A linear transition zone between both values is adopted in the range $0.8\varepsilon_{tu} \div \varepsilon_{tu}$ ($\varepsilon_{tu} = f_{fu}/E_f$), equivalent to $1.4\rho_{fb} \div \rho_{fb}$, which leads to:

$$\phi = \begin{cases} 0.55 & \rho_{fb} \\ 0.30 + 0.25 \ \rho_f/\rho_{fb} & \rho_{fb} < \rho_f < \rho_{fb} \\ 0.65 & \rho_f \leq 1.4\rho_{fb} \end{cases} \quad \text{(B7)}$$

B.3.1. Compression-controlled failure and transition zone

The same conditions and equations indicated in EC2/MC2020 for compression-controlled failure apply, taking into account that $\varepsilon_{cu} = 0.003$; f_{fd} is called f_{fu} in the code; and ε_{fd} is called ε_{fu}. Parameters η and λ of the concrete rectangular stress block, called α_1 and β_1 in the code adopt the following values:

$$\eta = 0.85$$

$$\lambda = \begin{cases} 0.85 & 21 \leq f_c' \leq 28 \\ 0.85 + 0.05\ (f_c' - 28)/7 & 28\ f_c' \leq 55 \\ 0.65 & f_c' \leq 55 \end{cases} \quad \text{(B8)}$$

The calculated M_n (M_{Rd} in previous equations) must be multiplied by the corresponding strength reduction factor ϕ.

B.3.2. Tension-controlled failure

The code indicates that the defined coefficients for the concrete rectangular stress block do not apply in this case. The code proposes a simplified and conservative lower bound for M_n based on assuming a neutral axis depth corresponding to the balanced condition, x_b. This way:

$$x_b = \frac{\varepsilon_{cu}}{\varepsilon_{cu} + \varepsilon_{fu}} d \quad \text{(B9)}$$

$$Mn = A_f \cdot f_{fd} \ (d - \beta 1 \cdot x_b) \quad \text{(B9)}$$

Disponible en **www.hormigonyacero.com**
https://doi.org/10.33586/hya.2025.4147

Fracture Monitoring in Encased Composite SFRC–Steel Beams Using DIC Under Static Loading

Monitorización mediante DIC del proceso de fractura de vigas mixtas de HRFA-acero estructural con perfiles embebidos bajo carga estática

Riccardo Zanon [a], Vaibhav W. Masih [b], Markus Schäfer [a], Sohanth T. Maganty [b], Ángel De La Rosa [c] & Gonzalo Ruiz [b,*]

[a] *Department of Engineering, University of Luxembourg, 6 rue Richard Coudenhove-Kalergi, L-1359 Luxembourg.*

[b] *ETSI Caminos, C. y P., Universidad de Castilla-La Mancha, Av. Camilo José Cela s/n, 13071 Ciudad Real, Spain.*

[c] *DIMME, Grupo de Durabilidad e Integridad Mecánica de Materiales Estructurales, Universidad Rey Juan Carlos, C. Tulipán s/n, 28933 Móstoles, Madrid, Spain.*

Recibido el 2 de septiembre de 2025; revisado el 4 de octubre de 2025, aceptado el 9 de noviembre de 2025

ABSTRACT

This study presents an experimental investigation into the crack initiation and propagation of full-scale load tests performed on encased composite steel-concrete beams, where the concrete is reinforced by conventional rebars together with high-strength steel fibers. Six beams were tested under three-point bending with quasi-static loading, including sagging and hogging configurations. One specimen from each configuration was subjected to various steps of sustained displacement to assess relaxation effects and observe time-dependent cracking phenomena. Full-field strain and crack evolution were monitored using a Digital Image Correlation (DIC) system alongside conventional instrumentation. The DIC system allowed high-resolution tracking of strain patterns, crack initiation and spacing, and crack mouth opening displacement at different load stages. These measurements were taken in a 660 mm wide region corresponding to the midspan. Results show that Steel Fiber-Reinforced Concrete (SFRC) was effective in controlling crack propagation and preventing concrete crushing in compression. At failure, sagging configurations exhibited several distributed cracks in the plastic hinge, and high ductility was achieved due to the favorable presence of the exposed steel flange on the tensile side. In hogging configurations, the steel profile was less effective in the tensile region, resulting in the formation of a dominant crack that concentrated damage at the ultimate state; however, these configurations also exhibited a ductile failure mode. Sustained loading did not significantly reduce the load-bearing capacity, although crack depth and opening did slightly increase. DIC proved effective in revealing strain redistribution and crack branching not captured by traditional sensors. The top SFRC layer of all the beams exhibited compressive strains of up to 1% without complete crushing or spalling, thus maintaining its functionality throughout the test. These findings confirm the validity of the compressive model for SFRC material outlined in Annex L of Eurocode 2, even for full-scale structures.

KEYWORDS: Encased composite SFRC--steel beams; DIC monitoring; crack width and spacing in composite structures; ductility of SFRC in compression.

RESUMEN

Este estudio presenta una investigación experimental sobre la iniciación y propagación de fisuras en ensayos a escala real realizados sobre vigas mixtas acero-hormigón con perfiles embebidos, donde el hormigón está reforzado con armaduras convencionales y con fibras de acero de alta resistencia. Se ensayaron seis vigas mediante flexión en tres puntos con carga cuasiestática, incluyendo configuraciones de flector positivo y negativo. Una viga de cada configuración fue

sometida a varias etapas de carga sostenida para evaluar efectos de relajación y observar fenómenos de fisuración dependientes del tiempo. La evolución completa de deformaciones y fisuras se monitorizó mediante un sistema de correlación digital de imágenes (DIC) junto con instrumentación convencional. El sistema DIC permitió un seguimiento de alta resolución de los patrones de deformación, la iniciación y espaciamiento de fisuras, y la apertura de la boca de las fisuras en diferentes etapas de carga. Estas mediciones se realizaron en una zona de 660 mm de ancho correspondiente al vano central. Los resultados muestran que el hormigón reforzado con fibras de acero (HRFA) fue eficaz en el control de la propagación de fisuras y en la prevención del fallo del hormigón en compresión. En el fallo, las configuraciones con momento positivo presentaron varias fisuras distribuidas en la rótula plástica, y se alcanzó una alta ductilidad gracias a la presencia beneficiosa del perfil de acero en la zona traccionada. En configuraciones con momento negativo, el perfil de acero fue menos eficiente en la región traccionada, lo que resultó en la formación de una fisura dominante que concentró el daño en el estado último; sin embargo, estas configuraciones también mostraron un modo de fallo dúctil. La carga sostenida no redujo significativamente la capacidad portante, aunque la profundidad y apertura de fisuras aumentaron ligeramente. El sistema DIC demostró ser eficaz para revelar redistribuciones de deformación y ramificaciones de fisuras no captadas por sensores tradicionales. La capa superior de HRFA en todas las vigas presentó deformaciones de compresión de hasta un 1% sin llegar a aplastamiento completo ni desprendimiento, manteniendo así su funcionalidad durante todo el ensayo. Estos hallazgos confirman la validez del modelo de compresión para el HRFA descrito en el Anexo L del Eurocódigo 2, incluso para estructuras a escala real.

PALABRAS CLAVE: Vigas compuestas encapsuladas de acero y hormigón reforzado con fibras de acero (SFRC); monitoreo mediante DIC; ancho y espaciamiento de fisuras en estructuras compuestas; ductilidad del SFRC a compresión.

* Persona de contacto / *Corresponding author*:
Correo-e / *e-mail*: gonzalo.ruiz@uclm.es (Gonzalo Ruiz)

How to cite this article: Zanon, R., Masih, V., Schäfer, M., Maganty, S., De la Rosa, Ángel, & Ruiz, G. (2026). Fracture Monitoring in Encased Composite SFRC--Steel Beams Using DIC Under Static Loading. *Hormigón y Acero*. 77(308):27-46. https://doi.org/10.33586/hya.2025.4147

1. INTRODUCTION

Steel–concrete composite systems are widely adopted in bridges, transfer girders, metro platforms, and high-rise structural cores due to their superior mechanical performance, fire resistance, and ductility. Fully encased configurations, where structural steel profiles are embedded within reinforced concrete, provide enhanced confinement and corrosion protection compared to concrete-filled tubes, leading to better performance under axial and flexural loading [1], [2], [3]. However, when high-strength concrete is employed in such encasement, it can introduce premature cover spalling and brittle failure modes [4], which compromise the ductility expected from composite interaction.

Steel Fiber-Reinforced Concrete (SFRC) has emerged as a promising alternative to traditional stirrups in composite members. The randomly distributed steel fibers bridge cracks and enhance tensile resistance, delay crack propagation, and improve post-peak load-bearing capacity [5], [6], [7], [8], [9]. These enhancements contribute significantly to both ultimate and serviceability limit states. The new Eurocode 2 Annex L (2022) officially includes constitutive models for SFRC in structural design [9], [10]. This update introduces residual strength-based compressive and tensile laws, which eliminate the need for traditional reinforcement under certain conditions, and allow for more efficient use of structural steel [8], [9].

Recent studies have confirmed the efficacy of SFRC in controlling crack widths, increasing energy absorption, and improving rebalancing of internal forces in coupon-scale elements [11]. Nonetheless, large-scale structural validation of these models, especially in beams with realistic reinforcement layouts and sustained loading conditions, remains limited. Understanding the fracture behavior at full scale is critical to confirming the applicability of Annex L provisions and to supporting SFRC-based design for high-performance infrastructure.

Steel fibers also enable the development of High-Technology Concrete (HTC), characterized by increased ductility, enhanced flexural strength, and superior strain hardening [9], [11]. HTC has been shown to delay localization and reduce early-age cracking. Its structural implementation, however, depends not only on material characterization but also on validating global and local responses under service-level actions such as relaxation and sustained loads. These conditions are typical of real structures but are rarely simulated in beam-scale experiments.

Traditional instrumentation, such as strain gauges and Linear Variable Differential Transformers (LVDTs), is limited to point-based measurements, lacking the spatial resolution needed to monitor early cracking, strain redistribution, or crack spacing [12]. In contrast, Digital Image Correlation (DIC) enables full-field strain tracking and crack opening measurement with sub-millimeter resolution.

DIC has been widely adopted in coupon-scale and small-component testing of concrete, composites, and fiber-reinforced systems, offering powerful tools for evaluating crack

opening, strain localization, and fatigue progression [13], [14]. Recent reviews have emphasized its growing application to large-scale structures, though its deployment in full-scale SFRC–steel composite beams remains limited due to experimental complexity and data processing challenges [14], [15].

In this context, the present study presents a full-scale experimental campaign using DIC to monitor the fracture behavior of SFRC-encased steel composite beams subjected to both monotonic and sustained loading. Six beams were tested under three-point bending, in both sagging and hogging configurations, to explore flexural performance under varying strain gradients. One beam from each configuration was subjected to several steps of sustained loading to evaluate time-dependent crack propagation and strain relaxation.

A preliminary version of this study was presented in conference format, focusing on global load–displacement responses and structural capacity [16]. The present work expands significantly on that study by incorporating high-resolution DIC tracking, sustained loading regimes, and quantitative crack spacing and Crack Mouth Opening Displacement (CMOD) analysis. Through this integration, we aim to bridge the gap between SFRC material characterization and structural-scale validation for design.

The key contributions of this work are as follows:

- Full-field monitoring of strain localization and crack evolution in SFRC–steel composite beams using DIC.
- Evaluation of CMOD, crack spacing, and ductility metrics under both static and sustained loading.
- Comparative fracture analysis between sagging and hogging configurations, capturing the influence of steel profile position on crack distribution and strain behavior.
- Experimental validation of the compressive model for SFRC proposed in Annex L of Eurocode 2 using structural-scale data.

Crack spacing was analyzed both manually and through DIC in a 660 mm midspan zone. Crack evolution was correlated with load–displacement trends, and localized strain drops were linked to crushing, fiber bridging, and crack bifurcation. CMOD values at failure ranged from 10 to 42 mm, with hogging beams exhibiting more localized crack openings. The DIC system proved essential in capturing detailed crack evolution, especially during sustained load holds where subtle strain redistribution and crack branching occurred. Unlike LVDTs, DIC provided spatial resolution of crack opening along the full beam depth and helped differentiate between fiber-dominated ductile failure and localized concrete crushing.

This study contributes to performance-based design approaches for SFRC composite systems by demonstrating how fiber-reinforced HTC beams behave under realistic loading conditions. The findings directly inform the extension of Eurocode 2 Annex L provisions to full-scale applications and support the use of DIC as a viable fracture monitoring tool in future standardization efforts.

The remainder of this paper is organized as follows: Section 2 describes the beam configuration, reinforcement, and HTC mix design; it also outlines the experimental methods, including DIC instrumentation and sustained loading protocol. Section 3 presents the results of load–displacement response, strain evolution, CMOD, and crack spacing. Section 4 discusses the implications for SFRC design and Annex L validation. Section 5 summarizes the key findings and offers future research directions.

2. MATERIALS AND METHODOLOGY

2.1. Test Specimen Configuration

The test specimens were designed as full-scale composite beams to represent filler beam decks commonly used in bridges. The cross-section geometry is compliant with filler beam decks covered by prEN 1994-2 [17]. Each specimen had a total length of 4400 mm and a constant rectangular cross-section measuring 650 mm in width and 330 mm in height, see Fig. 1.

The embedded steel profile used was a HEA260 made from S460M structural steel. It features a total flange width of 260 mm, an overall section depth of 250 mm, a flange thickness of 12.5 mm, and a web thickness of 7.5 mm. Tensile tests were conducted on both the web and the flange to determine their effective yield strength and rupture strength (see Table 2). Since all the beams tested were sourced from the same parent beam, the variation in material properties is

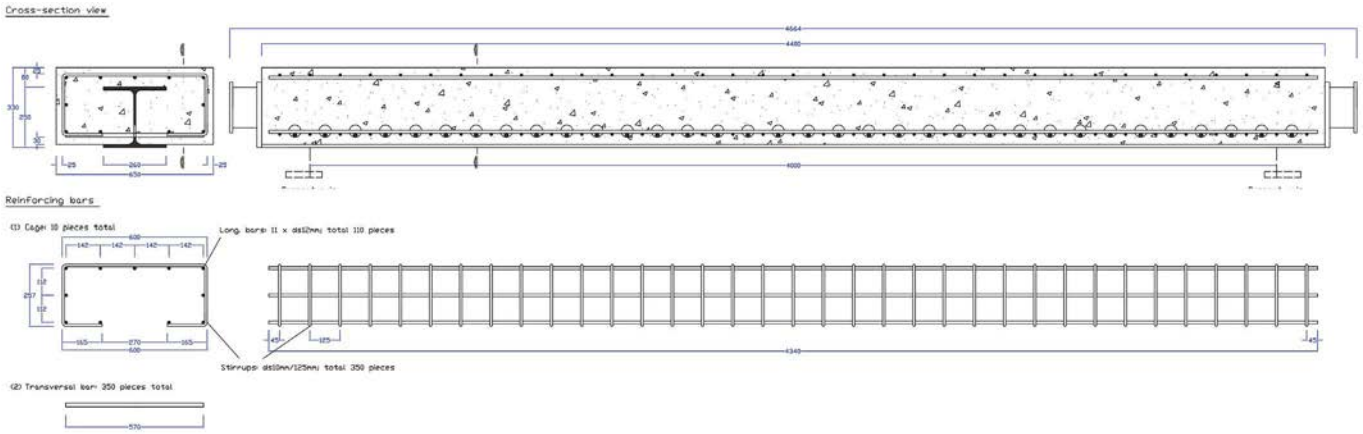

Figure 1. Cross and longitudinal section of the beam and reinforcement disposition.

minimal. The bottom flange is exposed and located beneath the concrete layer. Additionally, the concrete was reinforced with conventional reinforcement, which remained consistent along the entire length of the beam:

- 11 longitudinal rebars d_s 12 mm arranged above and below the steel section,
- 10 mm stirrups placed at 125 mm intervals, closed at the bottom by overlapping a transverse bar led through the web in diameter 16 mm,
- A concrete cover of 25 mm on the top and sides and 30 mm at the bottom.

Tensile tests were conducted on the longitudinal rebars, which were all manufactured from the same wire rod in a single production batch. This resulted in reduced variability among the tests, with the standard deviation of five specimens being 7.2 MPa (equating to 1.1% of the yield strength) and 4.1 MPa (or 0.57% of the ultimate strength) for the respective strengths measured.

2.2. High-Technology Concrete

The concrete used in this study was a steel fiber-reinforced HTC mix, formulated to balance enhanced mechanical performance with practical casting and pumping conditions. The formulation follows the industrial methodology validated by De La Rosa et al. [11], [18] for both quasi-static and dynamic regimes.

The HTC mix consisted of Portland cement (CEM I 52.5 R-SR 5), mineral filler, fine and coarse limestone aggregates, water, and two admixtures: a polycarboxylate-based superplasticizer and an air-entraining agent. Hooked-end steel fibers HE++75/35 (35 mm long, 0.75 mm diameter) were included at a dosage of 47.1 kg/m3 (0.6% vol.). The full mix composition is shown in Table 1.

TABLE 1.
Mix composition.

Component	*kg/m³*
Cement (CEM I 52.5 R-SR 5)	380
Fine aggregate (0/4 mm)	950
Coarse aggregate (4/12 mm)	525
Coarse aggregate (12/20 mm)	225
Limestone filler	90
Water	182
Superplasticizer	3.8
Air-entraining agent	1.52
Steel fibers (HE++75/35)	47.1

All specimens were stored under ambient indoor conditions for 5–6 months prior to testing. Mechanical characterization at the time of testing yielded compressive strength f_{cm}=55.9 MPa, modulus of elasticity E_c=33.3 GPa, and Poisson's ratio v=0.21. Characteristic residual flexural strengths determined from prismatic specimens (750 × 150 × 150 mm³) were: at CMOD 0.5 mm $f_{R,1k}$=2.9 MPa, and at CMOD 2.5 mm $f_{R,3k}$=2.6 MPa [16], [18].

A total of 6 beams were cast and tested under different loading conditions, including sagging, hogging, and sustained regimes. The beams were supported on elastomeric pads and tested using a three-point bending setup with a clear span of 4200 mm. Fig. 2 shows one of the beams during testing in hogging configuration, while Fig. 3 illustrates the sagging and hogging configurations.

TABLE 2.
Steel material properties used in beam specimens.

Component	*Nominal Class*	*$R_{p0.2}$[MPa]*	*Rm [MPa]*
Structural steel	S460M	480	612
Longitudinal rebars	B500B	624	720
Steel fibers (HE++75/35)	—	2150	—

TABLE 3.
Mechanical properties of the steel fiber-reinforced concrete mix.

Component	*Class*	*f_{cm} [MPa]*	*E_{cm} [GPa]*	*$f_{R,1k}$ [MPa]*	*$f_{R,3k}$ [MPa]*
SFRC Mix	C45/55 – 2.5c	55.9	33.3	2.9	2.6

2.3. Experimental Methods

2.3.1. Test Setup and Instrumentation

The experimental setup was designed to evaluate the fracture behavior of full-scale SFRC–steel composite beams under controlled static loading conditions. All beams were tested using a quasi-static three-point bending configuration with a clear span of 4200 mm, see Figs. 2 and 3. The primary objective of the setup was to capture the evolution of strain and crack patterns under both positive (sagging) and negative (hogging) bending moments using both conventional and full-field measurement techniques.

A servo-hydraulic actuator was used to apply vertical loads at midspan in displacement control mode. The initial displacement rate was 0.7 mm/min during the first hour, and later 2.5 mm/min to the end of the test. The actuator was connected to a high-capacity load cell to monitor real-time force application. To ensure accurate boundary conditions, the beams were supported on neoprene pads placed over steel rollers, enabling rotation and small horizontal displacements to simulate realistic support conditions (see Fig. 4).

LVDTs were strategically installed to record vertical displacements at several key locations along the beam span. A total of seven LVDTs were employed to capture global and local deflection profiles, midspan displacements, and differential deformations near the supports. The placement of these transducers is shown in Figure 4a and further detailed in Figure 5a.

Strain gauges (SGs) were affixed to both the concrete surface and the embedded steel-section to monitor longitudinal strains during loading. A total of 12 strain gauges were used per beam in the sagging configuration: six on the SFRC surface (top and bottom) and six on the steel flange/web to assess strain compatibility and stress redistribution between the composite materials. In the hogging setup, additional strain gauges were positioned to capture localized stress states near the compression zone, as seen in Figure 4b.

Complementing the conventional sensors, a 2D DIC system was installed to monitor the full-field strain distribution over a 660 mm zone centered at midspan the region of maximum bending moment. The DIC camera was mounted orthogonally to the beam surface and calibrated prior to testing. The speckle pattern required for DIC tracking was applied using a controlled screen-printing method [19] to ensure high contrast

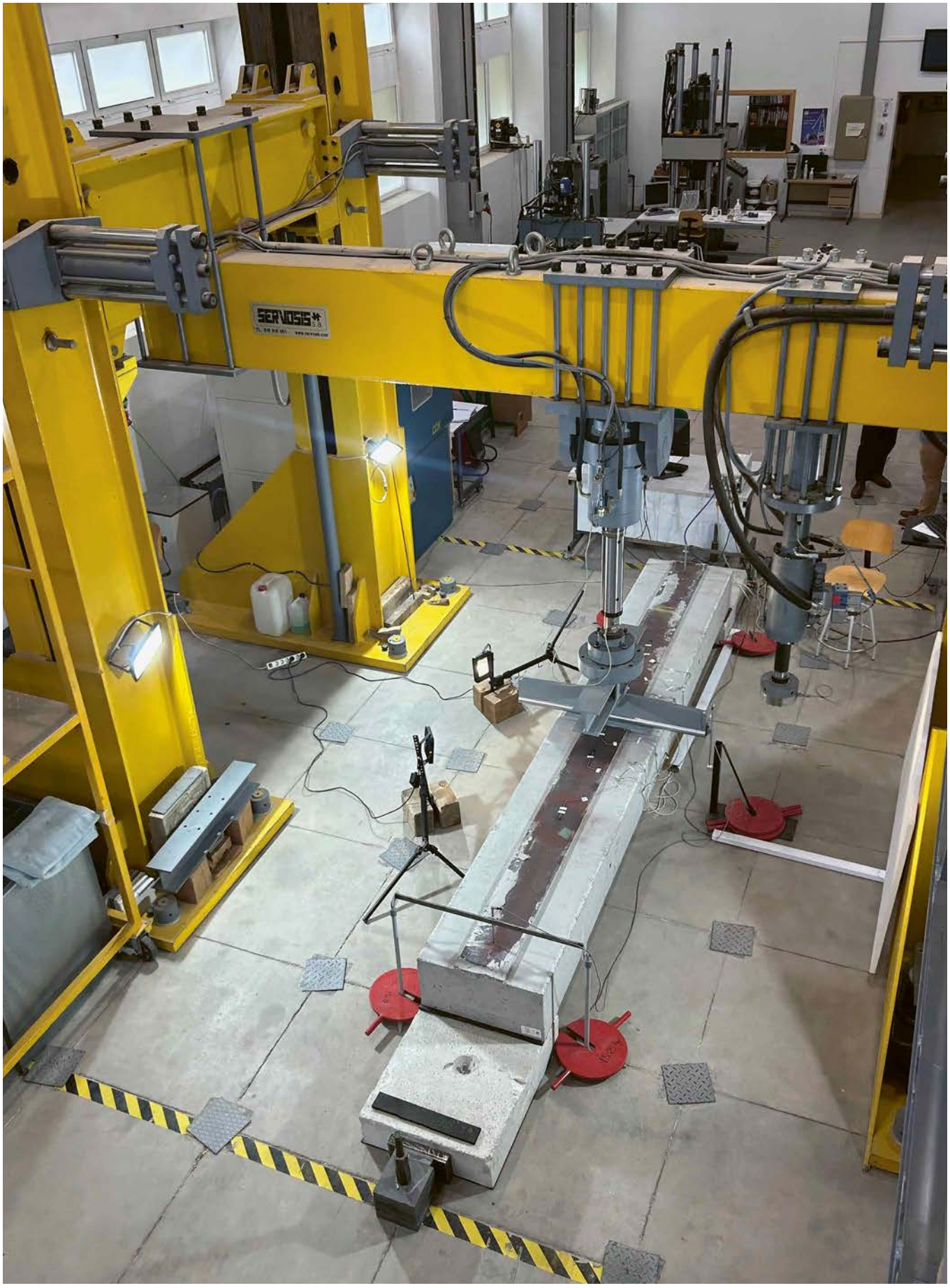

Figure 2: Beam being tested in hogging configuration.

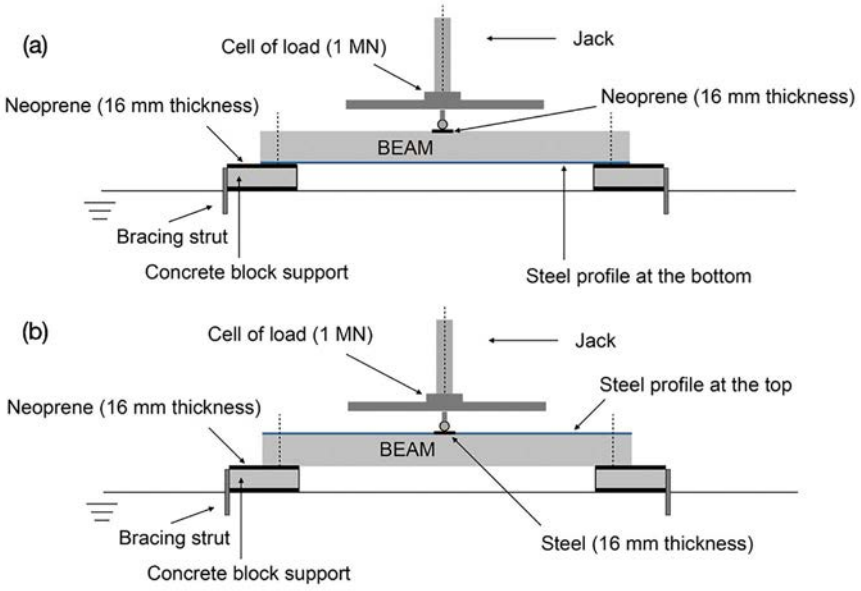

Figure 3. Experimental configurations for bending tests: (a) Sagging setup and (b) Hogging setup.

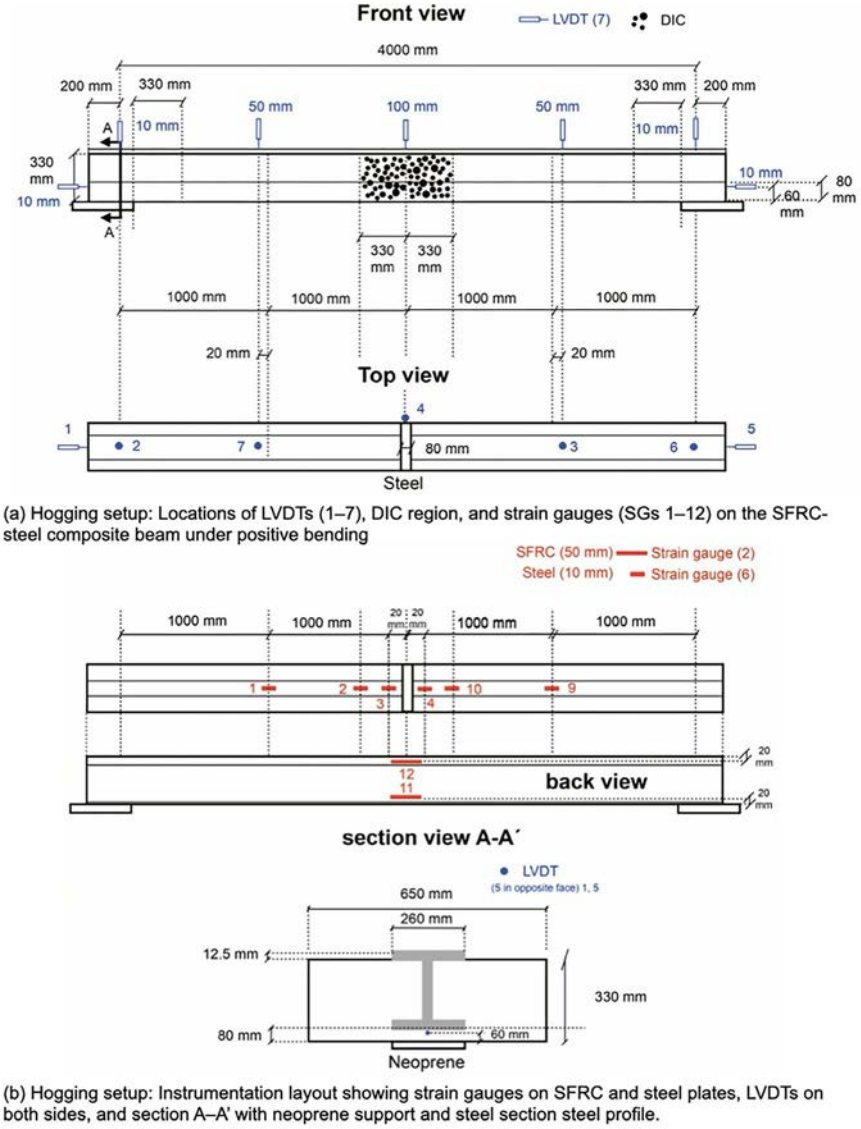

Figure 4. Experimental configurations for composite SFRC-steel beam tested under three-point bending: (a) Front and top views of the hogging setup showing LVDT locations, DIC region, and overall geometry of the SFRC, and (b) back and sectional views of the hogging setup showing strain gauge arrangement on SFRC and steel layers, and LVDT positioning at the supports.

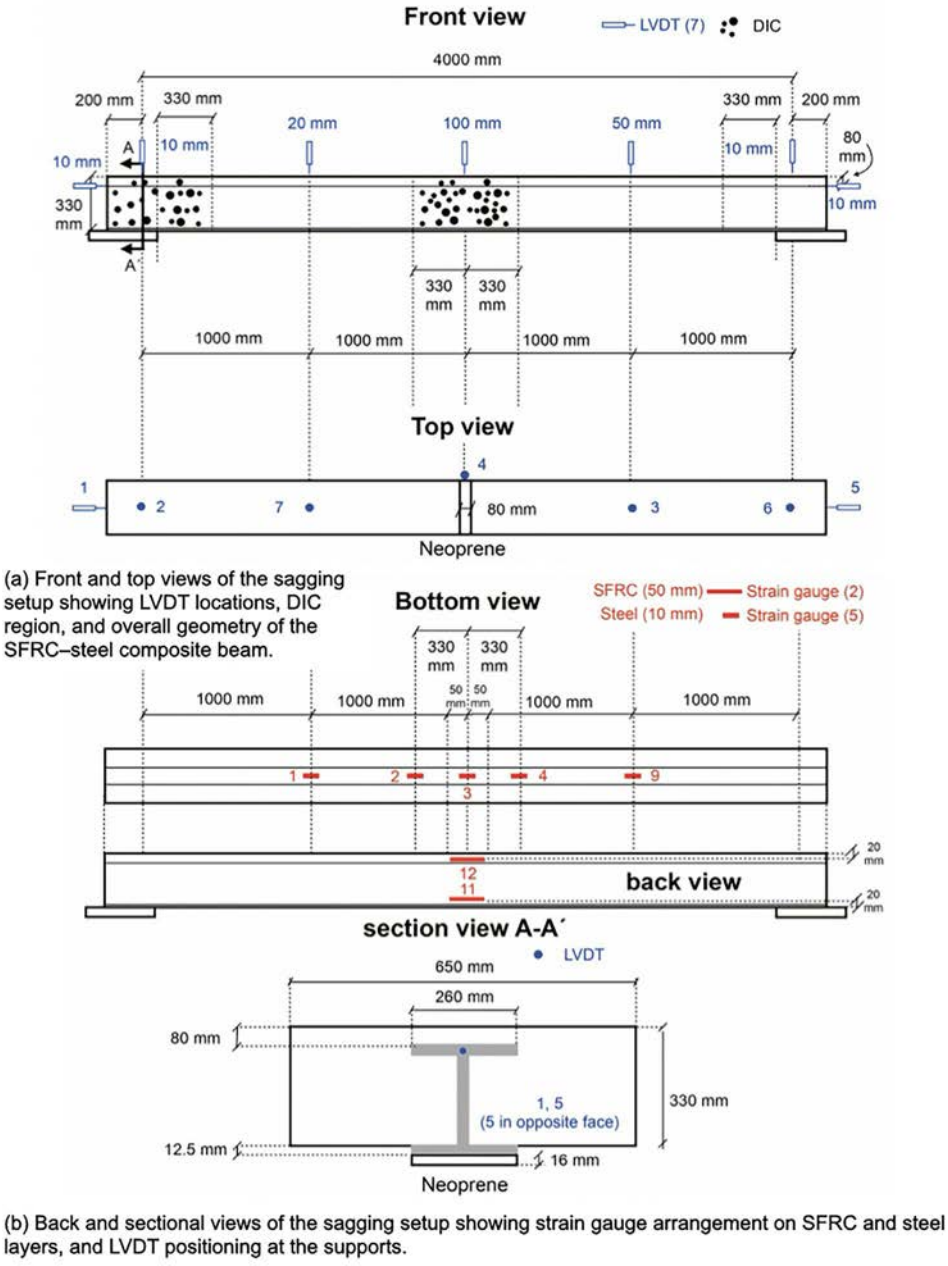

Figure 5. Instrumentation and geometry of the sagging configuration used for three-point bending tests on SFRC-steel composite beams: (a) Front and top views with LVDTs and DIC region, and (b) back and sectional views detailing strain gauge layout and support conditions.

and spatial consistency (Fig. 7). A fine polyester screen mesh with a predefined circular-dot stencil was held flush against the concrete surface, and matte black acrylic ink was deposited through the open apertures using standard flood squeegee passes. This process produced uniform dots of approximately 3 mm diameter and consistent inter-dot spacing, effectively mitigating overspray and dot coalescence typical of freehand spraying. The controlled application improves gray-level distribution and correlation robustness in large-area DIC [20].

Instrumentation layout diagrams (Fig. 5a and 5b) illustrate both front and rear views of the sagging beam configuration, clearly identifying LVDT positions, strain gauge locations, and the DIC region of interest.

In two beams (Beams 3 and 6), a sustained load protocol was introduced. The test procedure began with an initial ramp-up, starting at a velocity of 0.5 mm/min over a period of 40 minutes, followed by a 20-minute pause. This sequence was repeated three times, totaling three hours. The purpose of these three initial ramps was to achieve approximately 40% of the peak load. After the initial ramps, a new ramp was introduced, increasing the velocity to 1 mm/min for 20 minutes, followed by a 15-minute pause. This was succeeded by another ramp at a speed of 2 mm/min for 20 minutes, which was followed by a 15-minute pause. Finally, the test concluded with a last ramp at 2 mm/min until the end of the procedure. In total, the duration of this relaxation test was 4 hours and 40 minutes. This allowed assessment of strain redistribution and the effect of sustained stress on crack evolution and depth.

This comprehensive instrumentation scheme enabled multi-scale monitoring of the beam response, ranging from

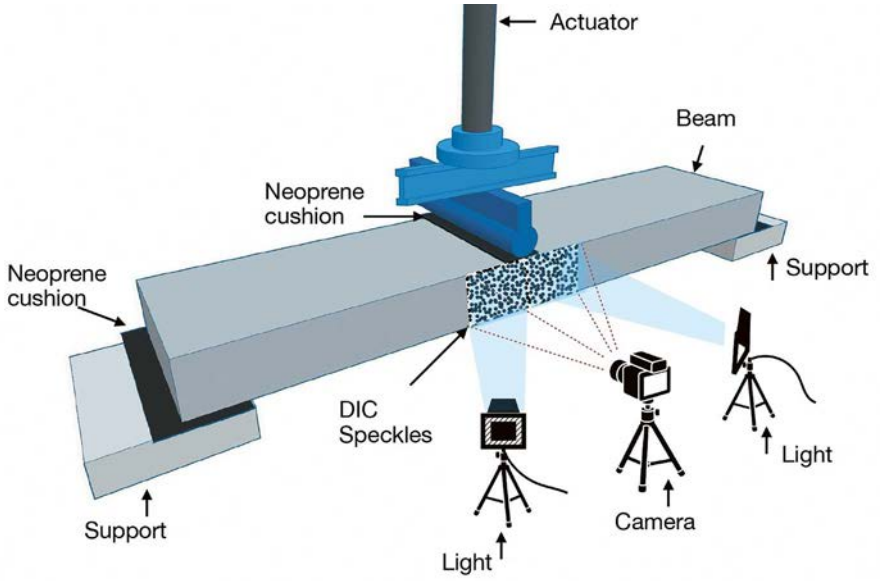

Figure 6. Setup of the components of the DIC system.

(a) Speckle pattern (3 mm, 85%–85%). (b) Speckle application on the beam surface.

Figure 7. Final speckle pattern and its application to the beam surface.

point-based strain and displacement measurements to full-field DIC analysis. The setup provided high-fidelity data for validating SFRC constitutive models under both service and ultimate load conditions, contributing to the structural-scale verification of Eurocode 2 Annex L provisions.

2.3.2. Digital Image Correlation (DIC) Methodology

A two-dimensional Digital Image Correlation (2D-DIC) system (ARAMIS Adjustable Base 2.3M) was used to capture full-field strain and displacement fields in the SFRC–steel composite beams during quasi-static and sustained loading. The system was deployed to monitor a 660 mm zone centered at midspan, which corresponds to the region of maximum flexural demand (see Fig. 6). This length was selected to match twice the beam depth, ensuring coverage of the expected crack formation zone.

The optical configuration employed a fixed industrial camera with a global shutter and a resolution of 1936 × 1216 pixels. A non-interchangeable lens, optimized for geometric stability, was used to provide consistent magnification and focus. Polarizing filters were installed on both the lens and illumination system to suppress glare and enhance speckle contrast. The camera was mounted perpendicular to the specimen surface using a rigid frame to avoid perspective distortion.

A speckle pattern consisting of 3 mm diameter black dots was applied to the concrete surface using the screen-printing technique described above. The pattern achieved approximately 85% coverage and 85% gray-level variation, which ensured high correlation quality during image post-processing. Several speckle designs were first trialed on a prototype wooden beam using the GOM live "pattern/correlation quality" check to compare performance [21]. The final pattern was selected based on stable facet tracking during preliminary sequences and a good calibration result (green indicator) after proper sensor warm-up and exposure setup. During testing, images were captured at defined load stages in 2D mode; the first image, taken at a preload of approximately 5 kN, served as the reference, and subsequent frames were correlated to obtain in-plane displacement and strain fields. Load-image synchronization was achieved via software time-stamps by ensuring synchronization between the timeline of the image captured and the progression of testing.

Image acquisition was performed at 1 Hz during quasi-static loading, and at 10 Hz during select 2-second bursts under sustained load conditions. These parameters provided a balance between temporal resolution and manageable data volume.

DIC analysis was conducted using the GOM Correlate software. A facet size of 35 × 40 pixels was used, defining the subset for displacement tracking. The strain fields obtained were processed using internal smoothing and filtering functions to enhance signal quality. The software's tracking tools were also used to measure CMOD and to map crack spacing along the midspan region.

CMOD was extracted using the two-point distance tool by placing markers on opposite sides of the crack mouth. The relative displacement between these markers was recorded continuously, allowing for sub-pixel resolution of crack opening throughout the loading protocol. Crack spacing was evaluated by identifying crack tips on sequential displacement contour maps and computing inter-crack distances.

This non-contact optical method was cross-validated with conventional point-based instruments such as LVDTs and strain gauges. CMOD and displacement values recorded by DIC were compared with those from mechanical sensors to ensure consistency. The DIC method also captured data in regions where traditional instrumentation could not be installed, especially near fiber-bridging zones or in regions with complex cracking.

Overall, the DIC system provided a high-fidelity, full-field dataset that complemented traditional instrumentation and enabled advanced fracture analysis of the composite beams. It proved especially valuable for evaluating strain localization, crack propagation under sustained loads, and ductility indicators that are critical to validating SFRC constitutive models at structural scale.

3. RESULTS AND ANALYSIS

3.1. *Load–displacement behavior*

Figure 8 presents the midspan load–displacement responses of specimens subjected to three-point bending. All specimens initially exhibit a linear response up to approximately 400–500 kN, corresponding to the elastic behavior of the composite section. Beyond this range, a nonlinear response emerges, indicating the onset structural steel and reinforcement yielding, and the extension of matrix cracking and crushing.

Post-yielding, most curves display either a plateau or a gradual increase in load capacity, suggesting strain hardening or redistribution of internal stresses facilitated by the reinforcement and embedded steel section. Distinct load drops followed by partial recoveries are observed in several specimens, indicative of localized cracking, fiber pull-out, or debonding, typical features in fiber-reinforced or ductile composite systems undergoing progressive damage [22], [23]. This type of damage generates a small release of mechanical energy stored in both the specimen and the loading frame. In such cases, both the specimen and the frame tend to slightly unload during tests conducted in position control. Note that in the load-displacement plots presented in the paper —such as Fig. 8— the displacement measurement reflects the reading from the LVDT using the strong floor as a reference. Consequently, the curve also illustrates the snap-back of the loading point during these load drops.

The peak load recorded across specimens ranges from approximately 600 kN to 730 kN, with notable variability. Most specimens retain significant residual load-bearing capacity beyond the peak, demonstrating favorable post-peak ductility. The average ultimate load capacities recorded for beams in sagging and hogging configurations are 719.2 kN and 664.3 kN, respectively.

Beams 3 and 6, tested in sagging and hogging configurations, respectively, were subjected to several steps of sustained loading, and present a reduction of ultimate load capacity by 2.4% and 2.0% in sagging and hogging, respectively, compared to the averages. We are uncertain about the causal relationship between the two phenomena; however, we believe the creep experienced by the fiber-reinforced concrete during the sustained loading may influence subsequent behavior.

The stepwise load drops observed beyond peak loading are attributed to the rupture of longitudinal steel rebars within the reinforcement cage, co-embedded with the steel section. These drops are more significant than previous ones and happen after the maximum load has been reached. They indicate a release of energy and a subsequent increase in stress on other elements, such as the steel profile and fiber-reinforced concrete. These rupture events were corroborated by audible cracking sounds synchronized with abrupt load reductions, confirming progressive failure of individual rebars. The load–displacement curves cluster into two distinct groups, as highlighted in Fig. 8: specimens in the sagging configuration consistently exhibit higher average ultimate loads (713.4 kN) compared to those in the hogging configuration (660.4 kN).

The ductility of the beams tested in the sagging configuration was consistently higher than that of those tested in the hogging configuration. Ductility was quantified using the displacement ductility ratio, as defined by Park et al. [24], which is expressed as the ratio of ultimate displacement (d_u) to yield displacement (d_y). This ratio serves as an indicator of the beam's capacity for inelastic deformation beyond initial yielding.

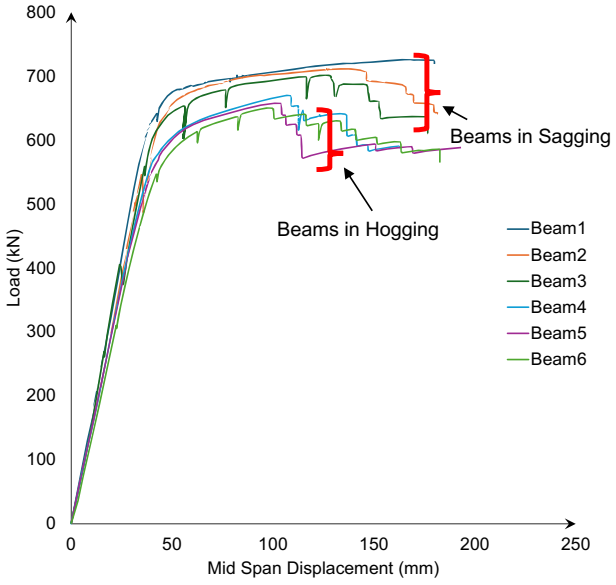

Figure 8. Load–displacement responses of all tested specimens under monotonic loading.

In the present study, the yield displacement (d_y) was identified on the ascending branch of the load–displacement curve as the displacement corresponding to 90% of the peak load, occurring just before the maximum load was reached. The ultimate displacement (d_u) was determined on the descending branch of the curve, where the load reduced to 90% of the peak load following the maximum point. While Park et al. [24] originally proposed the use of the 80% load level to define ultimate displacement, a 90% criterion was adopted

in this work. This modification was necessary because not all tests extended far enough to observe a drop to 80% of the peak load. Despite this adjustment, the 90% threshold provides a consistent and objective basis to evaluate post-peak ductility, especially under the constraint of incomplete post-peak data. A schematic illustration of the ductility measurement methodology is presented in Fig. 9.

Given that the load–displacement responses were nearly identical for the two specimens tested in each configuration, a single representative beam was selected from the sagging and hogging groups for ductility calculation. This allowed for a clear comparison of ductility ratios across configurations. Additionally, these values were compared with the ductility ratio of a beam subjected to sustained loading to assess the effect of loading history on deformation capacity. The results indicate that sustained loading led to a modest reduction in both maximum load and displacement at failure, suggesting some degradation in inelastic deformation capacity over time. However, the overall trend of higher ductility in sagging beams was maintained, potentially due to the favorable stress distribution and confinement conditions offered by the reinforcement layout in this configuration.

As evident from Table 4, the ductility factors are consistently higher for beams tested in the sagging configuration compared to those in the hogging configuration. Although the beam subjected to sustained loading does not exhibit a significant reduction in ductility factor, the corresponding load–displacement response indicates that beams tested under purely monotonic loading demonstrate greater absolute deformation capacity. This suggests that sustained loading may have a subtle effect on post-yield deformation, even if not fully captured by the ductility index alone.

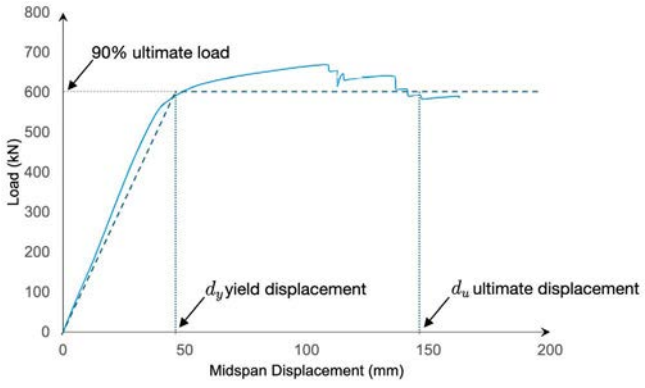

Figure 9. Illustration of ductility calculation based on the structural response curve.

TABLE 4.
Ductility ratios calculated for different beam types.

Specimen	d_u/d_y
Beam 2 (sagging)	3.88
Beam 3 (sagging, sustained loading)	3.83
Beam 4 (hogging)	2.79
Beam 6 (hogging, sustained loading)	2.78

3.2. *Evolution of strain contours and crack trajectories*

For Beam 1, the longitudinal strain contours (ϵ_{xx}) presented in Fig. 10 illustrate the evolution and propagation of cracks throughout the loading process. Immediately after crack nucleation, a brief reduction in tensile strain was observed, indicating localized stress relaxation. However, this strain quickly recovered due to the bridging action of the fibers, which effectively transferred stresses across the crack plane. Crack initiation events were accompanied by slight load drops; however, these were minimal and not clearly discernible in the global load–displacement curve. For instance, during stage 2, the initiation of a second crack caused a minor load drop of only 0.14 kN, underscoring the efficiency of the fibers in controlling crack growth and redistributing stresses.

Crack initiation and propagation occurred at an early stage within the linear elastic portion of the load response. The localized strain concentrations observed during these initial stages gradually widened as loading continued, leading to further crack development. Multiple fine cracks formed along the span and gradually opened until failure, demonstrating a distributed cracking mechanism instead of the formation of a single dominant crack. At the yielding stage, as shown in Fig. 10, DIC measurements indicate a strain of 1.0% in compression; however, the specimen remained intact without any visible spalling.

For Beam 2, the longitudinal strain contour plots presented in Fig. 11 reveal that multiple cracks formed at an even earlier stage compared to Beam 1. The overall cracking behavior and mechanisms observed in Beam 1 remain largely applicable here, including the influence of fibers in bridging cracks and redistributing stresses. However, a key observation for Beam 2 is that the material began to show signs of heavy crushing at a strain level of approximately 0.013. Despite this localized deterioration, no visible spalling was observed, and the beam maintained its structural integrity until ultimate failure.

This distinct load drop in Beam 2 response corresponds to localized crushing or deformation within the concrete compression zone shown in Fig. 12. Despite this damage, the presence of fibers ensures that the material remains cohesive, effectively acting as a cushioning layer that transfers loads to the steel beam at the bottom. The load decreases from 547.8 kN to 486.5 kN, representing a significant drop of 61.2 kN. Notably, following this initial load drop, the stiffness of the beam remains relatively stable, indicating that the fibers continue to bridge cracks effectively and preserve the overall structural integrity.

Beam 3, as illustrated in Fig. 13, shows the crack evolution under sagging conditions while being subjected to several steps of sustained loading, as described Section 2. The crack propagation and development closely resemble those observed in Beam 2. However, due to one of the sustained loading steps, a drop of approximately 2.4% is noted compared to the average load capacity of beams tested under static conditions in the sagging configuration. Crack initiation occurs early in the loading process, as depicted in Fig. 13, consistent with the behavior observed in Beams 1 and 2.

It is important to analyze the strain contours during the sustained loading period to better understand its effects on the beam under sagging conditions. Figure 14 presents strain contours at two distinct stages of sustained loading, highlighting a slight reduction in strain levels that corresponds with relaxation phenomena and a concurrent decrease in load val-

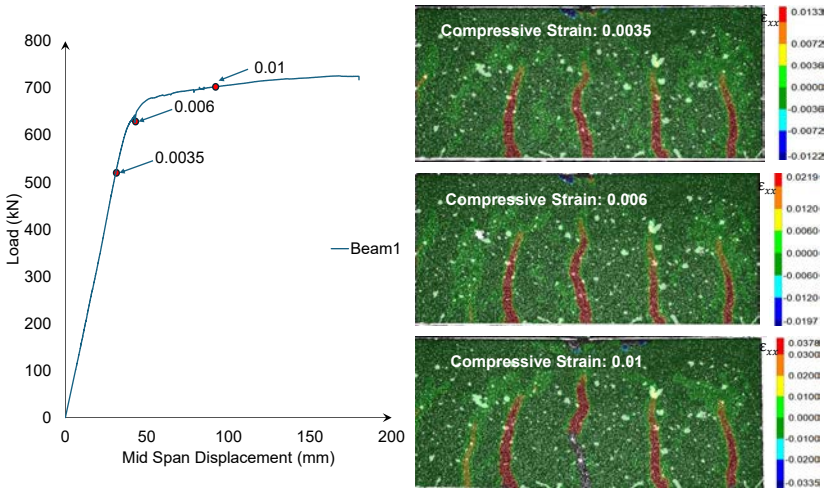

Figure 10. Longitudinal strain contour plots for Beam 1 at various loading stages, illustrating early multiple crack formation.

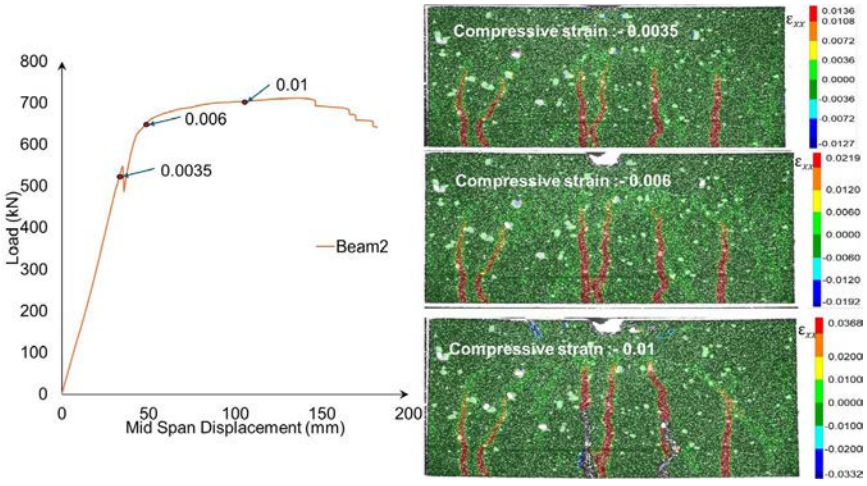

Figure 11. Longitudinal strain contour plots for Beam 2 at various loading stages, illustrating early multiple crack formation.

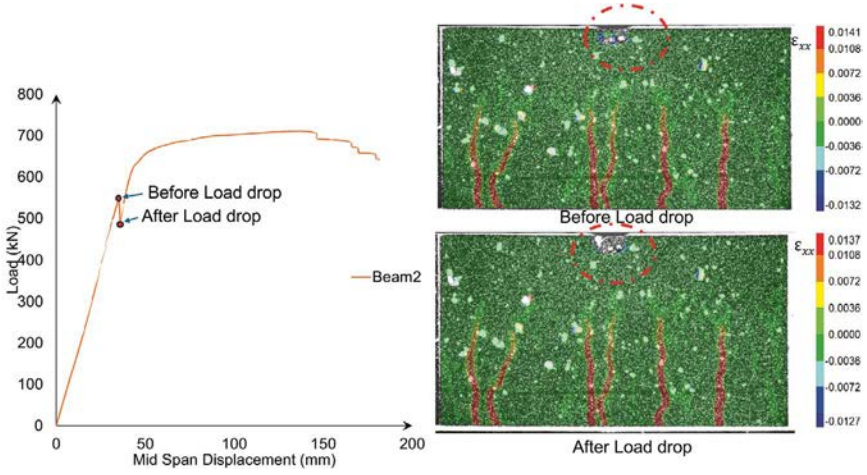

Figure 12. Longitudinal strain contour plots for Beam 2 before and after load drop.

ues. DIC analysis reveals that during this relaxation phase, crack depth increases notably by 7.8 mm, particularly at one dominant crack accompanied by branching as shown in Fig. 14. This crack progression is accompanied by a relaxation in the load response, which impacts the overall load-carrying capacity of the beam. At the onset of sustained loading, the beam carries a load of 271.4 kN, which decreases to 260.8 kN by the end of the 20-minute period. Additionally, crack branching was observed during the sustained load, indicating continued microstructural changes despite the reduced load.

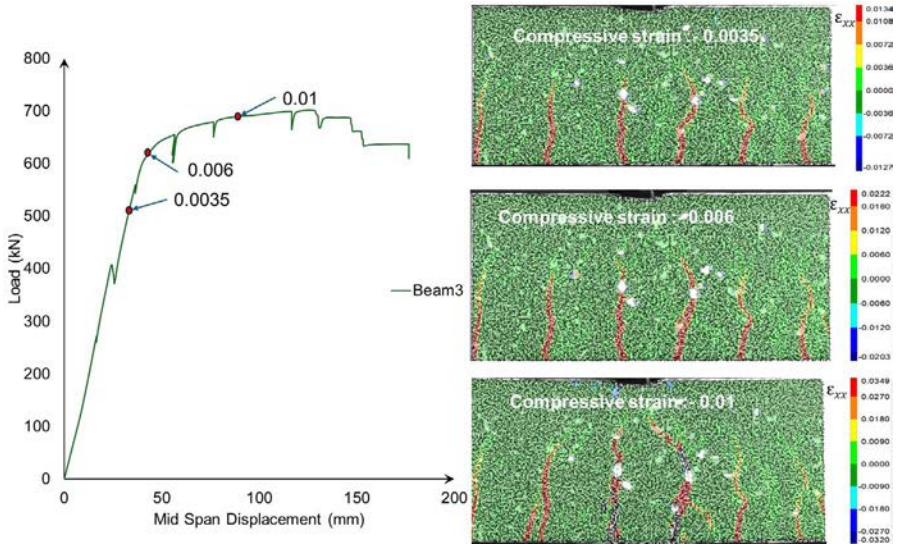

Figure 13. Longitudinal strain contour plots for Beam 3 at various loading stages, illustrating early multiple crack formation.

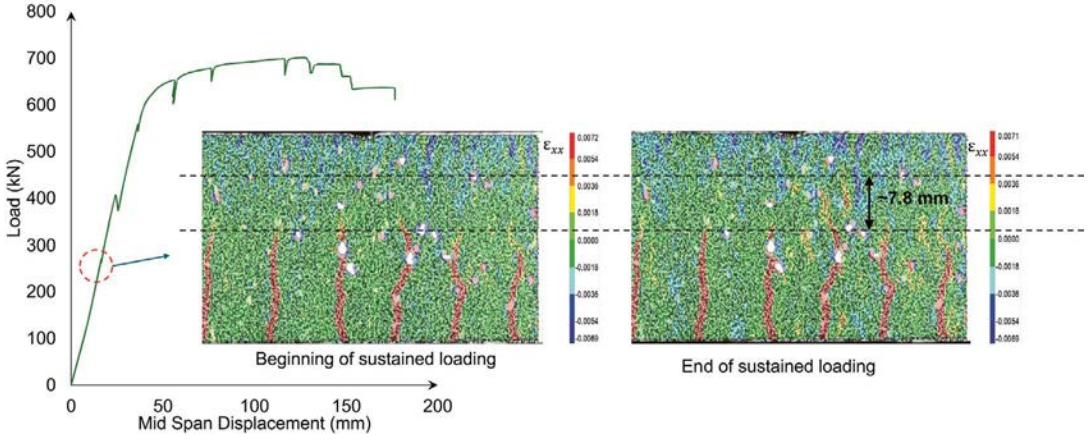

Figure 14. Longitudinal strain contour plots for Beam 3 before and after sustained loading at approximately 40% of the load peak.

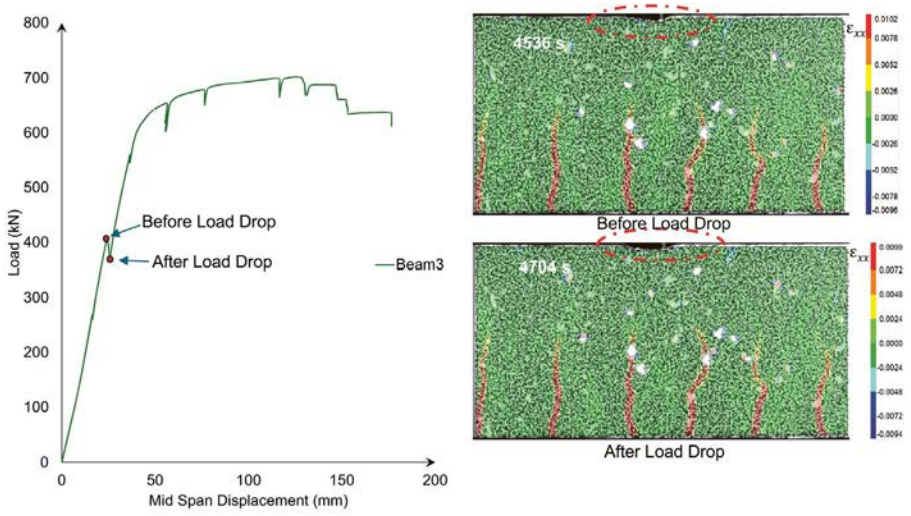

Figure 14. Longitudinal strain contour plots for Beam 3 before and after sustained loading at approximately 40% of the load peak.

Similarly, a noticeable load drop occurs in the initial stage of Beam 3's load response, akin to the behavior observed in Beam 2. Following this initial load drop, the stiffness of the beam remains largely unchanged, as reflected in the load response shown in Fig. 15. The load decreases from 407.2 kN to 372.4 kN, a total drop of 34.8 kN. Although no new crack

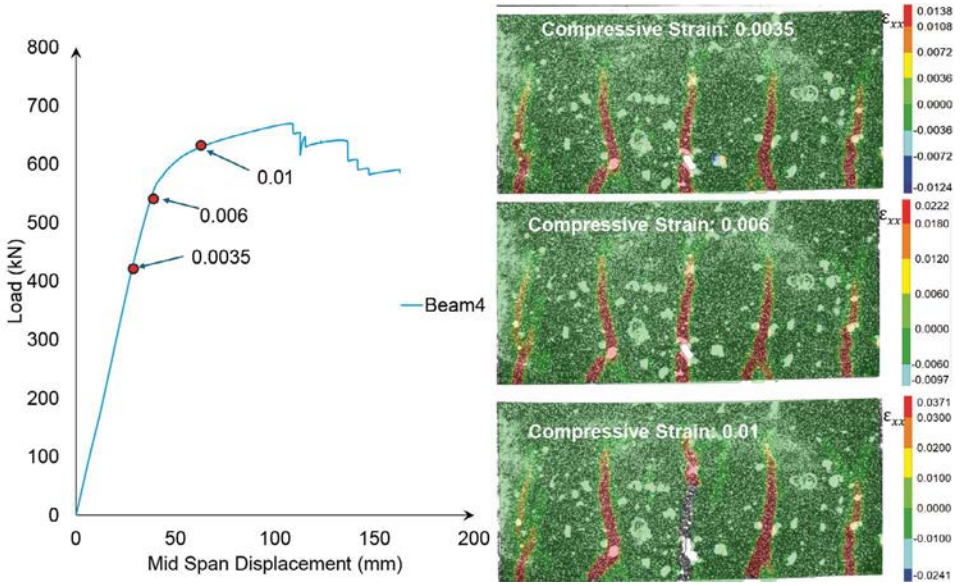

Figure 16. Longitudinal strain contour plots for Beam 4 (hogging) at various loading stages, illustrating early multiple crack formation.

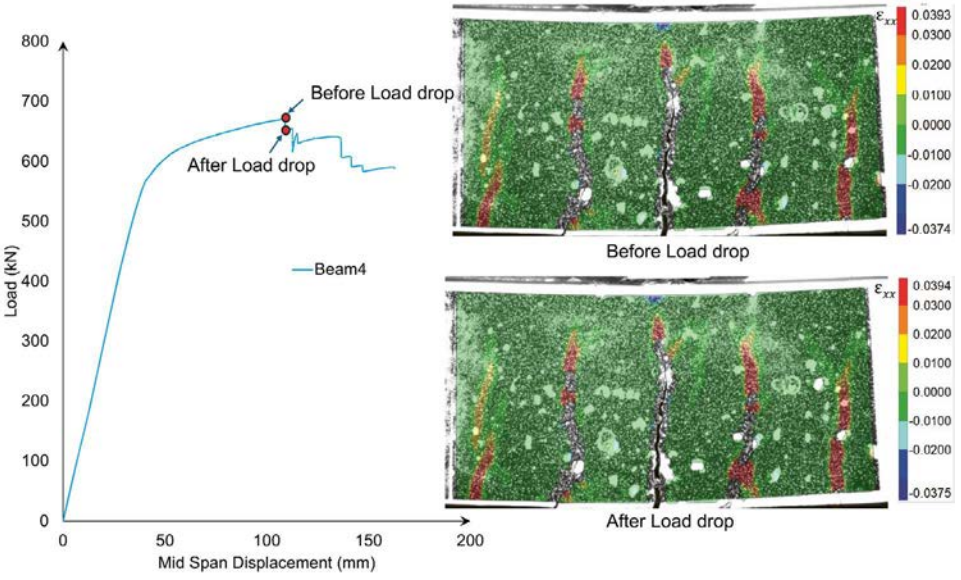

Figure 17. Longitudinal strain contour plots for Beam 4 (hogging) explaining the cause of the intermediate load drop that it experiences.

formation was detected through DIC analysis, some strain redistribution was observed.

From the response of Beam 4 shown in Fig. 16, it is evident that under hogging conditions crack initiation, as well as the formation of multiple cracks, occurs much earlier in the load response compared to the sagging configuration. Similar to what was observed in the sagging tests, the cracks that developed at the very beginning of loading continued to propagate and widen as the load increased, demonstrating a consistent cracking mechanism despite the different bending configuration.

The load drop in Beam 4 occurs only after the load response enters the nonlinear region and begins to plateau, as shown in Fig. 17. While no new cracks are observed during this stage, the sudden reduction in load can be attributed to localized debonding within the concrete matrix. This debonding is subsequently mitigated by the fibers, which bridge the cracks and help redistribute stresses, allowing the beam to maintain its structural integrity despite the loss in load capacity. One of the observations is that the load drop occurs at the ultimate load value in the case of hogging configuration in beams without sustained load.

The crack evolution and propagation in Beam 5, as illustrated in Fig. 18, closely mirror the behavior observed in Beam 4. Similar to Beam 4, crack formation in Beam 5 occurs at a very early stage of the load response, even while the response remains within the linear range. This early cracking pattern suggests that, under similar loading conditions, the hogging configuration promotes quicker crack initiation before the onset of significant nonlinear behavior.

Figure 19 presents the strain contours for Beam 6, where the pattern of crack initiation and propagation is largely consistent with the behaviors observed in Beams 4 and 5. The cracks form early in the loading process and progress in a

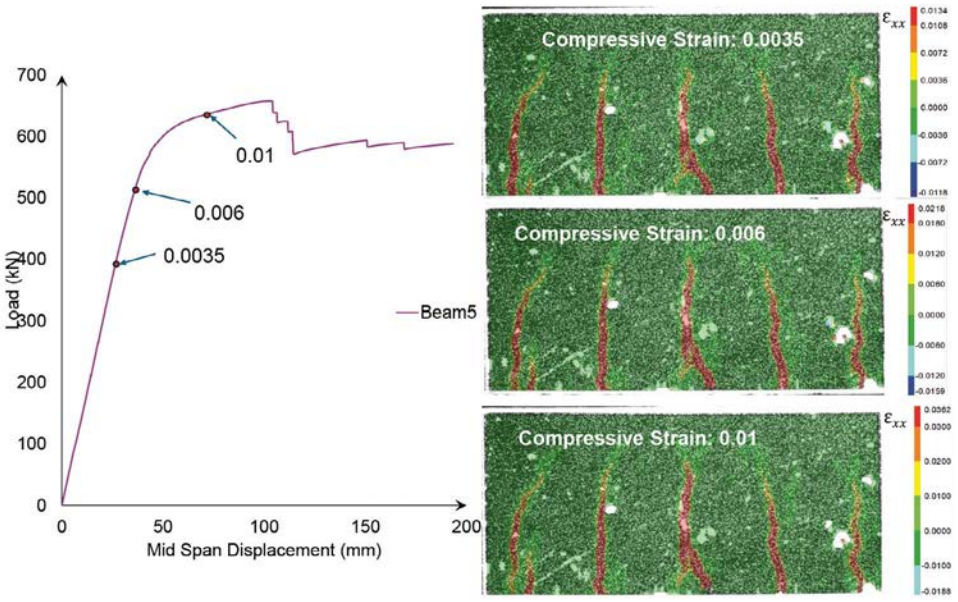

Figure 18. Longitudinal strain contour plots for Beam 5 (hogging) at various loading stages, illustrating early multiple crack formation.

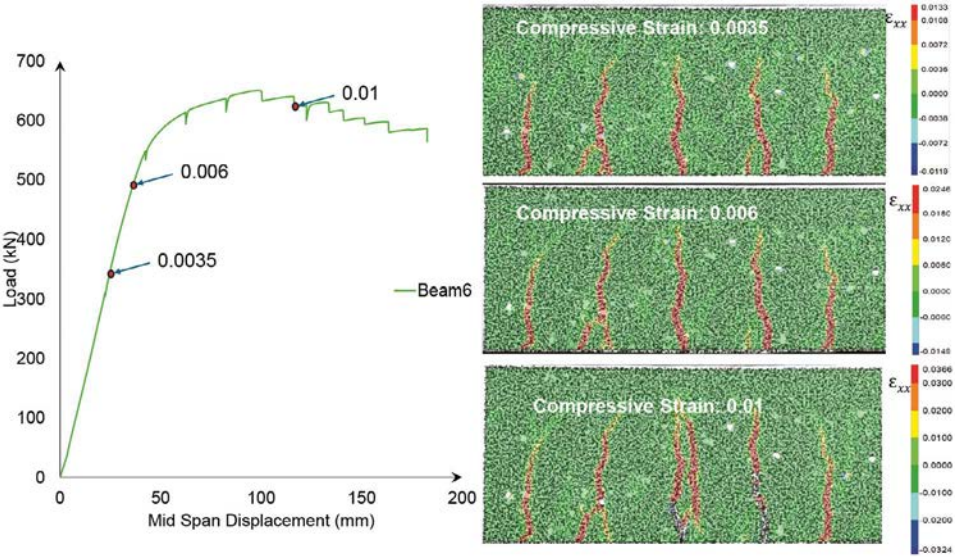

Figure 19. Longitudinal strain contour plots for Beam 6 (hogging) at various loading stages, illustrating early multiple crack formation.

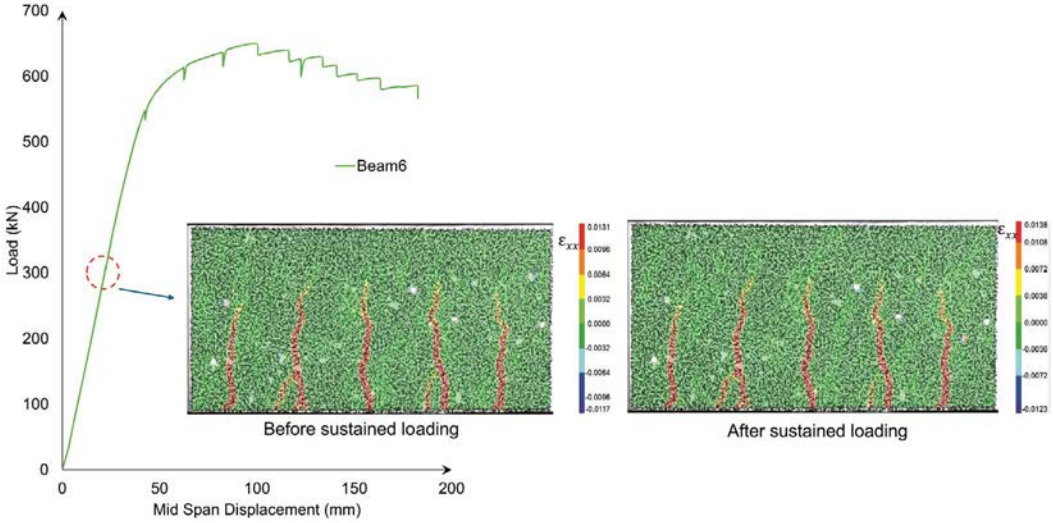

Figure 20. Longitudinal strain contour plots for Beam 6 (hogging) before and after sustained loading at approximately 40% of the load peak.

comparable manner, indicating a similar structural response under the given hogging configuration.

In the case of beams tested under hogging conditions, the concrete in the compression zone experiences very high strains, exceeding 1%, yet it remains intact without the crushing observed in beams tested in the sagging configuration. Before and after the sustained loading steps, no significant changes are observed in the crack patterns or their propagation in the hogging tests. However, both compressive and tensile strain levels show a slight increase, which can be attributed to creep effects during the sustained loading phases (see Fig. 20).

The load response of beams in the hogging configuration does not exhibit the distinct load drop observed in the sagging beams; instead, a gradual hardening behavior is evident. DIC analysis clarifies that the sharp load drop seen in the sagging case is linked to deformation of the concrete in the compressive zone directly beneath the point load. In contrast, under hogging conditions, the load transfer is primarily facilitated through the steel section, preventing localized crushing and contributing to the smoother, hardening-type response observed in these beams.

At an average strain level close to 0.013, the material in the compressive zone of the sagging beams begins to crush. Even though the concrete undergoes crushing, as shown in the final stage (Figs. 12 and 15), the presence of fiber reinforcement ensures that the crushed concrete behaves like a packing material, continuing to transfer load to the steel section. In contrast, in the hogging configuration, the beam maintains its structural integrity even at much higher compressive strain levels, reaching up to 4.14%, demonstrating the combined effectiveness of the fibers and the steel section.

3.3. *Evolution of compressive strains in the concrete compression zone throughout the load response.*

As mentioned in the introduction, the HTC used in these beam specimens has been shown to withstand exceptionally high levels of compressive strain. The addition of steel fibers improves the ductility of the concrete, enabling it to endure significantly greater strains compared to conventional mixes. Therefore, studying the evolution of compressive strain during the loading process is particularly important, as it provides experimental validation for the enhanced strain capacity of HTC, as previously reported by Ruiz et al. [9].

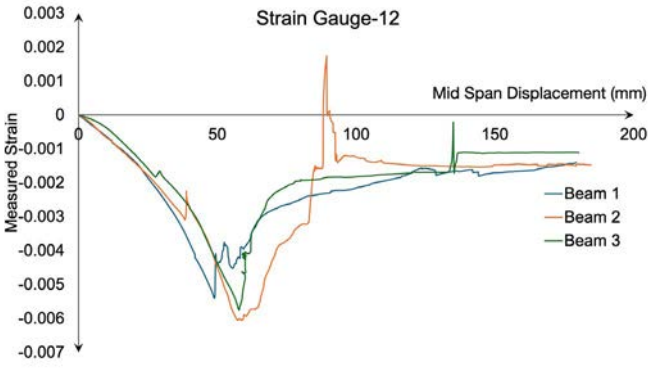

Figure 21. Recordings by the top strain gauge in compression.

Figure 21 shows the recordings of the top strain gauge in compression of all the beams tested in sagging. All the beams reach very high levels of compressive strain, way higher than what is usual for concrete structures, which have a limit of 0.35%, reaching roughly the 0.6% allowed in the Ultimate Limit State (ULS) by Annex L of the new Eurocode 2 [10]. The three beams consistently align with the readings taken via DIC, as shown in Figs. 10-13. However, the deformation and bending just below the actuator prevented the strain gauges from functioning properly beyond 0.6%. In spite of this, DIC measurements confirm that all the beams reach 1% compressive strain with no signs of crushing. Eventually, signs of crushing appear, but the fibers keep the concrete in place until the end of the tests.

In the hogging tests, the strain gauges failed to provide reliable measurements due to early cracking and concentrated rotation. However, the DIC results shown in Figs. 16-19 indicate that the levels of ductility in compression were similar to those in sagging.

3.4. *Crack mouth opening calculations*

Crack widths were calculated from displacement profiles by analyzing a selected section x–x, shown in Fig. 22, located at the bottom of the beam. The displacement profile was asymptotically matched on either side of the crack, and the crack opening was determined by subtracting the displacements immediately adjacent to the crack on the left and right sides.

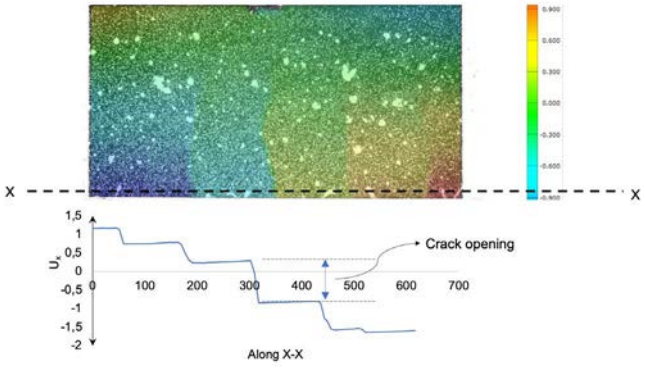

Figure 22. Displacement-based calculation of crack width at section x–x located at the beam bottom surface.

Figure 23 compares CMOD time histories obtained from DIC gauges placed across the crack mouth for four of the beams, grouped by bending regime (sagging left, hogging right) and by stage (monotonic loading up, relaxation down). In sagging at monotonic loading (Beam 1), several cracks open gradually at a similar slow rate until the hinge below the loading point forms, which coincides approximately with the initiation of the second loading ramp. Then the opening rate speeds up, and, eventually, there is a crack (marked as 2) that starts to localize most of the opening so that the rest of the nearby cracks (1 and 3) tend to close. Beam 4, tested in hogging at monotonic loading, behaves similarly, but the openings are higher, and the localization in crack 2 is more abrupt.

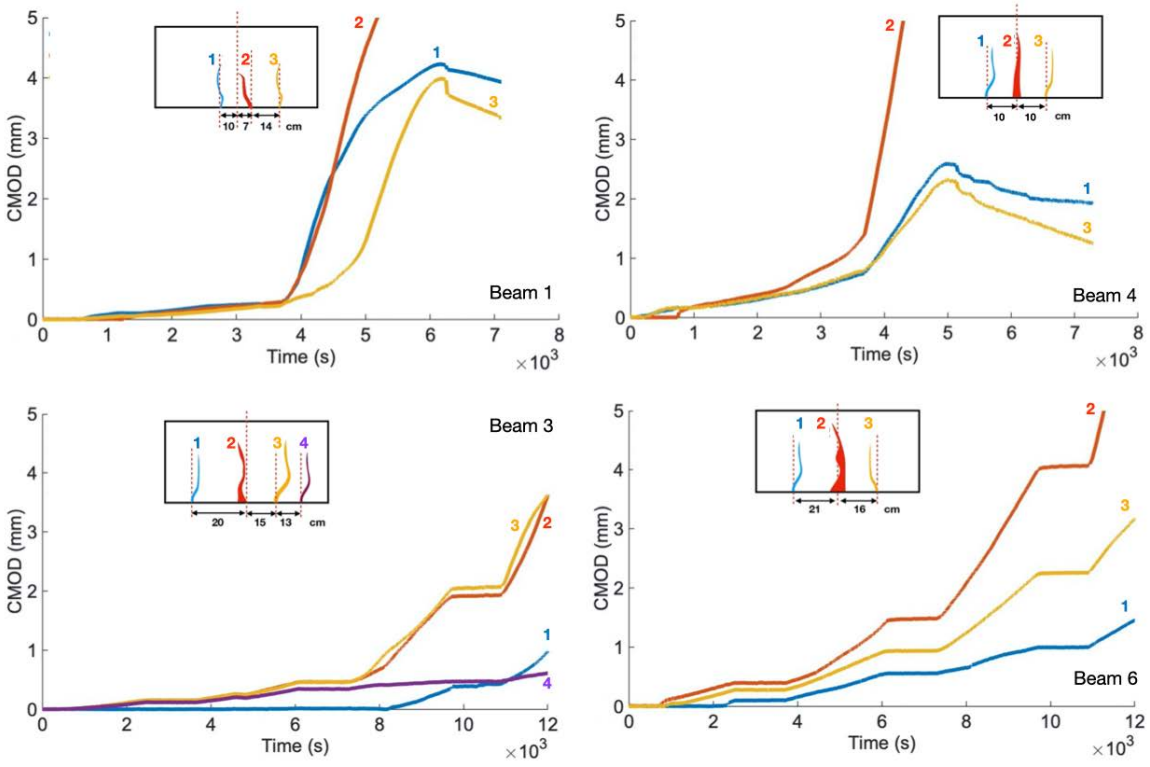

Figure 23. Comparison of CMOD development across sagging and hogging configurations in monotonic and relaxation loading.

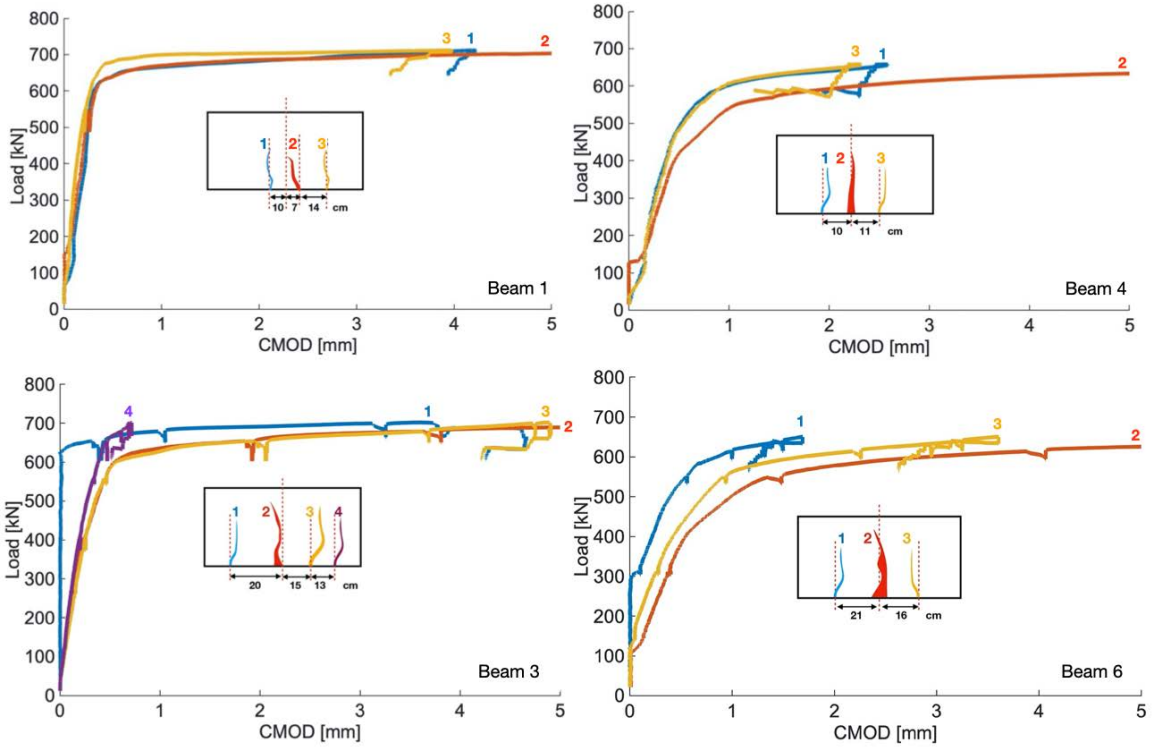

Figure 24. Comparison of Load-CMOD development across sagging and hogging configurations in monotonic and relaxation loading.

The lower line of subfigures in Fig. 23 presents the CMOD histories for two beams subjected to sustained loading. Beam 3, which is sagging, exhibits very slow crack growth during the periods of sustained load. However, it appears that the crack opening rate increases after the application of the same nearly constant displacement rate applied before the relaxation stage (5 mm/min). We believe this may be due to a slight progressive damage or creep at the matrix-fiber interface during the sustained stage. Similarly, Beam 6 shows a comparable behavior, but with higher openings and rates. This

is likely a result of the beam's section configuration, which places greater demands on the SFRC in the tensioned fibers.

Figure 24 shows the load-CMOD curves for the same beams and cracks as in Fig. 23. The curves of Beam 1 show that the openings are below 0.5 mm during the linear ramp-up, but start to grow significantly once the steel profile starts yielding. Eventually, all the opening localizes in crack 2, while the other studied cracks, 1 and 3, stall and even begin to close. Beam 4 follows the same trend as Beam 1, but shows wider openings and earlier localization in the central crack.

The load-CMOD plots for beams undergoing relaxation steps are displayed in the lower row of subfigures in Fig. 24. It is evident that the crack openings in these beams are wider compared to those in the beams that were subjected to monotonous loading. As mentioned above, this observation suggests a slight deterioration or creep at the matrix-fiber interface.

Table 5 presents the critical CMODs —at failure— (w_{Mc}) for the six beams tested. In the case of hogging, the critical crack opening is much larger than in sagging because of the absence of the steel section near the tensile fibers of the beam.

In the case of hogging, where the steel section is located at the top of the beam, a single-section failure is observed. Although multiple cracks may appear, only one section ultimately opens up until failure occurs. In contrast, when sagging takes place, the beam experiences widespread cracking. In all instances, there is one crack that becomes significantly larger than the others, ultimately leading to the failure of the beams.

In nearly all cases, the crack pattern remains largely unchanged, with no significant new crack initiations occurring beyond the initial portion of the load response, at least within the range captured by the DIC camera.

TABLE 5.
Critical crack openings at failure.

Specimen	w_{Mc} *[mm]*
Beam 1 (sagging)	10.20
Beam 2 (sagging)	16.87
Beam 3 (sagging)	21.15
Beam 4 (hogging)	30.08
Beam 5 (hogging)	40.99
Beam 6 (hogging)	42.10

3.5. *Crack Spacing Measurement Results*

Crack spacing was assessed using a combination of manual measurements and DIC post-processing. Figure 25 illustrates the schematic representation of the DIC region at midspan, highlighting how cracks were identified and inter-crack spacing was measured. The primary area of interest covered a 660 mm segment centered at midspan, which corresponds to the zone of maximum bending moment and was captured using DIC. Within this area, cracks were identified based on distinct separation lines in the displacement contour maps. The analysis included both major cracks and smaller microcracks that fell within the spatial resolution of the DIC system. For cracks located outside the DIC field of view, visual inspection and photographic documentation were used for manual mapping along the remaining beam length. Crack spacing was then calculated as the distance between successive cracks along the entire span, allowing for a comprehensive evaluation of crack distribution in both sagging and hogging configurations.

Each beam was segmented into four equal-length zones (0–110 cm, 110–220 cm, 220–330 cm, and 330–440 cm), and the number of visible cracks in each zone was recorded. Table 6 summarizes the total number of cracks and average spacing for six beams. Sagging beams (Beams 1–3) exhibited a more distributed cracking pattern, with an average spacing of approximately 12.9 cm, while hogging beams (Beams 4, 6, 7) showed slightly wider spacing, indicating a more localized cracking response.

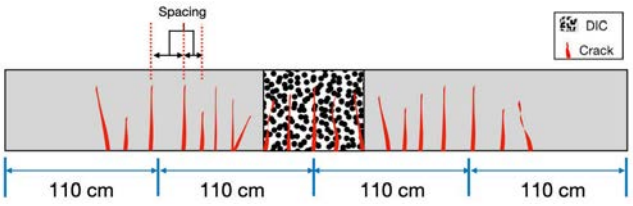

Figure 25. Schematic of crack spacing measurement zone showing DIC region and crack tip identification.

TABLE 6.
Total number of cracks and average spacing.

Specimen	*Number of cracks*	*Avg. Spacing [cm]*
Beam 1 (sagging)	20	12.90
Beam 2 (sagging)	21	12.95
Beam 3 (sagging)	9	12.84
Beam 4 (hogging)	24	10.11
Beam 6 (hogging)	15	14.46
Beam 7 (hogging)	18	14.00

To analyze the spatial distribution of cracking, Table 7 presents the number of cracks observed in each beam zone. In sagging specimens, cracks were more uniformly distributed across the central zones (Mid-Left and Mid-Right), suggesting effective strain redistribution through fiber bridging. In contrast, hogging beams exhibited pronounced clustering of cracks near midspan.

TABLE 7.
Zone-wise crack distribution across beam span.

Specimen	*Left 0–110 cm*	*Mid-Left 110–220 cm*	*Mid-Right 220–330 cm*	*Right 330–440 cm*
Beam 1	1	8	9	1
Beam 2	1	9	10	1
Beam 3	0	3	6	0
Beam 4	3	11	9	1
Beam 6	0	9	6	0
Beam 7	2	8	8	0

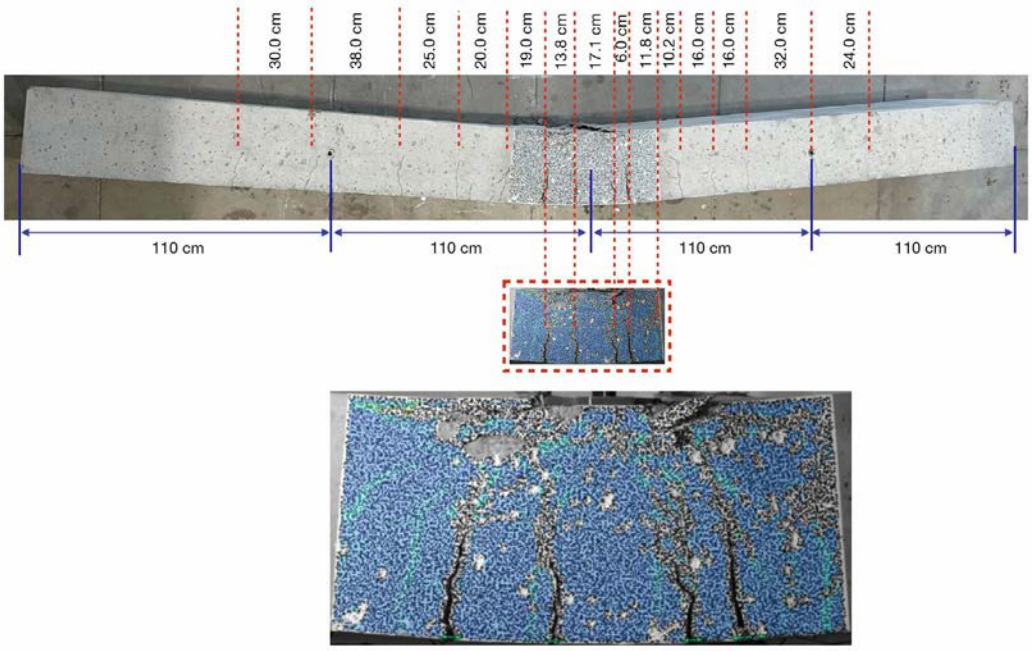

Figure 26. Crack spacing analysis for Beam 2 (Sagging configuration).

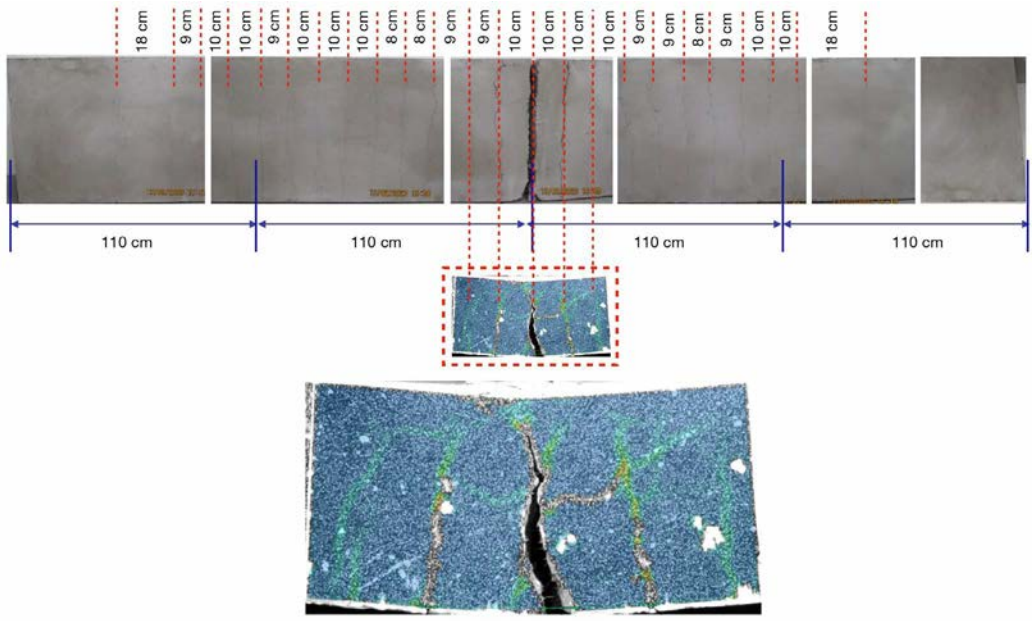

Figure 27. Crack spacing analysis for Beam 4 (Hogging configuration).

Figures 26 and 27 illustrate annotated crack maps obtained from DIC analysis for Beam 2 (sagging) and Beam 4 (hogging), respectively. The sagging configuration shows evenly distributed cracks across the midspan region, while the hogging case displays fewer but more dominant cracks forming closer to midspan.

Overall, the observed differences in crack spacing reflect the role of structural configuration and fiber contribution. Sagging beams, with the steel section located in tension, promote distributed cracking and effective fiber engagement. Conversely, hogging beams develop dominant cracks due to the higher contribution of SFRC in the tension zone, which cannot be redistributed to other cracks once a given crack reaches the decreasing point where fibers are pulled out.

4. DISCUSSION

The results obtained from the full-field DIC monitoring of SFRC–steel composite beams highlight several critical aspects of fracture behavior under static and sustained loading. In both sagging and hogging configurations, early crack initiation was observed within the serviceability load range where the structural behavior is approximately linear, with cracks progressively widening as loading continued. The distributed crack patterns in sagging beams, promoted by the tensile positioning of the steel section and enhanced fiber bridging, contrast with the more localized cracking observed in hogging specimens. This distinction is consistent with strain re-

distribution behavior and the availability of confinement near the tension zone.

The application of several steps of sustained loading introduced moderate changes in behavior, particularly in sagging beams. The overall reduction in peak load was limited (2–3%) and nonconclusive. DIC results revealed strain redistribution, increased crack depth (up to 7.8 mm) and opening rate, and branching phenomena not captured by conventional LVDTs. In contrast, hogging beams exhibited minimal change in crack patterns during sustained loading, but showed incremental increases in tensile and compressive strain values due to creep.

Compressive strain development shows the superior ductility of the HTC used in the study. All of the beams reached a 1% compressive strain with no visible crushing. Strain levels exceeding 1% were maintained in sagging specimens, although signs of matrix crushing appeared beyond this threshold. Despite the material being crushed, it continued to resist compression because of the fibers, and there was no spall failure in any case. Meanwhile, hogging beams withstood compressive strains well above 1% without visible crushing or spalling, thanks to the contribution of the stiff steel section located in compression. These observations align with prior reports on HTC and confirm its ability to endure large strains without brittle failure.

By allowing these higher strains, it is possible to optimize the materials' performance in composite structures. Specifically, this approach allows for the full utilization of the structural steel at ULS, as noted in previous papers [8], [9], [16]. Additionally, composite structural elements that leverage the significant ductility of SFRC in compression can reduce the carbon footprint by up to 40% when compared to alternative structural concrete solutions for the same structure, as demonstrated by some of the authors [25].

Annex L of the new Eurocode 2 [10] states that the maximum strain in any structural element made from SFRC is 0.6% under the ULS, compared to 0.35% for standard concrete. Additionally, the compressive model in Annex L shows that the SFRC used in our research, with compressive and flexural classes of C45/55 and 2.5c, respectively, can reach a strain of 0.89% in the Serviceability Limit State (SLS) [9]. Here, we demonstrate that these strain levels can be surpassed while the beams remain fully functional. Moreover, the beams examined in this paper achieve very high levels of compressive strain without any spalling in the top layer. These results confirm the material's reliability even under extreme loading conditions. Therefore, our study experimentally validates the principles outlined in Annex L at the structural level.

CMOD results further confirmed the structural distinction between configurations. Sagging beams displayed lower critical crack openings (10–21 mm) and distributed fracture mechanisms, whereas hogging beams reached crack openings up to 42 mm due to the lack of strain hardening in the tensile region. This behavior confirms the critical role of steel profile positioning in influencing crack propagation modes.

Moreover, the insights into crack development patterns and spacing gained during the campaign directly influence the design of composite beams and can help refine standard specifications on these topics. By understanding where and how cracks initiate and propagate in composite SFRC-structural steel structures, it is possible to optimize material placement and fiber reinforcement strategies to enhance durability and performance. This knowledge enables practical design adjustments that improve stress management.

Overall, the use of DIC in this experimental setup was highly effective for monitoring strain localization, crack spacing, and CMOD with excellent spatial and temporal resolution. Compared to traditional instrumentation, DIC offered valuable insights into strain redistribution, early microcracking, and crushing phenomena. However, there are challenges that need to be addressed in future studies, including the quality of the speckle pattern, uniformity of lighting, and limited coverage of the field of view. These issues could potentially be resolved by expanding to 3D-DIC or using synchronized multi-camera systems.

5. CONCLUSIONS

This experimental study investigated the fracture response of full-scale SFRC–steel composite beams under monotonic and sustained loading using a standard extensometry and a DIC system. The following conclusions can be drawn:

- *Strain Localization and Cracking*: DIC effectively captured early crack initiation, branching, and propagation. Sagging beams exhibited distributed cracking due to favorable tensile reinforcement conditions, while hogging beams displayed dominant, localized cracks.
- *CMOD and Crack Morphology*: CMOD values at failure ranged from 10 mm in sagging to over 40 mm in hogging beams. The presence of the steel section in tension promoted strain hardening and ductile behavior in sagging beams, while its position in compression in hogging beams limited tensile redistribution.
- *Compressive Strain Capacity*: The high-performance HTC matrix accommodated compressive strains well above 1% in sagging and hogging configurations without catastrophic failure, demonstrating enhanced ductility and compatibility with fiber-reinforced design models.
- *Sustained Loading Effects*: DIC revealed microstructural changes such as crack branching and increased crack depth, which were not evident through conventional instrumentation. Besides, CMOD histories reveal that the opening rate increases after a period of sustained loading, which could be attributable to deterioration or creep of the matrix-fiber interface.
- *Eurocode 2 Annex L Validation*: The experimental results confirm the applicability of Annex L residual strength-based compressive model and related strain limits in compression to full-scale SFRC composite beams. The strain and cracking behavior align well with design assumptions, supporting broader adoption in structural applications.
- *DIC as a Structural Monitoring Tool*: This study confirms the robustness and practicality of DIC in large-scale testing of composite beams. It offers a powerful complement to traditional sensors and paves the way for its inclusion in future monitoring guidelines and standards.

Future work should focus on exploring cyclic and fatigue behavior under varying load regimes, expanding to 3D-DIC setups, and validating numerical models for further generalization of these findings in the design and assessment of hybrid SFRC structures.

Acknowledgements

ArcelorMittal Global R&D. provided the funding for the tests. Additionally, this research received financial support from the *Ministerio de Innovación, Ciencia y Universidades* in Spain through grant PID2023-147971OB-C31, from the *Junta de Comunidades de Castilla-La Mancha* in Spain via grant SBPLY/24/180225/000003, and from the *Universidad de Castilla-La Mancha* and the ERDF through grant 2025-GRIN-38445.

Dedication

The authors dedicate this work to Professors Hugo Corres and Toni Marí in celebration of their seventieth anniversary and their remarkable, inspiring careers. In particular, Gonzalo Ruiz expresses heartfelt gratitude to Toni Marí for the many stimulating discussions on the applications of fracture mechanics to concrete technology, as well as for his kindness and friendship.

References

[1] B. Lai, J. Y. R. Liew, and A. L. Hoang, "Behavior of high strength concrete encased steel composite stub columns with C130 concrete and S690 steel," *Engineering Structures*, vol. 200, p. 109743, 2019, doi: 10.1016/j.engstruct.2019.109743.

[2] J. Zhao, Y. Sang, and F. Duan, "The state of the art of two-dimensional digital image correlation computational method," *Engineering Reports*, vol. 1, no. 8, p. e12038, 2019, doi: 10.1002/eng2.12038.

[3] B. Lai, J. Y. R. Liew, A. Venkateshwaran, S. Li, and M. Xiong, "Assessment of high-strength concrete encased steel composite columns subject to axial compression," *Journal of Constructional Steel Research*, vol. 164, p. 105765, 2020, doi: 10.1016/j.jcsr.2019.105765.

[4] A. Memarzadeh and M. Nematzadeh, "Axial compressive performance of steel reinforced fibrous concrete composite stub columns: Experimental and theoretical study," *Structures*, vol. 34, pp. 2455–2475, 2021, doi: https://doi.org/10.1016/j.istruc.2021.08.130.

[5] S. J. Foster and R. I. Gilbert, "Characterisation and structural design of steel fibre reinforced concrete," *Structural Concrete*, vol. 19, no. 1, pp. 121–132, 2018, doi: 10.1002/suco.201700156.

[6] G. Ruiz, Á. De La Rosa, S. Wolf, and E. Poveda, "Model for the compressive stress-strain relationship of steel fiber-reinforced concrete for non-linear structural analysis," *Hormigón y Acero*, vol. 69(S1), pp. 75–80, 2018, doi: 10.1016/j.hya.2018.10.001.

[7] G. Ruiz, Á. De La Rosa, and E. Poveda, "Relationship between residual flexural strength and compression strength in steel-fiber reinforced concrete within the new Eurocode 2 regulatory framework," *Theoretical and Applied Fracture Mechanics*, vol. 103, p. 102310, 2019, doi: 10.1016/j.tafmec.2019.102310.

[8] R. Zanon, M. Schäfer, G. Ruiz, Á. De La Rosa, and Q. Zhang, "Steel-fibre reinforced concrete in composite structures as a means to increase resistance and ductility," *Stahlbau*, vol. 91, no. 12, pp. 801–811, 2022.

[9] G. Ruiz, Á. De La Rosa, E. Poveda, R. Zanon, M. Schäfer, and S. Wolf, "Compressive behavior of steel-fiber reinforced concrete in Annex L of new Eurocode 2," *Hormigón y Acero*, vol. 74, no. 299–300, pp. 187–198, 2023.

[10] CEN, Eurocode 2, Design of concrete structures. Part 1-1: General rules – Rules for buildings, bridges and civil structures, prEN 1992-1-1: 2022. CEN–European Committee for Standardization, Brussels, Belgium, 2022.

[11] Á. De La Rosa, G. Ruiz, V. W. Masih, and R. Zanon, "Experimental study of the response to fatigue compression and indirect tensile loading in high-technology concrete," *Materials and Structures*, vol. 58, p. 207, 2025, doi: 10.1617/s11527-025-02731-9.

[12] M. Mahal, T. Blanksvärd, B. Täljsten, and G. Sas, "Using digital image correlation to evaluate fatigue behavior of strengthened reinforced concrete beams," *Engineering Structures*, vol. 105, pp. 277–288, 2015, doi: 10.1016/j.engstruct.2015.10.017.

[13] A. Baktheer and H. Becks, "Fracture mechanics based interpretation of the load sequence effect in the flexural fatigue behavior of concrete using digital image correlation," *Construction and Building Materials*, vol. 307, p. 124817, 2021, doi: 10.1016/j.conbuildmat.2021.124817.

[14] R. Janeliukstis and X. Chen, "Review of digital image correlation application to large-scale composite structure testing," *Composite Structures*, vol. 271, p. 114143, 2021, doi: 10.1016/j.compstruct.2021.114143.

[15] J. Holmes, S. Sommacal, R. Das, Z. Stachurski, and P. Compston, "Digital image and volume correlation for deformation and damage characterisation of fibre-reinforced composites: A review," *Composite Structures*, vol. 315, p. 116994, 2023, doi: 10.1016/j.compstruct.2023.116994.

[16] R. Zanon, M. Schäfer, G. Ruiz, Á. De La Rosa, V. W. Masih, and S. Wolf, "Experimental bending tests on encased steel-concrete composite beams with SFRC," in *11th international conference on fibre-reinforced concrete* (BEFIB 2024), Dresden, Germany, 2024. doi: 10.1007/978-3-031-70145-0_25.

[17] CEN, Eurocode 4, Design of composite steel and concrete structures. Part 1-1: General rules and rules for buildings, prEN 1994-1-2: 2022. 2022.

[18] Á. De La Rosa, G. Ruiz, V. M. Masih, and R. Zanon, "Innovative high-technology concrete mix design method integrating rheological properties and fracture mechanics," *Construction and Building Materials*, vol. 458, p. 139538, 2025, doi: 10.1016/j.conbuildmat.2024.139538.

[19] R. Henning, Water-based screenprinting today: Hands-on techniques to digital technology. New York: Watson-Guptill Publications, 2006.

[20] G. Crammond, S. W. Boyd, and J. M. Dulieu-Barton, "Speckle pattern quality assessment for digital image correlation," *Optics and Lasers in Engineering*, vol. 51, no. 12, pp. 1368–1378, 2013, doi: 10.1016/j.optlaseng.2013.03.014.

[21] *GOM GmbH ARAMIS User Manual Hardware*. GOM GmbH: Braunschweig, Germany, 2022.

[22] S. Li, H. Lv, T. Huang, Z. Zhang, J. Yao, and X. Ni, "Degradation of reinforced concrete beams subjected to sustained loading and multi-environmental factors," *Buildings*, vol. 12, no. 9, 2022, doi: 10.3390/buildings12091382.

[23] M. Shubaili, A. Elawadi, S. Orton, and Y. Tian, "Time-dependent behavior of reinforced concrete beams under high sustained loads," *Applied Sciences (Switzerland)*, vol. 12, no. 8, 2022, doi: 10.3390/app12084015.

[24] R. Park, "Ductility evaluation from laboratory and analytical testing," in *Proceedings of the Ninth World Conference on Earthquake Engineering*, 1988.

[25] S. Wolf, G. Ruiz, Á. De La Rosa, E. Poveda, M. Schäfer, and R. Zanon, "Ductility in compression of SFRC and its use with low CO_2 emissions green steel fibres," in Proceedings of FRC2023. Fiber Reinforced Concrete: From Design to Structural Applications. Joint ACI-fib-RILEM International Workshop, Phoenix, Arizona, 2023.

Disponible en **www.hormigonyacero.com**
https://doi.org/10.33586/hya.2025.4133

Why the Impact of Climatic Change on Reinforcement Corrosion Cannot Be Predicted at Present

Por qué el impacto del cambio climático no puede predecirse todavía.

Andrade Perdrix, Carmen[a]

[a] *Dr. In Industrial Chemistry. Distinguished Senior Researcher CIMNE. International Centre of Numerical Methods in Engineering (CIMNE)- Madrid-Spain.*

Recibido el 1 de junio de 2025; revisado el 22 de julio de 2025, aceptado el 22 de diciembre de 2025

ABSTRACT

Climate change calls into question the durability of infrastructures when environmental actions exceed those foreseen for their design. In the case of reinforcement corrosion, the main corrosion control parameter is the evaporable water content (retained water) of the concrete. Despite its importance that also affects other deterioration processes, data on its content in full-scale structures are scarce, in contrast to the numerous published references on laboratory experiments. This article presents values of the degree of saturation of specimens exposed to the weather and their impact on the corrosion potential, the resistivity of the concrete and the values of the corrosion rate. It can be deduced that the external conditions of temperature and RH are not the controlling factors of the corrosion process, but mainly rainfall. The results show that the only biunivocal relationship with the corrosion rate is that of resistivity, but a "function" has not yet been established that characterizes the environment to deduce its effects on the water content of the concrete and therefore on its resistivity. This lack of correlation of corrosion with the temperature and relative humidity outside calls into question the work published so far on the impact of climate change on infrastructures, since they are based on these external parameters and not on the water retained inside the concrete.

KEYWORDS: climate, corrosion, concrete, relative humidity, temperature, rain.

RESUMEN

El cambio climático cuestiona la durabilidad de las infraestructuras cuando las acciones ambientales exceden las previstas para su diseño. En el caso de la corrosión de las armaduras, el principal parámetro de control de la corrosión es el contenido de agua evaporable (agua retenida) del hormigón. A pesar de su importancia que también afecta a otros procesos de deterioro, los datos sobre su contenido en estructuras a escala real son escasos, en contraste con las numerosas referencias publicadas sobre experimentos de laboratorio. Este artículo presenta valores del grado de saturación de probetas expuestas a la intemperie y su impacto en el potencial de corrosión, la resistividad del hormigón y los valores de la velocidad de corrosión. Se puede deducir que las condiciones externas de temperatura y HR no son los factores controlantes del proceso de corrosión sino principalmente la lluvia. Los resultados muestran que la única relación biunívoca con la velocidad de corrosión es la de la resistividad, pero aún no se ha establecido una "función" que caracterizando el ambiente permita deducir sus efectos en el contenido en agua del hormigón y por tanto en su resistividad. Esta falta de correlación de la corrosión con la temperatura y humedad relativa exterior cuestiona los trabajos hasta ahora publicados sobre el impacto del cambio climático en las infraestructuras, ya que se basan en esos parámetros exteriores y no en el agua retenida en el interior del hormigón.

PALABRAS CLAVE: clima, corrosión, hormigón, humedad relativa, temperatura, lluvia.

* Persona de contacto / *Corresponding author*:
Correo-e / *e-mail*: candrade@cimne.upc.edu (Carmen Andrade Perdrix)

How to cite this article: Andrade, C. (2026). Why the Impact of Climatic Change on Reinforcement Corrosion Cannot Be Predicted at Present. *Hormigón y Acero*. 77(308):47-58. https://doi.org/10.33586/hya.2025.4133

1. INTRODUCTION

The classification of the exposure classes in present standards recognises the impact that the different environments have in the concrete durability, either on the concrete itself or onto the reinforcements [1]. This classification for preventing steel corrosion attends first to whether the concrete is carbonated or is chloride contaminated and, in the case of carbonation, it distinguishes the risk as a function of the water saturation. In the case of chloride attack, the main distinction is related to the possible chloride level, but chloride penetration depends on the degree of concrete saturation as well. In cases of other deterioration mechanisms as sulphate, or frost attack, or alkali-aggregate reaction, they also need a certain level of moisture to develop. Then, the concrete water content is the main factor for accelerating the deterioration processes, for steel corrosion as for concrete deterioration. That is, the degree of water saturation [2,3] or better named "water retention curve" is the controlling parameter for any prediction of the impact of climate in the concrete durability.

At present, such relationship has not been established because the difficulty to account for the water retained into the concrete, It can be measured: a) or by weighing (before and after a certain weather event), weight not feasible in a large structure or b) can be indirectly measured through the changes in concrete resistivity, but previous calibration is needed on the relation of the resistivity of a particular concrete and its water retained curve. Without the weight data it is not possible to predict the relation between the climatic events and the level of concrete water saturation. This was the main aim of a work undertaken around 20 years ago [2,3] planned to collect data on the several corrosion parameters as a function of the external climate.

In spite of the scarce data on weight variation with climatic events, there are an increasing number of studies claiming to predict the impact of the climate on concrete durability [4-11], based only in the increase in temperature and if this increase will accelerate the deterioration processes, or by considering only the external RH. It is of particular concern some reports [7,8] with these wrong assumptions. These studies are based on theoretical models not long term calibrated and with arbitrary or assumed input parameters. In the work mentioned [2,3] was noticed that an increase of temperature may lead through water evaporation into less internal humidity, in addition to emphasize that internal RH and external ones may significantly differ. These counter effects with the increase in temperature, were not considered in [4-10] calculations.

The water saturation in a concrete exposed to the atmosphere and rain after the period of drying after curing is the result of reaching an equilibrium with its surroundings, that depends on temperature, relative humidity, but mainly on the rain/snow regimes [2,3], and also on the possible use of deicing salts, that are hygroscopic. At present there is not a mathematical function linking the external climate parameters with the concrete water content (water retention curve) and therefore, the prediction of any climatic change is unfeasible.

In the particular case of carbonation, the process is dependent on the internal relative humidity (RH), presenting a maximum carbonation rate in intermediate values (around 60%), below or above which, the rate of carbonation decreases significantly. However, the internal RH is different than from the external one, sometimes is the double [2,3] because of the temperature and hysteresis effects. The predictions based on the external RH will lead to fully erroneous conclusions.

As an example of the complexity of the interaction of climatic events and the concrete [12], when it rains concrete absorbing water during the raining period depends on previous concrete internal relative humidity and on the temperature. Of the water absorbed, a part will evaporate depending on the external relative humidity and on the temperature, that may be different than during the rains. Absorption of water and evaporation cycle has hysteresis because the different speed in absorption-evaporation, which makes multiparametric the dependence with the climate of the annual water retention curve in a particular concrete. The water retention curve depends certainly on the temperature, but in a complex manner and then, the possible mathematical expression relating external climate and internal water retention also is complex and needs careful consideration of all the processes involved.

Works were undertaken around 35 years ago [2,3] advancing the understanding of the complex relation between environment and local climate by exposing concrete specimens outdoors and measuring the climatic events simultaneously with specimen weight and the corrosion parameters. In this paper results are given that were results collected in the specimens during more than 23 years. This long period already serves to deduce some general trends. Results of a carbonated specimens that serves to illustrate the general trends are shown for the whole testing period, and comparison between different specimens, in different exposure conditions, is made for a shorter period.

2. EXPERIMENTAL PROCEDURES

Specimens tested were of cylindrical shape (Figure 1) [2,3] with an embedded central bar. Their size is of 7.5cm x 15cm that tries to reproduce a cover depth of around 3 cm thick, not to low and not too high for having an averaged value of the possible hysteresis in the response to the weather change.

They were fabricated with ordinary portland cement in the proportions shown in Table 1. The Table also indicates the exposure conditions of each specimen from 1999 when they were 5 years old.

After their manufacturing the specimens were cured during 3 days under water and later, they were further dried until 28 days. Those containing chlorides added in the mix were introduced in a chamber at fixed RH/T regimes, while those non containing chlorides were carbonated at 100% CO_2 concentration until the weight was constant. When these specimens were fully carbonated, they were also introduced in chambers with fixed RH/T until they were around 5 years old (see Table 2).

On the humidity/temperature regimes that the specimens were submitted to, they are summarized in Table 2. The first years they were submitted to several laboratory conditions at fixed temperatures, T, and relative humidity, RH

TABLE 1.
Mix proportions, label, porosity (after 28 days of curing) and exposure conditions of the specimens considered in present paper.

Mix proportions	*label*	*w/c ratio*	*Porosity (% volume)*	*Preliminary Condition*	*Exposure condition after 5 years old*
350kg cement/m³	No. 2	0.5	5.7	carbonated	Exposed to rain
350kg cement/m³	No. 4	0.5	5.29	carbonated	Protected from rain
250kg cement/m³	No.13	0.5	7.6	carbonated	Exposed to rain
300 kg cement	No.23	0.6	12.44	3% $CaCL_2$ in the mixing	Exposed to rain

TABLE 2.
Regimes of humidity/ temperature

Time	28 days	Until 60 days life	Until almost 5 years life	Until almost 7 years life	From January1999 Until the end of the test
Action	Fabrication and curing	Carbonated: drying and carbonation Chlorides: exposure to fixed humidity and T chambers	Fixed RH/T in chambers	Outdoor exposure combined with several artificial wet-dry cycles	Outdoor exposure in two different places more or less exposed to rain

a) Aspect of the specimen.

b) Weighing.

c) Pluviometer.

d) Counter-electrode and sponge.

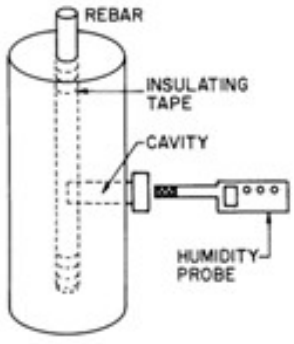

e) scheme of the specimen and of the hole.

f) Probe measuring internal RH and T.

Figure 1. Several features of the cylindrical specimens used for the testing.

until they were 5 years old. After this period, some of the specimens were exposed outdoors to natural atmosphere in Madrid-Spain. Madrid has a climate with relatively well marked seasons. It has a dry atmosphere which reaches values between 10-30% RH-IN during the summer when it seldom rains. Autumn and spring may be relatively mild (average temperatures of 14-15°C and average RH between 60-65%). There are intermittent rain periods during the year, with an average precipitation of around 420 mm/year (Figure 1c).

The weather conditions near the exposure site of the specimens were monitored by means of the same Vaisala hygrometric probe (RH and T) (Figure 1e and 1f) used for measu-

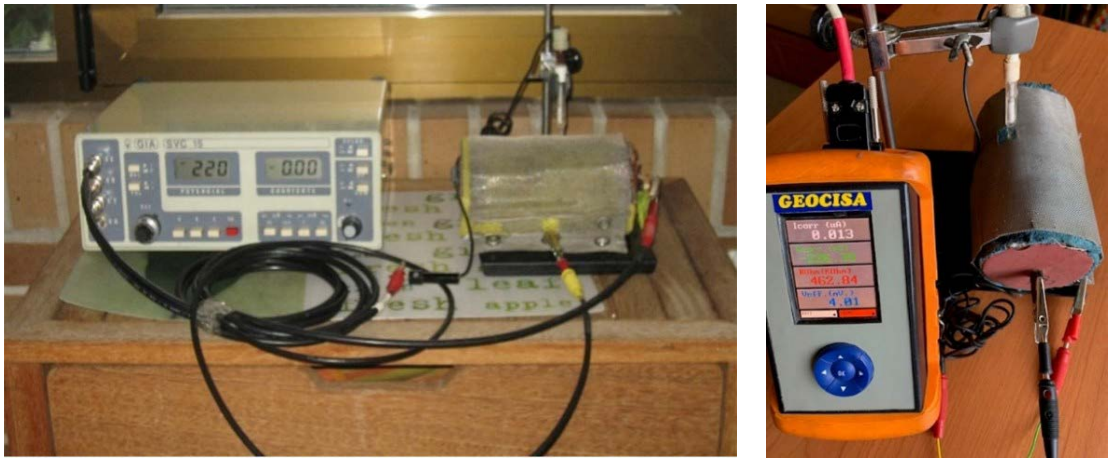

Figure 2. Left: Hand-made porTable potentiostat used during the first 20 years of testing period and specimen with the reference, counter and the plug to the bar as working electrode. Right: GECOR 10 corrosion-rate meter used in the most recent period.

ring the internal RH. For these conditions inside the concrete, the probe was introduced in the cavity shown in Figure 1e for a certain time [13]. This cavity was made by removing the concrete and inserting a metallic tube of the depth reaching the bar position but without metallic contact to it and having a plug. Following (13) this creates a small chamber whose air is in equilibrium to the internal concrete moisture content and that was assumed to represent the RH/T-INT. Rainfalls were measured through a simple pluviometer (Figure 1c).

To monitor the water content of the concretes, the specimens were weighed, as shown in Figure 1b, each time the corrosion parameters were measured. The water volumetric fraction is calculated from the weight taking as « dry » value obtained after the long dry period of Madrid summer (from July to September), which usually induced RH-INT of around 30%. The degree of saturation is calculated with respect to the total empty porosity, that was measured by Mercury porosimetry after 28 days wet curing.

2.1. Corrosion techniques

The corrosion parameters measured were:

- the corrosion potential (E_{corr}), using as reference a saturated *Ag/AgCl* electrode
- the corrosion rate (I_{corr}) using the Polarization Resistance (R_p) method. The equation for calculating the corrosion current was [2,3,14]:

$$I_{corr} = \left(\frac{\mu A}{cm^2}\right) = \frac{26}{\left(\frac{\Delta E}{\Delta I}\right) = \left(\frac{\Delta E}{\Delta I}\right)_{exp} - R_{oh}} \quad (1)$$

- Where the R_{oh} is the ohmic drop obtained in the recording of the current along testing time, that has to be discounted (as indicated in the denominator of equation (1) from the total value named "exp".
- the resistivity (ρ) is obtained from the ohmic drop R_{oh}, directly given by the corrosion rate meter, which was a hand-made portable potentiostat (Figure 2-left) and more recently through the GECOR10 (Figure 2-right). Figure 2 shows the specimen as well surrounded by the counter electrode in horizontal position to place the reference electrode in a small hole of the counter-electrode having a wet sponge (Figure 1d) in between the specimen and this counter-electrode. To obtain the resistivity from the ohmic drop given by the potentiostat a "geometrical factor" was applied (15).

The basis of the polarization resistance technique to measure the corrosion rate parameters are given in a Rilem Recommendation [14]. The calculation of the penetration depth (P_{corr}) is made through the integration of the evolution of the instantaneous corrosion rate with the time as also explained in this Recommendation.

$$P_{corr} = 11.6 \cdot \int_0^t I_{corr}\ (t)[dt \quad (2)$$

3. RESULTS

As a general illustration, first it will be given (Figure 3) the several parameters measured during the whole life of specimen no. 2 (see Table 1-350kg/m³ of cement and carbonated) while later, a particular period for 4 years was selected to illustrate more in detail the performance observed. This period of four years was selected to have a balanced number of data, because as being the measurements not from sensors, but from individual measurements, their representativeness depends on their periodicity or on whether the measurement is made during the day or the night. A lot of care has been taken when analysing the data to avoid bias if the regime of measurements is irregular.

3.1. Specimen carbonated with 350 kg/m³ cement during the whole testing period of 23 years

3.1.1. Weight evolution

In Figure 3 is shown the evolution of the weight of the specimen no.2. Cycling following the wet-dry seasonal and

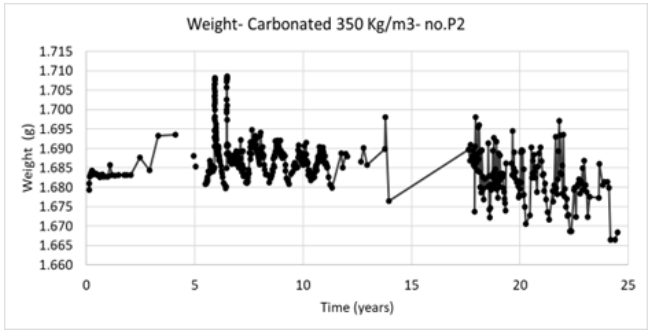

a) Weight evolution

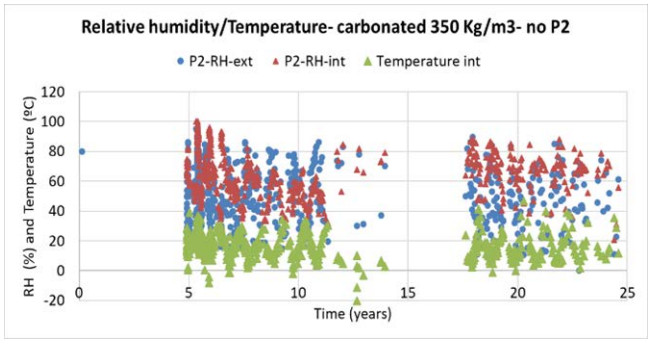

b) Relative humidity (external and internal) and internal temperature

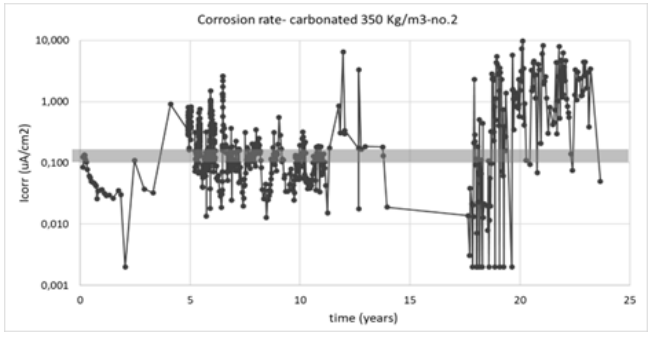

c) Corrosion rate

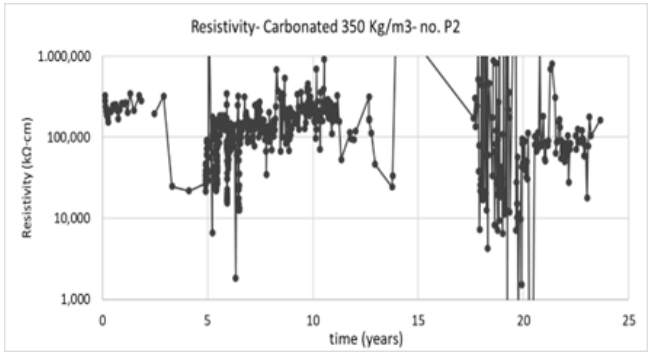

d) Resistivity

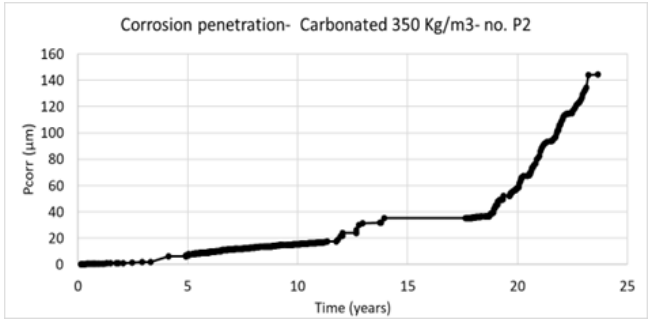

e) Corrosion penetration (accumulated corrosion)

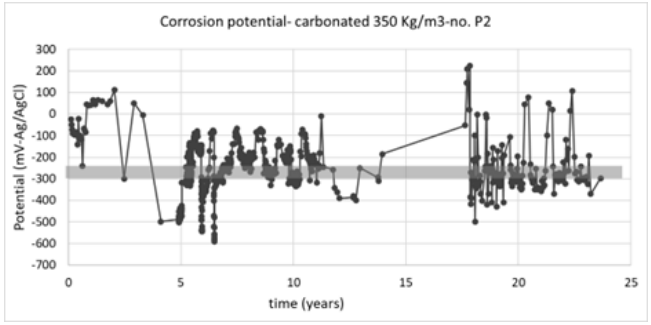

f) Corrosion potential

Figure 3. Climate and corrosion parameters in specimen no.2 (350 kg/m³ cement and carbonated).

daily periods are recorded. As the weight was started to be measured after the accelerated carbonation, the increase at the beginning was not due to the carbonation, but to the adaptation to reach moisture equilibrium with the particular chamber where the specimen was held until it was almost 5 years old (chamber at 20ºC and 80% RH in this case). After 5 years the specimen was removed from the chamber and placed outdoors and simultaneously tested by some artificial events to simulate "raining" (submerging the specimen under water). These immersion tests are noticed in the graph by a sharp increase in weight, followed by drying at the normal atmosphere. These cycles were made to understand the wetting and drying performance when rainfall is produced.

After being around 7 years old, the specimen was maintained outdoors for the rest of the testing without any perturbation from artificial wet-dry tests. The period between 7 to11 years life will be later illustrated in more detail. In the period of being around 14 to 17 years old the specimens were not measured, to retake the measurements until they were 23 years old.

Although from the beginning it was noticed a decrease in averaged weight with the time, it is more significant during this last period (17 to 23 years) that the weight evolves to be smaller than the original one (just after the accelerated carbonation). That is, it seems that the aging provokes a weight loss (attributed to the evaporation of the combined water likely because the increasing of the polymerization of the C-S-H) due to the evolution of hydration and the long periods of drying in Madrid summers, with increasing longer periods at high temperatures. It can be summarized that a weight of reference does not exist, because it may decrease with time. This evidence prevents a precise calculation of

the saturation degree (referred to the actual porosity that evolves) making more feasible to express the retained water content as "volumetric fraction", because the specimen volume remains, while the porosity evolves because of the aging effect.

3.1.2. RH/T evolution

It is shown in Figure 3b. These parameters were starting to be systematically recorded after 5 years of life with the period 14-17 years without records. As general feature there are cycles that follow the seasonal and the daily RH/T evolution simultaneously to the rain events. The RH inside the concrete is always higher than the external one in this specimen which is not protected from rain. The temperature inside and outside was very similar and that is why only the internal one is shown in the graph. This similarity was attributed to the metallic tube used to insert the RH/T probe that would thermically connect the exterior with the interior of the specimen.

There is a certain increase with time of the annually averaged temperature, but a noticeable increase cannot be concluded. The changes of RH also are similar all around the 23 years of testing (1992-2015).

3.1.3. Corrosion parameters

There are shown in Figure 3c (corrosion rate, I_{cor}), 3d (resistivity, ρ), 3e (corrosion penetration, P_{corr}) and 3f (corrosion potential. E_{corr}).

The corrosion rate (Figure 3c) after the initial carbonation was relatively low, because the specimens were in a chamber at 20°C and 80% RH, with then insufficient humidity to show active corrosion. When after 5 years, the specimen was exposed to the atmosphere and submitted to artificial wet-dry cycles, the corrosion rate increased following the natural and artificial changes of moisture, The maximum values were relatively high, above 5 µA/cm² [14]. In the last years of testing the oscillations were very significant following the moist periods, with values until around 10 µA/cm².

The evolution of the resistivity (Figure 3d) is completely parallel to that of the corrosion rate, but opposite: the corrosion rate decreases when the resistivity increases. There is a slight decrease from the initial values after carbonation to the last testing period, but it can be concluded that the average value is around 110 kΩ·cm with not high scatter.

The corrosion potential (Figure 3f) again shows a parallel, but opposite trend to the corrosion rate, with average values around -250-300 mV (*Ag/AgCl*). The most negative values reached -600 mV and the most positive were around +200 mV. Wide range typical of a carbonated concrete.

Finally, in Figure 3e gives values for Pcorr values which are the integration of the curve Icorr-time at each age (14). The trend is very illustrative of the two periods of conservation regimes: a first one inside a chamber with 80% RH and a low corrosion rate and a second stage at the atmosphere with much higher mean annual value of the Icorr. In this Figure, it is important to notice that not having data between 14 and 17 years the total corrosion penetration (140 µm) is smaller than the real value, because it was assumed that the corrosion rate in that period is small (0.02 µA/cm²) while the corrosion attack did not stop, but continue increasing.

3.2. Closer analysis of the climate effects on the period 7 to 11 years

The period between almost 7 to11 years is taken for a closer analysis on the detailed evolution of the corrosion parameters with respect to the evolution of the climate. First, we will comment on the climate evolution, then that of the weight and finally that of the corrosion parameters.

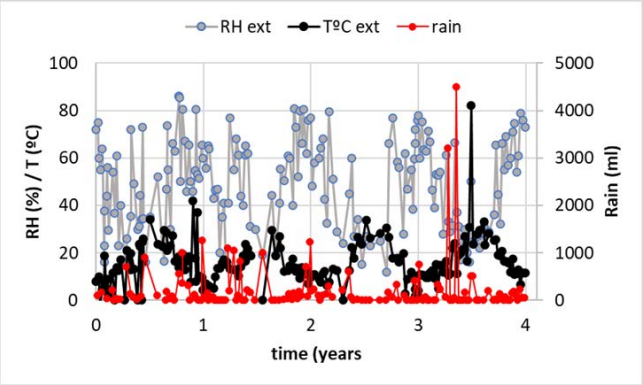

Figure 4. Evolution of weather parameters (RH-EXT, T-EXT and rain events) (the time axis has been started at 0 but the real time life was 4.8 years as in the rest of the Figures.)

Figure 4 depicts the evolution of the climatic (named external) parameters (T, RH-EXT and rainfall) showing the seasonal periods with the minimum values of RH-EXT when the temperature is maximum and vice versa. This record shows that the rain events have a transitory impact at short term by a sudden increase in the values of RH in the atmosphere, that later takes certain time to recover the average values. That is, the RH-EXT is temporarily increased during the rain events, introducing a bias in the RH-EXT. This disturbance by the rain appearance prevents to model a continuous evolution of the external climatic parameters, as the rainfalls are unexpected in intensity and duration. Several different alternative scenarios with respect to the duration and intensity of the rain are feasible but this complicates the detailed modelling very much.

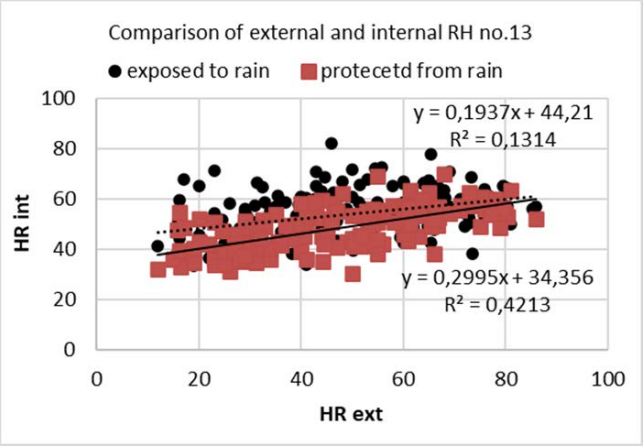

Figure 5. Comparison of RH-EXT and RH-INT of two twin specimens, one exposed to rain and the other sheltered from rain.

To illustrate better the effect of rain, Figure 5 shows the relation between RH-EXT and RH-IN in the case of two twin specimens, but one exposed and the other protected from rain. Not only the RH -IN is always higher than the RH-EXT, but that exposed to rain (black points) reaches higher RH-IN than the protected one (red colours) although with numerous days having similar values. However, given that the amount of retained water is very different in both, as shown in Figure 6, it can be deduced that RH is not a good indicator of the amount of water in a concrete exposed outdoors.

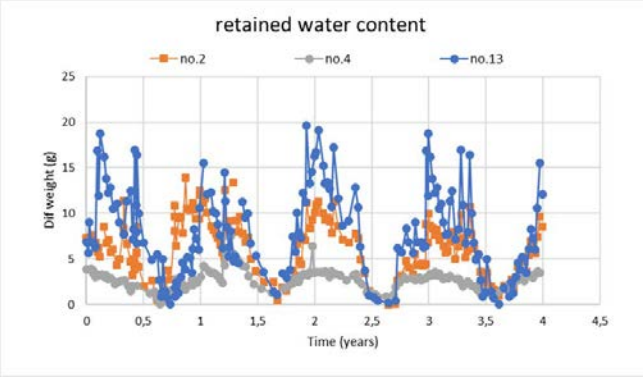

Figure 6. Evolution of retained water content of the specimens.

With respect to the weight evolution, Figure 6 depicts the change of volumetric fraction (weight divided by the volume of the specimen) of the specimens listed in Table 1 (three carbonated and one with chlorides in the mixing water) during the same period (6.8 to 10.8 years). The specimens submitted to rain, although present the same trend, they retain different amount of water, fact that can be explained by the different porosities and shape of their pore size distribution. The specimen sheltered from rain (in grey in the Figure) retains much less water.

Figure 7 shows the relation between the Fv and the internal RH, indicating the dependence but also showing how the same internal RH-INT is the consequence of very different water contents. The scatter is very high and the regression coefficients relatively low.

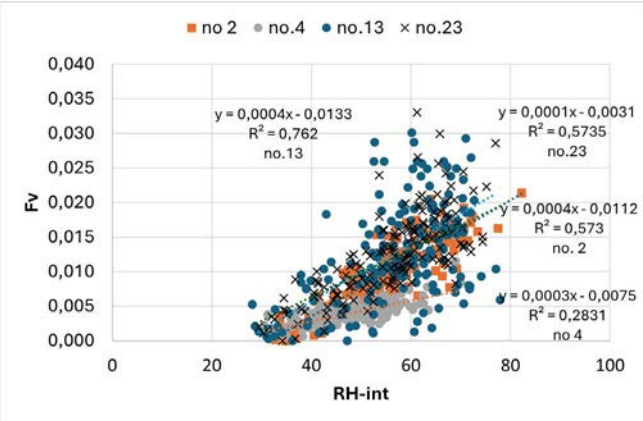

Figure 7. Relation between internal RH and volumetric fraction

Figure 8 shows the evolution of resistivity with time for the three specimens showing that they are different, mainly between being or not exposed to rain. Thus, the lowest values are recorded in the specimen no.13 having the lowest cement content and exposed to the rain. The specimen 4 has been always out of exposition to the rain and shows the highest values because it is drier and has never been wet after curing. The specimen number 2 is twin with the no.4 but shows resistivities similar to the specimen no.13 despite its higher cement content, but with much less difference between wet and dry periods.

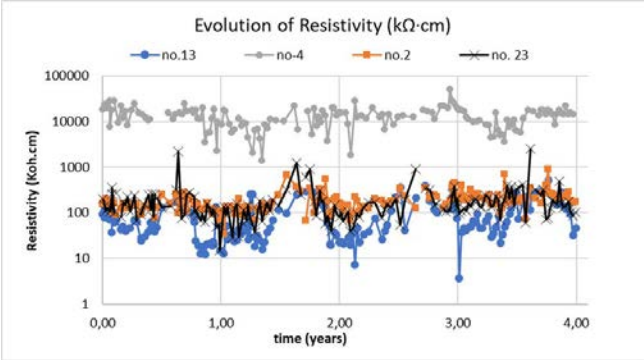

Figure 8. Evolution of Resistivity during the four years period.

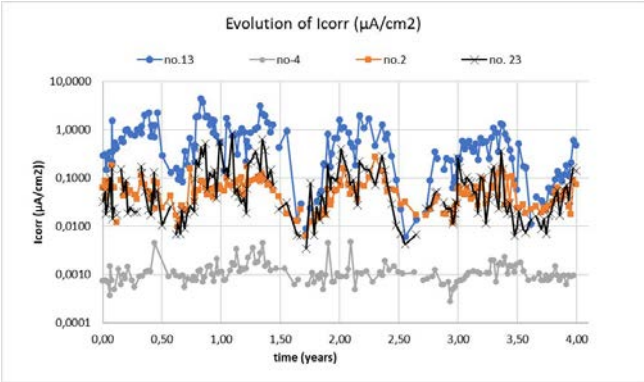

Figure 9. Evolution of corrosion current during the four years period.

The corrosion currents (Icorr) in Figure 9 shows the low values of the specimen protected from rain (average value of 0.001 µA/cm²) and the evolution with the seasonal events of those exposed to rain. The specimen showing the highest values is that with the lowest cement content carbonated (no 13 in the Figure), while that having 3% of chlorides in the mixing water (no.23 in the Figure and trend in black) does not show so high values. This is an important aspect to be emphasized as it is thought that the chloride contamination induces always higher values of corrosion rate than carbonated concrete, while here the results show the opposite (because the resistivity is higher in the chloride contaminated one as shown later). Then, the corrosion rates values would depend on the particular case (particular resistivity) and on the chloride content, being able to be smaller or higher than the carbonated condition.

4. DISCUSSION

As background, it is important to insist that the RH is the water vapour in the air, and then, water in gaseous phase. A vapour

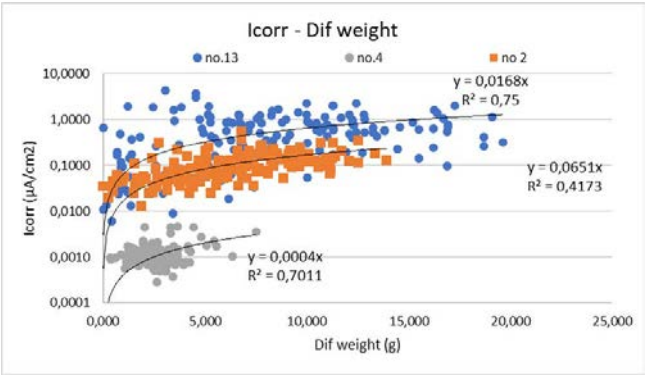

Figure 10. Relation between weight difference (retained water content) and corrosion current.

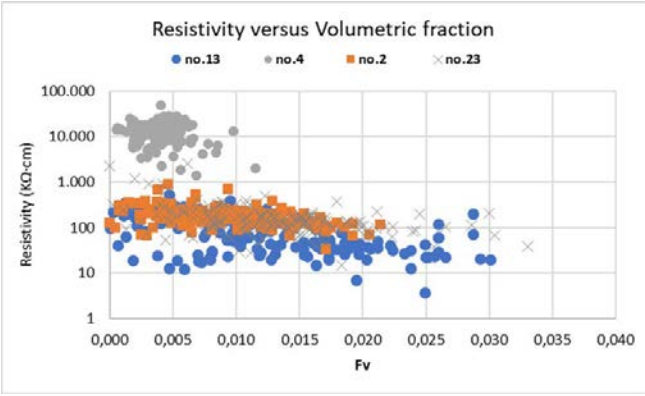

Figure 11. Resistivity of the three carbonated specimens as a function of the volumetric fraction

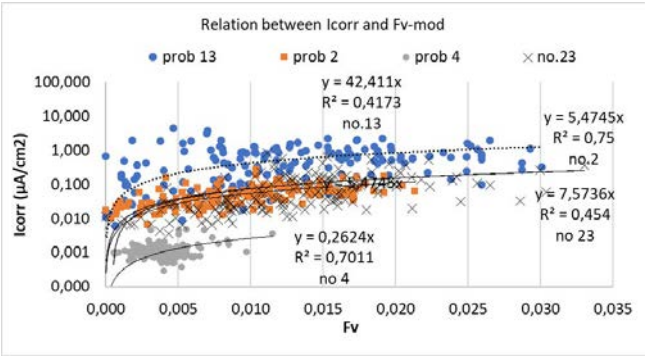

Figure12. Corrosion rate of three carbonated specimens as a function of the volumetric fraction.

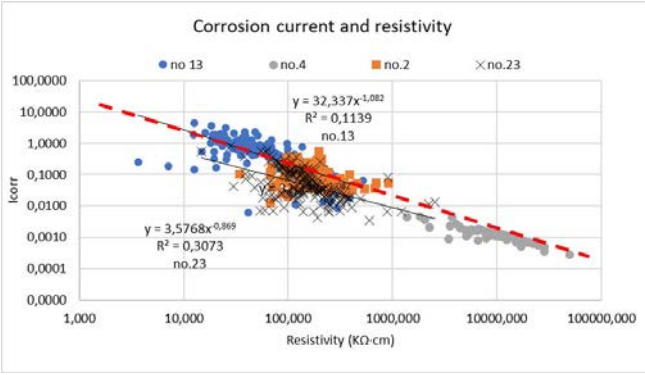

Figure 13. Corrosion rate as a function of resistivity of the four specimens. All the results fit with scatter but showing the trend of equation (3) [16].

does not provoke corrosion unless it condensates as water drops (liquid water or retained water). This is a usually forgotten aspect that makes many tests non-applicable to real concrete conditions when they are based on the RH value. The corrosion rate has to be related to the water content (saturation degree or volumetric fraction) and not to the RH, because this one is not univocally related to the water content when the temperature is not constant as is the case of natural exposure.

That is, the RH indicates the amount of water vapour in a cubic meter at a certain temperature, and that is why it is named "relative" and therefore, the total amount of vapour in the air (absolute humidity) may not change when the RH changes, because the RH is relative to the temperature. Also it is not related to the water content as for the same RH it might be very different water contents. This is because the system is continuously out of equilibrium due to the continuous evolution of the temperature and therefore the law of Kelvin-Laplace on the maximum pore radius filled with water at a certain RH, or Arrhenius law for changes with temperature, cannot be applied without simultaneous application of the corresponding kinetic laws, because the changes induced are not instantaneous.

An additional principle that is necessary to stress on the water exchange between the concrete and the atmosphere is the reason for the different F_v's when the rainfall on the specimens is the same. The F_v and the internal RH are a consequence of two different aspects: one is the inside and outside equilibrium of the water vapour (RH-INT) and of the capillarity produced when it is raining. Rain entries by capillarity into concrete and the rate of absorption followed by desorption is another key feature for the resulting F_v. Additionally, the amount of water retained by capillarity after a rain event depends on the temperature and the wind velocity which affects the evaporation rate. In summary, there are two fluids: the water vapour and the liquid water. Their exchanges follow different mechanisms which are dependent as well on the rates (kinetics) and critically, on the temperature.

Trying to understand the complex influence of the weather in the corrosion performance of the reinforcements, neglecting the external RH/T as the controlling parameter of the corrosion rate, analysis should progress on finding the acting controlling variable of the corrosion evolution. Figure 10 shows the relation between the weight difference and the corrosion current allowing to deduce that there is a dependence, but different for each specimen. Thus, the corrosion increases when the retained water is higher, but how high is the corrosion current varies in each specimen, again indicating the importance on the concrete porosity, and of the presence of chlorides with respect to the carbonation. In present specimens, the carbonated one with the lower amount of cement is that showing the highest corrosion currents, while, as mentioned, that having chloride in the mixing water presents in this case the lowest corrosion currents of the three exposed to rain.

The relation between the volumetric fraction and the resistivity is given in Figure 11, indicating again that there is a dependence but not with a unique relation.

The same happens when relating the corrosion rate to the F_v. (Figure 12). There is a dependency, but again not finding a unique relation to F_v., enabling to deduce that the microstructure of the concrete is as important as the climate parameters when trying to generalize the relation.

Other relationships of the corrosion current with the degree of saturation or the water volumetric fraction give similar trends, indicating the lack of a unique relation between corrosion current and water content. However, when plotting the corrosion current with respect to the resistivity, that unique relation appears as shown in Figure 13. Now it is possible to understand why the specimen with chlorides (no. 23) shows lower corrosion rates than the low quality carbonated one (no.13). It is because of the resistivity is higher in the chloride contaminated specimen. When they had similar values because of the degree of saturation, the corrosion rates may be similar.

The graph corrosion current-resistivity shows the trend (in red in the Figure) already identified [16] with a slope close to -1 and a value of resistivity of around 260 kΩ·cm for the corrosion current of 0.1 μA/cm² (boundary between active and negligeable corrosion). This trend has been confirmed by other researchers [17]. Then, the law behind the plot shown in expression (3) can be accepted as generic and universally applicable to concrete.

$$I_{corr} = \left(\frac{\mu A}{cm^2}\right) = \frac{26\ (K\Omega\cdot cm)}{\rho} \qquad (3)$$

It means that the corrosion rate evolves in parallel (mirror) to the resistivity which is its controlling parameter. However, to generalize the expression regarding the climate impact, as the resistivity of each specimen is different irrespective of the temperature (Figure 8), because it depends on the porosity of the specimens, it indicates the need to introduce a concrete microstructural parameter in any expression trying to relate the weather with the degree of water saturation or with the resistivity. Such function should be of the type indicated in expression (4) obtained from the [3] adding some factors, as indicated below.

$$I_{corr} = \left(\frac{\mu A}{cm^2}\right) = f_{ext}\cdot f_{un}\cdot f_p\cdot \frac{26\ (K\Omega\cdot cm)}{\rho} \qquad (4)$$

f_{ext} (factor modelling external weather)
f_{un} (factor of conversion of units to internal conditions)
f_p (factor modelling porous microstructure)

That is, for linking this unique relation [3] to the weather parameters it is necessary, apart from the external characterization, to link the resistivity to the concrete porosity (pore microstructure). It is necessary to formulate and find the mathematical expressions of the different factors. Without them any prediction will be purely theoretical. Unfortunately, we still lack of them. Any attempt to base the prediction of climatic change impact only in the external temperature or the RH-EXT alone will lead to erroneous conclusions. The still lack of full understanding of all interrelations between all involved climatic parameters and of the kinetics of the processes happening calls for rigorous collection of data on water retaining amounts in real condition, together with resistivity and corrosion current values.

4.1. Use of annual averaged values

The daily and seasonal evolution of the parameters introduces the difficulty of the short-term hysteresis on the evolution of all parameters, as soon as the temperature varies or the rainfall is produced. Next it is represented the annual average values that in principle seem are promising possibilities for future prediction.

The relation of the averaged corrosion rate with the average temperature is given in Figure 14. The average temperatures are very close. In spite of the few values, the regression coefficients are very poor indicating the lack of any correlation.

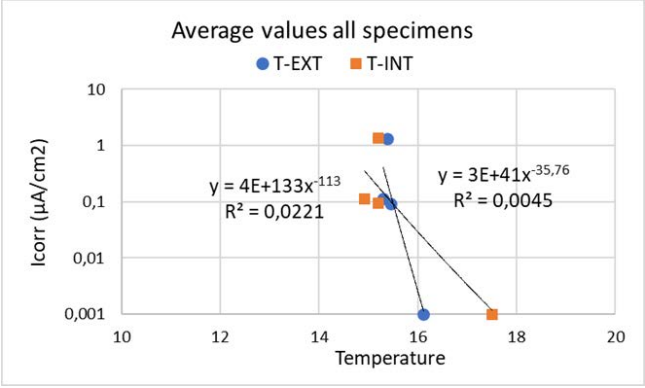

Figure 14. Relation of the averaged value of the corrosion rate of the four specimens with the temperature (T-EXT and T-INT).

Figure 15 shows the relation between external and internal RH with the resistivity and corrosion rate and Figure 16 shows the same but from the saturation degree (Sw). They conclusively indicate that, the external RH-EXT is not the correct parameter, showing a very high regression coefficient however with the RH-INT and the Sw, although they are few points. Why as mentioned, the RH-INT present a high regression coefficient in spite it represents the gas phase and not the liquid phase? Likely because it is an averaged value and not an individual one. The averaging would smooth the transitory evolution and then seem to reflect an equilibrium to the liquid content (degree of saturation)

A very high regression coefficient is also found if the parameter is the volumetric fraction as given in Figure 17, although with the corrosion current is much less precise, because there are aspects, as the chloride content or the previous amount of rust, that might influence the level of corrosion rate. These additional factors need to be studied in the future.

These results are very promising, although they are only four specimens (although in different conditions) are presented during only a period of 4 years. They indicate a strong correlation with the water retained inside the concrete. However, it has not been possible until now to find the univocal and significative function relating the external weather, including rain events, with the water retained in the concrete (vo-

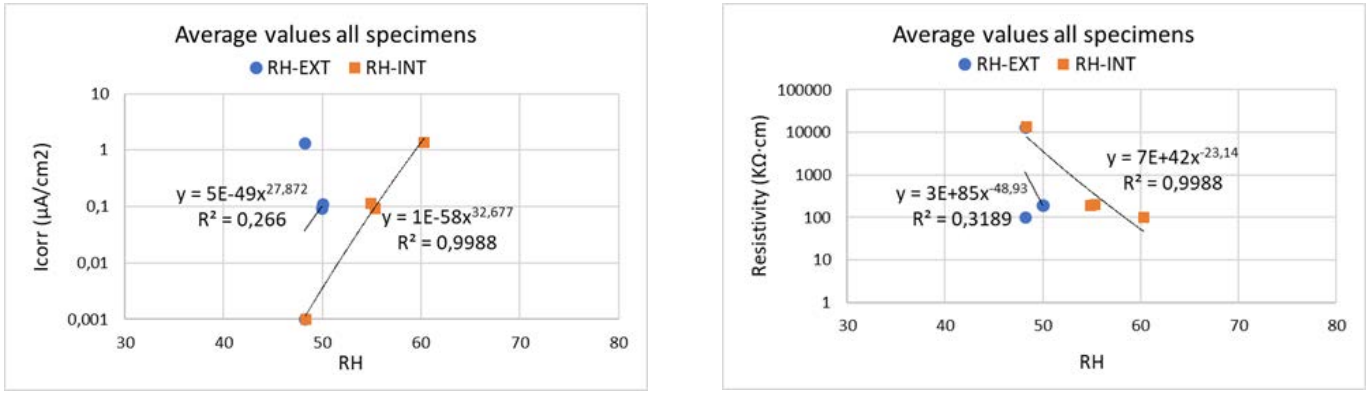

Figure 15. Relation of the averaged value of the corrosion rate and resistivity of the four specimens with the RH-EXT and RH_INT.

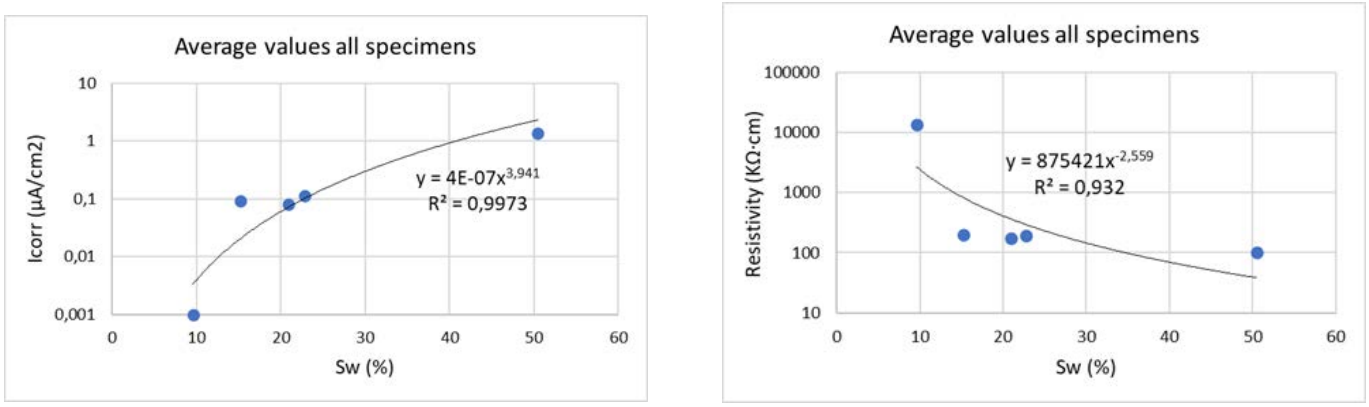

Figure 16. Relation of the averaged value of the corrosion rate and resistivity of the four specimens with the saturation degree (S_w).

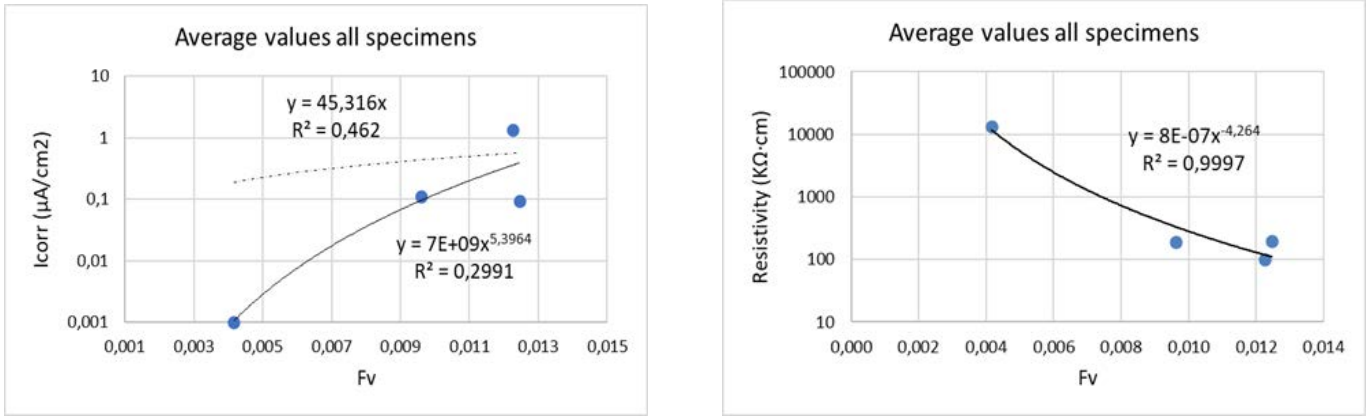

Figure 17. Relation of the averaged value of the corrosion rate and resistivity of the four specimens with the water volumetric fraction (F_v)

lumetric fraction) or the resistivity or the corrosion rate. To establish such function will be the next step in the research, extending the study to the whole period and to concrete elements other than these specimens.

Additionally, present results enable to state the incorrect procedure to base the prediction on the external, either temperature or RH, as has been assumed by all the studies claiming to predict the impact of the climatic change published until present [4-11]. It is particularly important a rectification of these conclusions, because until we have not the function relating univocally the external weather with the corrosion rate, it will not be possible to make a prediction with a minimum of precision. This conclusion applies as well to the prediction of the rate of carbonation, because the carbonation in itself is not damaging (even can be positive by fixing carbon dioxide). The only deleterious problem is the reinforcement corrosion.

5. CONCLUSIONS

The conclusions that can be reached from present results are:

1) The results do not allow yet to derive a general conclusion on the relation between external climatic parameters and the internal concrete conditions, because being exposed to the same weather regime, the specimens have retained different amount of water, attributed to their different pore size distribution (porous microstructure) and in consequence they show different resistivity and corrosion rate. The knowledge of the pore size distribution would help to have closer relations between climatic parameters and evolution of concrete water content, although the difficulty would remain as the pore size evolves as well with time because of hydration and carbonation.
2) There is not a unique relation between corrosion current and retained water (volumetric fraction), but it was found with the resistivity, confirming previous works. However, when averaging, not only the resistivity but the RH-INT, degree of water saturation and volumetric fraction, show the feasibility to deduce a strong relation to the corrosion rate.
3) Regarding the full expression to predict the impact in the reinforcement corrosion, in addition to find the external-internal impact, it seems critical the need to introduce a microstructural parameter (named here fp) into the possible function as indicated by (equation (4)):

$$I_{corr} = \left(\frac{\mu A}{cm^2}\right) = f_{ext} \cdot f_{un} \cdot f_p \cdot \frac{26\ (\mathrm{K\Omega \cdot cm})}{\rho} \qquad (4)$$

f_{ext} (factor modelling external weather)
f_{un} (factor of conversion of units to internal conditions)
f_p (factor modelling porous microstructure)

The resulting internal concrete conditions will be the interrelation between the concrete porous microstructure and the weather parameters. Any prediction considering climatic change based only in the increasing of temperature or variation of atmospheric RH will lead to erroneous conclusions. We need first to know which is the impact of climate on the internal concrete moisture conditions. Only after that advance, the impact of climatic change scenarios can be addressed.

Acknowledgement

For this paper I selected one of the most challenging subjects for me. One where I have more questions. It is a tribute of recognition and admiration to the contributions to the research area and the profession of Hugo Corres and Antonio Marí. Both are examples of perseverance and aspiration to excellence, in addition to their great vocation for teaching. They are also examples of going beyond our country's borders to compete internationally. I worked on a Spanish project on Rehabilitation, being Tony one of the partners, where he demonstrated his innovative spirit. With Hugo I have worked in several subjects for the last years, especially since his presidency at *fib* where his restless spirit has driven several innovative initiatives. This contact at *fib* has allowed me to establish a very enriching professional relationship, which continues to this day. Thank you, Hugo and Toni, for your contributions.

References

[1] EN 1992-1-1: (2024) Design of concrete structures. General rules and rules for buildings CEN Eurocode 2. Brussels.

[2] Andrade C., Sarría J., Alonso C. (1999) Relative humidity in the interior of concrete exposed to natural and artificial weathering. Cement and Concrete Research 29 1249-1259.

[3] Andrade C., Alonso C., Sarría J. (2002) Corrosion rate evolution in concrete structures exposed to the atmosphere. Cement and Concrete Composites 24 55-64.

[4] Stewart, M. G., Wang, X., & Nguyen, M. N. (2012). Climate change adaptation for corrosion control of concrete infrastructure. Structural Safety, 35, 29-39.

[5] De Larrard, T., Bastidas-Arteaga, E., Duprat, F., & Schoefs, F. (2014). Effects of climate variations and global warming on the durability of RC structures subjected to carbonation. Civil Engineering and Environmental Systems, 31(2), 153-164.

[6] Tran, N. L., Phan, V. P., & Valeriy, M. (2021). Investigating the corrosion initiation process in reinforced concrete structures under the impact of climate change. Architecture and Engineering, 6(2), 37-44.

[7] European Commission, Joint Research Centre, Dimova, S., Polo López, C.S., Sousa, M.L., Rianna, G., Bastidas-Arteaga, E., Nogal, M., Gervásio, H., Martorana, E., Reder, A. and Athanasopoulou, A., (2024) Impact of climate change on the corrosion of the European reinforced concrete building stock, Dimova, S., Polo López, C.S. and Sousa, M.L. editor(s), Publications Office of the European Union, Luxembourg, https://data.europa.eu/doi/10.2760/016004, JRC137288.

[8] Sousa M.L., Dimova S., Athanasopoulou A., Rianna G., Mercogliano P., Villani V., Nogal M., Gervasio H., Neves L., Bastidas-Arteaga E., Tsionis G.. (2020) Expected implications of climate change on the corrosion of structures, EUR 30303 EN, Publications Office of the European Union, Luxembourg, ISBN 978-92-76-20782-5, doi:10.2760/05229, JRC121312.

[9] Bastidas-Arteaga E., Stewart M. G. (2015) Damage risks and economic assessment of climate adaptation strategies for design of new concrete structures subject to chloride-induced corrosion. Structural Safety 52 40–53

[10] Bastidas-Arteaga E., Rianna G., Gervasio H., Nogal M. (2022) Multi-region lifetime assessment of reinforced concrete structures subjected to carbonation and climate change. Structures 45 886–899

[11] Saha M., Eckelman M. J. (2014) Urban scale mapping of concrete degradation from projected climate change. Urban Climate 9, 101–114

[12] Andrade C. Castillo A. (2010) Water content of concrete in natural atmospheres and its impact in the corrosion parameters. International RILEM Conference on Material Science- MATSCI, Aachen-Germany. Vol II, page 43.51- Springer Edition.

[13] Parrott, L. J. (1988). Moisture profiles in drying concrete. Advances in cement research, 1(3), 164-170.Parrott, L.J., Advances in Cement Research, vol.1, no.3, July (1988).

[14] Andrade C, Alonso C, Gulikers J, Polder R, Cigna R, Vennesland Ø, Salta M, Raharinaivo A, Elsener B. (2004). Test methods for on-site corrosion rate measurement of steel reinforcement in concrete by means of the polarization resistance method. RILEM TC 154-EMC: Electrochemical Techniques for Measuring Metallic Corrosion. Recommendations. Materials & Structures 37(273): 623-643.

[15] Morris W., Moreno E.I., Sagüés A.A., (1996) Practical evaluation of resistivity of concrete in test cylinders using a Wenner array probe, Cement and Concrete Research, 26, 1779-1787.

[16] Andrade C., Fullea J., Alonso C., (2000), The use of the graph corrosion rate-resistivity in the measurement of the corrosion current- Proceedings of the International Workshop on "Measurement and interpretation of the on-site corrosion rate. MESINA- RILEM Proc. No. 18. Ed. C. Andrade, C. Alonso, J. Fullea, J. Polimon and J. Rodriguez. Rilem Publications S.A.R.L. 157-166.

[17] Morris W., Vico A., Vazquez M., de Sanchez S.R., 2002, Corrosion of reinforcing steel evaluated by means of concrete resistivity measurements. Corrosion Science vol. 44, pp.81-99.

NUEVA VERSIÓN DE SOFiSTiK DISPONIBLE

Con la versión SOFiSTiK | 2026, la compañía refuerza su apuesta por flujos de trabajo claros y eficientes para el análisis y diseño estructural.
El software está totalmente basado en BIM y permite una coordinación inteligente, tanto en proyectos de puentes como de edificación, sin comprometer la integración con interfaces bien conectadas.

El usuario sigue siendo el centro del proceso: SOFiSTiK | 2026 ofrece la flexibilidad de elegir entre distintas plataformas para el modelado BIM integrado. Los datos de planificación pueden transferirse de manera fluida y sin pérdidas dentro de un proceso BIM abierto, permitiendo su uso posterior de forma eficiente.

Las nuevas funciones en las dos áreas clave de aplicación —puentes y edificación— son amplias e innovadoras. Entre ellas se incluyen:
- Verificaciones gráficas completas para puentes mixtos acero-hormigón.
- Nuevos métodos no lineales de integración paso a paso para el análisis dinámico.
- Una experiencia de usuario modernizada para la interfaz con Rhino.

En el ámbito del diseño de edificios, SOFiSTiK | 2026 incorpora mejoras en la alineación de elementos analíticos, resultados comprobables de transferencia de cargas y verificaciones de vigas integradas en el entorno BIM.

SOFiSTiK

Disponible en **www.hormigonyacero.com**
https://doi.org/10.33586/hya.2025.4140

Numerical Simulation of Full-Scale Load Tests on 50-Year-Old PC Bridge Deck Beams Under Flexural- and Shear-Dominant Failures

Simulación numérica de ensayos de carga a escala real en vigas de tablero de puente de hormigón pretensado (PC) con 50 años de antigüedad bajo fallos dominados por flexión y por cortante.

Mattia Anghileri[a,*] **& Fabio Biondini**[a]

[a] *Department of Civil and Environmental Engineering, Politecnico di Milano*
Piazza Leonardo da Vinci 32 – 20133 Milan, Italy.

Recibido el 8 de julio de 2025; revisado el 24 de agosto de 2025, aceptado el 2 de diciembre de 2025

ABSTRACT

Computational methods and modeling criteria for life-cycle design, assessment, maintenance, and management of aging structural systems require robust calibration and validation based on data and information gathered from existing structures and experimental tests. This paper provides a contribution along these lines based on criteria, methods, and tools for computational modeling and experimental validation of nonlinear finite element analysis of reinforced concrete (RC) and prestressed concrete (PC) structures. Structural modeling was developed with RC/PC beam finite elements and bi-dimensional finite elements for plane-stress analysis, formulated in accordance with the Modified Compression Field Theory. The formulations were applied to numerical simulation of full-scale load tests on 50-year-old PC bridge deck beams under different loading conditions intended to promote flexural- or shear-dominant failures. The models were informed by the results of laboratory tests on material mechanical properties and residual prestressing stress. The comparison of numerical and experimental results of full-scale load tests allows validation of the nonlinear analysis methods and structural modeling strategies and contributes to the successful implementation in practice of life-cycle-oriented models for deteriorating RC/PC structures.

KEYWORDS: PC bridge deck beams; full-scale load tests; nonlinear finite element analysis; experimental validation.

RESUMEN

Los métodos computacionales y los criterios de modelización para el diseño, evaluación, mantenimiento y gestión a lo largo del ciclo de vida de sistemas estructurales envejecidos requieren una adecuada calibración de parámetros y la validación de los modelos a partir de datos obtenidos de estructuras existentes y de ensayos experimentales.

Este trabajo contribuye en esta línea mediante la aplicación de criterios, métodos y herramientas para la modelización computacional y la validación experimental del análisis no lineal mediante elementos finitos de estructuras de hormigón armado (HA) y hormigón pretensado (HP).

La modelización estructural se realiza empleando elementos finitos de viga para HA/HP y elementos finitos bidimensionales para análisis en estado plano de tensiones, formulados de acuerdo con la Teoría Modificada del Campo de Compresiones (Modified Compression Field Theory).

Estas formulaciones se aplican a la simulación numérica de ensayos de carga a escala real realizados sobre vigas de tablero de puente de hormigón pretensado con 50 años de servicio, sometidas a distintas condiciones de carga destinadas a provocar modos de fallo dominados por flexión o por cortante.

Los modelos se calibran a partir de los resultados de ensayos de laboratorio sobre las propiedades mecánicas de los materiales y sobre el nivel residual del esfuerzo de pretensado.

La comparación entre los resultados numéricos y experimentales obtenidos en los ensayos de carga a escala real permite validar los métodos de análisis no lineal y las estrategias de modelización estructural, contribuyendo a la implementación práctica de modelos orientados al ciclo de vida para estructuras deterioradas de hormigón armado y pretensado.

PALABRAS CLAVE: Vigas de tablero de puente de hormigón pretensado; ensayo de carga a escala real; análisis no lineal por elementos finitos; validación experimental.

* Persona de contacto / *Corresponding author*:
Correo-e / *e-mail*: mattia.anghileri@polimi.it (Mattia Anghileri)

How to cite this article: Anghileri, M., & Biondini, F. (2026). Numerical Simulation of Full-Scale Load Tests on 50-Year-Old PC Bridge Deck Beams Under Flexural- and Shear-Dominant Failures. *Hormigón y Acero*. 77(308):59-70. https://doi.org/10.33586/hya.2025.4140

1. INTRODUCTION

Bridges and infrastructure facilities are frequently exposed to aggressive environments, leading to aging and structural deterioration processes that may seriously affect their life-cycle performance and residual lifetime (Biondini & Frangopol 2016, 2019). This critical situation is reflected in the high costs involved in many countries to restore or enhance the structural capacity and functionality of existing bridges and infrastructure facilities that are currently rated as structurally deficient (ASCE 2025). Risk-based methodologies for effective bridge prioritization are therefore fundamental to support a rational allocation of resources for inspection and diagnostic activities (Biondini et al. 2022). Moreover, the urgency of this situation is emphasized by bridge failure events that occurred worldwide in recent years with alarming frequency and involving different flexural- and shear-dominant failure mechanisms. Robust and efficient life-cycle-oriented design, assessment, and maintenance methods have been established and consolidated over the past decades to address these problems. However, for a successful implementation in practice and a reliable use to inform the evolution of standards and codes, life-cycle-oriented models and methods still require robust validation and accurate calibration based on experimental tests and data gathered from existing structures. These procedures are particularly challenging for reinforced concrete (RC) and prestressed concrete (PC) structures, especially bridges, mainly due to a wide range of deterioration processes and associated uncertainties.

Considering the structural analysis methods available in the literature, life-cycle analysis is applied in practice by using a variety of tools, models, and resources, whose representativeness and accuracy require proper verification. Advanced structural modeling and nonlinear structural analysis methods are frequently indispensable tools to accurately assess the lifetime structural performance, as well as to identify damage features and investigate the attainment of multiple limit states that characterize the structural response at the material and component level, such as concrete cracking, steel yielding, and concrete crushing. Moreover, structural modeling based on finite element formulations should guarantee the versatility of the methods to account for both flexural and shear mechanisms (Vecchio & Collins 1986; Kaufmann & Marti 1998; Collins, Bentz, & Sherwood 2008; Marí et al. 2015). However, robust validation and accurate calibration of these methods are generally difficult tasks because of the limited availability of experimental data on the long-term performance of in-service structures. In fact, despite experimental tests of corroded RC/PC beam specimens have been conducted and documented in the literature, experimental campaigns on existing bridges and full-scale members removed from in-service structures are very limited. There is therefore a strong need to validate life-cycle models properly accounting for the magnitude and spatial distribution of the uncertainties associated with geometrical quantities, mechanical properties, and exposure conditions that are typical of existing structures (Anghileri & Biondini 2025b). It is also important to establish and calibrate methodologies for daily engineering practice (Messina & Proverbio 2023). In the assessment of the structural performance of existing systems, discrepancies between the specified design properties and the actual characteristics can be significant due to several factors, including aleatory uncertainties, instantaneous and/or long-term variations, design variants and human errors in the construction phase. Gathering new data from both experimental tests and inspections of existing structures is therefore essential for the successful practical implementation of life-cycle methods (Biondini & Frangopol 2018).

In this paper, computational methods for nonlinear analysis of RC/PC structures are calibrated and validated using experimental results from the BRIDGE|50 research project, which includes multiple full-scale load tests on 50-year-old PC bridge deck beams under different loading conditions (Anghileri & Biondini 2021, 2022, 2023, 2025a, 2025b). Structural modeling is developed with two approaches associated with different levels of complexity and computational cost based on RC/PC beam finite elements and bi-dimensional finite elements for plane-stress analysis accounting for material nonlinearities. The numerical analyses are calibrated by the results of experimental laboratory tests on material mechanical properties and

(a) (b)

Figure 1. PC bridge deck beams: (a) Dismantling of the grillage bridge deck beams of the 50-year-old Corso Grosseto viaduct; (b) Storage of the beams at the testing site (corrosion damage visible at the beam ends).

residual prestressing levels. The results of the experimental validation are complemented by further numerical simulations aimed at investigating the residual structural capacity of the tested PC bridge deck beams and support proper planning of the ongoing full-scale load tests.

2. EXPERIMENTAL CAMPAIGN ON 50-YEAR-OLD PC BRIDGE DECK BEAMS

2.1. BRIDGE|50 research project

The BRIDGE|50 research project was established jointly by Politecnico di Milano and Politecnico di Torino under an agreement with public authorities and private companies to conduct a wide experimental campaign investigating the residual structural performance of a 50-year-old double-deck road viaduct located in Turin, Italy (Biondini, Manto et al. 2021; Biondini, Tondolo et al. 2021). The 80-span simply supported grillage bridge deck was formed by precast PC beams, including ten inner I-beams and two lateral U-box beams, with a top cast-in-situ RC slab (Savino et al. 2021). During the demolition of the viaduct after 50 years of service, several structural members were dismantled and preserved at a testing site, including 29 PC bridge deck beams (25 I-beams and four U-box beams) and two PC pier caps (Anghileri et al. 2020).

2.2. PC bridge deck beams

The dismantled PC bridge deck beams (Figure 1) are characterized by a length of about 19.50 m and a composite cross-section made of a precast PC I-beam and a top cast-in-situ RC slab. The precast beams are prestressed with twenty 7-wire steel strands arranged straight along the longitudinal axis of the beam. The nominal diameter of the steel strands is 12.7 mm (effective area 99 mm²). Stirrups with a diameter of 8 mm and spaced at 250 mm in the inner I-shaped cross-section and 100 mm in the rectangular cross-section at the beam ends have been evaluated based on data reported in the design documentation and results of pacometer tests. Visual inspection activities conducted on the dismantled beams allowed the identification of local damage in the end regions due to corrosion, with steel mass loss and concrete spalling and delamination, attributed to the inadequacy of bridge water conveyance system and use of road salts during the bridge lifetime (Beltrami et al. 2021; Carsana et al. 2022; Carsana, Redaelli, & Biondini 2023; Carsana, Biondini, & Redaelli 2025). However, despite the long-term exposure of the PC viaduct to an urban environment, no significant corrosion of the prestressing strands was observed by visual inspection of the failure regions of the tested beams. The effects of corrosion are therefore not considered in the experimental validation presented in this paper. Moreover, inspection activities performed after the full-scale load tests allowed the identification of the reinforcing steel layout in both the precast PC beam and cast-in-situ RC slab, which was not exhaustively reported in the original design documentation.

2.3. Material characterization

The actual material mechanical properties of the PC beams have been largely investigated with both non-destructive and destructive experimental tests (Anghileri et al. 2023). The concrete compressive and tensile strength and the elastic modulus have been estimated by means of laboratory tests carried out on several cylindrical specimens extracted from the dismantled PC beams. The material properties of both reinforcing steel bars and prestressing steel strands have also been estimated with laboratory tensile strength tests. Table 1 shows the sample mean and coefficient of variation (CoV) of material mechanical properties based on the outcomes of laboratory tests. In the numerical analysis, the elastic modulus of both reinforcing and prestressing steel is assumed to be 200 GPa

TABLE 1.
PC bridge deck beams: Sample mean and coefficient of variation (CoV) of material mechanical properties based on the outcomes of laboratory tests carried out on n samples.

Material	*Material properties*	*n*	*Sample mean*	*CoV*
Precast concrete beam	Compressive concrete strength, f_c	25	32.3 MPa	0.14
	Tensile concrete strength, f_{ct}	9	3.4 MPa	0.14
	Concrete elastic modulus, E_c	8	27.3 GPa	0.08
Cast-in-situ concrete slab	Compressive concrete strength, f_c	5	21.9 MPa	0.22
	Tensile concrete strength, f_{ct}	2	21.4 MPa	0.38
Prestressing steel strands	Steel yielding strength, f_{py}	8	1522 MPa	0.05
	Steel ultimate strength, f_{pu}	8	1763 MPa	0.03
Reinforcing steel bars	Steel yielding strength, f_{sy}	10	449 MPa	0.06
	Steel ultimate strength, f_{su}	10	685 MPa	0.06

and 195 GPa, respectively. Due to its significant role in the performance assessment, the residual prestressing stress σ_p was estimated using the strand cutting method based on the measurement of the strain on a cut prestressing strand (Savino, Tondolo et al. 2023). The initial prestressing stress, net of instantaneous and estimated long-term losses, as reported in the original technical design documentation, was σ_{pd}=836 MPa. However, the assessment of the residual prestressing stress after a lifetime of 50 years, based on the strand cutting method, led to about σ_p=582 MPa. This result may be attributed to higher instantaneous and/or long-term prestressing losses, as well as steel corrosion effects. The large number of experimental outcomes also allowed a probabilistic analysis based on statistical tests and regression analysis for the random variables associated with the material mechanical properties (Anghileri & Biondini 2025b). Moreover, the role of involved uncertainties and the effects of new data obtained from experimental tests have been investigated in Anghileri & Biondini (2025a) through Bayesian model updating.

2.4. Full-scale load test setup

The residual structural capacity of the PC bridge deck beams is investigated with full-scale load tests. The PC beams were tested with a steel reaction framework (Figure 2) under simple supports with a span length of about 19.00 m and loaded up to collapse. The applied load was transferred by two transverse steel beams to the PC beam. The experimental test setup was based on several sensors, including load cells, transducers, and displacement potentiometers installed to record the applied load, bending and shear strains, strand slips, support settlements, and vertical deflection (Tondolo et al. 2021, 2022). The reaction steel frame was designed to allow for a variable distance between the applied forces and to reproduce the in-service span of the PC bridge deck beams (Savino, Quattrone et al. 2023). Multiple full-scale load tests with different values of the shear span ratio $\alpha=a/l$ (i.e., a=shear span; l=half beam span) were conducted to study both bending and shear failures (Tondolo et al. 2025). In this paper, the experimental results of tests associated with shear span ratio $\alpha\approx$1.00, 0.68, 0.47, and 0.32 are considered to investigate the flexural and shear behavior of the PC beams.

3. FINITE ELEMENT MODELING OF PC BRIDGE DECK BEAMS

3.1. Finite element modeling of concrete structures

Finite element formulations for the nonlinear analysis of RC/PC structures have been proposed in the literature characterized by distinctive features such as the finite element discretization level, simplicity and robustness of the formulation, capability of properly describing the real structural behavior, accuracy of the solution process, and computational cost (Malerba 1998). The RC/PC beam finite element (BFE) formulation provides an effective trade-off among the abovementioned factors assuming the linearity of the cross-sectional strain field and accounting for the nonlinear constitutive laws of the materials, i.e., concrete, reinforcing steel, and prestressing steel. The BFE formulation neglects shear failures and bond-slip of steel.

To account for shear effects and local stress-diffusion phenomena, the Modified Compression Field Theory (MCFT) is adopted in this paper for the nonlinear plane-stress analysis of RC/PC structures. The MCFT is formulated based on a smeared rotating crack approach (i.e., cracks change orientation according to the direction of principal strains) and considers the cracked RC medium as an orthotropic material with its own constitutive laws. The critical crack direction is assumed to be normal to the principal tensile strain direction. Equilibrium, compatibility, and constitutive laws are formulated in terms of average stresses and average strains, and the directions of principal stresses and strains are considered coincident (Vecchio & Collins 1986). Among the various formulations proposed in the literature to account for shear effects of RC/PC structures, the MCFT was selected based on multiple factors, including the robustness of the formulation and the accuracy of the solution process (Vecchio 2001). The use of a specific type of finite element modeling approach (BFE or MCFT) should be guided by the expected governing behavior and failure mechanism. While both BFE- and MCFT-based models generally provide accurate results under flexure-dominated failures, significant deviations may arise when the structural response is governed by shear-dominat-

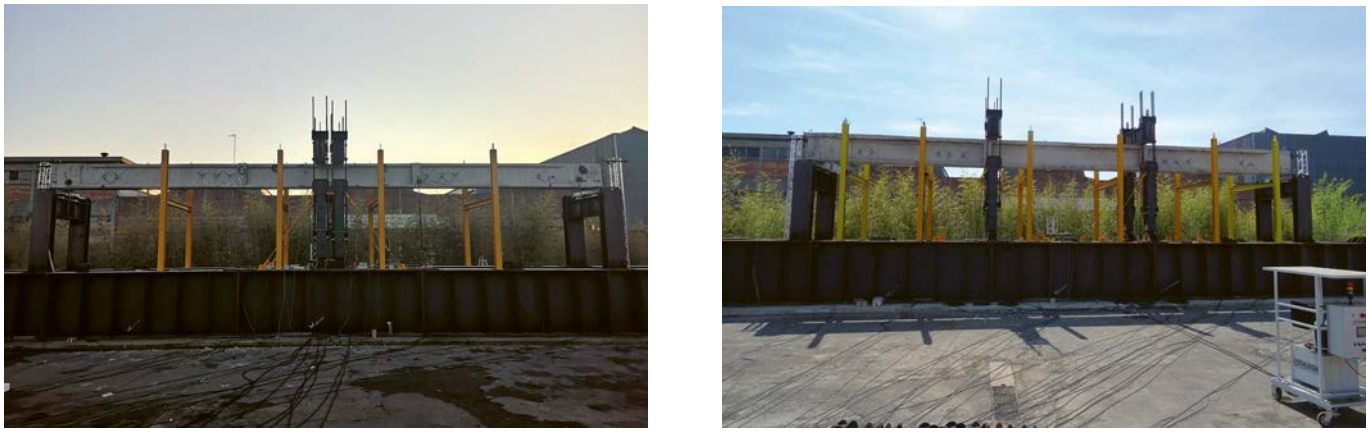

(a) (b)

Figure 2. Full-scale load tests: (a) Three-point bending test of PC beam without RC slab; (b) Four-point bending test of PC beam with RC slab.

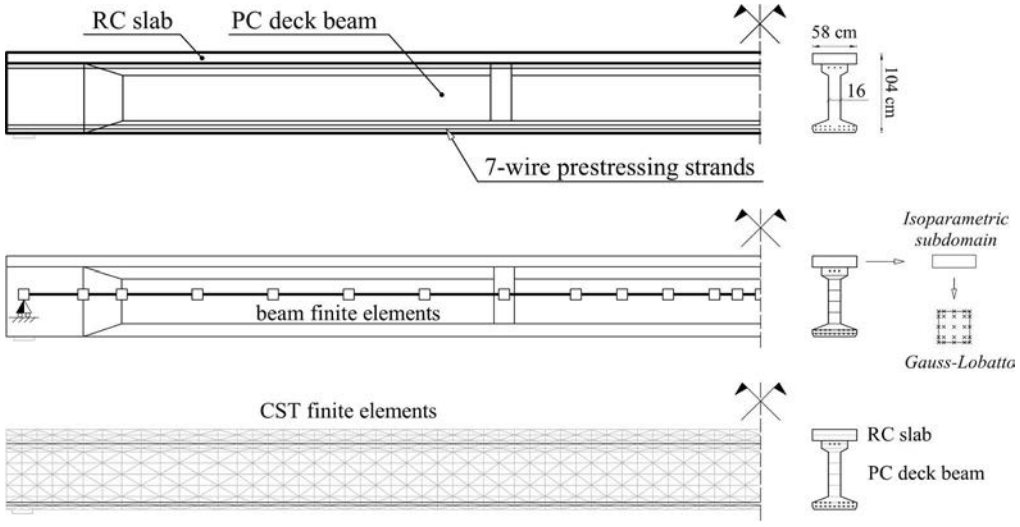

Figure 3. PC bridge deck beams: Longitudinal profile, structural modeling, and element discretization based on BFE model with isoparametric discretization and Gauss-Lobatto integration scheme and MCFT model with CST finite elements.

ed failures, which the BFE formulation is unable to capture. A proper model selection should also account for additional aspects, including importance of stress-diffusion effects near disturbed regions, required accuracy of the results at both local and system levels, capability to represent structures composed of multiple layers and/or realized at different stages, and balance between accuracy and computational costs.

3.2. BFE- and MCFT-based modeling of PC bridge deck beams

In this paper, both BFE- and MCFT-based formulations are validated based on the results of multiple full-scale load tests on PC bridge deck beams. In BFE modeling, the structure is discretized into beam finite elements, the member cross-section is subdivided into four-node isoparametric subdomains, and numerical integration is performed using a Gauss-Lobatto quadrature rule (Bontempi et al. 1995). The BFE model of the PC bridge deck beams is based on a discretization with 13 elements for half of the beam (Figure 3), with one outer element with rectangular cross-section at the support region, one adjacent element with linearly varying width of the beam web, and eleven inner elements with I-shaped cross-section. The beam cross-section is subdivided into nine quadrilateral isoparametric subdomains. Numerical integration is based on an 8×8 Gauss-Lobatto integration scheme. Moreover, eight sampling cross-sections are considered for each beam finite element.

In MCFT-based modeling, the structure is discretized into bi-dimensional constant strain triangle (CST) finite elements with smeared reinforcement representing the stirrups. The structural modeling is complemented by truss elements, attached to the concrete mesh, to reproduce discrete steel reinforcement and prestressing strands. The MCFT plane-stress finite element model of the PC beams is based on a discretization with 1128 CST finite elements for half of the beam under four-point loading (Figure 3). Two additional models based on a mesh with 1880 and 2256 CST finite elements are also considered for numerical analysis of non-symmetric load tests under three-point bending of a PC beam with or without the top slab, respectively. The stirrups are modeled as smeared reinforcement over the beam volume. Longitudinal

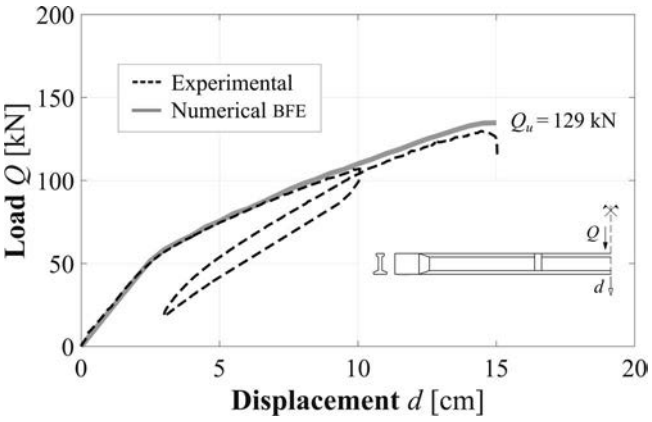

Figure 4. Experimental vs numerical (BFE) results in terms of load Q versus midspan displacement d of PC beam without RC slab under three-point bending test with shear span ratio α≈1.00.

bars and strands are modeled as truss elements built over the CST mesh. Separate nodal points are considered at the beam-slab interface with vertical and longitudinal links to model the beam-to-slab interaction (Anghileri & Biondini 2022, 2023). The model discretization and numerical integration were selected to achieve an optimal trade-off between accuracy of results and computational cost.

In the BFE model, the constitutive stress-strain relationships of concrete are based on the Saenz's model and an elastic-plastic law for concrete in compression and tension, respectively. In the MCFT-based model, for concrete in compression the Hognestad parabola is selected with compressive strength related to transversal principal strain to account for cracking effects. For concrete in tension, the behavior is linear up to cracking with a post-cracking softening branch accounting for the tension stiffening effect. These models were calibrated based on the results of laboratory tests, including eight uniaxial compressive tests on cylindrical concrete samples carried out to obtain complete stress-strain curves (Anghileri & Biondini 2025b). A bilinear hardening constitutive law is assumed for longitudinal reinforcing steel, transversal stirrups, and prestressing steel in both BFE- and MCFT-based models. Material mechanical properties and the residual prestressing level are based on the mean value of the outcomes of experimental laboratory tests (Table 1).

4. EXPERIMENTAL VALIDATION

4.1. Nonlinear structural analysis

The nonlinear structural analysis of the PC bridge deck beams was performed to validate the finite element formulations against the results of multiple full-scale load tests within the BRIDGE|50 research project. The nonlinear analyses were also used to investigate the role of the RC slab in the structural behavior of the PC beam and the transition from flexural to shear failure mechanisms. The experimental load protocol consisted of an initial loading phase up to concrete cracking, a pause under load to assess the concrete cracking pattern, followed by unloading, and a final reloading phase up to beam collapse. The nonlinear finite element analyses were carried out under monotonic loading. The BFE model was adopted to validate the numerical predictions against the experimental results of the full-scale three-point bending load test (α≈1.00) of the PC bridge deck beam without the top RC slab. The MCFT-based model was used to account for shear effects associated with four-point bending tests (α≈0.68, 0.47, 0.32) and the beam-slab interaction.

4.2. Three-point bending tests: Flexural failure

The testing program is currently ongoing. The first four load tests have been carried out with shear span ratio α≈1.00 (i.e., three-point loading) to favor a pure bending failure. Moreover, to study the behavior of the PC beam alone, one beam was tested under three-point loading up to failure after the removal of the top RC slab. Figure 4 compares BFE-based numerical results with the experimental outcomes in terms of load Q versus midspan displacement d, net of self-weight and prestressing, for the PC beam without top RC slab under three-point loading (α≈1.00). The experimental results included a preliminary loading phase up to Q=107 kN, a pause under load for assessment of the cracking pattern and dynamic testing, a subsequent unloading, and final reloading up to collapse (Q=129 kN). The tested beam exhibited structural failure that began with crushing in compression of the top RC slab at the critical region (midspan) and then propagated through the entire depth of the beam. After the full-scale load test, the PC beam was placed on supporting New Jersey barriers in the testing site to investigate concrete crack pattern and failure mechanism (Figure 5a). The close correspondence between numerical and experimental results validates the finite element formulation, the modeling strategies, and the results of the diagnostic activities. The structural response of the beam is also reproduced with high accuracy by using the MCFT-based structural model (Anghileri & Biondini 2025b).

Key factors to be investigated for the PC deck beams include the influence of the construction phases of the viaduct and the actual degree of collaboration between PC I-beams and top RC slab. In fact, the RC slab was cast with the PC deck beams already assembled and in place under the effects of beam self-weight and prestressing action. Therefore, considering the type of structural failure observed in the three-point bending tests of PC beams with RC slab (i.e., crushing of top slab and lack of connection between beam and slab at midspan at incipient collapse), the possible lack of interaction between beam and slab was considered using separate MCFT-based finite element models connected at the interface by means of links. In the longitudinal direction, links are considered rigid up to concrete cracking and elastic after cracking, with stiffness estimated to best fit the experimental results (Anghileri & Biondini 2025b). Figure 6 compares numerical and experimental results in terms of load Q versus midspan displacement d, net of self-weight and prestressing, for a PC beam with top RC slab tested under three-point loading. The PC beam with RC slab has been tested with a

(a) (b)

Figure 5. Failure mechanism after the full-scale load test based on three-point loading with shear span ratio $\alpha \approx 1.00$ of PC bridge deck beam (a) without top RC slab and (b) with top RC slab.

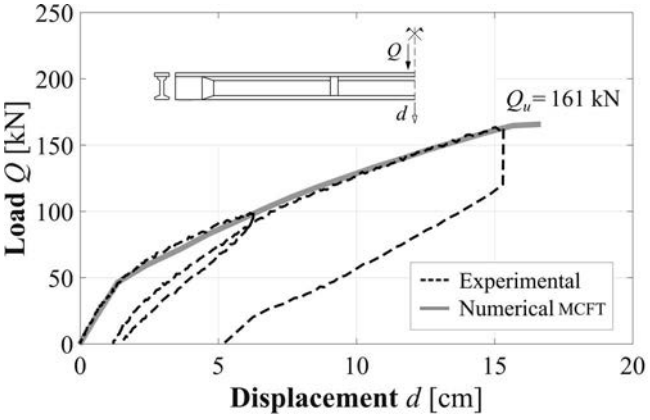

Figure 6. Experimental vs numerical (MCFT) results in terms of load Q versus midspan displacement d of PC beam with RC slab under three-point bending test with shear span ratio $\alpha \approx 1.00$.

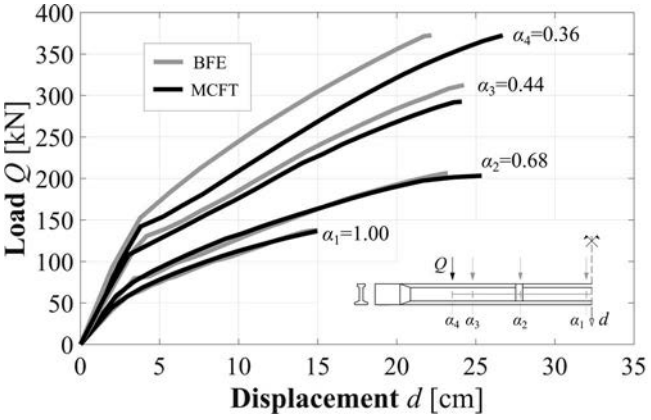

Figure 7. Load Q versus midspan displacement d of PC deck beam without RC slab: Comparison of BFE- and MCFT-based nonlinear analysis results for different values of the shear span ratio $\alpha = a/l$.

three-point bending test ($\alpha \approx 1.00$) using a first loading phase up to Q=100 kN, a subsequent unloading, and final load increase up to the collapse load Q=161 kN. The tested beam exhibited a structural failure associated with full crushing in compression of the top RC slab at midspan (Figure 5b).

The comparison of numerical and experimental results shows good agreement considering the pure bending failure of the tested beam. However, significant deviations may occur in the BFE model under four-point loading with reduced shear span ratios because of possible shear-dominant failures that the BFE formulation is unable to capture. Figure 7 compares the numerical results of the PC bridge deck beam without the top RC slab obtained using BFE- and MCFT-based models, in terms of load Q versus midspan displacement d, under four-point bending with different locations of the point loads. The results show that the reduction of the shear span ratio α leads to progressively larger deviations between the BFE and MCFT models, with a transition from flexural- to shear-dominated behavior and failure mechanisms. To this purpose, the MCFT-based model is used to investigate four-point bending tests.

4.3. Four-point bending tests: From flexural to shear failure

Additional tests have been performed under four-point loading with multiple shear span ratios to investigate the flexural-shear interaction and shear-dominant failure mechanisms. Figure 8 and Figure 9 show the numerical (MCFT) versus experimental comparison, in terms of load Q versus midspan displacement d, net of self-weight and prestressing, for the PC bridge deck with top RC slab tested under four-point loading with shear span ratio $\alpha \approx 0.68$ and $\alpha \approx 0.47$, respectively. The PC beam tested with span ratio $\alpha \approx 0.68$ was subjected to a preliminary loading phase up to Q=134 kN, a subsequent unloading and final reloading up to the collapse load Q=254 kN. The PC beam tested with span ratio $\alpha \approx 0.47$ has been associated with a single application of the load up to Q=363 kN. The failure of these PC beams occurred with full crushing in compression of the top slab in the critical region close to the applied load (Figure 10). It is worth noting that when passing from three-point to four-point bending tests, the slip between the precast beam and the top slab became less important, and the structural response tended

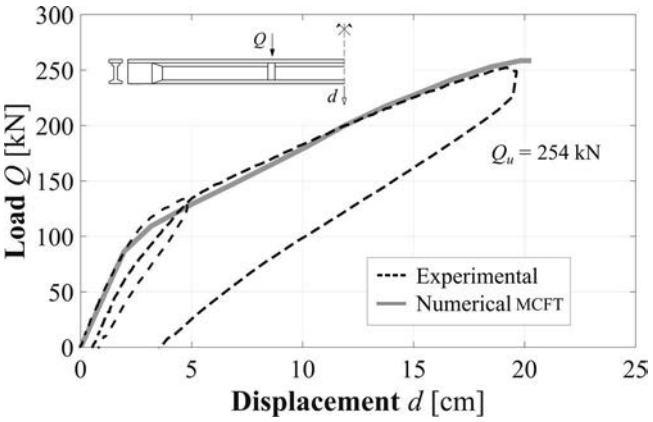

Figure 8. Experimental vs numerical (MCFT) results in terms of load Q versus midspan displacement d of PC beam with RC slab under four-point bending test with shear span ratio α≈0.68.

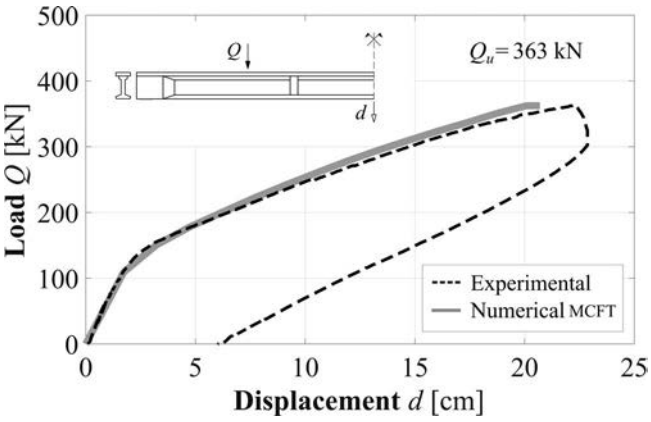

Figure 9. Experimental vs numerical (MCFT) results in terms of load Q versus midspan displacement d of PC beam with RC slab under four-point bending test with shear span ratio α≈0.47.

(a) (b)

Figure 10. Failure mechanism of the PC bridge deck beams with top RC slab under four-point loading with shear span ratio (a) α≈0.68 and (b) α≈0.47.

toward that of a monolithic beam-to-slab connection. Good agreement between numerical and experimental results has also been achieved considering different damage scenarios, associated with concrete cover removal and both reinforcing and prestressing steel cuts, for the validation of finite element formulations combined with damage modeling strategies (Anghileri & Biondini 2025b). Moreover, the large amount of data and experimental outcomes allowed the extension of the validation process on a statistical basis for a probabilistic description of the structural response of the investigated PC bridge deck beams (Anghileri & Biondini 2025a).

To investigate a shear-dominant failure mechanism, a full-scale load test with a three-point bending scheme and shear span ratio α≈0.32 was performed on a PC beam with top RC slab. The experimental load protocol consisted of a single loading phase up to the collapse load Q=723 kN. Figure 11 compares the experimental outcomes with the MCFT-based numerical results, net of self-weight and prestressing, in terms of applied load Q versus midspan displacement d. The tested PC bridge deck beam exhibited a structural failure that initiated with the formation of an inclined shear-dominant concrete crack developed from the region around the bearing support to the point of application of the load (Figure 12). The close agreement between numerical results and experimental outcomes validates the nonlinear finite element analysis. These results are complemented by numerical analyses aimed at further investigating the residual structural behavior of the tested PC beams under shear failure and at supporting appropriate planning of the ongoing full-scale load tests. As an example, Figure 13 shows the MCFT-based numerical results of three-point bending tests on a PC beam without top RC slab, in terms of load Q versus midspan displacement d, for different shear span ratios. In addition, Figure 14 shows the collapse load Q_u versus shear span ratio α with an indication of the estimated crack pattern at collapse.

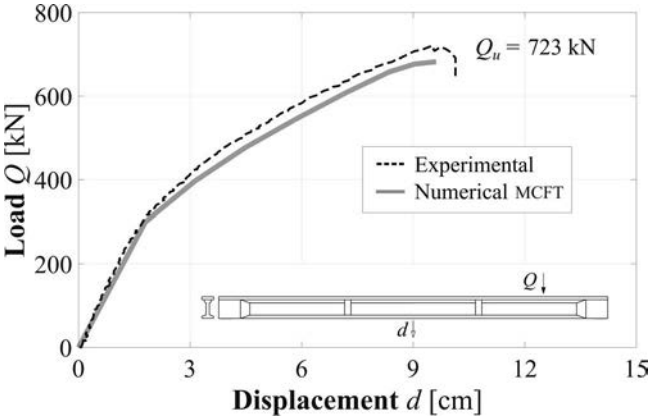

Figure 11. Experimental vs numerical (MCFT) results in terms of load Q versus midspan displacement d of PC beam with RC slab under three-point bending test with shear span ratio $\alpha \approx 0.32$.

5. CONCLUSIONS

The experimental validation and calibration of finite element models for nonlinear analysis of concrete structures based on BFE- and MCFT-based formulations have been presented. Structural modeling was developed using RC/PC beam finite elements and bi-dimensional finite elements for plane-stress analysis formulated in accordance with the MCFT and accounting for material nonlinearities associated with the constitutive laws of the materials, i.e., concrete, reinforcing steel, and prestressing steel. The calibration was based on the outcomes of laboratory tests on material mechanical properties and residual prestressing levels. The validation was based on multiple full-scale load tests on 50-year-old PC bridge deck beams under different loading conditions. The nonlinear structural analyses were used to accurately investigate the attainment of multiple limit states characterizing the structural response of the PC beams, including concrete cracking, steel yielding, and concrete crushing. The good agreement between experimental and numerical results allowed validation of the finite element formulations for PC beams with and without the top RC slab under both flexural and shear failure conditions. The role of the cast-in-situ RC slab in the structural capacity of PC bridge deck beams was also investigated considering the structural response of PC beams with and without the top RC slab under different shear span ratios. Based on the above, the main contributions of this paper include the calibration and validation of finite element formulations associated with the nonlinear analysis of concrete structures, using full-scale load tests on 50-year-old PC bridge deck beams under different loading conditions and failure modes. The formulations proposed provide a solid ground for a successful implementation in practice of life-cycle-oriented methods for design, assessment, maintenance, and management of aging RC/PC bridges. In addition, the results presented in this paper complement the experimental activities to further investigate the structural behavior of the tested PC bridge deck beams and support appropriate planning of the ongoing full-scale load tests. Future developments will be devoted to broadening and enriching the experimental results, further validating the finite element formulations under different exposure and damage conditions.

(a) (b)

Figure 12. Failure mechanism of the PC bridge deck beam with top RC slab under three-point loading with shear span ratio $\alpha \approx 0.32$.

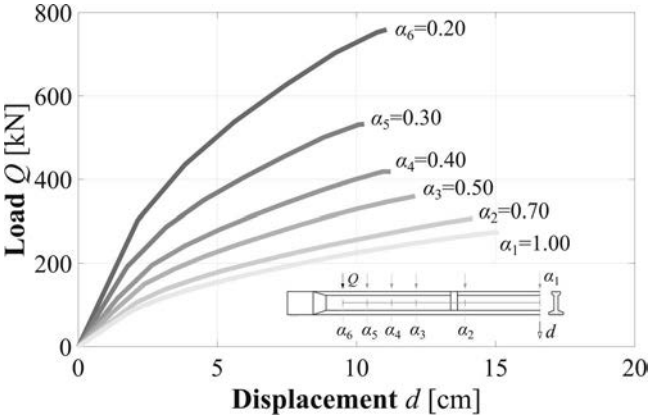

Figure 13. MCFT-based numerical results of three-point bending tests on PC beam without top RC slab: Load Q versus midspan displacement d for different values of the shear span ratio α.

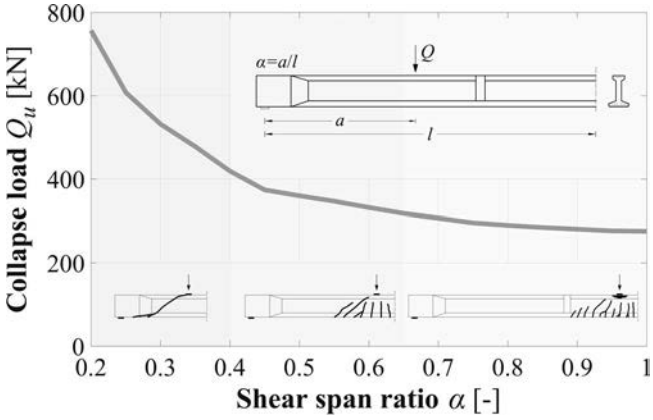

Figure 14. MCFT-based numerical results of three-point bending tests on PC beam without top RC slab: Collapse load Q_u versus shear span ratio α and crack pattern at collapse.

Acknowledgements

BRIDGE|50 is a research project based on a research agreement among universities, public authorities, and private companies. Members of the Management Committee: S.C.R. Piemonte (President); Politecnico di Milano (Scientific Coordinator); Politecnico di Torino (Scientific Responsible of the Experimental Activities); Lombardi Engineering (Secretary); Piedmont Region; City of Turin; Metropolitan City of Turin; TNE Torino Nuova Economia; ATI Itinera & C.M.B.; ATI Despe & Perino Piero; Quaranta Group. BRIDGE|50 website: https://www.bridge50.org.

This study has been partially supported by: (a) ReLUIS-CSLLPP 'Testing of guidelines for risk classification and management, safety assessment and monitoring of existing bridges', funded by the Italian Superior Council of Public Works – Consiglio Superiore dei Lavori Pubblici (CSLLPP); (b) ReLUIS-DPC 2024-2026 Research Project, funded by the Italian Department of Civil Protection – Dipartimento della Protezione Civile (DPC); and (c) RETURN Extended Partnership (multi-Risk sciEnce for resilienT commUnities undeR a changiNg climate), funded by the European Union Next-GenerationEU (National Recovery and Resilience Plan – NRRP).

References

[1] Anghileri, M., & Biondini, F. (2021). Nonlinear structural analysis of PC bridge deck beams. *1st Conference of the European Association on Quality Control of Bridges and Structures* (EUROSTRUCT 2021), Padua, Italy, August 29 - September 1, 2021. In: Pellegrino, C., Faleschini, F., Zanini, M.A., Matos, J.C., Casas, J.R., Strauss, A. (Eds.) *Lecture Notes in Civil Engineering*, 200, 2022, Springer, 1007–1017.

[2] Anghileri, M., & Biondini, F. (2022). Formulation and experimental validation of nonlinear finite element analysis of PC bridge deck beams. *11th International Conference on Bridge Maintenance, Safety and Management* (IABMAS 2022), Barcelona, Spain, July 11-15, 2022. In: Casas, J.R., Frangopol, D.M., Turmo, J. (Eds.), *Bridge Safety, Maintenance, Management, Life-Cycle, Resilience and Sustainability*. CRC Press, Taylor & Francis Group, London, UK, 1805–1812.

[3] Anghileri, M., & Biondini, F. (2023). Experimental validation of nonlinear finite element analysis of PC bridge deck beams based on the results of full-scale load tests. *Eighth International Symposium on Life-Cycle Civil Engineering* (IALCCE 2023), July 2-6, 2023, Milan, Italy. In: *Life-Cycle of Structures and Infrastructure Systems*, F. Biondini, D. M. Frangopol (Eds.), CRC Press, London, UK, 2085–2092 (Open Access).

[4] Anghileri, M., & Biondini, F. (2025a). Bayesian updating of the residual structural performance of existing concrete structures based on experimental tests. *Civil Engineering and Environmental Systems*, 42(2), 140–163.

[5] Anghileri, M., & Biondini, F. (2025b). Validation of life-cycle-oriented computational methods for nonlinear analysis of RC/PC structures based on experimental tests. *Structure and Infrastructure Engineering*, 21(7–8), 1193–1216.

[6] Anghileri, M., Biondini, F., Rosati, G., Savino, P., Tondolo, F., Sabia, D., Manto, S., Nivriera, M., Trincianti, C., Ventura, D., Monti, G., Legramandi, C., & Caruso, C. (2020). Deconstruction of the Corso Grosseto viaduct and setup of a testing site for full scale load tests. *10th International Conference on Bridge Maintenance, Safety and Management* (IABMAS 2020), June 28-July 2, 2020 (postponed to April 11-15, 2021), Sapporo, Japan. In: Yokota, H., Frangopol, D.M. (Eds.), *Bridge Maintenance, Safety, Management, Life-Cycle Sustainability and Innovations*. CRC Press/Balkema, Taylor & Francis Group, London, UK, 3365–3370.

[7] Anghileri, M., Rosati, G., Biondini, F., Savino, P., & Tondolo, F. (2023). Experimental tests for mechanical characterization of prestressed concrete bridge deck beams. *Eighth International Symposium on Life-Cycle Civil Engineering* (IALCCE 2023), July 2-6, 2023, Milan, Italy. In: *Life-Cycle of Structures and Infrastructure Systems*, F. Biondini, D. M. Frangopol (Eds.), CRC Press, London, UK, 2069-2076 (Open Access).

[8] ASCE (2025). Report card for America's infrastructure. A Comprehensive Assessment of America's Infrastructure, American Society of Civile Engineers (ASCE).

[9] Beltrami, C., Bianchi, S., Cervio, M., Anghileri, M., Felicetti, R., Quattrone, A., Chiara, M., Salza, B., & Masala, D. (2021). Bridge visual inspections: Experience of local authorities and the case study of the Corso Grosseto viaduct. *10th International Conference on Bridge Maintenance, Safety and Management* (IABMAS 2020), June 28-July 2, 2020 (postponed to April 11-15, 2021), Sapporo, Japan. In: Yokota, H., Frangopol, D.M. (Eds.), *Bridge Maintenance, Safety, Management, Life-Cycle Sustainability and Innovations*. CRC Press/Balkema, Taylor & Francis Group, London, UK, 3358–3364.

[10] Biondini, F., Ballio, F., di Prisco, M., Bianchi, S., D'Angelo, M., Zani, G., Capacci, L., Anghileri, M., Scalbi, A., & Ferreira, K. F. (2022). Bridge vulnerability and hazard assessment for risk-based infrastructure management. *11th International Conference on Bridge Maintenance, Safety and Management* (IABMAS 2022), Barcelona, Spain, July 11-15, 2022. In: Casas, J.R., Frangopol, D.M., Turmo, J. (Eds.), *Bridge Safety, Maintenance, Management, Life-Cycle, Resilience and Sustainability*. CRC Press, Taylor & Francis Group, London, UK, 1864–1873.

[11] Biondini, F., & Frangopol, D. M. (2016). Life-cycle performance of deteriorating structural systems under uncertainty: Review. *Journal of Structural Engineering*, 142(9), 1–17.

[12] Biondini, F., & Frangopol, D. M. (2018). Life-cycle performance of civil structure and infrastructure systems: Survey. *Journal of Structural Engineering*, 144(1), 06017008, 1–7.

[13] Biondini, F., & Frangopol, D. M. (2019). *Life-cycle design, assessment and maintenance of structures and infrastructure systems*. American Society of Civil Engineers (ASCE).

[14] Biondini, F., Manto, S., Beltrami, C., Tondolo, F., Chiara, M., Salza, B., Tizzani, M., Chiaia, B., Lencioni, A., Panseri, L., & Quaranta, L. (2021). BRIDGE|50 research project: Residual structural performance of a 50-year-old bridge. *10th International Conference on Bridge Maintenance, Safety and Management* (IABMAS 2020), June 28-July 2, 2020 (postponed to April 11-15, 2021), Sapporo, Japan. In: Yokota, H., Frangopol, D.M. (Eds.), *Bridge Maintenance, Safety, Management, Life-Cycle Sustainability and Innovations*. CRC Press/Balkema, Taylor & Francis Group, London, UK, 337–3344.

[15] Biondini, F., Tondolo, F., Manto, S., Beltrami, C., Chiara, M., Salza, B., Tizzani, M., Chiaia, B., Lencioni, A., Panseri, L., & Quaranta, L. (2021). Residual structural performance of existing PC bridges: Recent advances of the BRIDGE|50 research project. *1st Conference of the European Association on Quality Control of Bridges and Structures* (EUROSTRUCT 2021), Padua, Italy, August 29 - September 1, 2021. In: Pellegrino, C., Faleschini, F., Zanini, M.A., Matos, J.C., Casas, J.R., Strauss, A. (Eds.) *Lecture Notes in Civil Engineering*, 200, 2022, Springer, 997–1006.

[16] Bontempi, F., Malerba, P. G., & Romano, L. (1995). Formulazione diretta secante dell'analisi non lineare di telai in CA e CAP. *Studi e Ricerche, Graduate School for Concrete Structures 'F.lli Pesenti'*. 16, 351–386. Milan: Politecnico di Milano (In Italian).

[17] Carsana, M., Biondini, F., & Redaelli, E. (2025). Diagnostic procedure for corrosion assessment of existing concrete bridges: Experimental case study. *Structure and Infrastructure Engineering*, 21(7–8), 1117–1133.

[18] Carsana, M., Biondini, F., Redaelli, E., & Valoti, D.O. (2022). Corrosion assessment of 50-year-old PC deck beams. *11th International Conference on Bridge Maintenance, Safety and Management* (IABMAS 2022), Barcelona, Spain, July 11-15, 2022. In: Casas, J.R., Frangopol, D.M., Turmo, J. (Eds.), *Bridge Safety, Maintenance, Management, Life-Cycle, Resilience and Sustainability*. CRC Press/Balkema, Taylor & Francis Group, London, UK, 1797–1804.

[19] Carsana, M., Redaelli, E., & Biondini, F. (2023). Field and laboratory tests for corrosion assessment of existing concrete bridges. *Eighth International Symposium on Life-Cycle Civil Engineering* (IALCCE 2023), July 2-6, 2023, Milan, Italy (Keynote Paper). In: *Life-Cycle of Structures and Infrastructure Systems*, F. Biondini, D. M. Frangopol (Eds.), CRC Press, London, UK, 45–46 (Open Access).

[20] Collins, M. P., Bentz, E. C., & Sherwood, E. G. (2008). Where is shear reinforcement required? Review of research results and design procedures. *Structural Journal*, 105(5), 590-600.

[21] Kaufmann, W., & Marti, P. (1998). Structural concrete: Cracked membrane model. *Journal of Structural Engineering*, 124(12), 1467–1475.

[22] Malerba, P. G. 1998. *Analisi limite e non lineare di strutture in calcestruzzo armato*. Udine, Italy: International Centre for Mechanical Sciences, CISM (In Italian).

[23] Marí, A., Bairán, J., Cladera, A., Oller, E., & Ribas, C. (2015). Shear-flexural strength mechanical model for the design and assessment of reinforced concrete beams. *Structure and Infrastructure Engineering*, 11(11), 1399–1419.

[24] Messina, D., Proverbio, E. (2023). Effect of prestressing corrosion on failure in bridges. *Structural Concrete*, 24(1), 227–238.

[25] Savino, P., Anghileri, M., Chiara, M., Salza, B., & Quaranta, L. (2021). Corso Grosseto viaduct: Historical and technical overview. *10th International Conference on Bridge Maintenance, Safety and Management* (IABMAS 2020), June 28-July 2, 2020 (postponed to April 11-15, 2021), Sapporo, Japan. In: Yokota, H., Frangopol, D.M. (Eds.), *Bridge Maintenance, Safety, Management, Life-Cycle Sustainability and Innovations*. CRC Press/Balkema, Taylor & Francis Group, London, UK, 3345–3351.

[26] Savino, P., Quattrone, A., Sabia, D., Chiaia, B., Tondolo, F., Anghileri, M., Biondini, F., Rosati, G. (2023). Large-scale experimental testing of 50-year-old prestressed concrete bridge girder. *Eighth International Symposium on Life-Cycle Civil Engineering* (IALCCE 2023), July 2-6, 2023, Milan, Italy. In: *Life-Cycle of Structures and Infrastructure Systems*, F. Biondini, D. M. Frangopol (Eds.), CRC Press, London, UK, 2061–2068 (Open Access).

[27] Savino, P., Tondolo, F., Sabia, D., Quattrone, A., Biondini, F., Rosati, G., Anghileri, M., & Chiaia, B. (2023). Large-scale experimental static testing on 50-year-old prestressed concrete bridge girders. *Applied Sciences*, 13(2), 834.

[28] Tondolo, F., Biondini, F., Sabia, D., Rosati, G., Chiaia, B., Quattrone, A., Savino, P., & Anghileri, M. (2021). Experimental program and full-scale load tests on PC deck beams. *1st Conference of the European Association on Quality Control of Bridges and Structures* (EUROSTRUCT 2021), Padua, Italy, August 29 - September 1, 2021. In: Pellegrino, C., Faleschini, F., Zanini, M.A., Matos, J.C., Casas, J.R., Strauss, A. (Eds.) *Lecture Notes in Civil Engineering*, 200, 2022, Springer, 1045–1053.

[29] Tondolo, F., Sabia, D., Chiaia, B., Quattrone, A., Savino, P., Biondini, F., Rosati, G., & Anghileri, M. (2022). Full-scale testing and analysis of 50-year old prestressed concrete bridge girders. *11th International Conference on Bridge Maintenance, Safety and Management* (IABMAS 2022), Barcelona, Spain, July 11-15, 2022. In: Casas, J.R., Frangopol, D.M., Turmo, J. (Eds.), *Bridge Safety, Maintenance, Management, Life-Cycle, Resilience and Sustainability*. CRC Press, Taylor & Francis Group, London, UK, 1775–1782.

[30] Tondolo, F., Savino, P., Quattrone, A., Sabia, D., Anghileri, M., Biondini, F., Rosati, G., & Chiaia, B. (2025). Experimental tests inducing shear failure on PC bridge deck girders. *fib Symposium 2025, Concrete Structures: extend lifespan, limit impacts*, Antibes, France, June 16-18, 2025. In: fib Symposium Proceedings, The International Federation for Structural Concrete (fib), Lausanne, Switzerland, 1204–1212.

[31] Vecchio, F. J. (2001). Non-linear finite element analysis of reinforced concrete: at the crossroads?. *Structural Concrete*, 2(4), 201–212.

[32] Vecchio, F. J., & Collins, M. P. (1986). The modified compression field theory for reinforced concrete elements subjected to shear. *ACI Journal*, 83(2), 219–231.

CIRCULAR **CONCRETE**

Mucho más que hormigón

EN SIKA NO SÓLO MEJORAMOS EL HORMIGÓN. CREAMOS POSIBILIDADES.

Para ser más **sostenibles**, acceder a **mejores proyectos** y contar siempre con las tecnologías y aditivos necesarios para que tu hormigón sea exactamente lo que necesitas.
Por eso te ofrecemos la mayor gama de **soluciones a medida** y un equipo de especialistas que te acompaña en todo el proceso para lograr la combinación perfecta y **alcanzar tus objetivos**.

www.sikacircularconcrete.com

BUILDING TRUST

Disponible en **www.hormigonyacero.com**
https://doi.org/10.33586/hya.2026.4128

A Levels-of-Approximation Unified Mechanical Model for the Shear Strength of Slender and Short Reinforced and Prestressed Concrete Beams with Steel, FRP, or Fiber Reinforced Concrete

Un modelo mecánico unificado de niveles de aproximación para la resistencia a cortante de vigas esbeltas y cortas de hormigón armado y pretensado con acero, FRP o hormigón reforzado con fibras

Antoni Cladera[a,*], Eva Oller[b], Carlos Ribas[a], Juan Murcia-Delso[b], Noemí Duarte[b], Jesús Miguel Bairán[b]

[a] *Department of Industrial Engineering and Construction. Universitat de les Illes Balears, Spain.*
[b] *Department of Civil and Environmental Engineering. Universitat Politècnica de Catalunya, Spain..*

Recibido el 8 de mayo de 2025; revisado el 20 de diciembre de 2025, aceptado el 28 de enero de 2026

ABSTRACT

This paper presents a Levels-of-Approximation (LoA) unified mechanical model for the shear strength of slender and non-slender reinforced and prestressed concrete beams, with rectangular, T- or I-shaped sections. It applies to members reinforced with steel or fiber-reinforced polymer (FRP) bars, or fiber-reinforced concrete (FRC). Derived from the Multi-Action Shear Model (MASM), the model integrates the key shear transfer actions, including shear carried by the compression chord, residual tensile stresses across the critical crack, dowel action of longitudinal reinforcement and contributions from stirrups, if present.

Structured within the LoA framework, the model offers increasing complexity and accuracy for various structural design and assessment scenarios, from preliminary design (LoA 0) to detailed assessment (LoA III). Its adaptability is demonstrated through different extensions, including fatigue for RC beams without stirrups. The model is validated using 2,714 test results from 14 experimental databases, showing consistent predictions with reduced scatter, especially at higher LoAs.

This unified mechanical model provides a robust tool for both the design and assessment of structural concrete elements, offering a systematic approach to integrate advanced mechanical understanding with practical engineering needs.

KEYWORDS: Shear strength, structural concrete, mechanical model, reinforced concrete, prestressed concrete, FRP, SFRC, fatigue.

RESUMEN

Este artículo presenta un modelo mecánico unificado, estructurado bajo la metodología de Niveles de Aproximación (LoA, por sus siglas en inglés), para estimar la resistencia a cortante de vigas esbeltas y no esbeltas de hormigón armado y pretensado, con secciones transversales rectangulares, en T o en I. El modelo es válido para elementos reforzados con barras de acero o de polímeros reforzados con fibra (FRP), así como para hormigones reforzados con fibras (FRC). Derivado del *Multi-Action Shear Model* (MASM), el modelo integra los principales mecanismos de transferencia del

esfuerzo cortante, incluyendo la contribución de la cabeza comprimida, las tensiones residuales de tracción a través de la fisura crítica, el efecto pasador de la armadura longitudinal y la contribución de la armadura transversal, si la hubiera.

El modelo, estructurado en el marco de los Niveles de Aproximación, ofrece una complejidad y precisión crecientes para distintos escenarios de proyecto y evaluación estructural, desde el diseño preliminar (LoA 0) hasta la evaluación detallada (LoA III). Su adaptabilidad se demuestra mediante diversas extensiones, incluyendo el análisis a fatiga en vigas de hormigón armado sin estribos. La validación se ha realizado con 2.714 resultados experimentales procedentes de 14 bases de datos, mostrando predicciones consistentes y con baja dispersión, especialmente en los niveles más elevados de aproximación.

Este modelo mecánico unificado constituye una herramienta robusta tanto para el proyecto como para la evaluación de elementos estructurales de hormigón, proporcionando un enfoque sistemático que integra un conocimiento mecánico avanzado con las necesidades prácticas de la ingeniería.

PALABRAS CLAVE: Resistencia a cortante, hormigón estructural, modelo mecánico, hormigón reforzado, hormigón pretensado, FRP, SFRC, fatiga.

* Persona de contacto / *Corresponding author*:
Correo-e / *e-mail*: antoni.cladera@uib.es (Antoni Cladera)

How to cite this article: Cladera, A., Oller, E., Ribas, C., Murcia, J., Duarte, N., Bairán, J.M. (2026). A Levels-of-Approximation Unified Mechanical Model for the Shear Strength of Slender and Short Reinforced and Prestressed Concrete Beams with Steel, FRP, or Fiber Reinforced Concrete. *Hormigón y Acero*. 77(308):71-92. https://doi.org/10.33586/hya.2026.4128

1. INTRODUCTION

The long-standing debate on the shear strength of reinforced concrete (RC) members dates back to the earliest research in this field. As early as 1907, Mörsch identified three fundamental shear transfer actions or resisting mechanisms [1]: 1) shear stresses in the compression zone, 2) dowel action in the longitudinal reinforcement, and 3) tensile forces in the web reinforcement, if present. Faber introduced the arch effect as another crucial mechanism in a series of superb papers published in 1916 [2]. However, it was not until 1966 that Fenwick and Paulay [3,4], through ad-hoc experiments, systematically analyzed the principal mechanisms of shear resistance in RC beams and were the first to quantify their contributions experimentally. Their pioneering work also incorporated aggregate interlock across cracks and marked the first estimation of shear stress attributable to this mechanism. These findings became a foundational step for further research and were incorporated into the ACI-ASCE recommendations in 1973 [5].

Subsequent studies focused on quantifying the contributions of each shear transfer mechanism, particularly aggregate interlock [6–8]. Prof. Fritz Leonhardt, in his famous keynote address, highlighted that ultimate shear strength is influenced by more than 20 parameters [9]. Since then, researchers have developed increasingly sophisticated models to account for many of these factors, while practical design codes require simplifications. As Prof. Paul E. Regan observed in 1993 [10], simplifying the problem often involves neglecting secondary factors, but what is secondary in one case may be primary in another. An example of this balance is the ACI-318-19 design formula for shear strength [11], which is derived from six models based on different assumptions [12–17]. Of these, two prioritize aggregate interlock as the dominant mechanism [14,15], while the remaining four focus on shear stresses transferred by the compression zone.

In recent years, Campana et al. [18] proposed a novel methodology for evaluating shear transfer mechanisms during testing, combining detailed crack pattern analysis and crack kinematics. This approach allowed researchers to track the evolution of shear-transfer actions during different loading phases. Cavagnis et al. [19,20] and Huber et al. [21,22] enhanced this methodology by incorporating Digital Image Correlation techniques and advanced models of aggregate interlock. Cavagnis et al. demonstrated that the relative contributions of shear-transfer actions vary with beam geometry and loading conditions. For slender beams ($a/d > 2.5$), aggregate interlock predominates, whereas for short beams ($a/d < 2.5$), direct strut-and-tie mechanisms govern the behavior. This transition occurs at the vertex of the so-called Kani valley [23], where the dominant shear mechanism shifts with the slenderness ratio.

Recently, Montoya et al. [24] used the Digital Image Correlation (DIC) technique to measure the sliding and opening of cracks in six RC beams without transversal reinforcement. This enabled using the Walraven model to compute the stresses along cracks, and estimated a reduced contribution of the aggregate interlock across the shear crack in the web, until approximately 90%–98% of the total shear capacity according to six tests on RC beams without stirrups (Fig. 1b). At this loading level, a second, more horizontal branch of the critical shear crack forms (Fig. 1c) inside the compression chord, accompanied by significant sliding resulting in higher levels of shear stresses. These observations highlight a complementary relationship, rather than a contradiction, between models based on shear transferred through the compression chord [25–27] and those prioritizing aggregate interlock [28,29], including the branch of the crack in the compression chord.

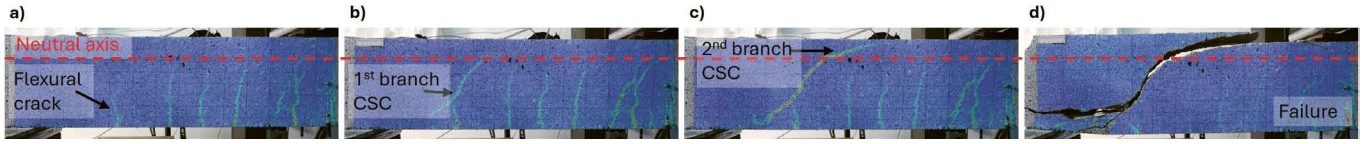

Figure 1. Crack pattern evolution in a RC beam, without stirrups, failing on shear.

A different methodology was employed by Bairán et al. [30], using optimized strut-and-tie models with concrete ties to understand shear transfer actions in RC beams without stirrups. This model considers stress transfer capacity across cracks by accounting for the inclination between the stress field and crack kinematics (opening and sliding). An experimental case study demonstrated that different shear-resisting actions dominate in different regions of the beam. For instance, aggregate interlock effectively transfers stresses in zones with near-vertical cracks. However, in areas with smaller bending moments and more inclined cracks, the stress components in the crack plane primarily induce direct tension with limited shear in the crack plane. Consequently, aggregate interlock becomes insufficient to carry the full shear force, and failure is governed by the compression zone's capacity.

In this context, two research groups—from the *Universitat Politècnica de Catalunya* and the *Universitat de les Illes Balears*—led by Prof. Antonio Marí, sequentially developed a mechanically derived shear strength model between 2014 and 2016. The initial development of the model began with efforts to explain the shear strength in ULS of beam-and-block floors [31] and beams reinforced with fiber-reinforced polymer (FRP) bars [32,33]. In both cases, it was observed that shear transfer in the compression zone was the dominant mechanism: in the first case, due to the prominence of the compression zone relative to the web width, and in the second case, due to the large crack widths in the web caused by the low modulus of elasticity of the FRP bars.

Building on these specific cases and integrating different transfer actions, as will be summarized in the following section, the general shear-flexural strength mechanical model for the design and assessment of reinforced concrete beams was formulated. This was initially applied to beams with rectangular cross-sections [34], then extended to T- and I-shaped beams [35], and finally to prestressed concrete beams [36]. Collectively, these contributions formed what we termed the Multi-Action Shear Model (MASM). The particular case of beams subjected to distributed loads was addressed in [37].

As the MASM presented closed-form equations for each shear transfer action, the model was simplified into the Compression Chord Capacity Model (CCCM), with the main premise that the shear transferred across the uncracked compression chord was the principal transfer action [38]. This simplified model also served as the base for the version developed for the ACI 318-19 update [16].

These mechanical models were further extended to address specific cases, including the shear strength of non-slender reinforced concrete beams [39], steel fiber reinforced concrete (SFRC) beams without stirrups [40], and the shear fatigue strength of RC members without stirrups [41]. Other applications included corrosion-damaged RC beams [42] and their long-time shear strength prediction [43,44], and prestressed concrete beams with FRP tendons [45]. The model was even adapted for punching shear of slabs [46,47], among other cases [48–50] not discussed here for the sake of conciseness. Moreover, a detailed discussion on open questions on shear behavior of structural concrete and the answers provided by mechanical models was recently published by Prof. Marí [51].

The 21 references cited earlier represent the culmination of approximately 12 years of dedicated and dynamic research. While these contributions were not always developed in a strictly sequential or comprehensive manner, each played a vital role in advancing the overall understanding of the subject. To bring coherence and clarity, this paper brings together those valuable insights into a unified mechanical model, structured in a logical progression—from the most general formulations to the more commonly encountered specific applications. Additionally, the work embraces the Level-of-Approximation (LoA) framework introduced in the Model Code 2010 [52], reinforcing a consistent and practical approach to model development.

The LoA framework ensures that the refinement of a design model corresponds to the required level of detail in the calculation process—whether for preliminary design, detailed design, or structural assessment—and considers the importance of the structural element in question [53]. For preliminary design, quick estimations are prioritized, requiring minimal calculation effort. In contrast, the strength assessment of existing structures often requires sophisticated models for accurate capacity evaluation, as decisions regarding reinforcement, rehabilitation, or demolition can carry substantial financial, social, and environmental implications. Accordingly, the complexity and effort involved in the design process increase with the LoA.

To maintain consistency across all LoAs, a unified physical model serves as the foundation, with conservative simplifications applied as the design complexity decreases. In this paper, the most refined model, corresponding to LoA III, is based on the Multi-Action Shear Model (MASM). From this formulation, the Compression Chord Capacity Model (CCCM) is transparently derived and proposed as LoA II. Further simplifications, tailored primarily for the design of new structures, constitute LoA I. Additionally, a preliminary design approach, referred to as LoA 0, is also discussed. This framework ensures coherent outcomes across different LoAs, with naturally more conservative results associated with lower levels of approximation, suitable for situations where data may be incomplete or imprecise.

This paper will present the LoAs in the logical sequence of their derivation (LoA III → II → I/0) although the intended use would be in the reverse order (LoA 0/I → II → III).

The key contribution of this work is the integration of the MASM and CCCM within a unified Level-of-Approximation framework. To the authors' knowledge, this is probably the first unified model capable of addressing a broad range of cases involving the shear strength of slender and short reinforced and prestressed concrete beams, with or without stirrups, considering

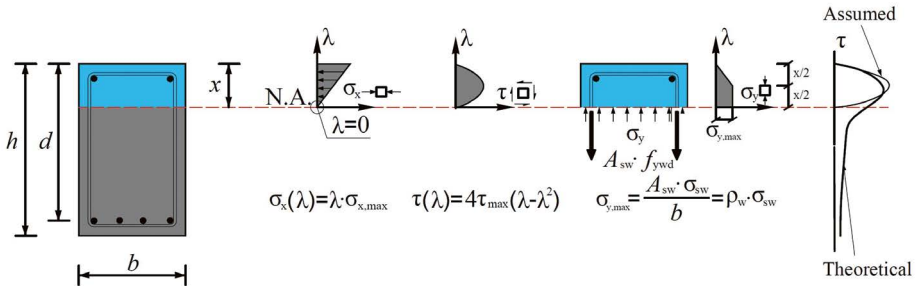

Figure 2. Considered distributions of stresses at the un-cracked concrete chord.

TABLE 1.
Summary of the equation for the LoA III: MASM

	Main expressions	
Shear strength	$V_{Rd} = V_{cu}+V_{su} \le V_{Rd,max}$	(1)
Concrete contribution	$V_{cu} = (v_c + v_w + v_l)\frac{f_{ct}}{\gamma_v}\cdot b\cdot d$	(2)
Shear reinforcement contribution	$V_{su} = (d_s-x)\ cot\theta\ \frac{A_{sw}}{s} f_{ywd}$	(3a)
	$V_s = (d_s-x)\ cot\theta\ \frac{A_{sw}}{s}\frac{f_{ywd}}{f_{ct}b\cdot d}$	(3b)
Maximum shear strength (strut crushing)	$V_{Rd,max} = \alpha_{cw}\ b_w\ z\nu_1\ f_{cd}\ \frac{cot\theta}{1+cot^2\theta}$	(4)
Contributing component	***Dimensionless expressions***	
Compression chord	$v_c = \zeta\left\{\left(0.70 + 0.18K_T + \left(0.20+0.50\ \frac{b}{b_w}\right)v_s\right)\ \frac{x}{d} + 0.02K_T\right\}\frac{b_{v,eff}}{b}K_p$	(5)
Cracked concrete web	$v_w = 167\ \frac{f_{ct}}{E_{cm}}\ \frac{b_w}{b}\left(1+\frac{2\cdot G_f\cdot E_{cm}}{f_{ct}^2\cdot d_0}\right)$	(6)
Longitudinal reinforcement (dowel effect)	$if\ \ v_s > 0 \rightarrow v_l = 0.23\ \frac{\alpha_e\cdot\rho_{l,b}}{1-x/d}$	(7a)
	$if\ \ v_s > 0 \rightarrow v_l = 0$	(7b)
Factors	***Expressions***	
Relative neutral axis depth	$\frac{x}{d} = \frac{x_0}{d} = \alpha_e\ \rho_{l,b}\left(-1+\sqrt{1+\frac{2}{\alpha_e\cdot\rho_{l,b}}}\right)$	(8a)
	$N_{Ed} > 0\ \ or\ P \rightarrow \frac{x}{d} = \frac{x_0}{d} + \Delta_{x/d} \le \frac{h}{d}$	(8b)
	$\Delta_{x/d} = \left(\frac{h}{d} - \frac{x_0}{d}\right)\left(\frac{h}{d}\right)\frac{\sigma_{cp}}{\sigma_{cp}+f_{ct}}$	(8c)
Effective flange width	$if\ x \le h_f \ \ \rightarrow \ \ b_{v,eff} = b_v = b_w + 2h_f \le b$	(9a)
	$if\ x > h_f \ \ \rightarrow \ \ b_{v,eff} = b_w + (b_v - b_w)\left(\frac{h_f}{x}\right)^{3/2}$	(9b)
Critical crack inclination	$cot\ \theta = \frac{0.85\ d_s}{(d_s-x)} \le 2.5$	(10)
Size and slenderness effect	$\zeta = \frac{2}{\sqrt{1+\frac{d_0}{200}}}\left(\frac{d}{a}\right)^{0.2}$	(11)
Parameter related to M_{cr} in T cross-section	$K_T = 0.1+ 0.9\ \frac{b_w}{b} + 2.5\ \frac{h_{f,tens}}{h}\left(\frac{b_{tens}-b_w}{b}\right)$	(12)
Parameter related to M_{cr} in prestressed members	$K_p = 1+ 0.3\ \frac{P\ cos\delta_p\ y_t}{f_{ct}\ bd^2}$	(13)

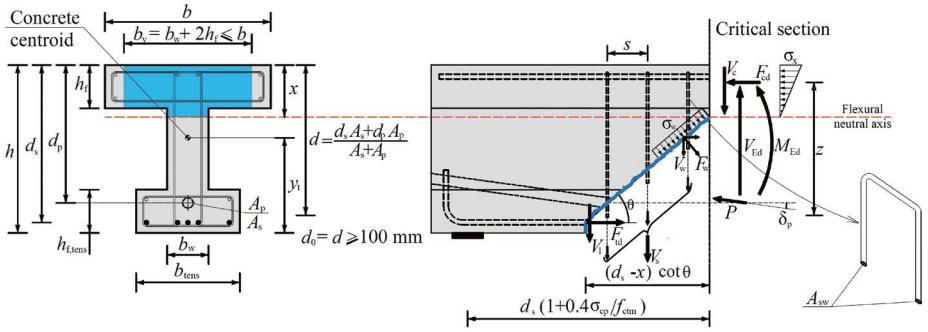

Figure 3. Graphical summary of the LoA III (MASM) with the definition of the basic parameters.

rectangular, T- or I-cross sections, with steel reinforcement, FRP reinforcement, or fiber-reinforced concrete. The extensions presented in this paper are primarily based on works previously published by the authors in separate contributions, which are here systematically compiled and adapted to ensure full internal consistency and practical applicability within the LoA framework, particularly at LoA II. This reorganization allows the different extensions to be applied in a homogeneous manner, providing a balanced compromise between mechanical accuracy and simplicity. In addition, in the specific case of beams internally reinforced with FRP bars—one of the earliest applications that motivated the development of the underlying mechanical model—the simplified formulation proposed at LoA II constitutes a new contribution, offering a more straightforward and fully integrated approach within the unified framework, now accounting for the successive developments of the general model.

2. BRIEF INTRODUCTION TO THE DERIVATION OF THE MULTI-ACTION SHEAR MODEL

The primary assumption of the Multi-Action Shear Model (MASM), supported by the empirical observations of many researchers [25,54,55], is that once the second branch of the critical crack develops, the load capacity does not significantly increase, as the softening of concrete in the compression zone begins.

Linking the onset of shear failure to the propagation of the second branch of the critical crack simplifies the problem significantly. This approach enables the formulation of a failure criterion based on concrete stresses in the compression chord, using Kupfer's biaxial failure envelope [56]. This criterion relies on the compressive and tensile strengths of concrete, parameters that exhibit less variability compared to those required in kinematic failure models.

In essence, the MASM assumes that the uncracked concrete in flexure experiences a multiaxial state of principal stresses (σ_1, σ_2), induced by the combined effects of shear force (τ), longitudinal bending stresses (σ_x), and vertical stresses (σ_y) from local effects (Figure 2), which collectively enhance the shear strength of the uncracked concrete. Building upon this assumption and applying classic mechanics principles, the MASM derives explicit equations (detailed in Section 3) for four shear transfer actions: shear transferred by the compression zone, shear transferred across the critical crack due to residual tensile stresses, shear transferred by dowel action of the longitudinal reinforcement, and shear transferred by the stirrups, if they exist. These actions are interdependent. For instance, the confinement stresses in the uncracked concrete, induced by stirrups, are accounted for when evaluating the shear contribution from the uncracked concrete, or the dowel effect is considered negligible if there are not stirrups. A comprehensive derivation of the MASM can be found in [29].

3. LEVEL OF APPROXIMATION III: THE MULTI-ACTION SHEAR MODEL (MASM)

Table 1, presenting Eqs. (1)-(13) and Figure 3, shows all the equations and factors needed to compute the shear strength of a reinforced or prestressed concrete member, with or without stirrups, with rectangular, T- or I-shaped cross-section. The key aspects and distinct features of this model will be highlighted

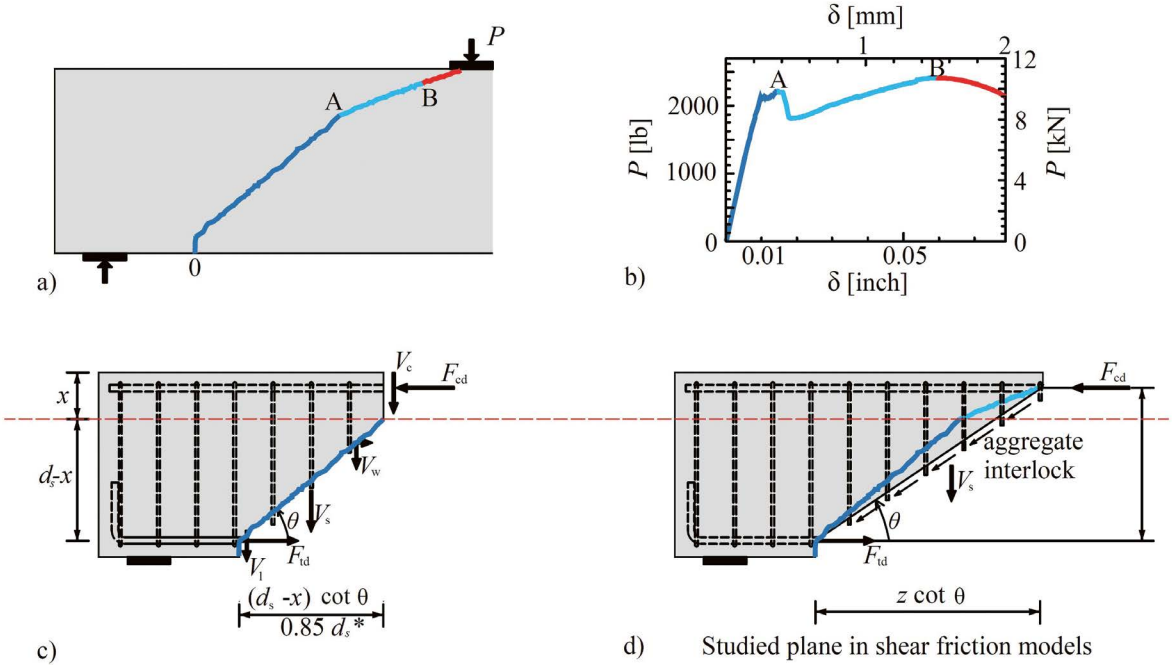

Figure 4. Qualitative scheme of crack propagation: a) crack trajectory [54]; b) load-displacement curve [54]; c) critical crack in MASM and simplified models; d) studied plane in shear friction models vs. the critical crack in MASM.

in the following subsections. Refer to the Notations section for the definition of the different parameters involved.

3.1. Relative neutral axis depth, x/d

The ratio of the neutral axis depth to the effective depth, x/d, is the key dimensionless parameter governing shear strength in the proposed model. For RC members, this parameter is determined by Eq. (8a), while for PC or RC members subjected to compressive axial loads, it is given by Eqs. (8b) and (8c).

As previously discussed and illustrated in Fig. 1, the shear critical crack (SCC) evolves from an initial flexural crack and develops in two distinct stages. This two-phase behavior has also been observed by other researchers during tests on notched specimens specifically designed to investigate mixed-mode crack propagation in reinforced concrete (see Figs. 4a and 4b) [54]. From Fig. 4, it becomes evident that internal forces may redistribute between stages 0-A and A-B of the load-displacement curve.

The MASM and its simplified models (Fig. 4c) focus on the crack stage corresponding to Point A in Fig. 4a, representing the onset of critical crack propagation. In contrast, models based on aggregate interlock or shear friction are typically concerned with the fully developed crack (Fig. 4d), where shear friction stresses are related to flexural strains, assessed at the level of the longitudinal reinforcement or at a specified depth in the web.

For quick estimations and to grasp the order of magnitude, typical x/d values as a function of the tensile reinforcement ratio, $\rho_{l,b}$, are $x/d \approx 0.20$ for lightly RC beams, $x/d \approx 0.25$ for conventionally RC beams, or $x/d \gtrapprox 0.35$ for heavily RC beams.

For PC members, Eqs. (8b) and (8c), derived in [36], apply. Notably, these formulas are straightforward and applicable to both prestressed members and members subjected to compressive loads. The increase in the neutral axis depth depends on the ratio $\frac{\sigma_{cp}}{\sigma_{cp}+f_{ct}}$, rather than solely on σ_{cp}.

The MASM (LoA III) has not been validated for members under tensile loads. However, the CCCM (LoA II) has been validated in such cases, as will be detailed in Section 4. For these scenarios, it is necessary to account for the concomitant bending moment, M_u, in the design sections [38].

3.2. Size and slenderness effect

The brittle nature of failure that occurs when the second branch of the critical crack propagates demands considering the size effect, which depends on the dimensions of the concrete region subjected to compressive and tensile stresses. To account for this, a combined size and slenderness factor is defined in Eq. (11). This factor integrates the size effect term proposed by the ACI Committee 446 [57] (first term in the equation) with a slenderness-dependent term, based on the shear span-to depth ratio, a/d, derived from empirical studies using genetic programming [58,59]. These studies demonstrated that the term $d/a^{0.21}$, simplified to $d/a^{0.2}$, accurately predicts the influence of slenderness. For accurate calculations in continuous beams or beams with distributed loads, it is recommended to refer to the definition of the shear span, a.

This integration represents a significant advancement, as it unifies the MASM and CCCM formulations while grounding the size effect treatment in a robust theoretical framework. In the original MASM formulation, an empirical factor proposed by other authors was adopted [25]. The updated approach is theoretically consistent, as the failure in the MASM is fully coherent with the failure explained by the fracture mechanics-based models [17,54,55].

3.3. Effective compression flange width

The influence of compression flanges on shear transfer mechanisms was thoroughly analyzed during the derivation of the MASM for T- and I-shaped beams [35]. However, to make the model more practical for everyday engineering applications, these effects were simplified into more compact expressions. In the MASM, the contribution of the compression flanges to shear strength is accounted for through an effective flange width, defined by Eqs. (9a) and (9b). This effective width depends on the section geometry and on the neutral axis depth. For further details, refer to the figure included in Table 1.

It should be noted that for rectangular beams, the effective flange width corresponds to the section width ($b = b_{v,eff} = b_w$). For L-shaped sections with a compression flange, the term $2h_f$ of Eq. (9a) is replaced by h_f, which represents the thickness of the compression flange.

3.4. Critical crack inclination

The inclination of the critical crack is a key parameter in evaluating shear strength, as it determines where the critical crack intersects the compression zone and affects the contribution of shear reinforcement, which depends on the number of stirrups intersecting the first branch of the critical crack. Based on experimental observations reported by the authors in [35], the horizontal projection of the first branch of the critical flexural-shear crack is assumed to be $0.85d_s$ (see Fig. 4c). This assumption corresponds to the crack inclination defined in Eq. (10).

Crack inclination is influenced by both the longitudinal and transverse reinforcement ratios, ρ_l and ρ_w, as these factors affect the strain distribution. However, longitudinal reinforcement has been found to have a more significant impact on crack inclination, as observed by other researchers [29,32]. For this reason, the MASM simplifies the analysis by focusing on the longitudinal reinforcement through its relationship with the neutral axis depth. This approach ensures the model remains straightforward and non-iterative, making it suitable for both design and assessment purposes.

As the longitudinal reinforcement ratio increases, the mean inclination angle of the critical crack decreases. This is consistent with the fact that for the same shear strain, the longitudinal tensile strain, ε_x, is lower when the longitudinal reinforcement ratio increases. For simplicity, the model assumes that the inclination angle of the critical crack is equal to the angle of the struts (θ), when verifying the maximum shear strength according to Eq. (4).

3.5. Position of the critical section and the critical point inside the compression chord

As the applied load increases, flexural cracks progressively develop with increasing bending moments. The critical crack is assumed to be the one closest to the zero bending moment point

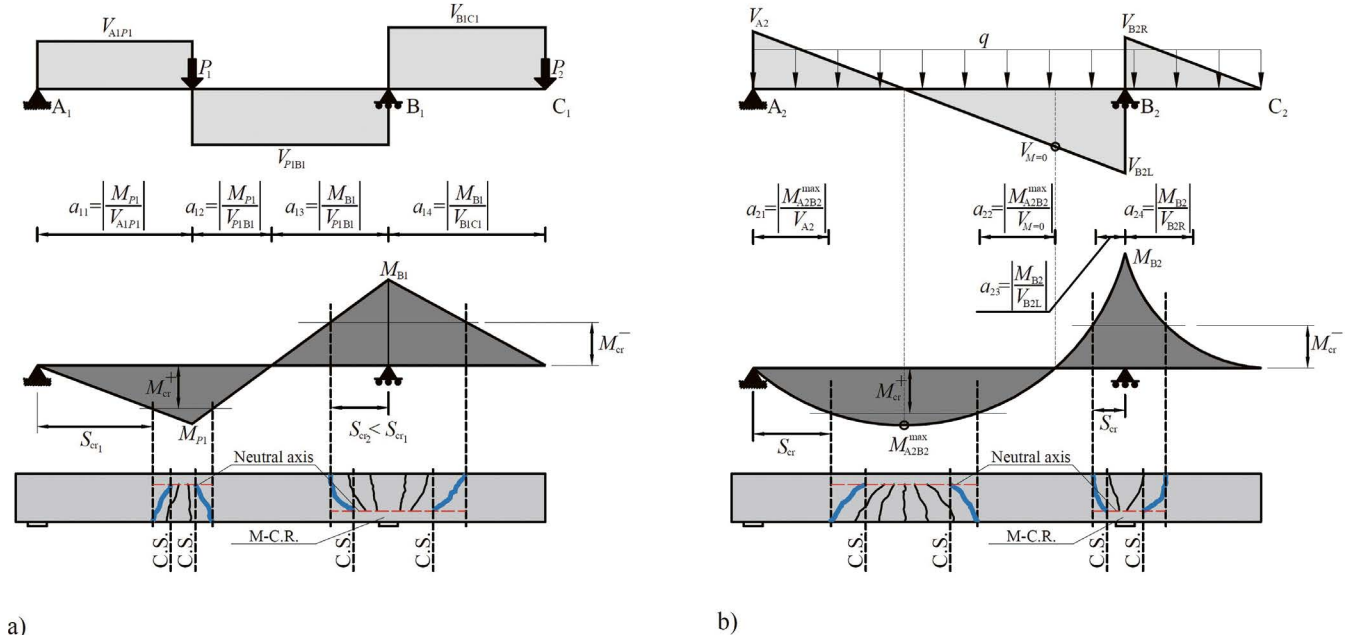

Figure 5. Location of critical section: a) Simply supported region and cantilever under concentrated loads; b) Simply supported region and cantilever under distributed loads.

Note: C.S.: critical section; M-C.R: multi-compressed region.

(see Fig. 1), initiating at the location where the bending moment diagram at failure reaches the cracking moment of the cross-section. The critical section, where equilibrium equations were set in the derivation of the model, is located at the point where this critical crack intersects the neutral axis depth (see Fig. 5).

Based on these considerations, and on the vertical crack horizonal projection defined in Section 3.4, the distance between the zero bending moment point and the initiation of the critical crack is $s_{cr} = M_{cr}/V_u$, and the critical section is positioned at $s_u = s_{cr} + 0.85d_s$. Typically, this distance slightly exceeds d_s, which is why, for design purposes, ds is used as the location to verify the shear strength of RC members.

In PC members, the higher cracking moment shifts the critical crack farther from the zero bending moment point compared to RC members. To address this, it is proposed to verify the shear strength at a section located at a distance $d_s(1+ 0.4\sigma_{cp}/f_{cm})$. The increased cracking moment in prestressed sections is incorporated into the mechanical model through the strength factor K_p (Eq. 13 in Table 1), while the influence of the compression or tensile flanges on the cracking loads is accounted for by factor K_T (Eq. 12). For RC beams without axial loads and rectangular cross-sections, $K_p = K_T = 1$.

The critical point within the compression chord, where failure is expected to initiate, corresponds to the location of maximum damage. Its position depends on the distributions of normal and shear stresses along the uncracked concrete chord. While this specific point is not directly used in the application of the MASM, it is of theoretical interest. Studies conducted by the authors [32] indicate that, assuming linear and parabolic distributions for the normal and shear stresses, respectively, the critical point is located at a distance of approximately $y \approx 0.425x$ from the neutral axis.

4. LEVEL OF APPROXIMATION II: THE COMPRESSION CHORD CAPACITY MODEL (CCCM)

The derivation of the CCCM equations (Table 2, Eqs. (14)-(21) and Figure 6) from MASM is detailed in Appendix A. To simplify the application of LoA II, the complete set of equations is provided, though many parameters (Eqs. 18a, 18b, 18c, 19a, 19b, 20 and 21) remain as defined for MASM in Table 1.

For RC beams, Eq. (18a) introduces a simplified expression for the relative neutral axis depth (term on the right), which shows good accuracy as demonstrated in [38]. A simplification for the expression of maximum shear strength is proposed in Eq. (17), with its derivation detailed in Annex A3.

The reduction of neutral axis depth for RC beams under tensile axial loads is addressed by Eq. (18d). While this approach simplifies the problem, the model still performs well, as shown in Section 7 and [60].

5. LEVEL OF APPROXIMATION I AND 0

In cases where lower computational effort is sufficient, LoA I provides a simplified alternative. Derived from LoA II (CCCM) as detailed in Appendix B, this approach assumes all cross-sections are rectangular, disregarding the beneficial effects of compression flanges. The model, outlined in Table 3 (Eqs. (22)-(28) and Figure 7), is applicable to RC and PC

TABLE 2.
Summary of the equations for the LoA II: CCCM

	Main expressions	
Shear strength	$V_{Rd} = V_{cu} + V_{su} \leq V_{Rd,max}$	(14)
Concrete contribution	$V_{cu} = \zeta \frac{x}{d} \frac{f_{ct}}{\gamma_v} b_{v,eff}\, d \prec V_{cu,min}$	(15)
	$V_{cu,min} = 0.18\left\{\zeta + \frac{100}{d_0}\right\} \frac{f_{ct}}{\gamma_v}\ b_w d$	(15a)
Shear reinforcement contribution	$V_{su} = 1.4\ (d_s - x)\ cot\theta\ \frac{A_{sw}}{s} f_{ywd}$	(16)
Maximum shear strength (strut crushing)	$V_{Rd,max} = \alpha_{cw}\ b_w\ z \nu_1\ f_{cd}\ \frac{cot\theta}{1+cot^2\theta} \approx 0.225\ f_{cd}\ b_w d$	(17)
Factors	***Expressions***	
Relative neutral axis depth	$\frac{x}{d} = \frac{x_0}{d} = \alpha_e\ \rho_{l,b} \left(-1 + \sqrt{1 + \frac{2}{\alpha_e \cdot \rho_{l,b}}}\right) \approx 0.75\ (\alpha_e\ \rho_{l,b})^{1/3}$	(18a)
	$N_{Ed} \neq 0\ \ or\ P \rightarrow 0 \leq \frac{x}{d} = \frac{x_0}{d} + \Delta_{x/d} \leq \frac{h}{d}$	(18b)
	$N_{Ed} > 0\ \ or\ P \rightarrow \Delta_{x/d} = \left(\frac{h}{d} - \frac{x_0}{d}\right)\left(\frac{d}{h}\right) \frac{\sigma_{cp}}{\sigma_{cp} + f_{ct}} > 0$	(18c)
	$N_{Ed} < 0 \qquad \rightarrow \Delta_{x/d} = 0.1\ \frac{N_{Ed}}{M_{Ed}} \frac{d_s}{d} < 0$	(18d)
Effective flange width	$if\ x \leq h_f \ \ \rightarrow \ \ b_{v,eff} = b_v = b_w + 2h_f \leq b$	(19a)
	$if\ x > h_f \ \ \rightarrow \ \ b_{v,eff} = b_w + (b_v - b_w)\left(\frac{h_f}{x}\right)^{3/2}$	(19b)
Critical crack inclination	$cot\ \theta = \frac{0.85\ d_s}{(d_s - x)} \leq 2.5$	(20)
Size and slenderness effect	$\zeta = \frac{2}{\sqrt{1 + \frac{d_0}{200}}} \left(\frac{d}{a}\right)^{0.2}$	(21)

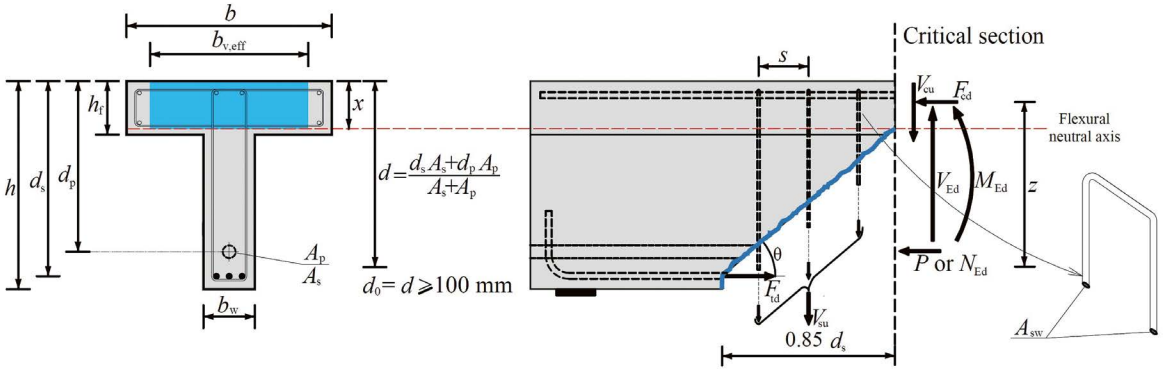

Figure 6. Graphical summary of the LoA II (CCCM) with the definition of the basic parameters.

elements with or without stirrups but does not account for tensile axial forces.

In the most complex case—a PC beam with an I-cross section and stirrups—LoA I requires only 7 equations and 12 variables, compared to the 18 equations and 21 variables used in LoA III (MASM, see Table 1). LoA II (CCCM) offers an intermediate level of complexity.

Eq. (24) defines the lower-bound shear strength for members with low longitudinal reinforcement, making it independent of the longitudinal reinforcement ratio. Due to its simplicity, this equation is designated as LoA 0. Note that within the brackets of Eq. (24), two size effects are considered: the compression chord size effect (ζ', left term) and the size effect due to the residual tensile stress transferred through the critical shear crack ($100/d_0$, right term).

6. UNCRACKED REGIONS IN BENDING

In highly prestressed, simply supported concrete beams—such as certain T- or I-shaped beams with minimal or no shear reinforcement—flexural cracking near the supports is often absent, even under significant loading. In these regions, the thin beam web experiences high shear stresses from the applied shear force, combined with compressive normal stresses induced by prestressing. This creates a biaxial stress state of compression and tension. When the principal stresses at the most critical point in the web exceed Kupfer's biaxial failure envelope [56], a diagonal crack forms across the entire beam height. Experimental evidence suggests that the cracking load in such cases is nearly identical to the ultimate load [61–63].

TABLE 3.
Summary of the Level of Approximation I procedure

	Main expressions	
Shear strength	$V_{Rd} = V_{cu} + V_{su} \leq V_{Rd,max}$	(22)
Concrete contribution	$V_{cu} = 1.35\zeta' \rho_{l,w}^{1/3} \frac{f_{ct}}{\gamma_v} b_w d(1+\Delta_{x/d}) \lessdot V_{cu,min}$	(23)
	$V_{cu,min} = 0.18\left\{\zeta' + \frac{100}{d_0}\right\} \frac{f_{ctm}}{\gamma_v} b_w d$	(24)
Shear reinforcement contribution	$V_{su} = 1.2 \frac{A_{sw}}{s} f_{ywd} d_s$	(25)
Maximum shear strength (strut crushing)	$V_{Rd,max} = 0.225 f_{cd} b_w d$	(26)
Factors	***Expressions***	
Prestressing effect	$N_{Ed} > 0 \;\; or \;\; P \rightarrow \Delta_{x/d} = \left(\frac{h}{d} - \frac{x_0}{d}\right)\left(\frac{d}{h}\right) \frac{\sigma_{cp}}{\sigma_{cp}+f_{ct}} > 0$	(27)
Size effect	$\zeta' = \frac{1.5}{\sqrt{1+\frac{d_0}{200}}}$	(28)

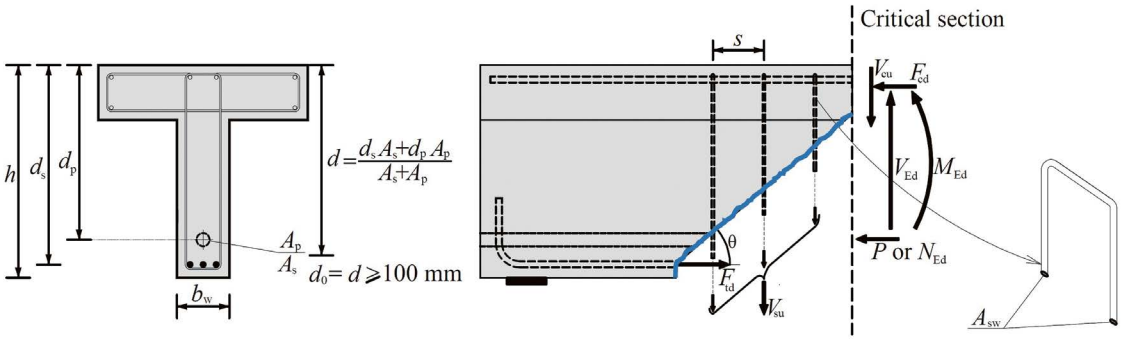

Figure 7. Graphical summary of the LoA I with the definition of the basic parameters.

As derived in [36], the shear strength under these conditions is given by Eq. (29):

$$V_{Rd} = \frac{I_c b_w}{S_c} 0.8 f_{ct} \sqrt{1+\alpha_1 \frac{\sigma_{cp}}{f_{ct}}} \tag{29}$$

The factor 0.8 in Eq. (29) accounts for the interaction between compressive and tensile stresses, as derived using Kupfer's failure envelope [36]. It is worth noting that some design codes omit this factor, which we consider a slightly unconservative approach.

For beams with transverse reinforcement, shear strength is calculated assuming the presence of flexural cracks. In such cases, the previously described levels of approximation (LoAs) should be used.

7. VALIDATION OF THE LOA 0, I, II AND III WITH EXPERIMENTAL DATABASES

The predictions of the defined Levels of Approximation (LoA) are validated against the ACI-DAfStb evaluation databases developed by ACI Subcommittee 445-D. These include RC beams without stirrups [64], RC beams with stirrups [65], PC beams without stirrups [66] and PC beams with stirrups [66]. Table 4 summarizes the primary statistics of the experimental-to-predicted strength ratios (V_{test}/V_{pred}).

For all comparisons in this paper, average concrete compressive strength and tensile steel strength values were used, with partial safety factors set to 1. For the concrete tensile strength, f_{ct}, and modulus of elasticity, E_c, the average values given in the Eurocode 2 of second generation [67] have been used (see Notations section for the exact definition).

Generally, as the LoA increases, both the mean V_{test}/V_{pred} ratio and its coefficient of variation (CoV) improve. LoA III demonstrates consistently low CoV across all databases, including the subsets of T-beams. In contrast, LoA I, which does not account for compression flanges, exhibits higher safety margins for T-beam subsets. Detailed comparisons with code-based methods are outside the scope of this paper but are available in [36,38]. Note that for PC beams without stirrups, each LoA is combined, depending on the cracking state for the predicted maximum load, with the shear strength for regions uncracked in bending.

Figure 8 illustrates the correlation between experimental results, V_{test}, and predictions for the four LoAs. The blue line represents perfect correlation, and dashed black lines indicate data trends, with R^2 values included. As observed, accuracy noticeably improves with higher LoA.

TABLE 4.
Comparison of tests results vs. predictions for different LoAs.

Database (or sub-database)	#	*LoA 0 ($V_{cu,min}$)*		*LoA I*		*LoA II*		*LoA III*	
		Mean	*CoV*	*Mean*	*CoV*	*Mean*	*CoV*	*Mean*	*CoV*
RC beams w/o stirrups	784	1.84	29.5%	1.27	22.9%	1.16	18.0%	1.03	17.8%
RC only T-beams w/o stirrups	64	2.19	35.6%	1.40	34.2%	1.09	22.2%	1.14	20.4%
RC beams with stirrups	170	1.53	22.4%	1.23	16.7%	1.14	14.2%	1.09	15.5%
RC only T-beams with stirrups	57	1.52	27.3%	1.34	15.1%	1.20	12.4%	1.21	12.7%
PC beams w/o stirrups	214	-	-	1.84	30.6%	1.21	22.8%	1.10	22.2%
PC only T-beams w/o stirrups	112	-	-	1.92	33.5%	1.21	21.8%	1.15	21.0%
PC beams with stirrups (115 with T-cross section)	117	-	-	1.48	23.2%	1.20	20.9%	1.10	14.4%

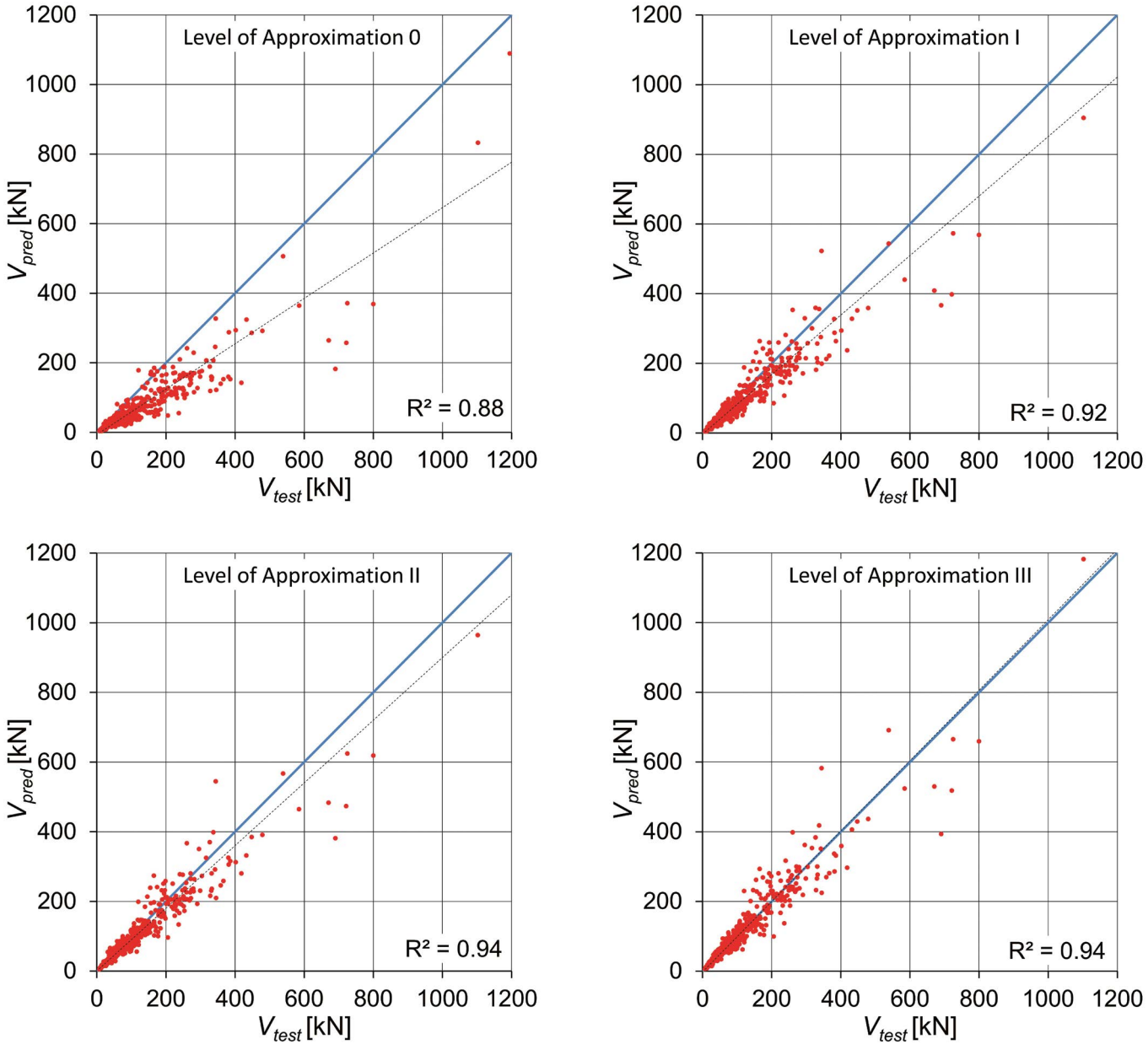

Fig. 8. Correlation between predictions and experimental results for RC beams w/o stirrups.

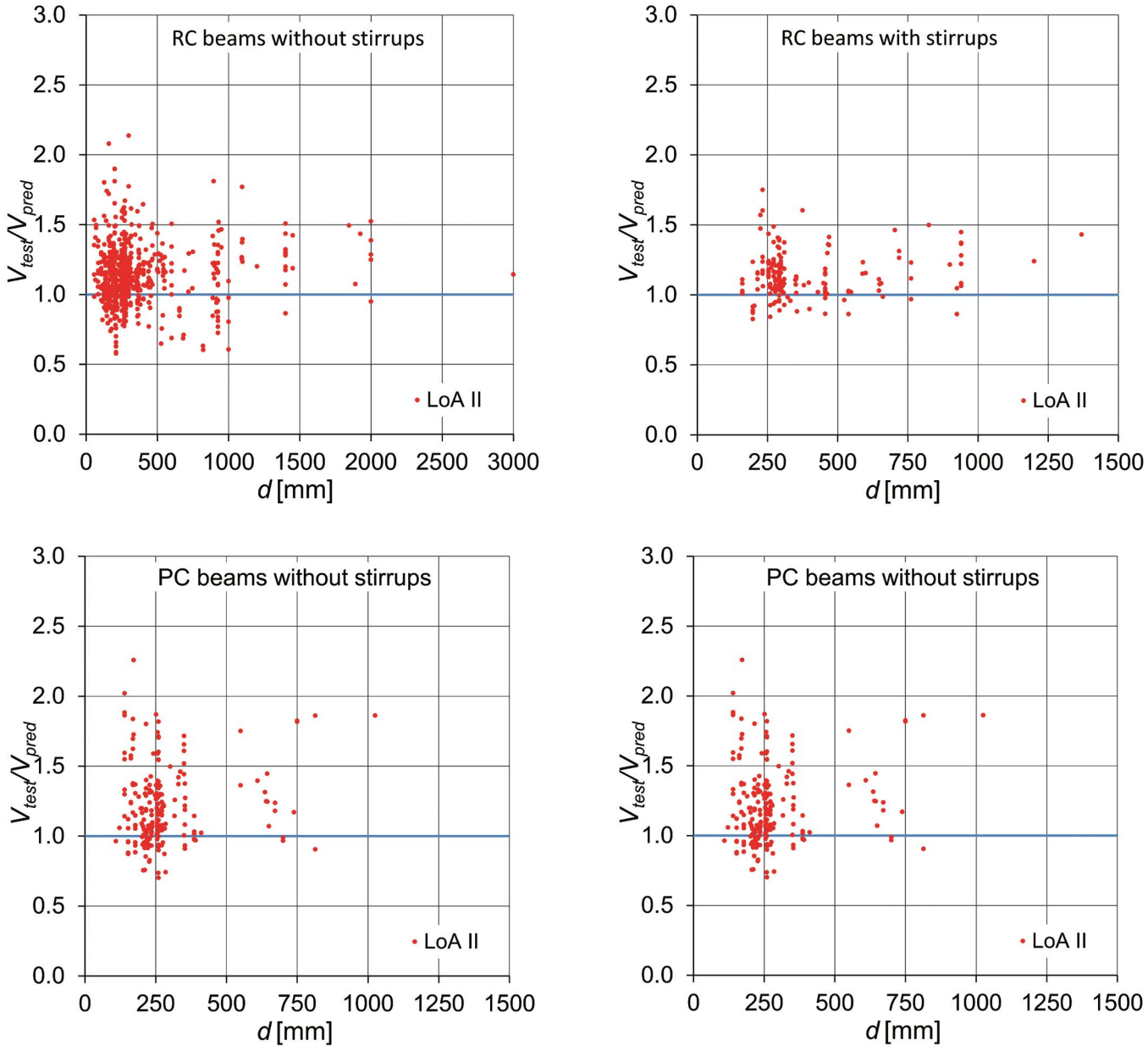

Figure 9. Correlation between LoA II and experimental results as a function of *d*.

Figure 9 shows the correlation between LoA II predictions and experimental results as a function of effective depth, *d*, for the four ACI-DAfStb databases. No significant trend against d is observed, confirming the appropriateness of the size effect factor.

It is worth noting that while the partial safety factor for concrete shear contribution is defined per Eurocode 2 (2nd generation) [67], this factor depends on the specific performance of the design model, as well as the uncertainties of its variables, so the direct interpolation to different models is, in general, not possible. Therefore, further reliability analyses are needed to calibrate the safety format of the presented LoAs for design purposes. As previously discussed, different shear mechanical models should be viewed as complementary rather than contradictory. For instance, for members with moderate or high amounts of shear reinforcement, variable-angle truss models based on plasticity offer a quick and practical design approach, particularly when torsion is present. For such members, a practical approach is to determine the maximum shear strength using either the models presented in this paper or variable-angle truss models based on plasticity, such as those included in the Eurocodes [67,68].

The LoA II (CCCM) incorporates the effect of axial tensile forces via Eq. (18d). To evaluate its predictive accuracy, two databases were analyzed. The first, from [69], includes 34 rectangular beams (a/d= 1.5–5.6) and 14 T-beams (a/d= 2.0). The second, from [70] contains 23 beams, some subjected to high axial tensile loads. Notably, Eurocode 2 predicts zero shear strength for 12 tests in this latter set, as noted in [60]. For the CCCM computations, the extension for non-slender beams presented in Section 8.1 has also been considered for beams with $a/d < 2.5$.

Figure 10 illustrates the V_{test}/V_{pred} correlations. For the first database (black and white circles), LoA II yields a mean ratio of 1.24 with a CoV of 21.1%. For the second (red circles), the mean ratio is 1.32 with a CoV of 13.8%. While these results are promising, it is crucial to note that under strong axial loads, $V_{cu,min}$ (Eq. (15b)) governs the prediction, as x/d may reduce to zero, rendering V_{cu} (Eq. (15a)) negligible. In such cases, the strong catenary effect could have had a significant impact on the shear strength, but this effect is outside the scope of this compact model. Careful application is advised in these scenarios.

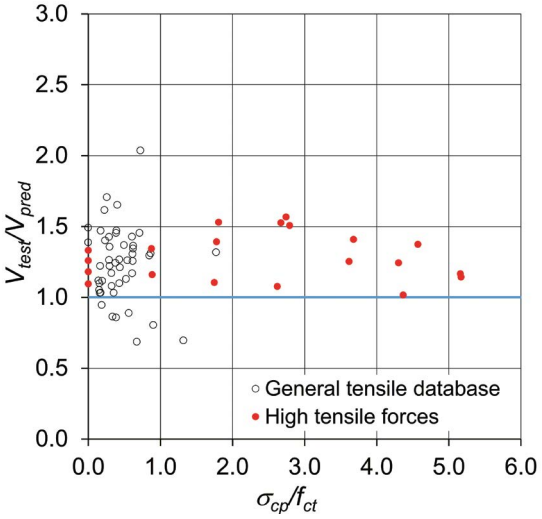

Figure 10. Correlation between LoA II predictions and experimental results as a function of non-dimensional tensile stress for the two databases.

8. MODEL EXTENSIONS

The following subsections present the key extensions developed by the authors. Each extension is summarized, followed by a brief comparison with the relevant databases for each case. For simplicity and computational efficiency, most extensions are based on LoA II, the Compression Chord Capacity Model.

8.1. Non-Slender Beams with and without stirrups

The shear strength of non-slender reinforced concrete beams, where $a/d \leq 2.5$, is enhanced due to arching action, as Kani [71] already showed in 1964. Existing shear design methods for such elements, including the strut-and-tie method (STM), show deviations from test results. The LoA II (CCCM), originally developed for slender beams, has been extended to non-slender beams. This extension incorporates the effects of non-planar strain distribution, the multi-compression stress state near the applied load, and the pre-determined position and inclination of the critical shear crack. The main equations for the extension are presented in Table 5 and Figure 11, with the full derivation provided in [39]. For any parameter or factor not listed in Table 5, the corresponding value from the CCCM (Table 2) should be used. This includes the relative neutral axis depth, x/d, for slender-beams.

The concrete contribution to shear strength is given by Eq. (30), which uses the shear strength for slender beams (dependent on x/d), multiplied by K_{ad}, a factor that accounts for the ratio between shear strengths in non-slender and slender beams (see Eq. 35).

To compute the contribution of the reinforcement to the shear strength, the relative neutral axis depth for non-slender beams must be determined. To account for the increase in neutral axis depth, a parabolic variation of x is assumed between a/d =2.5 (x_1=x, B-region) and a/d=0 (x_1=d), as seen in Eq. (36).

In non-slender beams, the critical shear crack develops straight and connecting the inner faces of the load to the support pads [72], with an inclination given by the shear-span-to-depth ratio, a/d, as seen in Eq. (37).

The web reinforcement contribution (Eq. 32) includes both vertical (stirrups) and horizontal reinforcement along the web. It is important to note that, in general, these reinforcements may not yield, and their stress contributions are considered using Eqs. (38a) and (38b).

To experimentally validate the proposed model for non-slender beams, the derived equations were used to predict the results of 486 tests. The datasets used for verification include: 222 tests on beams without web reinforcement [73], 178 tests on beams with vertical web reinforcement [74], and 86 tests on beams with horizontal and vertical web reinforcement [75]. The results are summarized in Table 6. Although some scatter is observed for RC beams without stirrups, the performance compares favorably to code procedures, as detailed in [39].

TABLE 6.
Comparison of tests results vs. predictions for non-slender beams.

Database	#	*LoA II*	
		Mean	*CoV*
RC beams w/o stirrups	222	1.47	29.5%
RC beams with vertical stirrups	178	1.19	19.4%
RC beams with vertical stirrups and longitudinal web reinforcement	86	1.37	22.1%

One fundamental contribution of the extension for non-slender beams is that it presents smooth continuity with LoA II for slender beams. This continuity is illustrated in Figure 12, which depicts results from Kani's renowned series of tests [23]. In these tests, key beam properties —such as width (154 mm), depth (610 mm), effective depth (539 mm), longitudinal reinforcement (ρ = 2.77 %, f_y =371.9 MPa), concrete and maximum aggregate size —were held relatively constant, while the shear-span-to-depth ratio, a/d, varied between 1 and 9. Because the beams were heavily reinforced longitudinally, flexural failures at midspan did not occur until a/d reached approximately 9 (beam 68 in Figure 12). The predictions for slender beams by LoA II (CCCM) are shown in red, while those for non-slender beams (a/d < 2.5) in blue. The figure highlights the satisfactory predictions and the consistency across both slender and non-slender beam cases.

TABLE 5.
Summary of the equations extended for non-slender beams

	Main expressions	
Shear strength	$V_{Rd} = V_{cu} + V_{su} \leq V_{Rd,max}$	(30)
Concrete contribution	$V_{cu} = \zeta \frac{x}{d} k_{ad} \frac{f_{ct}}{\gamma_v} b_{v,eff} d$	(31)
Web reinforcement contribution	$V_{su} = V_{swy} + V_{swx}$	(32)
Vertical web reinforcement	$V_{swy} = \frac{A_{swy}}{s_x} (d - x_1) \cot\theta \, \sigma_{swyd}$	(33)
Horizontal web reinforcement	$V_{swx} = 0.5 \frac{A_{swx}}{s_y} (d - x_1) \tan\theta \, \sigma_{swxd}$	(34)
Factors	***Expressions***	
Factor considering strength increase in non-slender beams	$k_{ad} = 1 + (2.5 - \frac{a}{d})^2$	(35)
Relative neutral axis depth	$\frac{x_1}{d} = \frac{x}{d} + (1 - \frac{x}{d})(1 - 0.4 \frac{a}{d})^2 \leq 1$	(36)
Critical crack inclination	$\cot\theta = \frac{a}{d} \geq 0.5$	(19a)
Stress at vertical and horizontal web reinforcement	$\sigma_{swy} = \frac{f_{ct} k_{ad}}{\rho_l} \frac{x_1}{d} \cot^3\theta \leq f_{ywd}$	(38a)
	$\sigma_{swx} = \frac{f_{ct} k_{ad}}{\rho_l} \frac{x_1}{d} \cot\theta \leq f_{ywd}$	(38b)

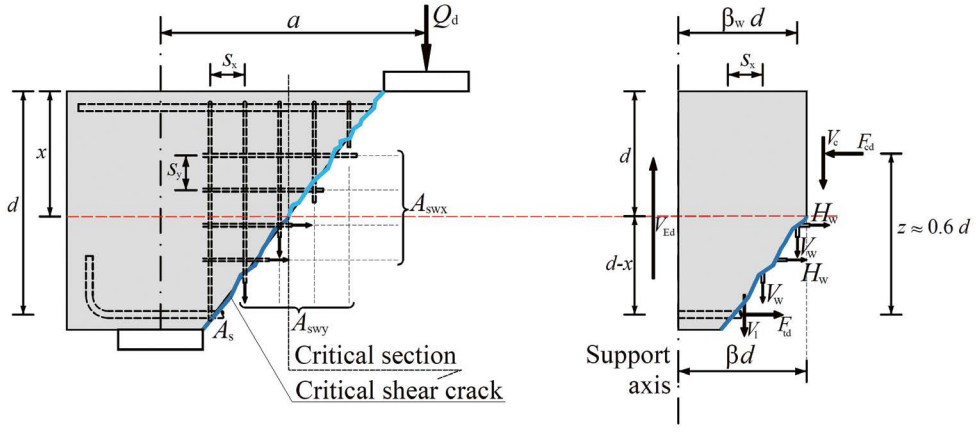

Figure 11. Graphical summary of the extension for non-slender beams.

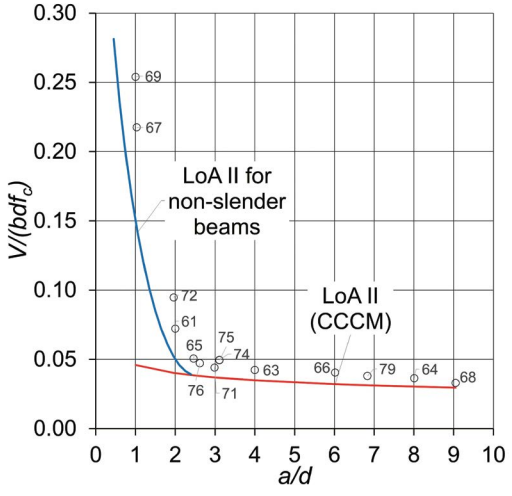

Figure 12. Predicted and observed strengths for Kani's RC beams [23].

8.2. Beams internally reinforced with FRP bars

For RC members reinforced internally with FRP bars—either longitudinal reinforcement alone or in combination with transverse FRP bars—crack widths tend to be larger than in beams reinforced with conventional steel bars [76]. This is due to the lower modulus of elasticity of FRP, which reduces aggregate interlock and increases the importance of shear transfer through the uncracked concrete chord. Notably, the development of MASM/CCCM models originated from this specific case [32,33].

For coherence with our other works, in this paper we propose using LoA II, i.e., the Compression Chord Capacity Model (Table 2), to also address this scenario. The modular ratio, α_e, should be computed considering the modulus of

elasticity of the FRP bars. Additionally, note that Eq. (15b), which defines $V_{c,min}$ is not applicable for RC beams reinforced internally with non-prestressed FRP bars. This equation assumed a significant contribution from shear transfer across the critical crack, v_w, which is less relevant in this context due to the material properties of FRP.

The contribution of the transversal FRP reinforcement, V_{fu}, is obtained using Eq. (16) but replacing the term f_{ywd} by σ_t, as defined in Eq. (39). This value accounts for two effects: 1) the tensile stress in FRP stirrups failing in the bent zone is assumed to be 45% of the ultimate strength of the straight portion of the bar, which corresponds to a mean value of the strength of the bent portion of the bar according to JSCE-97 [77] and ACI440.1R-15 [78] considering different ratios of the bent radius with respect to the bar diameter; and 2) σ_t represents the average stress of all stirrups crossing the critical crack, approximated as half of the stress in the most highly stressed stirrup.

$$\sigma_t = 0.225 \cdot f_{tu} \tag{39}$$

TABLE 7.
Comparison of tests results vs. predictions for beams with only FRP rebars.

Database (or sub-database)	#	*LoA II*	
		Mean	*CoV*
RC beams w/o stirrups	144	1.32	17.0%
RC beams with FRP stirrups	112	1.37	24.3%
PC beams with FRP tendons (with and w/o FRP stirrups)	55	1.13	25.8%

The LoA II model has been also extended for PC beams with FRP prestressing tendons, with and without FRP shear reinforcement [45]. The modifications described above for RC beams with FRP bars are applicable for this case, except that $V_{c,min}$ (Eq. 15b) is applicable in the case of PC beams with FRP prestressing tendons, as the prestressing action enhances the shear transfer across the critical crack. An additional particularity of beams with FRP tendons is that, as evidenced by experimental tests [79], they can potentially fail due to excessive slip of the tendon at the critical crack (shear-bond failure), owing to bond characteristics that are in many cases inferior to those of steel tendons. This type of failure will occur if the available bond length between the critical shear crack and the free end of the beam (l_{av}) is lower than the length required to develop the tensile force of the FRP tendon at the critical crack (l_{req}). Bond failure initiation will reduce the prestressing force and, as a result, the shear strength. This will also displace the position of the critical shear crack closer to the support. When $l_{av} < l_{req}$, an iterative procedure is needed to calculate the reduced value of the prestressing force P that will satisfy $l_{av}=l_{req}$ at the shear-bond failure. The available length l_{av} is the sum of the beam offset measured from the center of the support (e) and the position of the critical crack ($s_{cr} = M_{cr}/V_R$), while l_{req} is obtained by enforcing equilibrium along the bonded length and at the critical shear crack section [45]:

$$l_{req} = \frac{F_p}{u\ \tau_{max}} \tag{40}$$

$$F_p = \frac{M_{cr} + 0.85V_{cu}\ d + 0.2125V_{fu}\ d}{z} \tag{41}$$

where u is the nominal perimeter of the tendon, τ_{max} is the bond strength of the tendon, and F_p is the tensile force of the tendon at the critical crack.

A database of 55 tests has been used to assess the accuracy of the model extension for PC beams with FRP prestressing tendons. Most of the tests are on slender beams, but some non-slender elements (a/d<2.5) are also included in the database. Among the non-slender beams, there are beams without shear reinforcement which fail in shear in the absence of flexural cracking, due to the prestressing action. The correction factor for non-slender beams K_{ad} described in Eq. (35) was derived for the CCCM, and it is specific for beams cracked in flexure. An analogous correction factor $K_{ad,u}$ accounting for non-slender effects is proposed to modify the shear strength of uncracked beams V_{Rd} obtained with Eq. (29). The term $K_{ad,u}$ was derived in [45] based on an idealization of the arch and beam actions in non-slender uncracked beams:

$$K_{ad,u} = 1 + 2(1 - 0.4\ \frac{a}{d}) \geq 1 \tag{42}$$

The results of the model estimations for PC beams with FRP reinforcement are summarized in Table 6. As shown, the scatter of the results for PC beams is slightly higher than that for RC beams, consistent with trends observed for steel reinforcement. Notably, the model extension accounting for potential tendon slip is capable of predicting three out of the five shear-bond failures reported in the tests by [79], with the mean experimental-to-predicted strength ratio of 1.05 for these five tests and only one unsafe prediction (ratio < 1).

8.3. Steel Fiber Reinforced Concrete (SFRC) slender and non-slender beams without stirrups

The extension of the proposed model to slender and non-slender SFRC beams [40] was developed in collaboration with researchers from the University of Messina (Italy). The incorporation of steel fibers into concrete mixtures enhances shear behavior by delaying crack formation and improving the post-cracking tensile response. These enhanced mechanical properties significantly increase the shear strength of RC beams, as supported by numerous experimental studies [80–82].

The contribution of steel fibers was integrated into the equilibrium equations of the Multi-Action Shear Model (MASM). The residual tensile stresses of fiber reinforced concrete were addressed through a simplified formulation, which allowed the model to account for an improved compression chord contribution, direct shear transfer through the fiber-bridging effect along the critical shear crack, and enhanced dowel action provided by the fibers. Although these effects were initially modeled at the MASM level, the final expressions were compactly reformulated in [40], resulting in a practical LoA II procedure. The main equations for this extension are summarized in Table 8 and Figure 13, offering a

TABLE 8.
Summary of the LoA II for beams with Steel Fiber Reinforced Concrete without stirrups

	Main expressions	
Concrete contribution	$V_{cu} = [\zeta \frac{x}{d} k_{ad}(0.84-0.10 \frac{\sigma_{tu}}{f_{ct}})+0.08+1.10 \frac{\sigma_{tu}}{f_{ct}}] \frac{f_{ct}}{\gamma_v} b_{v,eff} d$	(43)
Maximum shear strength (strut crushing)	$V_{Rd,max} = \alpha_{cw} b_w z \nu_1 f_{cd} \frac{cot\theta}{1+cot^2\theta} \approx 0.225 f_{cd} b_w d$	(44)
Factors	***Expressions***	
Relative neutral axis depth	$\frac{x}{d} = \frac{x_0}{d} = \alpha_e \rho_{l,b} \left(-1+\sqrt{1+\frac{2}{\alpha_e \cdot \rho_{l,b}}}\right) \approx 0.75 (\alpha_e \rho_{l,b})^{1/3}$	(45)
Relative neutral axis depth	$\frac{\sigma_{tu}}{f_{ct}} = 2\eta_0 \eta_1 F_\tau \leq 1$	(46)

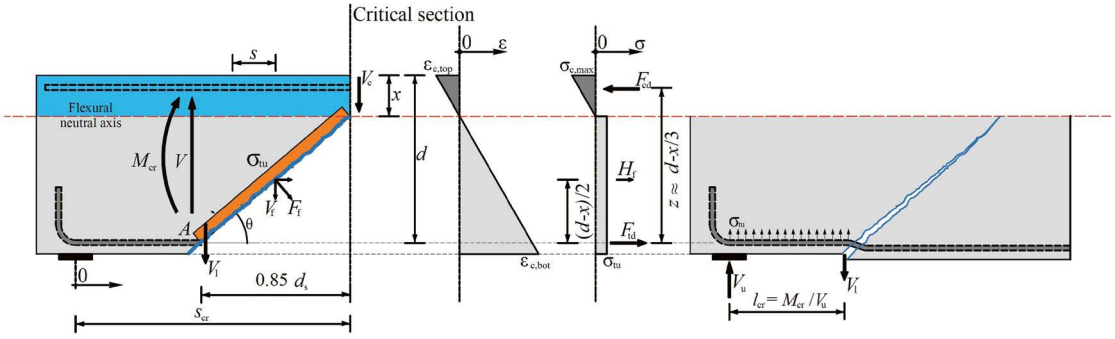

Figure 13. Graphical summary of the extension for SFRC beams without stirrups.

straightforward approach for designers while maintaining accuracy in predicting the shear strength of SFRC beams, both for slender and non-slender beams.

For non-slender SFRC beams, the Kad factor in Eq. (43), given by Eq. (35), adjusts the shear strength to account for arching action. Additionally, the concrete contribution is expressed as proportional to the relative neutral axis depth of an equivalent beam made with conventional concrete (Eq. (42)).

The non-dimensional average residual tensile stress of fibrous concrete in tension, σ_{tu}, is derived from the constitutive law proposed by Lim et al. [83] and is summarized in Eq. (46). Detailed definitions of the involved parameters are provided in the Notations section, while further derivations and explanations can be found in [40].

To validate this model, a database compiled by Lantsoght [80,84] was utilized. The structural parameters in the database vary over a wide range; however, the mechanical characterization of SFRC was not reported. Nevertheless, when experimental results for the post-cracking tensile stress of SFRC are available, they are often obtained using different experimental protocols, making homogenization of the data challenging [80]. Practical values of the fiber volume fraction (V_f) are used (0.5–1.5%), which result in workable mixes and serve the purpose of partially replacing conventional steel reinforcement.

Table 9 summarizes the correlation between experimental and predicted shear strengths for the entire database and specific subsets. The correlations are satisfactory, and they can be compared with those of different code procedures detailed in [40].

TABLE 9.
Comparison of tests results vs. Lantsoght database [80,84].

Database or subset	*#*	*LoA II*	
		Mean	*CoV*
All beams	488	1.17	23.8%
Only beams failing in shear according to the model (flexural check)	324	1.18	24.7%
Failing in shear with $a/d \geq 2.5$	223	1.15	25.6%
Failing in shear with $a/d < 2.5$	101	1.24	22.5%

8.4. RC beams without stirrups subjected to fatigue loads

Shear fatigue failures in reinforced concrete elements without shear reinforcement can govern the design of structures subjected to a high number of load cycles, such as wind towers, offshore structures, bridge decks, precast slabs for railways tracks, and similar applications.

The study of shear fatigue behavior in RC elements without shear reinforcement has a long history, and the associated failure modes are well understood. In 1958, Chang and Kesler [85,86] classified these failure modes into two main groups: the first involves fatigue failure of the longitudinal reinforcement under tension, while the second occurs when the compression zone at the top of the diagonal (shear) crack becomes too small to resist the applied load, due to combined compression and shear stresses.

The MASM/CCCM models define failure using Kupfer's envelope, which considers a combination of compressive and tensile stresses, although tensile stresses primarily govern. As such, the concrete contribution to shear resistance is consist-

ently expressed as a function of the concrete tensile strength in all proposed models (see Eqs. (2), (15), (23), (31), and (43)). This was the foundational assumption for extending the CCCM model (LoA II) to RC beams without stirrups subjected to fatigue loads [41].

Different approaches were employed to account for the reduction of the shear strength under fatigue loading. In the first one, the Model Code 2010 [87] expression for the degradation of concrete tensile strength due to the number of load cycles, N, was used. This relationship is expressed as shown in Eq. (47):

$$\sigma_{ct,max} = f_{ct}\left(1 - \frac{log\ N}{12}\right) \tag{47}$$

An alternative approach, based on Fernández-Ruiz et al. [88], applied Fracture Mechanics principles for quasi-brittle materials. This model considers the ratio of maximum to reference shear strength, V_{max}/V_{ref}, as a function of the load cycle ratio, $R = V_{min}/V_{max}$, and the number of load cycles, N, as expressed in Eq. (48):

$$\frac{V_{max}}{V_{ref}} = \eta \frac{1}{R + N^{\frac{1}{m}}(1-R)} \leq 0.5 \tag{48}$$

In this equation, m is an empirically derived coefficient equal to 17, and the threshold of 0.5 also refer to the average test response. The authors [88] recognized that these values could be adapted, if necessary, to respect a target safety level. The term η is a multiplying factor of static strength due to the loading rate, considered equal to 1 in [41] and in this paper, balancing two considerations: the implicit value of 0.9 suggested by Eurocode 2 [68] to reflect long-term effects on compressive strength, and the value of 1.1 proposed by Fernández-Ruiz et al. [88] to account for the increased concrete compressive strength observed in tests conducted at a loading rate of 1 Hz compared to failure times of approximately 1 hour in standard beam tests. Further details on this topic can be found in [41].

For facilitating the comparison with tests results, Eq. (48) can be reformulated in terms of V_{min}/V_{ref} (see Eq. 49):

$$\frac{V_{max}}{V_{ref}} = \eta N^{-1/m} + \frac{V_{min}}{V_{ref}}\left(1 - N^{-1/m}\right) \leq 0.5 \tag{49}$$

A database of fatigue tests on shear-critical beams, comprising 87 tests, was used to validate both approaches. This database, originally developed in [89], was later expanded and published in [88]. The primary results are summarized in Table 10.

The second method, which accounts for the load cycle ratio, R, provides slightly better and more consistent results across the entire range of log N values analysed (see Figure 14). Nevertheless, the differences between the two methods are minimal. Further empirical comparisons, presented in terms of Goodman diagrams, are available in [41].

TABLE 10.
Comparison of tests results vs. fatigue tests results.

Method	#	*LoA II*	
		Mean	*CoV*
LoA II with Eq (47)	87	1.15	14.6%
LoA II with Eqs. (48-49)	87	1.19	13.3%

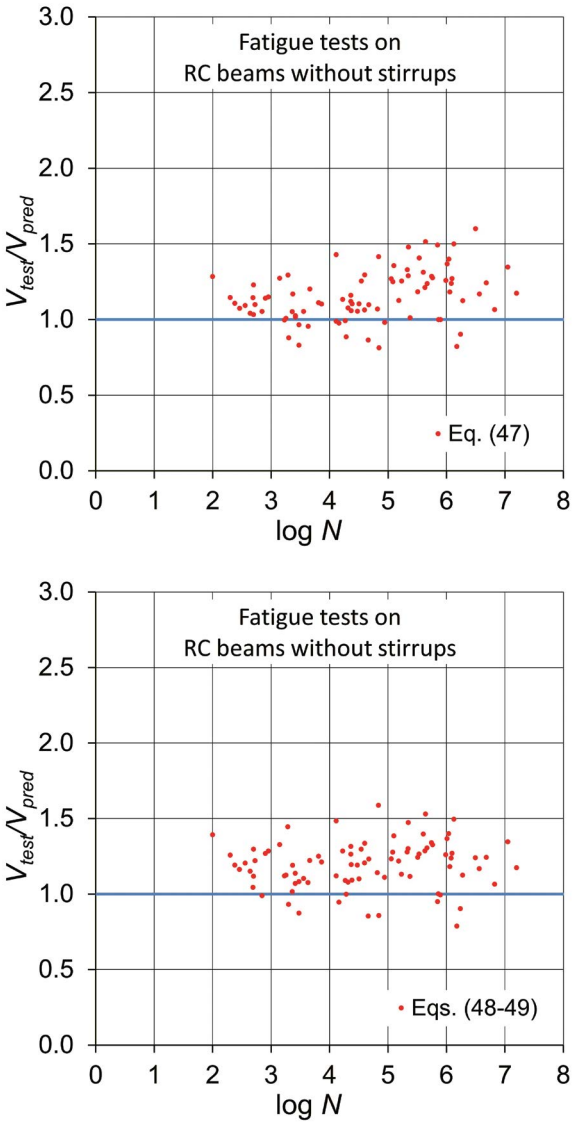

Figure 14. Correlation between predictions and experimental results for the two approaches considered for fatigue loads.

9. CONCLUSIONS

A unified mechanical model for the shear strength of slender and non-slender reinforced and prestressed concrete beams has been developed, applicable to beams with rectangular, T-, or I-shaped sections. Some distinct features of the presented model are:

- The model, based on the Multi-Action Shear Model (MASM), effectively integrates shear transfer actions such as compression chord contribution, residual tensile stresses across the critical crack, dowel action, and transversal reinforcement effects (if present).
- The Levels-of-Approximation (LoA) framework enables the application of the model in a wide range of structural design and assessment scenarios, with increasing complexity from LoA 0 (preliminary design) to LoA III (detailed assessment). Specifically, LoA III is based on the MASM,

and LoA II on the Compression Chord Capacity Model (CCCM). All LoAs provide continuous models for members with or without shear reinforcement.

- As highlighted in the introductory section of this paper, different mechanical approaches are valid for addressing the shear failure problem, and various models should be viewed as complementary rather than contradictory. For instance, for members with moderate or high amounts of shear reinforcement, variable-angle truss models based on plasticity offer a quick and practical design approach, particularly when torsion is present.
- The extension of LoA II (CCCM) to cover specific cases, such as the shear strength of non-slender beams, RC and PC beams reinforced with fiber reinforced polymers (FRP) bars, steel fiber reinforced concrete (SFRC) members, and fatigue loads for RC beams without stirrups, has been also presented.
- Validation of the model using 2,714 experimental tests from 14 databases has shown its accuracy and versatility, with improved prediction consistency and reduced scatter at higher LoAs.

This work contributes a robust tool for the design and assessment of structural concrete elements, offering a systematic approach that combines advanced mechanics with engineering practice. Looking ahead, future work will focus on conducting a comprehensive reliability analysis to assess the sensitivity and robustness of the model under varying conditions, particularly considering uncertainties in material properties, geometry, and loading. Such an analysis would be important for calibrating the models to the levels recommended by current standards and determining the most appropriate safety format, whether through partial safety factors or a global factor. Further research could also explore the application of the model to more complex geometries or hybrid materials, such as combinations of steel, FRP, and SFRC. Additionally, integrating the model into advanced structural design software could greatly enhance its usability in practical engineering scenarios.

Acknowledgements

This paper is dedicated to Prof. Antonio Marí, the leading force behind our 12 years of research on shear strength and the scientific father of the Multi-Action Shear Model. His guidance, wisdom, and vision have been an inspiration to all of us, and we owe him the deepest gratitude as our master, mentor and friend throughout these years. Additionally, we extend this dedication to Prof. Hugo Corres, whose insightful discussions and valuable contributions to the topic of shear strength have greatly enriched our work.

We would also like to acknowledge the financial support provided by grants TED2021-130272B-C21 / TED2021-130272B-C22 funded by MICIU/AEI/10.13039/501100011033 and the European Union Next Generation/PRTR, as well as grants PID2021-123701OB-C21 / PID2021-123701OB-C22 funded also by MICIU/AEI/10.13039/501100011033 and by ERDF/EU.

Notations

a	shear span, equal to $M_{Ed,max}/V_{Ed,max}$, where $M_{Ed,max}$ and $V_{Ed,max}$ are the maximum absolute values of the internal forces in the region between the maximum bending moment and the zero bending moment in which the considered section is located. This is equivalent to the distance from the support to the resultant of the loads producing shear at that support. Design values for uniformly distributed load, $a=0.25L$ (simple supported); $a=0.5L$ (cantilever); $a=0.2L$ (sagging moment regions in continuous beams); $a=0.15L$ (hogging moment regions in continuous members)
b	cross-section width. For T/I-sections, flexural effective compression flange width
b_{tens}	tensile flange width
$b_{v,eff}$	effective width for shear strength calculation
b_w	web width for T/I/L beams; for rectangular beams $b_w = b$
d	effective depth, $d=\frac{A_s d_s + A_p d_p}{A_s + A_p}$
d_0	minimum effective depth for size effect factor, d_0 = d≥100 mm
d_f	fiber diameter
d_{max}	maximum aggregate size
d_s	distance from maximum compressed concrete fiber to the centroid of mild steel tensile reinforcement. For elements with only prestressed reinforcement, $d_s = d_p$
d_p	distance from maximum compressed concrete fiber to the centroid of prestressing tendons placed at the tension zone
f_{cd}	design compressive strength of concrete
f_{ck}	characteristic compressive strength of concrete ($f_{ck} \leq 100$ MPa)
f_{cm}	mean compressive strength of concrete
f_{ct}	tensile strength of concrete, as per second generation of Eurocode 2 in this paper: $f_{ct}=f_{ctm}= 0.3f_{ck}^{2/3}$ if $f_{ck} \leq 50$ MPa, and $f_{ct}=f_{ctm}=1.1f_{ck}^{1/3}$ if $f_{ck} > 50$ MPa
f_{tu}	ultimate strength of FRP transverse reinforcement
f_{ywd}	design yield strength of shear reinforcement
h	overall cross-section depth
h_f	compression flange height. For haunched T/I/L beams, flange height + half the haunch
$h_{f,tens}$	tensile flange height. In T, I or L beams with haunches, $h_{f,tens}$ can be considered the flange height plus half the haunch
l_{av}	available bond length of prestressing tendon between critical shear crack and free end of the beam
l_c	critical fiber length, $\frac{\sigma_{fy} d_f}{2\tau_f}$
l_{req}	bond length required to develop the tensile force of prestressing tendon at the critical crack
s	stirrups spacing
u	nominal perimeter of FRP tendon.
x	neutral axis depth assuming zero concrete tensile strength
x_0	neutral axis depth for RC or PC members assuming $P = 0$
y_t	distance from the concrete section centroid to the most tensioned fiber
z	inner lever arm, approximate value $z \approx 0.9d$ may normally be used

A_c concrete cross-sectional area

A_p prestressing steel (tensile zone) cross-sectional area

A_s mild steel reinforcement (tensile zone) cross-sectional area

A_{sw} shear reinforcement cross-sectional area

E_{cm} secant modulus of elasticity of concrete, $E_{cm}=kE\ fcm^{1/3}$; for concrete with quartzite aggregates k_E = 9500 (value assumed in this paper)

E_s elastic modulus of mild reinforcement (200 GPa)

E_p elastic modulus of prestressing steel (195 GPa, if unspecified)

F_p tensile force of FRP tendon at critical crack.

F_τ fiber factor, $F_\tau=\beta_\tau\ V_f \frac{l_f}{d_f}$

G_f concrete fracture energy, $G_f = 0.028 f_{cm}^{0.18}\ d_{max}^{0.32}$

I_c second moment of area

K_{ad} factor that accounts for ratio between shear strengths of cracked non-slender and slender beams

$K_{ad,u}$ factor that accounts for ratio between shear strengths of uncracked non-slender and slender beams

K_p strength factor for axial load (including prestressing) and bending moment interaction

K_T strength factor for T/I-sections relative to rectangular beams

L_f fiber length

M_{Ed} design bending moment (positive)

N_{Ed} design axial/prestressing force (compression positive)

P prestressing tendon force after losses

S_c first moment of area above the centroid

V_{cu} concrete contribution to the shear strength

V_f volumetric percentage of fibers

V_{fu} shear FRP reinforcement contribution to the shear strength

V_{su} shear reinforcement contribution to the shear strength

V_{Ed} design shear force in the section

V_{Rd} design shear resistance of the member

$V_{Rd,max}$ maximum design shear resistance limited by strut crushing

α angle between shear reinforcement and beam axis perpendicular to the shear force

α_{cw} coefficient for stress in the struts: α_{cw}=1 for non-prestressed structures; $\alpha_{cw}=1+\sigma_{cp}/f_{cdfor}$ $0\le\sigma_{cp}\le0.25f_{cd}$; α_{cw}=1.25 for $0.25f_{cd}<\sigma_{cp}\le0.50f_{cd}$; and $\alpha_{cw}=2.5(1-\sigma_{cp}/f_{cd})$ for $0.50f_{cd}<\sigma_{cp}\le f_{cd}$

α_e modular ratio, $\alpha_e=E_s/E_{cm}$

α_l prestressing force transfer degree, which is ≤ 1.0 for pretensioned tendons, and equal to 1.0 for other types of prestressing

β_τ ratio of mean fiber-matrix shear stress to tensile strength, $\beta\tau=\tau_f/f_{ct}$. In the typical case of concrete matrix, β_τ adopts the value of 1.45 for hooked fibers and 0.70 for straight fibers. Mean value considered for crimped fibers

δ_p angle between prestressed tendon axis and beam axis

γ_v partial factor for concrete shear contribution. According to the 2nd generation of EC2, = 1.4 for persistent and transient design situation or fatigue. For accidental design situation 1.15. Necessary to carry out a reliability analysis to confirm these values.

η_0 fiber orientation factor, η_0 = 0.405.

η_1 fiber length efficiency factor. If $L_f \le l_c \rightarrow \eta_1 = 0.5$; otherwise $\eta_1=1-\frac{L_c}{2L_f}$

υ_1 strength reduction factor for concrete cracked in shear, υ_1 = 0.6 for $f_{ck} \le 60$ MPa and $\upsilon_1 = 0.9\text{-}f_{ck}/200$ for $f_{ck} > 60$ MPa

θ strut angle with respect beam axis

$\rho_{l,b}$ longitudinal tensile reinforcement ratio relative to effective depth d and the width b. For members with mild steel reinforcement and tendons, $\alpha_e\ \rho_{l,b}=\alpha_{e,s}\ \rho_{s,b}+\alpha_{e,p}\ \rho_{p,b}$ being $\alpha_{e,s}=E_s/E_{cm}$, $\alpha_{e,p}=E_p/E_{cm}$, $\rho_{s,b}=A_s/b_d$, $\rho_{p,b}=A_p/\ b_d$ and b the width of the cross-section. For the case of unbonded tendons, A_p = 0.

$\rho_{l,w}$ same as $\rho_{l,w}$ but relative to web width b_w

σ_{cp} concrete compressive stress at the centroid due to axial/prestressing load,$\sigma_{cp} = N_{Ed}/A_c$ (N_{Ed}>0 compression)

σ_{sy} steel fiber yield strength

σ_t mean value of the tensile stresses in the FRP stirrups crossing the shear critical crack

τ_f mean fiber-matrix shear stress. See definition of β_τ

τ_{max} bond strength of FRP tendon.

ζ combined size and slenderness effect factor (LoAs II and III)

ζ' size effect factor for LoA I, equal to ζ but assuming a/d = 4

References

[1] Mörsch E. Concrete-Steel Construction (Der Eisenbetonbau), authorized translation form the third German Edition. New York: The Engineering News Publishing Company; 1909.

[2] Faber O. Researches on Reinforced Concrete Beams with New Formulae for Resistance to Shear. Parts I, II, III and shear tests (1914 series). Concrete and Constructional Engineering (London) 1916;11:233–605.

[3] Fenwick RC. The shear strength of reinforced concrete beams. University of Canterbury, 1966.

[4] Fenwick RC, Paulay T. Mechanisms of shear resistance of concrete beams. ASCE J Struct Div 1968;94:2325–50.

[5] ACI-ASCE Committee 426. The Shear Strength of Reinforced Concrete Members. ACI Journal Proceedings, vol. 70, ACI; 1973, p. 1091–187.

[6] Walraven JC. Fundamental analysis of aggregate interlock. ASCE J Struct Div 1981;107:2245–70.

[7] Haskett M, Oehlers DJ, Mohamed Ali MS, Sharma SK. Evaluating the shear-friction resistance across sliding planes in concrete. Eng Struct 2011;33:1357–64. https://doi.org/10.1016/j.engstruct.2011.01.013.

[8] Walraven JC. Aggregate interlock: A theoretical and experimental analysis. Delft University, 1980.

[9] Leonhardt F. Shear and torsion in prestressed concrete. VI FIP Congresss Prague, vol. Session IV, 1970.

[10] Regan PE. Research on shear: a benefit to humanity or a waste of time? Structural Engineer 1993;71:337.

[11] Belarbi A, Kuchma DA, Sanders DH. Proposals for New One-Way Shear Equations for the 318 Building Code. Concrete International 2017;39:29–32.

[12] Li Y-A, Hsu TTC, Hwang S-J. Shear Strength of Prestressed and Nonprestressed Concrete Beams. Concrete International 2017;39:53–7.

[13] Park H-G, Choi K-K. Unified Shear Design Method of Concrete Beams Based on Compression Zone Failure Mechanism. Concrete International 2017;39:59–63.

[14] Reineck K-H. Proposal for ACI 318 Shear Design Members without Shear Reinforcement. Concrete International 2017;39:65–70.

[15] Bentz EC, Collins MP. Updating the ACI Shear Design Provisions. Concrete International 2017;39:33–8.

[16] Cladera A, Marí A, Bairán J-M, Oller E, Ribas C. One-Way Shear Design Method Based on a Multi-Action Model A compromise between simplicity and accuracy. Concrete International 2017;39:40–6.

[17] Frosch RJ, Yu Q, Cusatis G, Bažant ZP. A Unified Approach to Shear Design. Concrete International 2017;39:47–52.

[18] Campana S, Ruiz MF, Anastasi A, Muttoni A. Analysis of shear-transfer actions on one-way RC members based on measured cracking pattern and failure kinematics. Magazine of Concrete Research 2013;65:386–404. https://doi.org/10.1680/macr.12.00142.

[19] Cavagnis F, Fernández Ruiz M, Muttoni A. Shear failures in reinforced concrete members without transverse reinforcement: An analysis of the critical shear crack development on the basis of test results. Eng Struct 2015;103:157–73. https://doi.org/10.1016/J.ENGSTRUCT.2015.09.015.

[20] Cavagnis F, Fernández Ruiz M, Muttoni A. An analysis of the shear-transfer actions in reinforced concrete members without transverse reinforcement based on refined experimental measurements. Structural Concrete 2018;19:49–64. https://doi.org/10.1002/SUCO.201700145.

[21] Huber P, Huber T, Kollegger J. Investigation of the shear behavior of RC beams on the basis of measured crack kinematics. Eng Struct 2016;113:41–58. https://doi.org/10.1016/J.ENGSTRUCT.2016.01.025.

[22] Huber T, Huber P, Kollegger J. Influence of aggregate interlock on the shear resistance of reinforced concrete beams without stirrups. Eng Struct 2019;186:26–42. https://doi.org/10.1016/J.ENGSTRUCT.2019.01.074.

[23] Kani MW, Huggins MW, Wittkopp RR. Kani on shear in reinforced concrete. Dept. of Civil Engineering, University of Toronto; 1979.

[24] Montoya-Coronado LA, Ribas C, Ruiz-Pinilla JG, Cladera A. Time-history analysis of aggregate interlock in reinforced concrete beams without stirrups. Eng Struct 2023;283:115912. https://doi.org/10.1016/j.engstruct.2023.115912.

[25] Zararis PD, Papadakis GC. Diagonal shear failure and size effect in RC beams without web reinforcement. Journal of Structural Engineering 2001;127:733–42. https://doi.org/10.1061/(ASCE)0733-9445(2001)127:7(733).

[26] Tureyen AK, Frosch RJ. Concrete Shear Strength: Another Perspective. ACI Struct J 2003;100:609–15.

[27] Park HG, Kang S, Choi KK. Analytical model for shear strength of ordinary and prestressed concrete beams. Eng Struct 2013;46:94–103. https://doi.org/10.1016/j.engstruct.2012.07.015.

[28] Muttoni A, Fernandez-Ruiz M. Shear Strength of Members without Transverse Reinforcement as Function of Critical Shear Crack Width. ACI Struct J 2008;105:163–72.

[29] Collins MP, Bentz EC, Sherwood EG, Xie L. An adequate theory for the shear strength of reinforced concrete structures. Magazine of Concrete Research 2008;60:635–50.

[30] Bairán JM, Marí A, Cladera A. Analysis of shear resisting actions by means of optimization of strut and tie models taking into account crack patterns. Hormigón y Acero 2018;69:197–206. https://doi.org/10.1016/j.hya.2017.04.009.

[31] Ribas C, Cladera A. Experimental study on shear strength of beam-and-block floors. Eng Struct 2013;57:428–42. https://doi.org/10.1016/j.engstruct.2013.10.001.

[32] Marí A, Cladera A, Oller E, Bairán J. Shear design of FRP reinforced concrete beams without transverse reinforcement. Compos B Eng 2014;57:228–41. https://doi.org/10.1016/j.compositesb.2013.10.005.

[33] Oller E, Marí A, Bairán JM, Cladera A. Shear design of reinforced concrete beams with FRP longitudinal and transverse reinforcement. Compos B Eng 2015;74:104–22. https://doi.org/10.1016/j.compositesb.2014.12.031.

[34] Marí A, Bairán J, Cladera A, Oller E, Ribas C. Shear-flexural strength mechanical model for the design and assessment of reinforced concrete beams. Structure and Infrastructure Engineering 2015;11:1399–419. https://doi.org/10.1080/15732479.2014.964735.

[35] Cladera A, Marí A, Ribas C, Bairán J, Oller E. Predicting the shear–flexural strength of slender reinforced concrete T and I shaped beams. Eng Struct 2015;101:386–98. https://doi.org/10.1016/j.engstruct.2015.07.025.

[36] Marí A, Bairán JM, Cladera A, Oller E. Shear Design and Assessment of Reinforced and Prestressed Concrete Beams Based on a Mechanical Model. Journal of Structural Engineering 2016;142:04016064. https://doi.org/10.1061/(ASCE)ST.1943-541X.0001539.

[37] Marí A, Cladera A, Bairán J, Oller E, Ribas C. Un modelo unificado de resistencia a flexión y cortante de vigas esbeltas de hormigón armado bajo cargas puntuales y repartidas. Hormigón y Acero 2014;65:247–65. https://doi.org/10.1016/j.hya.2014.11.001.

[38] Cladera A, Marí AR, Bairán JM, Ribas C, Oller E, Duarte N. The compression chord capacity model for the shear design and assessment of reinforced and prestressed concrete beams. Structural Concrete 2016;17:1017–32. https://doi.org/10.1002/suco.201500214.

[39] Bairán JM, Menduiña R, Marí A, Cladera A. Shear strength of non-slender reinforced concrete beams. ACI Struct J 2020;117:277–89. https://doi.org/10.14359/51721369.

[40] Marí A, Spinella N, Recupero A, Cladera A. Mechanical model for the shear strength of steel fiber reinforced concrete (SFRC) beams without stirrups. Mater Struct 2020;53:28. https://doi.org/10.1617/s11527-020-01461-4.

[41] Cladera A, Ribas C, Oller E, Marí A. Shear fatigue strength of reinforced concrete members without transverse reinforcement according to the compression chord capacity model. Eng Struct 2020;211:110495. https://doi.org/10.1016/j.engstruct.2020.110495.

[42] Cladera A, Marí A, Ribas C. Mechanical model for the shear strength prediction of corrosion-damaged reinforced concrete slender and non slender beams. Eng Struct 2021;247:113163. https://doi.org/10.1016/j.engstruct.2021.113163.

[43] Frontera A, Cladera A. Predicción a largo plazo de la resistencia a cortante de vigas de hormigón armado basada en un modelo mecánico considerando la corrosión de la armadura. Hormigón y Acero 2024;75:79–90. https://doi.org/10.33586/hya.2024.3136.

[44] Frontera A, Cladera A. Long-term shear strength of RC beams based on a mechanical model that considers reinforcing steel corrosion. Structural Concrete 2023;24:25–40. https://doi.org/10.1002/suco.202200428.

[45] Oller E, Murcia-Delso J, Marí A, Legasa T. Theoretical Model for the Shear Strength of Prestressed Concrete Beams with FRP Tendons. Journal of Composites for Construction 2024;28. https://doi.org/10.1061/JCCOF2.CCENG-4390.

[46] Marí A, Cladera A, Oller E, Bairán JM. A punching shear mechanical model for reinforced concrete flat slabs with and without shear reinforcement. Eng Struct 2018;166:413–26. https://doi.org/10.1016/j.engstruct.2018.03.079.

[47] Marí AR, Fernández PG, Oller E, Cladera A. Punching-Shear Strength of Reinforced Concrete Slabs Subjected to Concentric Transverse Loads and In-Plane Tensile Forces. SP-357: Punching Shear of Concrete Slabs: Insights from New Materials, Tests, and Analysis Methods, American Concrete Institute; 2023, p. 139–59. https://doi.org/10.14359/51738764.

[48] Rius JM, Cladera A, Mas B, Ribas C. Shear behaviour of beams strengthened using different Ni-Ti-Nb shape memory alloy wire configurations and design proposal based on the compression chord Capacity model (CCCM). Eng Struct 2022;268:114724. https://doi.org/10.1016/j.engstruct.2022.114724.

[49] Cladera A, Montoya-Coronado LA, Ruiz-Pinilla JG, Ribas C. Shear strengthening of slender reinforced concrete T-shaped beams using iron-based shape memory alloy strips. Eng Struct 2020;221:111018. https://doi.org/10.1016/j.engstruct.2020.111018.

[50] Ribas González CR, D'Antino T, Sneed LH. Shear Strength Model for Reinforced Concrete Beams with U-Wrapped FRCM Composites Based on the Critical Shear Crack Width Evolution. Journal of Composites for Construction 2025;29:04025021. https://doi.org/10.1061/JCCOF2.CCENG-5040.

[51] Marí A. Questions on Shear Behavior of Structural Concrete and Answers Provided by Mechanical Models. The Challenge of Performance-Based Shear Design. Hormigón y Acero 2023;75:7–24. https://doi.org/10.33586/hya.2023.3116.

[52] Sigrist V, Bentz E, Ruiz MF, Foster S, Muttoni A. Background to the fib Model Code 2010 shear provisions – part I: beams and slabs. Structural Concrete 2013;14:195–203. https://doi.org/10.1002/suco.201200066.

[53] Muttoni A, Fernández-Ruiz M. Levels-of-Approximation Approach in Codes of Practice. Structural Engineering International 2012;22:190–4. https://doi.org/10.2749/101686612X13291382990688.

[54] Carmona JR, Ruiz G, del Viso JR. Mixed-mode crack propagation through reinforced concrete. Eng Fract Mech 2007;74:2788–809. https://doi.org/10.1016/j.engfracmech.2007.01.004.

[55] Yu Q, Le J-L, Hubler MH, Wendner R, Cusatis G, Bažant ZP. Comparison of main models for size effect on shear strength of reinforced and prestressed concrete beams. Structural Concrete 2016;17:778–89. https://doi.org/10.1002/suco.201500126.

[56] Kupfer HB, Gerstle KH. Behavior of concrete under biaxial stresses. Journal of the Engineering Mechanics Division 1973;99:853–66.

[57] Bažant ZP, Yu Q, Gerstle W, Hanson J, Ju JW. Justification of ACI 446 Proposal for Updating ACI Code Provisions for Shear Design of Reinforced Concrete Beams. Structural Journal 2007;104:601–10.

[58] Pérez JL, Cladera A, Rabuñal JR, Martínez-Abella F. Optimization of existing equations using a new Genetic Programming algorithm: Application to the shear strength of reinforced concrete beams. Advances in Engineering Software 2012;50:82–96. https://doi.org/10.1016/j.advengsoft.2012.02.008.

[59] Cladera A, Perez-Ordonez JL, Martinez-Abella F. Shear strength of RC beams. Precision, accuracy, safety and simplicity using genetic programming. Computers and Concrete 2014;14:479–501. https://doi.org/10.12989/cac.2014.14.4.479.

[60] Marí Bernat AR, Cladera Bohigas A, Bairán García JM. Effects of axial forces and prestressing on the shear strength of structural concrete members. Congreso de la de la Asociación Científico-Técnica del Hormigón Estructural (ACHE) 2017, 2017, p. 1–10.

[61] Evans RH, Schumacher EG. Shear Strength of Prestressed Beams Without Web Reinforcement. ACI Journal Proceedings 1963;60:1621–42. https://doi.org/10.14359/7907.

[62] Elzanaty AH, Nilson AH, Slate FO. Shear Capacity of Prestressed Concrete Beams Using High-Strength Concrete. ACI Journal 1986;83:359–68. https://doi.org/10.14359/10436.

[63] Choulli Y, Marí AR, Cladera A. Shear behaviour of full-scale prestressed i-beams made with self compacting concrete. Materials and Structures/Materiaux et Constructions 2008;41. https://doi.org/10.1617/s11527-007-9225-1.

[64] Reineck K-H, Bentz EC, Fitik B, Kuchma DA, Bayrak O. ACI-DAfStb database of shear tests on slender reinforced concrete beams without stirrups. ACI Struct J 2013;110:867–75.

[65] Reineck K-H, Bentz E, Fitik B, Kuchma DA, Bayrak O. ACI-DAfStb Databases for Shear Tests on Slender Reinforced Concrete Beams with Stirrups. ACI Struct J 2014;111:1147–56.

[66] ACI-DAfStb 617. ACI-DAfStb databases 2015 on shear tests for evaluating relationships for the shear design of structural concrete members without and with stirrups. Berlin: Beuth Verl; 2015.

[67] British Standards Institution BSI. BSI Standards Publication Eurocode 2 - Design of concrete structures. BSI Standards Publication 2023:408.

[68] Eurocode 2. EC2 Design of concrete structures. Part 1: General rules and rules for buildings. European Committee for Standardization (CEN); 2002.

[69] Fernández-Montes D, González Valle E, Díaz Heredia E. Influence of axial tension on the shear strength of floor joists without transverse reinforcement. Structural Concrete 2015;16:207–20. https://doi.org/10.1002/suco.201400063.

[70] Jørgensen HB, Hoang LC, Fabrin LS, Malgaard J. Influence of High Axial Tension on the Shear Strength of non-shear RC Beams. Proceedings of the International IABSE conference: Assessment, Upgrading, Refurbishment of Infrastructures, 2013.

[71] Kani G. The riddle of shear failure and its solution. ACI Journal Proceedings 1964;61:441–67.

[72] Vollum RL, Fang L. Shear enhancement in RC beams with multiple point loads. Eng Struct 2014;80:389–405. https://doi.org/10.1016/j.engstruct.2014.09.010.

[73] Reineck KH, Todisco L. Database of shear tests for non-slender reinforced concrete beams without stirrups. ACI Struct J 2014;111:1363–71. https://doi.org/10.14359/51686820.

[74] Todisco L, Reineck K-H, Bayrak O. Database with Shear Tests on Non-Slender Reinforced Concrete Beams with Vertical Stirrups. Structural Journal 2015;112:761–9.

[75] Todisco L, Bayrak O, Reineck KH. ACI-DAfStb database for tests on deep beams and comparisons with code provisions. Structural Concrete 2018;19:296–304. https://doi.org/10.1002/suco.201700061.

[76] Guadagnini M. Shear behavior and design of FRP RC beams. University of Sheffield, 2002.

[77] Japanese Society of Civil Engineers (JSCE). Recommendations for design and construction for concrete structures using continuous fibre reinforcing materials. vol. 23. 1997.

[78] ACI Committee 440. 440.1R-15, Guide for the Design and Construction of Structural Concrete Reinforced with Fiber-Reinforced Polymer (FRP) Bars. Farmington Hills MI: American Concrete Institute; 2015.

[79] Kueres S, Will N, Hegger J. Shear strength of prestressed FRP reinforced concrete beams with shear reinforcement. Eng Struct 2020;206:110088. https://doi.org/10.1016/j.engstruct.2019.110088.

[80] Lantsoght E. Database of Shear Experiments on Steel Fiber Reinforced Concrete Beams without Stirrups. Materials 2019;12:917. https://doi.org/10.3390/ma12060917.

[81] Minelli F, Conforti A, Cuenca E, Plizzari G. Are steel fibres able to mitigate or eliminate size effect in shear? Mater Struct 2014;47:459–73. https://doi.org/10.1617/s11527-013-0072-y.

[82] Dinh HH, Parra-Montesinos GJ, Wight JK. Shear Strength Model for Steel Fiber Reinforced Concrete Beams without Stirrup Reinforcement. Journal of Structural Engineering 2010;137:1039–51. https://doi.org/10.1061/(ASCE)ST.1943-541X.0000362.

[83] Lim TY, Paramasivam P, Lee SL. Bending Behavior of Steel-Fiber Concrete Beams. ACI Struct J 1987;84:524–36. https://doi.org/10.14359/2794.

[84] Lantsoght EOL. Database of experiments on SFRC beams without stirrups failing in shear. 2019. https://doi.org/10.5281/zenodo.2578060.

[85] Chang TS, Kesler CE. Fatigue Behavior of Reinforced Concrete Beams. ACI Journal Proceedings 1958;55:245–54. https://doi.org/10.14359/11352.

[86] Chang TS, Kesler CE. Static and Fatigue Strength in Shear of Beams with Tensile Reinforcement. ACI Journal Proceedings 1958;54:1033–57. https://doi.org/10.14359/11493.

[87] Fédération Internationale du Béton. fib Model Code for Concrete Structures 2010. vol. 1. Lausanne: Ernst & Sohn; 2013.

[88] Fernández-Ruiz M, Zanuy C, Natário F, Gallego JM, Albajar L, Muttoni A. Influence of Fatigue Loading in Shear Failures of Reinforced Concrete Members without Transverse Reinforcement. Journal of Advanced Concrete Technology 2015;13:263–74. https://doi.org/10.3151/jact.13.263.

[89] Gallego JM, Zanuy C, Albajar L. Shear fatigue behaviour of reinforced concrete elements without shear reinforcement. Eng Struct 2014;79:45–57. https://doi.org/10.1016/J.ENGSTRUCT.2014.08.005.

APPENDIX A:

Derivation of LoA II (CCCM) from LoA III (MASM)

A1. Detailed derivation of the main CCCM equation:

In LoA III (MASM), the general equation for the shear strength is given as:

$$V_{Rd} = V_{cu} + V_{su} = (v_c + v_w + v_l)\frac{f_{ct}}{\gamma_v} \cdot b \cdot d + V_{su}$$

Substituting the detailed components:

$$V_{Rd} = \zeta \left\{ \left[\left(0.70 + 0.18K_T + \left(0.20 + 0.50\frac{b}{b_w}\right)v_s\right)\frac{x}{d} + 0.02K_T \right] \frac{b_{v,eff}}{b} K_p + v_w + v_l \right\} \frac{f_{ct}}{\gamma_v} bd + V_{su}$$

For simplification, we assume $K_T = 1$, $K_P = 1$, and adopt safe average values of $v_w = 0.035$ and $v_l = 0.025$. Substituting these values:

$$V_{Rd} = \left\{ \zeta \left[\left(0.88 + \left(0.20 + 0.50\frac{b}{b_w}\right)v_s\right)\frac{x}{d} + 0.02 \right] \frac{b_{v,eff}}{b} + 0.035 + 0.025 \right\} \frac{f_{ct}}{\gamma_v} bd + V_{su}$$

To further simplify, the terms $v_w = 0.035$ and the constant 0.02 are incorporated in the x/d multiplier, assuming an average $z/d = 0.35$. Similarly, $v_l = 0.025$ is added to the vs factor, with an average v_s=0.25. For simplifying reasons, when introducing these constant values inside the parenthesis, the terms $b_{v,eff}/b$ and ζ have been considered equal to 1:

$$V_{Rd} = \left\{ \zeta \left[\left(0.88 + \frac{0.02}{0.35} + \frac{0.035}{0.35} + \left(0.20 + \frac{0.025}{0.35 \cdot 0.25} + 0.50\frac{b}{b_w}\right)v_s\right)\frac{x}{d} \right] \frac{b_{v,eff}}{b} \right\} \frac{f_{ct}}{\gamma_v} bd + V_{su} =$$

$$= \left\{ \zeta \left[\left(1.04 + \left(0.49 + 0.50\frac{b}{b_w}\right)v_s\right)\frac{x}{d} \right] \frac{b_{v,eff}}{b} \right\} \frac{f_{ct}}{\gamma_v} bd + V_{su} \approx$$

$$\approx \zeta \frac{x}{d}\frac{b_{v,eff}}{b}\frac{f_{ct}}{\gamma_v} bd + 0.5\zeta \left(1 + \frac{b}{b_w}\right)v_s \frac{x}{d}\frac{b_{v,eff}}{b}\frac{f_{ct}}{\gamma_v} bd + V_{su} =$$

$$\approx \zeta \frac{x}{d}\frac{f_{ct}}{\gamma_v} b_{v,eff} d + 0.5\zeta \left(1 + \frac{b}{b_w}\right)\frac{V_{su}}{\frac{f_{ct}}{\gamma_v} bd}\frac{x}{d}\frac{b_{v,eff}}{b}\frac{f_{ct}}{\gamma_v} bd + V_{su} =$$

$$= \zeta \frac{x}{d}\frac{f_{ct}}{\gamma_v} b_{v,eff} d + V_{su}\left[1 + 0.5\zeta \left(1 + \frac{b}{b_w}\right)\frac{x}{d}\frac{b_{v,eff}}{b}\right] = \zeta \frac{x}{d}\frac{f_{ct}}{\gamma_v} b_{v,eff} d + V_{su}[1 + \Delta_{Vcu}]$$

The term $\Delta_{Vcu} = 0.5\zeta \left(1 + \frac{b}{b_w}\right)\frac{x}{d}\frac{b_{v,eff}}{d}$ considers the increase in the concrete contribution to the shear strength due to the confinement caused by the stirrups to the compression chord concrete. An average value Δ_{Vcu}=0.4 is adopted to simplify the calculation procedure:

$$V_{Rd} = \zeta \frac{x}{d}\frac{f_{ct}}{\gamma_v} b_{v,eff} d + 1.4V_{su}$$

A2. Detailed derivation of the $V_{cu,min}$ expression

For some cases, v_w is an important shear contribution and the value adopted in A1 (v_w =0.035) is too conservative. This may happen for members, especially one-way slabs, with low values of d or low values of x/d (assumed $x/d < 0.2$ in the following). It has been considered that there is no shear reinforcement:

$$V_{cu,min} = (v_c + v_w)\frac{f_{ct}}{\gamma_v} bd =$$

$$= \left\{ \zeta \left[(0.70 + 0.18K_T)\frac{x}{d} + 0.02K_T \right] \frac{b_{v,eff}}{b} K_p + v_w \right\} \frac{f_{ct}}{\gamma_v} bd =$$

Assuming $K_T = 1$, $K_P = 1$, and substituting E_{cm} and G_f for a 25 MPa compressive strength concrete:

$$V_{cu,min} = \left\{\zeta\left[0.88\frac{x}{d} + 0.02\right]\frac{b_{v,eff}}{b} + 167\frac{f_{ct}}{E_{cm}}\frac{b_w}{b}\left(1 + \frac{2 \cdot G_f \cdot E_{cm}}{f_{ctm}^2 \cdot d_0}\right)\right\}\frac{f_{ct}}{\gamma_v} bd \approx$$

$$\approx \left\{\zeta\left[0.88\frac{x}{d} + 0.02\right]\frac{b_{v,eff}}{b} + 0.015\frac{b_w}{b}\left(1 + \frac{1206}{d_0}\right)\right\}\frac{f_{ct}}{\gamma_v} bd =$$

$$\approx \left\{\zeta\left[0.88\frac{x}{d} + 0.02\right] b_{v,eff} + 0.015 b_w\left(1 + \frac{1206}{d_0}\right)\right\}\frac{f_{ct}}{\gamma_v} d =$$

For simplicity, and from the safe side, we assume $b_{v,eff} = b_w$:

$$V_{cu,min} \approx \left\{\zeta\left[0.88\frac{x}{d} + 0.02\right] + 0.015\left(1 + \frac{1206}{d_0}\right)\right\}\frac{f_{ct}}{\gamma_v} b_w d =$$

$$\approx \left\{\zeta 0.88\frac{x}{d} + 0.02\zeta + 0.015 + \frac{18}{d_0}\right\}\frac{f_{ct}}{\gamma_v} b_w d \approx$$

This expression is intended for the cases in which v_c is small compared to v_w. For this reason, x/d will be assumed to be equal to 0.2. Moreover, for further simplicity, the terms 0.02ζ and 0.015 are disregarded:

$$V_{cu,min} \approx \left\{\zeta 0.176 + \frac{18}{d_0}\right\}\frac{f_{ct}}{\gamma_v} b_w d \approx \; 0.18\left\{\zeta + \frac{100}{d_0}\right\}\frac{f_{ct}}{\gamma_v} b_w d$$

A3. Simplification of the expression for maximum shear strength, $V_{rd,max}$

For the maximum shear strength given by the concrete strut capacity, assuming $\alpha_{cw} = 1$ (no axial force), $z = 0.9$d, $v_1 = 0.6$ (conventional concrete), and cot $= 1.85$ (average value between reinforced and prestressed concrete beams according to the databases):

$$V_{Rd,max} = \alpha_{cw} b_w z v_1 f_{cd}\frac{cot\theta}{1 + cot^2\theta} = 1 \cdot b_w \cdot 0.9d \cdot 0.6 f_{cd}\frac{1{,}85}{1 + 1{,}85^2} \approx 0.225 f_{cd} b_w d$$

APPENDIX B: Derivation of LoA I from LoA II (CCCM)

B1. Simplification of the concrete contribution

From Loa II (CCCM):

$$V_{cu} = \zeta\frac{x}{d}\frac{f_{ct}}{\gamma_v} b_{v,eff} d$$

The size effect, assuming a/d = 4, becomes:

$$\zeta' = \frac{2}{\sqrt{1 + \frac{d_0}{200}}}\left(\frac{1}{4}\right)^{0.2} \approx \frac{1.5}{\sqrt{1 + \frac{d_0}{200}}}$$

Assuming now rectangular cross-section ($b_{v,eff} = b_w$), $\frac{x}{d} = 0.75\,(\alpha_e\,\rho_l)^{1/3}$ and $\alpha_e = 6.0$ (corresponding to $f_{ck} = 35$ MPa):

$$V_{cu} = \zeta'\frac{x}{d}\frac{f_{ct}}{\gamma_v} b_{v,eff} d = \zeta' \cdot 0.75(6 \cdot \rho_l)^{1/3}\frac{f_{ct}}{\gamma_v} b_{v,eff} d = 1.35\zeta'\rho_l^{1/3}\frac{f_{ct}}{\gamma_v} b_w d$$

B2. Detailed simplification of the shear reinforcement contribution:

$$V_{su} = 1.4(d_s - x)\cot\theta\frac{A_{sw}}{s} f_{ywd} = 1.4(d_s - x)\frac{0.85 d_s}{d_s - x}\frac{A_{sw}}{s} f_{ywd} \approx 1.20\frac{A_{sw}}{s} f_{ywd}$$

Disponible en **www.hormigonyacero.com**
https://doi.org/10.33586/hya.2025.3973

Vigas armadas de acero en planta curva sometidas a carga concentrada y esfuerzo cortante

Steel I-Girders Curved in Plan Under Patch Loading and Shear Force

Enrique Mirambell[a, *], **Itsaso Arrayago**[a], **Jorge Bonilla**[a, b]

[a] *Departamento de Ingeniería Civil y Ambiental, Escuela Técnica Superior de Ingeniería de Caminos, Canales y Puertos de Barcelona, Universitat Politècnica de Catalunya (UPC), España.*
[b] *Departamento de Ingeniería Civil y Ambiental, Universidad de Brasilia (UnB), Brasil.*

Recibido el 10 de octubre de 2024; revisado el 26 de febrero de 2025, aceptado el 17 de marzo de 2025

RESUMEN

Las vigas armadas de acero en planta curva suelen utilizarse en puentes que se proyectan en zonas urbanas congestionadas, con requisitos de geometrías en planta complejas. El proyecto de puentes de vigas armadas en planta curva es más complejo que el de puentes rectos, debido a las dificultades que conlleva, tanto en proyecto como en ejecución, la consideración de la curvatura en planta del puente. Las versiones actual y futura del Eurocódigo 3 para estructuras de chapa (EN 1993-1-5) no abordan el proyecto de las vigas armadas curvas de acero, especialmente en lo relativo a su comportamiento frente a cargas concentradas -patch loading- y a esfuerzo cortante; en este sentido, las reglas de cálculo proporcionadas en dicha norma sólo son aplicables a vigas rectas. Por lo tanto, las guías actuales de proyecto no cubren adecuadamente el tipo estructural de vigas armadas de acero en planta curva sometidas a carga concentrada y a esfuerzo cortante, o si acaso proporcionan sólo una guía limitada y simplificada sobre cómo calcularlas. En este artículo se presenta un estudio numérico exhaustivo de vigas armadas curvas de acero en sección doble T, también llamada sección en I, sometidas a carga concentrada y esfuerzo cortante, considerando la no linealidad del material y la no linealidad geométrica, así como las imperfecciones iniciales. Los modelos numéricos se desarrollan mediante el software de elementos finitos ABAQUS y se validan frente a ensayos experimentales disponibles en la literatura. A partir de la evaluación de los resultados numéricos, se proponen recomendaciones prácticas para extender la aplicabilidad de las reglas de cálculo prescritas en la próxima versión de la norma EN 1993-1-5 para vigas armadas rectas al caso de vigas armadas de acero en planta curva.

PALABRAS CLAVE: Vigas armadas de acero en planta curva; cargasconcentradas -patch loading; esfuerzo cortante; carga crítica elástica de inestabilidad; resistencia última.

ABSTRACT

Curved steel plate girders are often utilized in bridges that are built in congested urban areas where complex plan alignments are required. However, the design of curved steel plate girder bridges is more complex than that of equivalent straight ones due to the difficulties associated to the simplification of the design procedures. The current and upcoming versions of Eurocode 3 for plated structures (EN 1993-1-5) do not address steel plate girders curved in plan, especially regarding their behavior against concentrated forces and shear. In that sense, the guidance provided for patch loading and shear design is only applicable to straight girders. Hence, current design guides seem not to cover curved plate girders subjected to patch loading and shear appropriately, or to provide only limited and simplified guidance on how to design them. Therefore, it is necessary to carry out more research in order to achieve a better understanding of the behavior of curved steel plate girders so that suitable design approaches can be developed. This paper presents a comprehensive numerical study on curved steel plate I-girders subjected to patch loading and shear, considering the material and geometric nonlinearities as well as initial imperfections. The numerical models are developed by means of the advanced finite element soft-

ware ABAQUS and validated against experimental tests available in the literature. From the assessment of the numerical results, practical recommendations are proposed to extend the applicability of the design provisions prescribed in the next version of EN 1993-1-5 for straight steel I-girders to the case of curved steel I-girders.

KEYWORDS: Steel I-girders curved in plan; patch loading; shear force; elastic critical buckling load; ultimate load.

* Persona de contacto / *Corresponding author*:
Correo-e / *e-mail*: enrique.mirambell@upc.edu (Enrique Mirambell)

Cómo citar este artículo: Mirambell, E., Arrayago, I., & Bonilla, J. (2026). Vigas armadas de acero en planta curva sometidas a carga concentrada y esfuerzo cortante. *Hormigón y Acero*. 77(308):93-115. https://doi.org/10.33586/hya.2025.3973

1. INTRODUCCIÓN

Las vigas armadas de chapa se utilizan habitualmente en puentes y grandes edificios, y pueden ser rectas o con curvatura en planta. En lo que se refiere a vigas curvas, la mayoría de las reglas de cálculo actuales se basan en formulaciones desarrolladas para vigas rectas, considerando en algún caso la influencia de la curvatura en planta [1-4].

El caso de carga concentrada en vigas armadas de acero, con sección transversal en doble T, es el caso de carga en el que una fuerza concentrada se impone perpendicularmente a través del ala de la viga, provocando normalmente un fallo local del alma de la viga en las proximidades del ala cargada. El problema asociado a la existencia de dicha carga concentrada puede resolverse mediante la disposición de rigidizadores transversales, aunque para algunas situaciones de proyecto, como es el caso de las cargas móviles, ésta no suele ser una solución práctica ni económica; un ejemplo de tal situación es el lanzamiento de puentes. Una de las primeras contribuciones en este campo fueron los modelos empíricos basados en un total de 11 ensayos de carga concentrada en vigas rectas realizados por Granholm [5] en 1960. Más concretamente, Lagerqvist [6] y Lagerqvist y Johansson [7] contribuyeron significativamente a este tema desarrollando una nueva formulación de cálculo para la resistencia a carga concentrada. Johansson et al. [8] desarrollaron y presentaron las nuevas reglas de cálculo que posteriormente se introducirían en el Eurocódigo 3 [9] para estructuras de chapa, donde la formulación de cálculo para carga concentrada seguía un procedimiento similar al propuesto por Lagerqvist [6] y Lagerqvist y Johansson [7], pero con algunas modificaciones. Posteriormente, Gozzi [10] desarrolló un programa experimental de tres ensayos con diferentes longitudes de carga y modelos de elementos finitos (EF) para estudiar las vigas armadas rectas sometidas a carga concentrada. Como resultado de esta investigación, se propuso un modelo de resistencia en estado límite último, que era una modificación del trabajo presentado por Lagerqvist [6]. Más recientemente, Graciano y Johansson [11], Kuhlmann y Seitz [12], Davaine y Aribert [13], Clarin [14], Kövesdi [15], y Kövesdi et al. [16] han llevado a cabo varios estudios en los que se investiga la resistencia a carga concentrada en almas de vigas armadas de acero rigidizadas longitudinalmente. Además, Chacón et al. [17-19] desarrollaron un extenso estudio numérico y experimental y presentaron un nuevo modelo mecánico para vigas armadas densamente rigidizadas, que condujo a una predicción satisfactoria de la capacidad de carga última de vigas armadas rectas sometidas a patch loading.

En lo que concierne al tipo estructural de vigas armadas curvas de chapa de acero, a lo largo de las últimas décadas se han realizado importantes estudios experimentales y numéricos. Basándose en los resultados de ensayos de veintisiete vigas, Nakai y Kotoguchi [20] desarrollaron un método analítico para evaluar la resistencia al pandeo lateral de vigas curvas con sección en doble T según un análisis de segundo orden, mientras que Nakai y Kitada [21] llevaron a cabo un extenso programa experimental consistente en treinta y dos vigas curvas con sección en doble T con alas compactas con el fin de determinar la resistencia última de vigas en planta curva sometidas a flexión, cortante y su interacción. Asimismo, Shanmugam et al. [22] llevaron a cabo varios ensayos en dos conjuntos de vigas curvas en doble T: un conjunto compuesto por perfiles laminados y otro dedicado a perfiles armados, en los que también se realizó un análisis no lineal por elementos finitos. Pi y Trahair [23] también desarrollaron un modelo curvo de elementos finitos curvos capaz de realizar análisis tridimensionales no lineales y de inestabilidad de vigas con curvatura en planta, que incluía el alabeo de las secciones transversales. Además, también se llevaron a cabo diversas investigaciones experimentales y numéricas sobre vigas mixtas acero-hormigón, con curvatura en planta. En estos estudios, se utilizaron vigas con secciones transversales compactas en las que alas y almas no abollaban elásticamente [24,25].

Pi et al. [26] desarrollaron modelos de análisis no lineal para estudiar el comportamiento de una viga armada en planta curva, mostrando un buen acuerdo con los resultados experimentales, mientras que Shanmugam et al. [2] llevaron a cabo una investigación experimental y numérica exhaustiva sobre vigas armadas curvas en planta. Como resultado de este estudio, se observó que la capacidad resistente de las vigas curvas disminuye al aumentar el valor de la curvatura en planta. Rodríguez [27] desarrolló un extenso estudio numérico sobre vigas armadas curvas de acero con sección en doble T, sometidas a carga concentrada, alcanzándose una muy buena concordancia entre los resultados derivados de los modelos numéricos y los resultados experimentales recogidos en la literatura [2]; posteriormente se realizó un extenso estudio paramétrico compuesto por 90 modelos numéricos, que dio lugar a diversas recomendaciones para el proyecto y cálculo de vigas armadas curvas, con sección transversal en doble T [27]. Bonilla et al. [4] también han presentado recientemente un estudio numé-

rico sobre vigas armadas de acero con curvatura en planta, con sección transversal en doble T, sometidas a carga concentrada, considerando las no linealidades del material y geométrica, así como las imperfecciones iniciales. Se propusieron recomendaciones prácticas para extender la aplicabilidad de las disposiciones de cálculo de las vigas armadas rectas al caso de vigas armadas curvas, con sección transversal en doble T.

Por otra parte, en lo que concierne al comportamiento frente a esfuerzo cortante, Mirambell et al. [3] presentaron un estudio numérico en el que se investigaba el comportamiento estructural de vigas armadas curvas de acero, con sección en doble T, sometidas a cortante. Esta investigación mostró que el esfuerzo cortante crítico elástico de vigas armadas curvas de chapa de acero con sección transversal en doble T aumenta con la relación a/R, siendo a la distancia entre rigidizadores transversales y R el radio de curvatura en planta. Esta conclusión es coherente con otras investigaciones relevantes recogidas en la bibliografía [28-32]. Los autores en [3] también proporcionaron recomendaciones para la aplicabilidad de las reglas de cálculo codificadas para vigas armadas rectas al caso de vigas armadas curvas, con sección transversal en doble T. Hendy et al. [33] presentaron un amplio estudio paramétrico realizado con un modelo de elementos finitos, con el objetivo de proponer nuevas reglas de cálculo para tableros de vigas múltiples de puentes mixtos acero-hormigón con curvatura en planta, mientras que Frankl y Linzell [34] desarrollaron estudios analíticos y numéricos para investigar los valores del coeficiente de abolladura por cortante de vigas armadas de acero, obteniendo expresiones útiles para su determinación que incluían los efectos de la curvatura horizontal.

A pesar de la considerable investigación sobre el comportamiento resistente de vigas armadas curvas de acero, con sección transversal en doble T, las versiones actual y futura de la norma EN 1993-1-5 [9,35] no ofrecen reglas de cálculo específicas para vigas armadas de chapa de acero con curvatura en planta. Y aunque la futura edición de la especificación prEN 1993-2 para puentes de acero [36] incluye cláusulas para el cálculo de vigas de acero en planta curva, no aborda específicamente la consideración de la carga concentrada y el esfuerzo cortante. Asimismo, AASHTO [37] considera la influencia de la curvatura en planta en la respuesta estructural de las vigas armadas curvas de acero, de sección transversal en doble T, pero lo hace de forma simplificada y empírica poniendo limitaciones a la separación entre arriostramientos. Estas observaciones son coherentes con las conclusiones extraídas anteriormente por otros autores [2,3,33], que han destacado sistemáticamente que las directrices y especificaciones de cálculo actuales parecen no contemplar las vigas armadas curvas sometidas a carga concentrada y esfuerzo cortante, o proporcionan únicamente una guía limitada y simplificada sobre cómo calcularlas, siendo a menudo inadecuadas o difíciles de utilizar. Esta situación conduce a un escenario en el que los proyectistas se ven obligados a establecer sus propias aproximaciones para el dimensionamiento y cálculo de vigas armadas curvas, utilizando reglas para vigas rectas en muchos casos, lo que potencialmente podría conducir a una falta de coherencia en el cálculo y a diseños excesivamente conservadores.

Este artículo pretende abordar la laguna existente en las disposiciones normativas en lo que concierne al dimensionamiento y cálculo de vigas armadas de chapa de acero en planta curva, sometidas a carga concentrada y cortante. El trabajo realizado facilitará la comprensión del comportamiento de dichas estructuras frente a estas acciones y permitirá evaluar la carga última de vigas armadas curvas con sección transversal en doble T, proponiendo una serie de recomendaciones útiles para el proyecto de vigas armadas curvas. Basando el trabajo de investigación en un extenso estudio paramétrico de elementos finitos utilizando el paquete informático ABAQUS [38], se evalúa la respuesta estructural de vigas armadas curvas de sección transversal en doble T frente a carga concentrada y esfuerzo cortante y se proponen, a posteriori, recomendaciones prácticas para la aplicación de las reglas de cálculo incluidas en la próxima versión de prEN 1993-1-5 [35] para vigas armadas rectas al caso de vigas armadas de acero curvas.

Notación

a, b	distancia entre rigidizadores transversales
b_f	ancho de ala
f_y	límite elástico
f_{yw}	límite elástico del alma
f_{yf}	límite elástico del ala
f_{ys}	límite elástico del rigidizador
h_w	altura del alma entre alas
t_w	espesor del alma
t_f	espesor del ala
l_y	longitud efectiva de carga
t_s	espesor de los rigidizadores transversales
S_s	longitud de apoyo rígido
E	módulo de Young
f_u	resistencia última a tracción
F_{cr} o $F_{cr,\text{EC-3}}$	carga crítica elástica de inestabilidad [35]
$F_{Rd,\text{EN1993-1-5}}$	resistencia de cálculo de acuerdo con la futura versión de EN 1993-1-5 [35]
$F_{u,exp}$	carga última experimental de las vigas armadas
$F_{cr,FE}$	carga crítica elástica de inestabilidad obtenida de un análisis de autovalores
$F_{u,FE}$	carga última numérica de las vigas armadas
R	radio de curvatura de la viga armada en planta
L	longitud de vano (longitud de arco en planta)
$V_{u,\text{EN 1993-1-5}}$	resistencia a cortante de acuerdo con la futura versión de EN 1993-1-5 [35]
$V_{u,num}$	resistencia última a cortante obtenida numéricamente
χ_F	factor de reducción debido a inestabilidad
$\bar{\lambda}_F$	esbeltez relativa para carga concentrada
χ_w	contribución del alma a la resistencia a abolladura por cortante
$\bar{\lambda}_w$	esbeltez relativa para abolladura por cortante
γ_{M1}	coeficiente parcial para la resistencia

2. SIMULACIÓN NUMÉRICA DE VIGAS ARMADAS DE ACERO

El modelo numérico para la reproducción de los ensayos de vigas armadas de chapa de acero se desarrolló utilizando el software de análisis por elementos finitos ABAQUS [38]. Para

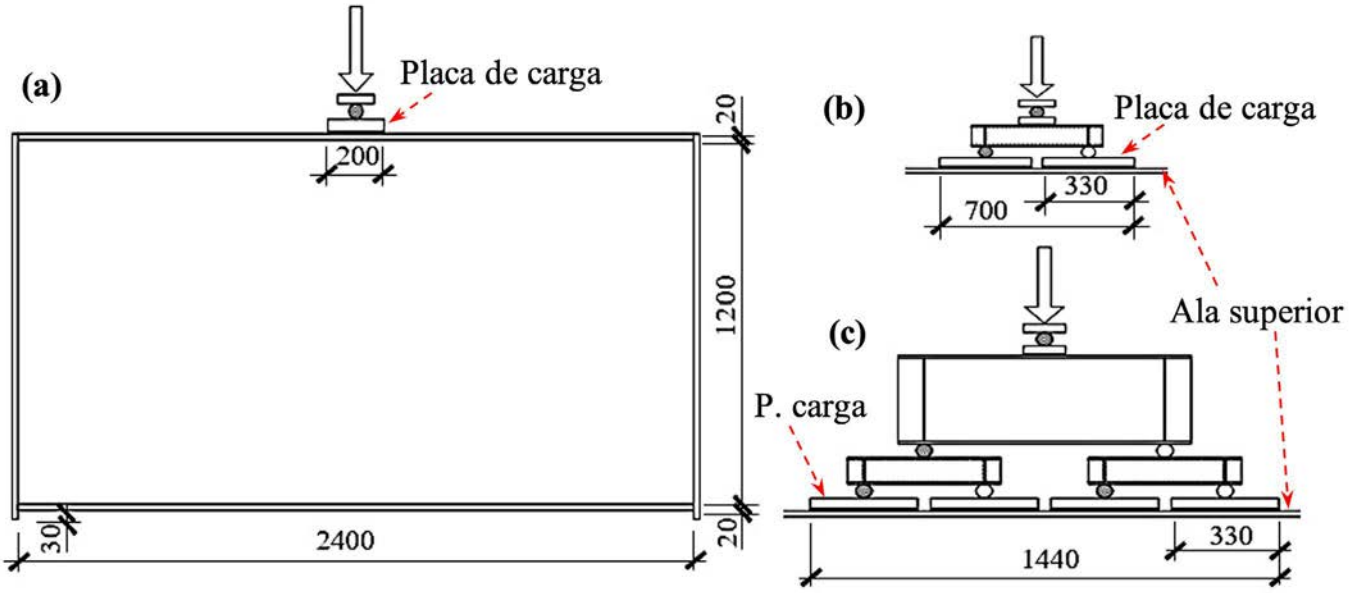

Figura 1. Dimensiones geométricas y montaje experimental para las tres vigas ensayadas [10]: (a) P200, (b) P700 y (c) P1440 (dimensiones en mm).

obtener resultados precisos de las simulaciones mediante los elementos finitos, en los modelos numéricos se tuvo en cuenta la geometría tridimensional de cada ensayo, así como las no linealidades relativas al material de acero y los efectos de segundo orden. La calibración y validación del modelo de elementos finitos de vigas armadas de chapa de acero sometidas a carga concentrada y esfuerzo cortante se llevó a cabo utilizando los ensayos de las vigas armadas rectas en sección en doble T descritas en Gozzi [10] y Chacón et al. [18], y los ensayos de las vigas curvas de Shanmugam et al. [2]. En las secciones siguientes se ofrece una breve descripción de estos ensayos y de las actuaciones experimentales.

2.1 Estudios experimentales para la calibración y validación de los modelos numéricos

2.1.1. Estudios experimentales de Gozzi

Gozzi [10] ensayó tres vigas armadas de chapa de acero con las mismas dimensiones de ala (ancho de ala b_f y espesor de ala t_f iguales a 450 mm y 20 mm, respectivamente) y de alma (altura de alma h_w y esesor de alma t_w iguales a 1200 mm y 6 mm, respectivamente). Los rigidizadores verticales de las secciones de apoyo presentaban las mismas dimensiones que las alas. El único parámetro que se varió en las vigas armadas ensayadas fue la longitud cargada S_s, que se supuso igual a 200 mm, 700 mm y 1440 mm; las vigas ensayadas se etiquetaron como P200, P700 y P1440 según la longitud S_s. La figura 1 muestra las dimensiones geométricas y el montaje del ensayo de las tres vigas analizadas. En los tres casos, se utilizaron placas de carga con un espesor igual a 40 mm, y se colocaron como se ilustra en la figura 1, para alcanzar las longitudes de carga S_s requeridas.

Para las tres vigas armadas se utilizó acero S355. Las propiedades del material se obtuvieron a partir de ensayos de tracción uniaxiales en las direcciones longitudinal y transversal con respecto a la dirección de laminación, tanto para las chapas de alma como para las de las alas. Los valores medios de f_y y f_u medidos a partir de los ensayos con probetas uniaxiales para el alma en la dirección longitudinal fueron de 371 MPa y 542 MPa, respectivamente. En la dirección transversal, estos valores medios fueron de 394 MPa y 543 MPa, respectivamente. Para las alas y rigidizadores, tanto en la dirección longitudinal como transversal, el valor de f_y fue de 354 MPa, y f_u fue igual a 519 MPa en la dirección longitudinal e igual a 521 MPa en la dirección transversal [10]. Las propiedades elásticas obtenidas en los ensayos fueron un módulo de Young de 185 GPa para el alma y de 200 GPa para las alas, y un coeficiente de Poisson de 0.3.

2.1.2.Estudios experimentales de Chacón et al.

Del programa experimental realizado por Chacón et al. [18], se eligieron tres vigas para la validación del modelo de elementos finitos desarrollado en esta investigación. La figura 2 muestra las dimensiones geométricas y el montaje de las vigas analizadas experimentalmente, etiquetadas como 1VPL2500 (a = 2500 mm y b = 0 mm), 1VPL750 (a = 750 mm y b = 875 mm) y 2VPL2500 (a = 2500 mm y b = 0 mm). Todas las vigas presentaban las mismas dimensiones de ala, alma y rigidizador transversal (b_f, t_f, h_w, t_w y t_s iguales a 200 mm, 20 mm, 500 mm, 4 mm y 20 mm, respectivamente), como puede apreciarse en la figura 2. Los límites elásticos f_{yf}, f_{yw} y f_{ys} fueron, respectivamente, 454 MPa, 325 MPa y 310 MPa para las dos primeras vigas (1VPL2500 y 1VPL750). Para la viga 2VPL2500, los valores de f_{yf}, f_{yw} y f_{ys} fueron iguales a 449 MPa, 210 MPa y 249 MPa, respectivamente. Para el módulo de Young y el coeficiente de Poisson se adoptaron los valores de 210 GPa y 0.3, respectivamente [18].

2.1.3. Estudios experimentales de Shanmugam et al.

Shanmugam et al. [2] desarrollaron un extenso programa experimental que incluía diez ensayos de vigas armadas de chapa de acero en planta curva. Para la validación del modelo numérico con vigas armadas curvas que aquí se realiza, se uti-

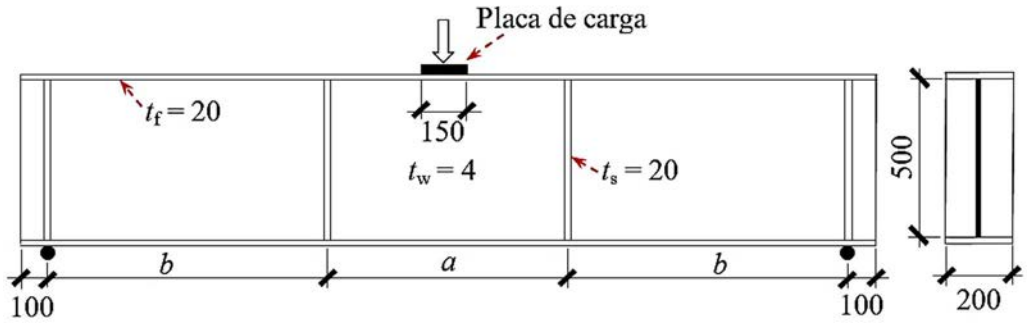

Figura 2. Dimensiones geométricas y montaje experimental para las tres vigas ensayadas [18]: 1VPL2500, 1VPL750 and 2VPL2500 (dimensiones en mm).

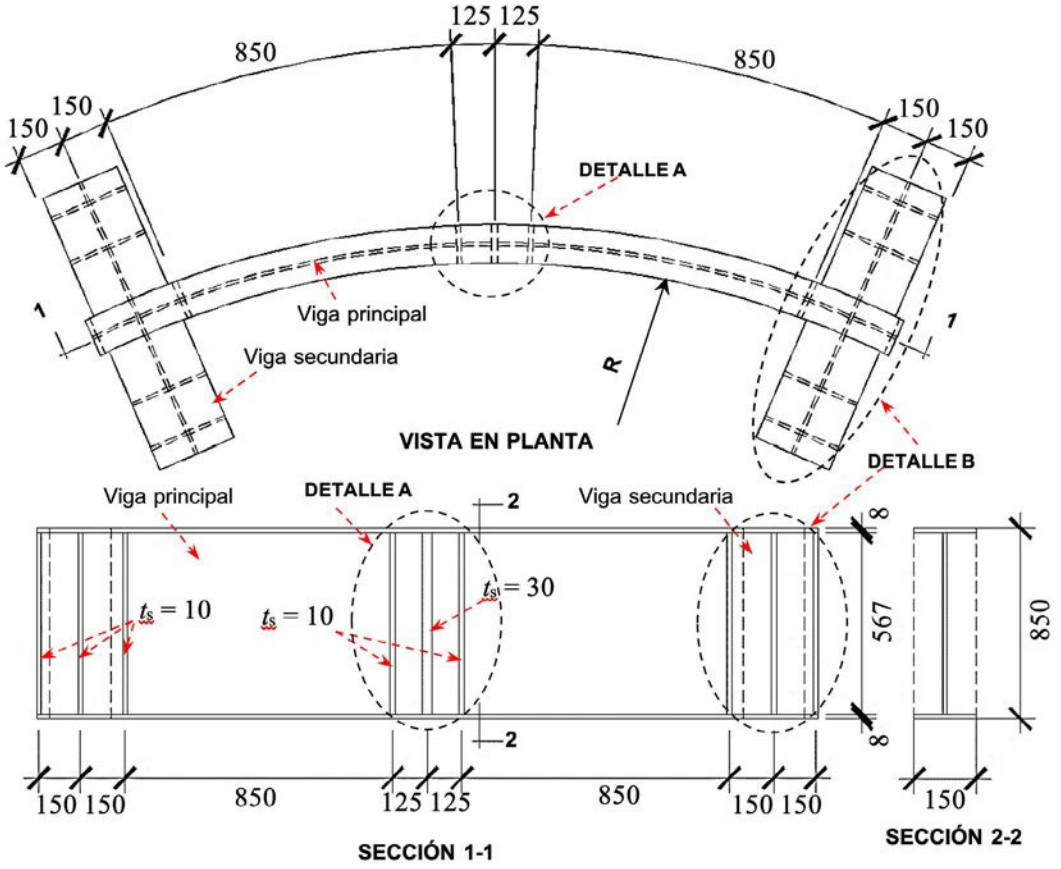

Figura 3. Vista en planta y detalles de la sección transversal de las vigas ensayadas por Shanmugam et al. [2].

lizaron las vigas C15W200 y C45W200 de la citada referencia, que presentaban radios de curvatura de 8600 mm y 2870 mm, respectivamente. Todas las vigas ensayadas tenían una luz total L de 2550 mm. Para todas las vigas, el canto total se mantuvo en 583 mm, con anchos de ala superior e inferior de 150 mm (ver figura 3). Los valores medios del espesor del ala (t_f) fueron, respectivamente, 8.32 mm y 8.2 mm para las vigas C15W200 y C45W200, mientras que los espesores medios del alma (t_w) y de los rigidizadores transversales (t_s) fueron, respectivamente, 2.2 mm y 10.03 mm para C15W200, y 1.95 mm y 9.20 mm para C45W200.

Los límites elásticos del acero f_{yw} y f_{yf} fueron, respectivamente, de 322 MPa y 375 MPa para la viga C15W200, y de 327 MPa y 367 MPa para la viga C45W200. Los módulos de Young del alma y del ala fueron de 216 GPa para C15W200, y de 213 GPa y 210 GPa, respectivamente, para la viga C45W200. La simulación de estas vigas se basó en el montaje experimental descrito en Shanmugam et al. [2], en el que las vigas secundarias se representaron mediante las condiciones de contorno adecuadas en los apoyos.

2.2. Modelización del material acero

El material acero se modelizó mediante el criterio de von Mises, utilizando la opción *PLASTIC disponible en ABAQUS [38] para simular su comportamiento no lineal. Para represen-

tar el comportamiento del acero en el espacio de tensiones de tres dimensiones se utilizó una regla de flujo plástico asociado y endurecimiento isotrópico. Para simular con precisión este comportamiento, ABAQUS sólo requiere la curva tensión-deformación uniaxial, que se representa mediante la curva tensión-deformación trilineal mostrada en la figura 4. Las propiedades del material acero de las vigas armadas utilizadas en la calibración de los modelos numéricos se recogen en las pertinentes referencias [2,10,18], asumiendo en todos los casos que la densidad del acero es de 7800 kg/m³. Para aquellos casos en los que los valores medidos de ε_u o f_u no estuvieran recogidos en [2,10,18], se consideraron las expresiones propuestas por Yun y Gardner [39] para su determinación.

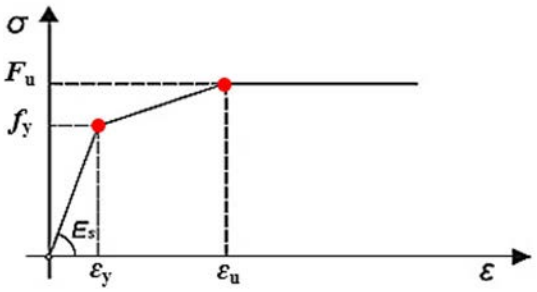

Figura 4. Relación tensión-deformación adoptada para el acero.

2.3. *Método de solución del análisis numérico*

El análisis de estabilidad de vigas armadas frente a carga concentrada mediante el software ABAQUS [38] se realiza en dos etapas. En primer lugar, se lleva a cabo un análisis de autovalores para establecer los modos de inestabilidad probables y guardarlos en un archivo de resultados que se utiliza posteriormente para determinar la imperfección geométrica inicial. En la segunda etapa del análisis, se introduce la imperfección obtenida del análisis previo utilizando la opción *IMPERFECTION, y a continuación se realiza un análisis no lineal postcrítico empleando el procedimiento RIKS.

En todos los casos, la carga se introdujo de forma incremental en el ala superior de las vigas, tal como se muestra en la figura 1, utilizando incrementos pequeños, en los que la magnitud de dichos incrementos era seleccionada automáticamente por ABAQUS [38,40] basándose en la condición de convergencia numérica. En este estudio, la carga se aplicó utilizando el algoritmo RIKS modificado [38,40], que se adopta comúnmente para predecir colapsos inestables y no lineales de estructuras. La base de este algoritmo es el método de Newton, en el que la solución final se obtiene como una serie de incrementos de carga con diferentes iteraciones que se realizan para obtener el equilibrio dentro de cada incremento, para lo cual ABAQUS [38,40] utiliza la longitud de arco a lo largo de la trayectoria de equilibrio estático en el espacio carga-desplazamiento. En este sentido, para capturar de forma eficiente la respuesta estructural carga-desplazamiento de inestabilidad frente a la actuación de la carga concentrada, es muy importante mantener el máximo incremento de longitud de arco pequeño durante la etapa de análisis de RIKS.

2.4. *Tipo de elemento finito, malla y condiciones inicial y de contorno del problema*

Para la discretización de las vigas se utilizó el elemento tipo lámina S4R disponible en la librería de elementos de ABAQUS, que ha demostrado un buen comportamiento en numerosas investigaciones previas para casos de inestabilidad similares [2,10,41]. Se realizó un análisis de sensibilidad de la malla con respecto al tamaño de los elementos de acuerdo con estudios previos [10,18], que dio como resultado la definición de una malla con una longitud de lado del elemento aproximada de 25 mm. Las placas de carga se modelaron con elementos sólidos C3D8R disponibles en ABAQUS como piezas separadas. En base a estudios numéricos previos de

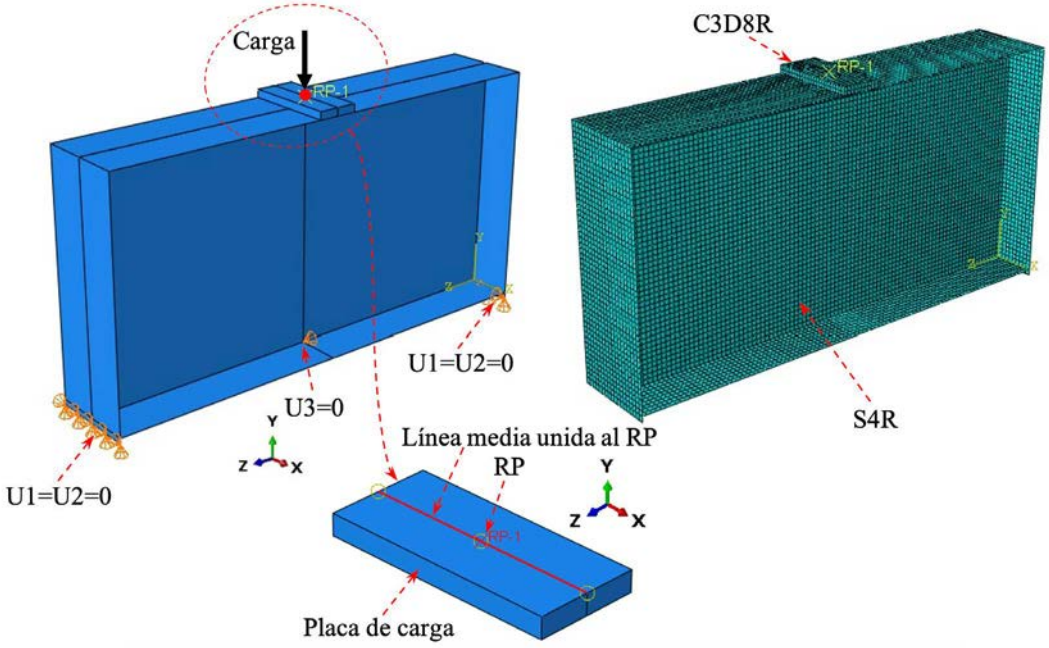

Figura 5. Condiciones de contorno y modelo de elementos finitos de la viga ensayada P200 [10].

vigas armadas de acero sometidas a carga concentrada [10], para la simulación de los ensayos de vigas, el contacto placa de carga-ala de la viga se consideró rígido, utilizando la opción *TIE CONSTRAINT disponible en ABAQUS. De acuerdo con lo expuesto por Gozzi [10], la carga se aplicó en un punto de referencia (RP) situado en la línea media (en la parte central de la placa de carga), tal como se muestra en la figura 5; no obstante, con el objetivo de reproducir de forma fidedigna los montajes reales de los ensayos, todos los nodos situados en la línea media se ligaron al punto de referencia, creando así una restricción de cuerpo rígido. En cuanto a las condiciones de contorno, se restringió el movimiento en las direcciones X e Y (U1=U2=0) en los apoyos de las vigas, tal como puede verse en la figura 5. Asimismo, y considerando la simetría de los ensayos, también se restringió el movimiento en la dirección Z de un nodo situado en el ala inferior, en el centro de las vigas ensayadas (U3 = 0), proporcionando el equilibrio requerido por el modelo numérico (ver figura 5).

Por último, se introdujeron imperfecciones geométricas iniciales como condiciones iniciales de las vigas ensayadas modelizadas. Dado que los modos de inestabilidad más bajos son los que, generalmente, proporcionan las formas de imperfección más críticas, generalmente éstas se escalan y se introducen en la geometría perfecta para crear la malla perturbada [40]. En este caso, se utilizaron los primeros modos de inestabilidad escalados a una amplitud máxima equivalente igual a la relación h_w/200, de acuerdo con las recomendaciones de prEN 1993-1-5 [35]. Debe tenerse en cuenta que la adopción de esta amplitud de imperfección equivalente supone la consideración en el análisis tanto de las imperfecciones geométricas iniciales como de las tensiones residuales, y esta metodología ha sido comúnmente adoptada en el desarrollo de modelos similares de elementos finitos en la literatura [3,10,27,42].

2.5. Validación del modelo de elementos finitos

La descripción del procedimiento y de las consideraciones tenidas en cuenta en el desarrollo del modelo de elementos finitos presentado en los apartados anteriores se ha basado en la viga ensayada P200 (Gozzi [10]). Para todas las vigas utilizadas en la validación del modelo numérico desarrollado, incluyendo las vigas P700 y P1440 del mismo autor, así como las vigas 1VPL2500, 1VPL750 y 2VPL2500 de Chacón et al. [18] y las vigas curvas C15W200 y C45W200 de Shanmugam et al. [2], se han considerado hipótesis y metodologías de trabajo equivalentes. Las geometrías, las propiedades de los materiales, las configuraciones de carga y las condiciones de contorno de las vigas antes mencionadas ya se han descrito en el apartado 2.1.

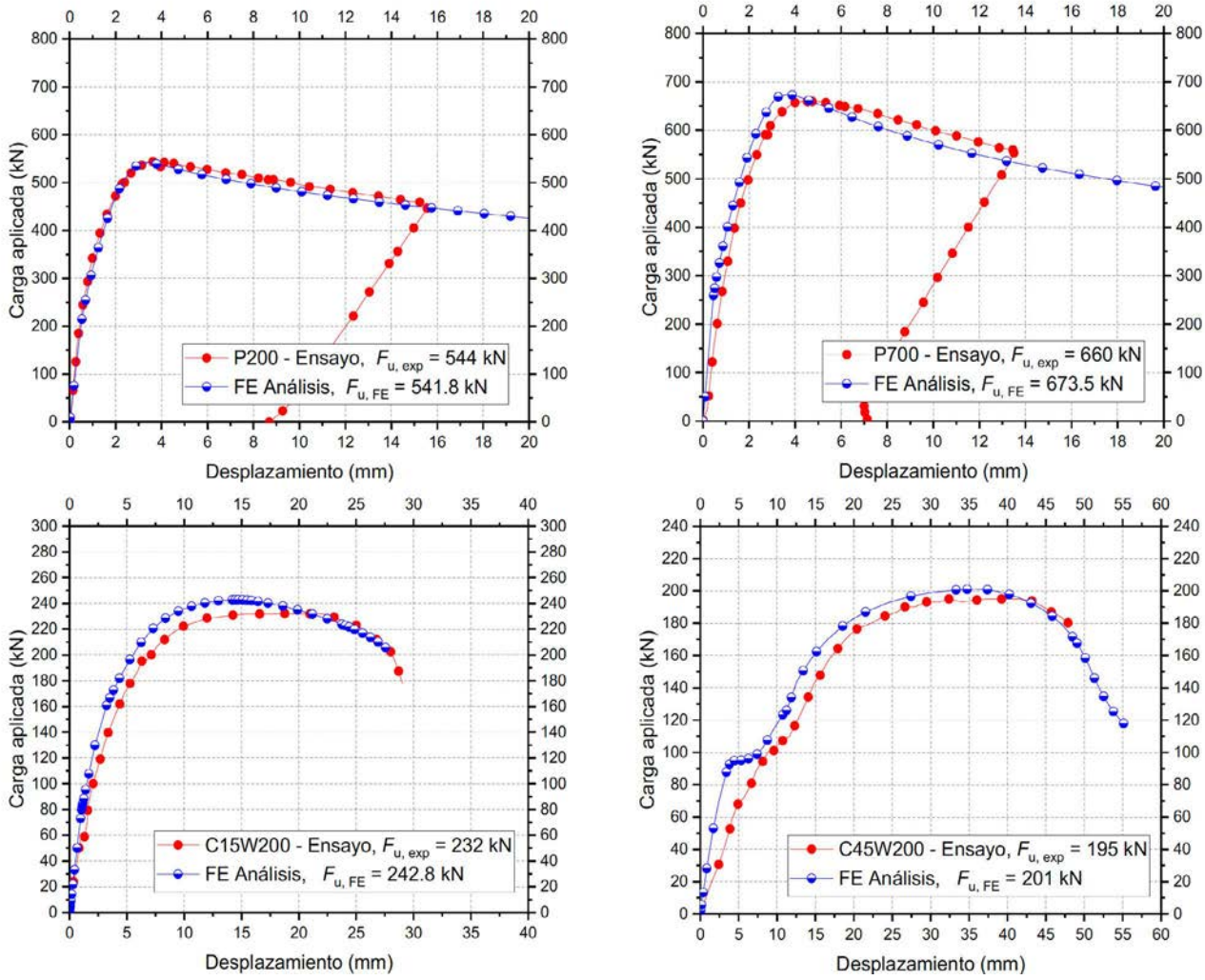

Figura 6. Comparación de las curvas carga-desplazamiento obtenidas experimental y numéricamente [2,10].

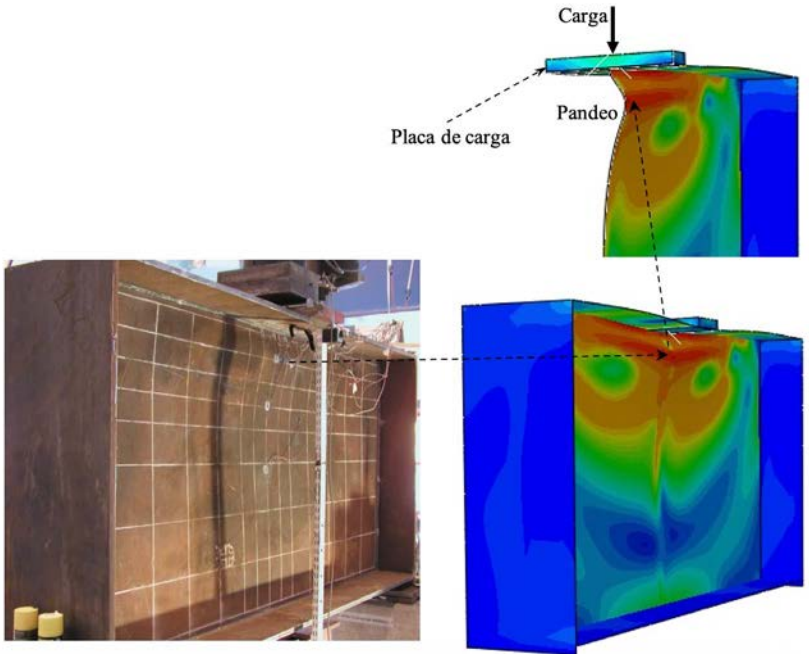

Figura 7. Comparación entre la deformada final obtenida experimentalmente [10] y la predicha por el modelo numérico, para la viga ensayada P200.

La tabla 1 presenta la comparación de las capacidades resistentes obtenidas experimental ($F_{u,exp}$) y numéricamente en este trabajo ($F_{u,FE}$). Puede observarse que se ha conseguido una muy buena concordancia entre los resultados experimentales y numéricos para todas las vigas ensayadas, ya que el valor medio de la relación $F_{u,exp}/F_{u,FE}$ es de 0.976, con un coeficiente de variación (COV) correspondiente de 0.016. Además, también se ha obtenido una excelente concordancia entre las curvas carga-desplazamiento vertical obtenidas a partir de los resultados experimentales y mediante los análisis numéricos realizados para todas las vigas (ver figura 6). Las formas típicas de deformación final observadas en los ensayos y las correspondientes a los modelos numéricos desarrollados pueden observarse en la figura 7 para el caso de la viga P200 [10], en la que se aprecia una buena concordancia del modo de fallo exhibido por la viga armada de acero.

TABLA 1.
Comparación de las cargas últimas experimentales y numéricas para la validación del modelo numérico.

Ensayos por	Viga ensayada	$F_{u,exp}$ (kN)	$F_{u,FE}$ (kN)	$F_{u,exp}/F_{u,FE}$
Gozzi [10]	P200	544	541.8	1.004
	P700	660	673.5	0.980
	P1440	808	842.2	0.959
Chacón et al. [18]	1VPL2500	217	225.2	0.964
	1VPL750	252	253.4	0.994
	2VPL2500	134	136.9	0.980
Shanmugam et al. [2]	C15W200	232	242.8	0.960
	C45W200	195	201.0	0.970
			Media	0.976
			COV	0.016

En base a los análisis comparativos anteriores entre los resultados experimentales y numéricos, puede concluirse que el modelo numérico desarrollado es fiable y capaz de predecir, con precisión, el comportamiento estructural de vigas armadas de chapa de acero sometidas a carga concentrada, incluyendo las vigas con curvatura en planta.

3. ESTUDIO PARAMÉTRICO DE VIGAS CURVAS SOMETIDAS A CARGA CONCENTRADA

Habiendo comprobado que el modelo numérico de elementos finitos desarrollado en este estudio para simular el comportamiento de vigas armadas frente a carga concentrada es capaz de reproducir los resultados experimentales y predecir las cargas últimas con precisión, se lleva a cabo a continuación un estudio paramétrico para evaluar la influencia de varios parámetros en la resistencia última de vigas curvas de acero frente a "patch loading".

3.1. Prototipos de las vigas analizadas

Se investigaron dos prototipos básicos de vigas curvas de acero para el estudio paramétrico. Por una parte, se consideraron (a) vigas sin rigidizadores transversales intermedios (Tipo I), y, por otra, (b) vigas con dos rigidizadores transversales intermedios (Tipo II), tal como se observa en la figura 8. Para considerar el efecto de los marcos transversales o arriostramientos laterales utilizados en situaciones reales como en puentes, se restringió el desplazamiento radial o lateral en los puntos identificados como 1 a 4, que se encuentran en los rigidizadores de los apoyos (ver figura 8).

3.2. Variables y rangos considerados en el estudio paramétrico

Para el estudio paramétrico de vigas armadas curvas de chapa de acero se adoptaron geometrías típicas, similares a las

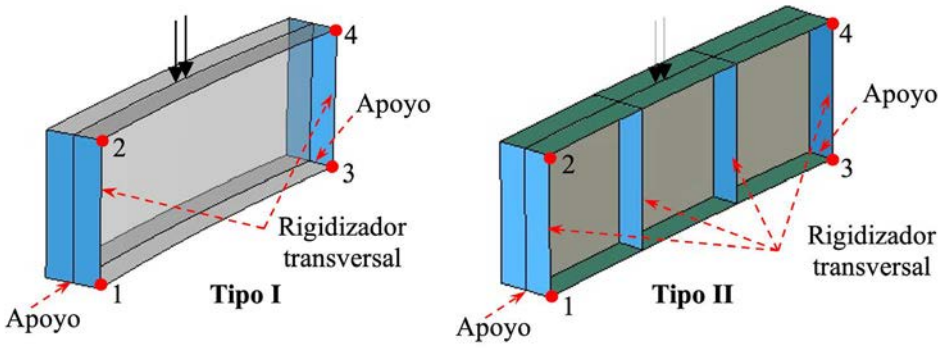

Figura 8. Prototipos de vigas armadas curvas investigadas en el estudio paramétrico.

TABLA 2.
Conjunto de variaciones consideradas en el estudio paramétrico.

Grupo	f_{yw} (MPa)	f_{yf} (MPa)	h_w (mm)	a (mm)	L(*)	t_w (mm)	$t_f \times b_f$ (mm²)	t_s (mm)	S_s (mm)	R (m)	Número de vigas
I	355	355	1000	1000, 2000, 3000	a	8,12	20 x 400	30	250, 500	∞, 500, 200, 100, 40, 20	72
II	355	355	2500	2500, 5000, 7500	a	12, 15	35 x 600	40	625, 1250	∞, 200, 100, 40, 20	60
III	355	355	4000	4000, 8000, 12000	a	15, 25	50 x 1000	60	1000, 2000	∞, 200, 100, 40, 20	60
										Número total de simulaciones numéricas (I-III):	192
IV	355	355	1000	1000, 2000	$3a$	8,12	20 x 400	30	500	∞, 200, 100, 40, 20	20
V	355	355	2500	2500, 5000	$3a$	12, 15	35 x 600	40	1250	∞, 200, 100, 40, 20	20
VI	355	355	4000	4000, 8000	$3a$	15, 25	50 x 1000	60	2000	∞, 200, 100, 40, 20	20
										Número total de simulaciones numéricas (IV-VI):	60
										Número total de simulaciones numéricas:	252

(*) La longitud de vano (L) se define como $L = a$ para los Grupos I, II y III, y $L = 3a$ para los Grupos IV, V y VI. En situaciones reales, L puede tomarse como la distancia entre diafragmas para los Grupos IV, V y VI.

mostradas en la figura 8; en la tabla 2 se resumen los valores y rangos de las propiedades y variables que influyen en la respuesta estructural de las vigas curvas frente a carga concentrada. El estudio paramétrico comprendió un total de 252 modelos numéricos, que se dividieron en los dos tipos mencionados anteriormente (vigas de Tipo I y Tipo II) y se subdividieron en seis grupos, en los que las vigas se agruparon en función de sus propiedades geométricas. Los Grupos I, II y III están formados por vigas de Tipo I, mientras que las vigas de Tipo II se analizan en los Grupos IV, V y VI. Para cada grupo perteneciente a las vigas de Tipo I, se consideraron tres valores diferentes de la relación de aspecto a/h_w (1.0, 2.0 y 3.0), así como dos valores diferentes de la esbeltez del alma h_w/t_w (83.33 y 125 para el Grupo I, 166.67 y 208.33 para el Grupo II, y 160 y 266.67 para el Grupo III). Al mismo tiempo, se consideraron seis valores de la relación a/R para las vigas del Grupo I (L = a para los Grupos I, II y III), y cinco valores para las vigas de los Grupos II y III. Alternativamente, se consideraron sólo dos valores de la relación a/h_w (1.0 y 2.0) para cada grupo perteneciente a las vigas Tipo II, y se consideró la misma esbeltez del alma adoptada en los grupos pertenecientes a las vigas Tipo I. Se adoptaron cinco valores de la relación L/R para las vigas de los Grupos IV, V y VI ($L = 3a$ para los Grupos IV, V y VI). Los valores de la relación L/R se movieron entre 0.0 (panel recto) y 0.6, y entre 0.0 y 1.2 (panel de alma con gran curvatura en planta) para las vigas pertenecientes a los Tipos I y II, respectivamente.

La base de datos numérica se construyó variando los siguientes parámetros: geometría del alma (altura h_w y espesor t_w), radio de curvatura R, y distancia entre rigidizadores transversales a. Los valores se eligieron a partir de proporciones realistas encontradas típicamente en puentes de vigas armadas de acero en planta curva (ver tabla 2). Dentro de cada grupo de vigas, la geometría de las alas (ancho b_f y espesor t_f), así como el espesor de los rigidizadores t_s, se mantuvieron constantes, tal como se indica en la tabla 2, mientras que se consideraron dos longitudes de carga diferentes S_s. En cuanto a las propiedades de los materiales, se utilizó en todos los casos y para todas las chapas que componen las vigas un grado de acero S355, de acuerdo con otros estudios paramétricos recogidos en la literatura [3,33]. Así, el límite elástico se fijó en 355 MPa ($f_{yw} = f_{yf} = f_{ys}$ = 355 MPa), y basándose en Yun y Gardner [39], se consideró un módulo de elasticidad de 210 GPa.

3.3. *Bases de la modelización*

La modelización por elementos finitos para el estudio paramétrico se realizó siguiendo los mismos principios utilizados en las simulaciones de los ensayos experimentales [2,10,18] para la calibración y validación de los modelos numéricos. En este apartado sólo se quiere prestar atención a tres aspectos:

- Se han tenido en cuenta las imperfecciones iniciales (como imperfección geométrica equivalente) considerando una geo-

metría imperfecta inicial siguiendo el primer modo propio con una amplitud máxima de h_w/200, siguiendo lo expuesto en [3,10,27,42] y de acuerdo con las recomendaciones de EN 1993-1-5, Anexo C, C.5, tabla C.2: Imperfecciones geométricas equivalentes (para paneles o subpaneles) [9].

- Tomando como referencia investigaciones previas [17,18], la carga se introdujo como una presión sobre el ala superior dentro de la longitud de carga S_s.
- El material de acero se modeló como un material elástico-perfectamente plástico de acuerdo con investigaciones previas [17,18].

3.4. Análisis de los resultados: patch loading-

3.4.1.Vigas armadas curvas de acero en I con esbeltez baja del alma (Grupo I)

En este apartado se analizan las vigas curvas en I de acero con pequeña esbeltez del alma (h_w/t_w = 83.3), pertenecientes al Grupo I, sometidas a carga concentrada. La figura 9 muestra algunas curvas típicas carga-desplazamiento vertical para vigas de acero en I en planta curva, con pequeña esbeltez de alma, mientras que la tabla 3 muestra los parámetros geométricos más relevantes de las diferentes vigas, así como las correspondientes cargas críticas elásticas de inestabilidad ($F_{cr,FE}$) y las cargas últimas ($F_{u,FE}$). Las cargas críticas elásticas ($F_{cr,FE}$) indicadas en la tabla se obtuvieron a partir de un análisis de autovalores, mientras que los valores de las cargas últimas ($F_{u,FE}$) se correspondían con los valores de las cargas pico observadas a partir de las curvas numéricas carga-desplazamiento vertical. Para estas vigas curvas con pequeña esbeltez del alma, se observa que el valor de la carga crítica elástica de inestabilidad ($F_{cr,FE}$) fue mayor que la carga última correspondiente ($F_{u,FE}$) (ver la tabla 3), mostrando así que no hay reserva de resistencia postcrítica. Además, a partir de los resultados mostrados en la tabla 3 y en la figura 9, se concluye que la carga última de las vigas disminuye a medida que el radio de curvatura disminuye, o cuando la curvatura en planta aumenta, y que este hecho ocurre independientemente de la relación de aspecto (a/h_w) considerada. Del mismo modo, se aprecia que la carga última también disminuye cuando aumenta la relación a/h_w para valores iguales o similares de L/R. Esto significa que la carga última disminuye al aumentar la separación entre rigidizadores, tal y como se ha puesto de manifiesto en investigaciones previas desarrolladas en vigas rectas sometidas a carga concentrada [18]. Por otro lado, puede observarse que para un valor dado de la relación de aspecto a/h_w (ver la tabla 3) no existen grandes variaciones de la carga crítica elástica de inestabilidad y de la carga última para vigas con pequeña curvatura en planta, es decir, con $L/R \leq 0.006$. La disminución más significativa de la carga última con respecto al valor correspondiente para panel plano de alma, es decir con $R = \infty$, se observó para la viga con la mayor curvatura en planta (L/R = 0.15) y con una relación de aspecto igual a 3.0, y la disminución observada de la resistencia fue de aproximadamente un 8%.

3.4.2. Vigas armadas curvas de acero en I con esbeltez alta y muy alta de alma (Grupos II y III)

En este apartado se analiza la respuesta a carga concentrada de vigas curvas de acero en I con esbelteces de alma alta y muy alta (h_w/t_w = 166.67 y 266.7), pertenecientes a los Grupos II y III, para las que se muestran curvas típicas carga-desplazamiento vertical en la figura 10. Para las vigas con esbelteces de alma alta y muy alta,

TABLA 3.
Resultados numéricos para vigas curvas en I, con esbeltez baja de alma (h_w/t_w = 83.3 Grupo I).

Espécimen	h_w (mm)	t_w (mm)	L/R	L(*) (mm)	a/h_w	$F_{cr,FE}$ (kN)	$F_{u,FE}$ (kN)
PL-I-1-12-1-25-∞	1000	12	0	1000	1.0	3084.87	1678.78
PL-I-1-12-1-25-500			0.002			3085.09	1669.20
PL-I-1-12-1-25-200			0.005			3085.92	1657.03
PL-I-1-12-1-25-100			0.01			3087.55	1626.88
PL-I-1-12-1-25-40			0.025			3100.62	1595.95
PL-I-1-12-1-25-20			0.05			3146.68	1567.79
PL-I-1-12-2-25-∞	1000	12	0	2000	2.0	1709.01	1570.10
PL-I-1-12-2-25-500			0.004			1709.62	1553.01
PL-I-1-12-2-25-200			0.01			1712.18	1543.68
PL-I-1-12-2-25-100			0.02			1721.39	1535.74
PL-I-1-12-2-25-40			0.05			1783.16	1472.36
PL-I-1-12-2-25-20			0.1			1981.31	1455.19
PL-I-1-12-3-25-∞	1000	12	0	3000	3.0	1416.65	1471.62
PL-I-1-12-3-25-500			0.006			1416.89	1456.64
PL-I-1-12-3-25-200			0.015			1420.50	1443.60
PL-I-1-12-3-25-100			0.03			1433.38	1418.34
PL-I-1-12-3-25-40			0.075			1517.52	1387.70
PL-I-1-12-3-25-20			0.15			1755.38	1352.87

Nota: La designación de especímenes corresponde a PL – Número del Grupo - h_w en m - t_w en mm - a en m - S_s en cm - R en m.
(*) En vigas pertenecientes al Tipo I no hay rigidizadores intermedios, por lo tanto L=a.

cuyos resultados se muestran en las tablas 4 y 5, respectivamente, se aprecia un aumento de la reserva de resistencia postcrítica en comparación con las vigas con esbelteces pequeñas de alma (Grupo I), ya que se observa que, en muchos casos, el valor de la carga de rotura es superior a la correspondiente carga crítica elástica de inestabilidad (ver las tablas 4 y 5). Esta reserva de resistencia postcrítica disminuye, sin embargo, a medida que aumenta la curvatura en planta. Los resultados numéricos de la carga última $F_{u,FE}$ para una viga recta (L/R = 0) con una relación de aspecto de a/h_w = 3.0, y una viga con un radio de curvatura muy pequeño (L/R = 0.375, R = 20 m) difieren significativamente, alcanzando esta diferencia un valor del 34.3% para las vigas con una esbeltez alta del alma (véase la tabla 4, especímenes: PL-II-2,5-15-7,5-62,5-∞ y PL-II-2,5-15-7,5-62,5-20). Realizando un análisis similar para los resultados de la tabla 5 para los especímenes con esbelteces de alma muy altas, considerando a/h_w = 3.0, en donde se comparan los resultados obtenidos para la viga recta (PL-III-4-15-12-100-∞) con los resultados de los especímenes que presentan curvaturas L/R iguales a 0.3 y 0.6 (especímenes: PL-III-4-15-12-100-40 y PL-III-4-15-12-100-20), las diferencias son del 35.8% y 44.8%, respectivamente. Esto corrobora el hecho de que, para los casos analizados, se produce una reducción considerable de la carga última a medida que aumenta la curvatura.

Cabe destacar que los resultados para $F_{cr,FE}$ y $F_{u,FE}$ observados y discutidos en las tablas 3, 4 y 5, para las vigas pertenecientes a los Grupos I, II y III, son similares a los observados para las vigas Tipo II (Grupos IV, V y VI, respectivamente). Por otra parte, debe indicarse que en los Grupos IV, V y VI, cuando la relación L/R fue mayor que 0.6, se observó que el colapso de estos especímenes fue debido al pandeo lateral. Por lo tanto, en estas vigas no se alcanzó el fallo por carga concentrada -patch loading-.

TABLA 4.
Resultados numéricos para vigas curvas en I, con esbeltez alta de alma (h_w/t_w=166.67 Grupo II).

Espécimen	h_w (mm)	t_w (mm)	L/R	L(*) (mm)	a/h_w	$F_{cr,FE}$ (kN)	$F_{u,FE}$ (kN)
PL-II-2.5-15-2.5-62.5-∞			0			2373.01	3156.03
PL-II-2.5-15-2.5-62.5-200			0.0012			2385.37	3080.90
PL-II-2.5-15-2.5-62.5-100	2500	15	0.0025	2500	1.0	2423.11	2968.11
PL-II-2.5-15-2.5-62.5-40			0.062			2678.30	2835.28
PL-II-2.5-15-2.5-62.5-20			0.125			3470.54	2728.31
PL-II-2.5-15-5-62.5-∞			0			1473.28	2831.21
PL-II-2.5-15-5-62.5-200			0.025			1529.20	2790.19
PL-II-2.5-15-5-62.5-100	2500	15	0.05	5000	2.0	1681.26	2740.99
PL-II-2.5-15-5-62.5-40			0.125			2312.14	2605.12
PL-II-2.5-15-5-62.5-20			0.25			3302.56	2357.26
PL-II-2.5-15-7.5-62.5-∞			0			1261.25	2719.38
PL-II-2.5-15-7.5-62.5-200			0.037			1334.07	2635.27
PL-II-2.5-15-7.5-62.5-100	2500	15	0.075	7500	3.0	1512.81	2527.73
PL-II-2.5-15-7.5-62.5-40			0.187			2144.52	2108.09
PL-II-2.5-15-7.5-62.5-20			0.375			3108.37	1785.35

(*) En vigas pertenecientes al Tipo I no hay rigidizadores intermedios, por lo tanto L=a.

TABLA 5.
Resultados numéricos para vigas curvas en I, con esbeltez muy alta de alma (h_w/t_w=266.67 Grupo III).

Espécimen	h_w (mm)	t_w (mm)	L/R	L(*) (mm)	a/h_w	$F_{cr,FE}$ (kN)	$F_{u,FE}$ (kN)
PL-III-4-15-4-100-∞			0			1595.13	3584.65
PL-III-4-15-4-100-200			0.02			1647.09	3425.89
PL-III-4-15-4-100-100	4000	15	0.04	4000	1.0	1795.25	3150.79
PL-III-4-15-4-100-40			0.1			2634.53	2755.78
PL-III-4-15-4-100-20			0.2			3924.27	2283.65
PL-III-4-15-4-100-∞			0			1092.92	3215.07
PL-III-4-15-4-100-200			0.04			1302.05	3008.56
PL-III-4-15-4-100-100	4000	15	0.08	8000	2.0	1656.25	2609.85
PL-III-4-15-4-100-40			0.2			2598.22	2312.34
PL-III-4-15-4-100-20			0.4			3866.85	1789.98
PL-III-4-15-4-100-∞			0			1011.57	3036.67
PL-III-4-15-4-100-200			0.06			1234.46	2902.79
PL-III-4-15-4-100-100	4000	15	0.12	12000	3.0	1580.86	2338.99
PL-III-4-15-4-100-40			0.3			2556.33	1948.99
PL-III-4-15-4-100-20			0.6			3832.85	1677.25

(*) En vigas pertenecientes al Tipo I no hay rigidizadores intermedios, por lo tanto L=a.

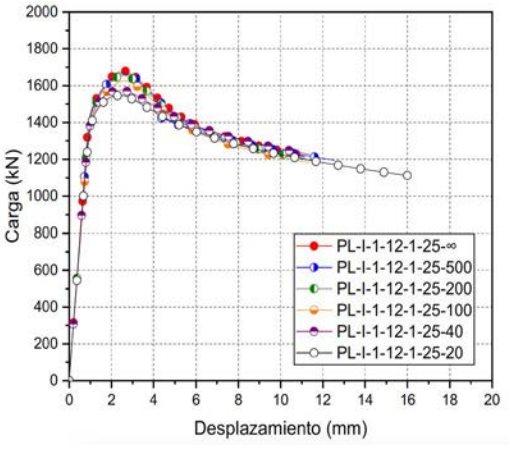

a) Grupo I, t_w = 12 mm, a = 1 m, S_s = 250 mm

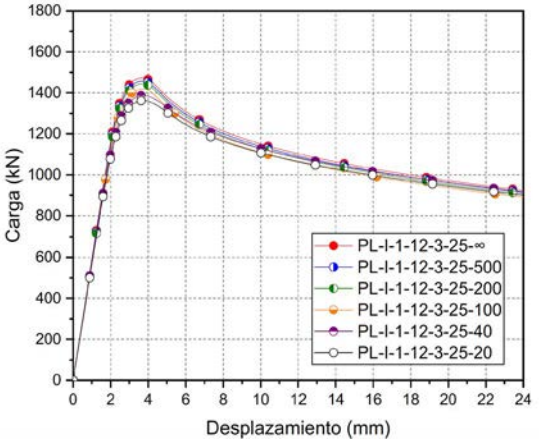

b) Grupo I, t_w = 12 mm, a = 3 m, S_s = 250 mm

Figura 9. Curvas carga-desplazamiento para vigas curvas de acero del Grupo I.

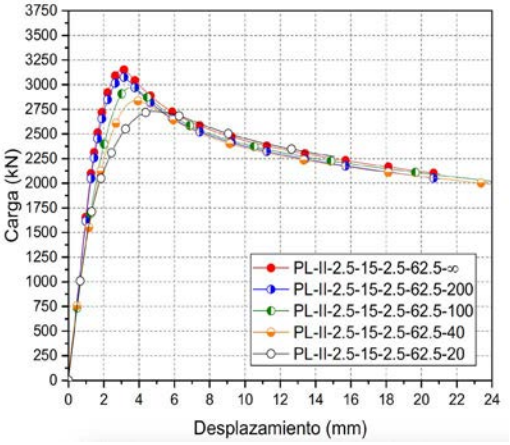

a) Grupo II, t_w = 15 mm, a = 2.5 m, S_s = 625 mm

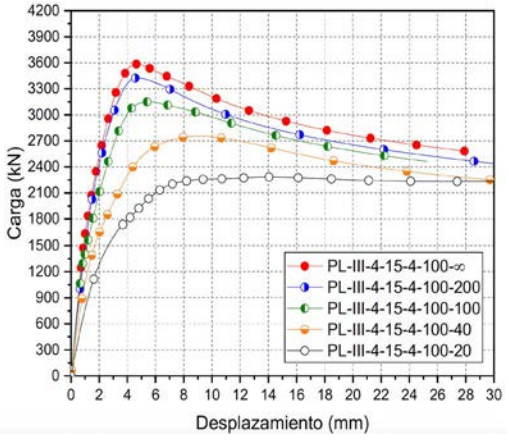

b) Grupo III, t_w = 15 mm, a = 4 m, S_s = 1000 mm

Figura 10. Curvas carga-desplazamiento para vigas curvas de acero de los Grupos II y III.

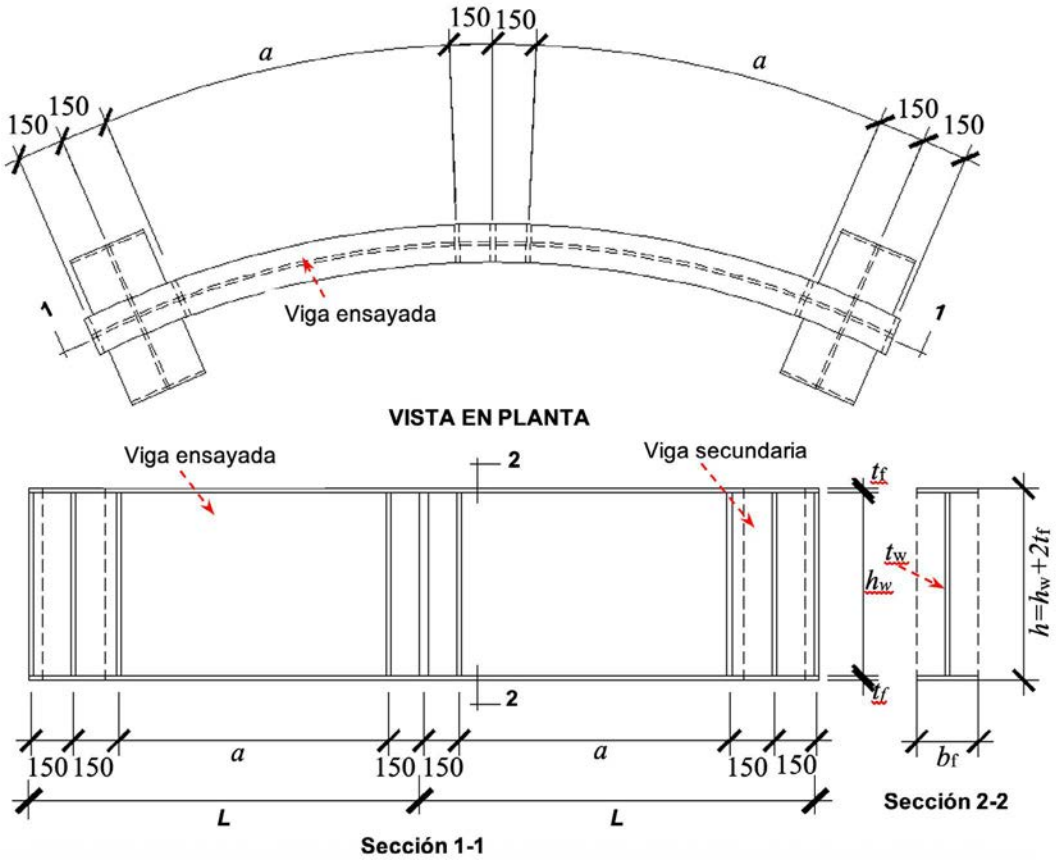

Figura 11. Dimensiones de las vigas curvas en I estudiadas.

4. ESTUDIO PARAMÉTRICO DE VIGAS CURVAS SOMETIDAS A CORTANTE

El modelo de elementos finitos desarrollado en este estudio era capaz de simular el comportamiento a cortante de vigas armadas de acero, reproduciendo los resultados experimentales y prediciendo las cargas últimas con precisión. Se realizó un estudio paramétrico para evaluar la influencia de varios parámetros y variables en la resistencia última a cortante de las vigas armadas curvas en I.

4.1. Prototipos de las vigas analizadas

Las simulaciones numéricas se realizan sobre vigas armadas curvas con sección en I, rigidizada transversalmente, tal como se muestra en la figura 11.

La base de datos numérica se construyó variando los siguientes parámetros: geometría del alma (altura h_w y espesor t_w), radio de curvatura R, y la distancia entre rigidizadores transversales a. Esta variación se eligió a partir de proporciones realistas que se encuentran típicamente en puentes de vigas de acero con planta curva (ver tabla 6). Además, la variación de estos parámetros permite estudiar la influencia de las variables adimensionales más relevantes relativas al comportamiento de las vigas curvas de acero en I sometidas principalmente a cortante, a saber, la relación de aspecto a/h_w, la esbeltez del alma h_w/t_w y la relación a/R siendo a la distancia entre rigidizadores transversales y R el radio de curvatura en planta de la viga.

Para cada grupo perteneciente a la Familia 1, se establece una esbeltez constante del alma, y se consideran tres valores diferentes de la relación de aspecto y cinco valores diferentes de la relación a/R, incluyendo el estudio de la viga recta ($a/R = 0$). Para cada grupo perteneciente a la Familia 2, se establece un valor constante de la esbeltez del panel de alma, y para cada valor de la relación de aspecto, se consideran cinco valores de la relación a/R, desde $a/R = 0$ (panel recto) hasta $a/R = 0.2$ (panel de alma con gran curvatura en planta).

En este estudio paramétrico, todas las vigas curvas analizadas son homogéneas, es decir, se asume el mismo límite elástico de 355 N/mm² para el alma y las alas. En la tabla 6 se resume el conjunto de variaciones de las variables consideradas en el estudio paramétrico, que dio lugar a un total de 70 vigas curvas analizadas.

La tabla 7 muestra los parámetros adimensionales más relevantes considerados en el estudio (h_w/t_w, a/R, a/h_w). Para todas las vigas analizadas, las dimensiones de las alas cumplen los requisitos de la Clase 1, con el objetivo de alcanzar un modo de fallo asociado al esfuerzo cortante.

4.2. Bases de la modelización

La modelización numérica por elementos finitos para el estudio paramétrico se realizó siguiendo los mismos principios descritos en los apartados 2 y 3.3, utilizándolos también para

TABLA 6.
Datos de las vigas curvas de acero consideradas en las simulaciones numéricas.

Variaciones de la base de datos numérica	Grupo				
	Familia-1			Familia-2	
	0	I	II	III	IV
Límite elástico f_y (N/mm²)	355	355	355	355	355
R (mm)	∞	∞	∞		
			240000		
	80000	160000	180000		
	60000	120000	120000	∞	∞
	40000	80000	90000	160000	160000
	30000	60000	80000	80000	80000
	26667	53333	60000	40000	40000
	20000	40000	55000	20000	20000
	15000	30000	45000		
	13333	26667	40000		
	10000	20000	30000		
h_w (mm)	1000	2000	3000	1000	1000
a (mm)	2000	4000	6000	2000	2000
	3000	6000	9000	3000	3000
	4000	8000	12000	4000	
t_w (mm)	12	12	15	8	4
t_s (mm)	30	30	30	30	30
Dimensiones del ala (mm)	450x45	600x45	900x70	500x45	500x45
Número de vigas por grupo	15	15	15	15	10
Simulaciones numéricas			70		

TABLA 7.
Variables y proporciones de las vigas curvas analizadas en las simulaciones numéricas.

Variaciones de la base de datos numérica	Grupo							
	Familia-1			Familia-2				
	0	I	II	III			IV	
h_w (mm)	1000	2000	3000	1000			1000	
h_w/t_w	83.33	166.67	200	125			250	
a/R	0	0	0	0	0	0	0	0
	0.05	0.05	0.05	0.01	0.02	0.03	0.01	0.02
	0.10	0.10	0.10	0.03	0.04	0.05	0.03	0.04
	0.15	0.15	0.15	0.05	0.08	0.10	0.05	0.08
	0.20	0.20	0.20	0.10	0.15	0.20	0.10	0.15
a/h_w	2	3	3					
	3	3	3	2	3	4	2	3
	4	4	4					
$b_f/2t_f$	5.00	6.67	6.43	5.56			5.56	

las simulaciones de los ensayos experimentales recogidos en [2,10,18] para la calibración y validación de los modelos numéricos de elementos finitos desarrollados en este estudio.

4.3. Análisis de los resultados: esfuerzo cortante

Las tablas 8, 9 y 10 muestran las características geométricas de los especímenes analizados y los resultados numéricos del esfuerzo cortante crítico elástico y de la resistencia última a cortante. Los esfuerzos cortantes críticos elásticos numéricos se han obtenido mediante el pertinente análisis de valores propios. Asimismo, también se muestran los valores de la resistencia última a cortante obtenidos según la expresión indicada en la norma EN 1993-1-5 [9], suponiendo que el panel del alma es recto; se considera tanto la contribución del alma como la de las alas.

4.3.1. Vigas curvas de acero en I con esbeltez de alma pequeña (h_w/t_w=83.33)

La figura 12 muestra las curvas esfuerzo cortante-desplazamiento (radial y vertical) para el caso de vigas armadas de acero en I con esbeltez de alma pequeña (Familia 1, Grupo 0). Para estas vigas con esbeltez del alma pequeña, se observa, como era de esperar, que el valor del esfuerzo cortante crítico elástico es mayor que el de la resistencia última a cortante. Por lo tanto, no existe reserva de resistencia, posterior a la

TABLA 8.
Resultados numéricos (esbeltez de alma baja (h_w/t_w=83.33) (Familia 1, Grupo 0).

Espécimen	h_w	t_w	a/R	a	Modelo numérico (kN)		EN1993-1-5 (kN)
	(mm)	(mm)		(mm)	V_{cr}	V_u	V_u
1-0-VC-1-12-00-2			0		3118.15	2216.20	
1-0-VC-1-12-05-2			0.05		3136.65	2218.30	
1-0-VC-1-12-10-2	1000	12	0.10	2000	3219.95	2179.00	2173.19
1-0-VC-1-12-15-2			0.15		3345.60	2136.60	
1-0-VC-1-12-20-2			0.20		3499.95	2098.20	
1-0-VC-1-12-00-3			0		2928.50	2172.50	
1-0-VC-1-12-05-3			0.05		2909.85	2163.40	
1-0-VC-1-12-10-3	1000	12	0.10	3000	3219.95	2139.40	1907.87
1-0-VC-1-12-15-3			0.15		3345.60	2111.40	
1-0-VC-1-12-20-3			0.20		3075.90	2082.40	
1-0-VC-1-12-00-4			0		2808.85	2089.40	
1-0-VC-1-12-05-4			0.05		2820.65	2080.00	
1-0-VC-1-12-10-4	1000	12	0.10	4000	2841.10	2071.30	1764.58
1-0-VC-1-12-15-4			0.15		2873.95	2048.40	
1-0-VC-1-12-20-4			0.20		2917.85	1964.50	

TABLA 9.
Resultados numéricos (esbeltez de alma alta (h_w/t_w=166.67) (Familia 1, Grupo 0).

Espécimen	h_w	t_w	a/R	a	Modelo numérico (kN)		EN1993-1-5 (kN)
	(mm)	(mm)		(mm)	V_{cr}	V_u	V_u
1-1-VC-2-12-00-4			0		1591.20	2910.00	
1-1-VC-2-12-05-4			0.05		1614.95	2870.00	
1-1-VC-2-12-10-4	2000	12	0.10	4000	1737.55	2631.70	2583.81
1-1-VC-2-12-15-4			0.15		1872.20	2342.00	
1-1-VC-2-12-20-4			0.20		2039.15	2209.30	
1-1-VC-2-12-00-6			0		1436.20	2819.50	
1-1-VC-2-12-05-6			0.05		1457.10	2722.80	
1-1-VC-2-12-10-6	2000	12	0.10	6000	1516.90	2526.50	2326.31
1-1-VC-2-12-15-6			0.15		1635.35	2446.20	
1-1-VC-2-12-20-6			0.20		1694.85	2348.30	
1-1-VC-2-12-00-8			0		1359.95	2805.90	
1-1-VC-2-12-05-8			0.05		1385.50	2708.00	
1-1-VC-2-12-10-8	2000	12	0.10	8000	1423.85	2551.70	2175.91
1-1-VC-2-12-15-8			0.15		1480.95	2385.70	
1-1-VC-2-12-20-8			0.20		1550.60	2327.90	

abolladura por cortante. Además, se observa que la resistencia última a cortante disminuye a medida que disminuye el radio de curvatura (o, lo que es lo mismo, a medida que aumenta la curvatura en planta), y este hecho se produce independientemente de la relación de aspecto considerada. Para esbelteces de alma bajas, la mayor disminución de la resistencia última a cortante en relación con el valor correspondiente para el panel de alma recta se obtuvo para la viga con la mayor curvatura en planta (a/R = 0.2) y con relación de aspecto igual a 4.0, y su valor fue de aproximadamente el 6%. Por el contrario, el esfuerzo cortante crítico elástico aumenta con el valor de la curvatura en planta. El mayor incremento sobre el valor correspondiente para el panel de alma recta se obtuvo para la viga con la mayor curvatura en planta (a/R = 0.2) y relación de aspecto igual a 0.2, y su valor fue de alrededor del 12%.

En cualquier caso, se concluye que los resultados numéricos de la resistencia última a cortante para las relaciones a/R = 0 (viga recta) y a/R = 0.05 (viga con curvatura muy pequeña en planta) son muy similares, siendo las diferencias despreciables. Esta conclusión puede extenderse también

TABLA 10.
Resultados numéricos (esbeltez de alma muy alta (h_w/t_w=200.00) (Familia 1, Grupo II).

Espécimen	h_w (mm)	t_w (mm)	a/R	a (mm)	Modelo numérico (kN)		EN1993-1-5 (kN)
					V_{cr}	V_u	V_u
1-2-VC-3-15-00-6			0		2052.25	5104.90	
1-2-VC-3-15-10-6	3000	15	0.10	6000	2373.65	4552.90	4508.02
1-2-VC-3-15-20-6			0.20		2883.40	4267.90	
1-2-VC-3-15-00-9			0		1931.80	4820.40	
1-2-VC-3-15-10-9	3000	15	0.10	9000	2040.25	4211.10	4026.13
1-2-VC-3-15-20-9			0.20		2334.80	3966.60	
1-2-VC3-15-00-12			0		1877.75	4773.50	
1-2-VC-3-15-10-12	3000	15	0.10	12000	1938.80	4512.60	3761.77
1-2-VC-3-15-20-12			0.20		2140.70	4032.90	

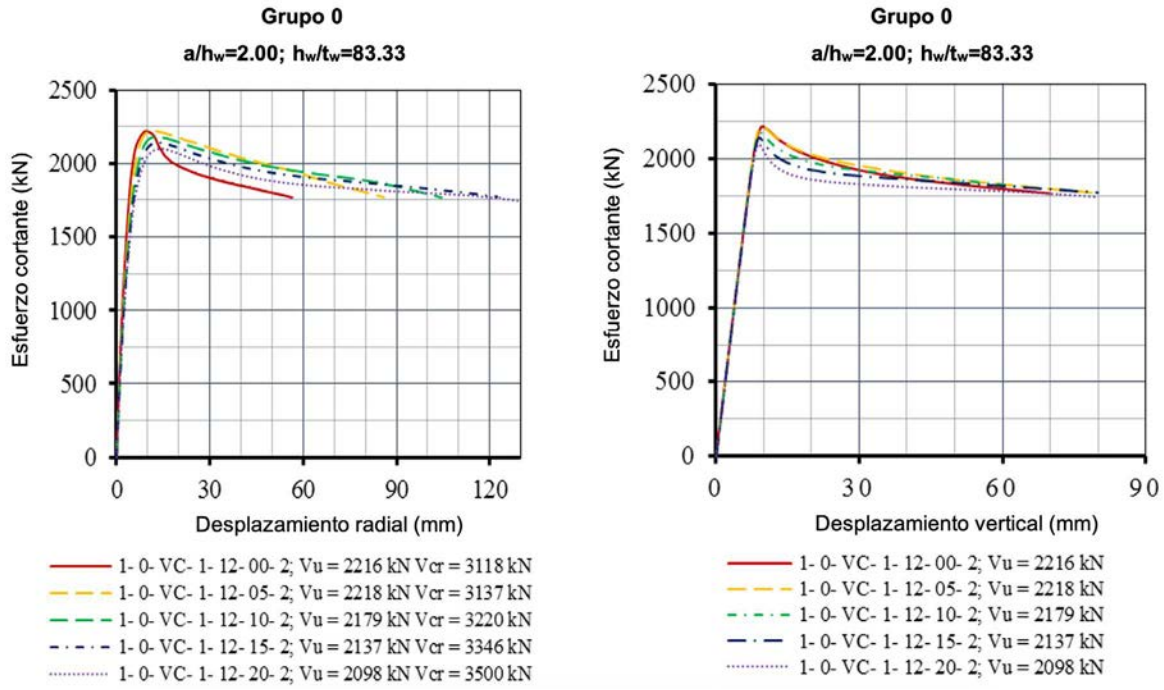

Figura 12. Curvas esfuerzo cortante-desplazamiento (radial y vertical) (h_w/t_w = 83.33).

para vigas curvas con relación a/R = 0.1, ya que la diferencia entre la resistencia última a cortante para la viga curva y la resistencia última a cortante para la viga recta es muy pequeña, inferior al 1.7%. Esta diferencia es aún menor a medida que aumenta la relación de aspecto.

La respuesta estructural de estas vigas curvas de acero en I, independientemente de la relación de aspecto y de la curvatura en planta, fue prácticamente lineal hasta valores del esfuerzo cortante próximos al 90% de la resistencia última a cortante.

4.3.2. Vigas curvas de acero en I con esbeltez de alma alta y muy alta (h_w/t_w = 166.67-200.00)

En la figura 13 se muestran las curvas esfuerzo cortante-desplazamiento vertical obtenidas a partir del modelo numérico para las vigas pertenecientes a la Familia 1 y a los Grupos I y II. De nuevo, se observa que cuanto mayor es la curvatura en planta de la viga curva, menor es la resistencia última a cortante y mayor es el esfuerzo cortante crítico elástico. Es importante destacar que los paneles curvos de alma son capaces de desarrollar el campo diagonal de tracciones y ofrecer reserva de resistencia postcrítica. A modo de ejemplo, la viga curva analizada con relación de aspecto a/h_w = 4, esbeltez del alma h_w/t_w = 200 y a/R = 0.2 muestra una reserva de resistencia postcrítica, relacionada con su esfuerzo cortante crítico elástico, cercana al 88% (ver la tabla 10, viga 1-2-VC-3-15-20-12). Cuanto mayores sean la esbeltez y la relación de aspecto del panel de alma curva, mayor será la reserva de resistencia postcrítica.

La reserva de resistencia postcrítica disminuye a medida que aumenta la curvatura en planta. Los resultados numéricos de la resistencia última a cortante para las rela-

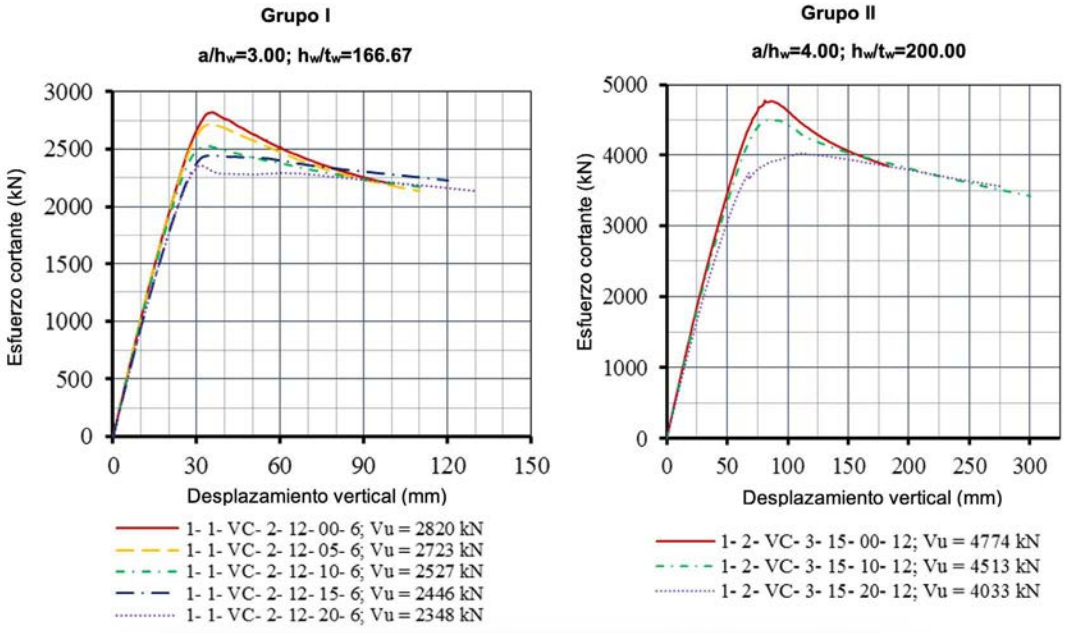

Figura 13. Curvas esfuerzo cortante-desplazamiento vertical (h_w/t_w = 166.67/200).

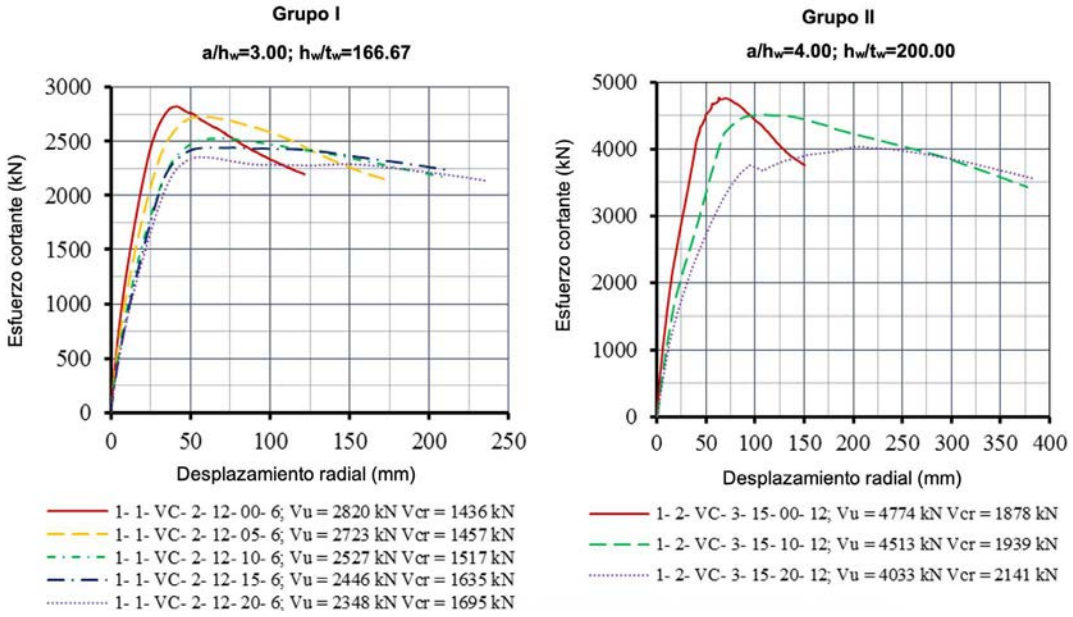

Figura 14. Curvas esfuerzo cortante-desplazamiento radial (h_w/t_w = 166.67/200).

ciones a/R = 0 (viga recta) y a/R = 0.05 (viga con curvatura muy pequeña en planta) son muy similares, siendo las diferencias inferiores al 3.5%. Esto ocurre para paneles de alma curva con esbelteces de alma altas y muy altas. Sin embargo, los valores de resistencia última a cortante para vigas en las que a/R > 0.1 difieren significativamente de los resultados para paneles de alma recta. A modo de ejemplo, la resistencia última a cortante de la viga curva con relación de aspecto a/h_w = 4, esbeltez del alma h_w/t_w = 200 y a/R = 0.2 (Grupo II) es de 4033 kN, mientras que la resistencia última a cortante de la viga recta es de 4774 kN, siendo la reducción de la resistencia a cortante cercana al 15%. La respuesta estructural de las vigas curvas con curvatura en planta elevada (a/R > 0.1) es claramente diferente de la respuesta estructural de la correspondiente viga recta.

Esto también puede apreciarse en la figura 14, en donde se muestran las curvas esfuerzo cortante-desplazamiento radial para algunas vigas analizadas. Por ejemplo, comparando las curvas esfuerzo cortante-desplazamiento radial para la viga analizada con relación de aspecto a/h_w = 4 y esbeltez del alma h_w/t_w = 200, para panel recto y curvo con a/R = 0.2 (curvatura en planta elevada) respectivamente, se concluye que, aumentando la relación de aspecto y la esbeltez del alma del panel, la respuesta del panel curvo es claramente no lineal ya a partir de niveles bajos de esfuerzo cortante, y diferente de la respuesta cuasi-lineal de la viga recta.

Cabe destacar que, como se ha observado previamente para todas las relaciones de esbeltez analizadas, el esfuerzo cortante crítico elástico aumenta con la relación a/R. Ello se

debe al efecto estabilizador de la curvatura, la cual genera tensiones de membrana que estabilizan el alma, reduciendo las deformaciones fuera del plano y aumentando la rigidez. Este incremento de la rigidez del alma frente a inestabilidades locales a causa de la curvatura en planta retrasa el inicio de la abolladura por cortante.

5. EVALUACIÓN DE LAS FORMULACIONES DE CÁLCULO DE EN 1993-1-5 RESPECTO A LOS RESULTADOS NUMÉRICOS

5.1. Carga concentrada - patch loading

En este apartado se presentan las reglas de cálculo para la verificación de vigas armadas rectas frente a carga concentrada recogidas en la próxima versión de la norma europea prEN 1993-1-5 [35] y se evalúan frente a los resultados numéricos obtenidos en el estudio paramétrico. Se realiza un análisis comparativo entre los resultados predichos por la formulación prEN 1993-1-5 [35] para vigas rectas, en términos de carga crítica elástica de inestabilidad y carga de rotura, y los resultados numéricos de vigas armadas curvas, proponiéndose a continuación recomendaciones prácticas.

De acuerdo con prEN 1993-1-5 [35], la resistencia de cálculo de vigas armadas con almas rigidizadas o no rigidizadas frente a carga concentrada debe obtenerse mediante la aplicación de las ecuaciones (1)-(8), en las que todos los parámetros han sido definidos anteriormente. Debe tenerse en cuenta que estas ecuaciones se prescriben sólo para vigas rectas, y que en [35] no se hace mención explícita a su aplicabilidad para la predicción de la resistencia frente a carga concentrada de vigas armadas curvas de acero.

$$F_{Rd,EN1993\text{-}1\text{-}5} = \frac{\chi_F \, l_y \, t_w \, f_{yw}}{\gamma_{M1}} \tag{1}$$

$$\chi_F = \frac{1.0}{\varphi_F + \sqrt{\varphi_F^2 - \bar{\lambda}_F}} \leq 1.0 \tag{2}$$

donde:

$$\varphi_F = \tfrac{1}{2}\left(1 + \alpha_{F0}\,(\bar{\lambda}_F - \bar{\lambda}_{F0}) + \bar{\lambda}_F\right) \tag{3}$$

$$\bar{\lambda}_F = \sqrt{\frac{l_y \, t_w \, f_{yw}}{F_{cr}}} \tag{4}$$

$$\alpha_{F0} = 0.75 \;\; ; \;\; \bar{\lambda}_{F0} = 0.50$$

$$F_{cr} = 0.9 \, k_F \, E \, \frac{t_w^3}{h_w} \tag{5}$$

$$k_F = 6 + 2\left(\frac{h_w}{a}\right)^2 \tag{6}$$

$$l_y = S_s + 2\, t_f \left(1 + \sqrt{m_1}\right) \quad \text{con} \quad l_y \leq a \tag{7}$$

donde:

$$m_1 = \frac{b_f}{t_w} \tag{8}$$

Es importante puntualizar que las expresiones (6) y (7), utilizadas para determinar el coeficiente de pandeo k_F y la longitud efectiva de carga l_y que se presentan aquí, están prescritas en [35] sólo para el tipo de aplicación de carga estudiado en esta investigación, es decir, carga aplicada a través del ala y resistida por esfuerzo cortante en el alma. Para otros tipos de aplicación de la carga, el apartado 8.1 de prEN 1993-1-5 [35] ofrece las pertinentes definiciones de k_F y l_y. Además, debe tenerse en cuenta que el coeficiente parcial para la resistencia γ_{M1} que aparece en la ecuación (1) se ha tomado como 1.0, a efectos comparativos en esta investigación.

5.1.1. Predicción de la carga crítica elástica de inestabilidad

En este apartado se presenta la evaluación de la predicción de la carga crítica elástica de inestabilidad de las vigas armadas curvas de acero en sección en I, utilizando la expresión prescrita en prEN 1993-1-5 [35] (es decir, la ecuación (5)) para vigas armadas rectas. Basándose en los resultados numéricos presentados en el apartado 3.4, se observa que la carga crítica elástica de inestabilidad de vigas armadas con paneles de alma curva es mayor que la de las vigas con paneles de alma recta equivalentes, calculadas utilizando la expresión (5), siempre que la esbeltez del alma y la relación de aspecto del panel de alma sean las mismas. Teniendo en cuenta lo anterior, los autores sugieren que la carga crítica de vigas armadas con paneles curvos se determine aproximadamente utilizando la conocida expresión de la teoría clásica para vigas con paneles de alma recta prescrita en prEN 1993-1-5 [35] para un alma equivalente con la misma esbeltez y relación de aspecto del panel, lo que conduce a valores que estarán del lado seguro.

La figura 15 muestra una comparación de las cargas críticas elásticas de inestabilidad derivadas del modelo numérico ($F_{cr,FE}$) y de la expresión recogida en prEN 1993-1-5 [35], Ec. (5) ($F_{cr,EC\text{-}3}$) para todas las vigas analizadas en el estudio paramétrico. El valor medio de la relación $F_{cr,FE}/F_{cr,EC\text{-}3}$ y el correspondiente coeficiente de variación (COV) se presentan también en las figuras para los diferentes Grupos considerados en el estudio paramétrico (ver la tabla 2 y la figura 11) agrupados por las mismas relaciones h_w/t_w y a/h_w. Se puede observar que, en muchos casos, la ecuación (5) tiende a subestimar, de forma excesiva, la carga crítica de las vigas armadas curvas de acero de sección en I, dando lugar a resultados notablemente dispersos; no obstante, la predicción de la carga crítica es, en general, razonable.

5.1.2. Predicción de la carga última

En este apartado se presenta la evaluación de la formulación de prEN 1993-1-5 [35] para la estimación de la resistencia frente a carga concentrada de vigas armadas con paneles rectos de alma cuando se aplican a vigas armadas en planta curva. La figura 16 presenta las relaciones $F_{u,FE}/F_{Rd,EN\ 1993\text{-}1\text{-}5}$ para todas las vigas curvas de acero con sección en I analizadas en el estudio paramétrico en función de la esbeltez del alma (h_w/t_w) y de la relación de aspecto (a/h_w), donde $F_{u,FE}$ es la carga última obtenida mediante el modelo numérico de elementos finitos y $F_{Rd,EN\ 1993\text{-}1\text{-}5}$ es la resistencia frente a carga concentrada, obtenida mediante la aplicación de las ecuaciones (1)-(8). En la figura 16 se puede observar que la predicción de la carga última $F_{Rd,EN\ 1993\text{-}1\text{-}5}$, aplicando prEN 1993-1-5 [35], tiende a subestimar la resistencia última de las vigas curvas, y

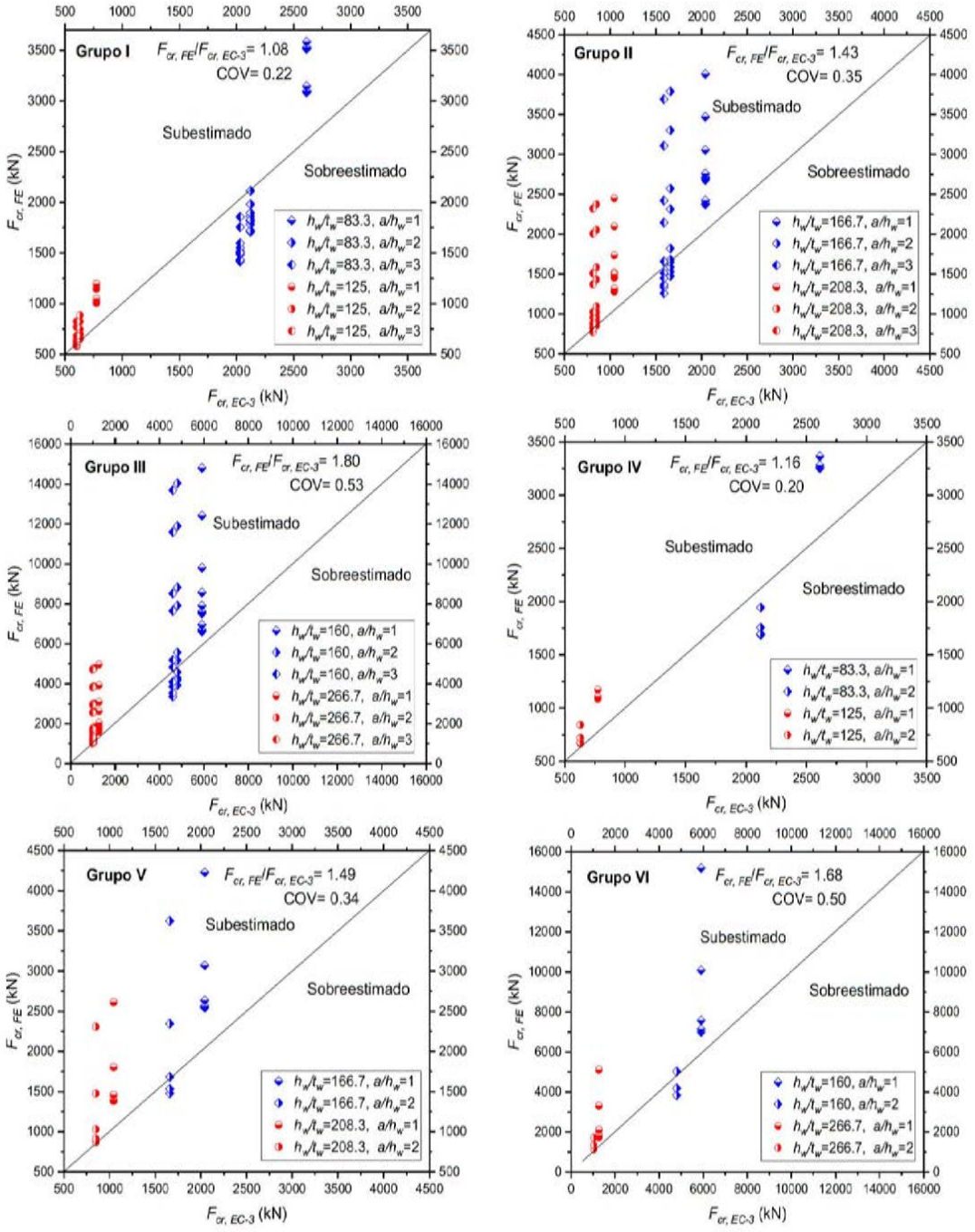

Figura 15. Predicción de la carga crítica elástica de inestabilidad. Comparación de los resultados de $F_{cr,EC-3}$ vs. $F_{cr,FE}$.

de forma excesivamente conservadora en muchos casos. Para vigas curvas con una esbeltez del alma relativamente baja, es decir, para relaciones h_w/t_w iguales a 83.3 y 125, prEN 1993-1-5 [35] subestima el valor de la carga de rotura para todos los casos (véase la figura 16(a)). Por otro lado, también se puede apreciar en la figura 16(a) que hay varias vigas curvas para las que la aplicación de la prEN 1993-1-5 [35] lleva a sobrestimar los resultados numéricos, principalmente para vigas con esbelteces de alma altas y muy altas (concretamente, para valores de h_w/t_w iguales a: 160, 166.7, 208.3 y 266.7). La figura 16(b) muestra las relaciones $F_{u,FE}/F_{Rd,EN\ 1993\text{-}1\text{-}5}$ para las vigas curvas en I de acero analizadas en función de su relación a/h_w, y en donde no se observa una tendencia clara entre la relación $F_{u,FE}/F_{Rd,EN\ 1993\text{-}1\text{-}5}$ y la relación de aspecto. Obsérvese que las relaciones de aspecto (a/h_w) en la figura 16(b) son iguales a 1.0, 2.0 y 3.0 para los Grupos I, II y III, y a 1.0 y 2.0 para los Grupos IV, V y VI.

La figura 17(a) muestra valores de la relación $F_{u,FE}/F_{Rd,EN\ 1993\text{-}1\text{-}5}$ para vigas armadas curvas de Tipo I (véase la figura 8) pertenecientes a los Grupos I, II y III, en función de la relación L/R. Se puede apreciar que, para relaciones $L/R < 0.3$, prEN 1993-1-5 [35] subestima el valor de la carga de rotura de las vigas curvas. De forma similar, la figura 17(b) ofrece la relación $F_{u,FE}/F_{Rd,EN\ 1993\text{-}1\text{-}5}$ en función de la curvatura L/R

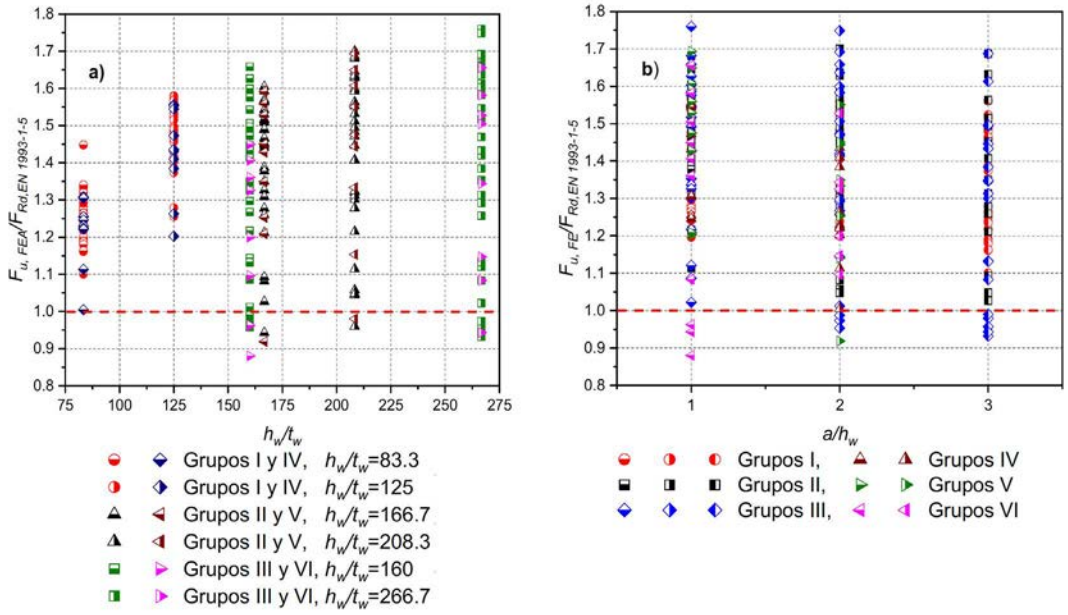

Figura 16. Predicción de la carga última: a) $F_{u,FE}/F_{Rd,EN\ 1993\text{-}1\text{-}5}$ vs. h_w/t_w; b) $F_{u,FE}/F_{Rd,EN\ 1993\text{-}1\text{-}5}$ vs. a/h_w.

para vigas de Tipo II pertenecientes a los Grupos IV, V y VI, en donde se observa un comportamiento similar de predicción de la carga última cuando $L/R < 0.3$, resultando en una estimación conservadora de la capacidad de la viga. Por lo tanto, basándose en los resultados anteriores, se puede concluir que la carga última de las vigas armadas curvas de acero sometidas a carga concentrada se puede determinar de forma aproximada y conservadora utilizando las reglas de cálculo recogidas en prEN 1993-1-5 [35] para vigas rectas, siempre que $L/R < 0.3$. De acuerdo con las referencias relevantes [2], y a modo orientativo, puede decirse que la relación L/R suele estar en el rango de 0.0 (vigas rectas) a 0.1 en realizaciones de puentes de carretera con curvatura en planta. Por lo tanto, los resultados presentados en esta investigación revelan que la resistencia a la carga concentrada de las vigas con curvatura en planta que se encuentran habitualmente en la práctica puede determinarse utilizando las reglas de diseño prescritas en prEN 1993-1-5 [35], para vigas rectas equivalentes.

5.2. *Esfuerzo cortante*

En este apartado se presentan las reglas de cálculo para la verificación de las vigas armadas rectas frente al esfuerzo cortante que se recogen en la próxima versión de la norma europea prEN 1993-1-5 [35] y se evalúan frente a los resultados numéricos obtenidos en el estudio paramétrico. Se realiza un análisis comparativo entre los resultados predichos por la formulación prEN 1993-1-5 [35] para vigas rectas, en términos de la carga crítica elástica de inestabilidad y el esfuerzo cortante último, y los resultados numéricos de las vigas armadas curvas de acero, a partir de los cuales se proponen recomendaciones prácticas.

Según la norma prEN 1993-1-5 [35], la resistencia última a cortante debe calcularse como

$$V_{b,Rd} = V_{bw,Rd} + V_{bf,Rd} \leq \frac{\eta f_{yw} h_w t_w}{\sqrt{3}\,\gamma_{M1}} \tag{9}$$

en donde $V_{bw,Rd}$ representa la contribución del alma a la resistencia a cortante, dada por

$$V_{bw,Rd} = \frac{\chi_w f_{yw} h_w t_w}{\sqrt{3}\,\gamma_{M1}} \tag{10}$$

y $V_{bf,Rd}$ representa la contribución de las alas. El coeficiente η considera los efectos del endurecimiento por deformación y su valor recomendado para grados de acero de hasta S460 es 1.20. El coeficiente de reducción χ_w para la contribución del alma a la resistencia a cortante depende de la esbeltez reducida del alma que se obtiene mediante la siguiente expresión

$$\bar{\lambda}_w = 0.76\sqrt{\frac{f_{yw}}{\tau_{cr}}} \tag{11}$$

La tensión tangencial crítica de abolladura por cortante τ_{cr} se obtiene según la teoría clásica con el coeficiente de pandeo k_τ para condiciones de borde simplemente apoyado. Cabe señalar que el coeficiente parcial para la resistencia γ_{M1} que figura en las ecuaciones (9) y (10) se ha tomado como 1.0, a efectos comparativos en esta investigación.

5.2.1. *Predicción del esfuerzo cortante crítico elástico de abolladura*

Tal como se ha comentado anteriormente, de acuerdo con los resultados numéricos, el esfuerzo cortante crítico elástico para los paneles de alma curva es mayor que el esfuerzo cortante crítico para el panel de alma recta correspondiente, siempre que la esbeltez del alma y la relación de aspecto del panel de alma sean iguales. Por lo tanto, el valor del esfuerzo cortante crítico para paneles curvos puede determinarse utilizando la conocida expresión de la teoría clásica para paneles de alma recta. Ello conducirá a comprobaciones que estarán del lado seguro. En la tabla 11 se muestran los valores del esfuerzo cortante crítico elástico derivados del modelo numérico y de la expresión establecida en prEN 1993-1-5 [35] para algunas

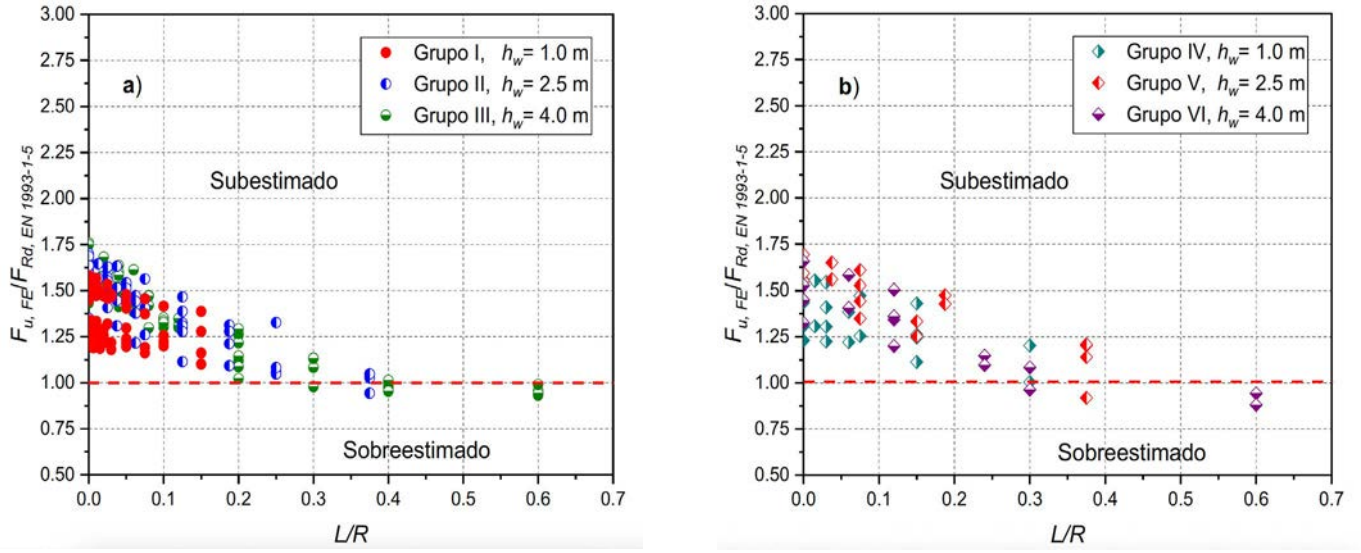

a) Vigas de Grupos I, II y III (Tipo I)

b) Vigas de Grupos IV, V y VI (Tipo II)

Figura 17. Resultados de $F_{u,FE}/F_{Rd,EN\ 1993\text{-}1\text{-}5}$ vs. curvatura L/R.

vigas analizadas en el presente estudio, incluidas en los grupos III y IV de la Familia 2 (ver las tablas 6 y 7). Se observa que los valores obtenidos según prEN 1993-1-5 son claramente inferiores a los obtenidos numéricamente, debido a que el panel de alma se considera con todos los bordes simplemente apoyados. Se ha realizado un estudio adicional relativo a la determinación de los esfuerzos cortantes críticos considerando condiciones de borde empotrado para el panel de alma y del coeficiente de abolladura por cortante $k_{\tau,ff}$ adecuado. Se puede observar en la tabla 11 que los valores de los esfuerzos cortantes críticos elásticos asumiendo condiciones de contorno de bode empotrado son muy próximos a los obtenidos mediante el modelo numérico.

5.2.2. Predicción de la resistencia última a cortante

Se realiza un análisis comparativo entre los valores de las 70 vigas curvas analizadas, obtenidos numéricamente y de acuerdo con prEN 1993-1-5 [35], asumiendo tales vigas curvas como rectas.

La figura 18(a) muestra los valores de $V_{u,num}/V_{u,EN\ 1993\text{-}1\text{-}5}$ para todas las vigas armadas curvas analizadas, en función de la esbeltez del alma. No se observa una tendencia clara entre los resultados obtenidos y el parámetro de esbeltez. Por otro lado, la figura 18(b) muestra los mismos valores $V_{u,num}/V_{u,EN\ 1993\text{-}1\text{-}5}$ para todas las vigas armadas curvas analizadas, en función de la relación de aspecto. En cierto modo, puede observarse que a medida que aumenta la relación de aspecto del panel del alma, aumentan los valores de $V_{u,num}/V_{u,EN\ 1993\text{-}1\text{-}5}$, concluyendo que la obtención de la resistencia última a cortante para las vigas armadas curvas de acero mediante la expresión indicada en prEN 1993-1-5 [35] conduce a resultados más fiables cuando aumenta la relación de aspecto.

La figura 19(a) muestra los valores de la relación $V_{u,num}/V_{u,EN\ 1993\text{-}1\text{-}5}$ para las 45 vigas analizadas pertenecientes a la Familia 1, en función de la relación a/R. Para relaciones $a/R \leq 0.1$, todos los valores de $V_{u,num}/V_{u,EN\ 1993\text{-}1\text{-}5}$ son superiores a la unidad. Por lo tanto, en base a los resultados obtenidos, se concluye que la resistencia a cortante de las vigas curvas puede determinarse utilizando las reglas de cálculo establecidas en prEN 1993-1-5 [35] para vigas rectas siempre que la relación $a/R \leq 0.1$. Los resultados presentados en la figura 19(b), relativos a las vigas curvas de la Familia 2, refuerzan claramente la conclusión, incluso para vigas curvas con una esbeltez del alma elevada. Para vigas analizadas en las que $a/R \leq 0.1$, el valor mínimo de la relación $V_{u,num}/V_{u,EN\ 1993\text{-}1\text{-}5}$ es de 0.98, y se ha obtenido para la viga curva con relación de aspecto 2.0 y esbeltez de alma 125.

TABLA 11.
Resultados numéricos y según prEN 1993-1-5 [35] del esfuerzo cortante crítico elástico.

Grupo – a/h_w	V_{cr} numérico	V_{cr} prEN1993-1-5	V_{cr} $k_{\tau,ff}$ (empot.)	$V_{cr,num}/V_{cr,EN1993}$	$V_{cr,num}/V_{cr,k,ff}$
	(kN)				
Grupo III-a/h_w=2	952.30	616.11	1008.70	1.55	0.94
Grupo III-a/h_w=3	887.45	562.12	933.10	1.58	0.95
Grupo III-a/h_w=4	866.95	543.22	906.70	1.60	0.96
Grupo IV-a/h_w=2	121.39	77.01	126.09	1.58	0.96
Grupo IV-a/h_w=3	112.72	70.26	116.64	1.60	0.97

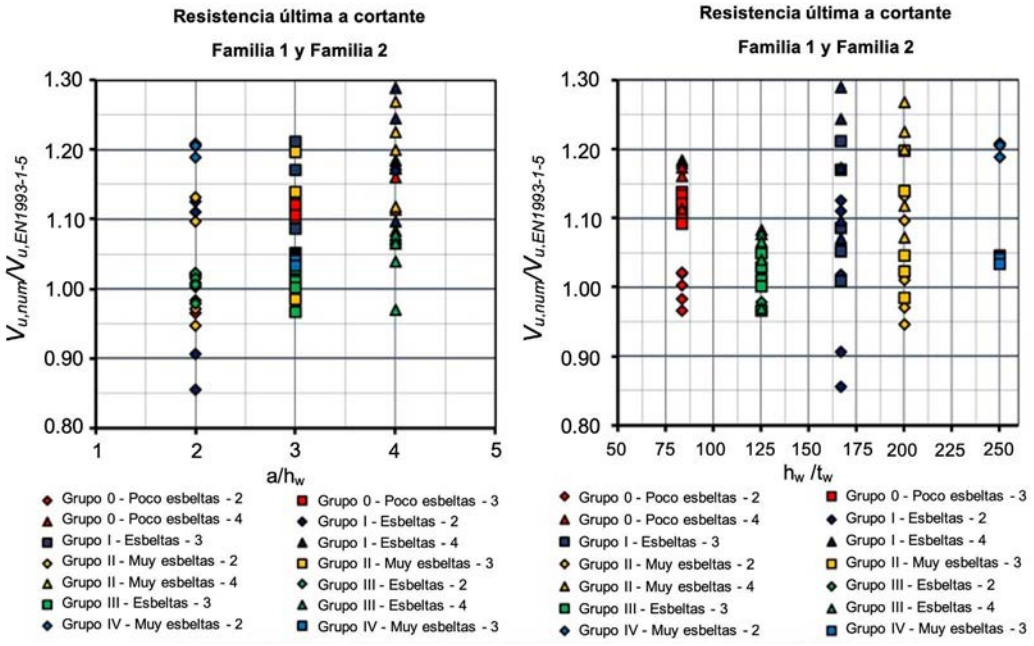

Figura 18. Resultados de $V_{u,num}/V_{u,EN1993\text{-}1\text{-}5}$: a) Esbeltez del alma h_w/t_w. b) Relación de aspecto a/h_w.

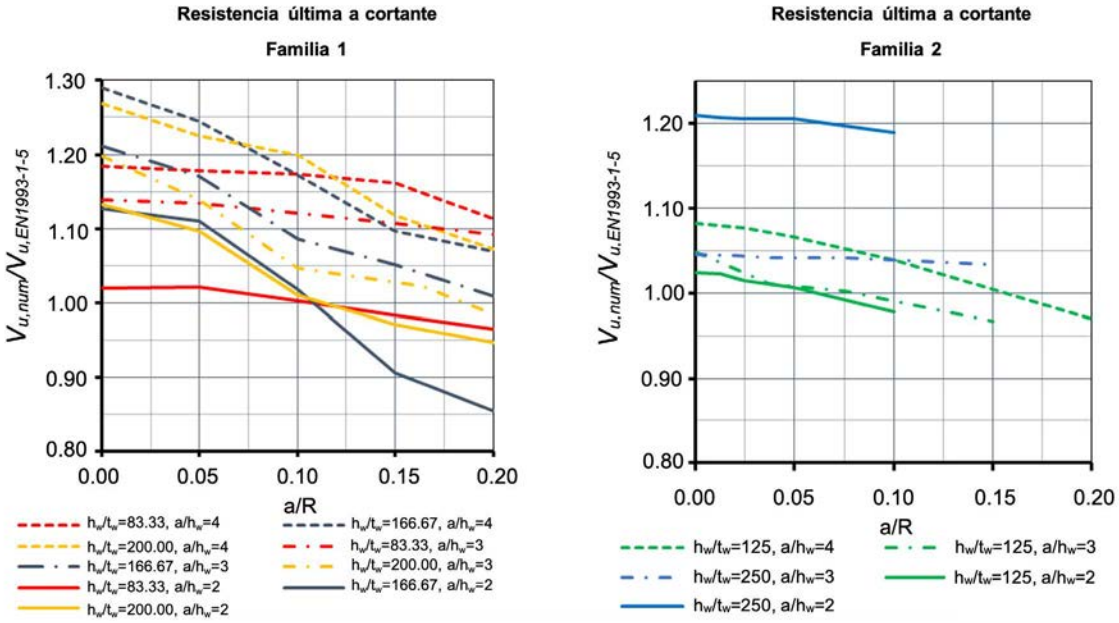

Figura 19. Resultados de la relación $V_{u,num}/V_{u,EN1993\text{-}1\text{-}5}$ vs. a/R: a) Vigas Familia 1. b) Vigas Familia 2.

6. CONCLUSIONES

La futura edición de la norma prEN 1993-2 [36] incluye alguna cláusula para el cálculo de vigas armadas de acero en planta curva; no obstante, no aborda específicamente el dimensionamiento y comprobación de dichas vigas curvas frente a carga concentrada y esfuerzo cortante, a sabiendas de que éste es un tipo estructural utilizado habitualmente en el diseño de puentes y edificios singulares. Este tema tampoco se trata en la actual ni en la próxima edición de la norma europea para el cálculo de elementos estructurales de chapa EN 1993-1-5 [9,35], no ofreciendo ninguna orientación para el cálculo de vigas armadas en planta curva con sección transversal en I, sometidas a carga concentrada -patch loading- y a esfuerzo cortante. Con el objetivo de cubrir esta laguna, en este trabajo de investigación se ha desarrollado un extenso análisis numérico no lineal para estudiar el comportamiento estructural de vigas armadas de acero con sección transversal en I, en planta curva, sometidas a carga concentrada y esfuerzo cortante, que ha permitido, posteriormente, ofrecer recomendaciones de diseño para este tipo estructural.

Los modelos de elementos finitos desarrollados se validaron frente a los resultados experimentales disponibles en la bibliografía, referentes a vigas armadas de chapa de acero rectas y curvas sometidas a carga concentrada. Se observó una muy buena concordancia entre los resultados derivados de los modelos numéricos y los resultados experimentales, ya que aquéllos predijeron con exactitud las relaciones carga-desplazamiento vertical y los modos de fallo de las vigas armadas rectas y con curvatura en planta, con un valor medio de la relación $F_{u,exp}/F_{u,FE}$ experimental-numérica igual a 0.976 y un coeficiente de variación de 0.016.

Tras la pertinente validación de los modelos numéricos, con el objetivo de poder evaluar la resistencia última frente a carga concentrada -patch loading- de vigas armadas curvas de acero en sección en I, se llevó a cabo un amplio estudio paramétrico que incluía 252 modelos numéricos. Como resultado de este estudio paramétrico, se pueden extraer varias conclusiones: (1) la carga crítica elástica de inestabilidad de las vigas armadas curvas aumenta a medida que aumenta la relación entre la longitud de vano y el radio de curvatura de la viga en planta L/R; (2) la predicción de la carga crítica elástica utilizando la formulación de prEN 1993-1-5 [35] para vigas armadas rectas tiende a estimar de forma conservadora los valores obtenidos numéricamente, y arroja resultados significativamente dispersos; (3) la carga última disminuye cuando disminuye el radio de curvatura. Teniendo todo ello en cuenta, se puede extraer una recomendación práctica de diseño, concluyendo que la resistencia última de las vigas armadas curvas de acero en sección en I se puede determinar utilizando las reglas de cálculo prescritas en prEN 1993-1-5 [35] para vigas armadas rectas, siempre que $L/R < 0.3$. Esta conclusión es válida para los límites de la relación de aspecto $a/h_w \leq 3.0$ y de la esbeltez del alma $h_w/t_w \leq 266.7$ que se han adoptado en esta investigación.

Asimismo, para poder evaluar la resistencia última a cortante de vigas armadas curvas de acero en sección en I, se realizó un amplio estudio paramétrico que incluía 70 modelos numéricos. Se pueden extraer varias conclusiones: (1) el esfuerzo cortante crítico elástico para las vigas armadas curvas aumenta al aumentar la relación a/R, siendo a la distancia entre rigidizadores transversales y R el radio de curvatura en planta de la viga; (2) las vigas armadas curvas de acero en sección en I pueden desarrollar la acción de campo diagonal de tracciones cuando se ven sometidas a cortante. El modelo mecánico aplicable a vigas armadas rectas de acero con sección en I puede extenderse al caso de vigas armadas curvas de acero con sección en I. Se produce una reducción de la reserva de resistencia postcrítica de los paneles de alma de las vigas curvas con el aumento de la curvatura en planta, es decir, con el aumento de la relación a/R; (3) los resultados numéricos derivados del estudio paramétrico permiten concluir que las curvaturas horizontales de las vigas curvas que suelen encontrarse en la práctica no influyen significativamente en la resistencia a cortante, en comparación con los resultados relativos a las vigas armadas rectas.

En base a los resultados obtenidos, se concluye que la resistencia a cortante de vigas armadas curvas de acero en sección en I puede determinarse utilizando las reglas de cálculo establecidas en prEN 1993-1-5 [35] para vigas rectas, siempre que la relación $a/R \leq 0.1$. Estas conclusiones se apoyan implícitamente en la consideración de los siguientes límites para la relación de aspecto $a/h_w \leq 4$ y de la esbeltez del alma $h_w/t_w \leq 200$ para las vigas armadas curvas de acero en sección en I analizadas en este estudio.

Referencias

[1] Structural Stability Research Council—Task Group 14. Horizontally curved girders—A Look to the future., in: 1991 Annu. Report, SSRC Work., Chicago, IL, 1991.

[2] N.E. Shanmugam, M. Mahendrakumar, V. Thevendran, Ultimate load behavior of horizontally curved plate girders, J. Constr. Steel Res. 59 (2003) 509–529. https://doi.org/10.1016/S0143-974X(02)00043-3.

[3] E. Mirambell, E. Rodríguez, A. Rodríguez, A numerical study of curved steel I-girders subjected to shear, in: B.Y.& Y. Cai (Ed.), Eighth Int. Conf. STEEL Alum. Struct., Hong Kong, 2016.

[4] J. Bonilla, E. Mirambell, I. Arrayago, Numerical analysis of curved steel plate girders subjected to patch loading, Eng. Struct. 297 (2023) 117015. https://doi.org/10.1016/j.engstruct.2023.117015

[5] C.A. Granholm, Tests on girders with extremely thin web plates, Report 202, Inst. för Byggnadsteknik, Göteborg, 1960.

[6] O. Lagerqvist, Patch loading - Resistance of steel girders subjected to concentrated forces, Doctoral thesis 1994:159D, Luleå University of Technology, ISRN: HLU-TH-T- -159-D--SE, 1994.

[7] O. Lagerqvist, B. Johansson, Resistance of I-girders to Concentrated loads, J. Constr. Steel Res. 39 (1996) 87–119. https://doi.org/10.1016/S0143-974X(96)00023-5

[8] B. Johansson, R. Maquoi, G. Sedlacek, New design rules for plated structures in Eurocode 3, J. Constr. Steel Res. 57 (2001) 279–311. https://doi.org/10.1016/S0143-974X(00)00020-1

[9] European Committee for Standardization (CEN). EN 1993-1-5. Eurocode 3 – Design of Steel Structures – Part 1-5: Plated structural elements, Brussels, Belgium, 2006.

[10] J. Gozzi, Patch Loading Resistance of Plated Girders - Ultimate and serviceability limit state, PhD. Thesis, Luleå, 2007.

[11] C. Graciano, B. Johansson, Resistance of longitudinally stiffened I-girders subjected to concentrated loads, J. Constr. Steel Res. 59 (2003) 561–586. https://doi.org/10.1016/S0143-974X(02)00046-9

[12] U. Kuhlmann, M. Seitz, Longitudinally stiffened girder webs subjected to patch loading, in: Steelbridge 2004, Int. Symp. Steel Bridg., Millau, France, 2004.

[13] L. Davaine, J.M. Aribert, Launching of steel girder bridge, in: Proc. Fourth Eur. Conf. Steel Compos. Struct. Eurosteel 2005, Maastricht, Netherlands, 2005.

[14] M. Clarin, Plate buckling resistance - Patch loading of longitudinally stiffened webs and local buckling, Doctoral thesis 2007:31, Luleå University of Technology, ISRN: LTU-DT--07/31--SE, 2007.

[15] B. Kövesdi, Patch loading resistance of slender plate girders with longitudinal stiffeners, J. Constr. Steel Res. 140 (2018) 237–246. https://doi.org/10.1016/j.jcsr.2017.10.031

[16] B. Kövesdi, B.J. Mecséri, L. Dunai, Imperfection analysis on the patch loading resistance of girders with open section longitudinal stiffeners, Thin-Walled Struct. 123 (2018) 195–205. https://doi.org/10.1016/j.tws.2017.11.030

[17] R. Chacón, E. Mirambell, E. Real, Hybrid steel plate girders subjected to patch loading, Part 1: Numerical study, J. Constr. Steel Res. 66 (2010) 695–708. https://doi.org/10.1016/j.jcsr.2009.12.005.

[18] R. Chacón, E. Mirambell, E. Real, Transversally stiffened plate girders subjected to patch loading. Part 1. Preliminary study, J. Constr. Steel Res. 80 (2013) 483–491. https://doi.org/10.1016/j.jcsr.2012.06.008.

[19] R. Chacón, E. Mirambell, E. Real, Transversally stiffened plate girders subjected to patch loading. Part 2. Additional numerical study and design proposal, J. Constr. Steel Res. 80 (2013) 492–504. https://doi.org/10.1016/j.jcsr.2012.06.001

[20] H. Nakai, H. Kotoguchi, A study on lateral buckling strength and design aid for horizontally curved I-girder bridges, in: Proc. Japan Soc. Civ. Eng. 339, 1983: pp. 195–205. https://doi.org/https://doi.org/10.2208/jscej1969.1983.339_195.

[21] H. Nakai, T. Kitada, Experimental study on ultimate strength on bending strength of web plate of horizontally curved girder bridges, in: Proc. Japan Soc. Civ. Eng. 340, 1983: pp. 19–28.

[22] N.E. Shanmugam, V. Thevendran, J.Y. Richard Liew, L.O. Tan, Experimental study on steel beams curved in plan, J. Struct. Eng. 121 (1995) 249–259. https://doi.org/10.1061/(ASCE)0733-9445(1995)121:2(249).

[23] Y.L. Pi, N.S. Trahair, Nonlinear elastic behaviour of I-beams curved in plan, J. Struct. Eng. 123 (1997) 1201–9. https://doi.org/10.1061/(ASCE)0733-9445(1997)123:9(1201)

[24] V. Thevendran, N.E. Shanmugam, S. Chen, J.Y. Richard Liew, Experimental study on steel–concrete composite beams curved in plan, Eng. Struct. 22 (2000) 877–89. https://doi.org/10.1016/S0141-0296(99)00046-2

[25] V. Thevendran, N.E. Shanmugam, S. Chen, J.Y. Richard Liew, Nonlinear analysis of steel–concrete composite beams curved in plan, Finite Elem. Anal. Des. 32 (1999) 125–39. https://doi.org/10.1016/S0168-874X(99)00010-4

[26] Y.L. Pi, M.A. Bradford, N.S. Trahair, Inelastic analysis and behaviour of steel I-beams curved in plan, J. Struct. Eng. 126 (2000) 772–9. https://doi.org/10.1061/(ASCE)0733-9445(2000)126:7(772)

[27] A. Rodriguez, Estudio de la inestabilidad frente a cargas concentradas de vigas armadas de acero, MSc. Thesis, Universidad Politécnica de Cataluña, 2016.

[28] C.G. Culver, N. Mariani, J. Mozer, D. Brogan, Instability of Horizontally Curved Members-Shear Buckling of Cylindrical Web Panels, Carnegie-Mellon University, Report to Pennsylvania Department of Transportation, 1972.

[29] J.S. Davidson, Nominal Bending and Shear Strength of Curved Steel I-Girder Bridge Systems, PhD. Thesis, Auburn University, Auburn, AL, USA, 1996.

[30] S.C. Lee, C.H. Yoo, Strength of curved I-girder web panels under pure shear, J. Struct. Eng. 125 (1999) 847–853. https://doi.org/10.1061/(ASCE)0733-9445(1999)125:8(847)

[31] D.W. White, A.H. Zureick, N. Phoawanich, S.K. Jung, Development of Unified Equations for Design of Curved and Straight Steel Bridge I Girders, Final report to American Iron and Steel Institute Transportation and Infrastructure Committee, Professional Services Industries, Inc., and Federal Highway Administration, Atlanta (GA), School of Civil and Environmental Engineering, 2001.

[32] Zureick, A.H., "Horizontally Curved Steel I-Girders. Chapter 9, Guide to Stability Design Criteria for Metal Structures", 5 Edition, Structural Stability Research Council, T.V. Galambos (ed.), McGraw-Hill, New York, 365-382, 1998.

[33] C.R. Hendy, M. Cai, J.P. Martins, F. Ljubinkovic´, L.S. da Silva, New design rules for plate girders curved in plan, in: Proc. Inst. Civ. Eng. – Bridg. Eng., Bridge Engineering, 2020. https://doi.org/https://doi.org/10.1680/jbren.19.00057.

[34] B.A. Frankl, D. Linzell, Validation of modified shear buckling coefficients for horizontally curved steel plate girders, J. Constr. Steel Res. 168 (2020) 106009. https://doi.org/https://doi.org/10.1016/j.jcsr.2020.106009.

[35] European Committee for Standardization (CEN). prEN 1993-1-5. Eurocode 3 – Design of Steel Structures – Part 1-5: Plated structural elements, Brussels, Belgium, 2020.

[36] European Committee for Standardization (CEN). prEN 1993-2. Eurocode 3 – Design of steel structures — Part 2: Steel Bridges, Brussels, Belgium, 2022.

[37] AASHTO(American Association of State Highway and Transportation Officials), LRFD, Bridge design specifications, Seventh Edition, Washington, DC, USA, 2014.

[38] ABAQUS, User's Manual, Version 6.14-1, (2014) 224.

[39] X. Yun, L. Gardner, Stress-strain curves for hot-rolled steels, J. Constr. Steel Res. 133 (2017) 36–46. https://doi.org/https://doi.org/10.1016/j.jcsr.2017.01.024.

[40] ABAQUS, Theory manual, Version 6.14-1, Dassault Systèmes Simulia Corp, Providence, RI, USA, 2014.

[41] J. Gozzi, A. Olsson, A. Talja, Cold-formed stainless steel profiles subjected to bending and concentrated forces -Test results, numerical modelling and design guidance, in: RFCS Contract RFCS-CR-03018, ComBri-Report-CTICM-005, CTICM, France, 2006.

[42] D. Zeka, J.-A. Boutzas, Patch loading resistance of welded I-beams – with respect to misaligned web stiffeners, KTH Royal Institute of Technology, Stockholm, Sweden, 2016.

Disponible en **www.hormigonyacero.com**
https://doi.org/10.33586/hya.2025.4044

Robustez estructural de edificios en España. Investigaciones recientes en la Universitat Politècnica de València

Structural Robustness of Buildings in Spain. Recent Research at the Universitat Politècnica de València.

Lisbel Rueda-García[a,*], Brais Barros[a], Manuel Buitrago[a], José M. Adam[a]

[a] *Universitat Politècnica de València, Camí de Vera s/n, 46022, Valencia, Spain.*

Recibido el 22 de diciembre de 2024; revisado el 23 de febrero de 2025, aceptado el 16 de abril de 2025

RESUMEN

El incremento constante de eventos extremos hace necesario contar con edificios robustos capaces de soportar daños iniciales locales sin que se produzca una propagación de fallos que afecte a toda o gran parte de la estructura. Este artículo analiza el estado actual de la normativa y la investigación en España sobre robustez estructural de edificios, más concretamente aquella llevada a cabo en la *Universitat Politècnica de València*, proporcionando una visión global sobre robustez tanto para profesionales del sector como investigadores. Aunque el Código Estructural español menciona la necesidad de edificios robustos, carece de indicaciones claras sobre su implementación, lo que lleva a la posible adopción de normativas internacionales, como el Eurocódigo 1 Parte 1-7 o la UFC 4-023-03 de EE.UU. Estas normativas contemplan diferentes estrategias para diseñar edificios robustos, entre las que destacan el método de las fuerzas de atado, el método de los caminos de carga alternativos y el diseño de elementos clave. Las características principales de estos métodos también se describen en este artículo. A nivel de investigación, España presenta avances significativos ya que existen importantes proyectos que introducen estrategias innovadoras tanto para mejorar la robustez de estructuras existentes como para frenar el colapso una vez éste se ha iniciado. Estos proyectos destacan el potencial nacional en el desarrollo de enfoques avanzados y efectivos en materia de robustez.

PALABRAS CLAVE: robustez estructural, colapso progresivo, normativas, investigación, España.

ABSTRACT

The constant increase in extreme events requires robust buildings capable of withstanding initial local damage without causing propagation of failures that could affect the entire structure or a significant part of it. This article examines the current state of regulations and research on building structural robustness in Spain, more specifically that carried out at the *Universitat Politècnica de València*, offering a comprehensive overview for both industry professionals and researchers. Although the Spanish Structural Code mentions the need for robust buildings, it lacks clear guidance on implementation, leading to the possible adoption of international standards, such as Eurocode 1 Part 1-7 or the U.S. UFC 4-023-03. These standards consider various strategies for designing robust buildings, highlighting the tying forces method, the alternative load path method, and the design of key elements. The main features of these methods are also described in this article. In terms of research, Spain shows significant progress since important projects introduce innovative strategies to enhance the robustness of existing structures or arrest collapse once initiated. These projects highlight the national potential in developing advanced and effective robustness approaches.

KEYWORDS: structural robustness, progressive collapse, standards, research, Spain.

* Persona de contacto / *Corresponding author*:
Correo-e / *e-mail*: lisruega@upv.es (Lisbel Rueda García)

Cómo citar este artículo: Rueda-García, L., Barros, B., Buitrago, M. & Adam, J.M. (2026). Robustez estructural de edificios en España. Investigaciones recientes en la Universitat Politècnica de València. *Hormigón y Acero*. 77(308):117-129. https://doi.org/10.33586/hya.2025.4044

1. INTRODUCCIÓN

Los edificios son vulnerables a las devastadoras consecuencias de eventos extremos provocados por accidentes, tales como explosiones o impactos de vehículos, ataques terroristas, el envejecimiento y los fenómenos meteorológicos extremos. En concreto estos últimos son cada vez más habituales: en el período 2000-2019 se registraron 7348 desastres naturales frente a los 4212 de 1980-1999 [1]. Estos sucesos a menudo causan daños locales en elementos estructurales críticos, dando lugar a una cadena de fallos que conducen al colapso parcial o total del edificio, un fenómeno conocido como "colapso progresivo" (figura 1).

Figura 1. Edificio federal A.P. Murrah tras un ataque terrorista perpetrado con una furgoneta cargada de explosivos (Oklahoma, 1995) [2].

En los últimos años, la prensa ha destacado una serie de colapsos progresivos notorios [3]. Entre los más significativos, ya sea por la cantidad de víctimas, la magnitud de los daños o el impacto social en su momento, se encuentran casos clásicos como Ronan Point (Londres, 1968) y Capitán Arenas (Barcelona, 1972); el cuartel de los Marines de EE.UU. (Beirut, 1983); la Asociación Mutual Israelita Argentina (Buenos Aires, 1994); el edificio Federal A.P. Murrah (Oklahoma, 1995); los grandes almacenes Sampoong (Seúl, 1995); las Torres Gemelas del World Trade Center (Nueva York, 2001); y el centro comercial Achimota Melcom (Acra, 2012).

Los estudios sobre el colapso progresivo de estructuras comenzaron a principios de la década de 1940, cuando Lord Baker analizó el comportamiento de los edificios dañados por bombardeos en Londres durante la Segunda Guerra Mundial [4]. El colapso del bloque de apartamentos Ronan Point (Londres, 1968) marcó un hito a partir del cual los códigos de construcción y las recomendaciones de diseño empezaron a considerar el riesgo de colapso progresivo. Sin embargo, fue solo después del colapso del edificio Federal A.P. Murrah (Oklahoma, 1995) y de las Torres Gemelas del World Trade Center (Nueva York, 2001) cuando hubo una gran alarma social y se desarrollaron nuevas normas y recomendaciones. La comunidad científica también comenzó a mostrar un interés sostenido en el estudio de este campo. Esto se observa en la tendencia al alza en el número de publicaciones científicas anuales relacionadas con el campo del colapso progresivo de edificios. Según datos de Scopus, en el año 1969 se registraron 3 publicaciones relacionadas, pasando a 123 en el año 1996, 138 publicaciones en el año 2002 e incrementándose exponencialmente desde entonces, registrándose hasta 1647 documentos en el año 2024 (véase el apartado 3.2.1 de este artículo).

Como se ha mencionado, las normativas relacionadas con el colapso progresivo comenzaron a desarrollarse tras el devastador colapso del edificio Ronan Point en 1968. En consecuencia, las regulaciones sobre robustez estructural son relativamente recientes. Para reducir la vulnerabilidad de los edificios al colapso progresivo, se introdujo en las normas de diseño el concepto de "robustez", entendido como la insensibilidad de la estructura a un fallo local. Las normativas más avanzadas en el ámbito de la robustez estructural, como las normas o guías estadounidenses UFC 4-023-03 [5], GSA 2016 [6] o ASCE/SEI 76-23 [7], o la norma europea EN 1990:2023 [8] y EN 1991-1-7:2018 [9], junto con los informes del JRC asociados (*Reliability background of the Eurocodes* [10] y *Guidance on the design for structural robustness* [11]), así como algunos códigos específicos de materiales, como los códigos de hormigón estructural EN 1992-1-1:2023 [12] y *fib* Model Code 2020 [13], tienen como objetivo garantizar la continuidad de las estructuras, permitiendo que las cargas soportadas por los elementos portantes que fallen se transfieran a los elementos adyacentes. Las normas se enfocan en abordar fallos causados por eventos desconocidos, aplicando enfoques de análisis independientes de la causa (los llamados "threat-independent analysis"), y que se centran más en las consecuencias, a nivel estructural, que cualquier evento podría producir. Este enfoque garantiza que las estructuras puedan resistir y redistribuir las cargas de manera segura, independientemente del origen del fallo, promoviendo un diseño más robusto frente a una amplia variedad de escenarios imprevistos. Estos códigos incluyen diversas filosofías de diseño, que varían en complejidad, como el método de las fuerzas de atado, el de los elementos clave o el de los caminos de carga alternativos (se explican en

detalle en el apartado 2.3), e incluso filosofías de muy reciente desarrollo como la segmentación. Para determinar qué enfoque o enfoques de diseño deben aplicarse (en cuanto a complejidad se refiere), las normativas clasifican los edificios en distintas categorías según las consecuencias asociadas a su uso, considerando factores como el propósito del edificio (residencial, educativo, sanitario, etc.), el número de pisos y el grado de ocupación.

En la práctica actual de los proyectos y obras, la aplicación de los códigos de robustez se encuentra aún en una fase incipiente debido a su relativamente reciente introducción y falta de tradición en su aprendizaje y uso. Aunque la normativa vigente establece pautas, muchos profesionales no han interiorizado completamente estos nuevos estándares. Esto genera incertidumbre sobre las consecuencias que tendrían eventos accidentales no previstos en los edificios actuales. La adopción efectiva de estas normativas requerirá un proceso gradual de formación y ajuste en la práctica profesional, así como un consenso claro sobre las pautas a seguir a nivel normativo.

En este artículo se presenta un resumen detallado de la normativa vigente en España, las principales filosofías de diseño estructural y el panorama actual de la investigación en robustez estructural. Con este enfoque, se busca ofrecer una guía práctica para los profesionales del sector, ayudándoles a comprender las normativas aplicables, los fundamentos de las filosofías de diseño actuales y cómo implementarlas adecuadamente. Además, se pretende proporcionar a la comunidad investigadora una visión general del estado del conocimiento en este campo y destacar las investigaciones realizadas en España, más concretamente en la *Universitat Politècnica de València*, que han alcanzado un reconocimiento significativo a nivel mundial. En última instancia, este trabajo enfatiza la importancia de garantizar el cumplimiento normativo y promover una mayor seguridad en nuestros edificios, contribuyendo así a una construcción más confiable y resiliente.

2. ESTADO DE LA NORMATIVA EN ESPAÑA

2.1. Código Estructural

La normativa más reciente en el ámbito estructural en el contexto español es el Código Estructural [14], vigente desde 2021. A pesar de su reciente publicación, el Código Estructural hace una breve mención a la consideración de la robustez en las estructuras. En concreto, la norma establece en su Artículo 5.2.1.3, sobre "Exigencia de robustez y redundancia", que las estructuras "*deberán ser proyectadas de manera que cualquier evento extraordinario no produzca consecuencias desproporcionadas respecto a la causa original*". Asimismo, se indica que, "*cuando así lo establezca la propiedad, el proyecto deberá contemplar la selección de un esquema estructural y un diseño conceptual que asegure que la eliminación accidental de un elemento o de una parte limitada de la estructura origina daños proporcionados y limitados, de forma que, además, el resto de la estructura no afectada sea capaz de asegurar la estabilidad mínima de la misma*". Finalmente, afirma que los procedimientos incluidos en el Código "*no son suficientes para el cumplimiento de esta exigencia*".

El Artículo 5.2.1.3 del Código Estructural, aunque exige que las consecuencias de cualquier evento no sean desproporcionadas, da lugar a una interpretación muy abierta de la norma y no detalla el grado de exigencia de este requisito de robustez. En su lugar, y cuando trata de concretar la exigencia en forma de requisito concreto, deja la decisión en manos de la propiedad. Incluso así, cuando la propiedad lo exija, el código no da procedimientos o estrategias para asegurar la robustez de las estructuras. Parece ser que, para estos casos, de aproximación general o específica cuando la propiedad lo requiera, el código exige y da pie a seguir otras recomendaciones de robustez más detalladas para poder cumplir esta exigencia. En el ámbito español, una opción razonable sería recurrir a la normativa europea, que ofrece un desarrollo más avanzado sobre esta materia.

2.2. Normativa europea

En esta sección se recogen los aspectos normativos más relevantes de los códigos europeos actuales en materia de robustez estructural que son de aplicación en España: el Eurocódigo 1 Parte 1-7 sobre acciones accidentales (EN 1991-1-7:2018) [9] y aquellos Eurocódigos de la segunda generación actualmente publicados que tratan la robustez en edificios (el Eurocódigo 0 EN 1990:2023 [8], y el Eurocódigo 2 de hormigón estructural, EN 1992-1-1:2023 [12]), junto con los informes del *Joint Research Centre* (JRC) asociados (*Reliability background of the Eurocodes* [10] y *Guidance on the design for structural robustness* [11]).

El EN 1991-1-7:2018 [9] expone una serie de estrategias a considerar en el proyecto de estructuras frente a acciones accidentales para limitar la extensión de un fallo localizado debido a una causa no especificada (Artículo 3.1). Estas estrategias son tres, que son las comúnmente adoptadas a nivel mundial y que se explican en detalle en la sección 2.3 de este artículo: (i) el método de las fuerzas de atado; (ii) el método de los caminos de carga alternativos, y (iii) el método de diseño de elementos clave. En la segunda generación de los Eurocódigos, el Eurocódigo 0 (EN 1990:2023 [8]) aborda en el Artículo 4.4 y el Anexo E los requerimientos básicos para la robustez de estructuras, presentando un planteamiento muy similar al indicado en el EN 1991-1-7:2018 [9], aunque menos específico que éste. Como novedad, el EN 1990:2023 [8] contempla, como enfoque de diseño, la segmentación.

El uso de cada una de estas estrategias de diseño para mejora de la robustez depende de la clase de consecuencia en la que se clasifique el edificio (Artículo 3.4 del EN 1991-1-7:2018 [9]). Se establecen tres clases según la gravedad de las consecuencias del fallo de la estructura: CC1 a CC3, de menor a mayor gravedad de las consecuencias de fallo.

El Anexo A del EN 1991-1-7:2018 [9], de carácter informativo, profundiza más en las reglas y métodos para el proyecto de edificios para que soporten una extensión del fallo localizado por una causa no especificada sin un colapso desproporcionado. En primer lugar, proporciona una correspondencia entre tipos o usos de edificios y las clases de consecuencias, que se resume en la Tabla 1 (para más ejemplos acudir a la Tabla A.1 del EN 1991-1-7:2018 [9]).

En función de la clase de consecuencia en la que se clasifique un edificio determinado, el EN 1991-1-7:2018 [9] recomienda una serie de estrategias a adoptar que deberían "proporcionar al

TABLA 1.
Ejemplos de clasificación de diferentes tipos de edificios según las clases de consecuencias (adaptado de la Tabla A.1 del EN 1991-1-7:2018 [9]).

Clase de consecuencia	*Ejemplos de tipos de edificios*
CC1	• Viviendas unifamiliares ≤ 4 alturas • Edificios de uso agrícola
CC2a Grupo de Riesgo bajo	• Viviendas unifamiliares de 5 alturas • Hoteles, bloques de viviendas y oficinas ≤ 4 alturas • Edificios industriales ≤ 3 alturas • Edificios de venta al por menor ≤ 3 alturas y ≤ 1000 m² en cada altura • Edificios de uso educativo ≤ 1 altura
CC2b Grupo de Riesgo alto	• Hoteles, edificios residenciales y oficinas entre 5 y 15 alturas • Edificios de venta al por menor entre 4 y 15 alturas • Edificios de uso educativo entre 2 y 15 alturas • Hospitales ≤ 3 alturas • Aparcamientos ≤ 6 alturas
CC3	• Edificios indicados en 2b que excedan el nº de alturas • Edificios con un alto flujo de acceso público • Estadios con aforo > 5000 espectadores • Edificios con mercancías peligrosas

edificio un nivel aceptable de robustez para soportar un fallo localizado sin un efecto desproporcionado". Esta clasificación, que se resume a continuación, también se encuentra detallada en el informe publicado recientemente por el JRC [10].

- CC1. No es necesario tener en cuenta consideraciones adicionales sobre robustez, siempre y cuando el edificio haya sido diseñado en base al resto de Eurocódigos (Normas EN 1990 a EN 1999).
- CC2a. Aparte de lo indicado para CC1, deberían proporcionarse atados horizontales efectivos (método de las fuerzas de atado).
- CC2b. Aparte de lo indicado para CC1, se deberían proporcionar atados horizontales y verticales efectivos; o bien, asegurar (método de los caminos de carga alternativos) que tras la retirada ficticia de cualquier pilar y cualquier viga soportando un pilar (para pilares apeados) o cualquier sección nominal de un muro portante, el edifico permanece estable y el daño local no excede un cierto límite (v.g. colapsos). Además, cuando la retirada ficticia de tales columnas y secciones de muros produzca una extensión del daño que supere el límite aceptado, tales elementos deberían designarse como "elementos clave" (método de los elementos clave). El valor recomendado del límite de fallo local admisible es el menor valor entre un 15% del forjado o 100 m², en cada una de dos alturas adyacentes.
- CC3. Se requiere un estudio más detallado, llevando a cabo una estimación sistemática del riesgo, teniendo en cuenta tanto los peligros previsibles como los no previsibles (Anexo B del EN 1991-1-7:2018 [9]).

El EN 1990:2023 [8] muestra una recomendación menos detallada de los métodos de diseño a utilizar, pero añade el método de la segmentación en los edificios clasificados como CC2. Adicionalmente a lo indicado por EN 1991-1-7:2018 [9] para CC3, sugiere considerar eventos potenciales de fallo inicial, así como la propagación del fallo.

Mientras que las normas mencionadas proporcionan una serie de reglas prescriptivas para el atado horizontal y vertical de los elementos, y dan una breve indicación sobre cómo abordar el diseño de los elementos clave, no facilitan pautas para la aplicación del método de los caminos de carga alternativos, lo que obliga a acudir a otras normas internacionales. La sección 2.3 de este artículo profundiza en ello.

Como material adicional al presentado, conviene destacar la existencia de la guía sobre robustez estructural desarrollada por el CEN/TC 250 Working Group 6 sobre robustez con la participación del JRC (*Guidance on the design for structural robustness* [11]) que constituye un recurso valioso, ya que ofrece un resumen detallado del estado actual de la normativa y del conocimiento en la materia; así como el *fib* Model Code 2020 [13] sobre hormigón estructural, que contiene un enfoque más general del tema de la robustez, incluyendo una posible estrategia práctica para el proyecto, así como una propuesta de requisitos de fiabilidad para los elementos clave.

2.3. Estrategias de proyecto

Existen varios grupos de métodos de diseño que pueden identificarse fácilmente en la normativa de aplicación en España; tres de ellos son ampliamente reconocidos y se explican en detalle a continuación. Los métodos de las fuerzas de atado y de los caminos de carga alternativos consideran la posibilidad de fallos locales, mientras que el método de diseño de elementos clave se orienta a prevenir el fallo local de elementos críticos.

Por otro lado, como se ha indicado en la sección 2.2, el reciente EN 1990:2023 [8] ha incorporado como método de diseño la segmentación, entendida como la separación de la estructura en partes distintas mediante uno o más elementos estructurales más débiles, de modo que cada parte pueda colapsar de forma independiente sin comprometer la seguridad de las demás. A pesar de ello, las normativas vigentes en España e internacionales aún no incluyen directrices específicas para su aplicación, ni se ha abordado en informes técnicos relevantes, como el del JRC sobre robustez [15]. Por el momento, su desarrollo permanece en un ámbito predominantemente científico.

Finalmente, las normas contemplan un último método para el estudio de edificios de la clase de consecuencia más alta (CC3) consistente en la evaluación de riesgos, que envuelve un

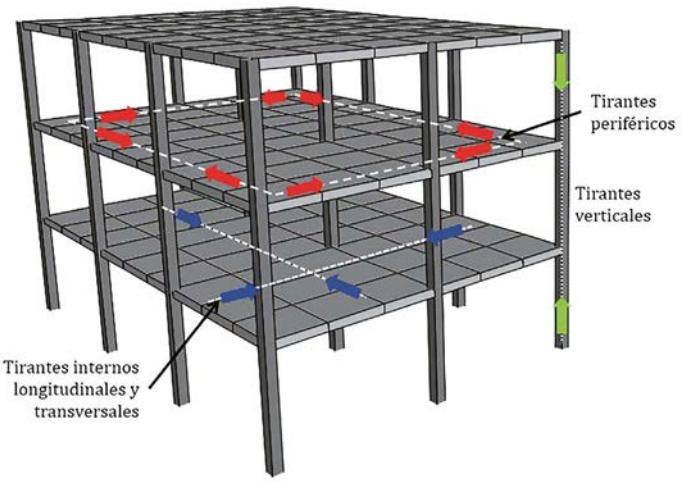

Figura 2. Fuerzas de atado en una estructura porticada.

análisis más complejo (ver Anexo B del EN 1991-1-7:2018 [9] y sección 3.10 del *Reliability background of the Eurocodes* [10] del JRC).

Por los motivos expuestos, se desarrollan en este artículo únicamente los tres métodos habituales mencionados.

2.3.1. Método de las fuerzas de atado

Las reglas de las fuerzas de atado se recomiendan comúnmente en las normativas internacionales para estructuras con bajo riesgo de colapso progresivo. Estas reglas están orientadas a proporcionar niveles mínimos de atado, continuidad y ductilidad, aunque normalmente no se realiza una verificación explícita de esta última característica [3]. El enfoque de las fuerzas de atado se emplea en numerosos códigos como EN 1991-1-7:2018 [9], ASCE/SEI 76-23 [7] y UFC 4-023-03 [5]. Este método suele clasificarse como un "enfoque de diseño indirecto", ya que la resistencia al colapso progresivo se considera de forma implícita, mediante la provisión de niveles mínimos de resistencia, continuidad y ductilidad.

En general, el atado se asegura mediante la implementación de atados horizontales y verticales, logrados a través de la prescripción de una fuerza de atado mínima, que suele ser consistente en las distintas normativas. No es posible cuantificar con precisión el aumento en los niveles mínimos de robustez proporcionado por las distintas reglas de fuerzas de atado, ya que uno de los desafíos asociados a la robustez estructural es la carencia de una medida cuantitativa concreta de ésta [16,17]. Aun así, se acepta generalmente que el atado tiene un efecto positivo en la robustez de las estructuras [18,19]. No obstante, algunos códigos, como GSA 2013 [6], excluyen este enfoque de diseño, debido a que se ha demostrado que las rotaciones requeridas en los elementos para aportar el necesario comportamiento de catenaria son inalcanzables en algunos casos.

Las normativas que incluyen el método de las fuerzas de atado, como EN 1991-1-7:2018 [9], indican la carga de tracción mínima que deben soportar los atados, en función de las características geométricas de la estructura y de las cargas que recibe en la situación de proyecto accidental. Además, los códigos especifican el área donde deben concentrarse los atados. Existen diferentes enfoques en cuanto a su disposición: el código EN 1991-1-7:2018 [9], por ejemplo, indica que los atados deben ser continuos y colocarse lo más cerca posible de los bordes de los forjados y de las líneas de pilares y muros, asegurando una distribución efectiva de las cargas. En contraste, UFC 4-023-03 [5] excluye la fuerza de atado en las vigas internas y de borde. Esta decisión se basa en la capacidad reducida de las vigas de desarrollar las grandes rotaciones necesarias para asegurar el desarrollo completo de la acción de catenaria. Este atado, en cambio, se recomienda disponerlo únicamente en los forjados, elementos con mayor capacidad de rotación, para así desarrollar el atado interno a través de la acción de membrana. De esta forma, las rotaciones requeridas para una adecuada redistribución de fuerzas pueden ser significativamente menores, evitando así el problema de la rotación insuficiente de las vigas que se indicaba anteriormente. En la figura 2 se muestra un esquema de la distribución de los diferentes atados en una estructura porticada de acuerdo con las indicaciones de la UFC 4-023-03 [5].

Los atados pueden implementarse de diversas formas, dependiendo del tipo de estructura y de los materiales empleados. Los atados pueden estar compuestos de perfiles laminados de acero, barras de refuerzo en losas de hormigón, o malla de acero y láminas de acero en forjados compuestos de acero y hormigón (siempre que se conecten directamente a las vigas de acero mediante conectadores). En muchos casos, es común emplear una combinación de estos tipos de atados para lograr una distribución más efectiva de la fuerza de atado.

En términos generales, el método de las fuerzas de atado es sencillo de aplicar, lo cual lo convierte en una opción práctica para mejorar la robustez estructural en el diseño frente a eventos extremos no identificados. En el caso específico de la norma EN 1991-1-7:2018 [9], el cálculo de las fuerzas de tracción necesarias en los tirantes se realiza mediante una serie de fórmulas básicas, detalladas en los apartados A.5 y A.6 de la norma. Estas fórmulas permiten determinar con rapidez el nivel de tracción requerido en los distintos elementos de atado de la estructura. Una vez calculadas estas fuerzas de tracción, se verifica si la armadura obtenida por medio de las reglas de diseño habituales, o los elementos estructurales en sí, pueden soportar dichas tracciones. En caso de que la resistencia de estos elementos resulte insuficiente, se procede a reforzarlos hasta alcanzar los valores mínimos exigidos por la norma. De esta manera, el método permite asegurar un nivel básico de resistencia sin necesidad de procedimientos de cálculo complejos.

Cabe destacar que el recientemente publicado Eurocódigo 2 sobre diseño de estructuras de hormigón (EN 1992-1-1:2023 [12]) incluye en su articulado (en concreto en el Artículo 12.9) una serie de prescripciones para el sistema de atado en edificios de hormigón. Dichas fórmulas son similares a las contenidas en el EN 1991-1-7:2018 [9].

2.3.2. Método de los caminos de carga alternativos

Los caminos de carga alternativos, o ALPs (del inglés "alternate load paths"), se pueden describir como rutas dentro de una estructura a través de las cuales las cargas pueden redistribuirse tras la pérdida de un elemento (ver figura 3), permitiendo a la estructura soportar fallos locales sin comprometer su estabilidad global [20]. Este enfoque tiene como objetivo demostrar explícitamente la robustez de la estructura ("enfoque de diseño directo") mediante el análisis bajo condiciones de daño

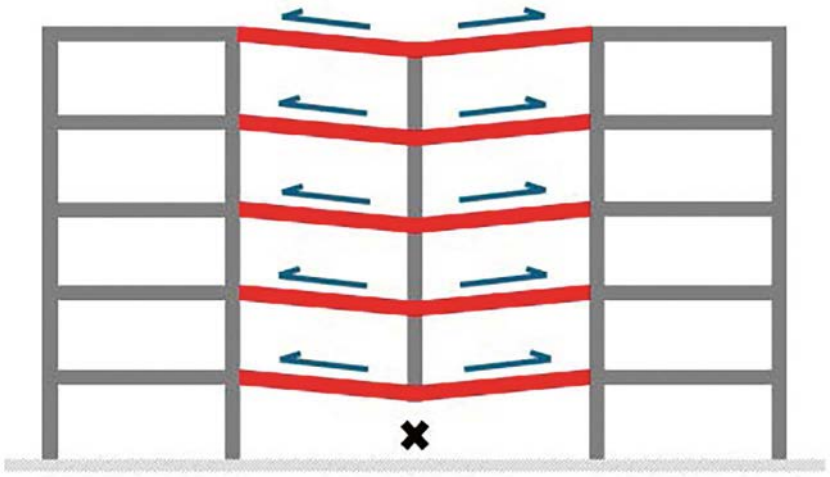

Figura 3. Esquema ilustrativo del funcionamiento de los caminos de carga alternativos, destacando específicamente el mecanismo de acción de catenaria.

preestablecidas, evaluando la capacidad de la estructura para redistribuir las cargas adicionales que provienen de las áreas afectadas por el daño local [3].

Tanto el Código Estructural [14] como el EN 1991-1-7:2018 [9] coinciden en que se debe asegurar que la eliminación accidental de un elemento, un solo elemento, no desemboca en el colapso progresivo de la estructura. Sin embargo, no dan indicaciones sobre cómo abordar este análisis. Es posible recurrir a otros códigos, como la UFC 4-023-03 [5], para obtener directrices específicas sobre la implementación de este método, y así poder seleccionar elementos de la estructura, estratégicamente ubicados, para proceder al análisis de retirada de elementos.

Un dato importante para la aplicación del método de los ALPs que proporcionan algunos códigos es la ubicación de los elementos estructurales que deben ser retirados para verificar la robustez del edificio. Según las indicaciones de la UFC 4-023-03 [5], se deberán retirar las columnas externas que se muestran en la figura 4a, que atienden a los siguientes criterios:

- Retirar, como mínimo, una columna cerca del centro del lado corto, otra cerca del centro del lado largo y otra en una esquina.
- Retirar columnas en áreas donde la geometría en planta varíe significativamente, como en reducciones abruptas de la longitud de un vano o en esquinas reentrantes.
- Si en el paño asociado a la columna retirada, de dimensiones L x l, existe una columna situada a una distancia menor al 30% de la dimensión mayor del paño (L), ésta debe retirarse simultáneamente (ver ejemplo de la figura 4a).
- Realizar el análisis para cada localización definida anteriormente en los siguientes niveles: (a) primer piso sobre el nivel del suelo; (b) piso inmediatamente debajo del tejado; (c) piso a media altura, y (d) piso ubicado por encima de una unión entre columnas o cambio de sección en la columna.

Además, se deberán retirar columnas internas en el caso de estructuras que posean estacionamientos subterráneos o áreas de acceso público no controlado (como "halls" públicos), donde se recomienda retirar columnas internas cercanas al centro de los lados corto y largo, así como en esquinas (figura 4b). Esta retirada solo debe realizarse en el nivel donde se encuentre el estacionamiento o el área de acceso no controlado. Si alguna otra columna está situada a menos del 30% de la dimensión mayor del vano asociado desde el lugar de retirada, debe también retirarse simultáneamente.

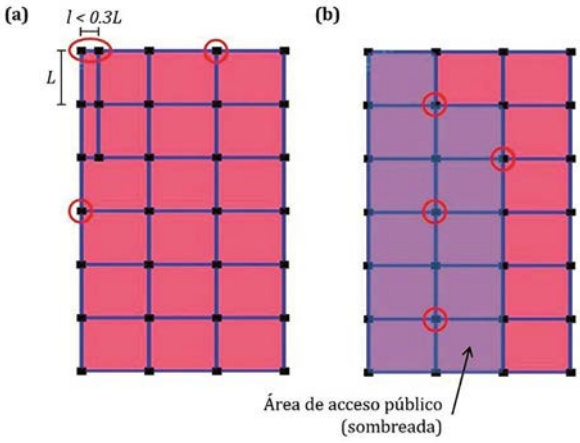

Figura 4. Esquema de la localización en planta de las columnas a retirar según la norma UFC 4-023-03 [5]: (a) Retirada de columnas interiores; (b) Retirada de columnas exteriores. Figura elaborada a partir de las indicaciones de la UFC 4-023-03 [5].

Aunque los fundamentos de este método son claros, en la práctica el análisis mediante ALP requiere diversas suposiciones y simplificaciones que pueden llevar a soluciones de diseño o evaluación con distintos niveles de robustez [3]. Algunos de los aspectos a considerar para este análisis incluyen la precisión en la introducción de los efectos dinámicos, la no linealidad de los materiales, efectos de la velocidad de deformación, grandes deformaciones de los elementos, y la capacidad de deformación de las conexiones [18]. Aunque el uso de modelos numéricos dinámicos no lineales ofrece mayor precisión, estos son complejos y más exigentes en términos computacionales. El grado de refinamiento de los modelos de análisis requerido por la normativa dependerá de la categoría de riesgo en la que se clasifique la estructura.

La normativa UFC 4-023-03 [5] permite, en ciertos tipos de estructuras, acudir a modelos más simples como son los modelos estáticos lineales y no lineales. Para ello proporciona reglas sobre cómo amplificar la carga aplicada para tener en cuenta, indirectamente en los modelos lineales, el efecto de la no linealidad estructural (geométrica) y de materiales, así como los efectos dinámicos característicos de fallos ocasionados por eventos extremos. Por otro lado, tal y como indican [3,15], existen otras alternativas para llevar a cabo el análisis de los ALPs de forma simplificada, como el análisis estático incremental no lineal ("pushdown"), como el propuesto por Izzuddin et al. [21] en su metodología de evaluación de robustez basada en la ductilidad, que ha sido reconocido como una herramienta eficaz y ha sido aplicado en varios tipos de estructuras [22–24]. De forma alternativa, para evitar tanto el uso de análisis dinámicos como de factores de amplificación dinámica, se desarrolló el método energético, que permite derivar una curva de capacidad dinámica a partir de un análisis estático de tipo "pushdown" [25,26].

Es evidente que el método de los ALPs proporciona resultados más fiables sobre la robustez de la estructura objeto de análisis que, por ejemplo, el método de las fuerzas de atado; de ahí que sea el método más empleado en investigaciones en este campo, pese a su complejidad.

2.3.3. Método de los elementos clave

El método de los elementos clave se recomienda en códigos y guías como un método de último recurso cuando el método de los ALPs no es capaz de demostrar una redistribución de cargas suficiente en la estructura. Este enfoque se centra en identificar los elementos clave, es decir, aquellos elementos estructurales cuyo fallo podría activar un colapso progresivo, y rediseñarlos para resistir cargas accidentales con el fin de evitar fallos locales en cada uno de estos elementos.

De acuerdo con la norma EN 1991-1-7:2018 [9], el diseño de elementos clave forma parte del enfoque de los ALPs para estructuras de la Clase de consecuencia 2b. En estas estructuras, cuando la retirada ficticia de ciertas columnas o secciones de muros conduce a una extensión del daño que excede el límite aceptado (el menor valor entre un 15% del forjado o 100 m², en cada una de dos alturas adyacentes, según EN 1990:2023 [8] y EN 1991-1-7:2018 [9]), tales elementos deben designarse como "elementos clave". En el caso de estructuras de Clase de consecuencia 3, consideradas de alto riesgo, en las que se requiere una estimación sistemática del riesgo, una evaluación de riesgos podría requerir, entre otras medidas, que ciertos elementos o grupos de elementos se diseñen como elementos clave.

Según esta norma, un elemento clave debe ser capaz de soportar una acción accidental de cálculo (A_d) aplicada en direcciones tanto horizontal como vertical (no simultáneamente). Para estructuras de edificación, el valor recomendado de A_d es 34 kN/m².

En contraste, la norma UFC 4-023-03 [5] adopta un enfoque diferente al del EN 1991-1-7:2018 [9]. Esta norma establece de forma sistemática que, en los edificios pertenecientes a las categorías de riesgo más altas (III y IV de dicha norma), además de asegurar el cumplimiento de los ALP, se debe mejorar la resistencia local de todas las columnas perimetrales en la planta baja. El enfoque de diseño en esta norma es asegurar un mecanismo de fallo dúctil de los elementos clave.

3. AVANCES EN INVESTIGACIÓN

3.1. Estadísticas de publicaciones sobre robustez

Al igual que ha pasado con las normativas existentes, las cuales han sufrido un gran desarrollo en el campo de la robustez estructural, el creciente interés por el campo de la robustez ha provocado un notable incremento del número de publicaciones. Con el fin de cuantificar estas tendencias se ha empleado la base de datos Scopus para recopilar todas las investigaciones del área. Para filtrar la búsqueda se ha utilizado como criterio de búsqueda que estuviesen contenidas en el título, el resumen o en las palabras clave el siguiente conjunto de palabras: ("Building") ***AND*** ("Robustness" ***OR*** "Collapse" ***OR*** "Failure") ***AND*** ("Structure") y además las búsquedas se han limitado al ámbito de ingeniería.

Figura 5. Número de publicaciones por año sobre robustez usando la base de datos Scopus.

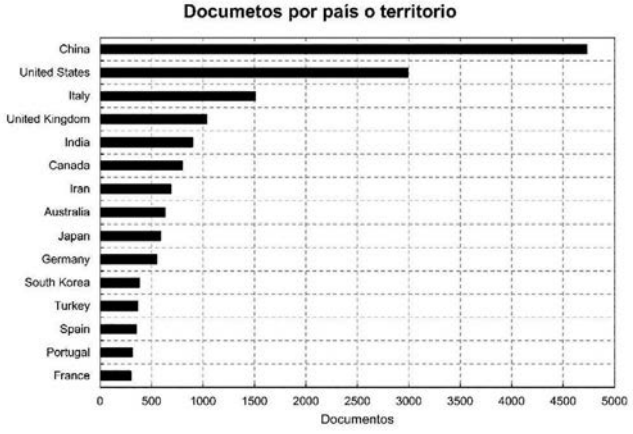

Figura 6. Número de publicaciones sobre robustez por países usando la base de datos Scopus.

Figura 7. Foto de uno de los ensayos llevados a cabo en el proyecto ENROOT.

Como resultado se han obtenido un total de 18.420 documentos. En la figura 5 pueden observarse el número de publicaciones anuales donde se percibe claramente como a partir del año 2000 el crecimiento es casi exponencial. Actualmente en 2024 se ha llegado a su máximo de publicaciones anuales con más de 1500 documentos de los cuales el 62.9% son artículos de investigación y 31.7% artículos de conferencia.

Si desgranamos estos documentos por país de origen podemos ver una clara hegemonía de China seguido de EEUU, que son los países con más publicaciones, con más de 4728 y 2991 respectivamente (ver figura 6). España se encuentra en el puesto 13 de los países con más publicaciones con un total de 353 documentos.

Tal y como se mencionó anteriormente, la mejora de la robustez de las estructuras puede darse siguiendo dos enfoques diferentes: buscar soluciones estructurales para una amenaza concreta o bien buscar la mejora de la robustez sin tener en cuenta la amenaza, es decir, teniendo en cuenta solo sus consecuencias (fallo de una columna, viga etc.). El primer tipo de investigación es el más abundante en el ámbito nacional, donde pueden encontrarse un amplio abanico de investigaciones sobre sismo [27–31], explosiones [32–34] y fuego [35– 38] entre otras amenazas. No obstante, este artículo se centra en el estudio de investigaciones sobre la robustez estructural, con el enfoque de independencia de la amenaza, las cuales son más escasas. En concreto, el siguiente apartado se centra en las investigaciones llevadas a cabo en la *Universitat Politècnica de València* (UPV).

3.2. Estudios de robustez en la Universitat Politècnica de València

Dentro de las investigaciones de robustez desde un enfoque independiente de la amenaza se ha establecido una clasificación atendiendo a si son investigaciones llevadas a cabo en subconjuntos (o subensamblajes o subestructuras), es decir, unidades estructurales más pequeñas que representan la interacción entre algunos elementos clave de la estructura general, como columnas, vigas y conexiones, o bien si son investigaciones que contemplan el edificio completo a escala real. Dentro de estos últimos se han subdividido las investigaciones en función de si conllevaban el ensayo experimental del edificio o no.

3.2.1. Estudios sobre subconjuntos

Como se ha señalado previamente, existe un elevado número de publicaciones que analizan o emplean elementos estructurales o subconjuntos aislados en el estudio de fenómenos específicos. Este enfoque es comúnmente utilizado en las etapas iniciales de investigación de un fenómeno, particularmente para evaluar aspectos relacionados con la robustez estructural. En este contexto, efectos como la acción de membrana o la catenaria en estructuras de hormigón y acero han sido ampliamente estudiados mediante subconjuntos antes de proceder a la realización de ensayos a escala real [39–42]. Sin embargo, en otros tipos de estructuras, como las de madera, que han recibido menos atención en estudios de robustez, este tipo de ensayos específicos no se han llevado a cabo de manera sistemática.

La UPV fue beneficiaria del proyecto ENROOT, financiado por la Generalitat Valenciana, que trató sobre la robustez de estructuras de madera mediante el diseño y la evaluación de sus conexiones. Para ello se evaluó experimentalmente la robustez de dos conexiones ampliamente utilizadas en el sector mediante el uso de subconjuntos estructurales para aislar y analizar el problema con mayor detalle. Estos subconjuntos estaban compuestos por tres columnas (incluyendo la columna eliminada) y dos vigas, las cuales se sometieron a cargas verticales en la columna central para simular la pérdida de la columna (figura 7). En este proyecto también se ensayaron diseños mejorados de las citadas

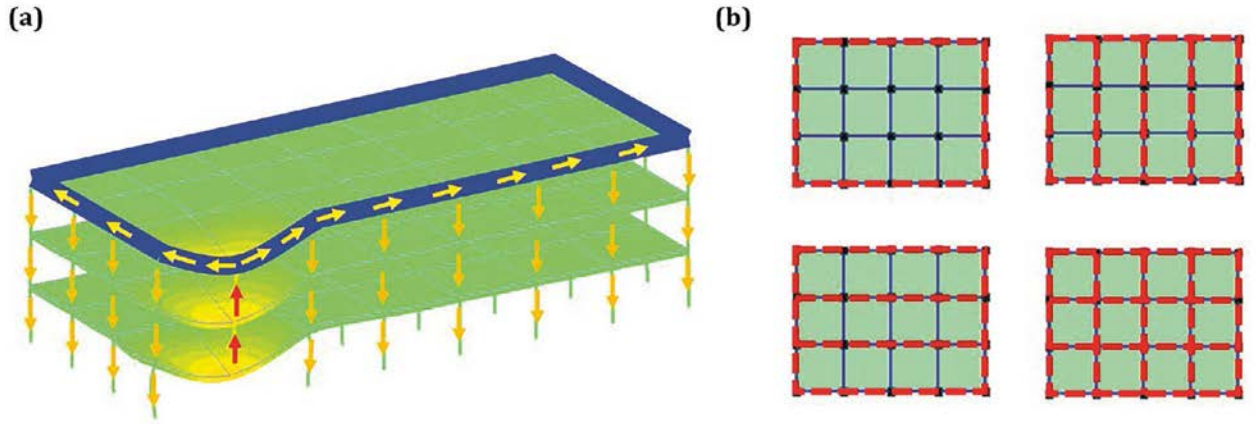

Figura 8. Método de refuerzo del proyecto ENHANCE: (a) Esquema del funcionamiento estructural; (b) Ejemplos de posibles disposiciones de la viga de refuerzo en cubierta.

conexiones que serán optimizados para conseguir la mejor configuración posible.

3.2.2. Estudios teóricos de robustez sobre edificios

Hay múltiples investigaciones sobre edificios que abordan distintos aspectos de la robustez estructural sin necesidad de acudir a la experimentación, empleando únicamente simulaciones numéricas que siempre han venido validadas previamente en base a ensayos experimentales. En este contexto, en la UPV se han desarrollado estudios como el presentado por Caredda et al. [43] que desarrolla una metodología para definir posibles configuraciones de segmentación basadas en fusibles estructurales para detener la propagación horizontal del colapso en edificios. Por otro lado, también se encuentran investigaciones más centradas en el análisis estructural como [17], donde se propone una metodología práctica para evaluar la robustez estructural de edificios de hormigón armado combinando una estrategia de modelización eficiente y unos índices de robustez adecuados. En concreto, en este estudio se compararon cuatro índices de tipo "reserve-based", que son aquellos basados en estimar la capacidad de carga restante de un sistema estructural después de un fallo inicial [44] y que han demostrado ser particularmente adecuados para evaluar la efectividad de las medidas que buscan garantizar la disponibilidad de ALPs. Se llegó a la conclusión de que, teniendo en cuenta la precisión y el tiempo de cálculo, el índice propuesto por Bao et al. en [26] es el más práctico, ya que requiere sólo un análisis estático no lineal de tipo "pushdown", pero considera los efectos dinámicos mediante el principio basado en la energía. Este método ha sido utilizado para evaluar el nivel de daño en componentes y comparar soluciones de refuerzo.

También se están desarrollando en la UPV cuatro proyectos que abarcan la simulación de edificios completos. El primero de estos proyectos es ENTIRE que trata sobre el desarrollo de nuevos sistemas estructurales de estabilización para prevenir el colapso progresivo de edificios. Estos sistemas de estabilización se basan en el uso de elementos de estabilización de columnas que funcionan bajo cargas de compresión axial, de forma similar a como lo hacen los apuntalamientos en vaciados o excavaciones. Con conexiones adecuadas a los pilares, puenteando el pilar que falla y estabilizando los pilares adyacentes a éste, se permite que los tirantes funcionen a plena capacidad bajo las acciones catenarias en vigas (o de membrana en forjados) provocadas por el fallo de un elemento portante, evitando así el colapso progresivo [45].

Otro de los proyectos financiados es EVOLVE, llevado a cabo gracias a la financiación de la Generalitat Valenciana, que estudia cuando las normativas actuales pueden contribuir a un colapso desproporcionado en estructuras de hormigón armado. Para ello se está trabajando en una metodología de evaluación del rendimiento para determinar cuándo una mayor conectividad y continuidad pueden aumentar el riesgo de colapso desproporcionado en las estructuras de hormigón armado. Para ello se han calibrado modelos computacionales que son capaces de simular todas las fases del colapso, incluyendo el agrietamiento, la separación de elementos y la colisión de escombros. Con estos modelos se determinan los niveles óptimos de continuidad para mejorar la robustez de los edificios [46].

La UPV también ha sido financiada por la Generalitat Valenciana para desarrollar el proyecto ENHANCE, el cual consiste en el desarrollo de un novedoso planteamiento de rehabilitación de edificios existentes basado en colgar los forjados del tejado para garantizar que cumplen los últimos requisitos de robustez estructural (figura 8). Para ello en este proyecto se están estudiando, mediante modelización computacional, distintas disposiciones de viga de refuerzo con el fin de explorar la eficacia y limitaciones de este sistema. Este estudio numérico será complementado con una campaña experimental donde se validarán los resultados obtenidos mediante el ensayo de subconjuntos.

Por último, la propia UPV ha financiado el proyecto ENFORCE, cuyo objetivo es proporcionar una herramienta de fácil manejo para evaluar el riesgo de colapso de edificios existentes en la Comunitat Valenciana. Se utilizarán simulaciones numéricas de diseños típicos cuidadosamente definidos para evaluar el efecto de diversos parámetros clave sobre la robustez estructural de los edificios. Estos resultados se utilizarán para definir categorías de riesgo que permitan una clasificación de edificios a escala urbana más precisa que la que puede conseguirse basándose en la información proporcionada en códigos actuales. Con esta información se pretende elaborar mapas de riesgo de colapso de los principales núcleos urbanos de la Comunitat Valenciana que sirvan de apoyo a la toma de decisiones sobre la mejora de la robustez de los edificios existentes. Las inundaciones ocurridas en Valencia el 29 de octubre de 2024, las cuales tuvieron un im-

Figura 9. Fotos del edificio con el cerramiento de tabiquería ensayado con la financiación de la beca Leonardo.

Figura 10. Foto de edificio de hormigón prefabricado ensayado con la financiación dentro del proyecto PREBUST [51].

pacto devastador en la región, evidencian la necesidad de contar con este tipo de recursos para optimizar la toma de decisiones.

3.2.3. *Campañas experimentales sobre edificios*

La UPV destaca a nivel mundial por sus campañas experimentales de edificios a escala real para el estudio de la robustez. El primero de los especímenes ensayados fue realizado gracias a la financiación de la Beca Leonardo de la Fundación BBVA. En este proyecto se empleó un edificio-probeta a escala real (figura 9), en el cual se ensayaron diferentes escenarios de fallo en sus columnas de esquina [47]. Como fruto de esta investigación se evaluaron los caminos de carga alternativos que se pueden desencadenar debido al fallo de las columnas de esquina. Además, debido a la naturaleza del ensayo (retirada repentina de una columna) se pudieron considerar los efectos dinámicos del escenario de fallo [47,48]. La campaña experimental también incluyó un ensayo en el cual se disponían cerramientos de tabiquería con el fin de estudiar su influencia en los caminos de carga alternativos [49]. Posteriormente se desarrolló un trabajo de simulación computacional con el objetivo de analizar situaciones de diseño accidentales y evaluar los caminos de carga alternativos para establecer recomendaciones prácticas para las situaciones de diseño [50].

El segundo de los especímenes se realizó dentro del proyecto PREBUST financiado por el Ministerio de Ciencia e Innovación. La campaña experimental conllevó el desarrollo de un edificio-probeta a escala real de dos alturas de 2.6 m y unas dimensiones en planta de 15×12 m² (figura 10). Dicho edificio fue sometido a diversos escenarios de fallo de retirada repentina de columna de esquina y columnas de medianería para analizar las rutas de carga alternativas. Durante los ensayos se adquirieron datos de un total de 106 sensores, incluidos 59

Figura 11. Foto del edificio de hormigón prefabricado construido dentro del proyecto ENDURE antes del ensayo.

Figura 12. Foto del edificio de hormigón prefabricado construido dentro del proyecto ENDURE tras el ensayo.

galgas extensiométricas, 38 transductores de desplazamiento y 9 acelerómetros. Los resultados obtenidos del ensayo mostraron una respuesta estructural gobernada por la acción de Vierendeel con una clara contribución de los forjados. A partir de los resultados de las pruebas se analizó en detalle el comportamiento estructural y se obtuvieron factores de amplificación de la carga para tener en cuenta los efectos dinámicos no lineales [51,52].

El último de los tests llevados a cabo por la UPV ha sido realizado gracias a la financiación *Consolidator Grant del European Research Council*, con un presupuesto de 2.5 millones de euros, para la ejecución del proyecto ENDURE. Este proyecto desarrolla una nueva filosofía dentro de la robustez. Mientras que la mayoría de las investigaciones se centran en la mejora de la continuidad para evitar la propagación de un fallo local, este proyecto se basa en el concepto de segmentación estructural. Para ello desarrollan el concepto de fusible estructural con el fin de parar la propagación del colapso una vez se ha iniciado y evitar daños desproporcionados tras un fallo inicial (ver figura 11).

Dicho edificio fue diseñado mediante un enfoque basado en jerarquía, el cual emplea conexiones de rigidez parcial y un sistema estructural con columnas fuertes capaz de aislar el fallo a una zona pequeña del edificio. Con esta filosofía, los fallos en las conexiones siempre se van a dar antes que en las columnas. Esto garantiza que el colapso siempre se limite a los componentes inmediatamente adyacentes a los directamente implicados en el fallo inicial [53]. La campaña experimental fue complementada con computación numérica mediante *Applied Element Method* (AEM). Se realizaron dos modelos, uno siguiendo el enfoque basado en jerarquía y otro siguiendo un enfoque convencional de diseño. El enfoque basado en jerarquía consiguió limitar el colapso a las inmediaciones del fallo inicial mientras que el diseño convencional propagaba el colapso al resto de la estructura. Estos resultados fueron validados por lo observado en la campaña experimental donde el colapso se limitó a las zonas adyacentes del fallo inicial (ver figura 12) validando por lo tanto la eficacia del diseño basado en fusibles.

4. CONCLUSIONES Y FUTURAS APROXIMACIONES

La robustez estructural es un tema de creciente interés tanto a nivel nacional como internacional, dada su importancia para garantizar la seguridad de las estructuras frente a eventos extremos.

Aunque las normativas en esta materia son relativamente recientes, se han dado importantes avances en su desarrollo. En España, el Código Estructural exige considerar la robustez en el diseño, pero proporciona escasas indicaciones prácticas sobre cómo abordar este desafío, lo que nos lleva a recurrir a otras normativas como el Eurocódigo 1 Parte 1-7, que establece reglas para diseñar con criterios de robustez, o incluso a normativas de otros países, como la estadounidense UFC 4-023-03, cuando se requiere mayor detalle.

Las normas de robustez se basan principalmente en tres estrategias de diseño: (i) el método de las fuerzas de atado, donde se proporciona un nivel mínimo de atado vertical y horizontal en las estructuras para ofrecerles continuidad en caso de fallo de un elemento estructural;

(ii) el método de los caminos de carga alternativos, consistente en garantizar que la estructura es capaz de generar vías alternativas para la transmisión de las cargas mediante el análisis de diferentes escenarios de fallo, y (iii) el método de los elementos clave, que identifica los elementos clave en el colapso de una estructura y los rediseña para resistir cargas accidentales con el fin de evitar fallos locales en cada uno de estos elementos.

La elección del método más adecuado depende de las posibles consecuencias asociadas al colapso de la estructura.

En el ámbito de la investigación, el número de estudios en robustez ha aumentado significativamente. A nivel nacional, España cuenta con proyectos innovadores que abren nuevos horizontes en materia de robustez. Algunos ejemplos son los proyectos desarrollados en la *Universitat Politècnica de València*, como ENDURE, que implementa fusibles estructurales en estructuras de nueva construcción para frenar el colapso una vez iniciado, y el proyecto ENHANCE, que desarrolla una solución de refuerzo estructural para edificios existentes que involucra y aprovecha toda la estructura, en su conjunto, en la resistencia al colapso progresivo. Estas iniciativas destacan el potencial nacional en el desarrollo de enfoques avanzados y efectivos en materia de robustez estructural.

Agradecimientos

Los autores desean expresar su más sincero agradecimiento al profesor Antonio Marí, cuya excepcional trayectoria académica y humana ha sido una fuente de inspiración para colegas y estudiantes a lo largo de los años. Este artículo, elaborado en reconocimiento a su dedicación incansable y en agradecimiento por la valiosa amistad que nos une, forma parte de un homenaje merecido a su destacada labor y al impacto duradero de su legado.

Este trabajo no habría sido posible sin el apoyo de la Generalitat Valenciana por la subvención otorgada al proyecto ENHANCE (CIPROM/2022/47), así como al MCIN/AEI/10.13039/501100011033 y a la "Unión Europea Next-GenerationEU/PRTR" por la financiación recibida a través de la beca postdoctoral IJC2020-042642-I. Asimismo, los autores agradecen el apoyo recibido para el desarrollo del proyecto ENTIRE, financiado en el marco de la convocatoria de Ayudas para Primeros Proyectos de Investigación (PAID-06-22) del Vicerrectorado de Investigación de la Universitat Politècnica de València. De igual manera, este artículo forma parte del proyecto ENFORCE, financiado por la convocatoria PAID-06-24 del mismo Vicerrectorado.

Referencias

[1] CRED UNDRR, The human cost of disasters: an overview of the last 20 years (2000-2019), 2020.

[2] FBI Federal Bureau of Investigation, Oklahoma City Bombing, (n.d.). https://www.fbi.gov/history/famous-cases/oklahoma-city-bombing#Additional-Information (accessed December 9, 2024).

[3] J.M. Adam, F. Parisi, J. Sagaseta, X. Lu, Research and practice on progressive collapse and robustness of building structures in the 21st century, Eng Struct 173 (2018) 122–149. https://doi.org/10.1016/j.engstruct.2018.06.082.

[4] J.F. Baker, E.L. Williams, D. Lax, The Design of Framed Buildings against High-Explosive Bombs., in: The Civil Engineer in War, Thomas Telford Ltd, London, 1948: pp. 3: 80-112. https://doi.org/10.1680/ciwv3.45170.0006.

[5] Department of Defense (DoD), Unified Facilities Criteria (UFC) Design of Buildings to Resist Progressive Collapse, 2024. http://dod.wbdg.org/.

[6] GSA, Alternate Path Analysis and Design Guidelines for Progressive Collapse Resistance, General Services Administration, Washington DC, USA, 2016.

[7] ASCE/SEI 76-23, Standard for Mitigation of Disproportionate Collapse Potential in Buildings and Other Structures, 2023.

[8] CEN, EN 1990:2023 - Eurocode - Basis of structural and geotechnical design, Brussels, 2023.

[9] CEN, EN 1991-1-7 - Eurocode 1, Actions on structures - Part 1-7 General Actions - Accidental actions, Brussels, 2018.

[10] V. T, D. S, S. ML, M. J, M. G, K. U, T. A, J. R, J. W, S. T, F. P, S. D, S. JD, S. P, S. M, F. M, C. P, Z. B, T. P, K. J, M. M, A. J, S. R, K. J, B. T, M. J, A. D, S. J, Reliability background of the Eurocodes, (2024). https://doi.org/10.2760/9482837 (online).

[11] A. J, A. M, B. B, B. F, C. R, D. J, I. B, M. P, M. T, O. A, P. F, S. J, S. ML, T. T, C. R, T. T, S. ML, Guidance on the design for structural robustness, (2024). https://doi.org/10.2760/525706 (online),10.2760/4945167 (print).

[12] CEN, EN 1992-1-1:2023. Eurocode 2 - Design of concrete structures - Part 1-1: General rules and rules for buildings, bridges and civil engineering structures, 2023.

[13] International Federation for Structural Concrete (fib), fib Model Code for Concrete Structures (2020), Lausanne, 2024.

[14] Gobierno de España, Código Estructural BOE Real Decreto 470/2021, 2021.

[15] A. J, A. M, B. B, B. F, C. R, D. J, I. B, M. P, M. T, O. A, P. F, S. J, S. ML, T. T, C. R, T. T, S. ML, Guidance on the design for structural robustness, (2024). https://doi.org/10.2760/525706 (online),10.2760/4945167 (print).

[16] E. Díaz-Pavón Cuaresma, J. León González, J. Ley Urzáiz, Robustez estructural: la cualidad que echó de menos Ribera en 1905, Hormigón y Acero 68 (2017) 171–183. https://doi.org/10.1016/j.hya.2017.04.011.

[17] A. Setiawan, D. Cetina, N. Makoond, M. Buitrago, J.M. Adam, Practical methodology for quantifying the structural robustness of RC building structures, Structures 70 (2024) 107898. https://doi.org/10.1016/j.istruc.2024.107898.

[18] Arup, Review of international research on structural robustness and disproportionate collapse, 2011.

[19] Y. Li, X. Lu, H. Guan, L. Ye, An improved tie force method for progressive collapse resistance design of reinforced concrete frame structures, Eng Struct 33 (2011) 2931–2942. https://doi.org/10.1016/j.engstruct.2011.06.017.

[20] A. Elshaer, H. Mostafa, H. Salem, Progressive collapse assessment of multistory reinforced concrete structures subjected to seismic actions, KSCE Journal of Civil Engineering 21 (2017) 184–194. https://doi.org/10.1007/s12205-016-0493-6.

[21] B.A. Izzuddin, A.G. Vlassis, A.Y. Elghazouli, D.A. Nethercot, Progressive collapse of multi-storey buildings due to sudden column loss — Part I: Simplified assessment framework, Eng Struct 30 (2008) 1308–1318. https://doi.org/10.1016/j.engstruct.2007.07.011.

[22] A.G. Vlassis, B.A. Izzuddin, A.Y. Elghazouli, D.A. Nethercot, Progressive collapse of multi-storey buildings due to sudden column loss—Part II: Application, Eng Struct 30 (2008) 1424–1438. https://doi.org/10.1016/j.engstruct.2007.08.011.

[23] K. Khandelwal, S. El-Tawil, Pushdown resistance as a measure of robustness in progressive collapse analysis, Eng Struct 33 (2011) 2653–2661. https://doi.org/10.1016/j.engstruct.2011.05.013.

[24] G. Mucedero, E. Brunesi, F. Parisi, Nonlinear material modelling for fibre-based progressive collapse analysis of RC framed buildings, Eng Fail Anal 118 (2020) 104901. https://doi.org/10.1016/j.engfailanal.2020.104901.

[25] G. Xu, B.R. Ellingwood, An energy-based partial pushdown analysis procedure for assessment of disproportionate collapse potential, J Constr Steel Res 67 (2011) 547–555. https://doi.org/10.1016/j.jcsr.2010.09.001.

[26] Y. Bao, J.A. Main, S.-Y. Noh, Evaluation of Structural Robustness against Column Loss: Methodology and Application to RC Frame Buildings, Journal of Structural Engineering 143 (2017). https://doi.org/10.1061/(ASCE)ST.1943-541X.0001795.

[27] M.V. Requena-Garcia-Cruz, A. Morales-Esteban, P. Durand-Neyra, Assessment of specific structural and ground-improvement seismic retrofitting techniques for a case study RC building by means of a multi-criteria evaluation, Structures 38 (2022) 265–278. https://doi.org/10.1016/j.istruc.2022.02.015.

[28] S. Villar-Salinas, S. Pacheco, J. Carrillo, F. López-Almansa, Influence of high axial compression ratios in RC columns on the seismic response of MRF buildings, Structural Engineering and Mechanics 90 (2024) 51–70.

[29] M.-V. Requena-Garcia-Cruz, A. Morales-Esteban, P. Durand-Neyra, B. Zapico-Blanco, Influence of the constructive features of RC existing buildings in their ductility and seismic performance, Bulletin of Earthquake Engineering 19 (2021) 377–401. https://doi.org/10.1007/s10518-020-00984-z.

[30] R. Moreno-Gonzalez, J.M. Bairan, Seismic Damage Assessment for Waffled-Slabs Reinforced Concrete (RC) Buildings in Barcelona, International Journal of Architectural Heritage 7 (2013) 116–134. https://doi.org/10.1080/15583058.2011.616619.

[31] B. Guaygua, A.J. Sánchez-Garrido, V. Yepes, Life cycle assessment of seismic resistant prefabricated modular buildings, Heliyon 10 (2024) e39458. https://doi.org/10.1016/j.heliyon.2024.e39458.

[32] A.P. Santos, R. Castedo, L.M. López, M. Chiquito, J.I. Yenes, A. Alañón, E. Costamagna, S. Martínez-Almajano, Reinforced Concrete Building with IED Detonation: Test and Simulation, Applied Sciences 12 (2022) 7803. https://doi.org/10.3390/app12157803.

[33] R. Castedo, A.P. Santos, A. Alañón, C. Reifarth, M. Chiquito, L.M. López, S. Martínez-Almajano, A. Pérez-Caldentey, Numerical study and experimental tests on full-scale RC slabs under close-in explosions, Eng Struct 231 (2021) 111774. https://doi.org/10.1016/j.engstruct.2020.111774.

[34] M. Chiquito, L.M. López, R. Castedo, A. Pérez-Caldentey, A.P. Santos, Behaviour of retrofitted masonry walls subjected to blast loading: Damage assessment, Eng Struct 201 (2019) 109805. https://doi.org/10.1016/j.engstruct.2019.109805.

[35] E. Garcia-Castillo, I. Paya-Zaforteza, A. Hospitaler, Fire in heritage and historic buildings, a major challenge for the 21st century, Developments in the Built Environment 13 (2023) 100102. https://doi.org/10.1016/j.dibe.2022.100102.

[36] J.A. Capote Abreu, D. Alvear, M. Lázaro, J. Crespo, I. Fletcher, S. Welch, J. Torero, Modelado de las solicitaciones de los elementos estructurales de hormigón en edificios de gran altura en incendios reales, Informes de La Construcción 63 (2011) 83–91. https://doi.org/10.3989/ic.09.005.

[37] E. Garcia-Castillo, I. Paya-Zaforteza, A. Hospitaler, Analysis of the fire resistance of timber jack arch flooring systems used in historical buildings, Eng Struct 243 (2021) 112679. https://doi.org/10.1016/j.engstruct.2021.112679.

[38] E. Menéndez, L. Vega, Analysis of the behaviour of the structural concrete after the fire at the Windsor Building in Madrid, Fire Mater 34 (2010) 95–107. https://doi.org/10.1002/fam.1013.

[39] N. Stathas, S.N. Bousias, X. Palios, E. Strepelias, M.N. Fardis, Tests and Simple Models of RC Frame Subassemblies for Postulated Loss of Column, Journal of Structural Engineering 144 (2018). https://doi.org/10.1061/(ASCE)ST.1943-541X.0001951.

[40] S.-B. Kang, K.H. Tan, Behaviour of precast concrete beam–column sub-assemblages subject to column removal, Eng Struct 93 (2015) 85–96. https://doi.org/10.1016/j.engstruct.2015.03.027.

[41] D.-Y. Kong, Y. Yang, S. Li, B. Yang, J.Y.R. Liew, Experimental and Analytical Study on Progressive Collapse of 3D Composite Floor System under Corner Column Loss, Journal of Structural Engineering 148 (2022). https://doi.org/10.1061/(ASCE)ST.1943-541X.0003288.

[42] D.-Y. Kong, Y.-F. Lyu, Y.-R. Dong, H. Wang, Y. Yang, Large-scale test of a 3D steel moment-resisting frame with composite slab subject to penultimate interior column loss, J Constr Steel Res 201 (2023) 107763. https://doi.org/10.1016/j.jcsr.2022.107763.

[43] G. Caredda, N. Makoond, M. Buitrago, J. Sagaseta, M. Chryssanthopoulos, J.M. Adam, Enhancing building robustness through a fuse-based segmentation framework, Developments in the Built Environment 19 (2024) 100515. https://doi.org/10.1016/j.dibe.2024.100515.

[44] U. Starossek, Measures of robustness and collapse resistance, in: Progressive Collapse of Structures, n.d.: pp. 129–140. https://doi.org/10.1680/pcos.61682.129.

[45] M. Buitrago, G. Sempértegui, N. Makoond, J.M. Adam, New structural stabilisation systems to prevent building progressive collapse, in: 31st Int. Work. Intell. Comput. Eng., Vigo, 2024: pp. 256–263.

[46] N. Makoond, A. Setiawan, S.L. Orton, J.M. Adam, The effect of continuity reinforcement on the progression of collapse in reinforced concrete buildings, Structures 61 (2024) 105981. https://doi.org/10.1016/j.istruc.2024.105981.

[47] J.M. Adam, M. Buitrago, E. Bertolesi, J. Sagaseta, J.J. Moragues, Dynamic performance of a real-scale reinforced concrete building test under a corner-column failure scenario, Eng Struct 210 (2020) 110414. https://doi.org/10.1016/j.engstruct.2020.110414.

[48] J. Garzón-Roca, J. Sagaseta, M. Buitrago, J.M. Adam, Dynamic Punching Assessment of Edge Columns after Sudden Corner Column Removal, ACI Struct J 118 (2021). https://doi.org/10.14359/51728195.

[49] M. Buitrago, E. Bertolesi, J. Sagaseta, P.A. Calderón, J.M. Adam, Robustness of RC building structures with infill masonry walls: Tests on a purpose-built structure, Eng Struct 226 (2021) 111384. https://doi.org/10.1016/j.engstruct.2020.111384.

[50] M. Buitrago, E. Bertolesi, J. Garzón-Roca, J. Sagaseta, J.M. Adam, A Parametric Computational Study of RC Building Structures under Corner-Column Removal Situations, Applied Sciences 10 (2020) 8911. https://doi.org/10.3390/app10248911.

[51] M. Buitrago, N. Makoond, J.J. Moragues, J. Sagaseta, J.M. Adam, Robustness of a full-scale precast building structure subjected to corner-column failure, Structures 52 (2023) 824–841. https://doi.org/10.1016/j.istruc.2023.03.146.

[52] M. Buitrago, J. Sagaseta, N. Makoond, A. Setiawan, J.M. Adam, Robustness of a full-scale precast building structure after edge column failure, Eng Struct 326 (2025) 119495. https://doi.org/10.1016/j.engstruct.2024.119495.

[53] N. Makoond, A. Setiawan, M. Buitrago, J.M. Adam, Arresting failure propagation in buildings through collapse isolation, Nature 629 (2024) 592–596. https://doi.org/10.1038/s41586-024-07268-5.

cotca, s.a.

C/ Balmes 200 5è 2ª
08006 – Barcelona
A08574816

tlf. 93.218.71.46
info@cotca.com
www.cotca.com

ASISTENCIA TÉCNICA

Se ocupa de dar al cliente el soporte técnico necesario para conseguir el óptimo desarrollo de todas las fases de la obra.

PATOLOGIA

Realiza todo tipo de estudios de catalogación de daños y definición de estado actual de edificios, aportando estudios de riesgos y propuestas de actuación.

CONTROL DE CALIDAD / OCT

Actividades destinadas a medir y comprobar los niveles de calidad reales, contrastando toda la información con la normativa vigente.

INGENIERÍA

Asesoramos a nuestros clientes en toda la cadena de valor de la ingeniería estructural y de la construcción.

Metro de Lima – Perú
2025

Torre de refrigeración de Puertollano
2008

Chimeneas Central Térmica Sant Adrià del Besòs
2018

Hospital de la Santa Creu i Sant Pau de Barcelona
2026

Acueducto de Tardienta
2019

OCT Viviendas Casernes de Sant Andreu IMHAB 2024

Disponible en **www.hormigonyacero.com**
https://doi.org/10.33586/hya.2025.4132

Ensayos no destructivos o moderadamente destructivos para la caracterización de los materiales componentes de la obra de fábrica de ladrillo

Non-Destructive or Minor Destructive Tests for the Characterization of the Component Materials of Brick Masonry

Albert Cabané Cañas[a] , **Luca Pelà**[b] , **Pere Roca Fabregat**[b, *]

[a] *Doctor, investigador, Universitat Politècnica de Catalunya.*
[b] *Doctor, profesor catedrático, Universitat Politècnica de Catalunya.*

Recibido el 23 de mayo de 2025; revisado el 8 de julio de 2025, aceptado el 1 de agosto de 2025

RESUMEN

Se presenta la aplicación a los componentes de la obra de fábrica (ladrillos y mortero en juntas) de un conjunto de técnicas de ensayo no destructivas (NDT) o moderadamente destructivas (MDT) para la medida experimental in situ de la resistencia a compresión del material. El estudio se orienta principalmente al caso de obra de fábrica histórica de ladrillo macizo y mortero hidráulico de cal, prestándose asimismo cierta atención al mortero de cemento Portland. Las tècnicas investigadas comprenden el ensayo penetrométrico (PPT), el ensayo de extracción de tornillo helicoidal (HPT), el esclerómetro (Rebound Hammer, RH), el ensayo velocidad del pulso ultrasónico UPV) y la técnica SonReb, basada en la combinación de estos dos últimos ensayos. Se presta también atención al ensayo de doble embolo (Double Punch Test, DPT) sobre muestras de juntas de mortero a pesar de su carácter más destructivo.

Para las técnicas PPT y HPT se proponen unas correlaciones empíricas, derivadas de la ejecución de un gran número de ensayos, para correlacionar los parámetros medidos (profundidad de penetración y fuerza de extracción respectivamente) con la resistencia a compresión de ladrillos y mortero. Por otra parte, se ha comprobado que el método SonReb, basado en la integración de resultados obtenidos con esclerómetro y ultrasonidos, es aplicable, con ciertas precauciones metodológicas y utilizando una correlación específica, para la estimación de la resistencia a compresión del ladrillo cerámico macizo.

PALABRAS CLAVE: Obra de fábrica de ladrillo, ladrillo cerámico macizo, mortero de cal, ensayo no destructivo (NDT), ensayo moderadamente destructivo (MDT), resistencia a compresión, correlación empírica.

ABSTRACT

The study presents the application of a set of non-destructive testing (NDT) or minor destructive testing (MDT) techniques to masonry components (bricks and mortar joints) for the experimental in-situ measurement of the material's compressive strength. The study focuses primarily on the case of historic masonry construction made of solid brick and lime mortar, with some attention also paid to Portland cement mortar. The techniques investigated include the penetrometer test (PPT), the helical screw pullout test (HPT), the sclerometer (Rebound Hammer, RH), the ultrasonic pulse velocity test (UPV), and the SonReb technique, based on a combination of the latter two tests. Attention is also paid to the double punch test (DPT) on mortar joint samples, despite its more destructive nature.

For the PPT and HPT techniques, empirical correlations derived from a large number of tests are proposed to relate the measured parameters (penetration depth and pullout force, respectively) with the compressive strength of bricks

and mortar. Furthermore, the SonReb method, based on the integration of results obtained with sclerometers and ultrasounds, has been shown to be applicable, with certain methodological cautions and using a specific correlation, for the estimation of the compressive strength of solid ceramic bricks.

KEYWORDS: Brick masonry, solid ceramic brick, lime mortar, non-destructive test (NDT), minor destructive test (MDT), compressive strength, empirical correlation.

* Persona de contacto / *Corresponding author*:
Correo-e / *e-mail*: pere.roca.fabregat@upc.edu (Pere Roca Fabregat)

Cómo citar este artículo: Cabané, A., Pelà, L., & Roca, P. (2026). Ensayos no destructivos o moderadamente destructivos para la caracterización de los materiales componentes de la obra de fábrica de ladrillo. *Hormigón y Acero*. 77(308):131-143. https://doi.org/10.33586/hya.2025.4132

1. INTRODUCCIÓN

La evaluación resistente de las construcciones existentes requiere disponer de un conocimiento suficiente sobre las propiedades mecánicas de los materiales estructurales que las conforman. Tales propiedades proporcionan un dato de partida fundamental para el desarrollo de los análisis estructurales orientados a verificar el desempeño de las estructuras ante acciones gravitatorias y horizontales de sismo y viento. Asimismo, estos análisis son necesarios para concluir sobre la necesidad y el alcance de posibles intervenciones de refuerzo. Con todo, la caracterización de las propiedades de los materiales en estructuras existentes topa con dificultades importantes. Por una parte, los materiales de tales estructuras, y especialmente de las estructuras antiguas, pueden presentar niveles muy importantes de variabilidad y dispersión, por lo que una caracterización exhaustiva, basada en la toma de muestras, puede resultar inviable debido al gran número de muestras potencialmente necesario. Esta dificultad se agrava cuando además se pretende que las muestras respeten los formatos geométricos estandarizados definidos por normativas vigentes orientadas hacia la construcción de estructuras de nueva planta. La necesidad de limitar el número de muestras y, asimismo, de limitar sus dimensiones geométricas, conduce frecuentemente a preferir el empleo de criterios no estandarizados tanto en lo relativo a la representatividad del número de muestras como en relación a los formatos y tamaños de las muestras. En cualquier caso, estas dificultades pueden resolverse parcialmente mediante el empleo de técnicas de ensayo mecánico en laboratorio, adecuadamente calibradas, aplicables sobre muestras no estándares de pequeñas dimensiones. Alternativamente, es posible aplicar ciertas técnicas de ensayo no destructivo (NDT) o moderadamente destructivo (MDT) que, sin inducir daño o bien casando un daño muy limitado y fácilmente reparable, permiten obtener una estimación suficientemente fiable de las propiedades mecánicas fundamentales. En cualquier caso, las técnicas MDT y NDT pueden combinarse con un uso limitado de ensayos destructivos (DT) en laboratorio sobre muestras. Del uso combinado de técnicas MDT, NDT i DT resulta un enfoque que, gracias a la repetibilidad de los ensayos MDT y NDT, gracias al carácter más directo y fiable de los ensayos DT y gracias a la posible redundancia de las medidas, permite alcanzar un nivel mucho más elevado de fiabilidad y representatividad.

Las dificultades mencionadas en relación a la medición de las propiedades mecánicas de los materiales resultan aún más críticas en el caso de construcciones históricas o patrimoniales construidas de obra de fábrica de ladrillo o piedra. La necesidad de limitar el número de muestras y su tamaño resulta aún más acusada debido a las fuertes restricciones que el respeto hacia los valores culturales y patrimoniales introduce sobre el potencial daño causado por los procedimientos de inspección. Ello puede restringir drásticamente la posibilidad de extraer muestras para ensayo destructivo en laboratorio, siendo necesario recurrir de forma intensiva a las técnicas MDT y NDT.

El Comité Científico Internacional sobre Análisis y Restauración de Estructuras del Patrimonio Arquitectónico de ISCARSAH, perteneciente a la organización internacional ICOMOS (Consejo Internacional de Monumentos y Sitios) y formado por más de 300 expertos procedentes de una multitud de países, aprobó en Septiembre de 2024 un documento sobre análisis y conservación del patrimonio arquitectónico ("Guidelines for the Analysis, Conservation and Sttructural Restoration of Architectural Heritage" [1]) en el que, además de aportar definiciones rigurosas sobre estos tipos de ensayos (DT, NDT y MDT), establece algunas recomendaciones sobre cómo utilizarlos y combinarlos. Según el documento de ICOMOS/ISCARSAH, los ensayos destructivos deben utilizarse de forma estrictamente limitada y controlada. Solo deben realizarse cuando la información necesaria no pueda obtenerse por otros medios o cuando sean indispensables para calibrar los métodos MDT y NDT. Las técnicas DT deben emplearse preferiblemente en zonas poco visibles o con escaso valor patrimonial, minimizando el daño ocasionado y sin debilitar o comprometer la resistencia de los elementos estructurales. Por las mismas razones, el número de muestras debe minimizarse y, en general, restringirse a las partes de la estructura con menor valor patrimonial.

De acuerdo con ICOMOS / ISCARSAH [1], la posible ganancia que un ensayo DT pueda proporcionar en información debe compensar ampliamente el daño y la pérdida de valor patrimonial causado en la estructura. En otras palabras, es preciso que la ganancia en información posibilite realmente

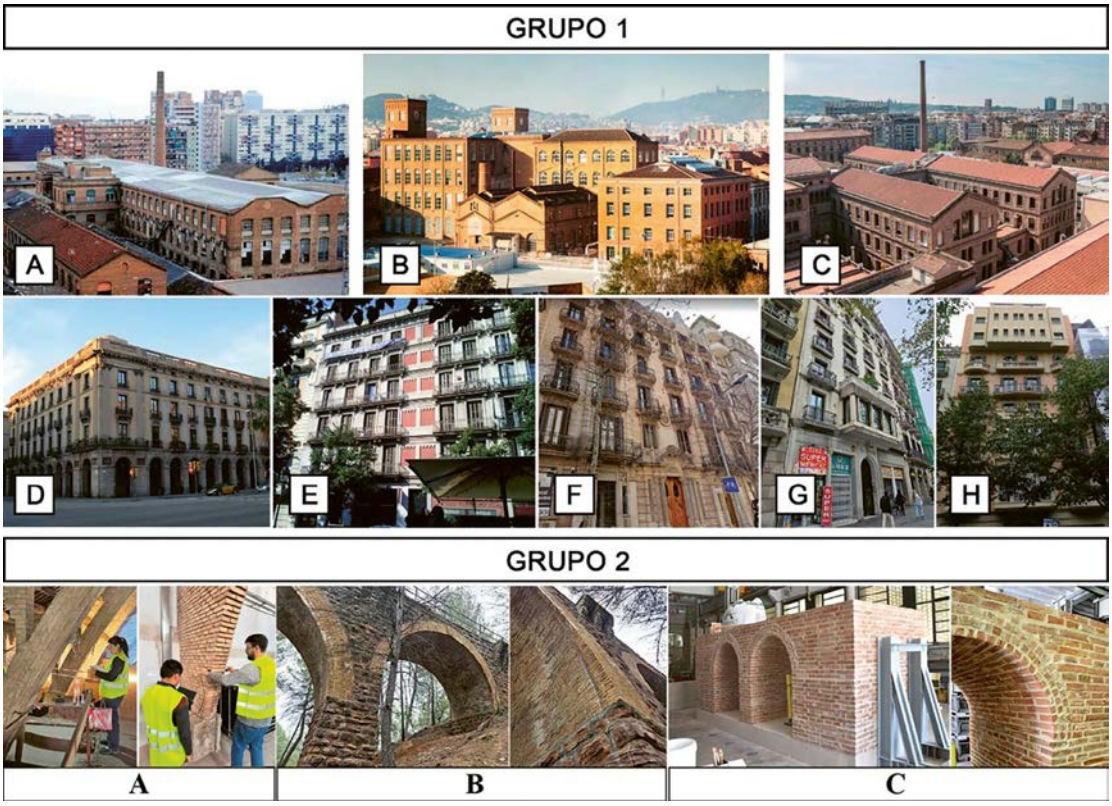

Figura 1. Casos de estudio considerados en la presente investigación. Primer grupo: edificio industrial de 1878 (a); edificio industrial de 1910-1920 (b); edificio industrial de 1927 (c); edificio residencial de 1840 (d); edificio residencial de 1880 (e); edificio residencial de 1905 (f); edificio residencial de 1910 (g); edificio residencial de 1930 (h). Segundo grupo: bodega construida a principios del siglo XX (A); puente histórico multiarco de Joncadella (B); puente construido en laboratorio (C).

una reducción del alcance de la intervención y de su impacto en la autenticidad de la estructura, de forma que esta reducción compense muy ampliamente la alteración causada por el ensayo destructivo. Ciertamente, la experiencia demuestra que intervenciones basadas en un conocimiento deficiente pueden fácilmente ocasionar un elevado impacto negativo en la autenticidad y en el valor patrimonial de la estructura.

El presente estudio relaciona una serie de técnicas de ensayo MDT y NDT aplicadas a los materiales componentes de la fábrica de ladrillo. En particular, se estudia la posibilidad de aplicar tales técnicas al ladrillo macizo cerámico y al mortero (de cal hidráulica o de cemento Portland) de las juntas. Las técnicas investigadas son el ensayo penetrométrico (PPT), el ensayo de extracción de tornillo helicoidal (HPT), el esclerómetro (Rebound Hammer, RH), los ultrasonidos (ensayo velocidad del pulso ultrasónico UPV) y la técnica SonReb, basada en la combinación de estos dos últimos ensayos. A estas técnicas cabe añadir la técnica de ensayo de doble émbolo (Double Punch Test, DPT) que, aunque es estrictamente un ensayo destructivo (DT) por cuanto requiere extraer una muestra de junta de mortero, causa de hecho un daño muy reducido y fácilmente reparable, por lo que podría, bajo ciertas condiciones, clasificarse como MDT.

El conocimiento de la resistencia a compresión de ladrillos y morteros, estimada mediante los ensayos mencionados, posibilita obtener una estimación la resistencia a compresión de la obra de fábrica como material compuesto a partir de expresiones empíricas disponibles que, como en el caso de la fórmula del Eurocódigo 6 [2] y de CTE DB-SE-F [3], permiten calcular este último valor a partir de la resistencia de los componentes (mortero y ladrillo). Por otra parte, los autores han desarrollado técnicas moderadamente destructivas o MDT basadas en la extracción de pequeñas probetas cilíndricas de fábrica compuesta sobre las cuales realizar ensayos a compresión o a corte en laboratorio ([4], [5]).

El presente artículo expone las características y la metodología de empleo de cada una de las técnicas investigadas. Se indican algunas precauciones o consideraciones que es preciso tener en cuenta para optimizar el uso de las técnicas en elementos de obra de fábrica, basadas en la experiencia de los autores. Asimismo, se presentan las correlaciones empíricas que ha sido posible derivar para relacionar la resistencia a compresión del material con el parámetro realmente medido (profundidad de penetración en PPT o fuerza de arranque en HPT). En el caso de las medidas con esclerómetro o ultrasonidos, la estimación de la resistencia a compresión resulta de la integración combinada de las medidas a través de la técnica SonReb.

2. MATERIALES ANALIZADOS

La investigación que se presenta se ha centrado en el análisis de la resistencia a compresión de los materiales componentes

obra de fábrica de ladrillo, prestando especial atención al caso de la obra de fábrica histórica. Los materiales componentes investigados son los ladrillos cerámicos macizos y los morteros de cal hidráulica o de cemento Portland. Se han investigado ladrillos de distinto tipo, incluyendo ladrillos fabricados por extrusión mecánica y fabricados manualmente, éstos últimos tanto modernos como históricos, extraídos de muros de obra de fábrica existentes. Las juntas de mortero se manufacturaron en el laboratorio o bien se recolectaron de edificios históricos de obra de fábrica.

En el caso de las muestras formadas en laboratorio, éstas fueron extraídas de muros construidos a propósito y posteriormente desmantelados.

Se construyeron dos tipos de muros, combinando ladrillos fabricados por extrusión con mortero de cemento y ladrillos de fabricación manual con mortero de cal hidráulica, estos últimos orientados a representar, en la medida posible, una obra de fábrica de tipo histórico. Se construyeron dos muros de cada tipo. En los artículos de García-Ramonda et al. [6] y Huang et al. [7] puede hallarse más información al respecto. Por otra parte, se examinaron ocho muros de obra de fábrica distintos, pertenecientes a un grupo de siete edificios históricos, con el fin de adquirir ladrillos y juntas de mortero (figura 1). Los edificios investigados incluyen complejos industriales y edificios residenciales. Todos estos edificios fueron construidos a finales del siglo XIX o a principios del siglo XX.

Los morteros producidos en el laboratorio se fabricaron con dos aglomerantes diferentes. En primer lugar, se utilizó un mortero de cal hidráulica premezclado comercial clasificado como M5 según EN 998-2:2018 [8]. Este mortero premezclado se alteró incorporando relleno de piedra caliza para disminuir su resistencia a la compresión, con el objetivo de replicar un mortero histórico de baja resistencia, según el procedimiento propuesto por Segura et al. [9]. En segundo lugar, se utilizó mortero de cemento premezclado disponible en el mercado clasificado como M7.5 según [8].

La resistencia a compresión de los morteros utilizados en la construcción de los muros en laboratorio se evaluó según EN 1015-11:2020 [10] ensayando cubos de 40 × 40 × 40 mm³ fabricados con el mismo material empleado para los muros. Los ensayos de compresión en el mortero de cal hidráulica, realizados de acuerdo con esta normativa, proporcionaron una resistencia a la compresión f_m de 3.54 MPa y 3.47 MPa (respectivamente para cada muro), con un coeficiente de variación del 19.4 % y 20.1 %. A su vez, la resistencia a la compresión del mortero de cemento alcanzo un valor de 7.64 MPa y 5.59 MPa (para cada muro) con un coeficiente de variación del 32.7 % y 8.6 %.

Por otra parte, se han estudiado ladrillos provenientes de un segundo grupo de estructuras de obra de fábrica correspondientes a una bodega histórica formada por varias naves (caso A), un puente multiarco (puente de Joncadella de la línea ferroviaria de Manresa a Súria, caso B) y un modelo experimental de puente de dos arcos recientemente construido en laboratorio (caso C). Las propiedades mecánicas de los ladrillos del puente de Joncadella, así como del puente experimental han sido también medidas en laboratorio mediante ensayos destructivos. Sin embargo, debido a restricciones relacionados con el valor patrimonial, no ha sido posible extraer material sobre el cual aplicar tales ensayos en el primer caso de estudio. Puede hallarse más información sobre los materiales ensayados en los artículos previos de los autores ([11] y [12])

3. ENSAYOS DESTRUCTIVOS EN LABORATORIO

3.1. Procedimientos de ensayo

Los ensayos destructivos realizados para la medida de la resistencia a compresión, realizados sobre probetas o muestras de mortero y muestras de ladrillo, han sido ejecutados en el Laboratorio de Tecnología de Estructuras y Materiales de Construcción (LATEM) de la Universidad Politécnica de Cataluña.

Las muestras de ladrillo se prepararon de acuerdo con los procedimientos especificados en la norma europea EN 772-1:2011+A1:2016 [13]. De los ladrillos enteros se obtuvieron muestras de 100 × 100 × 40 mm³ utilizando una sierra de mesa equipada con chorro de agua. Posteriormente, las muestras se sometieron a un proceso de secado en horno a temperatura constante de 105 ± 5 °C durante 24 horas. Se prepararon y analizaron un total de 125 muestras de ladrillo.

Las muestras de junta de mortero se prepararon y ensayaron de acuerdo con los procedimientos especificados en la norma alemana DIN 18555-9:2019-04 [14] y en el documento 778-3R de la Unión Internacional de Ferrocarriles (UIC) [15]. Muchas de las muestras extraídas presentaban baja consistencia y cohesión, no siendo factible realizar ensayos en muestras con las dimensiones de 50 × 50 mm² que aconseja la norma alemana. El espesor de las muestras, correspondiente al espesor de la junta, se midió con un calibrador. Las muestras se ensayaron el mismo día de la extracción, sin secado previo, para asegurar un grado de humedad similar al de la pared existente. Se preparó y ensayó un total de 416 muestras de juntas de mortero. Las muestras se ensayaron con émbolos de carga de 20 mm de diámetro. Siguiendo las indicaciones de Pelà et al. [16, 17] y Matysek et al. [18], las muestras se dotaron de una capa de yeso en polvo de 1 mm de espesor, interpuesta entre la muestra y los émbolos, para regularizar las superficies de apoyo y asegurar una carga homogénea. En uno de los edificios industriales investigados fue posible extraer y ensayar en laboratorio muestras cúbicas de 40 × 40 × 40 mm³ de un relleno interior existente en muros de múltiples hojas.

3.2. Resultados obtenidos en ladrillo y mortero

Los ensayos realizados sobre probetas de ladrillo correspondientes a los muros construidos en laboratorio o de ladrillos extraídos del primer grupo de edificios han permitido medir valores de resistencia a compresión media (para los distintos tipos de ladrillos ensayados) dentro del rango de 16.8 MPa a 52.7 MPa, con dispersiones situadas entre 3.5% y 21%. Para los ladrillos modernos confeccionados por extrusión o con molde se han obtenido resistencias medias de 52.7 MPa y 17.4 MPa respectivamente, con dispersiones de 2.4% y 8.6% respectivamente. En los ladrillos provenientes de edificios históricos

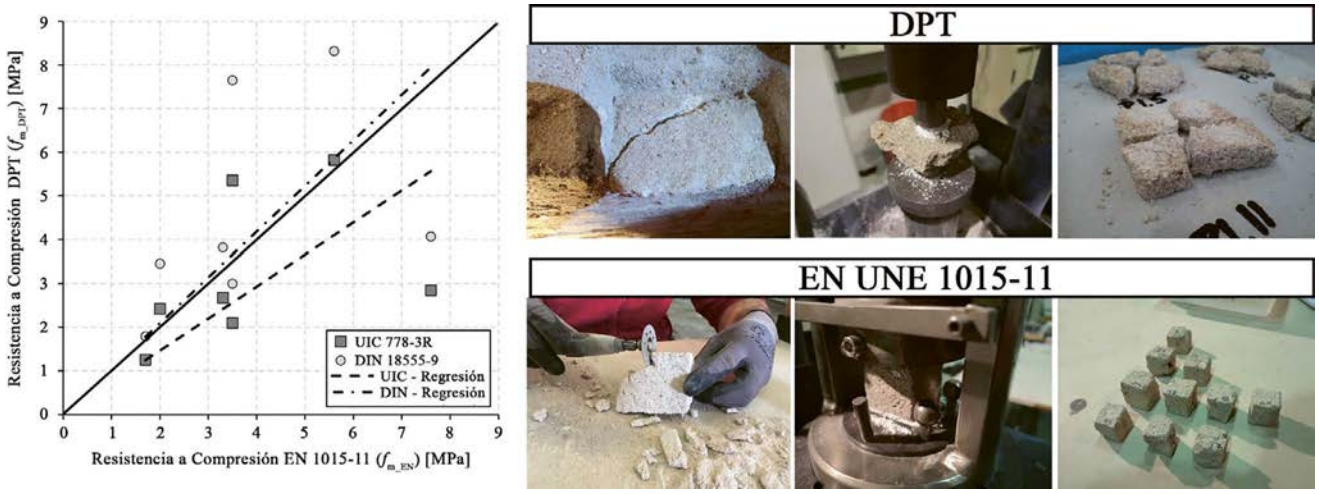

Figura 2. Regresión lineal que relaciona los valores de resistencia a la compresión de DPT y EN 1015-11:2020 [8] en muestras de mortero. En los ensayos DPT la resistencia a compresión se evalúa según los criterios de las normas DIN 18555-9:2019-04 [12] y el documento UIC 778-3R [15].

(primer grupo) se han obtenido resistencias medias situadas entre 16.8 y 35.4 MPa, con dispersiones en el rango de 12% a 23%. El valor de resistencia de 35.4 MPa, correspondiente a un único edificio del siglo XIX, es excepcionalmente alto en comparación con los valores medidos en otros edificios, cuyas resistencias se sitúan normalmente en el rango de 15 a 20 MPa. Una descripción más detallada de los resultados según tipos de ladrillos y edificios puede hallarse en Cabané et al. [11].

En el mortero, la resistencia media medida mediante DPT y calculada de acuerdo con DIN 18555-9:2019-04 [17] varía entre 0.37 N/mm² y 13.3 N/mm² en función de su procedencia, situándose los valores más frecuentes en el rango de 2 MPa a 4 MPa. Como en el caso de los ladrillos, el artículo de Cabané et al. [11] proporciona una relación detallada de las resistencias obtenidas.

En relación al segundo grupo de estructuras analizadas, la resistencia a compresión media medida experimentalmente en ladrillos del segundo y del tercer caso de estudio alcanzó valores normalizados de 27.7 y 22.6 MPa respectivamente. La resistencia media en probetas de mortero, sólo medida en el tercer caso, alcanzó un valor de 5.7 MPa.

3.3. *Comparación de valores de resistencia a compresión en mortero*

La campaña experimental en mortero permitió comparar las resistencias a la compresión obtenidas con DPT y en especímenes estándar según EN 1015-11:2020 [10] (figura 2) obtenidas de la misma fase constructiva de un edificio existente. La norma DIN 18555-9:2019-04 [14] y el documento UIC 778-3R [15] proporcionan diferentes criterios para la evaluación de la resistencia a la compresión basada en DPT. Por esta razón, la figura 2 incluye líneas de tendencia correspondientes al uso de las dos normas. La figura 2 también indica la línea de 45° correspondiente a igualdad entre resistencias obtenidas con probetas estandarizadas y con DPT.

Como se puede observar en la figura, los valores de resistencia a la compresión medidos con DPT son mayores que los que se han obtenido mediante el ensayo de probetas estandarizadas. Esta discrepancia se puede atribuir a la variación en el tamaño y las condiciones de fraguado de las muestras de mortero. Es importante notar que las condiciones de fraguado del mortero en probetas cúbicas estandarizadas difieren significativamente de las condiciones que el mortero experimenta en las juntas de los muros. Las muestras estandarizadas se obtuvieron cortando en seco probetas cúbicas de 40 mm de lado obtenidas de masas de mortero de cal extraídos de los muros de piedra irregular. Por el contrario, las juntas de mortero permanecen embebidas en la obra de fábrica, en contacto directo con ladrillos porosos y con una exposición superficial mínima al ambiente circundante.

Debido a que los valores obtenidos con DPT son más representativos de las condiciones físicas y tensionales que caracterizan a las juntas de mortero en muros, en los siguientes apartados éstos han sido considerados como de referencia para su comparación con los ensayos MDT y NDT. Por otra parte, se adopta el criterio de DIN 18555-9:2019-04 [14] para la valoración de los resultados del ensayo DPT debido a que, tal y como muestra la figura 2, da lugar a una mejor correlación con los resultados obtenidos con el ensayo a compresión de probetas estándar.

Es preciso notar también que las juntas de mortero ensayadas con DPT presentaban espesores muy variables (entre 12 y 17,6 mm). Como indican Pelà et al. [17], la evidencia empírica muestra que existe una relación inversamente proporcional entre la resistencia a la compresión y el espesor de la probeta. Debido al limitado grueso de las muestras, el estado de tensión es multiaxial debido a que el material que envuelve el área cargada introduce un efecto de confinamiento.

4. TÉCNICAS DE ENSAYO NO DESTRUCTIVO O MODERADAMENTE DESTRUCTIVO INVESTIGADAS

Como ya se mencionó, las técnicas MDT investigadas incluyen cuatro tipos de ensayos (figura 3), correspondientes al ensayo de penetrómetro (Pin Penetration Test, PPT), ensayo de extracción de tornillo helicoidal (HPT), esclerómetro (Rebound

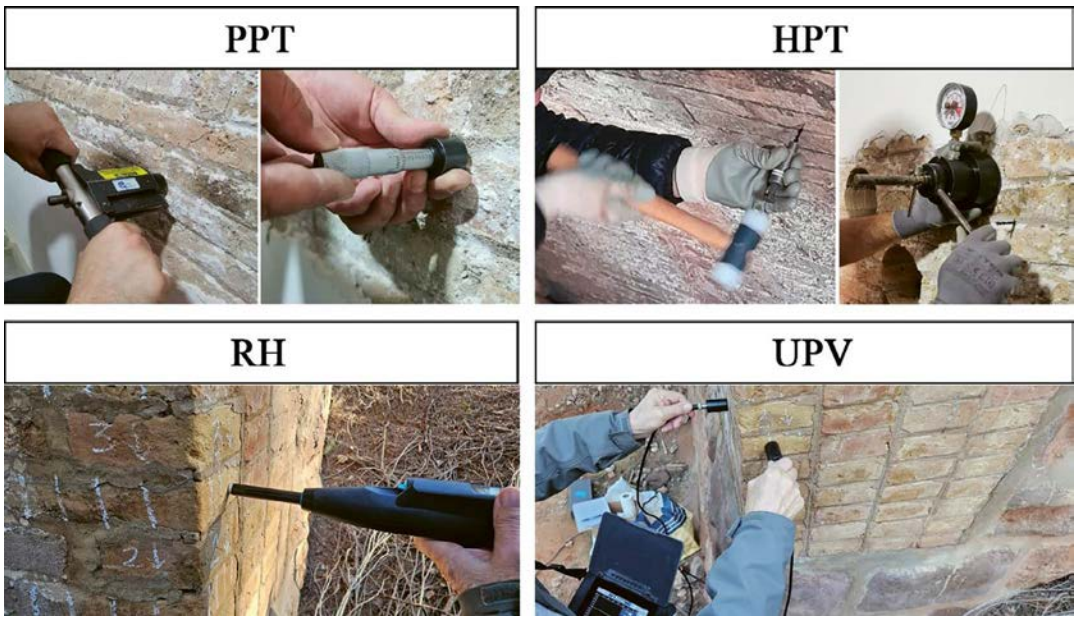

Figura 3. Principales pasos de las técnicas MDT investigadas: Ensayo de penetrómetro (PPT), Ensayo de extracción de tornillo helicoidal (HPT), Esclerómetro (RH) y el Ensayo de velocidad de pulso ultrasónico (UPV).

Hammer, RH) e inspección mediante ultrasonidos (ensayo velocidad del pulso ultrasónico, UPV). A ello hay que añadir la técnica SonReb, utilizable en ladrillos, orientada a mejorar la precisión de las medidas de la resistencia a compresión combinando los resultados del esclerómetro con los del ensayo de velocidad de pulso ultrasónico.

En el primer grupo de casos se llevaron a cabo un total de 498 medidas de PPT y 343 de HPT, incluyendo medidas realizadas tanto in situ como en laboratorio. Las 498 medidas de PPT incluyen 151 en ladrillos y 347 en juntas de mortero, mientras que las 343 medidas de HPT incluyen 114 en ladrillos y 229 en juntas de mortero. En el segundo grupo de estructuras se realizaron un total de 50 medidas de HPT en juntas de mortero y 240 de RH más 72 de UPV en ladrillos.

5. ENSAYO PENETROMÉTRICO (PPT)

5.1. Descripción de la técnica de ensayo

El ensayo mediante penetrómetro (Pin Penetration Test, PPT) es un método MDT desarrollado específicamente para evaluar la resistencia a la compresión del hormigón, mortero y ladrillo, siguiendo las recomendaciones de las normas ASTM C803/C803M [19] y BSI 1881-207:1992 [20]. El ensayo puede realizarse mediante un dispositivo fabricado por James Instruments Inc., conocido como Windsor Pin Test System®. El dispositivo puede aplicarse en las superficies expuestas de los ladrillos y de las juntas de mortero con espesor mínimo de 10 mm. Se procede insertando en el dispositivo una aguja de acero de 3 mm de diámetro y con extremo cónico. El dispositivo debe posicionarse de forma perpendicular a la superficie. A continuación, se activa el gatillo mientras se mantiene un contacto firme entre el dispositivo y la superficie. El fabricante de la herramienta indica que el dispositivo tiene suficiente fuerza como para ensayar hormigón con resistencia máxima a la compresión de 46.1 MPa, y morteros con una resistencia a la compresión en el rango de 0.8 a 50.7 MPa. Una vez clavada de la aguja, ésta se retira cuidadosamente utilizándose un soplador de aire de bulbo para eliminar cualquier material restante dentro del agujero. Se procede entonces a la lectura de la profundidad de penetración mediante un micrómetro. Dado que el mecanismo de resorte interno puede degradarse con el tiempo debido al uso repetido, se requiere una calibración al inicio de cada campaña. La calibración se realiza disparando contra una placa metálica de referencia.

Los estudios realizados por los autores han demostrado que profundidades de penetración comprendidas entre 6 mm y 11.5 mm pueden correlacionarse de forma fiable con la resistencia a la compresión del mortero. Por otra parte, se confirma que se deben realizar al menos 10 mediciones en diferentes juntas horizontales de mortero para una misma área muestreada.

5.2. Estimación de la resistencia a compresión mediante PPT

La campaña experimental anteriormente descrita ha permitido obtener una correlación entre la profundidad de penetración y la resistencia a la compresión medida a partir ensayos destructivos sobre probetas (figura 4). Se ha aplicado un tratamiento unificado para ladrillos y mortero, hallándose una correlación única para ambos materiales. En la figura 4, los distintos puntos representan la relación entre la resistencia a compresión media (en MPa) y la profundidad de penetración (en mm) para muestras ensayadas in situ, tanto en muros históricos como en los muros construidos en el laboratorio. Las líneas horizontales o verticales asociadas los distintos puntos indican las desviaciones estándar obtenidas.

La correlación (figura 4) se ha extendido a los valores más elevados obtenidos (del orden de 52.7 MPa), a pesar de que el

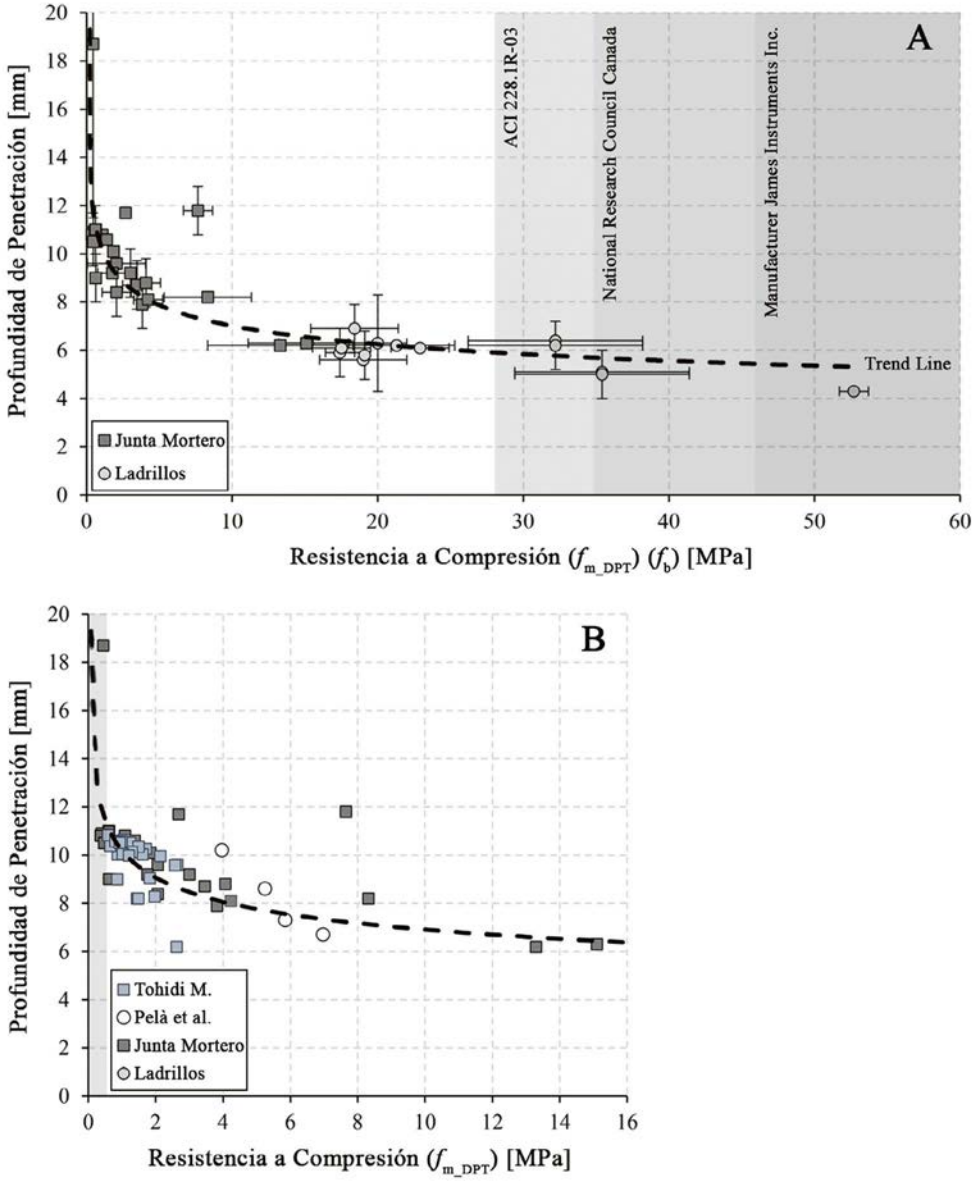

Figura 4 - Correlación empírica entre la resistencia a la compresión y la profundidad de penetración medida con PPT en ladrillos y morteros. (a) Resistencia media experimental, incluyendo barras de desviación y línea de tendencia. Los valores que exceden los límites máximos recomendados se indican mediante sombreado. (b) Gráfico extendido hasta 16 MPa de resistencia DPT, incluyendo datos experimentales adicionales provenientes de la literatura científica disponible [14, 19, 23].

fabricante del dispositivo de ensayo recomienda no utilizarlo para materiales con una resistencia superior a 46.1 MPa. Estos valores también exceden el rango máximo de aplicación sugerido por el Consejo Nacional de Investigación de Canadá [21] (con valor límite entre 30 y 40 MPa) y por ACI 228.1R-03 [22] (que establece un límite de 28 MPa). El área que excede estos umbrales se indica en el gráfico mediante un sombreado. Es preciso notar asimismo que de la calibración se ha excluido un valor atípico que presentaba una posición divergente con respecto a los demás valores experimentales.

La correlación puede ajustarse mediante la ecuación (1), resultando un coeficiente de correlación de 0.82, que es mucho mayor que los que se obtendrían si se adoptaran dos curvas de ajuste separadas para mortero y ladrillo (que serían de 0.62 y 0.42 respectivamente). En la ecuación (1), f_c representa la resistencia a la compresión del ladrillo o la resistencia DPT del mortero (en MPa), y d indica la profundidad de penetración en milímetros.

$$f_c = \left(\frac{10.2}{d}\right)^{1/0.17} \quad (1)$$

La figura 4 también muestra que la profundidad de penetración tiende a aumentar bruscamente para valores muy bajos de resistencia a la compresión. Esta tendencia dificulta la medición de valores de resistencia muy bajos con suficiente resolución. Además, para altas resistencias a la compresión, variaciones muy pequeñas en la penetración dan lugar a variaciones elevadas del valor de resistencia estimado. La presente investigación sugiere que, para garantizar su fiabilidad, el método solo

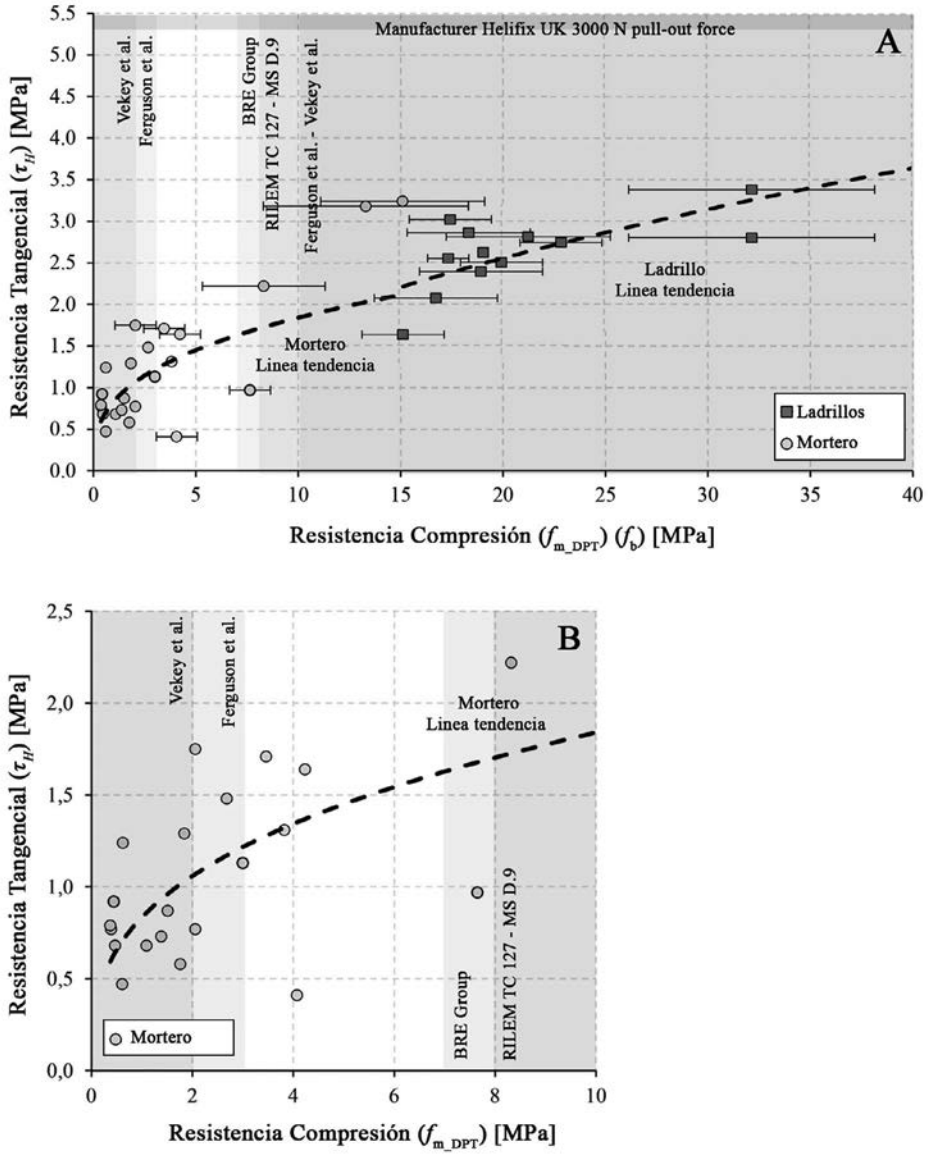

Figura 5. (a) Correlación empírica entre la resistencia a compresión y la resistencia tangente, tanto para ladrillo como para mortero, derivada del presente programa experimental. (b) Extensión de la correlación hasta resistencia de 10 MPa. El gráfico incluye datos experimentales adicionales extraídos de la literatura científica disponible [14, 19, 26, 27, 28, 30].

debería emplearse, en principio, para penetraciones situadas en el rango de 6.0 mm a 11.5 mm, que corresponden, utilizando la ecuación (1), a resistencias a la compresión comprendidas entre 0.5 MPa y 22.7 MPa, respectivamente.

6. ENSAYO DE EXTRACCIÓN DE TORNILLO HELICOIDAL (HPT)

6.1. Descripción de la técnica de ensayo

El ensayo de extracción de tornillo helicoidal (HPT) es un método moderadamente no destructivo desarrollado para la caracterización in situ de mortero de baja resistencia según las recomendaciones de RILEM TC 127-MS D.9 [24]. Helifix Company UK produce las herramientas necesarias y las hélices utilizadas con el nombre ResiTie®.

El ensayo requiere, en primer lugar, formar un orificio piloto de pequeño diámetro en las juntas de mortero o en los ladrillos ensayados. Para crear orificios piloto en los ladrillos, se utiliza un taladro de martillo rotatorio equipado con una broca para obra de fábrica. En ambos casos, el orificio perforado tiene una profundidad de 35 mm. Basándose en investigaciones previas sobre morteros de baja resistencia [16, 23, 25], los autores consideran preferible ejecutar un orificio piloto de 3 mm de diámetro en contraste con el diámetro de 4 o 4.5 mm recomendado por Vekey y Ferguson [24, 26, 27]. Por otra parte, se prefiere un orificio piloto de 4 mm de diámetro para los ladrillos, en contraste con los 5 mm especificados por Ferguson et al. [28].

Tras la formación del orificio piloto, se introduce en él un tornillo helicoidal de acero inoxidable de 1/4 pulgada (6.3

mm) de diámetro mediante una herramienta auxiliar. La herramienta se martillea cuidadosamente mientras se mantiene en posición horizontal, lo que provoca que el tornillo helicoidal se inserte en el orificio piloto girando y enroscándose en el material. El proceso continúa hasta que la penetración alcanza una profundidad de 30 mm. Tras de la inserción, el tornillo se extrae mediante una llave de prueba de carga (LTK). La llave coarta la rotación del tornillo durante la extracción, causando el fallo por corte del material ensayado. La carga máxima alcanzada durante el ensayo proporciona la fuerza de extracción. Se utiliza un manómetro integrado en la herramienta para leer la carga de extracción con precisión de lectura de 100 N. Tal y como sugiere Ferguson [26], y tal y como han confirmado BRE [29] y RILEM TC 127-MS D.9 [24], es preciso ejecutar al menos 10 pruebas HPT para ensayar un mismo mortero, siendo este número suficiente para distinguir entre diferentes morteros.

6.2. Estimación de la resistencia a compresión

Para relacionar la resistencia a compresión del material con la fuerza de extracción medida con HPT, Vekey et al. [27] han propuesto una correlación empírica. Debe notarse que, como indica RILEM TC 127-MS D.9 [24] y como también han observado Vekey et al. [30], la correlación entre la fuerza de extracción y la resistencia no es lineal.

Basándose en una interpretación mecánica, Benedetti et al. [25] han propuesto una ecuación para relacionar la resistencia a las tensiones tangenciales (τ_H) causadas en la extracción con la fuerza aplicada (F). Tal relación (ecuación 2) depende de la longitud de empotramiento (L) y el diámetro externo (D_e) de la hélice.

$$\tau_H = \frac{F}{\pi \cdot D_e \cdot L} \tag{2}$$

Existe un número muy limitado de investigaciones previas sobre la aplicación de HPT en muestras de ladrillos y morteros [16, 23, 27, 28, 29, 30]. Los ensayos obtenidos en la presente investigación han permitido obtener una correlación empírica entre la resistencia a la tensión tangencial y la resistencia a compresión de estos materiales (figura 5). Para la determinación de esta correlación también se han tenido en cuenta los resultados experimentales publicados por Vekey [30], Ferguson et al. [28], Ferguson [26], Vekey et al. [27] y Pelà et al. [16, 23]. La figura 5 presenta la relación obtenida entre la resistencia a la compresión media y la resistencia tangencial para muestras ensayadas ya sea dentro de la misma sección de muro (en el caso de edificios existentes) o en especímenes de laboratorio. Los valores se presentan en el gráfico como un punto, que denota el valor medio, junto con una línea que indica la desviación estándar.

En la literatura científica se proponen diferentes rangos óptimos de resistencia a compresión para la aplicación fiable de HPT. Ferguson et al. [28, 29] indican un rango de resistencia de 2 MPa a 10 MPa; Vekey et al. [27] especifican un rango de 3 MPa a 10 MPa; BRE [29] especifica una resistencia máxima de 7 MPa; a su vez, RILEM TC 127-MS D.9 [24] recomienda un valor máximo de 8 MPa. Las áreas que superan los umbrales recomendados se indican en la figura 5 mediante sombreado.

La figura 5 muestra asimismo las líneas de tendencia de potencia que relacionan la resistencia y la resistencia tangencial. De forma similar a lo que se ha comentado para PPT, se propone una curva de ajuste unificada para mortero y ladrillo. La función de ajuste (ecuación 3) presenta un coeficiente de correlación de 0.78. En esta ecuación, fc indica la resistencia a la compresión del ladrillo o mortero (obtenida en este último caso mediante DPT) y τ_H designa la resistencia tangencial, obtenida mediante la ecuación (2). La figura 5b proporciona una extensión de la correlación para valores superiores de hasta 10 MPa.

$$f_c = \left(\frac{\tau_H}{0.83}\right)^{1/0.37} \tag{3}$$

La mayoría de los datos se ajustan aceptablemente a la línea de tendencia de la Ecuación (3), excepto aquellos relacionados con los bloques de AAC de Ferguson et al. [28] y con los valores de mortero de Ferguson [26] y Vekey et al. [27]. Estos resultados sugieren que, además de la resistencia a la compresión, es posible que otras propiedades del mortero o del ladrillo influyan en las fuerzas de extracción medidas experimentalmente.

7. ESCLERÓMETRO (REBOUND HAMMER, RH)

7.1. Descripción del método

El esclerómetro es una técnica de ampliamente utilizada para estimar la resistencia a la compresión y la dureza superficial del hormigón. Los protocolos estándar se especifican en las normas ASTM C805/C805M [31], EN 12504-2 [32], EN 13791 [33] e ISO 1920-7 [34]. Para el presente estudio se ha empleado dispositivo Silver Schmidt OS8200® tipo N, fabricado por Screening Eagle Technologies. Este dispositivo funciona mediante una masa accionada por resorte que se desplaza a lo largo de una guía y golpea un émbolo de acero, el cual resulta comprimido contra la superficie ensayada. Tras el impacto, se crea una onda de compresión que se propaga a través del émbolo, cuya reflexión provoca el rebote de la masa, de forma que la energía absorbida durante el impacto produce una deformación local de la superficie. El índice de rebote, conocido como valor Q y a menudo denominado coeficiente de restitución, se determina calculando la raíz cuadrada de la relación entre las energías cinéticas previa y posterior al impacto. La energía absorbida por el material durante el impacto puede correlacionarse con sus propiedades de amortiguamiento, que a su vez pueden considerarse relacionadas con la resistencia a la compresión del material.

La posible aplicación del RH a ladrillos cerámicos requiere ciertas precauciones. En el caso de los ladrillos es preciso seleccionar cuidadosamente los puntos de impacto de forma que exista suficiente espesor entre éstos y las superficies del ladrillo. Las normas estipulan unas distancias mínimas a los bordes (25 mm según la norma EN 12504-2) [32] y 50 mm según ASTM C805/C805M [31] e ISO 1920-7 [34]) que no siempre son factible en ladrillos debido sus restricciones dimensionales. La

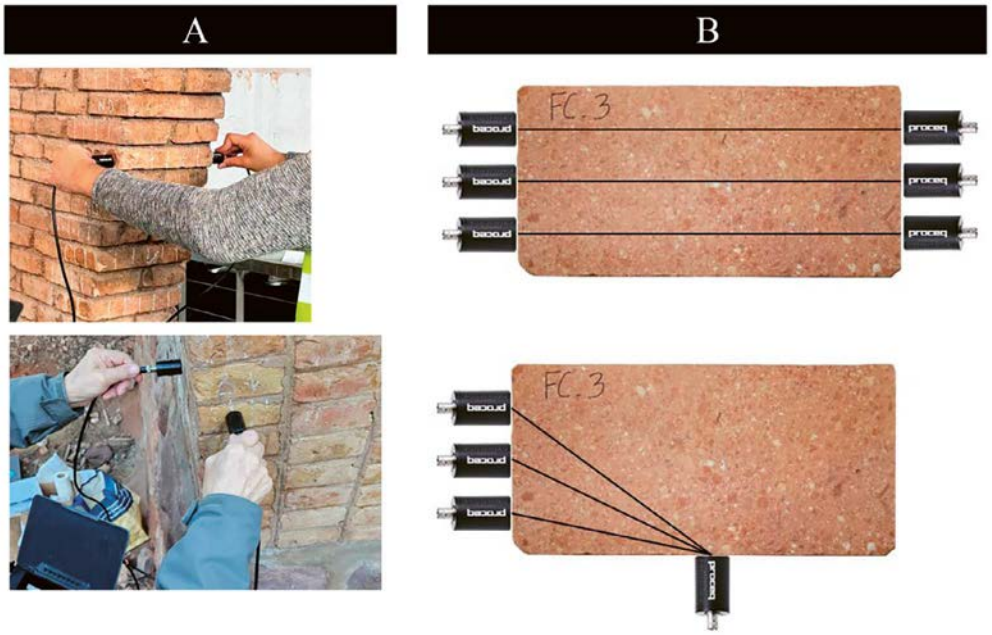

Figura 6. Procedimiento de prueba directa de UPV a través de la longitud para el caso de estudio A (a) y procedimiento de prueba semidirecta de UPV para los casos de estudio B y C del grupo 2 (b).

metodología de ensayo que se propone consiste, en primer lugar, en subdividir el canto de cada ladrillo en seis secciones iguales, mientras que la testa puede dividirse en cinco secciones. Con ello se busca mantener una separación mínima de 25 mm entre los puntos de impacto, según lo recomendado por las normas. Para minimizar la influencia de las irregularidades de la superficie en los resultados, éstas se pulen mediante una piedra de amolar suministrada por el fabricante.

Antes de la prueba, los puntos de impacto se marcan sistemáticamente en cada superficie preparada. Posteriormente, el dispositivo Schmidt se posiciona por estimación visual y se mantiene firmemente en una orientación perpendicular con respecto a la superficie. Luego, el émbolo del instrumento se presiona gradualmente contra la superficie asegurando su perpendicularidad. Si el impacto produce un aplastamiento localizado o se produce cerca de un vacío superficial, la medición se considera inválida y se excluye de análisis posteriores. Los resultados finales del ensayo se obtienen calculando la mediana de los valores Q según lo prescrito por la norma EN 12504-2 [32].

7.2. Estimación de la resistencia a compresión

La ecuación (4), proporcionada por el fabricante del dispositivo y correspondiente a la curva del percentil 10º inferior ha sido deducida a partir de datos exhaustivos recopilados a través de diversas investigaciones. El fabricante indica que el dispositivo es capaz de ensayar muestras de hormigón con resistencias a la compresión situadas entre 10 MPa y 100 MPa, correspondientes a valores Q de 22 a 75. Además, la norma EN 13791 [33] proporciona una tabla de referencia que correlaciona la resistencia a la compresión del hormigón con el número de rebote Q en el percentil 10º.

$$f_c = 2.77 \cdot e^{0.048Q} \quad (4)$$

8. ULTRASONIDOS (VELOCIDAD DEL PULSO ULTRASÓNICO, UPV)

El ensayo de velocidad de pulso ultrasónico (UPV) es un método no destructivo comúnmente empleado para evaluar la velocidad de propagación de pulsos de ondas de tensión longitudinales a través del hormigón. El UPV también ha sido aplicado recientemente en los materiales componentes de la obra de fábrica [36, 37]. Los procedimientos estandarizados para los ensayos de UPV se describen en las normas ASTM C597 [39] y EN 12504-4 [38].

Para el presente estudio se ha utilizado el dispositivo Ultrasonic Pundit 200®, fabricado por Proceq Technologies. Este instrumento genera y detecta pulsos ultrasónicos a través de un par de transductores electroacústicos, los cuales comprenden un generador de pulsos y un amplificador receptor. Los transductores utilizados en esta investigación operan a una frecuencia de 250 kHz, la cual corresponde a una longitud de onda de 14.8 mm, que puede considerarse adecuada para materiales con un tamaño máximo de grano de 7 mm. Se garantiza así que la longitud de onda sea menor que el espesor mínimo de la muestra y mayor que el tamaño del grano promedio, cumpliendo así los requisitos fundamentales para una prueba ultrasónica fiable. La prueba UPV mide el tiempo que tarda un pulso ultrasónico en atravesar el material. La velocidad del pulso se calcula dividiendo la longitud del recorrido entre los transductores por el tiempo de recorrido registrado. El adecuado contacto entre los transductores y la superficie del ladrillo requiere la aplicación de un agente de acoplamiento y de una presión firme para minimizar las cavidades superficiales y mejorar la transmisión de la señal. En la presente investigación, todas las pruebas se realizaron siguiendo las recomendaciones de la norma EN 12504-4 [38], la cual recomienda realizar un mínimo de tres mediciones por ladrillo.

En la ejecución de las pruebas puede adoptarse una configuración de transmisión directa, colocando los transductores directamente enfrentados (caso analizado A del grupo 2) o bien de transmisión semidirecta, con un transductor colocado en el canto del ladrillo y el otro en la testa adyacente (casos B y C del grupo 2). La figura 6 describe el procedimiento. En la presente investigación, las pruebas UPV se realizaron en seis ladrillos diferentes para cada conjunto de posiciones. En el caso A, se tomaron mediciones en tres puntos distribuidos uniformemente a lo largo de cada ladrillo (figura 6a). Para los casos B y C, las pruebas se realizaron en cuatro puntos distribuidos en superficies adyacentes, combinando un punto de medición en el canto con tres puntos en la testa, lo que resulta en tres mediciones combinadas por ladrillo (figura 6b).

A pesar de disponer de una propuesta de correlación, la experiencia de los autores muestra que el UPV resulta poco fiable cuando se utiliza de forma exclusiva para la medida de la resistencia a compresión de los ladrillos cerámicos. Ello puede explicarse debido a la heterogeneidad de estos materiales. Por ello, en la presente investigación, el pulso ultrasónico sólo se ha utilizado en el contexto del método SonReb, combinando sus medidas con las de los ultrasonidos.

9. ENSAYO SONREB EN LADRILLOS

9.1. Descripción de la técnica

El método SonReb es una técnica de ensayos no destructivos que combina los ensayos de velocidad de pulso ultrasónico (Ultrasound Pulse Velocity, UPV) y de esclerómetro (Rebound Hammer, RH) con la finalidad de medir la resistencia a compresión del hormigón. Al integrar los resultados de ambos métodos, el ensayo SonReb mejora la fiabilidad de las estimaciones de resistencia, ofreciendo una mayor precisión en comparación con cada ensayo individual. La técnica SonReb ha quedado formalizada en las directrices del Comité RILEM TC 43 CND (1993) [40] para la determinación in situ de la resistencia del hormigón. Estas directrices establecen una correlación general entre la resistencia a la compresión del hormigón, los valores de RH y las mediciones de UPV. Esta relación empírica ayuda a mitigar las incertidumbres introducidas por cada técnica y es especialmente útil cuando no es posible obtener muestras de material en las que ejecutar ensayos destructivos de laboratorio.

9.2. Estimación de la resistencia a compresión

Para obtener una precisión satisfactoria en las predicciones de resistencia es necesario aplicar técnicas específicas de análisis matemático. En este sentido, han sido propuestos diversos métodos. Los modelos comúnmente utilizados incluyen formulaciones tanto lineales (ecuación 5) como no lineales (ecuación 6). En estas ecuaciones, $f_{c,}$est representa la resistencia a la compresión estimada, RH se refiere al valor Q del martillo de rebote, UPV representa la velocidad del pulso ultrasónico en m/s, y a, b y c son constantes.

$$f_{c,est} = a+b\cdot RH+c\cdot UPV \quad (5)$$

$$f_{c,est} = a\cdot RH^{b}\cdot UPV^{c} \quad (6)$$

Es preciso notar que, si bien el método SonReb se ha aplicado y verificado ampliamente para el hormigón, no existen investigaciones previas que hayan evaluado su uso en obra de fábrica y, particularmente, en ladrillos cerámicos. En este sentido, la investigación que se presenta en este artículo constituye una primera exploración de su aplicación a este material.

A partir de estudios experimentales previamente realizados por los autores (Cabané et al. [41]), se propone una correlación lineal (ecuación 7) para estimar la resistencia a compresión de ladrillos cerámicos. Los experimentos previamente realizados han mostrado que esta ecuación proporciona una aproximación fiable para la caracterización mecánica in situ de este tipo de ladrillos. Los coeficientes de la ecuación (7) han sido determinados mediante análisis de regresión en base a los resultados experimentales obtenidos por los autores previa eliminación de algunos valores considerados anómalos [41].

$$f_{c,est} = a+b\cdot RH+c\cdot UPV=-55+0.68\cdot RH+0.02\cdot UPV \quad (7)$$

A efectos de aplicar el método SonReb, la tabla 1 resume las medianas de los valores Q medidos con la prueba de HR y el UPV en ladrillos. Todos los valores se presentan con su correspondiente coeficiente de variación entre paréntesis. Dada la posible anisotropía de los ladrillos, y según el estudio de Cabané et al. [42], las técnicas han sido siempre aplicadas a lo largo de una única dimensión de ladrillo, correspondiente a su longitud (soga). Las mediciones de HR en los ladrillos se tomaron en el canto o en la testa y las mediciones de UPV se realizaron a lo largo (soga) del ladrillo mediante un procedimiento directo o semidirecto. No se pudieron obtener mediciones de UPV en una cierta zona (designada como zona A.2) del Caso A.

TABLA 1
Resumen de los valores de resistencia a la compresión de ladrillo estimados mediante el método SonReb y mediante ensayos destructivos a compresión según EN 772-1 [13].

Caso	*Resistencia a compression [MPa]*		*Diferencia*
	SonReb $f_{c,est}$	*EN 772-1 [13]* f_b	
A.1	24.3	28.1	14%
A.2	24.0	27.7	13%
A.3	33.5	38.6	13%
B	22.7	26.3	14%
C	29.1	33.6	13%

La tabla 1 presenta los valores de resistencia a la compresión medida mediante SonReb, determinada con la ecuación (7), y medida mediante ensayo a compresión en laboratorio sobre probetas cúbicas de 40 × 40 × 40 mm³. En este último caso se proporcionan valores normalizados. El valor de resistencia a la compresión normalizada, f_b se ha derivado aplicando dos factores de forma: un factor inicial de 1.65 para correlacionar la

probeta de 40 × 40 × 40 mm³ con la muestra estandarizada de 100 × 100 × 40 mm³ (de acuerdo con EN 772-1 [13]), y un segundo factor de 0.7 (también según [13]), para obtener la resistencia a la compresión normalizada, f_b. En ausencia de datos obtenidos con UPV, la resistencia a la compresión estimada de los ladrillos en el caso A.2 se ha determinado utilizando la ecuación (4) con los resultados de la prueba RH. Tal y como muestra la tabla 1, el método SonReb ha funcionado correctamente y ha permitido obtener estimaciones satisfactorias de la resistencia a compresión. Tales estimaciones aproximan correctamente los valores medidos mediante el ensayo destructivo a compresión. Con todo, se observa un error de estimación sistemático del orden del 14%, lo cual puede atribuirse al carácter impreciso de los factores de forma utilizados en la conversión de la resistencia. Ello sugiere la posibilidad de mejorar la estimación de la resistencia normalizada multiplicando la resistencia medida mediante SonReb por un factor del orden de 1.35, lo cual reduciría el error a un 1%, Con todo, esta modificación no dispone por el momento de la suficiente generalidad, por lo que su adopción requiere investigaciones adicionales extendidas a más casos de estudio y a otros tipos de ladrillos.

10. CONCLUSIONES

Se han presentado un conjunto de técnicas de carácter no destructivo o moderadamente destructivo para la estimación de la resistencia a compresión de los materiales componentes de la obra de fábrica. El estudio se ha centrado en la medida de la resistencia en obra fábrica de ladrillo cerámico macizo recibida con mortero de cal o de cemento Portland, prestando especial atención al caso de las fábricas históricas. Las técnicas investigadas han sido el ensayo penetrométrico (PPT), el ensayo de extracción de tornillo helicoidal (HPT), el esclerómetro (Rebound Hammer, RH), el ensayo velocidad del pulso ultrasónico UPV) y la técnica SonReb, basada en la combinación de estos dos últimos ensayos. A pesar de su carácter más destructivo, pues exige extraer muestras de mortero de juntas, también se ha prestado atención al ensayo de doble émbolo (Double Punch Test, DPT), el cual es de gran utilidad para el estudio de fábricas existentes.

Se constata que hasta el momento se ha prestado una atención muy escasa a la aplicación de las técnicas mencionadas a los componentes de la obra de fábrica (ladrillo y mortero), habiendose dedicado casi todo el esfuerzo investigador previo al hormigón. Con todo, y aunque el hormigón presenta características muy disímiles de las del mortero en juntas y los ladrillos, la experiencia previa en este material resulta muy valiosa y permite extraer aspectos metodológicos y formulísticos de alto interés para su posible aplicación a estos materiales. Con todo, la investigación realizada ha permitido derivar protocolos y técnicas, orientados a optimizar y garantizar tanto la ejecución de los ensayos como su postproceso, específicamente aplicables a los componentes de la obra de fábrica.

En el caso de los ensayos PPT y HPT ha sido posible obtener correlaciones empíricas satisfactoriamente significativas para correlacionar los parámetros físicos medidos (profundidad de penetración y fuerza de extracción respectivamente) con la resistencia a compresión de los componentes. En ambos casos ha sido posible obtener una correlación unificada para ladrillo y mortero. Ha sido posible asimismo establecer un rango de uso óptimo, excluyendo rangos de valores de resistencia a compresión excesivamente bajos o altos para los cuales los ensayos pierden fiabilidad o resolución.

Finalmente, se ha comprobado que la técnica SonReb, basada en la combinación de medidas con esclerómetro (RH) y ultrasonidos (UPV) y hasta el momento solo utilizada en hormigón, puede ser asimismo aplicada con éxito para la medida de la resistencia a la compresión de ladrillos macizos cerámicos. Tal aplicación exige considear algunas precauciones metodológicas, así como una reformulación de las correlaciones normalmente empleadas para el hormigón.

Entre las distintas técnicas investigadas, el método SonReb es la que se vislumbra como más fiable para estimar la resistencia compresion de ladrillos. Con todo, se consdiera que la mejor aproximación, y la que ofrece mayor fiabilidad, es la que consiste en combinar distintas técnicias con la finalidad de obtener información redundante y corroborar resultados.

Las técnicas y expresiones matemáticas propuestas han sido calibradas en base a una variedad amplia de casos de estudio caracterizados por rangos extensos de valores de resistencia de mortero y de ladrillo, por lo que en principio se consideran adecuadamente validadas. Con todo, su extensión a otros entornos geográficos (caracterizados por el uso de materiales y/o técnicas constructivas muy distintas) podría requerir una mayor validación extendida a un número mayor de casos de estudio. Por otra parte, no puede descartarse que los factores climáticos (como temperatura y humedad) puedan tener alguna influencia sobre las medidas experimentales, aspecto que debería ser específicamente estudiado.

Agradecimientos

Los autores agradecen la financiación obtenida del Ministerio de Ciencia e Innovación del Gobiero Español, de la Agencia Española de Investigación y de los Fondos Europeos de Desarrollo Regional (ERDF) a través del proyecto PONT3 *Anticipating failure propagation of ageing bridges through a cost-effective interdisciplinary approach*, con número de referencia PID2021-124236OB-C32. Luca Pelà agradece el apoyo recibido del programa de investigación AGAUR - ICREA Acadèmia del Departamento de Investigación y Universidades de la Generalitat de Cataluña.

Los autores han escrito este artículo como un sentido homenaje a los profesores Antonio Marí y Hugo Corres, a quienes consideran maestros de varias generaciones de estudiantes, profesionales e investigadores de la ciencia del hormigón estructural. El tercer autor desea expresar su gran gratitud hacia Antonio Marí por el apoyo recibido a lo largo de su carrera universitaria y por el gran ejemplo que para él ha significado como científico, como maestro y como persona de profunda humanidad.

Referencias

[1] ISCARSAH/ICOMOS, Guidelines for the analysis, conservation and structural restoration of architectural heritage (2024).

[2] CEN European Committee for Standardization (2013), EN 1996-1-1:2011+A1:2013 Eurocode 6 - Design of masonry structures - Part 1-1: General rules for reinforced and unrein-forced masonry structures.

[3] Código Técnico de la Edifiacación. Documento Básico SE-F. Seguridad Estructural.Ministerio de Fomento, Direccion General de Arquitectura, Vivienda y Suelo, 2019.

[4] J. Segura, L., Pelà, P. Roca, A. Cabané, Experimental analysis of the size effect on the compressive behaviour of cylindrical samples core-drilled from existing buildings, Construction and Building Materials, (2019), 228, 116759. https://doi.org/10.1016/j.conbuildmat.2019.116759.

[5] D. Marastoni, L. Pelà, A. Benedetti, P. Roca, Combining brazilian tests on masonry cores and double punch test for the mechanical characterization of historical mortars, Construction and Building Materials, (2016), 112, pp. 112-127. https://doi.org/10.1016/j.conbuildmat.2016.02.168.

[6] L. Garcia-Ramonda, L. Pelà, P. Roca, G. Camata, Experimental cyclic behaviour of shear masonry walls reinforced with single and double layered Steel Reinforced Grout, Constr. Build. Mater. 320 (2022) 1–36. https://doi.org/10.1016/j.conbuildmat.2021.126053.

[7] D. Huang, A. Albareda, O. Pons, Experimental and Numerical Study on Unreinforced Brick Masonry Walls Retrofitted with Sprayed Mortar under Uniaxial Compression, Buildings. 13 (2023). https://doi.org/10.3390/buildings13010122.

[8] European Committee for Standardization (CEN), EN 998-2:2018 Specification for mortar for masonry. Part 2: Masonry mortar, (2018).

[9] J. Segura, D. Aponte, L. Pelà, P. Roca, Influence of recycled limestone filler additions on the mechanical behaviour of commercial premixed hydraulic lime based mortars, Constr. Build. Mater. 238 (2020). https://doi.org/10.1016/j.conbuildmat.2019.117722.

[10] European Committee for Standardization (CEN), EN 1015-11:2020 Methods of test for mortar for masonry - Part 11: Determination of flexural and compressive strength of hardened mortar, (2020).

[11] A. Cabané, L. Pelà, P. Roca, Laboratory and in-situ mechanical characterization of masonry components by comparing destructive and minor destructive testing techniques, Construction and Building Materials, (2024), 41, 134473. https://doi.org/10.1016/j.conbuildmat.2023.134474.

[12] A. Cabané, L.Pelà, P. Roca, Experimental mechanical characterization of masonry in existing buildings using NDT and MDT techniques. Proceedings of the 14th International Conference on Structural Analysis of Historical Constructions, 2025.

[13] European Committee for Standardization (CEN), EN 772-1:2011+A1:2016 Methods of test for Masonry Units - Part 1: Determination of Compressive Strength, (2016).

[14] Deutsche Norm, DIN 18555-9:2019-04 Testing of mortar containing mineral binders - Part 9: Determining the compressive strength of hardened mortar, (2019).

[15] Railway Technical Publications (UIC), Leaflet 778-3R: Recommendations for the inspection, assessment and maintenance of masonry arch bridges, (1995).

[16] L. Pelà, P. Roca, A. Aprile, Combined In-Situ and Laboratory Minor Destructive Testing of Historical Mortars, Int. J. Archit. Herit. 12 (2018) 334–349. https://doi.org/10.1080/15583058.2017.1323247.

[17] L. Pelà, A. Benedetti, D. Marastoni, Interpretation of experimental test on small specimens of historical mortars, in: Jerzy Jasieńko (ed) (Ed.), Struct. Anal. Hist. Constr., Wroclaw, Poland, 2012.

[18] P. Matysek, S. Seręga, S. Kańka, Determination of the Mortar Strength Using Double Punch Testing, Procedia Eng. 193 (2017) 104–111. https://doi.org/10.1016/j.proeng.2017.06.192.

[19] American Society for Testing and Materials (ASTM), ASTM C803/C803M-18 Standard Test Method for Penetration Resistance of Hardened Concrete, (2018). https://doi.org/10.1520/C0803_C0803M-18.

[20] Standard British (BSI), BS 1881-207:1992 Testing concrete. Recommendations for the assessment of concrete strength by near-to-surface tests, (1992).

[21] National Research Council Canada, Review of Non-Destructuve Test Methods for Assessing Strength, Serviceability and Deterioration in Buildings, (1993).

[22] ACI 228.1R-03, In-Place Methods to Estimate Concrete Strength Reported, ACI Comm. Reports. (2003) 44.

[23] L. Pelà, P. Roca, A. Aprile, Comparison of MDT techniques for mechanical characterization of historical masonry, Struct. Anal. Hist. Constr. Anamn. Diagnosis, Ther. Control. - Proc. 10th Int. Conf. Struct. Anal. Hist. Constr. SAHC 2016. (2016) 769–775. https://doi.org/10.1201/9781315616995-104.

[24] R.C. de Vekey, RILEM TC 127-MS: Test for masonry materials and structures. MS-D.9 determination of mortar strength by the screw (helix) pull-out method, Mater. Struct. 30 (1997) 325–327. https://doi.org/10.1007/BF02480682.

[25] A. Benedetti, M. Tarozzi, Interpretation formulas for in situ characterization of mortar strength, Constr. Build. Mater. 242 (2020) 118093. https://doi.org/10.1016/j.conbuildmat.2020.118093.

[26] W.A. Ferguson, Further Data on the Screw Pull-out Test for the In-situ Measurement of the Strength of Some Masonry Materials, Mason. Int. 9 (1995) 25–30.

[27] R.C. de Vekey, M. Sassu, Comparison of non-destructive in-situ mechanical test on masonry mortars: The PNT-G method and the helix method, in: Proc. 11th Int. Brick Block Mason. Conf., Tongji University, Shanghai, China, 1997: pp. 376–384. http://www.hms.civil.uminho.pt/ibmac/1997/376.pdf.

[28] W.A. Ferguson, J. Skandamoorthy, The screw pull-out test for the in-situ measurement of the strength of masonry materials, in: Proc. 10th Int. Brick Block Mason. Conf., Calgary, Canada: Masonry Council of Canada, 1994: pp. 1257–66.

[29] BRE Group, Digest421 Measuring the compressive strength of masonry materials: the screw pull-out test, 1997. https://www.brebookshop.com/details.jsp?id=325216.

[30] R.C. de Vekey, In-Situ Tests for Masonry, in: Proc. 9 Th Int. Brick Block Mason. Conf., Berlin, Germany, 1991: pp. 620–627.

[31] ASTM American Society for Testing and Materials (2018), C805/C805M-18 Standard Test Method for Rebound Number of Hardened Concrete. https://doi.org/10.1520/C0805_C0805M-18.

[32] CEN European Committee for Standardization (2022), EN 12504-2 Testing concrete in structures - Part 2: Non-destructive testing. Determination of rebound number.

[33] CEN European Committee for Standardization (2020), EN 13791:2020 Assessment of in-situ compressive strength in structures and precast concrete components.

[34] ISO International Standard (2004), ISO 1920-7 Testing of concrete - Part 7: Non-destructive test on hardened concrete.

[35] Proceq, Screening Eagle (n.d.), The Silver Schmidt Reference Curve.

[36] N. Makoond, L. Pelà, C. Molins (2019), Dynamic elastic properties of brick masonry constituents, Construction and building Materials 199, p. 756-770. https://doi.org/10.1016/j.conbuildmat.2018.12.071.

[37] N. Makoond, A. Cabané, L. Pelà, C. Molins (2020), Relationship between the static and dynamic elastic modulus of brick masonry constituents, Construction and Building Materials 259, p. 120386. https://doi.org/10.1016/j.conbuildmat.2020.120386.

[38] CEN European Committee for Standardization (2022), EN 12504-4:2022 Testing concrete in structures - Part 4: Determination of ultrasonic pulse velocity.

[39] ASTM American Society for Testing and Materials (2022), C597-22 Standard Test Method for Pulse Velocity Through Concrete. https://doi.org/10.1520/C0597-22.

[40] RILEM TC 43CND (1993), Draft recommendation for in situ concrete strength determination by combined non-destructive methods, Mater Struct 26 43–49.

[41] A. Cabané, T. Seneschal, L. Pelà, P. Roca (2025) Non-Destructive Evaluation of Solid Fired Clay Brick Strength Using the SonReb Method, Under review in Construction and Building Materials.

[42] A. Cabané, L. Pelà, P. Roca (2022) Anisotropy and compressive strength evaluation of solid fired clay bricks by testing small specimens, Construction and Building Materials 344 128195. https://doi.org/10.1016/j.conbuildmat.2022.128195.

ACHE

MONOGRAFÍAS

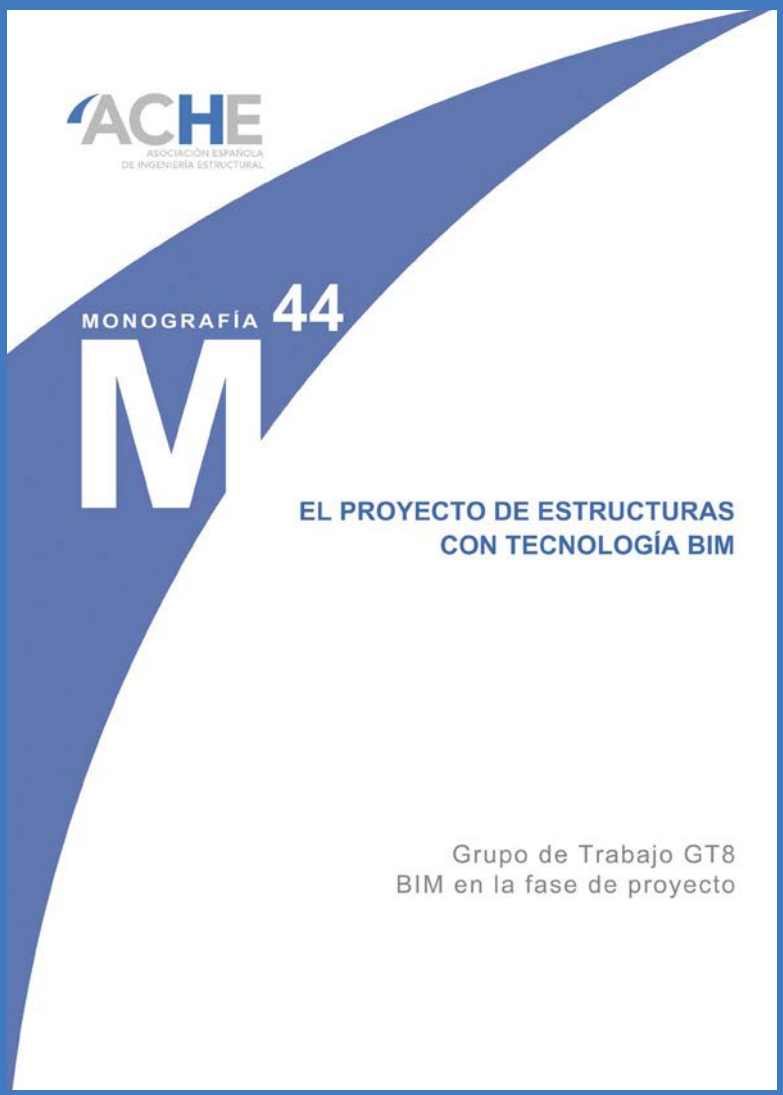

SECRETARÍA DE ACHE
Tel.: 91 336 66 98
www.e-ache.com

Disponible en **www.hormigonyacero.com**
https://doi.org/10.33586/hya.2025.4097

Sustainable Concrete Structures – Design Approaches for Materials and Components

Estructuras de hormigón sostenibles: enfoques de diseño para materiales y componentes

Harald S. Müller[a]

[a] *Prof. Dr.-Ing., SMP Ingenieure im Bauwesen GmbH, Karlsruhe, Germany*

Recibido el 19 de mayo de 2024; revisado el 11 de noviembre de 2024, aceptado el 5 de marzo de 2025

ABSTRACT

Changes in the current use of concrete materials and design approaches are mandatory in order to comply with the requirement for sustainable future concrete structures. On this background, the article indicates the design of sustainable concrete mixes (green concretes or eco-concretes) and the structural components made from them. Such concretes are characterized by a pronouncedly reduced CO_2 footprint compared to conventional structural concretes made with Portland cement clinker. After an introduction to the sustainability problems of today's structural concretes, the basic approaches for the development of sustainable concretes are presented. The specific parameter Concrete Sustainability Potential is introduced, which combines the main effecting parameters such as environmental impact, service life (durability) and performance (strength). An overview of possibilities available today for producing sustainable concrete mixtures is given. For good reasons emphasis is placed on such sustainable concretes, in which a large proportion of the cement is replaced by rock powders. Further, adequate service life design for concretes and concrete components is indicated, as the corresponding calculations play a decisive role in view of sustainable concrete structures. Finally, a new and innovative relationship for sustainability design is introduced. This concept is equally applicable to concrete as a material and to components made from it. The article concludes with considerations on the implementation of this new concept in practice.

KEYWORDS: Sustainable concrete, concrete composition, cement replacement, service life design, sustainability.

RESUMEN

Los cambios en el uso actual de los materiales de hormigón y los enfoques de diseño son obligatorios para cumplir con el requisito de futuras estructuras de hormigón sostenibles. En este contexto, el artículo aborda el diseño de mezclas de hormigón sostenibles (hormigones verdes o eco-hormigones) y los componentes estructurales fabricados con ellas. Tales hormigones se caracterizan por una huella de CO_2 significativamente reducida, en comparación con los hormigones estructurales convencionales fabricados con clínker de cemento Portland.

Tras una introducción a los problemas de sostenibilidad de los hormigones estructurales actuales, se presentan los enfoques básicos para el desarrollo de hormigones sostenibles. Se introduce el parámetro específico Potencial de Sostenibilidad del Hormigón, que combina los principales parámetros que lo afectan, como el impacto medioambiental, la vida útil (durabilidad) y el rendimiento (resistencia). Se ofrece una visión general de las posibilidades disponibles en la actualidad para producir mezclas de hormigón sostenibles. Por razones fundadas, se hace hincapié en este tipo de hormigones sostenibles, en los que una gran proporción del cemento se sustituye por polvo de roca. Además, se señala la importancia del diseño adecuado de la vida útil del hormigón y de sus componentes, ya que los cálculos correspondientes desempeñan un papel decisivo en la sostenibilidad de las estructuras de hormigón.

Por último, se introduce una relación nueva e innovadora para el diseño sostenible. Este concepto es igualmente aplicable al hormigón como material y a los componentes estructurales fabricados con él. El artículo concluye con consideraciones sobre la aplicación de este nuevo concepto en la práctica.

PALABRAS CLAVE: Hormigón sostenible, composición del hormigón, sustitución del cemento, diseño de la vida útil, sostenibilidad.

* Persona de contacto / *Corresponding author*:
Correo-e / *e-mail*: h.mueller@smp-ing.de (Harald Müller)

How to cite this article: Müller, H. (2026). Sustainable Concrete Structures – Design Approaches for Materials and Components. *Hormigón y Acero*. 77(308):145-154. https://doi.org/10.33586/hya.2025.4097

1. PROBLEM STATEMENT

The decisive advantages of concrete - comparatively high strength and durability combined with high availability in huge quantities and cost-effective production anywhere in the world - are up to nowadays not even remotely matched by any other building material. For this reason, concrete became by far the most important building material of the modern industrial age. It has made possible the economic development of the industrial nations over the last 100 years. With an annual production volume of currently approx. 8 billion m³ of concrete, economic development worldwide would not be possible without it.

However, a very unfavourable factor is the high CO_2 emission associated with concrete production which results mainly from the cement manufacturing. It was not until the turn of the millennium when the awareness was raised that the production of cement is one of the most energy-intensive and CO_2-intensive industries in the world, surpassed today only by energy production through the burning of fossils, the transport vector and the steel production. It is estimated that the cement industry is currently responsible for about 7-8 % of the global man-made CO_2 emissions.

These emissions have to be tremendously reduced, as a contribution of the concrete industry, so that the international agreement to limit global warming to a maximum of 1.5 degrees Celsius above pre-industrial level can be reached. This target was set in the Paris Agreement of 2015 to prevent the worst effects of the climate change. It is therefore not surprising that many strategies have been developed, in particularly in the past decade, to significantly reduce the CO_2 footprint associated with concrete construction.

When thinking of a solution to this sustainability problem, a first idea could be to strive for a tremendous reduction of the use of concrete. However, as can be seen from the above, this is absolutely impossible. Such an approach would cause fundamental economic problems for the entire world.

The second idea consisting of completely replacing cement with another binding agent cannot be implemented either. To date, there is no alternative binder that could even come close to the positive properties of Portland cement clinker. And, if one considers the huge quantities of suitable base materials for binder production that have to be available all over the world, this idea is also ruled out from the outset.

The above leaves the third solution consisting of retaining conventional cement production but capturing the CO_2 emissions. The technology of capturing CO_2 is well developed since a couple of years. Currently it is being tested in a few pilot projects in cement production. If this technology proves successful, it will probably last decades before every cement plant in the world has been converted accordingly. Further, it must also be accepted that the price of cement will rise significantly. At present, it is roughly assumed that the price of cement will double.

In view of the alternatives for avoiding CO_2 emissions in concrete production described above, which cannot be implemented for various reasons, the only remaining option for the coming years is to reduce CO_2 emissions by making suitable changes to the composition of cement and concrete. Various strategies can be adopted, which are discussed in this article.

First, as an important tool the Concrete Sustainability Potential is introduced that combines the governing parameters environmental impact, service life (durability) and performance (strength). Further, an overview of the possibilities available today for producing sustainable concrete mixtures having an improved CO_2 footprint is given. Hereby, emphasis is placed on such eco-concretes for which a large proportion of the cement is replaced by rock powders.

As the parameter service life of components and structures plays a decisive role in the context of sustainability associated with the use of concrete, the procedure of an adequate service life design is indicated as well. Finally, a new and innovative relationship for sustainability design is introduced. This concept is equally applicable to concrete as a material and to components made from it.

2. THE SUSTAINABILITY POTENTIAL ASSOCIATED WITH THE USE OF CONCRETE

From the facts indicated in the previous chapter, it becomes evident that at first sight the concrete composition must be fundamentally changed. In particular the content of Portland cement clinker, which is associated with extremely high CO_2 emissions, must be reduced or must be substituted as far as possible by more environmentally friendly binders.

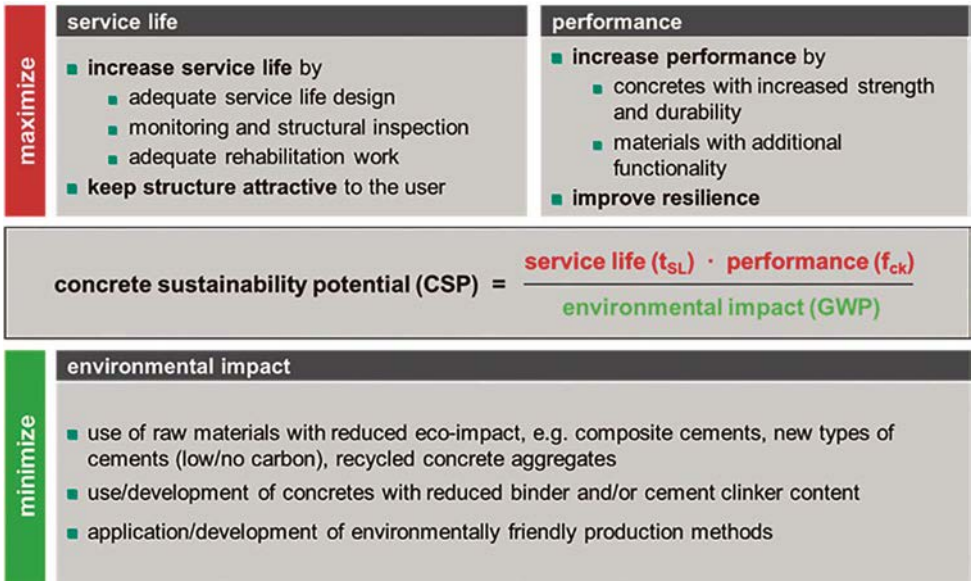

Figure 1. Overview of approaches and tools to develop sustainable concretes.

However, when evaluating the sustainability of concrete, the CO_2 emissions alone cannot be addressed. For example, if one single high CO_2 emission is associated with the production of a high-quality concrete that may withstand all critical exposures for many decades without repair or replacement, then the initial adverse emission has to be evaluated differently. Further high performance and durability are required from the building material itself in the case of structures, which, however, cannot be guaranteed in principle by ecologically optimized concrete. Therefore, the parameters of performance and service life must be considered equally with the environmental impact in a balance sheet related to sustainability. Taking these considerations into account, the Concrete Sustainability Potential (CSP) was introduced as defined by equation (1), see [1, 2]:

$$\text{concrete sustainability potential (CSP)} = \frac{\text{service life } (t_{SL}) \text{ . performance } (f_{ck})}{\text{environmental impact (GWP)}} \quad (1)$$

Herein, f_{ck} is the characteristic strength of the concrete in [MPa] representing the possible performance of the material, t_{SL} is the potential service life of the concrete under the specific environmental actions to be expected in the lifetime of the building member in years [a], and GWP is the environmental impact associated with the production of the concrete including all raw materials expressed by the lead parameter Global Warming Potential (GWP) in eq. kg CO_2; for further details see [2].

Equation (1) represents a simple tool to quantify the advantages and disadvantages of a specific concrete type regarding its potential as a sustainable material. The exploitation of this potential during the design and construction process depends on the designer and user of the building or structure. It should be noted that equation (1) may also be applied to structural components.

According to equation (1), three basic approaches to sustainable use of concrete exist: The first is the optimization of the composition of the concrete regarding its environmental impact while maintaining an equal or better performance and service life; the second is the improvement of the concrete's performance at equal environmental impact and service life; the third is the optimization of the service life of the building material and the building structure at equal environmental impact and performance. A combination of the above-mentioned approaches appears reasonable.

Figure 1 provides an overview of various methods for maximizing the service life and the performance of concrete and concrete structures and for minimizing environmental influences and thus improving sustainability:

- In terms of service life, structural monitoring and structural inspection as well as applying sustainable repair work are particularly suitable methods for increasing the service life of a structure. In this way, the building also retains its attractiveness for the user. The service life assessment at the stage of design is also of great importance. If a structure is only used for a short period of time, for example in industrial construction, a significantly lower quality of concrete is acceptable than for structures which are used over long periods of time, as is the case with structures of great economic importance (tunnels, bridges, dams). Note that currently the higher the quality of concrete the higher the associated CO_2 emissions.
- In terms of concrete performance, higher strength results in lower material consumption for the same load-bearing capacity of components. Further, an increase in durability is advantageous because the service life of the structure is extended and early repair is avoided. Improved overall resilience also leads to lower CO_2 emissions when using concrete.
- There are essentially three different ways to reduce the environmental impact by reducing CO_2 emissions. Firstly, concrete raw materials should be used that have a lower CO_2 footprint from the outset. It is also beneficial to use recycled concrete as aggregate. Furthermore, efforts must be made to use as little Portland cement clinker as possible. Finally, the overall CO_2 emissions can also be reduced by optimizing the production of concrete and its transport.

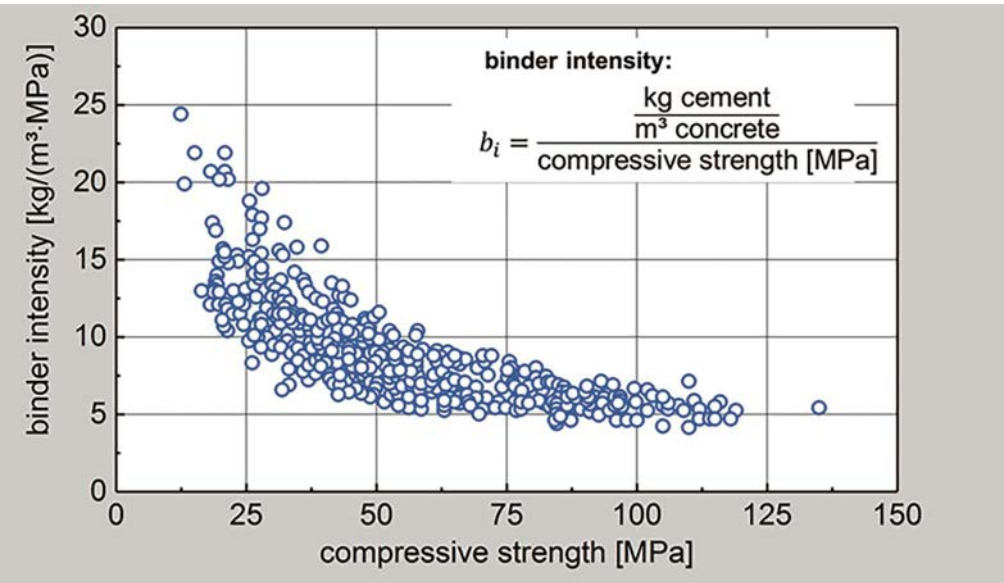

Figure 2. Efficiency of the used amount of binder in typical structural concretes depending on the strength of concrete [3].

Related to the environmental impact, i.e. the use of raw materials with reduced eco-impact, e.g. composite cements, new types of cements (low/no carbon footprint), recycled concrete aggregates and the use/development of concretes with reduced binder and/or cement clinker content, chapter 3 of this paper indicates further details.

As the use of Portland cement is indispensable for producing structural concrete today, the question arises as to what the most efficient way is when applying this binder in view of minimizing the environmental impact. In this context a concrete data evaluation by Damineli et al [3] is very revealing. They have defined a so-called binder intensity, and have plotted this binder intensity over the compressive strength (see Figure 2).

The decreasing binder intensity with increasing compressive strength, as may be depicted in Figure 2, indicates that the use of Portland cement is the more efficient (sustainable) the higher the strength is. This is the more pronounced as for higher strength concrete the cross-section of members may be reduced, i.e. a reduction in mass consumption is achieved at a given load-bearing capacity.

Figure 2 also indicates that for normal and low-s strength concrete the amount of cement used for these concretes is not necessary for the reason of strength, however, it is beneficial for workability and durability reasons. This means that a large amount of cement may be saved, if workability and durability are guaranteed by other measures. This would be very efficient in view of sustainability as roughly 90 % of all concretes used in practice have a compressive strength between 20 and 50 MPa.

From Figure 2 the general conclusion may be drawn that either the reduction of the binder content of ordinary strength concrete or the use of high strength concrete lead to a sustainable use of concrete. The concept of reducing the binder content for ordinary structural concrete while keeping its advantageous technical properties is further analysed in the subsequent chapter 3 of this paper.

3. DESIGN OF SUSTAINABLE CONCRETE MIXES

3.1. Approaches for sustainable mixes

In order to meet the requirements of sustainability concerning concrete as a building material, the currently used concrete compositions must be fundamentally changed. In particular, the Portland cement clinker (PC), which is associated with extremely high CO_2 emissions, must be substituted as far as possible by more environmentally friendly binders, for example, secondary cementitious materials (SCM) and/or new types of hydraulic binders. Further, substitution with inert fines of aggregates is also a very promising approach to significantly reduce the carbon footprint of concrete mixes.

Figure 3 summarizes the different strategies for clinker replacement by subdividing these strategies into four different kinds of approaches. The composition of ordinary structural concrete in volume parts is indicated by the first column (left). Apart from the aggregates which comprise a volume of approx. 70 vol %, the remaining 30 vol % are filled by water, cement (or substitute products), additives and admixtures.

Approach 1 (see Figure 3) shows a pronounced replacement of the cement by SCM additives. The materials blast furnace slag (BFS) and fly ash (FA) being often used today must be viewed critically. BFS is a by-product of steel production. Therefore, its availability is limited and BFS may never replace PC due to the huge amount of PC which is needed worldwide. FA is a waste-product resulting from coal combustion. However, the energy generation from coal combustion is extremely problematic due to the high associated CO_2 emissions. Therefore, this type of energy is coming to an end in a continuously increasing number of countries. This means that FA will become more and more scarce in the concrete industry and will no longer be available at some point

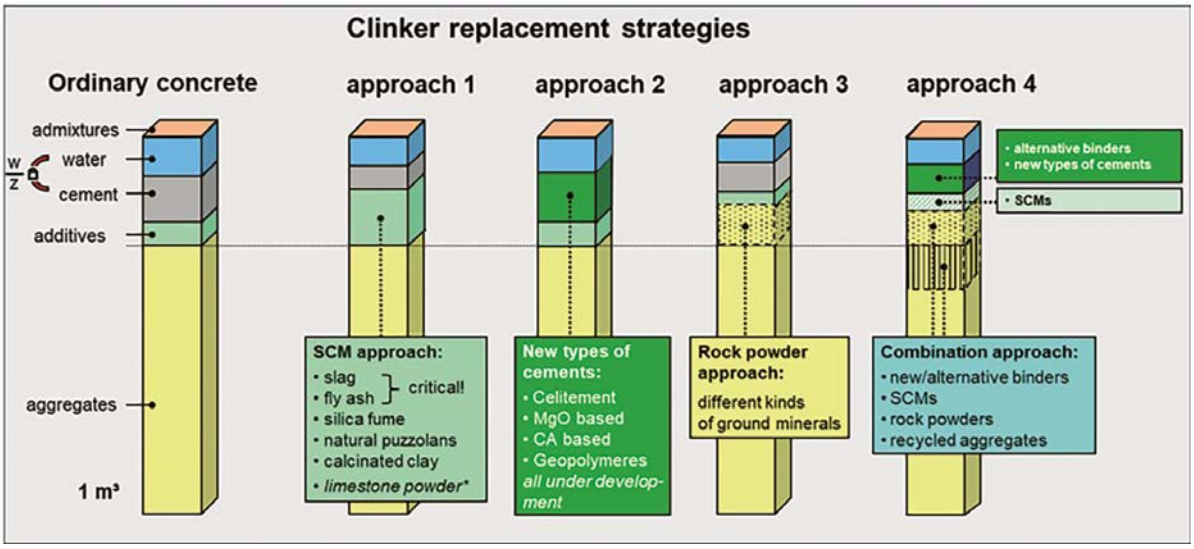

Figure 3.Strategies and examples for the reduction or replacement of Portland cement clinker for the production of structural concrete.

in time. Silica fume (SF) is also a by-product having a very limited availability in the market. The other SCM mentioned in Figure 3 (approach 1) can be expected to increasingly enter the market. However, there is still a considerable need for research in the area of calcinated clays.

Approach 2 (see Figure 3) assumes that Portland cement clinker will be completely replaced by new types of cement/binder. In addition to the product Celitement these are primarily MgO- and CA (= CaAl)-based binders as well as geopolymers. Intensive research is currently being carried out related to these binders. Despite some successes and promising approaches, however, it must also be noted that no binder has yet been developed or is under development which, in terms of its technical properties, is equivalent to the product Portland cement clinker.

Approach 3 (see Figure 3) is characterized by the fact that a large proportion of the cement is replaced by finely ground inert aggregates. The underlying idea is that these aggregates form the necessary fines in the concrete mix to ensure the cohesion and the processing of a concrete mix, and also contribute to the concrete strength, which is, however, mainly provided by the remaining Portland cement clinker. This approach, which dispenses completely with the use of SCM, is further described below.

Approach 4 indicated in Figure 3 is a combination of the approaches 1 to 3 with the additional use of recycled aggregates for concrete production. The amount of recycled aggregates may cover a large part of the total aggregates.

An alternative to these four approaches is the CO_2 avoidance strategy by carbon capture and storage (CCS) or carbon capture and use (CCU) concepts being under development in some countries. These concepts allow the conventional production of PC as the associated CO_2 emissions are captured by applying available technologies. Although this is a promising approach, it must be noted that there are numerous technical, economic and social problems associated with it. It is very unlikely that a sufficiently large volume of PC may be produced by applying these technologies, in particular not until 2050, when the zero CO_2 emission target should be reached in Europe.

Approach 1 is mainly used by the cement industry to significantly reduce the mass proportion of Portland cement clinker in the binder for concrete. As a result, there is a very wide range of more environmentally friendly, standardized binders/cements for concrete on the market today. Approaches 2 and 3 are in the focus of the current research. This research is entering new areas that is not the case with the cement industry approaches, as it has to stay within the framework of established regulations and codes with its modified binders in order to be able to serve the needs of the market.

3.2. Rock powder approach

As already mentioned above, approach 3 was scientifically investigated in more detail by [1, 4]. One of the main reasons for this was the positive result of preliminary investigations, which showed that it is possible in principle to reduce the cement content of concrete from over 300 kg/m³ to values of around 100 kg/m³ if the missing cement quantity is replaced by aggregate powders without losing any of the concrete's essential properties. A further positive aspect is that rock powders are available or may be easily produced in large amounts anywhere in the world.

However, this change in the composition of concrete, i.e. the replacement of cement with rock powders is associated with considerable complications. Elaborated particle packing density model approaches must be used to determine the composition of the fines properly. To ensure sufficient workability – the water content of the concrete must be drastically reduced to prevent the water-cement ratio from increasing too much when the cement content reduces – extensive preliminary tests with various superplasticizers proved necessary. Note that superplasticisers have been chemically designed in order to work with cement particles and not with fine aggregate particles which have different molecular surface properties.

Concrete composition			
component		ord	green
type of cement	-	42,5 R	52,5 R
cement	[kg/m³]	320	113
water		192	87
paste content	[Vol.-%]	29	13
w/c ratio (eff.)	[-]	0,60	0,64
quartz powder 1	[kg/m³]	-	96
quartz powder 2		-	120
sand 0/2		550	955[1)]
gravel 2/8		635	480
gravel 8/16		640	505
plasticizer		-	6,5

[1)] splitted in two fractions 0.1/1 and 1/2 mm

Concrete properties			
parameter		ord	green
compr. strength f_{cm}	[N/mm²]	38,4	76,9
modulus of elast. E_c		33700*	38030
spl. tensile str. $f_{ctm,sp}$		2,9*	2,3
flex. strength $f_{ctm,fl}$		4,4*	4,9
inverse carbonation resistance R_{ACC}^{-1}	[(10⁻¹¹ m²/s) /kg/m³]	13,4	18,9
chloride migration coefficient $D_{RCM,0}$	[10⁻¹¹ m²/s]	2,5	2,0
CDF frost spalling	[g/m²]	< 1500	2760
Global Warming Potential	[equ.kg CO_2 /m³]	285	135

* according to *fib* Model Code 2010

Figure 4. Comparison of ordinary concrete C30/37 ("ord") and green concrete ("green", cement replacement by rock powder) – concrete compositions (left) and concrete properties (right).

Figure 4 summarizes important results of the extensive investigations given in [4]. It shows the composition (left) of a standard structural concrete ("ord") and a green concrete ("green") produced according to approach 3. The right part of Figure 4 shows the concrete properties determined in each case. While the strength parameters and the stiffness of the green concrete are even better compared to ordinary concrete, the lower resistance to carbonation and the insufficient frost resistance in particular are deficits. However, it appears that these disadvantages can also be compensated to a large extent by further developments. On the other hand, such a green concrete could already be used wherever no frost attack is given. Its GWP is reduced to a value of approx. 50 % compared to that of an ordinary concrete (here GWP considers all materials and processes).

A rather particular aspect has to be considered when comparing the compositions and the properties of conventional and green concrete produced by the rock powder approach. While the water-cement ratio increases from 0.60 to 0.64, the compressive strength increases from 38.4 to 76.9 MPa as well (see Figure 4). This is in contrast to Abram's well-established law, which states that with increasing water-cement ratio the compressive strength is decreasing. This means that green rock powder-type concretes behave differently than normal concretes, and that well-established relations for normal concretes are not necessarily valid for these types of green concrete.

3.3. *Problems associated with sustainable concretes*

The positive development of hydraulic binders for concrete with regard to environmental issues due to the increasing substitution of Portland cement clinker is accompanied by a certain disadvantage resulting from the novelty or the lack of experience with these products, respectively. Thus, for classical concrete, whose binder consists essentially of Portland cement clinker and/or granulated blast furnace slag, a very large number of scientific studies are available with regard to a wide variety of material properties, as well as extensive long-term observations and practical experience. These findings have been reflected in material models and design approaches available to the design engineer. Since this is not the case for concretes with new binders, the necessary performance tests to ensure safety and durability are of great importance when building with these new types of concretes.

4. APPLICATION OF SERVICE LIFE DESIGN APPROACHES

4.1. *Basic considerations and overview*

The service life of concrete structures is a decisive parameter with regard to the sustainable use of concrete (see also Eq. 1). The reason for this is that the use of concrete is inevitably associated with critical emissions and the use of natural resources. In other words, the less new concrete is used, the less adverse emissions are produced. It is therefore sustainable if the service life of existing structures is extended and new buildings are not built. On the other hand, social and economic development requires new and needs-oriented concrete structures.

Taking into account the durability of concrete, emissions and the consumption of resources increase significantly when the planned service life of a structure increases. It is therefore crucial to select the concrete composition in such a way that the durability achieved for the concrete corresponds to the intended service life. This applies both to a long service life, as is the case with large infrastructural structures (e.g. tunnels, bridges, dams), and to a planned short service life of a concrete structure, as is often the case for industrial constructions.

As for sustainability reasons the concrete composition must be adapted to the planned service life for a construction, it is not possible to apply the currently valid guidelines

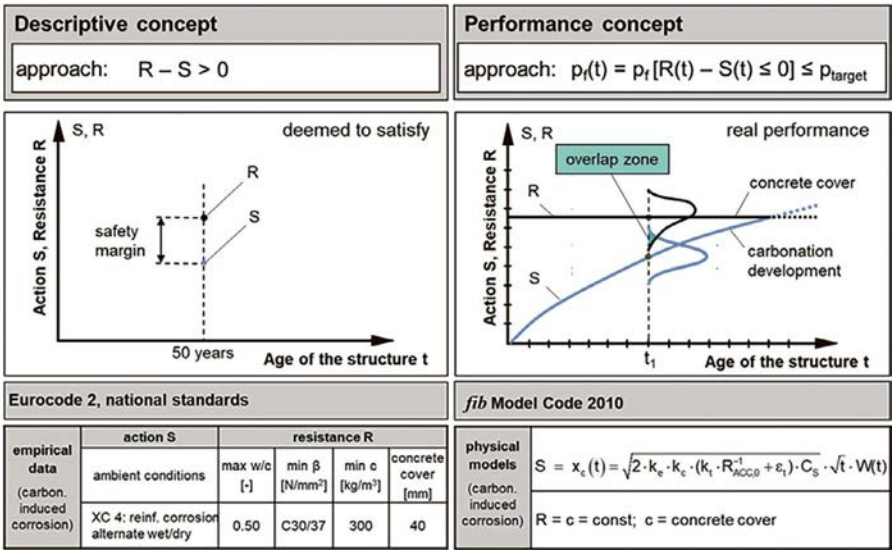

Figure 5. Design for durability for carbonation-induced reinforcement corrosion; left: descriptive approach as used in codes (CEN, national) being not suited for the adaption to the real service life in order to optimize sustainability (the age of 50 years is fixed); right: performance approach which allow to consider any particular service life (the age t is a variable parameter).

[5] because the specifications/requirements are designed for a fixed service life of 50 years. In addition, the information on the effecting/environmental conditions and the material properties/concrete compositions is only given in verbal form and characteristic values in tables, and is not described by mathematical-physical time functions.

The required material laws or degradation models, respectively, which describe the loss of durability, i.e. the decreasing resistance to the environmental loads in mathematical-physical form, depending on age and environmental conditions, are provided in the fib Model Code 2010 or the fib Model Code 2020. They can be used, for example, to specify specific lifetimes/usage periods and to calculate from this information the corresponding requirements for the concrete properties or the concrete composition, respectively.

4.2. Principle and methodology of service life design

In the engineering design for service life, actions (S) and resistances (R) are related to each other in mathematical form, analogous to a static-constructive design. The actions are environmental conditions or exposures that are divided into classes. The resistances are partly structural requirements (e.g. concrete cover), but in particular the material properties. They are described either by concrete technology parameters (e.g. water/cement ratio, cement content) and minimum design requirements or corresponding material parameters (e.g. diffusion coefficient). The consideration of failure probabilities is indispensable. The applied probabilistic methods in combination with the description of the concrete behaviour by means of degradation models enable the solution of complex practical problems.

The two different basic concepts for the design for service life are illustrated in Figure 5 using the example of carbonation-induced corrosion of steel reinforcement. The conventional or descriptive concept, as it is mostly used in guidelines (e.g. [5] and national application documents), assumes that sufficient durability of the structure over 50 years is guaranteed if minimum or maximum values for the water/cement ratio, concrete strength, cement content and concrete cover are complied with (Figure 5, left). The choice of limit values for the concrete composition is based on the results of scientific studies in conjunction with many years of experience with the behaviour of concrete structures in practice. In English, this concept is appropriately characterized as "deemed to satisfy" due to the existing uncertainty.

Action and resistance are only specified qualitatively when applying the descriptive concept in the case of a general attack. Therefore, the designing engineer does not know how large the safety margin, i.e. the difference (R - S), actually is. It is also not possible for him to quantitatively estimate how the affecting parameters, e.g. concrete cover or concrete composition, are to be changed if a structure is to be used for only 20 years or 150 years, for example.

In contrast, the performance concept, often referred to as the probabilistic approach (Figure 5, right), enables a quantitative prediction of the changing durability over time. This is also illustrated by the fact that the action/resistance axis and building age axis can be scaled in the diagram. Actions and resistances are generally described by time functions. For the selected example of carbonation-induced reinforcement corrosion, the action function describes the progress of carbonation over time. The resistance function is time-constant here because it reflects the concrete cover.

A very important feature of the performance concept is that the respective scatter (see the distribution functions shown in Figure 5, right) must be taken into account for the action and resistance functions. With increasing time, there is a growing overlap of the scattering curves and thus an increasing probability of failure or corrosion p_f.

The design process is summarized in Figure 6. In the upper part, the governing functions are given. The values of the probability of failure $p_f(t)$ are converted into reliability indices $\beta(t)$, which is merely a mathematical operation. The greater the probability of failure or the area of overlap (= extent of corrosion) according to Figure 5, the lower the

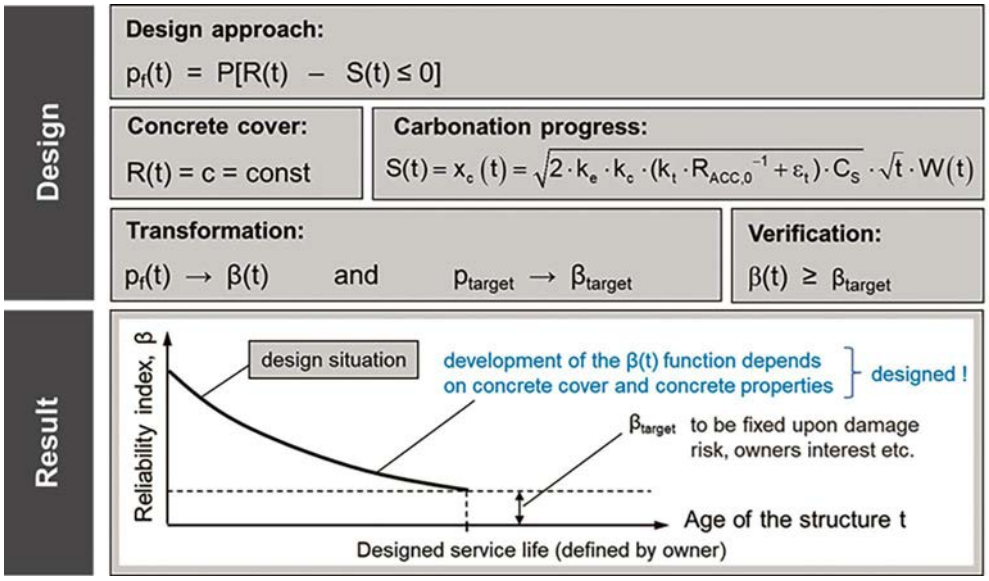

Figure 6. Principle of probabilistic service life design for the example of carbonation induced corrosion.

reliability, i.e. the *β(t)* function decreases monotonically with time, as shown in Figure 6 (lower part).

In a design, the designed service life and the permissible probability of failure at this point in time are taken from guidelines or specified by the owner of the structure. The curves for the action and the resistance can be shifted accordingly or dimensioned in such a way that the desired limit state, i.e. the desired combination of service life and probability of failure, is exactly fulfilled. This ensures that the best possible sustainability is achieved with regard to the use of concrete.

A fully probabilistic service life design requires both a complete functional description of the action and the resistance for a considered durability-relevant process, and further special statistical analysis tools. Detailed data on the concrete used and the scatter values for the input parameters (see S-function in Figure 5, bottom right), i.e. the type of distribution function, mean value and standard deviation, must be known.

4.3. Further aspects

From the point of view of the methodology and the required input parameters, the two concepts compared in Figure 5 represent two extreme cases of durability design. To date, the information required for a fully probabilistic service life design is only available for carbonation and chloride-induced reinforcement corrosion [2, 6]. For all other processes of degradation of concrete, there are essentially only descriptive design concepts based on findings from scientific investigations and experience. In view of the complexity of the various degradation processes, it will probably last decades before full probabilistic prediction models will have been developed for all durability-relevant concrete properties [7].

Between the two basic concepts shown in Figure 5, various intermediate stages can be located, the development of which is currently being worked on intensively [7]. It is becoming apparent that the descriptive concept in national and international guidelines (Figure 5, left) will be replaced by extended concepts considering e.g. partial safety factors, or performance tests. Design engineers will have design tables or diagrams at their disposal that enable simple engineering design for durability, see [8].

5. DESIGN TOOL FOR SUSTAINABILITY OF CONCRETES AND COMPONENTS

The Concrete Sustainability Potential as defined by equation (1) is a useful tool for making comparative considerations when selecting or specifying a concrete in advance of a construction project. This tool makes it possible to identify a specific concrete with a high sustainability potential that also meets the required technical specifications. However, in order to be able to carry out an engineering design of a concrete for sustainability, equation (1) must be reformulated for various reasons. This also applies to the case that equation (1) is used for the design of components, which is possible in principle as well.

In design, target values have to be related to an upper or a lower limit. Hence, the inverse of the Concrete Sustainability Potential shall be considered. Further, it is very difficult to give limiting values for a property like sustainability, as it is not based on a defined physical dimension like strength or stresses or strains. Hence, relative values should be determined in which as a consequence the dimensions are cancelled. Further, as the concrete strength is the basis for the design of a member, and is calculated from the requirements regarding the load-bearing capacity, it is kept constant and thus cancelled for the design for sustainability.

Taking the afore-mentioned considerations into account, the general format for verification of concrete environmental

performance is proposed with equation (2), which defines a limit state, see [2]:

$$ELS_{cal} = \frac{\left[\frac{\sum EI}{SL}\right]_{eco}}{\left[\frac{\sum EI}{SL}\right]_{ref}} \leq ELS_{predefined} \leq 1.0 \qquad (2)$$

ELS_{cal} is the calculated concrete environmental performance limit state, $ELS_{predefined}$ is the limit value that defines the *ELS* criteria, *EI* is the environmental impact of concrete and concrete production and *SL* is the service lifetime.

The index *ref* indicates the value calculated for a reference concrete. The index *eco* indicates the value calculated for a concrete for which an optimization has been carried out in such a way that the predefined limit state criterion ($ELS_{predefined}$) is fulfilled.

For practical application, equation (2) can also be simplified, for example by focusing the limit state consideration exclusively on the CO_2-eq emission. In such case, $\sum EI = CO_2$-eq mass per cubic metre [kg/m³] of concrete and $SL = 1.0$. For more details, see [9, 10, 11].

Figure 7 shows an example of dimensioning according to equation (2). First, different concretes must be compared with each other in terms of their sustainability potential given on the y-axis, see Figure 7, diagram top left. As a result, a specific ecologically optimized concrete can be selected. A further step is to optimize the structural component in terms of maximizing the load-bearing capacity while minimizing the concrete consumption (see Figure 7, diagram top right). Both considerations and optimizations lead to an optimized environmental impact for the finally used structural component.

The next step in this design approach is to consider the service life (see Figure 7). Ideally, a probabilistic design for service life is carried out. The diagram at the bottom left in Figure 7 shows the result of such a design, whereby the reliability index given on the y-axis decreases with increasing time under service. At the end of the defined service life, the given reliability limit state is reached.

In the last step of design, the limit state for sustainability must be defined. Due to the structure of the equation (2), this limit state can be expressed by any number between 0 and 1. Since with regard to the reduction of CO_2 emissions, the desirable limit state of zero emissions cannot be achieved immediately but rather through a degressive development over time, the assessment can be based on corresponding progressions, taking into account the calendar year. The diagram at the bottom right of Figure 7 shows the curves for three different annual reduction rates for CO_2 emissions.

This concept for sustainability assessment and design presented here is innovative and new. It can be considered as a basis and framework, and as a starting point for further developments. So far, there is no practical experience in the application of this concept. It is to be expected that the application of this concept in the practice of concrete construction will certainly lead to further improvements in the coming years.

6. CONCLUDING CONSIDERATIONS

The concrete construction industry faces significant challenges, which primarily consist of reducing the CO_2 footprint of concrete construction without negatively influencing the technical performance and the superior durability of the produced structures. Even though environmentally optimized concretes are readily available today and techniques to produce much slimmer and mass-reduced structures have been proposed, these techniques are rarely implemented in every-

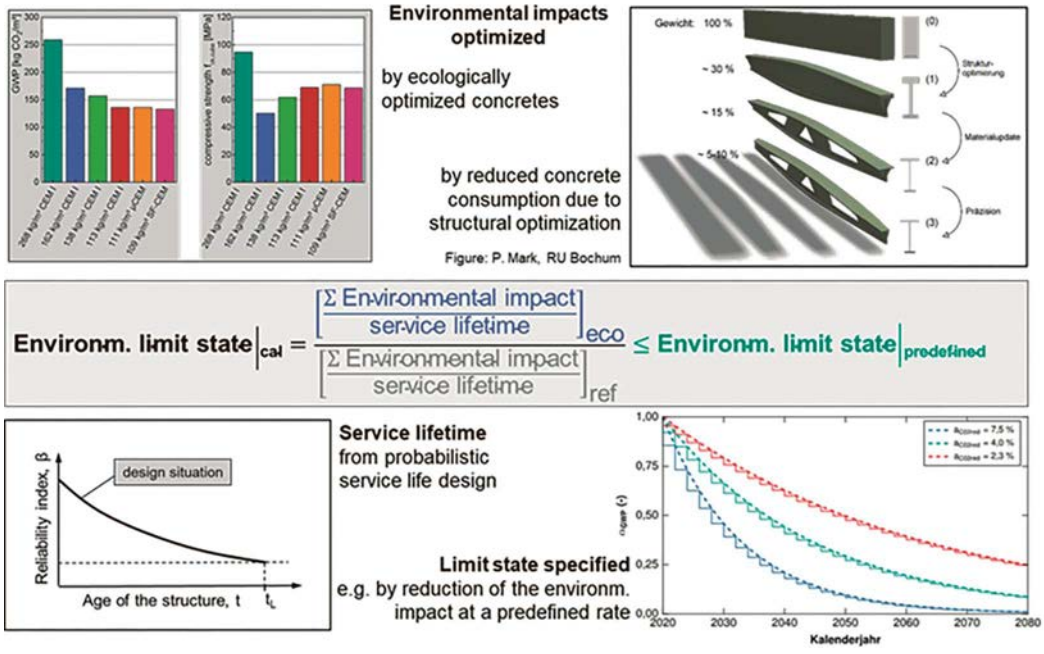

Figure 7. Example for design of concrete members by means of the design equation for sustainability as given in [2].

day construction as suitable incentives and the necessary knowledge are lacking.

Nevertheless, it is the designer who plays the decisive role on the way to an efficient reduction of the GWP and such the protection of the global climate. The design aids proposed with equation (1) and equation (2) are initial approaches, still to be further developed, for demonstrating the sustainability of materials and components. However, such proofs will only find their way into practice when a core problem that still exists today is overcome. This is because nearly all measures that lead to a significant improvement in sustainability are ultimately still associated with higher costs. As long as this does not change, the cost pressure in the competitive economic environment means that the desired, major progress will fail to materialize.

Ultimately, this deficit can only be eliminated by enforcing sustainable measurement with normative specifications. Since the CO_2 emissions associated with the production of concrete components can be calculated with the tools available today, one concept could be, for example, to price the CO_2 emissions, as is currently already the case with emissions trading. It will be interesting to see what solution politicians come up with in this regard. The necessary tools have already been provided by the research community.

References

[1] Müller, H. S., Haist, M., Moffatt, J. S.: Environmental impact, performance and service lifetime – pillars of sustainable concrete construction. Proceedings of the International Conference on Concrete Sustainability (ICCS16), Madrid, Spain, 2016

[2] fib Model Code for Concrete Structures 2020. International Federation for Structural Concrete (fib), Lausanne, Switzerland, 2023

[3] Damineli, B.L., Kemeid, F.M., Aguiar, P.S., John, V.M.: Measuring the eco-efficiency of cement use. Cement and Concrete Composites 32, 2010, pp. 555-562

[4] Müller, H. S., Moffatt, J. S., Vogel, M., Haist, M.: A new generation of sustainable structural concretes – Design approach and material properties. Proceedings of the International Conference Central Europe Towards Sustainable Building (CESB19), Prague, Czech Republic, 2019

[5] EN 1992-1-1:2004-12/AC:2010-11 (Eurocode 2): Design of concrete structures – Part 1-1: General rules and rules for buildings. CEN, Brussels, 2010

[6] fib Model Code for Concrete Structures 2010. International Federation for Structural Concrete (fib), Wiley c/o Verlag Ernst & Sohn, Berlin, 2013

[7] Müller, H. S., Boumaaza, M.: Modeling concrete properties: New approaches in MC2020. Structural Concrete (24), 2023, H. 4

[8] Müller, H. S., Anders, I., Breiner R., Vogel, M.: Concrete: treatment of types and properties in fib Model Code 2010. Structural Concrete, Vol. 14, No. 4, 2013, pp. 320-334

[9] Haist, M., Bergmeister, K., Curbach, M., Mark, P., Müller, C., Müller, H.S. et al.: Climate Limit State (CLS) for Building Structures – a possible companion of ULS and SLS Limit States: Proceedings of the fib International Congress, Oslo, Norway, June 12-16, 2022

[10] Haist, M., Bergmeister, K., Curbach, M., Forman, P., Gaganelis, G., Gerlach, J., Mark, P., Moffatt, J., Müller, C., Müller, H.S., Reiners, J., Scope, C., Tietze, M. and Voit, K.: Nachhaltig konstruieren und bauen mit Beton. BetonKalender, eds K. Bergmeister, F. Fingerloos and J.-D. Wörner, 2022, pp. 421-531

[11] fib Bulletin NN: Background document to Chapter 14 "Concrete" of the fib Model Code 2020. To be published in 2024

Disponible en **www.hormigonyacero.com**
https://doi.org/10.33586/hya.2025.4098

Sound Conceptual Design for Sustainability in bridges

Diseño conceptual para la sostenibilidad en puentes

Akio Kasuga[a]

[a] *Dr. Senior Principal Researcher. The University of Tokyo. Department of Civil Engineering. School of Engineering*

Recibido el 7 de mayo de 2024; revisado el 11 de noviembre de 2024, aceptado el 5 de marzo de 2025

ABSTRACT

How did the great bridge designers of the past leave behind such wonderful structures in an age before computers and thick standards? This has been the author's question for many years. It was known that the three elements of Roman beauty also applied to bridges. But that alone is not a sufficient explanation. And when the world set sustainability as a new goal, it turned out that it could be successfully explained by introducing the idea of structural sustainability. This paper explains the conceptual design of Japanese bridges in terms of structural elegance and structural sustainability.

KEYWORDS: Structural sustainability, conceptual design, structural elegance, bridge.

RESUMEN

¿Cómo lograron los grandes diseñadores de puentes del pasado dejar estructuras tan magníficas en una época sin computadoras ni normativas extensas? Esta ha sido una pregunta que el autor se ha planteado durante muchos años. Se sabía que los tres principios de belleza de la arquitectura romana también se aplicaban a los puentes, pero esto por sí solo no es una explicación suficiente. Cuando el mundo estableció la sostenibilidad como un nuevo objetivo, se descubrió que esta pregunta podía explicarse con éxito introduciendo el concepto de sostenibilidad estructural. Este artículo analiza el diseño conceptual de los puentes japoneses en términos de elegancia y sostenibilidad estructurales.

PALABRAS CLAVE: Sostenibilidad structural, diseño conceptual, elegancia structural, Puente.

* Persona de contacto / *Corresponding author*:
Correo-e / *e-mail*: kasuga@concrete.t.u-tokyo.ac.jp (Akio Kasuga)

How to cite this article: Kasuga, A. (2026). Sound Conceptual Design for Sustainability in Bridges. *Hormigón y Acero*. 77(308):155-165. https://doi.org/10.33586/hya.2025.4098

1. INTRODUCTION

The last 44 years of the author's career as a bridge designer have seen significant technological developments. And the author has been fortunate enough to witness this process first hand. From calculators to personal computers, from linear to non-linear analysis, from drafters to CAD and BIM, and new structures and materials, the technological developments have been impressive in every way. Figure 1 shows the evolution of the number of pages in Japanese concrete and road bridge standards and the number of pages in calculation documents for conventional three-span box girder bridges. The handwritten calculations, which were about 300 pages in 1980 when the author started working on bridges, are now ten times that number, and most of them are typed by computer. Have we really improved our technical potential as well as the number of these pages?

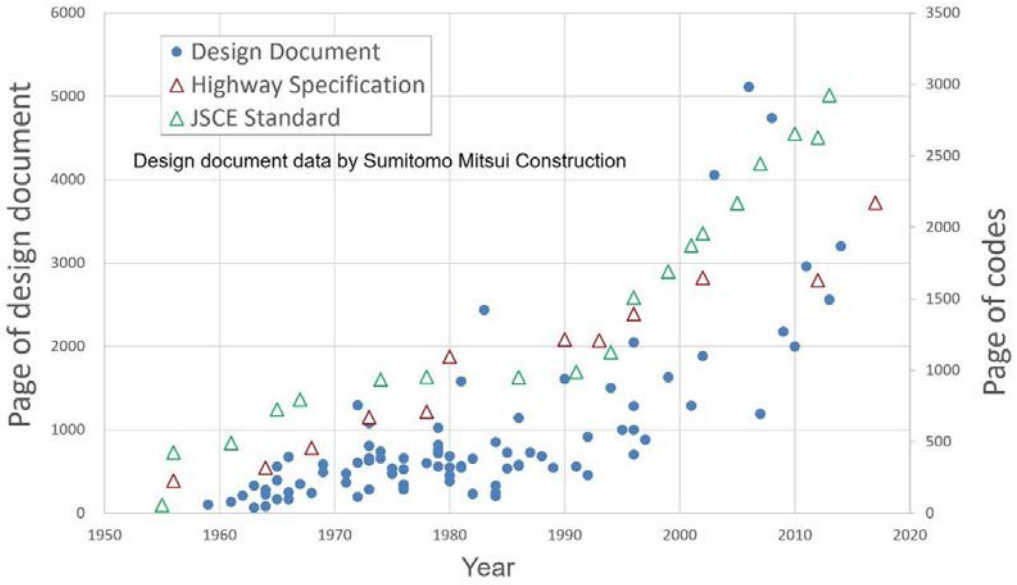

Figure 1. Changes in the number of pages of standards and design documents.

When the author was young, I used to think a lot while drawing lines on a drafting board, and there was no e-mail or mobile phone. FEM was linear, of course, but it was expensive, so I worked out how to optimise it by simple analysis and formulation. Now, however, we are in an age where we can turn to computers right from the start and use the power of computers in large models in abundance. And we can get to the optimum solution in a short time. Today's engineers should have more time to think along these lines, but in reality this does not seem to be the case. The next job is waiting for them. In other words, design productivity has improved dramatically since the author's time, but I can't help feeling that something important is being lost. I believe it is conceptual design. Conceptual design does not need thick standards or computers. This has been proven historically by great bridge designers. In the extreme, conceptual design is a process where all you need is a piece of paper and a pencil and you can think in your head and come up with the optimum solution. The author belongs to a generation that practised conceptual design by always carrying a 5 mm graph paper and a pencil (Figure 2).

Against this historical background, the new value of sustainability has entered design in the 2000s. This paper reconsiders what is appropriate conceptual design with examples and discusses conceptual design for sustainability.

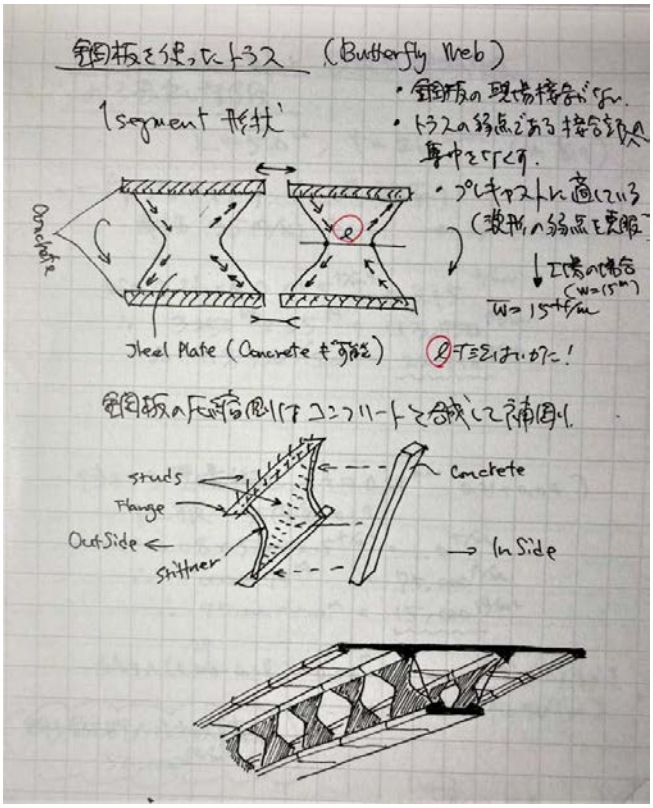

Figure 2. Sketch of butterfly web in conceptual design.

2. CONCEPTUAL DESIGN

Figure 3 shows the life cycle of a structure. Conceptual design, which occurs at the beginning of the design process, involves a rough optimisation of the object to meet performance requirements and constraints. Performance requirements include safety, serviceability and durability as specified in the standards. Performance is then given in the design so that these performance requirements are met during the life cycle of the structure. Constraints, on the other hand, differ from project to project and it is necessary to derive a structure that satisfies cost, construction time, bridge alignment, etc. As the performance requirements and constraints differ in their physical quantities, the design becomes a multivariable optimisation problem. And since most of the variables are related to CO_2 emissions, it is necessary to discuss how

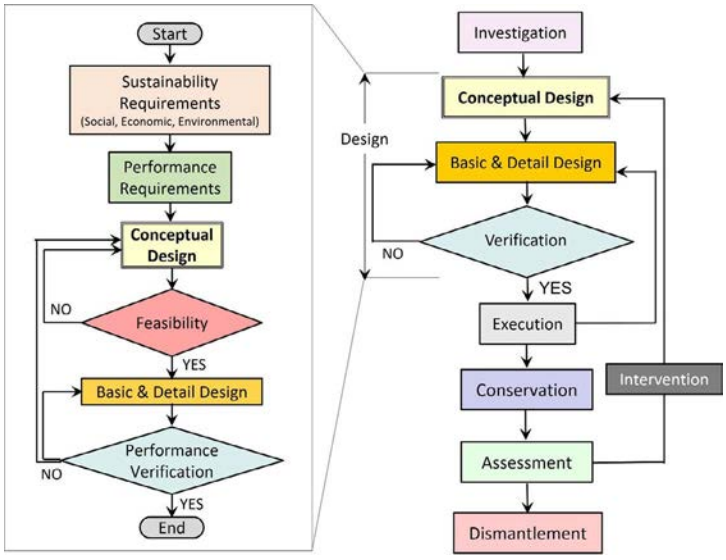

Figure 3. Conceptual design in life cycle flowchart.

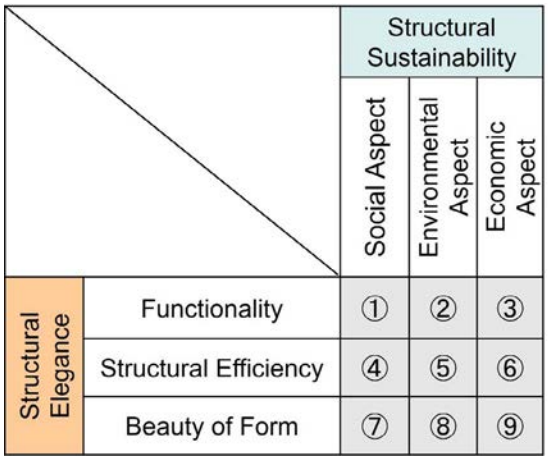

Figure 4. Matrix of structural elegance and structural sustainability.

to optimise them. The Special Activity Group has been organised in 2024 across all fib committees. This discussion will continue within this group. The design will now include the new constrains (performance) of CO_2 emission reduction. In other words, we have an increasingly multivariable and complex puzzle to solve.

The clues to solving this puzzle can be considered in two categories. One is structural elegance and the other is structural sustainability. Structural elegance consists of three elements. They are the same as the three elements of architectural beauty identified by the Roman Vitruvius: utilitas (useful), firmitas (sturdy) and venustas (beautiful). Applied to bridges, they are "functionality", "structural efficiency" and "beauty of form" respectively. The author has identified these as the three elements of structural elegance in bridges [1]. The three elements of structural sustainability are the same as the three aspects of sustainability, social, economic and environmental aspects. Each element attributed to the structure is then specifically defined as structural sustainability.

The three elements in these two categories are considered in a three by three matrix (Figure 4). There are nine possible combinations of each element and four main keywords that can be considered to reduce CO_2 emissions. The first is 'lightweight structure'. If this can be achieved through structural ingenuity without increasing the strength of the materials, a significant reduction in CO_2 emissions can be achieved. Of course, this also reduces costs. The second is 'accelerated construction'. Although shortening the construction period generally increases costs, it is known that shortening the construction period can significantly reduce indirect CO_2 emissions when the impact of construction on surrounding social activities is taken into account [2]. The third is 'rational force flow'. A structure designed to minimise the flow of forces from the point of loading to the point of support of the structure is material minimising. This means that CO_2 emissions are also minimised. This principle is particularly important for cable supported structures. The fourth is 'minimum environmental impact' construction. By minimising the environmental impact of construction sites, CO_2 emissions are minimised and biodiversity is protected.

In the following chapters, the 3x3 matrix of structural elegance and structural sustainability will be used to explain how the four keywords for reducing CO_2 emissions contribute to conceptual design, using actual examples from Japan.

3. STRUCTURAL ELEGANCE

It is difficult to translate structural elegance into Japanese. If I had to guess, I would say 'iki and miyabi'. In English it would be 'chic and graceful'. The best example of 'iki and miyabi' in Japanese architecture is shrine and temple architecture. The warping of the eaves and the depth of the eaves, originally imported from China and refined to the highest degree, are the result of the Japanese aesthetic sense, the former by reducing the warping and the latter by deepening the eaves to suit the rainy climate. The connections between the columns and the beams are of nail-less construction, with the beams penetrating the columns, a so-called seismic isolation structure that allows seismic forces to escape to a moderate degree. In addition, the clay walls have the function and strength to retain an appropriate level of moisture and are an excellent material that can be kneaded and reused. Although made of wood, it has a 1,000-year lifespan and is truly a masterpiece of functionality, structural efficiency and beauty of form.

3.1. Functionality

The most important function of a bridge, such as a road bridge, is to allow vehicles to pass. Another important element of functionality is how well it blends into the surrounding terrain and environment. Another aspect that attracts attention is how well the environment is maintained during

Figure 5. Seiun Bridge (2004).

Figure 6. Installation of precast member using suspension cables.

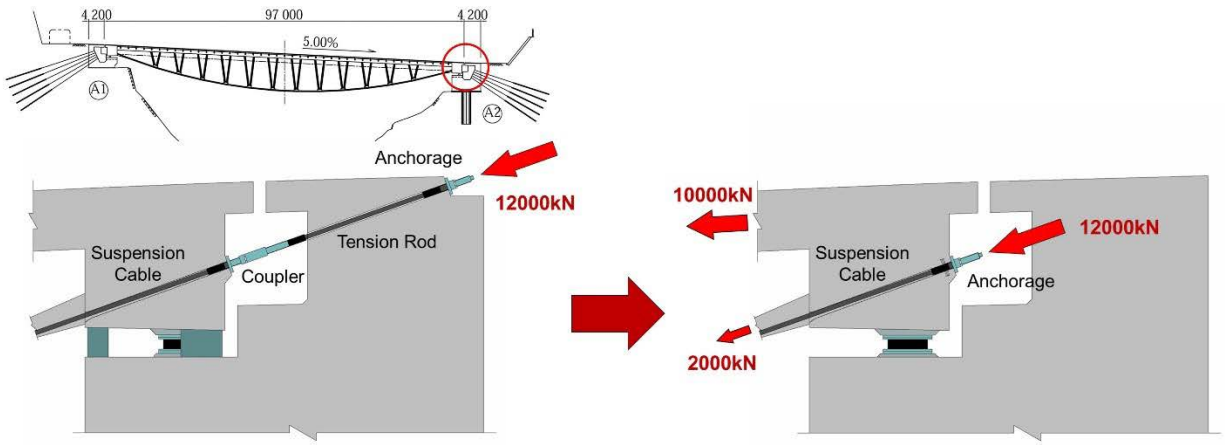

Figure 7. Structural system conversion.

construction, which can also be considered as a function. It is natural for a thing with a superior function to take on a beautiful form. It is important to be able to explain the need for functionality, while at the same time being able to imagine a structure that is in harmony with its surroundings. The pursuit of functionality requires a very high level of skill.

The Seiun Bridge [3], shown in Figure 5, had difficult constraints. The bridge is located in a national park and as no piers could be placed in the river, even during construction, it was necessary to build a 90m single span bridge. Both abutment locations were also difficult to secure construction yards due to the steep mountains. In such terrain, an arch bridge is generally adopted. However, an arch bridge was excluded due to their high environmental impact, as they significantly alter the terrain during excavation of the arch abutments. A special erection method using a suspension structure was then adopted (Figure 6). The anchoring forces of the suspension structure are released on completion and transferred as prestressing forces to the girders to construct the simple girder (Figure 7). All components of the girders were also prefabricated in the factory as precast and transported to the site. Of course, during construction, analyses were carried out using the large deformation theory, although the structure was concrete. These solutions under severe constraints are considered to be an important functionality and are positioned in ② of the matrix. And the key word is 'minimum environmental impact'.

3.2. Structural efficiency

Structural efficiency is the most obvious element and can be summarised as structural rationality and simple force flow. Structural efficiency is important to ensure that the flow of forces is clear and that forces are transmitted through the shortest possible distance, so that no additional bending moments or shear forces are generated. And bridge engineers can read this philosophy through the structure without explanation when they look at it. Structural efficiency is something that cannot be faked against professionals.

Figure 8 shows a good example of structural efficiency, the Katsushika Harp Bridge. The road spans the canal in an S-shape, which limits the location of the bridge piers. Cable-stayed bridges were then chosen to reduce the weight of the superstructure. The problem is the location of the main towers and the arrangement of the stay cables. Therefore, the main tower is located at the inflection point of the S-shape, which makes the stay cables point-symmetric and eliminates the out-of-plane horizontal component of the stay cable forc-

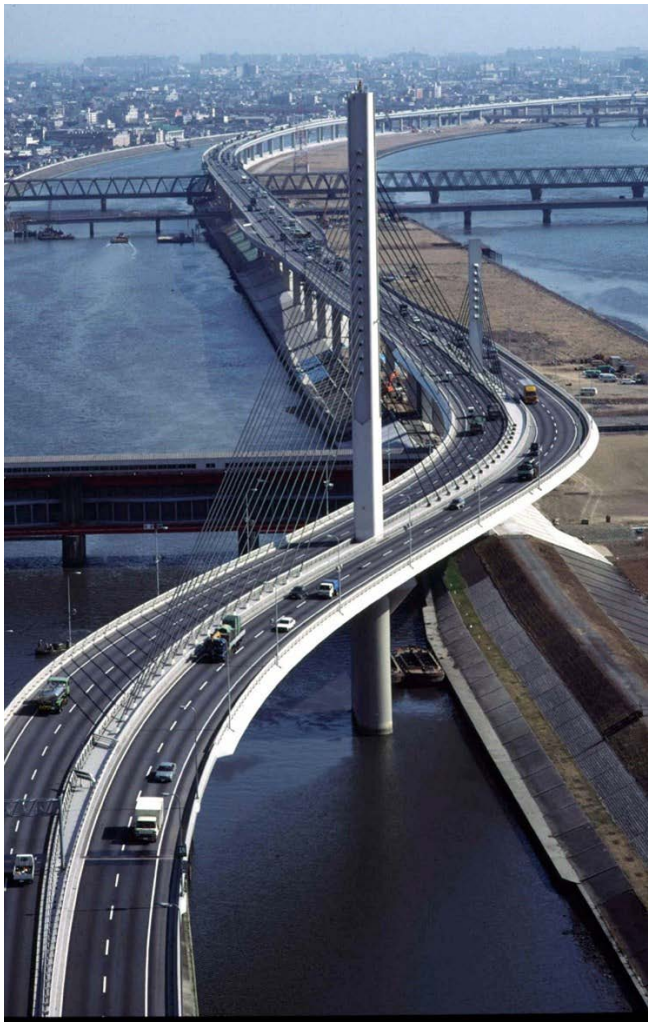

Figure 8. Katsushika Harp Bridge with S-shaped planar alignment.

es. This allowed the main tower to be a single column rather than a frame structure. It is a small but very elegant solution. In addition, due to the limitations of the pier positions, the main towers are arranged at different heights, resulting in a three-span structure. It is positioned in ⑥ of the matrix and the keyword is 'rational force flow'.

3.3. *Beauty of form*

Structural Elegance cannot be described by this beauty of form alone. The essence lies in the functionality and structural efficiency mentioned above. Therefore, it is considered to be only a subsidiary role. And it is fundamental that the beauty of form can be explained structurally. Beauty of form is a matter of personal preference and subjectivity. And unlike functionality and structural efficiency, which are commonly understood by bridge engineers in different countries, beauty of form is influenced by the specific culture of each climate and ethnic group. Beauty of form can only be developed through exposure to many examples. But it requires a structural background.

The Furukawa Viaduct [4], shown in Figure 9, is a 3 km long motorway built in an urban area. It was built using the precast segmental method, but because of the urban area

Figure 9. Furukawa Viaduct with factory fabricated segments.

around it, it was prefabricated and transported at a precast plant 100 km away. Trailers on Japanese roads are normally restricted to a maximum weight of 30 tonnes. Therefore, if a beam with a span of 35 m and a width of 17 m is precast in its entire cross section, the segment width will be 1.9 m. The total number of segments would then be 1,900. In order to reduce the number of segments and thus the transport, a special shape called the U-shaped core segment was conceived (Figure 10). This gave a segment width of 2.6 m and reduced the number of segments to 1300. The decks were cast-in-place, using precast panels instead of formwork. The deck is then constructed in five days. This is the same speed as forming a U-shaped core segment into a girder. Erection costs were also reduced because the weight of the segments suspended from the erection beams was reduced by 60%.

The social impact of the viaduct construction in the city has been minimised and the view from under the bridge is reminiscent of the eaves of Japanese temples and shrines. It can be positioned at ⑦ of the matrix, where beauty of form and social aspect merge. The key word in the conceptual design is 'accelerated construction' through 'lightweight structure'.

4. STRUCTURAL SUSTAINABILITY

The concept of sustainability has been introduced from the fib Model Code 2010 and placed at the centre of the Model Code 2020 [5]. The author felt that when talking about sound conceptual design, it is sometimes not possible to explain it well using only structural elegance. How were the great bridge designers of the past able to build such holistic structures in an era before computers and thick standards? The answer to this question has been a longstanding theme for the author. The three elements of Roman beauty would, of course, have been recognised by them. But that was not enough. It turned out to be well explained by adding the concept of sustainability, which takes into account the economic aspirations, environmental considerations and social impact

Figure 10. Erection of U-shaped core segments.

caused by the structure. This is structural sustainability [1]. The two categories of elegance and sustainability are structure-driven. From now on, bridge designers are needed who can project these into the conceptual design.

4.1. Economic aspect

As infrastructure, bridges are naturally expected to be economically viable. And the quest for economic efficiency is largely driven by the structure. This is all the more true when the constraints are severe. Minimising life-cycle costs, not just initial costs, is now the order of the day. Guidelines against chloride attack were established in Japan in 1984. Since then, measures have been taken to increase concrete cover in areas where chloride attack is a concern. Durability considerations are never about minimising initial costs, but an optimum solution over the life cycle. In Japan, reinforced concrete slabs on motorways built more than 60 years ago have deteriorated by deicing salt and are being replaced with new slabs at great cost. Material minimisation in the 1960s was not an optimal solution. Two examples of the pursuit of initial cost minimisation are presented below.

The first is the Katsurajima Viaduct [6] (Figure 11). This bridge was constructed using the incremental launching method. At the time of the contract, the bridge was a full-section double-cell concrete box girder, which meant that the weight of the main girder was high and the cost of erection during launching was also high. It was therefore necessary to reduce the weight of the main girder for launching. The solution was to change the main girder to a corrugated steel web and to construct the overhanging slab after launching, thereby reducing the weight of the main girder during launching by half (Figure 12). In addition, the external cables used during construction were re-installed and re-used for the completed girder. These measures resulted in significant cost savings. This, together with rational erection, is posi-

Figure 11. Katsurajima Viaduct by incremental launching of core segments.

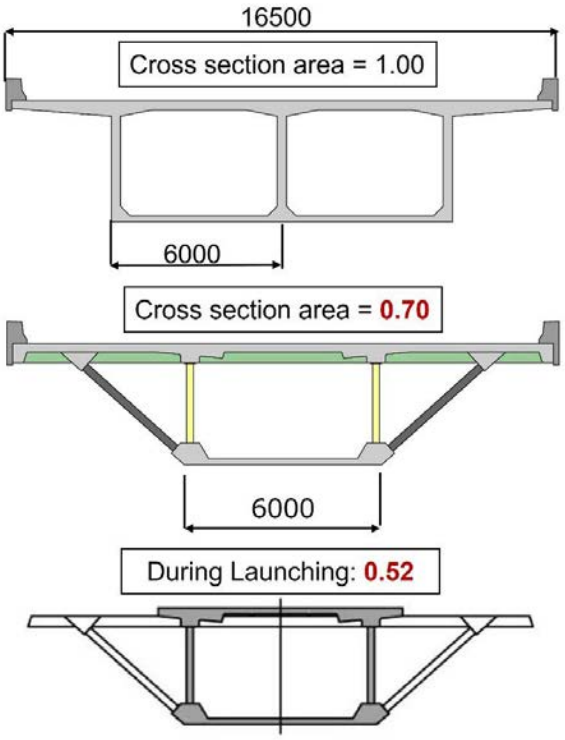

Figure 12. Lightweight structure during incremental launching.

tioned at ③ in the matrix. The key word in the conceptual design is 'lightweight structure'.

The second is the Kakehashi Ichigou Bridge [7], an arch bridge with a span of 155 m (Figure 13). In a design-build competition, it was superior to the steel arch bridge proposal in terms of cost. The main difficulty with this bridge is that the road alignment is curved and deviates from the axis of the arch (Figures 14, 15). The client's masterplan proposal included a higher amount of concrete for the arches and abutments to widen the arches to match the road alignment. However, by reducing the four piers on the arches to two, the amount of concrete was reduced without widening the arches. The amount of concrete was reduced by 20% in the superstructure and 30% in the substructure. This bridge is located at ⑨ in the matrix and the key concept of the design is 'lightweight structure'.

The two examples described above represent the realisation of structural sustainability through lightweight structure. However, material considerations and thoughtful detailing are important to ensure durability for life cycle optimisation.

4.2. Social aspect

Bridge construction and maintenance have a significant impact on social activities in the vicinity of the site. This includes noise and vibration caused by construction activities, as well as traffic congestion and detours due to construction restrictions. In particular, traffic congestion and detours indirectly result in additional CO_2 emissions. And it has been reported that these CO_2 emissions are highly dependent on the construction period and in some cases far exceed the direct CO_2 emissions from construction [2]. This section begins with a

Figure 13. Kakehashi Ichigou Bridge with concrete arch.

Figure 14. Deviation of arche and curved girder.

project of minimising the impact on social activities around a construction site by shortening the construction period.

The Takubogawa Bridge [8], shown in Figure 16, is surrounded by a primary school and a kindergarten. The construction of the piers and foundations had already been completed in a separate project, but the weight of the concrete box girder bridge at the time of the contract award required new reinforcement due to new seismic standards. The operator, the Highway Company, wanted a lighter superstructure and a shorter construction period to minimise the impact on the surrounding area. Naturally, this was to be achieved with a concrete structure. The solution proposed was the butterfly web [9]. The butterfly web can reduce the weight

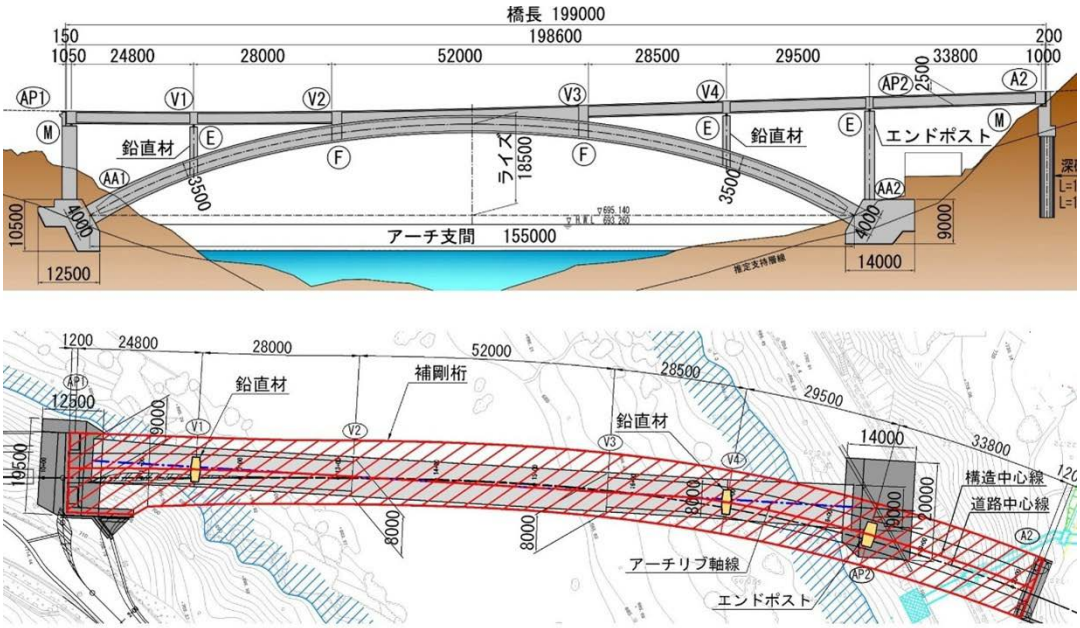

Figure 15. General view of design and build scheme.

Figure 16. Takubogawa Bridge with butterfly web.

of the main girder by 15%. This weight reduction reduces the number of main girder segments from eight to five per cantilevering. It also eliminates the need for additional reinforcement of the substructure. The reduction in construction time and the avoidance of reinforcement work due to the weight reduction could minimise the impact on surrounding social activities. Positioned in ① of the matrix, the key word in the conceptual design is 'accelerated construction' through 'lightweight structure'.

Not all social aspects can be measured in terms of CO_2 emissions. Another example is the Yamakiri Ichigou Viaduct [10] (Figure 17). The bridge was surrounded by a village on one side and a citrus grove on the other. The basic design at the time of the contract was for construction on falsework. However, the piling for the falsework was carried out using the down the hole hammer method, which had a significant risk of spreading dust into the surrounding area. The 45m span was too short for the cast-in-place cantilevering meth-

Figure 17. Yamakiri Ichigou Viaduct in a difficult surrounding environment.

Figure 18. Precast segment cantilevering with erection girder.

Figure 19. Seishun Bridge with double suspension cables.

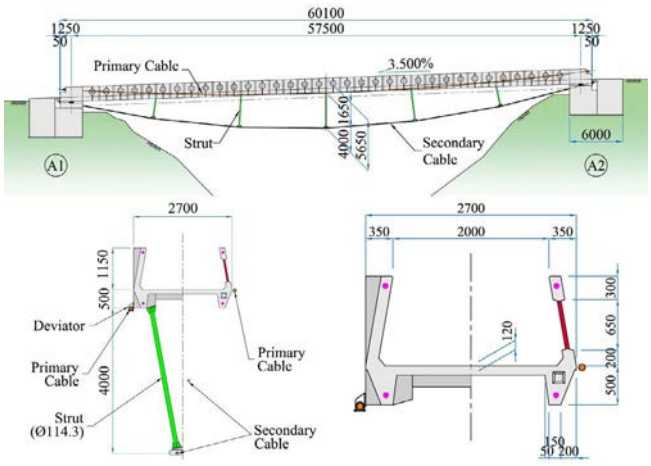

Figure 20. General view of Seishun Bridge.

od. In the end, a precast segment cantilevering was chosen, with the earthworks section behind the abutment as the fabrication yard (Figure 18). To reduce weight during erection, the overhanging slabs were constructed after the girders had been erected. Dust risks were avoided and the impact on social activities in the neighbourhood was minimised by having the fabrication yard on site. This case can be placed at ④ in the matrix. And the key concept of the conceptual design is 'accelerated construction'.

4.3. Environmental aspect

The biggest environmental challenge is the reduction of CO_2 emissions towards carbon neutrality of concrete structures. And from now on, attention must also be paid to the protection of biodiversity in order to minimise the impact of construction on the surrounding environment. Two case studies from different perspectives are presented below.

The first is the Seishun Bridge [11], a pedestrian bridge (Figure 19). This bridge was designed to connect a junior high school with a sports field and was tendered in a design-build competition. The constraints were that it should be a single span of approximately 60 m across a valley, that no anchors should be left in the ground and that the longitudinal gradients should not exceed 5%. And first of all, the stress ribbon bridge disappeared from our proposal. The author had the know-how of the Seiun Bridge mentioned in 3.1. However, the method of erecting members from the bottom up using a suspension structure was unstable until the load was finally applied. For this bridge, a new construction method was considered in which the members were erected from top to bottom, and a new type of structure, the double suspension structure, was adopted (Figure 20). All loads during erection were carried by the upper primary cables and lifted upwards by the lower secondary cables to achieve the required girder alignment (Figure 21). The anchor forces are then released and transferred to the girders as prestressing forces, as in the Seiun Bridge, to make it a simple girder. After construction, the author knew that there was a wheelchair-bound student at the junior high school and that the completion of this bridge would make it easier for him to get to the playground. This bridge is very dear to the author's heart. Positioned at ⑤ in the matrix, the key words are 'rational force flow' and 'minimum environmental impact'.

Figure 21. Adjustment of girder alignment using secondary cables.

Figure 22. Mukogawa Bridge with lightweight structure.

The second is the Mukogawa Bridge [12], the ultimate lightweight bridge (Figure 22). The client's basic design was a conventional concrete box girder. The constraints were that the 80m high piers in the river had to be circular with a diameter limit of 5m. A shorter construction period was also required. A structural problem in the basic design was that the piers were unbalanced due to seismic forces being concentrated on the lower piers. To solve this problem, it was necessary to reduce the weight of the girders to eliminate the unbalance of the piers. The piers were half precast using 50Mpa concrete (Figure 23). This method allowed the construction speed of the piers to be halved. The main girders were changed by extradosed bridges with butterfly webs. The construction time of the superstructure was reduced by 270 days because the number of segments was halved by using butterfly webs. As a result, the girders and piers were 20% and 50% lighter, and CO_2 emissions were reduced by 13% and 50% respectively. Although the cost was higher than that of a conventional box girder, it can be placed at ⑧ in the matrix in that it shortened the construction period and gave a slender, beautiful form to the surrounding environment. The key word, of course, is 'lightweight'.

5. CONCLUSIONS

In the days of Freyssinet, Torroja, Finsterwalder, Maillart and others, there was no concept of sustainability. Nor were there computers or thick standards of detail. So why were they able to leave behind great structures? Because they were able to invest enough energy and time in conceptual design to find the optimum solution that would be sustainable.

The examples of conceptual design described in this paper have been implemented in the past. They mean that there is still a lot we can do to improve structural sustainability. CO_2 emissions of the past structures are not quantified but will be in the future through LCA.(Life Cycle Assessment) Struc-

Figure 23. Half precast erection of 80m high pier.

tural elegance is verified as a performance requirement other than beauty of form. Structural sustainability, on the other hand, is often treated as a measure to satisfy constraints rather than performance requirements. There is an urgent need to discuss how to find a multivariable optimisation solution with different physical quantities. Sound conceptual design is an indispensable element for LCA optimisation. Within Commission 1 of fib, the Task Group 1.5 on Structural Sustainability is active [13]. A bulletin for sound conceptual design for structural sustainability will be published this year.

How can conceptual design skills be developed? The author's answer is to actually see a great object and listen to the 'language' through the structure that it speaks to you. It is a conversation about why the structure is the way it is, how it was built and why it works. Imagine for yourself, and talk to the designer through the structure, how it can be explained in terms of structural elegance and structural sustainability. That way you can hone your own skills. I think that is the only way.

References

[1] Kasuga, A., Structural sustainability leading to structural elegance, IABSE Symposium Nara Keynote Lecture, 2015

[2] Haist, M.; Bergmeister, K.; Fouad, N.A.; Curbach, M.; Deiters, M.V.; Forman, P.; Gerlach, J.; Hatzfeld, T.; Hoppe, J.; Kromoser, B.; Mark, P.; Müller, C.; Müller, H.S.; Scope, C.; Schack, T.; Tietze, M.; Voit, K.: Nachhaltiger Betonbau - Vom CO 2 - und ressourceneffizienten Beton und Tragwerk zur nachhaltigen Konstruktion; In: Bauphysik-Kalender, Schwerpunkt: Nachhaltigkeit, Fouad, Nabil A. (Eds.), Ernst & Sohn, Berlin, 2023, pp. 259-363

[3] Kasuga, A., Noritsune, T., Yamazaki, K., and Kuwano, M. DESIGN AND CONSTRUCTION OF COMPOSITE TRUSS BRIDGE USING SUSPENSION STRUCTURE, fib Symposium Budapest, 2005

[4] Ikeda, S., Ikeda, H., Mizuguchi, K., Muroda, K. and Taira, Y. DESIGN AND CONSTRUCTION OF FURUKAWA VIADUCT, fib Congress Osaka, 2002

[5] Kasuga, A. Evolution of fib model codes: Mastering challenges and encountering new ones, Structural Concrete, 2023, pp 4336-4340

[6] Aoki, K., Nakamura, A., Morohashi, A. and Kasuga, A. Corrugated Steel Web Bridge with Ribs and Struts. Design and Construction of The Katsurashima Viaduct, fib Congress Naples, 2006

[7] Kasuga, A. CONSTRUCTION OF ARCH BRIDGES IN JAPAN, fib Symposium Prague, Keynote Plenary Lectures, 2011

[8] Ashizuka, K., Miyamoto, K., Kata, K. and Kasuga, A. Construction of a Butterfly Web Bridge, fib Symposium Stockholm, 2012

[9] Kasuga, A. Effects of butterfly web design on bridge construction, Structural Concrete, 2018, pp128-142

[10] Shibata, T., Asai, H., Fujioka, T., Kasuga, A. and Sakai, K. Application of sustainability design to an existing viaduct in a hilly area, Structural Concrete, 2017

[11] Kasuga, A., Sakao, H., Taira, Y., and Kuwano, M. DESIGN AND CONSTRUCTION OF DOUBLE SUSPENSION STRUCTURE, fib symposium Dubrovnik, 2007

[12] Samizo, J., Fukuda, M., Kasuga, A., and Mizuno, K. DESIGN AND CONSTRUCTION OF THE MUKOGAWA BRIDGE, fib Symposium Copenhagen,2015

[13] https://fib-international.org/commissions/com1-concrete-structures.html

Disponible en **www.hormigonyacero.com**
https://doi.org/10.33586/hya.2025.4099

Exploring the Multifaceted Aspects and Benefits of Structural Health Monitoring

Exploración de los aspectos y beneficios multifacéticos del seguimiento del daño estructural

Giuseppe Mancini[*,a], **M. Longo**[a], **D. La Mazza**[a]

[a] *SACERTIS Ingegneria S.r.l., Roma, Italy.*

Recibido el 2 de junio de 2024; revisado el 18 de febrero de 2025, aceptado el 18 de febrero de 2025

ABSTRACT

The degradation and failures of structures present considerable threats to both the economy and society, underscoring the need to address safety risks and maintenance deficiencies. These issues, combined with the aging of structures and progressive deterioration, require improved structural safety assessment methods and strategies to ensure accurate evaluation of the remaining service life. Structural Health Monitoring (SHM) is crucial in addressing these challenges. These systems primarily ensure safety concerning Ultimate Limit States and protect lives. Additionally, they offer benefits such as supporting proactive maintenance, monitoring traffic load variations, understanding structural behaviour under different conditions, and evaluating the effectiveness of retrofitting interventions. In this paper three case studies, related to reinforced or prestressed concrete bridges monitored in continuous and in real time by Sacertis Ingegneria, showcase the effectiveness of SHM systems demonstrating how these systems can effectively identify behavioural variations due to different causes, supporting the maintenance and safety of aging infrastructures.

KEYWORDS: Structural health monitoring, existing bridges proactive maintenance, structural behaviour.

RESUMEN

La degradación y las fallas en las estructuras representan amenazas significativas tanto para la economía como para la sociedad, lo que resalta la necesidad de abordar los riesgos de seguridad y las deficiencias en el mantenimiento. Estos problemas, junto con el envejecimiento de las estructuras y su deterioro progresivo, requieren métodos y estrategias mejoradas para la evaluación de la seguridad estructural, asegurando una valoración precisa de la vida útil remanente.

La Monitorización de la Salud Estructural (SHM) juega un papel fundamental en la gestión de estos desafíos. Estos sistemas garantizan principalmente la seguridad en relación con los Estados Límite Últimos y la protección de vidas humanas. Además, proporcionan beneficios como el apoyo al mantenimiento proactivo, el monitoreo de variaciones en las cargas de tráfico, la comprensión del comportamiento estructural bajo diferentes condiciones y la evaluación de la eficacia de las intervenciones de refuerzo.

En este artículo se presentan tres casos prácticos relacionados con puentes de hormigón armado o pretensado, monitorizados de manera continua y en tiempo real por Sacertis Ingegneria. Estos casos evidencian la eficacia de los sistemas SHM, demostrando cómo pueden identificar variaciones en el comportamiento estructural debido a diversas causas, apoyando así el mantenimiento y la seguridad de las infraestructuras envejecidas.

PALABRAS CLAVE: Monitoreo de la salud structural, puentes existentes mantenimiento proactive, comportamiento estructural.

* Persona de contacto / *Corresponding author*:
Correo-e / *e-mail*: giuseppe.mancini@sacertis.com (Giuseppe Mancini)

How to cite this article: Mancini, G., Longo, M., & La Mazza, D. (2026). Exploring the Multifaceted Aspects and Benefits of Structural Health Monitoring. *Hormigón y Acero*. 77(308):167-174. https://doi.org/10.33586/hya.2025.4099

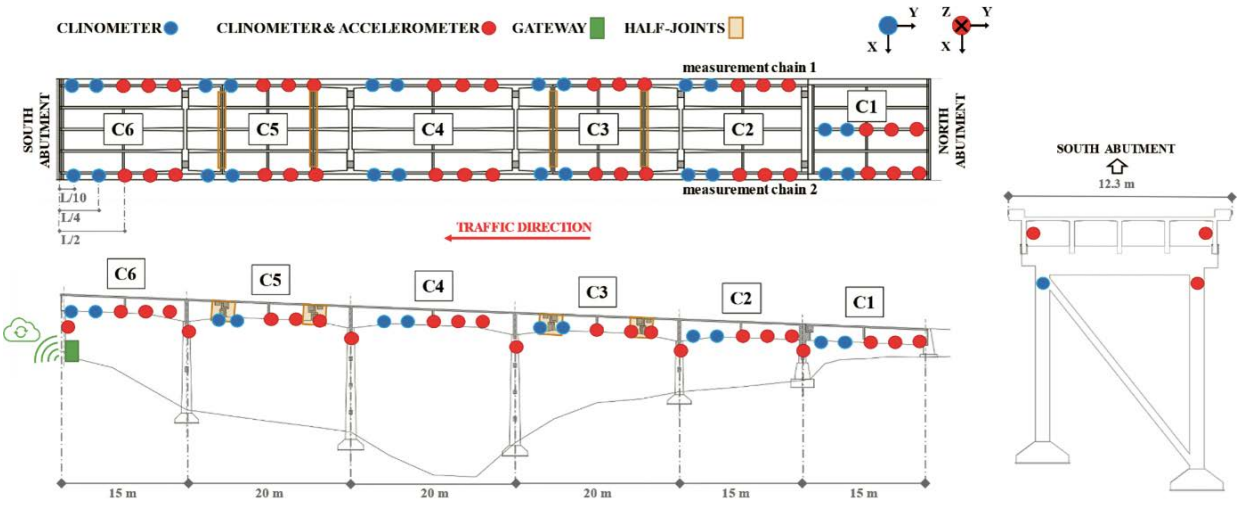

Figure 1. Monitoring for proactive maintenance - Case study geometry and SHM system.

1. INTRODUCTION

The deterioration and malfunction of structures and infrastructures, pose significant risks to both the economy and society [1]. Recent years have witnessed a growing number of disasters highlighting the urgent need to address safety risks and maintenance deficiencies [2]. These issues, compounded by the ageing of structures and progressive deterioration processes, necessitate an improvement of structural safety assessment methods and strategies to ensure the remaining design service life of these structures is accurately evaluated.

A key strategy in addressing these challenges is the implementation of Structural Health Monitoring (SHM) systems [3] [4][5].

The primary purpose of SHM systems is to ensure safety in relation to Ultimate Limit States and protect human lives. However, they also offer numerous additional benefits, including support for proactive maintenance, monitoring of traffic load variations, comprehensive understanding of structural behaviour under different operational conditions, evaluation of retrofitting interventions effectiveness, and more [6][11].

In this paper, three case studies under continuous monitoring by Sacertis, a leading Italian company in the field of structural health monitoring, are presented. These case studies demonstrate how a monitoring system can be effective in identifying behavioural variations due to distinct causes and specifically:

- The first case demonstrates how a SHM system can be used to apply a proactive maintenance-based approach on a structure. The system provides real-time data on structural health, allowing for early detection of minor issues that, if left unaddressed, could lead to significant damage. This enables maintenance teams to perform targeted interventions, addressing problems early and preventing them from developing into larger, more costly issues. Proactive maintenance not only enhances the safety and reliability of the structure but also optimizes maintenance resources and reduces overall lifecycle costs.
- The second case illustrates how a SHM system enables comprehensive characterization of a structure, capturing variations in behaviour due to seasonal temperature and environmental conditions changes. This global understanding of a structure performance is critical for accurate assessment and management. For instance, SHM data can reveal how a bridge performance changes with temperature fluctuations or how it responds to different environmental conditions over time. This detailed characterization helps engineers develop more precise maintenance and reinforcement strategies, tailored to the specific needs of the structure.
- The third case shows how a SHM system can play a crucial role in evaluating the effectiveness of reinforcement interventions. When a structure undergoes reinforcement, it is essential to assess whether the intervention has successfully restored or improved its structural integrity. SHM systems provide continuous data on the performance of the reinforced structure, allowing engineers to verify the effectiveness of the intervention and make any necessary adjustments. This approach ensures that maintenance efforts are both efficient and effective, ultimately enhancing the safety and longevity of the structure.

2. MONITORING FOR PROACTIVE MAINTENANCE

2.1. The case study

The case study is a highway reinforced concrete bridge built in the late 1960s, located in Northern Italy [12]. The viaduct has a total length of 105m and it is made of 6 span; the deck is a girder with five longitudinal beams and three transversal beams and it is 10.5m wide. The static scheme shows the presence of half joints creating an alternance of supporting and supported spans (span no. 3 and 5 supported spans). The first span is the only one simply supported between pier and abutment.

Figure 2. Case study 1 - Monitoring timeline.

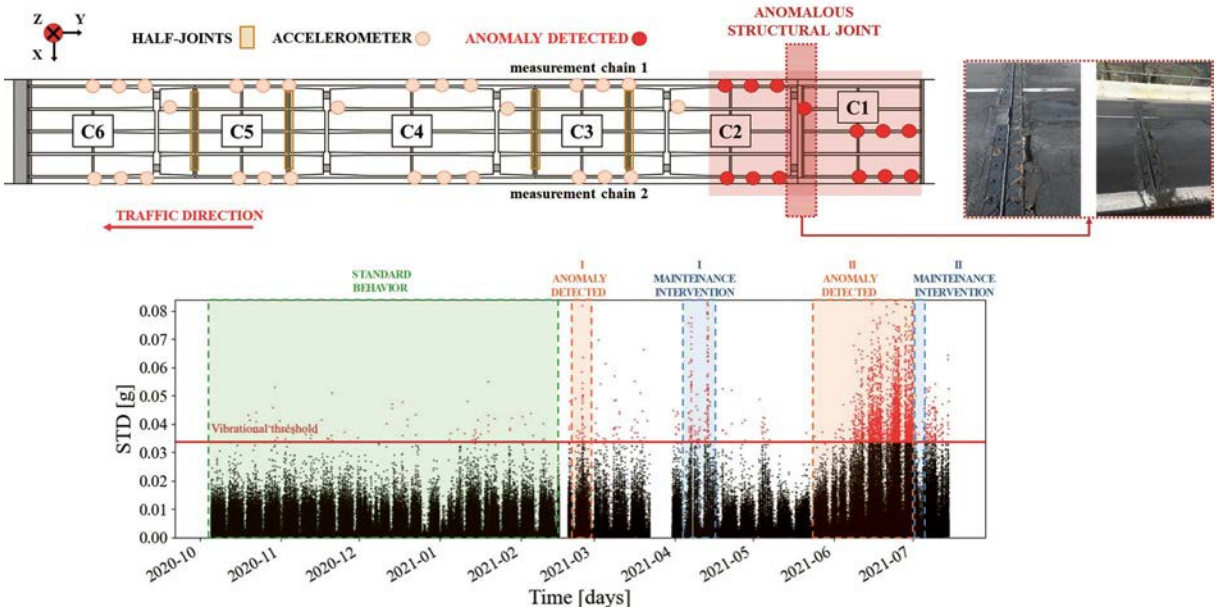

Figure 3. Case study 1 – Vibration anomalies.

The primary beams have a total depth of 2.7 meters, while the reinforced concrete slab has a constant thickness of 0.20m. The geometry of the case study is shown in Figure 1.

A permanent monitoring system was installed on the bridge in 2019 to control its static and dynamic behaviour over time. The system consists of MEMS biaxial inclinometers and triaxial accelerometers, located on the edge beams. The sensors are wired and connected to a local gateway, which collects data before storing them in the cloud. The layout of the SHM system is shown in Figure 1: for each span and each edge beam, 5 inclinometers and 3 accelerometers are positioned at key points for a comprehensive diagnostic of the static and dynamic behaviour (near the supports, at the quarters, and in midspan). The accelerometers sample at 100Hz along three orthogonal axes: the Z-axis (vertical), the Y-axis (longitudinal in the plane of the deck), and the X-axis (transversal in the plane of the deck). Clinometers, on the other hand, acquire data when queried by the gateway according to a polling cycle and measure along the two axes lying in the horizontal plane (X-axis and Y-axis).

2.2. Monitoring history

Bridge monitoring started in 2019 with a Model-Driven approach, following the timeline described in Figure 2. Initially, just after the installation of the monitoring system, static load tests were performed by loading each span of the bridge with two 40-ton trucks in different configurations (both symmetric and asymmetric). Data recorded by inclinometers during these tests, combined with modal information extracted from accelerometers under operational conditions, were used to update the numerical model of the structure. A digital twin of the bridge, representative of its real behaviour, was thus obtained. From this model, damage indicators (DIs) were selected to monitor any appearance of damage over time.

Some damage scenarios were hypothesized and simulated on the numerical model, obtaining the critical values for each of the selected DIs, which are monitored over time with automatic controls running both at the gateway (semi real-time controls) and cloud (medium-long period controls) levels. Alongside these DIs and their related Model-Driven thresholds, Data-Driven Indicators were also chosen and initialized with appropriate algorithms running at various frequencies automatically, responsible for detecting any change in the bridge behaviour (anomaly detection) compared to what was recorded during the initial training period. In this case, thresholds are computed using statistical or more advanced machine learning approaches.

Among the Data-Driven Indicators, one was selected and monitored over time to recognize eventual impulsive and short-term anomalous vibrations related to high-energy events occurring in specific areas of the bridge (e.g., near the supports, on a specific beam, on abutments or piers, etc.). This indicator is calculated with an algorithm that processes data recorded by accelerometers and computes, in semi real-time, synthetic parameters to recognize short-term vibrational events with very high energy (e.g. standard deviation over 1

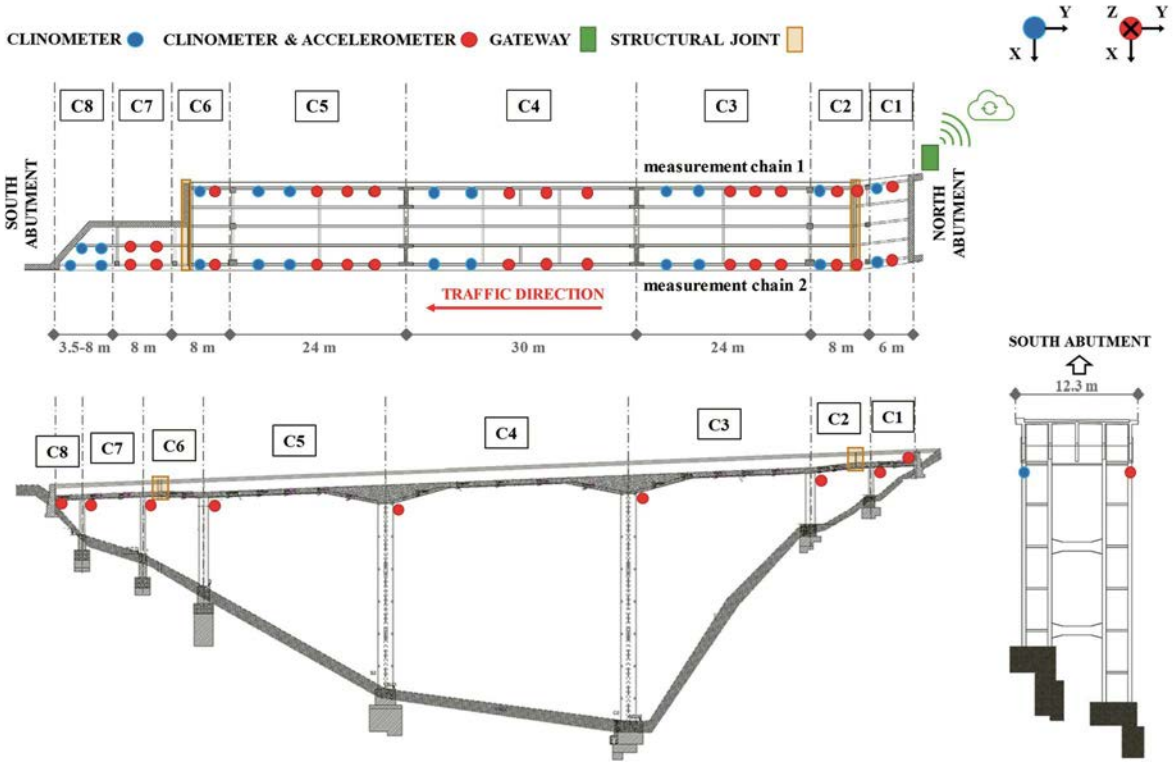

Figure 4. Case study 2: Geometry and SHM system.

second of sampling). The robustness of the control is ensured by working on groups of sensors, preventing the notification of false positives due to anomalies in sensor signals. The algorithm was activated after defining the vibrational baseline behaviour of the structure over a consistent 3-month training period, computing thresholds with a data-driven approach, and proved effective in triggering maintenance interventions.

Indeed, in February 2021, about 3 months after the activation of the Anomaly Indicator, the SHM system notified the exceedance of the thresholds for a group of sensors located near the expansion joint between spans C1 and C2, indicating an anomalous increase in vibration levels in that area. The other Key Performance Indicators (both static and dynamic, Model and Data-Driven) did not show any alerts or anomalies.

The anomaly detection triggered a site inspection, which revealed several defects along the entire pavement and significant local damage to the expansion joint where the anomaly was identified. This confirmed that the acceleration impulses due to vehicular traffic were accurately correlated with poor road surface conditions and local damage. As a result, proactive maintenance interve-tions were initiated, and the structural joints were promptly replaced in April 2021.

However, the intervention was not fully effective. By June 2021, the viaduct still showed increased STD values, progressively spreading across the entire deck. The Sacertis SHM system alerted the road operator in near-real time about potential damage. It was confirmed that poor installation conditions of the joints, with bitumen flowing within the joints, were hindering proper structural thermal expansion. A second intervention was required in July 2021. After this intervention, structural vibrations returned to standard values.

The anomaly detection procedure uncovered vibrational anomalies and localized damages, ultimately verifying the effectiveness of maintenance interventions. These findings supported asset management in optimizing proactive maintenance strategies.

3. CONTINUOUS MONITORING FOR A COMPREHENSIVE STRUCTURE BASELINE CHARACTERIZATION

3.1. The case study

The viaduct is a reinforced concrete structure built in the late 1950s and located in Northern Italy [13]. It spans approximately 118 meters in total length, segmented in three independent portions by two structural joints. The external sections measure respectively 18m (2 spans) and 8m (1 span), while the central one is 92m long and is composed by 5 continuous spans (longest span 32m). The deck girder is composed of 5 beams with variable height from 2.9m to 3.7m, and a slab with a thickness of 0.27m. The pier frames feature two H-shaped concrete cross sections, jointed by transverse beams, as depicted in Figure 4.

The monitoring system is composed by a wired network of 67 biaxial MEMS clinometers and 38 triaxial MEMS accelerometers, installed on the edge beams in the key points for a comprehensive diagnostic of the static and dynamic behaviour as shown in Figure 4, except for spans C7 and C8 that, due to installation difficulties, have a dedicated sensors layout. Two

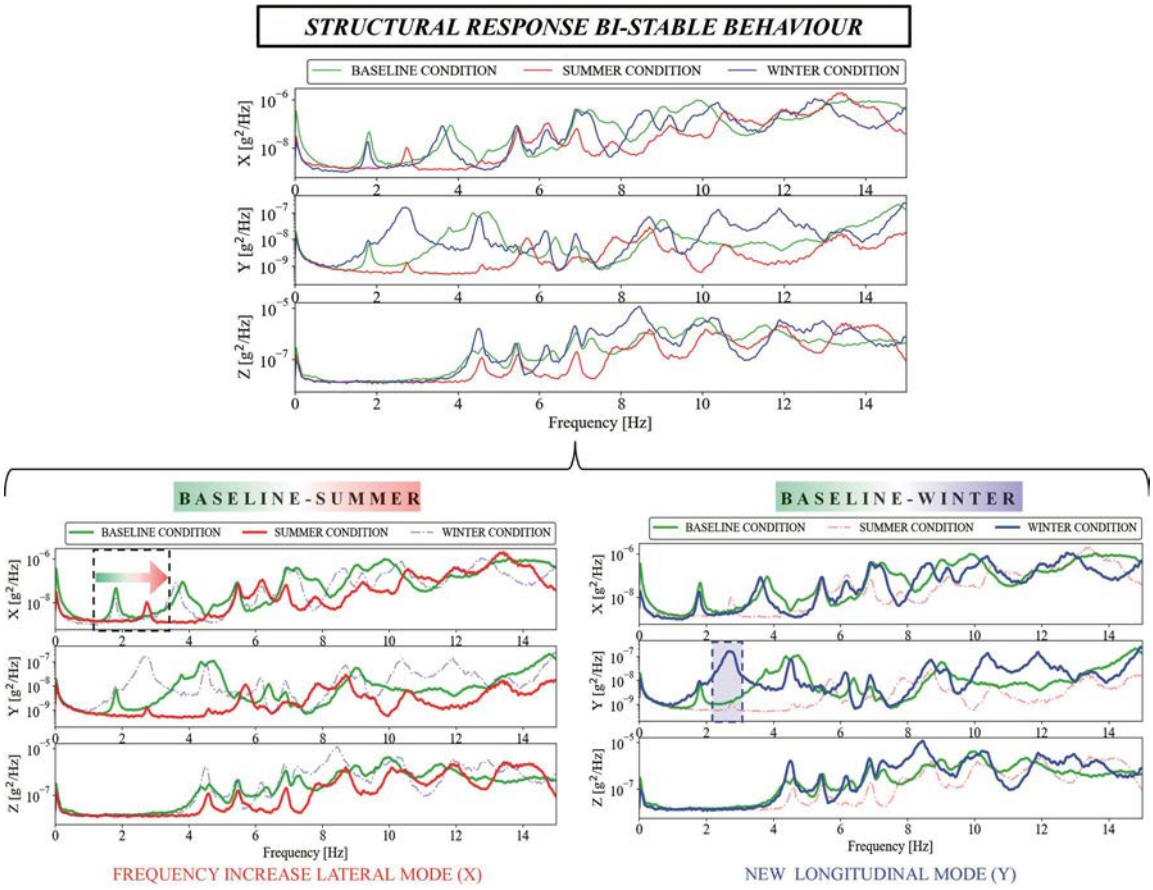

Figure 5. Case study 2 - Seasonal dynamic configurations.

networks managed by the same IoT gateway enable the collection of both slow-varying data and dynamic data: the former uses a power-line-based architecture, and the latter employs a CAN-BUS network. The data are pre-processed and filtered at the gateway level, with only significant information sent to the cloud for further analysis and long-term storage. The biaxial MEMS clinometers installed on the viaduct sample at 208Hz and measure along two orthogonal axes: Y-axis (longitudinal in the plane of the deck), X-axis (transversal in the plane of the deck). Accelerometers sample at 100Hz and measure along three orthogonal axes: Z-axis (vertical), Y-axis (longitudinal in the plane of the deck), X-axis (transversal in the plane of the deck). Anomaly conditions detected by different sensors, correlated in space and time, along with multi-parameter cross-checks, enhance the SHM system reliability by minimizing false alarms. When thresholds are exceeded, alerts are sent to the cloud with attached severity metadata for appropriate handling.

3.2. *Monitoring history*

In the case of this application as well, a Model-Driven approach was chosen as monitoring strategy. The system was installed in the summer of 2019, and after an initial characterization period, both Model and Data-Driven algorithms for selected KPIs were activated. The monitoring of the structure dynamic behaviour was conducted in both the time and frequency domains, aiming to track vibrational levels (time-domain) and modal parameters (frequency-domain).

Thanks to these controls, this case study serves as an example of how a permanent monitoring system can be more effective and advantageous than a discrete one. Additionally, the importance of a Model-Driven approach for gaining complete knowledge of the bridge is demonstrated, highlighting the need for a structural interpretation by technical and specialized personnel to comprehensively diagnose any anomalies triggered by the system.

Before delving into why this case study exemplifies the benefits of continuous monitoring, it is necessary to provide a brief description of the monitoring history of the structure.

After three months from the installation of the system, the baseline of the structure was established. By focusing on accelerometers data, the main vibration modes of the structure were identified and characterized with the relative modal parameters. This dynamic information, along with data obtained from specific proof loading tests, was used to feed a genetic algorithm to update the numerical model, making it representative of the actual behaviour of the structure. The baseline was established in autumn (Table 1), and the natural frequencies were used as a reference for activating an automatic control to monitor any variations in their values (thresholds were set based on both damage simulations on the FEM model and Data-Driven approaches). The choice of a permanent monitoring system demonstrated its advantages by highlighting the presence of different dynamic configurations of the bridge that change based on external thermal conditions. Continuous monitor-

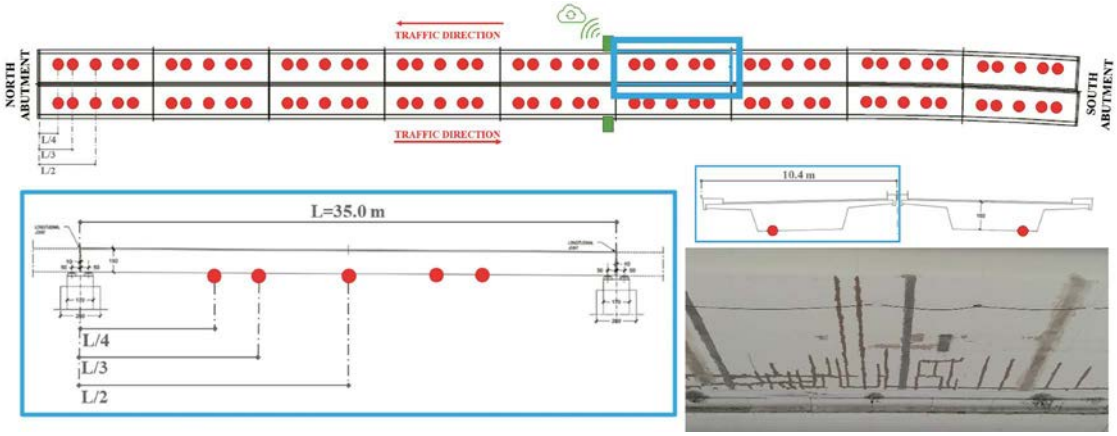

Figure 6. Case study 3 – Geometry, SHM system and view of the cracking pattern after the inspection.

TABLE 1.
Case study 2 - Frequency values in different seasonal conditions.

MODE OF VIBRATION	SPRING/AUTUMN FREQUENCY [Hz]	SUMMER FREQUENCY [Hz]	WINTER FREQUENCY [Hz]
Lateral	1.83	2.80	1.80
Longitudinal	-	-	3
Flexural	4.40	4.77	4.60
Flexural	8.60	9.40	8.45

ing of frequency values over time revealed a modification in the modes of vibration during the winter season, when a longitudinal mode appeared, as shown in the PSD of Figure 5, along with slight modifications to other minor modes of vibration. This new dynamic configuration persisted only for a few months: once the winter season ended and temperatures began to rise, a return to the baseline configuration was observed in the spring season.

With the arrival of summer, the structure experienced a new thermal condition, resulting in a new and previously unobserved dynamic behaviour. In this season, the lateral mode showed a considerable increase in frequency value and a change in the modal shape, as highlighted in Figure 5.

With the help of the FEM model, the observed variations in the modes were correctly interpreted, identifying the structural reasons for these changes. Numerical simulations demonstrated that the bridge undergoes different static schemes based on external thermal conditions and the varying states of the expansion joints, which were modelled with non-linear links. By adjusting the stiffness of these links for all translational degrees of freedom (in both the horizontal and vertical planes) according to the state of the joints (closure/opening) over a year, the three different configurations were reproduced. For example, in summer, the longitudinal expansion of the deck likely causes the joints to close, leading to a global stiffening of the structure. This effect would be even more pronounced if debris were present inside the joints.

In conclusion, this case study proved how continuous monitoring, combined with a Model-Driven approach, can effectively and accurately characterize the structure. If discrete dynamic tests were performed instead, there could be a misunderstanding, mistaking changes in dynamic parameters due to temperature for modifications induced by damage.

4. MONITORING FOR ASSESSING THE EFFICACY OF RETROFITTING INTERVENTION

4.1. The case study

The structure is a highway prestressed concrete bridge located in Northern Italy and constructed in the early 1980s [14]. The bridge consists of two independent decks, one per carriageway, each featuring nine simply supported 35m spans, for a total length of 315m. The cross section of the deck is a prestressed concrete slab with a constant depth of 1.5m and two transversal cantilevers. Figure 6 shows a view of the bridge.

The SHM system was installed to monitor the evolution of the structural behaviour tracking an eventual damage progression because, during a periodic inspection, it was found a widespread crack pattern in the midspan region of a span. The concrete cracking was attributed to tendon failure due to structural aging, the corrosive effects of deicing salts and the increased weight and volume of traffic loads.

To restore bearing capacity and safety levels, it was designed a deck strengthening intervention using an external prestressing system placed on the bottom surface of the slab.

The SHM system enabled to monitor the bridge behaviour pre-, during and post-intervention. In the short term, it was used to avoid traffic closure while awaiting reinforcement and to measure structural effects associated with repairing. In the long term, it monitored structural response evolution, facilitating more efficient condition-based maintenance instead of traditional time-based methods.

The SHM system was designed to monitor both static and dynamic behaviour in continuous. It consists of MEMS biaxial clinometers and triaxial accelerometers, located near the edg-

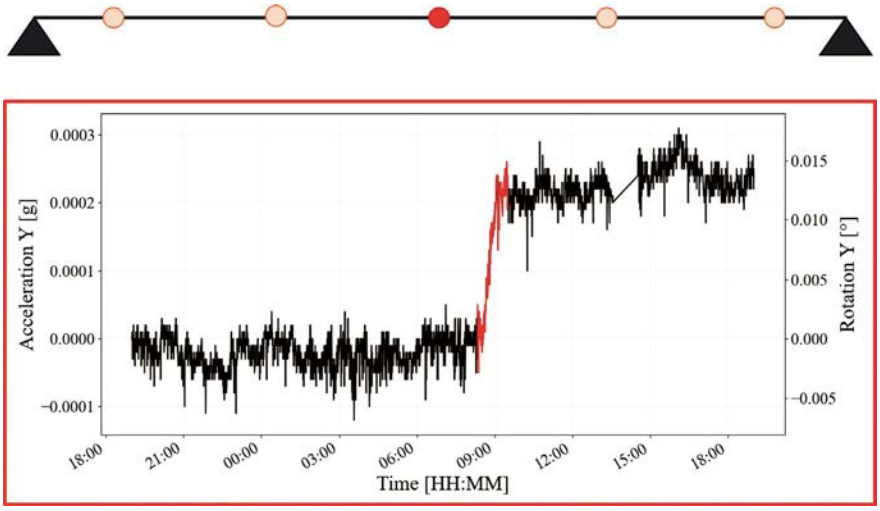

Figure 7. Case study 3 - static response after the retrofitting intervention.

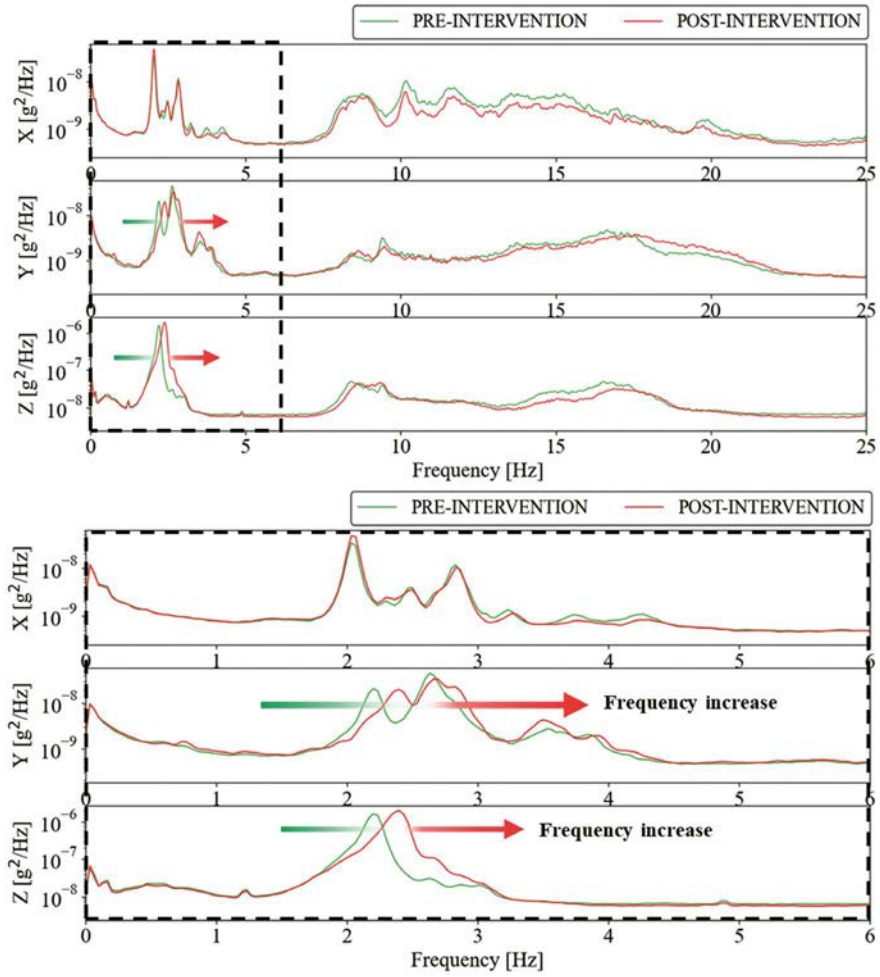

Figure 8. Case study 3 - dynamic response after the retrofitting intervention.

es of the bottom surface of the slabs. Sensors are wired and connected to a gateway per carriageway for the collecting and the pre-processing of the data before their storage into a cloud system. The layout of the SHM system is shown in Figure 6: for each span, 5 clinometers and 5 accelerometers (for a total amount of 90 sensors per carriageway) are positioned at the quarters, the thirds and the midspan. Accelerometers sample at 100Hz along three orthogonal axes: Z-axis (vertical), Y-axis (longitudinal in the plane of the deck), X-axis (transversal in the plane of the deck). Clinometers, instead, acquire when queried from the gateway according to a polling cycle and have only the two axes laying in the horizontal plane (X-axis and Y-axis).

4.2. Monitoring history

The system installed before of retrofitting intervention allowed to control the structural response changes during and after the activities both from static and dynamic point of view. Figure 7 and Figure 8 summarize an overview of the main results obtained analysing the data collected by sensors:

- Clinometers detected a sudden rotation shift following the application of external prestressing. Starting from the measured rotations, it was then possible to reconstruct the deformed shape due to external prestressing by calculating the midspan camber and comparing it with the one predicted by the designer to evaluate the effectiveness of the intervention. Notably, the intervention was executed without any traffic closing on the viaduct, enabling the sensors to capture deformations caused by moving vehicles. Figure 7 shows tilt measurements in the middle-span.
- Accelerometers data were used to assess the deck natural frequencies pre- and post-maintenance. Figure 8 displays the Power Spectral Density (PSD) curves for X (transverse), Y (longitudinal), and Z (vertical) directions. It can be noted an increase of the frequency values observed especially in the Y and Z axes, reflecting the stronger influence of prestressing on the Y-Z plane.

From an overall analysis of the response, it emerged that, following the retrofitting intervention, the safety levels of the structure were restored in accordance with the provisions of the current regulations. The change in behaviour was observed significantly both from a static perspective (clinometers) and dynamic perspective (accelerometers). This allowed for a near real-time confirmation of the effectiveness and proper execution of the planned interventions, increasing confidence in the repaired structure.

5. CONCLUSIONS

Many infrastructures in Europe and around the world have reached or are close to reaching their designed lifespan. This situation presents a challenge for Road Administrators to find a reliable strategy for managing these aging structures, ensuring safety levels, and planning retrofitting interventions when needed. One possible solution is to install monitoring systems on the most critical infrastructures to continuously track any unfavourable trends in their behaviour.

Following this concept, this paper presents some real-life examples of how powerful the application of a Structural Health Monitoring (SHM) system can be in obtaining useful information about the behaviour of structures, aiding in their management. The paper focuses not only on the primary damage detection objective but also on all the benefits that can arise from the application of a permanent monitoring system. This idea is supported by three different case studies, which respectively highlight how monitoring was effective in triggering ordinary maintenance interventions, evaluating the efficacy of a retrofitting intervention, and gaining comprehensive knowledge of the structure. This is indispensable to prevent misclassification problems and to correctly identify deviations from a baseline that might not be unique but variable under different external thermal conditions, as demonstrated in the second case study proposed in the paper. The benefits of adopting a monitoring system are even greater if a Model-Driven approach is utilized. This approach aids in interpreting the results of monitoring, setting damage scenarios on the relevant performance indicators, and identifying the real causes of anomalies detected by the system, discerning damage from all other possible causes of changes in the system behaviour.

References

[1] CEDR, TEN-T (Roads), (2017). 2017 Performance Report.

[2] ib Bulletin No. 109 (2023). Existing concrete structures life management, testing and structural health monitoring - State-of-the-art-report. ISBN 978-2-88394-171-7.

[3] Farrar, C. R., Worden, K., (2012). Structural Health Monitoring: A Machine Learning Perspective. Wiley, ISBN 9781119994336.

[4] A. Cury, D. Ribeiro, F. Ubertini, M. Todd, (2022). Structural Health Monitoring Based on Data Science Techniques. Springer International Publishing, ISBN 9783030817152.

[5] Lynch J. P., Sohn H., Wang, M.L., (2014). Sensor Technologies for Civil Infrastructures, Volume 2: Applications in Structural Health Monitoring. Woodhead Publishing Series in Civil and Structural Engineering. ISBN 9781782422426.

[6] Strauss A., Bigaj-van Vliet A., Daró P., Van Meerveld H., (2022). Condition-states and low limit maintenance thresholds of transport infrastructures in an European Context, fib Congress Oslo. ISBN 9782940643158 - ISSN 26174820.

[7] Daró, P., Alovisi, I., Mancini, G., Negri, S., Bigaj-van Vliet, A., van Meerveld, H., (2022). Lessons learned from proactive maintenance practices for concrete bridges, fib Congress Oslo. ISBN 9782940643158 – ISSN 2617-4820.

[8] Alovisi, I., La Mazza, D., Longo, M., Lucà, F., Malavisi, M., Manzoni, S., Melpignano, D., Cigada, A., Darò, P., Mancini, G. (2022). New Sensor Nodes, Cloud, and Data Analytics: Case Studies on Large Scale SHM Systems. Struc-tural Integrity 21:457-484.

[9] Darò, P., Alovisi, I., Mancini G., Longo M., La Mazza D., Cigada A., (2023). Dense sensing on roadway bridges network: new approach to data-informed assessment. https://doi.org/10.1002/cepa.2024.

[10] Alovisi, I., Cigada, A., La Mazza, D., Longo, M., (2023). Bridges continuous dense monitoring network: A framework to support the infrastructures assessment and management process. In Proceedings of the 11th International Conference on Bridge Maintenance, Safety and Management, IABMAS 2022. ISBN 9781003322641.

[11] Darò, P., De Cicco, B., La Mazza, D., Longo, M., Chiariotti, P., Manzoni, S., Cigada, A. Mancini, G. (2023). Thermal Effects on Bridges Dynamic Behaviour. In: Limongelli, M.P., Giordano, P.F., Quqa, S., Gentile, C., Cigada, A. (eds) Experimental Vibration Analysis for Civil Engineering Structures. EVACES 2023. Lecture Notes in Civil Engineering, vol 432. Springer, Cham. https://doi.org/10.1007/978-3-031-39109-5_76.

[12] Basone, F., Cigada, A., Darò, P., Lastrico, G., Longo, M., Mancini, G. (2023). Concrete Bridges Continuous SHM Using MEMS Sensors: Anomaly Detection for Preventive Maintenance. In: Rizzo, P., Milazzo, A. (eds) European Workshop on Structural Health Monitoring. EWSHM 2022. Lecture Notes in Civil Engineering, vol 253. Springer, Cham. https://doi.org/10.1007/978-3-031-07254-3_47.

[13] La Mazza, D., Basone, F., Longo, M., Darò, P., Cigada, A. (2023). Anomaly Detection Through Long-Term SHM: Some Interesting Cases on Bridges. In: Noh, H.Y., Whelan, M., Harvey, P.S. (eds) Dynamics of Civil Structures, Volume 2. Conference Proceedings of the Society for Experimental Mechanics Series. Springer, Cham. https://doi.org/10.1007/978-3-031-05449-5_7.

[14] Cigada, A., Lucà, F., Malavisi, M., Mancini, G. (2021). Structural Health Monitoring of a Damaged Operating Bridge: A Supervised Learning Case Study. In: Pakzad, S. (eds) Dynamics of Civil Structures, Volume 2. Conference Proceedings of the Society for Experimental Mechanics Series. Springer, Cham. https://doi.org/10.1007/978-3-030-47634-2_19.

Disponible en **www.hormigonyacero.com**
https://doi.org/10.33586/hya.2025.4100

On Conceptual Design, Assessment of Existing Structures, Research and Standards

Sobre diseño conceptual, evaluación de estructuras existentes, investigación y normas.

Aurelio Muttoni[a, b, c]

[a] *Professor Emeritus, Ecole Polytechnique Fédérale de Lausanne, Switzerland.*
[b] *Founding partner, Lurati Muttoni Partner, Studio d'ingegneria SA, Mendrisio, Switzerland.*
[c] *Founding partner, Muttoni Partners Ingénieurs Conseils SA, Ecublens, Switzerland.*

Recibido el 4 de junio de 2024; revisado el 11 de noviembre de 2024, aceptado el 18 de febrero de 2025

ABSTRACT

The author has had the good fortune to be active for the past four decades almost uninterruptedly as a designer, researcher, teacher, and standards-writer. Over this time, he has been observing a tendency for an increased degradation of the profession, with the segregation between education, research, and practice. It is the opinion of the author that each of these fields has been experiencing individual advances isolated from a holistic view of the profession, compromising the evolution and, consequently, the impact of civil engineers in society. Consequently, the profession is becoming less and less attractive for bright and motivated young people. It is the opinion of the author that such trend can only be inverted by placing more emphasis on the creative and intellectual components in each of the fields of education, research, and practice, as well as by bridging the gaps between them. These considerations are supported by personal experience which is shared in this article by presenting some instances of conceptual designs.

KEYWORDS: Conceptual design, dimensioning, assessment, research, standards.

RESUMEN

El autor ha tenido la suerte de trabajar durante las últimas cuatro décadas casi ininterrumpidamente como diseñador, investigador, profesor y redactor de normas. Durante este tiempo, ha observado una tendencia a la degradación creciente de la profesión, con la segregación entre educación, investigación y práctica. En opinión del autor, cada uno de estos campos viene experimentando avances individuales aislados de una visión holística de la profesión, comprometiendo la evolución y, consecuentemente, el impacto de los ingenieros civiles en la sociedad. En consecuencia, la profesión resulta cada vez menos atractiva para los jóvenes brillantes y motivados. En opinión del autor, esta tendencia sólo puede invertirse haciendo más hincapié en los componentes creativos e intelectuales de cada uno de los ámbitos de la enseñanza, la investigación y la práctica, así como colmando las lagunas existentes entre ellos. Estas consideraciones se apoyan en la experiencia personal, que se comparte en este artículo presentando algunos ejemplos de diseños conceptuales.

PALABRAS CLAVE: Diseño conceptual, dimensionamiento, evaluación, investigación, normas.

* Persona de contacto / *Corresponding author*:
Correo-e / *e-mail*: aurelio.muttoni@epfl.ch (Aurelio Muttoni)

How to cite this article: Muttoni, A. (2026). On Conceptual Design, Assessment of Existing Structures, Research and Standards. *Hormigón y Acero*. 77(308): 175-190. https://doi.org/10.33586/hya.2025.4100

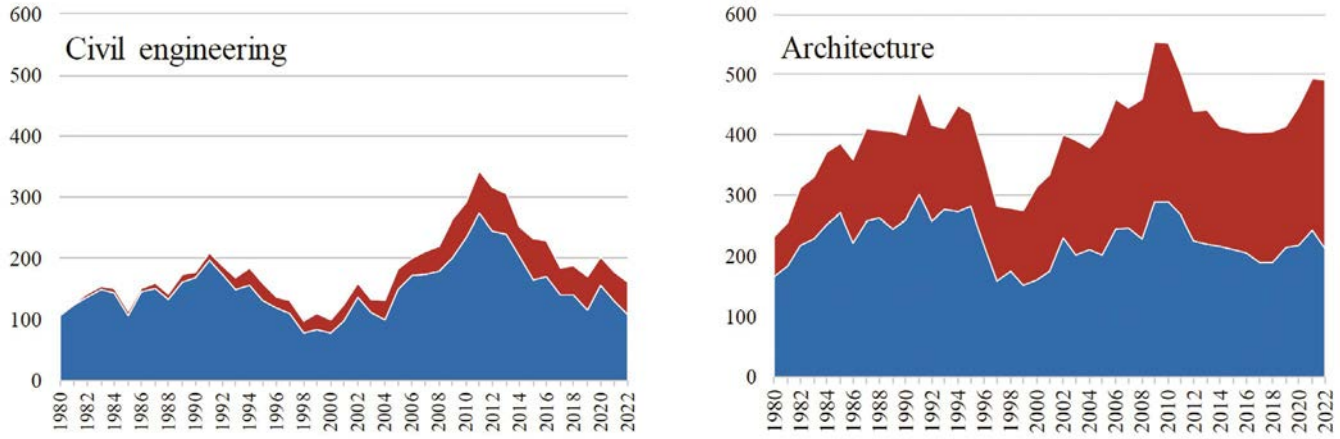

Figure 1. Number of students in civil engineering and architecture starting their curricula at both technical universities in Switzerland (male in blue; female in red, data by the Swiss Federal Office of Statistics).

1. INTRODUCTION

Several great structural engineers of the last century have already emphasised the importance of structural design in the work of engineers (Maillart [1], Nervi [2], Freyssinet [3], Torroja [4], Schlaich [5]). Although the profession of civil engineering shares the same roots as those of architecture (until the 18th century, they were simply referred to as builders), the separation became necessary with the industrial revolution. At that moment, construction using relatively expensive materials (cast iron and steel, and later reinforced concrete) made necessary to calculate and dimension them, which required new skills and specific education. However, for at least a century now, the scientific side of structural engineering (analysis, verification, dimensioning) has taken over [6] and nowadays, our masters' warning is even more justified. If we compare ourselves with our architect colleagues, with whom we still share the design and project activity, the evolution of the last few decades has been rather unfavourable. The trend in students' number in both disciplines bears witness to this (Figure 1). Although the trends were similar until recently, and essentially correlated with the economic situation in the construction industry, for some time now we have been witnessing a reverse trend (see Figure 1).

We should be concerned by the fact that our profession is seen by young people, perhaps wrongly, as being too technocratic, having little to do with solving society's challenges, and attracts therefore fewer and fewer young people. It is also worth mentioning that, unlike architecture, where in some universities, more than half the students are female (Figure 1), our profession is having difficulty attracting young women.

The challenges of climate changes and artificial intelligence, with all their risks and opportunities, make it more urgent to reflect on the current situation and possible outcomes. The thesis developed in this text is that engineers should once again be able to free up more time for design and project-related activities, and with more creativity in all activities.

2. ABOUT DESIGN, CONCEPTUAL DESIGN, AND CREATIVITY

First of all, what is the most noble and interesting activity of the engineer, and what should be the added value of the engineer's activity to the society?

According to Wikipedia, "*engineers, as practitioners of engineering, are professionals who invent, design, analyse, build and test machines, complex systems, structures, gadgets and materials to fulfil functional objectives and requirements while considering the limitations imposed by practicality, regulation, safety and cost*" [7]. Interestingly, in this definition, the creative component of engineer's work is listed at the beginning of the engineer's activity. With this respect, the etymology is also interesting: the word *engineer* (Latin ingeniator) is derived from the Latin words "*ingeniare*" (to invent, to plan, to devise) and "*ingenium*" (cleverness, therefore, "*engineer*" has the same etymology as "*genius*").

Design is a word that has among civil engineers, especially in English, a too broad meaning that often lends itself to confusion. To avoid misperceptions, the word '*design*' should be reserved for the creative and intellectually noble part of the engineer's activity, while another definition should be reserved for the technical part, associated with dimensioning and verification. Current standards for structural engineering have also contributed to the misperception surrounding the word *design*. In fact, *design values* used in our standards [8,9] have very little to do with design, being rather values needed to dimension a new structure or assess an existing one (the definitions "valor de cálculo" in Spanish, "Bemessungswert" in German, "valeur de calcul" in French and "valore di calcolo" in Italian correspond better to the concept than the English term "design value").

To overcome this misperception related to the word design (here again, this is mainly a problem of the English language: in German, Italian, and French, we respectively differentiate Gestaltung / Bemessung; progetto / dimensionamento; projet / dimensionnement and certainly other languages also make this distinction), the definition of *conceptual design* was introduced at the end of last century when a congress called "Conceptual De-

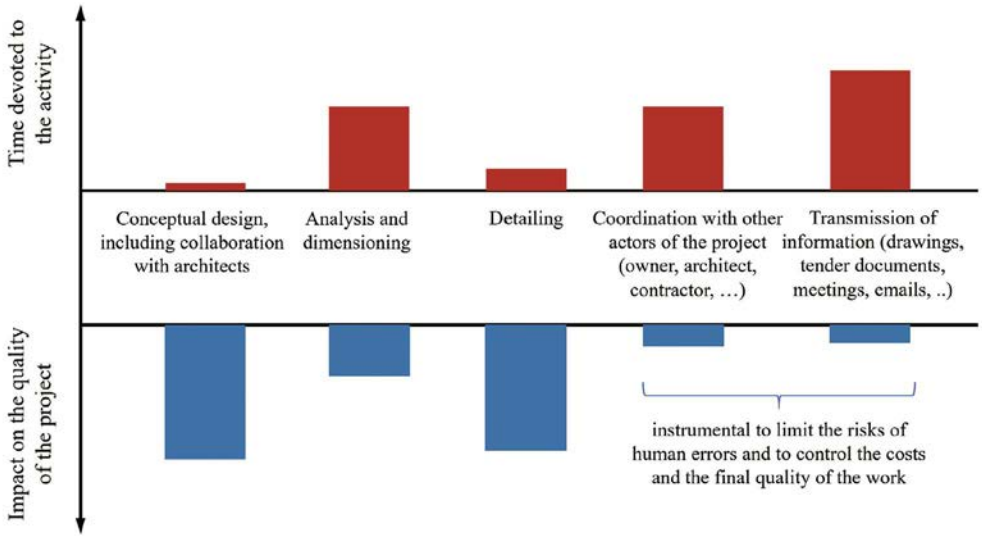

Figure 2. Significance of conceptual design in terms of time devoted and impact on the quality of the structure compared to other engineer's activities.

sign of Structures" was organised by Jörg Schlaich at Stuttgart for the International Association for Shell and Spatial Structures in 1996 [10].

With this respect, the International Federation for Structural Concrete (*fib*) took the initiative, based on a precursor idea by Hugo Corres, to organise a series of symposia on Conceptual Design every two years. The first event took place in Madrid in 2019 followed by the symposia in Attisholz (Switzerland) in 2021 and in Oslo in 2023, to be pursued by events in Rio de Janeiro in 2025 and in Italy in 2027.

When we initiated the 2021 symposium with my colleague Joseph Schwartz, we discussed much about what conceptual design is (and what is not). During the symposium, it became evident that the variety of definitions of conceptual design was no less than the number of participants at the conference. However, we believe that conceptual design should be defined to avoid the risk that at the end, everything is considered belonging to it (in fact, to avoid again the confusion related to the term "design"). For this reason, we have tried to formulate a definition in our contribution to the book "Conceptual Design of Structures" [11]:

> "*The term Conceptual Design of Structures denotes the intellectual activity of developing a highly appropriate structural solution - in terms of structural system, shape, materialization, construction method, detailing, etc. – for a given purpose in a defined context. When related to buildings, it follows the programmatic idea of a reconciliation between the discipline of engineering and architecture through the reciprocal integration of load-bearing structure and architectural design concept, with a unified understanding of the interplay of form and load-bearing capacity. This activity is nurtured by knowledge of the functioning of structures and of construction history - although it should never be limited to uncritically applying already known solutions*".

The experience and the success of the Conceptual Design Symposia organized by *fib* have shown the need to increase the importance of creativity in the contemporary work of structural engineers. Current and future challenges related to sustainability aspects, to a better distribution of resources in the world, to the correct use of artificial intelligence (increasing the beneficial results and minimising the threats), to the lack of attractiveness of our profession among the younger generations, to the decreasing motivation and increasing frustration of some designers confirm these needs and make a rethinking of our priorities even more important. The structural project and the creativity required to improve it should be at the heart of our commitment. Creativity is also a key aspect to make structural engineering more interesting, to ensure the engineer's contribution as a significant added value, to keep current colleagues motivated in our field and to attract more talented young people to our profession.

All the phases starting from the initial conceptual design to the final execution in the construction site of a structure for a building or for an engineering work such as a bridge require a broad range of skills, the collaboration of many actors within an engineering office, as well as collaboration and interaction with many external actors. Personal experience shows that the creative part is often the most rewarding and has often the most impact on the final quality of a structure, even though it requires relatively little time commitment (Figure 2). In the examples shown in Figure 3, the initial phase of structural conceptual design, starting with the study of the context, the analysis of needs, the proposal of a few sketches up to a pre-dimensioning (typically a very simple manual calculation), took relatively little time, but was then followed by other phases in which everyone's commitment and perseverance were equally decisive in achieving the final quality of a structure. With this respect, detailing plays also a major role and without a professional coordination with other actors (owners, architects, contractors, other specialists, …) and an efficient transmission of knowledge between them, it would be impossible, nowadays, to successfully finalise a project. In addition, efficient coordination and transmission of information are instrumental to limit the risks of human

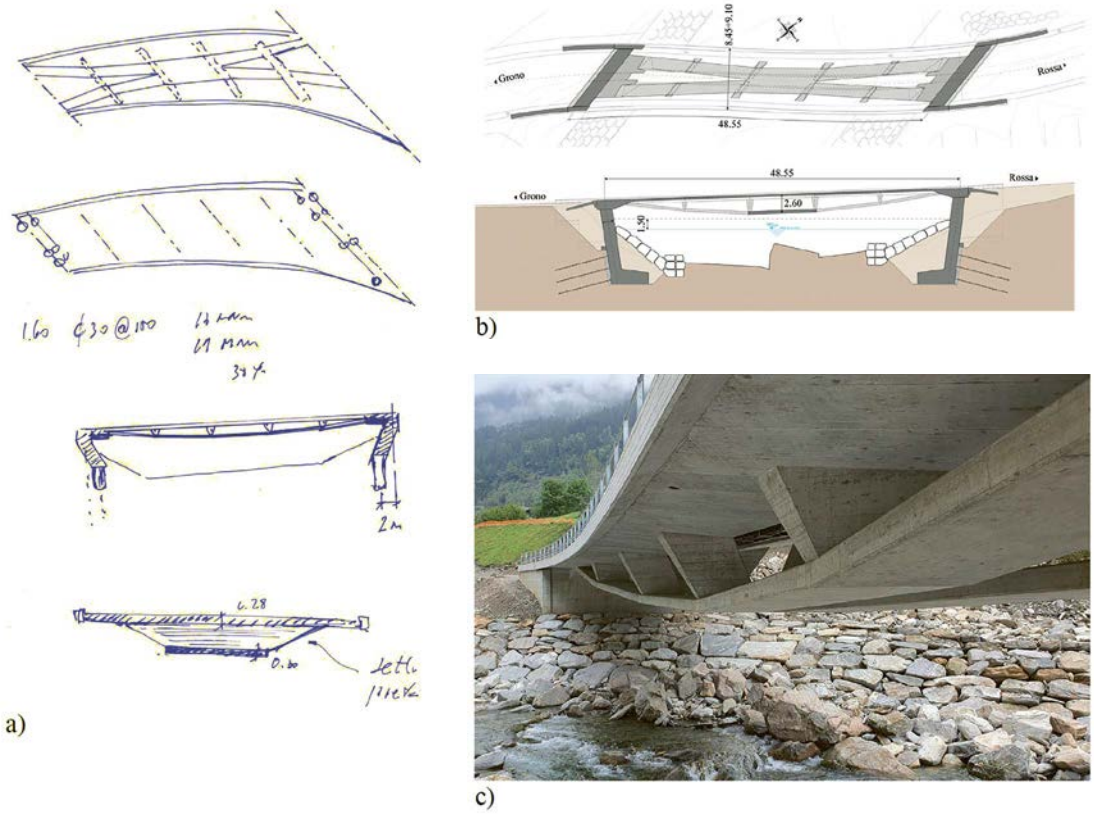

Figure 3. Bridges Auriglia and Loveira over the Calancasca river, Southern Switzerland, (a) sketches for the conceptual design of the Loveira bridge, (b) final design of the Auriglia bridge and (c) photo of the Auriglia bridge (Lurati Muttoni Partner civil engineers, A. Muttoni structural designer) [12].

errors and to control the costs and the final quality of the work. It is therefore fair to acknowledge everyone's contribution, but neither should one fall into the temptation of wanting to quantify contributions only in terms of time and effort. Unlike architectural projects, which have many similarities with our own projects, and where the author of the project is clearly defined, in engineering projects there is often a tendency to keep the role of the *author of the conceptual design* quiet. This is clearly counterproductive. Without falling into the opposite excess, which is common in other fields, where only the author of the project is often mentioned, in our structural projects, this role should be emphasised more so as to motivate young colleagues to be more involved in *conceptual design of structures*. We should therefore speak more often of '*design author*' for engineering works, '*author of structural design*' for buildings in which there is a real creative contribution on the part of the engineer, or simply of '*structural designer*'.

Still with respect to Figure 2, according to the experience of the author, the situation has deteriorated in the last decades. The introduction of new technologies, accelerating phases such as analysis and the preparation of drawings, instead of liberating more time for the creative component of the profession, has been used to coordination and administrative tasks. This trend must absolutely be inverted since these technological advances will continue (see for instance artificial intelligence). The risk is that the weight of the creative component of our profession will further decrease with time.

Civil engineers should take action and use the new technologies in their favour, for instance using the automation for repetitive and administrative tasks and improving the quality of the projects by dedicating more time to the intellectually challenging tasks instead of searching to reduce the time devoted to the project.

In the design of structures, a clear definition of the required function and a knowledge of possible construction methods and their economic costs, planning and environmental implications are necessary. In addition, an ability to analyse the constraints and particularities of the site with the landscape and the built environment, a deep understanding of how structures work and a good knowledge of construction history are essential. In this context, it is not a question of adopting uncritically well-known solutions, but of taking inspiration from them, adapting, optimising, and developing them to better meet the requirements of the new project. A creative contribution leads to an evolution of the adopted structural solution. In structural design, revolutionary and disruptive solutions are rare, but continuous evolution is possible and desirable. It is often a question of studying with a critical and curious eye, and, of course, of understanding known solutions, so as to be able to improve them. Our own previous projects are often a privileged source of inspiration because the potential for improvement is better known as a result from the lessons learnt during the completion of the

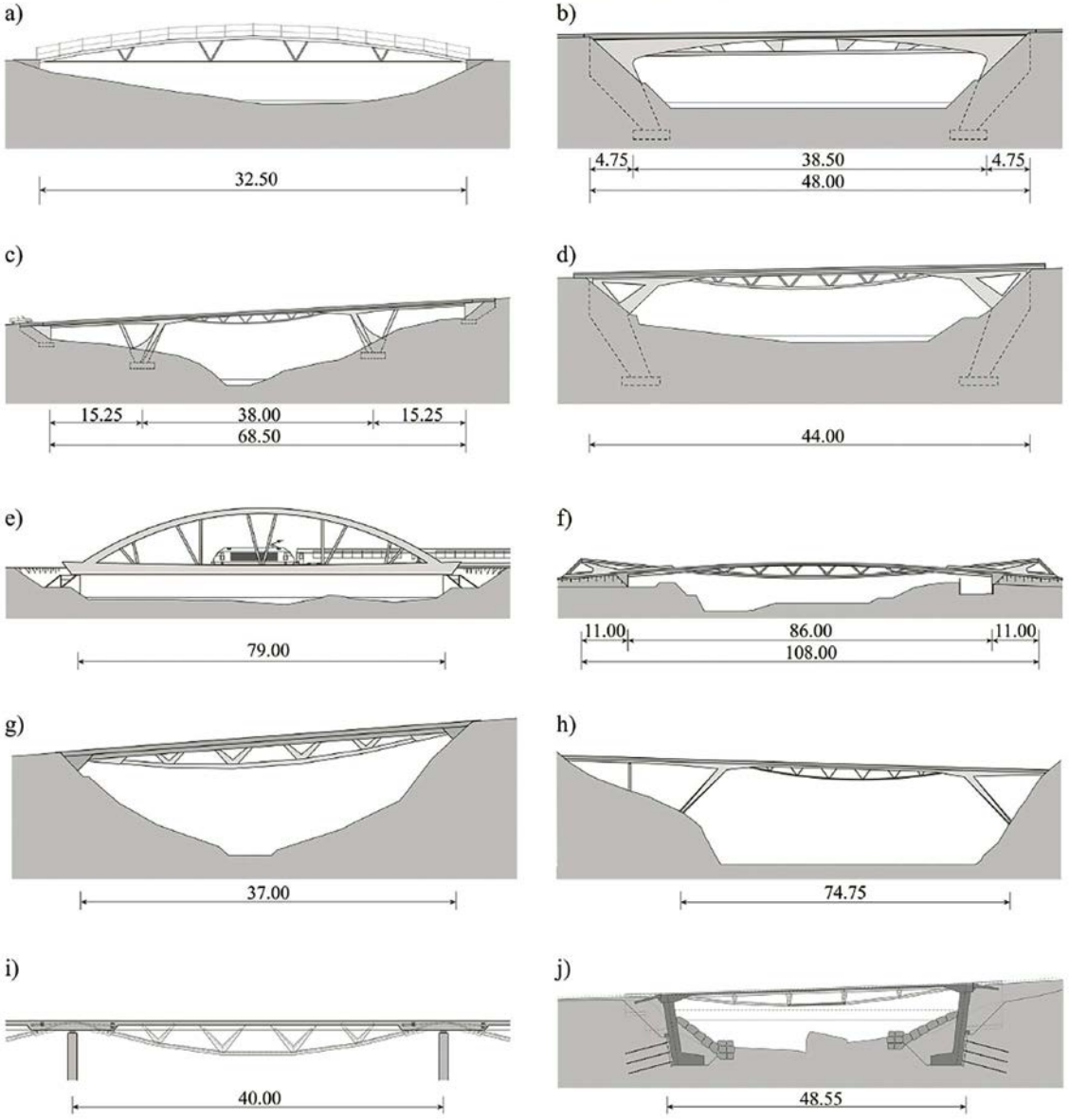

Figure 4. Development of under-spanned structures and bowstrings for footbridges and bridges; (a) pedestrian bridge over the River Ticino at Faido, Switzerland, 1987; (b) bridge over the river Brenno at Loderio, Switzerland, 1993-94; (c) Bridge at Odogno, Sitzerland, 1995-96; (d) Bridge over the Ticino river at Villa Bedretto, Switzerland, 1996, (e) Design competition for a railway bridge in Switzerland, 1992; (f) Design competition over a river in Senigallia, Italy, 1995; (g) Competition for a bridge in Corticiasca, Switzerland, 1997; (h) Project for a Bridge over the Reddalskanalen, Norway, 1996; (i) Study for continuous bridges in Norway, 1997; and (j) Bridge Auriglia over the Calancasca river, Switzerland, 2018-2021 (see also [13,15,12]).

work. Never being completely satisfied with what we have designed and realised is an approach that makes it easier to find a better solution for the next projects. Nevertheless, every project is different, in the sense that the sites, challenges and constraints are different.

Sometimes, innovative solutions result from a desire to improve a project for a very specific situation and can then be adapted for very different cases. The road bridge shown in Figure 3, for instance, is the result of a long evolution that began three decades before when the aim was to design for a client with very limited means the most economical and lightest footbridge possible. The initial idea of a very slender bowstring had the advantage of very simple fabrication, but the problem of being too sensitive to variable loads. To solve such issue, V-shaped tubular connecting elements were introduced between the top chord and the tie-rod made of reinforcing bars. The result was a structure that was halfway between an under-spanned structure and a Vierendeel beam (Figure 4a, [13]). It is interesting to note that Mamoru Kawaguchi arrived at a similar solution a few years later for his Inachus bridge at Beppu, Japan, but following a completely different path (in that case, it was the removal of some diagonals in a lenticular truss that led to the same structural solution [14]). The great efficiency of the first footbridge built in 1987, designed when I was still a PhD student, then persuaded me that bridges and other structures could be built adopting the same structural solution. A few years later, the opportunity arose to apply the same idea to the construction of a road

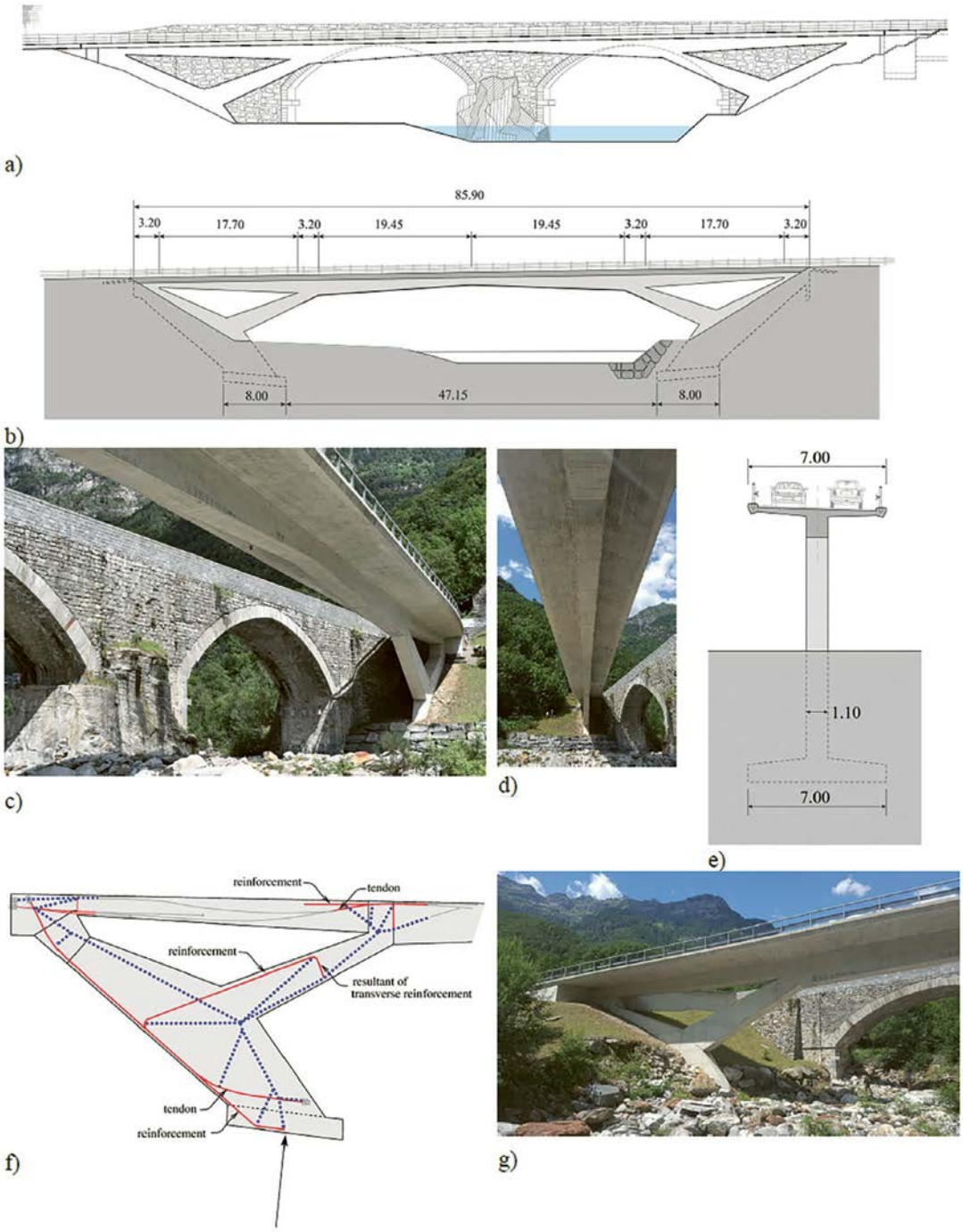

Figure 5. Verzasca Bridge at Frasco, Switzerland; (a) elevation showing the existing masonry bridge; (b) scheme of the system; (c), (d) and (g) photos; (e) cross section; and (f) strut-and-tie model of the abutment (Lurati Muttoni Partner civil engineers, A. Muttoni structural designer, with Michele Arnaboldi architect) [17].

bridge (figure 4b). The short length of the structure (only 50 m) meant that an integral solution, with neither expansion joints nor mechanical bearings, was suitable. The deck was therefore clamped in two piers to form a frame. The choice of material, prestressed concrete for both the deck and the bottom chord, meant that the V-shaped tubular elements of the footbridge were replaced by trapezoidal reinforced concrete walls. A visually different solution, but identical from a functional point of view (these elements were designed using the strut-and-tie method, as if they were two linear elements). Several projects for road and rail bridges as well as roof structures in steel, reinforced concrete, and mixed structures for a wide variety of situations, were subsequently completed adopting and adapting the same principle (Figure 4, [13,15]).

A similar development took place with the idea of inclining toward the span the two piers of the frame shown in figure 4b. In this bridge, this solution had been adopted to facilitate earthworks and the construction of the foundations due to the presence of a road nearby. Positioning the foundations offset from the end of the bridge also had the

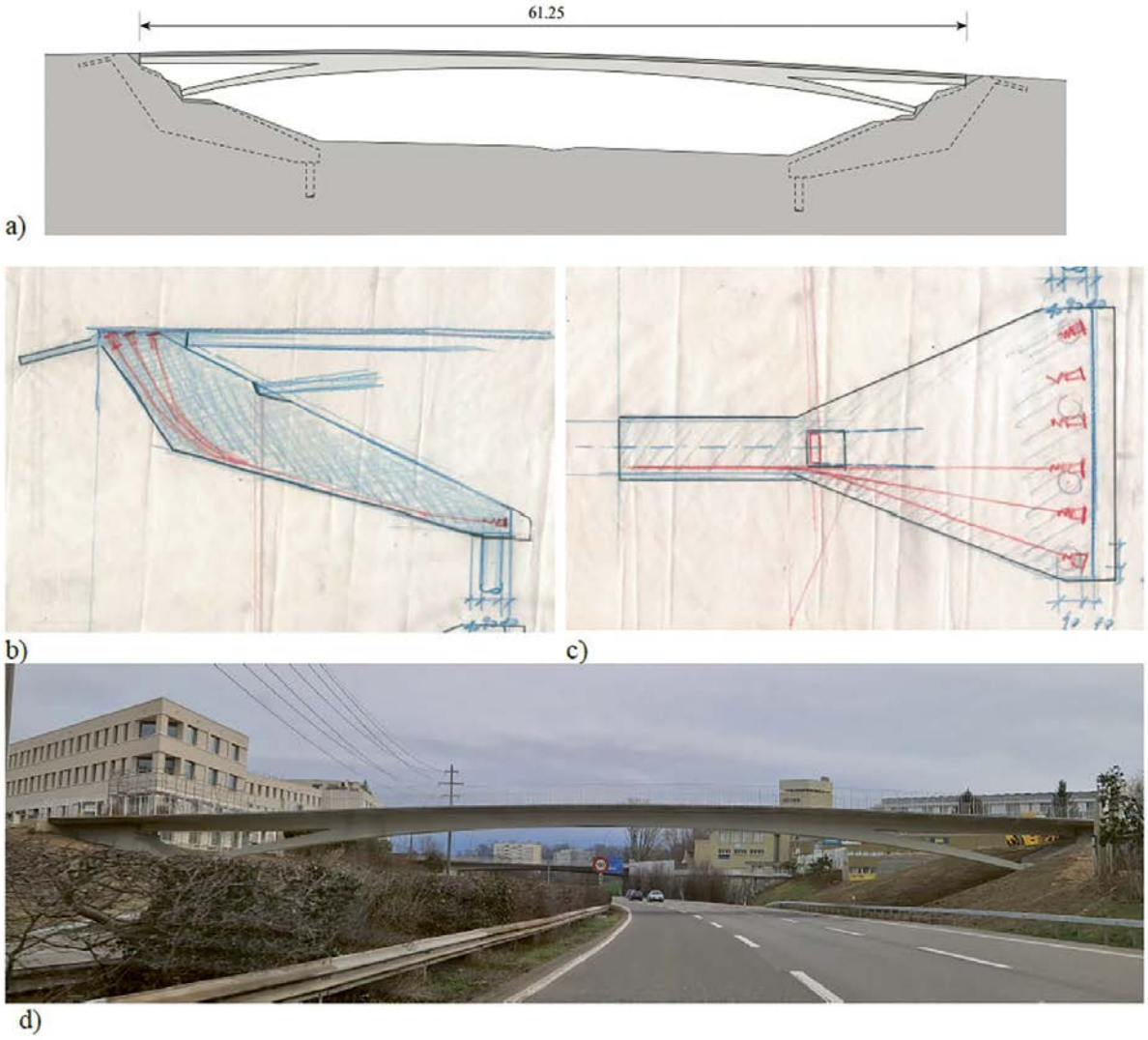

Figure 6. Footbridge "Cèdres" near Lausanne, Switzerland, (a) Scheme of the system, (b-c) conceptual design including study of the prestressed abutments (A. Muttoni structural designer), (d) view of the finished structure (MC2 engineers, Cano Lasso Architects, Muttoni and Fernandez engineers, completed 2024).

advantage of reducing the horizontal thrust, thus reducing the risk of horizontal settlement of the foundations, which is particularly problematic for frames with short piers. This principle has been used for other projects (see, for instance, the bridge in Figure 4d).

The project Figure 5 was proposed as a variant to the original project consisting of widening a historic masonry bridge adding a new deck slab in concrete, which would have significantly altered the appearance of the bridge and given rise to considerable costs due to the need of strengthening it. The idea was therefore to create a new structure that was as slender as possible, and with a relatively long span over the river in order to preserve the view of the old bridge and its support on the rock in the middle of the river, but with enough character to avoid appearing banal. The old bridge could then be used for soft mobility. The choice for the new structure was therefore made to clamp the deck in two inclined piers to form a frame, but to place the piers that connect the foundations to the deck mostly in the ground, allowing them to almost disappear. The slenderness of the deck is further enhanced using two support struts. Here again, the idea to incline the piers was adopted in a different situation and was instrumental to achieve the goals of a structure that is as slender as possible and of buried, low-profile abutments, while requiring limited earthworks. The piers-struts-deck system was designed as a monolithic structure in which all the shapes and dimensions were defined based on the internal forces that could be studied using the strut and tie method (see Figure 5) and the stress field approach. Evidently, the great builders such as Maillart, Freyssinet, Nervi, Torroja and others were able to conceive similar structures and forms based on intuition and calculation, but today, we can do so with the most modern means [16].

As the site did not allow for the new bridge to be situated too far from the existing one, it was designed to limit the presence of structural elements close to the masonry bridge. The main structure was therefore designed as thin as possible (1.10 metres) and positioned on the axis of the bridge, where the bridge deck slab essentially functions as two cantilevers on either side.

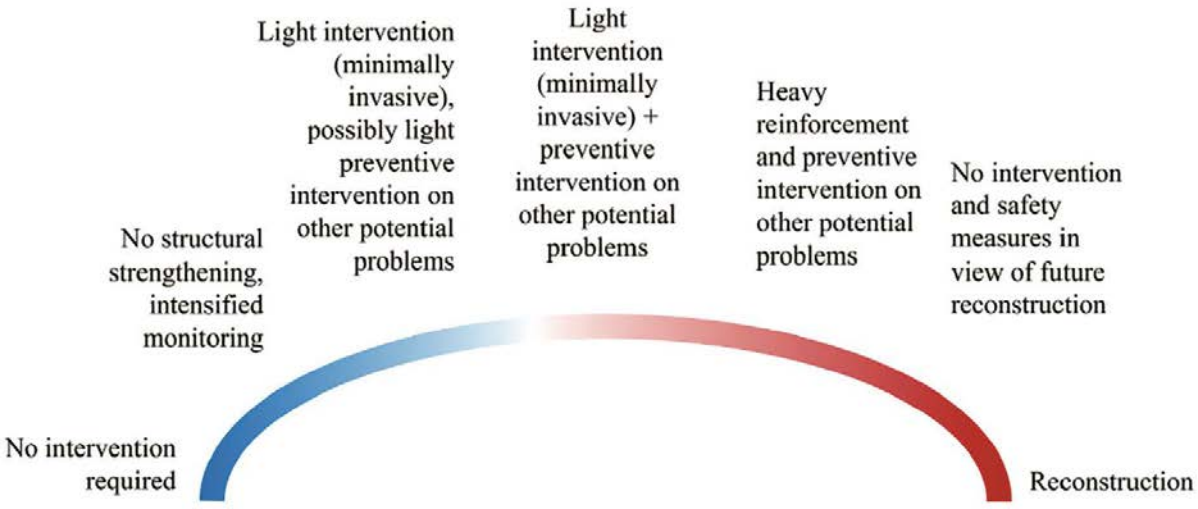

Figure 7. Possible options for interventions on existing structures.

The same design principle could be applied in a more recent project, consisting of a very slender footbridge over the motorway near Lausanne, Switzerland. The initial project, resulting from a design competition, with a ribbon stretched over the motorway, had to be abandoned because of (1) the difficulties of draining of the water from the deck onto the motorway, and (2) the considerable tensile forces of the stress ribbon, which would have had to be anchored in a very poor ground. The idea was therefore to replace the stress ribbon with a very slender arch (Figure 6). Here, the thrust of the structure is carried by abutments in the form of pre-stressed recumbent piers. Once again, the same principle was adopted, where the geometry of the whole system is designed to cancel out the horizontal thrust so that the whole structure can be supported on vertical piles.

The two examples in Figures 5 and 6 show that the same idea can evolve into completely different projects. Solutions can be adapted to the requirements and constraints of different situations, and to the aims of different projects. This is clearly demonstrated in the case of project competitions, where for the same situation and the same requirements, the different participants come up with completely different projects. These projects highlight the importance of structural design, which required relatively little time for these projects, but which strongly influenced them.

3. DESIGN OF INTERVENTIONS ON EXISTING STRUCTURES

In several advanced societies, the centre of gravity of the structural engineer's activity is shifting from the design of new structures to the assessment and intervention on existing ones. This new activity undoubtedly requires specific knowledge and, perhaps also for this reason, a new professional figure specialised in existing structures is emerging. With this respect, it is important to keep in mind that the new knowledge specifically related to assessment and intervention on existing structures should be seen as an addition to, and not a substitute to that required for the design of a new structure. In addition, knowing how to design, how to build and, not less important, how it was designed, dimensioned, and built in the past, is crucial to correctly assess an existing structure (being able to quickly identify hidden defects and to intervene correctly).

The fact that there is less and less construction of new structures in some Countries can be a problem in this respect. Personal experience shows that young engineers who have never had the opportunity to design a bridge tend to have an overly academic and analytical approach. When they begin to assess an existing bridge, they too often neglect a crucial initial phase consisting on a sufficiently holistic qualitative approach, including (i) the identification of inherent weaknesses in the structure, (ii) the considerations on the governing "*assessment situations*" (performed with a qualitative analysis of the critical details perhaps supplemented by some very simplified preliminary quantitative verifications), and (iii) the identification of the main involved uncertainties. Unfortunately, some young engineers tend to immediately focus on the aspects they know best and that they are able to analyse, perhaps neglecting others that are more problematic. In assessments, we all too often see detailed analyses and verifications when the real problems are most likely elsewhere.

It is therefore interesting to note that this shortcoming is analogous to the one previously discussed for the design of new structures, where the creative part of the conceptual design is too often neglected and the analytical part is overdone, resulting in lengthy and not always necessary calculation notes.

When the inspection and assessment of an existing structure reveals problems or weaknesses, the following questions arise: to intervene or not? Preserve or replace? In fact, as shown in Figure 7, the choice is much wider, from doing nothing to demolishing and rebuilding. This choice must al-

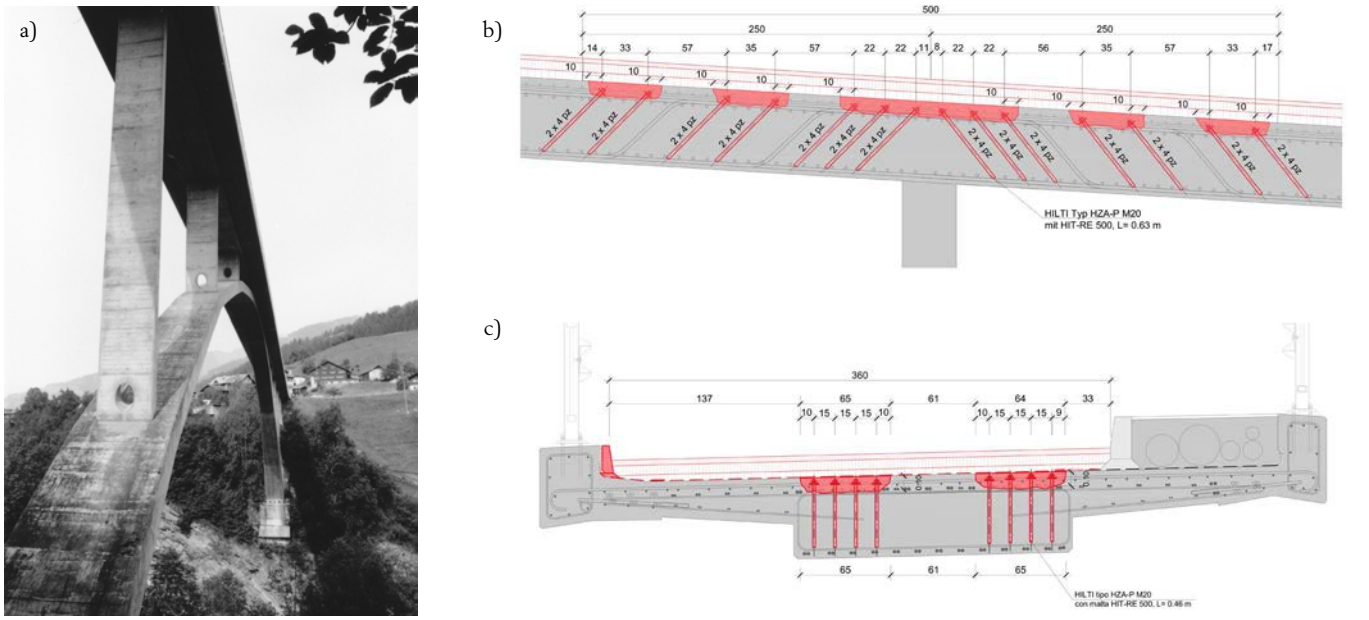

Figure 8. Valserrhein bridge Uors-Surcasti in the Swiss Alps; (a) view of the bridge designed by Christian Menn, 1962; (b) longitudinal section and (c) cross section of the deck showing the strengthening details (Lurati Muttoni Partner, 2022).

ways be balanced, trying to avoid any conflict of interest, and above all must always be made based on plausible options and well-defined projects. For instance, in some cases, wanting to preserve an existing structure at all costs, even when the interventions become major, often with considerable risks in terms of the lifespan of the intervention (unfortunately, little is said about failed interventions, which leave a structure that has undergone major intervention still in poor condition after only two or three decades), is neither economic nor sustainable. On the contrary, when a structure of quality can be repaired using simple, effective, long-lasting, and economical interventions, it is also not responsible to replace the structure or to heavily intervene. Once again, the choices are easier if one avoids prejudices and ideological approaches (such as repairing is better than rebuilding because it is more sustainable). If in doubt, it is best to compare two options studied in detail, with a well-balanced comparison of costs, risks, final quality, residual lifespan, environmental aspects, duration of works, impact on users, and so on. The heritage value, in terms of the quality of the structure itself or as a historical witness, shall also be considered in this assessment (the recent guideline by the Swiss Federal Road Administration [18] to account for these aspects in case of bridges and other engineering works is a useful help).

When structural strengthening proves to be necessary, the designer may be tempted to affirm the new intervention with a strong and visible gesture, even when a less invasive retrofitting would be possible. Designers should not fall into that temptation. In an analogous and curious exercise, what would people say if orthopaedists would make their work visible? This is not to say that the intervention shall always be hidden, but the designer should always ask himself the question: does the intervention, in addition to restoring the necessary level of safety, really make the structure better? Also, from an architectural point of view? In the case of a positive answer, strong character and visually invasive interventions are possible, but they should always be designed with great care, and must always allow the architectural quality of a fine new structure to be achieved.

In the case of the bridge shown in Figure 8, for instance, the need to retrofit against shear the deck of an arch bridge designed by Christian Menn in the early 1960s led the engineer commissioned to propose several reinforcement variants: (1) vertical steel rods anchored in the deck slab and in steel sleepers under the deck; (2) longitudinal steel girders under the deck; (3) addition of intermediate piers to reduce spans; (4) an under-spanned system applied under the deck and (5) concreting large capitals under the deck in the area near the piers. Each of these interventions would have had a considerable visual impact on a bridge of very high quality, designed by one of the greatest bridge designers of his generation, and which represents a fine example of the art of building in the early 1960s. For this reason, the owner searched for a second opinion and called for other less architecturally invasive solutions to be proposed. It was against this backdrop that we were able to propose and carry out a strengthening that was very respectful from an architectural point of view. The new shear reinforcement is made up of post-installed reinforcing bars embedded in inclined boreholes. The anchor heads were sealed with mortar, so that the strengthening work is barely visible once completed. By using a new technique, developed in collaboration with a specialized company, it was possible to propose a method that respects the existing structure.

4. ANALYSIS, DIMENSIONING, AND ASSESSMENT: NEW VS. EXISTING STRUCTURES

In the example shown above, the quantity of post-installed reinforcement could be greatly reduced by using detailed

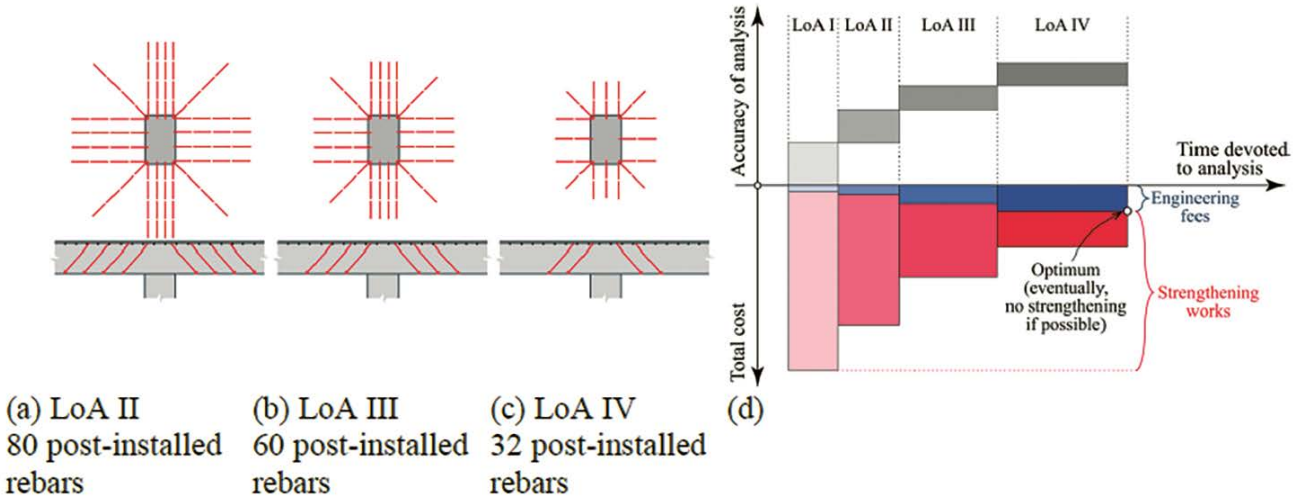

Figure 9. Strengthening necessary to ensure the safety level with respect to punching shear in a slab-column connection, applying the LoA (a) II, (b) III, (c) IV and (d) accuracy of the verification and costs associated with re-quired strengthening works as a function of the required time for analyses for different levels of approximation (LoA) (adapted from [19, 20]).

verification methods. This situation is well known and occurs frequently. This means that the methods of analysis, dimensioning and verification should be adapted to the engineer's task. This is not necessarily specific to existing structures. For new structures too, it is always reasonable to start with approaches and calculations that are as simple as possible, and to refine them only when this is necessary or can lead to an optimisation of the resulting project.

It is to account for this matter of fact that the so-called levels of approximation (LoA) approach was introduced in standards (we speak of levels of approximation, and not levels of refinement, because we start from the idea that all calculations by the engineer are always an approximation of reality). The idea is very simple and actually corresponds to what engineers with sufficient experience have always done: they first start with a very simplified but sufficiently conservative calculation. If one realises that in any case the verification is satisfied (for example because the failure mode underlying the verification is not governing), or if in any case the economic impact of the conservative verification is limited, one can stop the calculation after the first level of approximation (LoA I) and move on.

If, on the other hand, when dimensioning a new structure, the necessary dimensions (e.g., concrete thicknesses or the required amount of reinforcement and/or prestressing) are too important, then it may be reasonable to move to a higher LoA. The same applies to the assessment of an existing structure: if low LoAs show that structural strengthening is necessary, it is worthwhile to move to higher LoAs that perhaps allow it to be demonstrated that a strengthening is not necessary. Moreover, even if this is still indispensable, the use of higher LoAs for sizing the strengthening can result in considerable savings (Figure 9).

Despite the fact that this approach has been used by engineers implicitly since time immemorial, it was first implemented explicitly in a standard only some 20 years ago at national level [20], then adopted internationally in the *fib* MC2010 [21] and more systematically in the *fib* MC2020 [8] and in the second generation of the European Standard for concrete structures [9] (although not using explicitly the term "Level of Approximation" in the latter).

For critical existing structures, the more refined and general model will be used (higher levels of approximation), whereas for the design of simple new structures, in the vast majority of cases, the use of a simplified version of the model is sufficient (low levels of approximation). In this context, a misunderstanding must be avoided: the statement '*low levels of approximation for new structures and higher levels of approximation for existing structures*' is incorrect. Even in the assessment of existing structures, one will always start with the lowest levels of approximation, either because perhaps such a verification shows a sufficient level of safety (and then the verification stops there), or because the level of knowledge of the structure is too low, and then it is wiser to invest the time in on-site investigations rather than perhaps unnecessary verifications. High levels of approximation are only justified in existing structures when they allow avoiding expensive interventions or limit their cost [19]. On the other hand, high levels of approximation may also be justified for new structures, e.g., when they allow complex cases to be solved, very important structures to be dimensioned, or for economy when the number and repetitiveness of structural elements justifies it.

5. ABOUT RESEARCH VS. PRACTICE AND RESEARCH VS. DESIGN

It is a matter of fact that the gap between research and practice (and between research and education as well as between

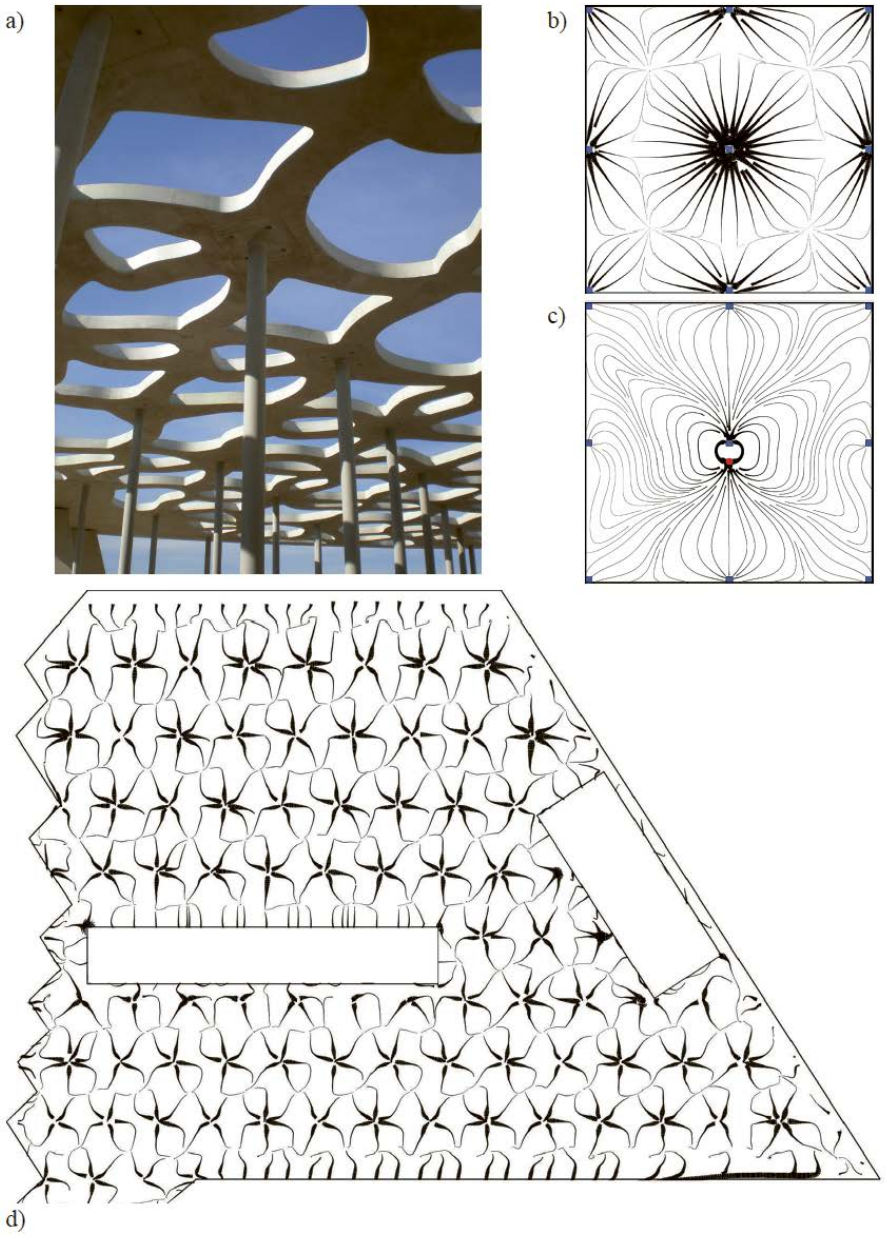

Figure 10. (a) Canopy of the Jan Michalski Foundation dedicated to writing and literature at Montricher, Switzerland; (b) shear field for a flat slab under uniformly distributed load and (c) under a concentrated load near to the internal column; and (d) shear field of the canopy (with Mangeat-Wahlen architects, Muttoni and Fernández civil engineers, A. Muttoni structural designer) [22].

education and practice) has increased significantly in the last decades. The reason seems to be evident: universities are ranked mostly based on the quantification of their scientific production, increasing the pressure over researchers to publish (*publish or perish*). In addition, in an increasing number of universities, new professors are selected mostly based on their (quantitative) scientific production or their potential to succeed in the field, making young professors to be comprehensively more motivated to publish than to invest their time in teaching or in professional and standardization activities. This system means that the most important skills for a young professor today are those of a science journalist (ability to quickly produce good quality texts describing the results of research) rather than those of a researcher capable of producing new ideas. Furthermore, the generation of professors which has been appointed with these criteria is more and more involved in the selection process of new colleagues and will tend to perpetuate the system.

In some universities, in an attempt to solve the problem resulting from the lack of knowledge of some young colleagues on the practical realities, teaching is delegated to colleagues who are essentially active in practice, but not or very little involved in research (professors of practice). This is a false good solution: it presents an increased risk of further segregation between teaching and research, which should, in an ideal situation, be mutually enriching.

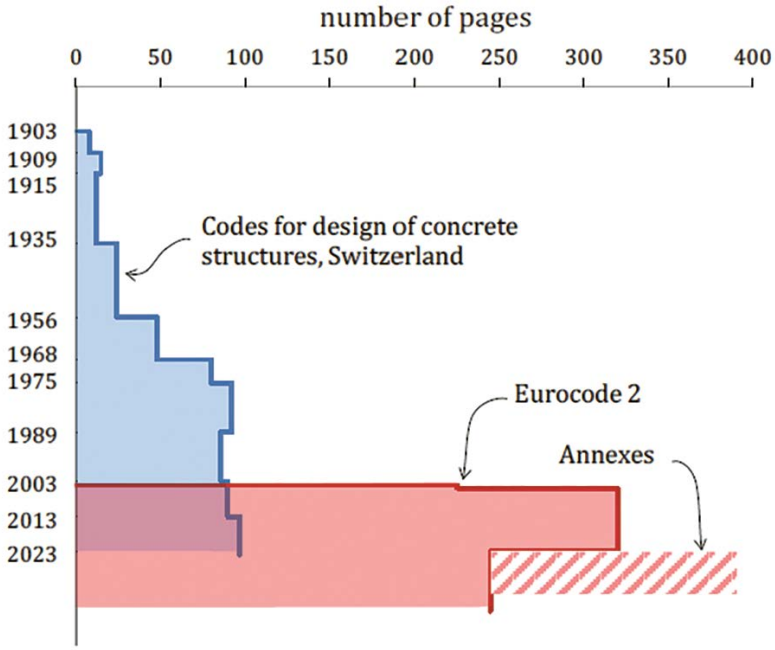

Figure 11. Evolution of number of pages of the Swiss standard for concrete structures and the equivalent Eurocode (adapted from [20])

Starting from the pessimistic reading in the previous paragraph, it is necessary to find ways out. Again, one must start from the reading of the situation in order to be able to propose promising solutions. Publications of research results are unfortunately seen as the most obvious outcome of research, but in this respect, there is a flagrant confusion between ends and means. One should publish to disseminate knowledge and the result of research. Thus, publication is nothing more than a means to an end, which is to increase knowledge and, in our case, to improve our structures in terms of economy, reliability, constructability and sustainability.

Another important issue concerns the interaction between design and research. On the one hand, design and practice, as mentioned earlier, should influence structural engineering research, especially with regard to research topics. On the other hand, research also has an influence on the projects, in terms of analysis, dimensioning, choice of materials and other essential points. This influence takes place in structural engineering mainly through standards. In addition, research can also contribute to new structural solutions or the tools derived from research can help to find structural forms that are more efficient and more in keeping with the actual behaviour of the chosen material. This is for instance the case of the project shown in Figure 10.

The architectural idea behind this project was to suspend from a canopy covering an area of around 6000 m² the small houses that accommodate the writers in residence at the foundation. This structure therefore forms the suspension points for the small houses, but also has the function of creating a space that links them to the library, an exhibition room, an auditorium, and the common services. For the canopy, the designers (architects and engineers) hesitated a great deal between a grid of beams and a perforated slab: neither of these solutions could adequately meet the challenges of the project. After lengthy discussions, the designers came up with a new structure (neither a perforated slab nor a grid of beams). The material (in this case concrete) is arranged according to the trajectories that follow in a slab the application of loads toward the supports formed by a forest of tall, slender columns. This is the result of research carried out by the structural designer since the 1980s into the actual behaviour of slabs and the analogies with shells. In fact, in slabs, it is possible to trace shear fields (the main direction of the shear force) which represent in fact the path of the loads to the supports. For simple cases (see the uniformly loaded flat slab supported on nine points shown in Figure 10b), the shear field is fairly predictable (the loads converge directly towards the supports). On the contrary, for slightly more complex situations, the shear field describes intriguing paths that may even seem counter-intuitive (see for example Figure 10c with the same slab loaded by a single concentrated load near to the centre column). For the Jan Michalski foundation canopy, we therefore calculated the shear field of a solid slab (Figure 10d) and arranged the material of the new structure along the paths followed by the loads. The result is a structure that highlights the central position of the support columns towards which the ribs converge (and which also support the suspended houses), but which does not show a grid that would be inconsistent with the architectural idea.

This is an interesting example where not only the shape, but the structural system also can be generated to better meet the architectural challenges from considerations how the structure works. It is also a nice example where a creative work is issued from research in structural engineering as well as from intensive discussions between the architect and the structural designer.

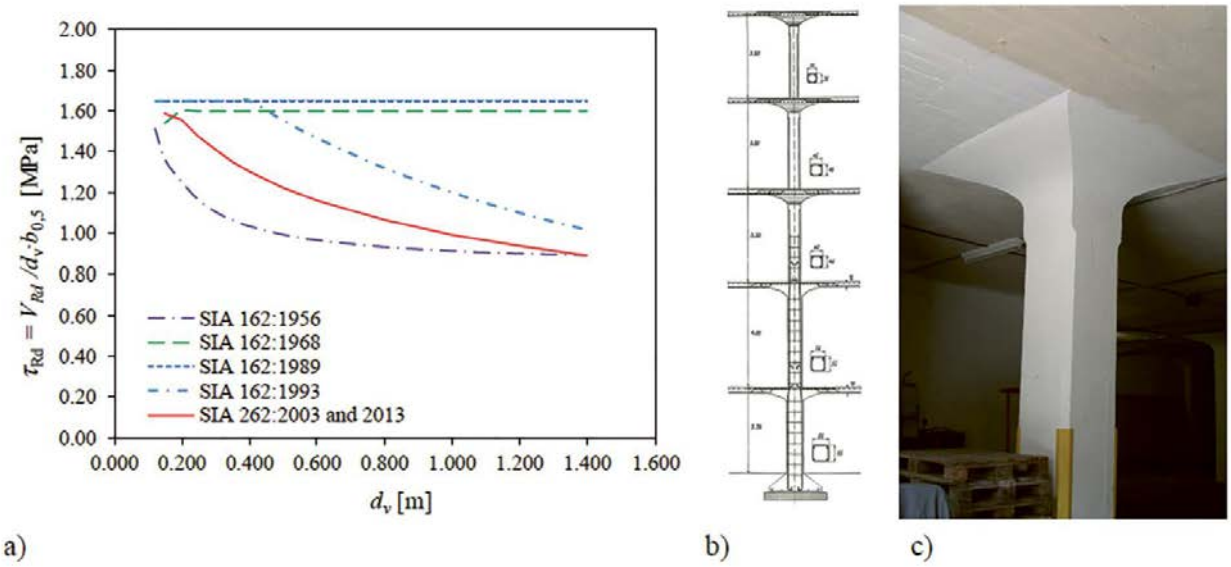

Figure 12. (a) normalized punching shear resistance as a function of the effective depth according to the Swiss codes since 1956 (f_{ck} = 30 MPa, c/d = 1.25, ρ = 0.75%); (b) mushrooms slabs with capitals according to Maillart and (c) Magazzini Generali at Chiasso Switzerland, 1924-25.

6. WHY ARE STANDARDS MORE AND MORE COMPLEX, AND WHAT CAN WE DO TO AVOID THEM BEING DIFFICULT TO USE?

"*Standards are more and more complex, uneasy to use, and lead to more and more uneconomic structures*": this is a statement that we often hear and perhaps also share. Does it correspond to reality? What is the reason? How do we get out of it?

It is a matter of fact that standards are becoming increasingly complex and exhaustive. Figure 11 shows the evolution of the number of pages of the Swiss standard for concrete structures since its first edition in 1903. In comparison, the number of pages of the same European standard is also shown. It is interesting to note that when, in the 1930s, the number of pages doubled (from 12 to 24), the famous engineer Robert Maillart made the following comments [1]:

> *"Unfortunately, the provisions of the standards mislead engineers or force them to apply them mechanically, particularly when they are used during the training of engineers and when they are imposed by control officers. A general relaxation of the rules, giving greater responsibility to the engineer, would go a long way towards improving the quality of our buildings. Simple design is also possible and sufficient. The rational evaluation of its results leads to structures with an identical and uniform level of safety compared to those designed by the thoughtless application of building standards considering all their details."*

What would Robert Maillart say today? Was he right? Before answering these questions, it is also useful to understand the reasons for these changes.

Let's start with the fact that current standards are often more conservative (and potentially less economic) than those of a few decades ago. Figure 12a shows the example of the punching resistance of reinforced concrete slabs according to Swiss standards, from 1956 until the latest edition in 2013. Firstly, how did Swiss engineers do it before 1956, when the 1903 and 1935 standards did not even mention punching? The answer is simple, the shape of the capitals over supporting columns was defined in such a way as to limit shear stresses around the column (the Maillard capitals shown in Figures 12b and c had a hyperbolic shape, for example, so as to keep the shear stress constant regardless of the distance from the column axis) while in foundation slabs, when it was not possible to vary the thickness of the slab, bent up bars were placed to effectively carry the shear forces. From the 1950s onwards, it was thought to simplify the construction methods (flat floors and no more bent up bars): the problem of shear and punching in columns supported slabs was thus created out of nothing and had to be dealt with in the standards. For beam shear, Ritter and Mörsch had already proposed models and solutions more than a century ago, but for punching, the problem is more complex, so it was essential to calibrate empirical formulae or models (as it is today) by means of laboratory tests. To limit the cost of punching tests, it was decided to test only the part of the plate subjected to hogging moments, and the thickness was limited to avoid too large specimens and too high forces involved, thus implicitly creating two problems: the membrane effect was neglected (on the side of safety), and the size effect was not accounted for (it is now known that it is not on the side of safety at all). In addition, one wanted to test shear, not bending, so the tests of those years were conducted on elements that were heavily reinforced in bending. It is interesting to

note in figure 12a that all editions of the Swiss standard gave practically the same punching resistance for thin slabs (this is no coincidence, they were calibrated on the same slabs). Furthermore, the first 1956 standard already had a kind of size effect, but this was purely by chance. In fact, at that time, it was based on the idea that the shear resistance depends on the thickness of the plate h, and not on the effective depth d, so that as the thickness increases, the *h/d* ratio decreases and there is therefore a reduction in strength when normalising it to the effective depth (this effect was further enhanced in the Swiss standard of 1956 by considering the control perimeter at a distance h from the column edge). In the years that followed, however, it was rightly decided to consider the effective depth *d* for the calculation of resistance, but without considering the size effect, simply because it was not yet known for reinforced concrete structures, or because since in the 1970s there have been doubts as to its relevance for practical cases.

When it was finally realised that the size effect and the reduction in resistance for poorly reinforced slabs should be accounted for, there were two possibilities for the following standards: either a very simple formulation is maintained by calibrating it for thick lightly reinforced slabs (which would, however, be overly conservative and give uneconomical solutions for thin slabs or/and highly reinforced in bending), or a necessarily more complex formulation is sought that can account for the majority of cases found in practice. In most cases, the latter solution has been chosen, or with some compromises, explaining the fact that in some cases, codes are overly conservative.

Figure 12 highlights yet another problem: thick flat slabs and footings built in Switzerland between 1968 and 2003, and especially up to 1993, are potentially unsafe in relation to today's knowledge. This means that for the assessment of existing structures, it is useful to have more refined calculation methods than those used for the dimensioning of new structures if one wants to avoid systematically carrying out costly retrofitting's. This explains the resurgence of research into punching, and shear in general, over the last three decades or so (P. Regan, for example, asked the rhetorical question "*Research on shear: a benefit to humanity or a waste of time?*" to explain this in 1993 [23]). It was in this context, for example, but also to account in a more rational manner for the size effect and the influence on punching resistance of a low level of flexural reinforcement, that the author of these lines developed the Critical Shear Crack Theory from 1985 onwards [24, 25, 26], subsequently implemented in several national [27] and international standards [21, 8, 9] (research in this field was subsequently carried out even more intensively, see [28] for an overview, after being confronted with several tragic accidents, as it will be shown later, see Figure 13, [29, 30, 31]).

The same story about an increase in complexity and supposed conservativeness could be told for other standards and for other cases (shear of slabs without shear reinforcement, shear of prestressed beams, anchorage length and laps of reinforcement bars, etc).

To return to Maillart's concerns, we should not forget that he was writing in the 1930s, addressing engineers of a small country, when civil engineers had a rather uniform and high level of training, when the problems to be solved were simpler and more homogeneous, and when the level of knowledge was certainly less developed. In addition, a fundamental difference compared to today is that, because of their more limited knowledge and a society with fewer constraints, engineers took on much more responsibility and relied more on what we call "common sense" or "engineering judgement". Today, the situation has changed dramatically: taking responsibility for deviations from a standard is less and less common (also because the consequences of potential problems have become more severe) and at the same time, some engineers do not hesitate to go to the limit of what is allowed by a standard, even when this does not make much sense (this is rather justified by some level of unconsciousness related to the lack of knowledge of the limitations of the current standards). This means that more and more limits and cases have to be defined and treated in the standards.

While we can certainly feel a certain nostalgia for the freedom engineers enjoyed at Maillart's time, we must bear in mind that our standards are aimed at a multitude of users (it is estimated that half a million engineers will use the Eurocodes in a near future) who operate in very different situations.

When we began working on the 2nd generation of the Eurocode for concrete structures (the author of these lines chaired the working group that drafted the main part) [9], one of the main aims was to improve the ease of use of the standard, and in this context, we asked ourselves the following question: should this standard be able to resolve 80-90% of cases in a simple manner, or should it be able to resolve a large proportion of the cases that engineers are faced with today? The answer is not easy: in the first case, the use of the standard would be easier for most cases, but would enormously complicate the work of engineers, who would often have to deal with situations not considered in the standard. Finally, we have once again come to the conclusion that the approach based on levels of approximation enables ordinary cases to be solved simply, and more unusual cases to be solved in a way that is inevitably more complex.

To be effectively effective, the Levels of Approximation Approach (LoAA) needs proper implementation in standards. In fact, it is crucial that when an engineer moves from one LoA to the following one, an important part of the calculation can be kept unchanged. Ideally, it is necessary that at each step, only certain parameters are refined. Therefore, care must be taken in the derivation of the code provisions: it is necessary to start with the general model at the highest level, and then to simplify the equations at lower levels as we go along, ensuring that certain parameters are not calculated from the beginning, but chosen on the basis of different considerations.

What are the disadvantages of this approach? Firstly, freedom is given to the designer (the standard is therefore less prescriptive, which can also be seen as an advantage by some, and a disadvantage by others). For example, some colleagues fear that the client will always demand the highest LoA, in the sense that this is often their interest when fees are fixed (see figure 9d). On the other hand, this fear depends on the type of contract the designer has and the importance he wants and can give to common sense in these considera-

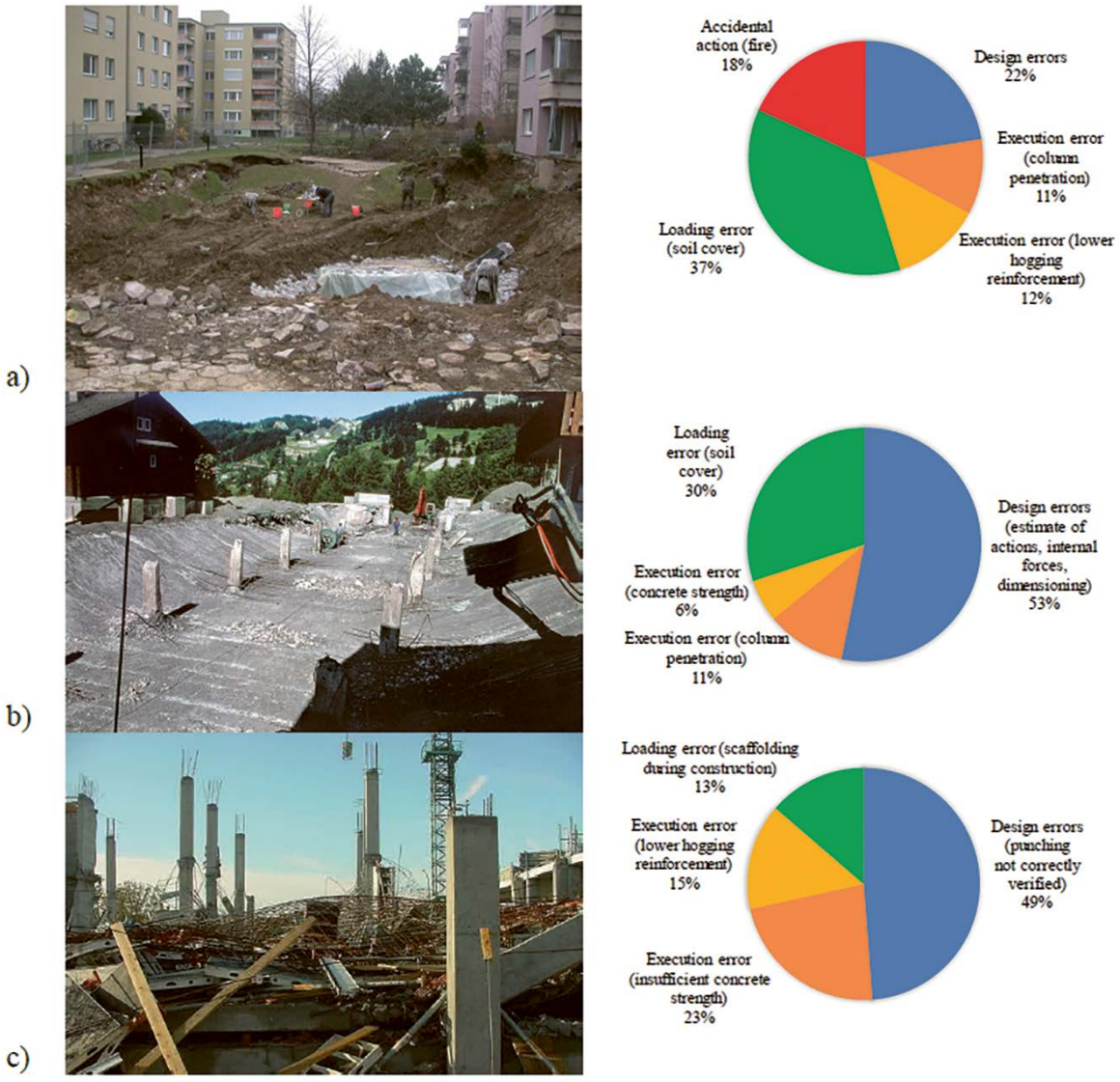

Figure 13. Quantification of the causes of collapses due to punching: (a) Gretzenbach accident in Switzerland, 2004 [29]; (b) Bluche Accident in Switzerland, 1981 [30]; and (c) Cagliari Accident in Italy, 2004 [31].

tions. It is therefore essentially for this reason that the 2nd generation of Eurocode 2 [9] does not explicitly mention the concept of Levels of Approximation but is nevertheless formulated to allow such an approach.

Another disadvantage of the method is that with the LoAA, standards become longer (since there is a repletion of provisions on the same content) and, at first sight, more complex and more difficult to use. Nevertheless, this is only the first impression, and the reality is exactly the opposite: the LoAA is, once the method is understood, extremely effective in reducing calculation time in the vast majority of cases and allowing the study of cases that cannot be investigated with too general or concise standards.

Another advantage of being able to carry out an initial check in a simplified way relates to the reliability of our work and the probability of making calculation errors. The latter is a real concern, if we think, for example, of the increasingly limited time available for analysis and verification. If we look again at the Figure 2 and consider the trend over the last few decades, we can only conclude that other activities, such as coordination, meetings, communications, and the drafting of documents that are not always essential, are taking up more and more time. Deadlines are also getting shorter and shorter, and the likelihood of misunderstandings is increasing due to the increasingly complex way in which projects are organised. In addition, experienced engineers have less and less time to devote to the supervision and accompaniment of their younger colleagues, who in turn are increasingly using complex and sophisticated tools that are not always transparent or fully mastered, so the likelihood of error increases. In this context, we should not forget that, if it is true that a serious problem on site or the collapse of a structure is often the result of the accumulation of several errors, it is also true that calculation errors often represent a significant proportion of

the causes of a collapse (Figure 13).

For all these reasons, refined methods are needed to solve today's problems, for example in the efficient assessment of existing structures, but at the same time, having simple and easily understandable tools is essential to limit risks and save time that can be devoted preferably to quality design.

7. CONCLUSION

Based on the author's experience and observing the evolution of the profession over the past decades, today's situation has several unsatisfactory aspects. In this context, the strong commitment of schools and professional organisations is necessary to make structural engineering more attractive to the younger generation, but not sufficient. A great deal also depends on the examples we set and pass on to the younger generation, and this depends essentially on the activity and attitude of every one of us.

The main thesis of this contribution is that the intellectual and creative component of structural engineering should be more emphasized and gain more attention.

References

[1] Maillart R. (1938), Current issues in reinforced concrete construction (in German: Aktuelle Fragen des Eisenbetonbaues), Schweizerische Bauzeitung, Zurich, Switzerland.

[2] Nervi P. L. (1945), Scienza o Arte del costruire? , Edizioni della Bussola, Rome, Italy.

[3] Freyssinet E. (1993), Un amour sans limite, Collection of writings 1936-1958, Editions du Linteau, Paris, France.

[4] Torroja E. (1957), Razón y Ser de los Tipos Estructurales .

[5] Schlaich, J. (1992), Can Conceptual design be taught?, The Structural Engineer.

[6] Muttoni, A., The Art of Structures (2011), EPFL Press, Lausanne, Switzerland.

[7] Wikipedia, https://en.wikipedia.org/wiki/Engineer (accessed 10.05.2024).

[8] fib Model Code for Concrete Structures (2023).

[9] CEN (2023), EN 1992-1-1, Eurocode 2 - Design of concrete structures - Part 1-1: General rules and rules for buildings, bridges and civil engineering structures.

[10] Conceptual Design of Structures (1996), Proceedings of the International Symposium, University of Stuttgart / International Association for Shell and Spatial Structures.

[11] Muttoni A. and Schwartz J. (2024), Conceptual design of structures in practice, research, and teaching, chapter of the book "Conceptual design of structures", Birkhäuser publishing.

[12] Muttoni A., Lurati F., Muttoni L., Rezzonico M. (2022), Two bridges in southern Switzerland with under-spanned concrete girders, Structural Concrete in Switzerland, Swiss report for the fib Congress in Oslo, Norway.

[13] Muttoni A. (1997), Bridges with an innovative system (in German: Brücken mit einem innovativen statischen System», Schweizer Ingenieur und Architekt, Zurich.

[14] Lázaro L., Domingo A., Abel J., Kawaguchi K., Gantes C. (2021) Mamoru Kawaguchi, Innovation and Tradition in Structural Design, International Association for Shell and Spatial Structures.

[15] Muttoni A., Lurati F. (2023), Under-spanned bridges: a suitable solution for efficiency and sustainability, Proceedings of the fib Conceptual design symposium, Oslo, Norway.

[16] Muttoni A., Schwartz J., Thürlimann B. (1996), Design of Concrete Structures with Stress Fields, Springer Science & Business Media.

[17] Muttoni A., Muttoni L., Lurati F. (2010), The new bridge at Frasco over the Verzasca River, Structural Concrete in Switzerland, Swiss report for the fib Congress in Washington DC, USA.

[18] Engineering Structures on National Roads as Cultural Assets (2023) (in French : Les Ouvrages d'Art des Routes Nationales en qualité de Bien Culturels), Guidline of the Swiss Federal Road Administration.

[19] Muttoni A., Lurati F., Faria D., Simões J., Fernández M. (2023), Assessment of Existing Bridges: The Swiss Experience of the Last Three Decades, Proceedings of Italian Concrete Conference 2022, DOI: 10.1007/978-3-031-43102-9_38.

[20] Muttoni A. (2003), Introduction to the Swiss Code SIA 262 (in French and German), Documentation SIA, Swiss Society of Engineers and Architects SIA, Zurich, p. 5-9.

[21] fib Model Code for Concrete Structures 2010 (2013).

[22] Muttoni A., Fernandez Ruiz M. (2014), Concrete Canopy of "Maison de l'Ecriture" in Montricher, Structural Concrete in Switzerland, Swiss report for the fib Congress in Mumbai, India.

[23] Regan P.E. (1993), Research on shear: a benefit to humanity or a waste of time?, The Structural Engineer.

[24] Muttoni A. and Schwartz J. (1991), Behaviour of beams and punching in slabs without shear reinforcement, Proceeding of the IABSE Colloq., Stuttgart, Germany.

[25] Muttoni A. (2003), Shear and punching strength of slabs without shear reinforcement, Bet. Stahlbetonbau, [in German].

[26] Muttoni A. (2008), Punching shear strength of reinforced concrete slabs without transverse reinforcement, ACI Struct. J.

[27] Swiss Society of Engineers and Architects (2003), Code 262 for Concrete Structures.

[28] Muttoni A., Simões J.T. (2023), Shear and punching shear according to the Critical Shear Crack Theory: background, recent developments and integration in codes, IBRACON Structures and Materials Journal.

[29] Muttoni A., Fürst A., Hunkeler F. (2005), Slab collapse of the undergound garage Standenacker in Gretzenbach, Published Report (in German: Deckeneinsturz der Tiefgarage am Staldenacker in Gretzenbach).

[30] Guandalini S., Muttoni A. (2008), Study of the collapse of a car park slab, in "Structural safety of covered car parks" (in French: Sécurité structurale des parkings couverts), Document D02226, Swiss Society of Engineers and Architects, Zurich, Switzerland.

[31] Muttoni A. (2009), Investigation of the collapse of the structure of a shopping centre in Selargius (Cagliari, Italy) on 28 October 2004, unpublished report.

Acknowledgements

Some of the thoughts described in this text came to light during long and frequent discussions with my friend and colleague Hugo Corres, with whom I share a passion for the profession. This text is dedicated to him on the occasion of his 70th birthday.

Disponible en **www.hormigonyacero.com**
https://doi.org/10.33586/hya.2025.4101

An Overview on Floating Structures and the Role of Engineering

Una disertación sobre las estructuras flotantes y el papel de la ingeniería

Arianna Minoretti[a,*], **Tor Ole Olsen**[b]

[a] *PhD, Department of Civil and Environmental Engineering, Faculty of Engineering, Norwegian University of Science and Technology, Norway, orcid.org/0009-0008-2432-4946; Senior Principal Engineer, Technology and Development Department, Norwegian Public Roads Administration, Norway*

[b] *Dr. Techn. Olav Olsen AS, Vollsveien 17A, 1366 Lysaker, Norway*

Recibido el 1 de junio de 2024; revisado el 4 de febrero de 2025, aceptado el 25 de febrero de 2025

ABSTRACT

This article presents a brief history of floating structures, and their links with recent opportunities given by offshore developments. The role of engineering designers is then analysed too, highlighting how these types of structures resemble the idea of design where engineering and architecture meet in a convivium of functionality and beauty. The role of designers is therefore transported to the present day, where the lack of space on land and the environmental requirements of reduction for land use demands finding alternatives such as floating structures. In a complex scenario where the art of engineering meets the challenges of the marine environment, influencing each other, the article discusses which is the new role of engineers. Drawing from the teachings on the philosophy of structures and, in particular, from the essence of Eduardo Torroja Miret's work, the article analyses the challenges for the design of floating structures in a complex environment and uses the basic theory of conceptual design to outline a new necessary profile of a designer, aware of the complexity and multiculturalism of the new context in which he operates.

KEYWORDS: floating structures, environmental impact, engineering role.

RESUMEN

En este artículo se presenta una breve historia de las estructuras flotantes, que enlaza en con las recientes opciones que ofrecen los desarrollos offshore. Posteriormente se analiza el papel de los ingenieros, destacando cómo en este tipo de estructuras se plasma la idea de diseño en el cual ingeniería y arquitectura se encuentran en un convivio de funcionalidad y belleza. El papel de los ingenieros se traslada, por tanto, a la actualidad, donde la falta de espacio y las exigencias ambientales de reducción del uso del suelo empujan a encontrar alternativas como las estructuras flotantes. En un escenario complejo donde el arte de la ingeniería se enfrenta a los desafíos del medio marino, influyéndose mutuamente, el artículo analiza cuál es el nuevo papel de los ingenieros. A partir de las enseñanzas sobre la filosofía de las estructuras y, en particular, de las ideas de Eduardo Torroja Miret, el artículo analiza los desafíos para el diseño de estructuras flotantes en un entorno complejo y resalta la importancia del diseño conceptual en el perfil del ingeniero, consciente de la complejidad y multiculturalidad del nuevo contexto en el que se desenvuelve.

PALABRAS CLAVE: estructuras flotantes, impacto ambiental, papel de la ingeniería.

* Persona de contacto / *Corresponding author*:
Correo-e / *e-mail*: arianna.minoretti@vegvesen.no (Arianna Minoretti)

How to cite this article: Minoretti, A., & Ole Olsen, T. (2026). An overview on floating structures and the role of engineering. *Hormigón y Acero*. 77(308): 191-196. https://doi.org/10.33586/hya.2025.4101

1. INTRODUCTION

Floating structures have been an alternative to ground-based structures since ancient times, with a long tradition as temporary solutions.

Their design demand engineers to optimize structural design, and require a combination of structural behaviour intuition and advanced structural analysis. Typically extreme actions combined with structural shapes have led to proposals where the essence and beauty of the Engineering emerge as a whole design.

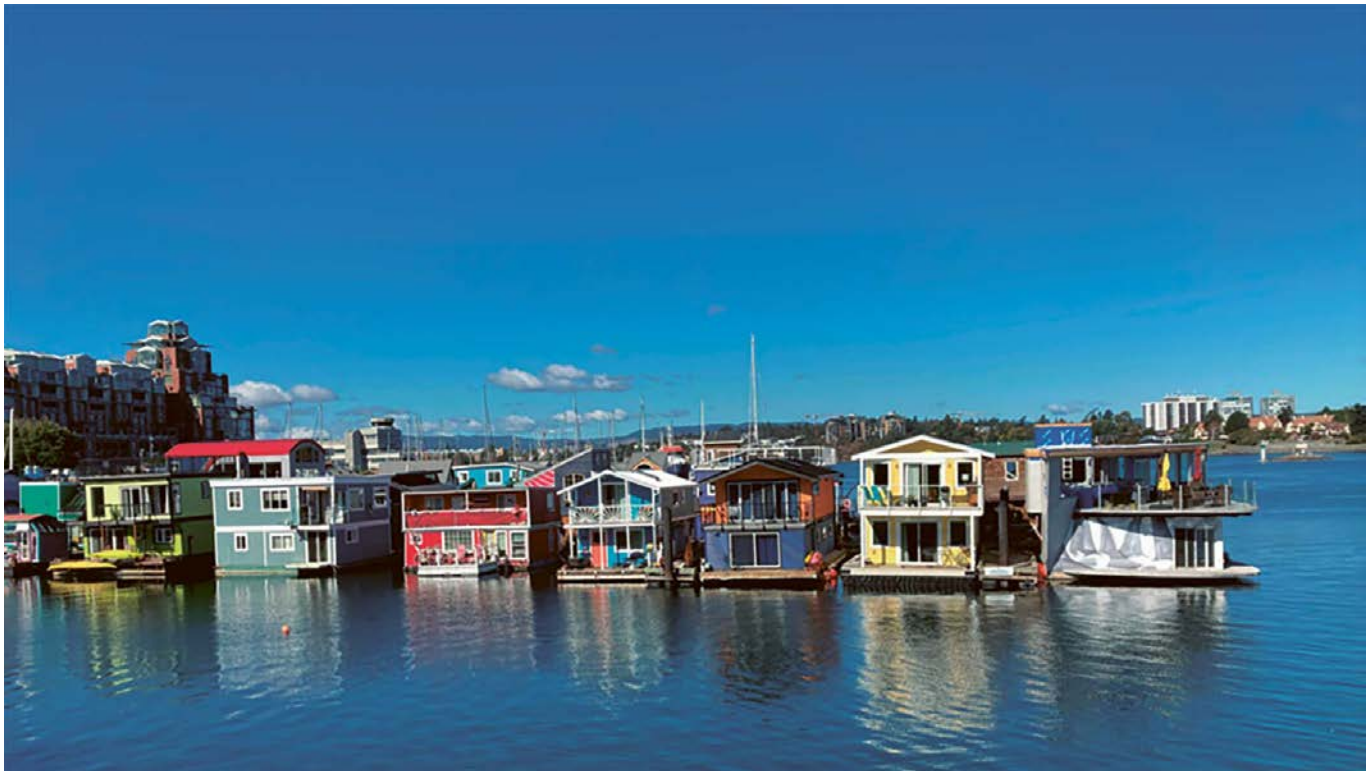

Figure 1. Fisherman's Wharf, Victoria, BC, Canada - Ronin, Unsplash.

Nowadays, technological development, especially in the offshore field, has brought new possibilities for floating structures as permanent structures. In addition, the recent environmental policies push for a reduction in the use of land. This has brought a flourish of proposals for different types of floating structures in different fields such as transportation, housing, energy, and food production. In this new horizon of possibilities, the enthusiasm must be calmed by a new awareness of the role of engineering which, in the complexity of today's panorama, calls for a new role for the designer.

2. BRIEF HISTORY OF FLOATING STRUCTURES

Building on the water has always been a necessity. Starting from floating houses (Figure 1), as an ancient way of inhabitant protection, or where communities lived on fishing activities, multiple examples around the world show how floating constructions for civil use have changed to adapt to different needs.

New reasons, among them climate challenges, imply a technological effort in areas such as the Netherlands, to build large floating settlements.

The development of floating structures involves several fields, depending on the needs to be met. Floating bridges have served as a temporary solution, especially for military purposes, as the historical Xerxes's floating boat bridge which was used during the second Persian invasion of Greece in 480 BC (Tavana and Khanjani 2013), and then became an alternative for permanent constructions since around 1940, for example with the Hobart bridge in 1943 (Lee and Wood 1981). 1940 is also the construction year of Lake Washington Floating Bridge, closed in 1989, in Seattle, US.

Since then, other floating bridges have been constructed around the world. Among them, are the two Norwegian floating bridges Bergsøysund (1992) and Nordhordland (1994), in Figure 2.

Floating docks are also military solutions turned into permanent use. Mulberry Harbour, used during the Second World War by the British, is an example of a military application (Landis 1997). Among the permanent constructions of this type, the floating container terminal at Valdez, Alaska, built in 1982, is the largest of its kind and is an example of how concrete is a promising material for use in this exposed environment.

Concrete durability has been successfully evidenced also in offshore applications (Fernandes et al. 2008) and, in the last 50 years, new solutions have been developed both for material properties and their technological applications. For instance, elements connecting the tension leg platforms to the seabed, called tethers, were installed for the first time in the '80s in the UK continental shelf in the Hutton oil field (Mercier et al. 1982) and then in several other installations.

The technological advances in marine operations necessary for the installation of these constructions and the maturity of newly developed technologies, such as seabed connection systems (tethers), led to the development of several studies for deep-water crossings (Minoretti and Olsen 2020). Around 2014, after the first study for crossing the Sognefjord (Skorpa 2010), Norway started a series of studies and tests to cross the deep and large fjords along its west coast, along the E39 route from Kristiansand to Trondheim (Minoretti and Bakken 2016).

Figure 2. Nordhordland bridge – Aas Jakobsen.

Among the structures proposed, floating bridges, hybrid suspension bridges on tension leg platforms and submerged floating tube bridges (SFTB) have been evaluated. Actual proposals for submerged floating tube bridges origins in an old conceptual design from the end of the 19th century (Minoretti and Olsen 2020). The tube structure is submerged but floating at a defined position below the water level. For long crossings, the structure needs to be vertically stabilized by floating pontoons or tethers, connecting the structure to the seabed (Minoretti et al 2019).

In this solution, the submerged structure takes advantage of the buoyancy to counterbalance the vertical loads (that is why it is also named 'Archimedes bridge') and concurrently lowers the main sea load on the structure just with the submergence. In a vision where the structure takes advantage of the natural laws, the SFTB recalls the solutions where the project equation marries the simplicity and correctness of nature (Livio 2017). Nevertheless, this crossing solution has been proposed several times in the last century, for different applications (Fib bul.96 2020) in lakes and sea crossings, but it has not been built yet.

Hybrid existing solutions are the Statpipe shore approach SFTB, a twin rectangular 670 meters SFTB built in 1982 in Kalstø, Norway, to protect two gas pipelines, and the Söderströmstunnel (Figure 3) in Stockholm, Sweden. This is a subsea tunnel built in 2015 that relies on groups of piles for the foundations, due to the poor soil characteristics, and therefore having a static behaviour as an SFTB on columns support.

Other types of floating structures have been developed and implemented, such as floating facilities (restaurants, stages, airports) and floating production installations (for energy production - Figure 4 - or food production). Technology is allowing us to broaden our horizons and the designers are working to implement new solutions.

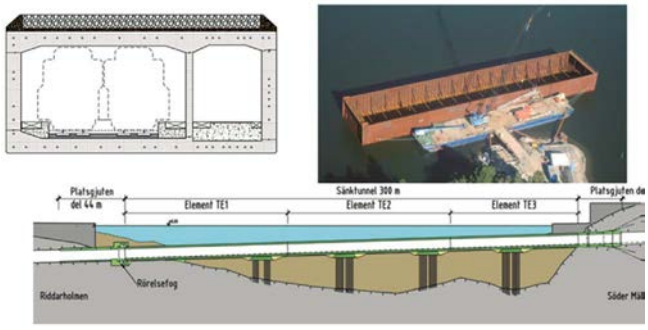

Figure 3. Söderströmstunnel - cross-section, concrete casting afloat and longitudinal section, Trafikkverket.

2.1. The role of Engineering

Certainly, the high technical specialization required in the design of these constructions, combined with their functionality in the past linked almost predominantly to the industrial sector, has attracted many engineers to the ranks of designers of floating structures. Furthermore, floating structures are among those types of constructions where the design of the structure simultaneously defines the aesthetics of the construction. As with bridge structures, technique and aesthetics come together in the design of floating structures, and the role of engineers as designers enter the dimension of beauty's rigor defined by Pier Luigi Nervi (Leslie 2017).

Figure 4. Walden Floating PV, National Renewable Energy Lab.

The role of structural engineers has been distinguished by the general role of designer only in the last 150 years (Shteto, 2021) and, before that, the structure and the architecture had undistinguished roles within the process of creation.

Floating structures are among those structures where the structural design has a general design role, because, once defined, it shapes also the main architecture and defines, with a major role, the aesthetic of the construction. Along this process, to answer to the defined need, engineers conceive a functional solution to withstand the local specific load conditions, shaping the aesthetical function of the structure at the same time. To say it with Eduardo Torroja's words, in floating structures, the structural part answers all the equations required for the project (Torroja et al.1958).

Borrowing Torroja's words again, structural intuition becomes of paramount importance, as the conceptual design leads the way for the solution's success.

The role of conceptual design has gained more and more importance, recognizing the essential role of designers in the front-end phase, in the scientific and technical communities. For this reason, the International Federation for Structural Concrete (Fib) has been organizing, since 2019, the Fib Symposium of Conceptual Design of Concrete Structures. The Symposium, by an initiative of Prof. Hugo Corres Peiretti, took place for the first event at the Torroja Institute in Madrid, with the vision of bringing together the different professionals around the reflection on the role of conceptual design and the importance of sharing knowledge with new young generations. Again through input from Prof. Corres, in his role as president of the Fib, the Fib YMG (Young Member Group) was created (Figure 5). Four years later, the Symposia slogan invited the young members on a reflection on the future: 'The challenges ahead are more serious than before, therefore future conceptual designers must be better than the existing ones'.

Figure 5. Prof. Corres with YMG of Fib.

3. THE NEW CHALLENGES

3.1. Future challenges are for sure important and urgent.

Sea levels rising (source https://climate.nasa.gov/vital-signs/sea-level) are putting pressure on several nations, which can no longer rely on protective solutions that are now technically reaching their limit and economically unsustainable. In addition, exhausted areas (Wang and Wang, 2015) are pressing to find new solutions, that could be flexible to accommodate future changes in space and fast to build. There is a need to make available areas near existing settlements or to return lands to nature in areas that are now saturated, reconstructing a habitat that was erased in times of little awareness of environmental impact. In the governmental plans for construction expansion, the imperative reduction of produced emissions and of land use darkens the horizon, threatening with stagnation in the construction sector. Along the coastal areas, land has become more expensive,

Figure 6. Sorenga seawater pool, Oslo - Dr. Techn. Olav Olsen.

bringing a need to relocate logistic installations and production plants.

For these reasons, water has been seen as a new expansion area, both for relocating facilities near the shore or to extend the existing ones (Figure 6), or for new energy production installations, but also for civil and transportation purposes.

Floating structures present in addition several favourable characteristics (Fib bull. 91). They are flexible and they could be conceived as modular for future change. They are in principle resistant to earthquakes as they are base-isolated, and they are not exposed to risks for sea-level rising. They could reduce the noise impact in the surroundings for the population inland and they require a use of land limited to eventual areas of connection with land or to anchorages or foundations.

On the other hand, floating structures could have to withstand harsh environmental conditions, especially if the structure is exposed to open sea. Particular challenging situations, like a tsunami or subsea landslides, could compromise the integrity of the structure and therefore the design of these structures requires a very high technical level and an excellent knowledge of local design situations. Situations where the buoyancy of the structure is compromised must be considered by experienced designers and, in the design, robustness and redundancy must be used wisely.

However, the success or failure of floating structures is not only a matter of structural response to design conditions. Operating in the sea (or lake) environment, the structure must be conceived taking into consideration the local environmental characteristics of the area, in terms of biological marine life, and must be designed considering the possible benefits that the structure could generate for the local environment, in addition to minimizing the possible negative impact on the surroundings.

Floating concrete installations could provide new colonization areas for local species but could also be areas for invasive and indigenous species that could compromise the survival of local species. In addition, the release of material from the concrete surface could endanger local species in the long term, so careful testing especially in the use of new materials should be planned. The presence of floating structures and artificial lighting could represent a barrier to migration for some species or attract them in the proximity of the light source. Floating structures connecting different habitats, such as floating bridges, could represent a favourable connection for the spreading of species, with positive or negative consequences. The effect of noise produced during the construction, installation and the life of the structures, should be evaluated also in terms of effects on marine species. Specific studies (Follestad et al. 2022; Multiconsult 2023) demonstrated the importance of involving environmental experts from the early stage of the design, to build a knowledge of the local environment and work on the environmental challenges to transform them into opportunities, whenever possible.

As an example, for the study of an SFTB on the Bjørnafjord crossing, in Norway (Minoretti et al. 2016), the pontoons were studied as floating green islands (Figure 7), able not only to guarantee the structural performance needed but also to create a shelter for the nesting of local species.

The environment therefore becomes a new equation in the perspective of the design, with a multiplicity of competence needed to bring into the general picture at the base of a successful design concept.

4. THE NEW ROLE OF ENGINEERING

The new conceptual design is more difficult than before, as the Fib symposium stated in 2023. Starting from bridging engineering and architecture, the new designers need to be aware of the complexity of the environment we operate in.

Figure 7. Study for an SFTB with pontoons for the Bjørnafjord crossing in Norway, Statens vegvesen.

Floating structures can be a real opportunity if we just do not make the same mistake made with land-based constructions, where the indiscriminate construction has ignored the socio-environmental implications and has led us to today's desperate and often unsuccessful attempts to remedy past mistakes.

The new conceptual design starts from the knowledge of the project's needs and of the local characteristics where the project will operate, embracing a multidisciplinary perspective and recognizing the need for the involvement of a range of experts from various disciplines. Among them, environmental experts, who must be involved from the early stages of the project, to transform the environmental challenges into possibilities and provide long-term value to the construction. Lasting value is the bearer of true sustainability.

References

[1] Aslaksen, Erik 2015. 'The Relationship between Engineers and Society: Is It Currently Fulfilling Its Potential?: An Invited Discourse'. Journal and Proceedings of the Royal Society of New South Wales 148: 28–43. https://doi.org/10.5962/p.361726

[2] Fernandes, J., T. Bittencourt, and P. Helene 2008. 'A Review of the Application of Concrete to Offshore Structures'. American Concrete Institute, ACI Special Publication, 377–92

[3] Fib bulletin. 91, 2019. Floating concrete structures. State-of-the-art-report. ISBN 978-2-88394-134-2

[4] Fib bulletin. 96, 2020. Guidelines for Submerged Floating Tube Bridges. Guide to good practice. ISBN 978-2-88394-144-1

[5] Follestad A., J. Järnegren, E. Johannes Mul, C. Rosten and F. Thomassen Singsaas 2022. Environmental impacts of floating bridges, Norwegian Institute for Nature Research, Report 2057, ISBN: 978-82-426-4840-2

[6] Landis, J. W. 1997. Operation Mulberry: A Floating Transportable Harbor for World War II Normandy Invasion, Woodhead Publishing Series in Civil and Structural Engineering, Macro-Engineering, Woodhead Publishing, Pages 25-52, ISBN 9781898563334, https://doi.org/10.1016/B978-1-898563-33-4.50006-9

[7] Lee, T. R., and L.J. Wood 1981. 'Adjustment in the Urban System: The Tasman Bridge Collapse and Its Effects on Metropolitan Hobart'. Progress in Planning 15: 63–150 https://doi.org/10.1016/0305-9006(81)90002-7

[8] Leslie T, 2017. Beauty's Rigor: Patterns of Production in the Work of Pier Luigi Nervi. Publisher: University of Illinois Press. ISBN: 0252041127

[9] Livio, 2017. La sezione aurea, Rizzoli.

[10] Mercier, J.A., R.G. Goldsmith, and L.B. Curtis 1982. 'The Hutton TLP: A Preliminary Design'. Journal of Petroleum Technology 34, no. 01: 208–16. https://doi.org/10.2118/10647-PA.

[11] Minoretti A. and A. Bakken 2016. Mega-Bridge Concepts for Bjørnafjord Crossing in Norway, Bridges 2016 At Coventry (UK), Volume: Bridge Design & Engineering

[12] Minoretti A., A. Myhr, S. A. Haugerud, J. Sekse, T. Fjell 2016. Presented at IABSE Congress: Challenges in Design and Construction of an Innovative and Sustainable Built Environment, Stockholm, Sweden, 21-23 September 2016, pp. 1875-1882

[13] Minoretti A., Egeland Eidem M., and T. Egeberg Aasland 2019. "The Submerged Floating Tube Bridge for the Norwegian Fjords." Paper presented at the The 29th International Ocean and Polar Engineering Conference, Honolulu, Hawaii, USA, June 2019.

[14] Minoretti A., T. O. Olsen 2020. The Submerged Floating Tube Bridge: History of a new Structure. Presented at IABSE Symposium: Synergy of Culture and Civil Engineering – History and Challenges, Wrocław, Poland, 7-9 October 2020, published in IABSE Symposium Wroclaw 2020, pp. 430-437

[15] Multiconsult, 2023. Measurements of underwater noise at floating bridges and ferries, Report 10245203-01-RIMT-RAP-001

[16] Shteto, G 2021. 'The Aesthetics of Structure', Master Thesis.

[17] Skorpa L. 2010. A feasibility study: Crossing of the Sognefjord with a fixed connection. Presented at IABSE Symposium: Large Structures and Infrastructures for Environmentally Constrained and Urbanised Areas, Venice, Italy, 22-24 September 2010, pp. 760-761

[18] Tavana, H., and M. Khanjani 2013. 'Reducing Hydroelastic Response of Very Large Floating Structure: A Literature Review'. International Journal of Computer Applications 71: 13–17. https://doi.org/10.5120/12353-8658

[19] Torroja, E., Polivka, J. J., & Polivka, M. 1958. Philosophy of Structures (DGO-Digital original, 1). University of California Press. https://doi.org/10.2307/jj.8501169

[20] Wang, C. M., and B. T. Wang, 2015. 'Great Ideas Float to the Top'. Large Floating Structures: Technological Advances, 1–36. Singapore: Springer, 2015. https://doi.org/10.1007/978-981-287-137-4_1.

Disponible en **www.hormigonyacero.com**
https://doi.org/10.33586/hya.2025.4103

A Retrospective and Prospective View on Teaching Conceptual Design of Structures

Una visión retrospectiva y prospectiva sobre la enseñanza del diseño conceptual de estructuras

Leonardo Todisco[a]

[a] *Prof. Dr., Universidad Politécnica de Madrid, Spain*

Recibido el 21 de junio de 2024; revisado el 23 de febrero de 2025, aceptado el 24 de febrero de 2025

ABSTRACT

The paper begins with personal reflections on the, often underestimated, role and responsibilities of structural designers in the context of sustainability. The integration of the sustainability framework within the construction industry must begin at the Conceptual Design stage, as early decisions profoundly impact the sustainability of the entire project. The paper then introduces criteria to develop a sound structural concept, emphasizing the need to integrate diverse disciplines. While past concerns focused primarily on safety and economy, today's emphasis on sustainability demands a more holistic and multidisciplinary approach. Structural designers must balance and prioritize inherently contradictory criteria to devise an appropiate structural concept. Next, the paper addresses the essential ingredients of a sound Conceptual Design: creativity, experience and knowledge. Education plays a vital role in fostering these qualities. The paper traces the origin and evolution of the course "Tipología Estructural", which was originally introduced by Eduardo Torroja in the 1953-54 academic year. Torroja was a pioneer in teaching Conceptual Design at academic level, integrating diverse knowledge areas and hands-on design experience. His visionary course, which continues today with updated contents and methodology, uses a project-based learning to foster creativity and practical problem-solving skills. This approach prepares students to effectively tackle structural design challenges in the framework of sustainability.

KEYWORDS: sustainable design, holistic approach, conceptual design, teaching, structural typology.

RESUMEN

El artículo comienza con reflexiones personales sobre el papel y las responsabilidades, a menudo subestimadas, de los diseñadores estructurales en el contexto de la sostenibilidad. La integración del marco de sostenibilidad en la industria de la construcción debe iniciarse en la fase de Diseño Conceptual, ya que las decisiones tempranas impactan profundamente la sostenibilidad de todo el proyecto. A continuación, se introducen criterios para desarrollar un concepto estructural sólido, destacando la necesidad de integrar diversas disciplinas. Mientras que en el pasado las preocupaciones se centraban principalmente en la seguridad y la economía, el enfoque actual en la sostenibilidad exige un enfoque más holístico y multidisciplinario. Los diseñadores estructurales deben equilibrar y priorizar criterios inherentemente contradictorios para desarrollar un concepto estructural óptimo.

Posteriormente, el artículo aborda los elementos esenciales de un Diseño Conceptual sólido: creatividad, experiencia y conocimiento. La educación desempeña un papel fundamental en el desarrollo de estas cualidades. Se rastrea el origen y la evolución del curso "Tipología Estructural", introducido originalmente por Eduardo Torroja en el año académico 1953-54. Torroja fue un pionero en la enseñanza del Diseño Conceptual a nivel académico, integrando diversas áreas del conocimiento y la experiencia práctica en el diseño. Su curso visionario, que continúa impartiéndose con contenidos y metodologías actualizados, utiliza un enfoque de aprendizaje basado en proyectos para fomentar la creatividad y las habilidades prácticas de resolución

de problemas. Esta metodología prepara a los estudiantes para abordar eficazmente los desafíos del diseño estructural en el marco de la sostenibilidad.

PALABRAS CLAVE: diseño sostenible, enfoque holístico, diseño conceptual, enseñanza, tipología estructural.

* Persona de contacto / *Corresponding author*:
Correo-e / *e-mail*: leonarodo.todisco@upm.es (Leonardo Todisco)

How to cite this article: Todisco, L. (2026). A Retrospective and Prospective View on Teaching Conceptual Design of Structures. *Hormigón y Acero*. 77(308):197-206. https://doi.org/10.33586/hya.2025.4103

1. ON THE RESPONSIBILITY OF THE STRUCTURAL DESIGNERS

Sustainability has become a crucial concern in the construction sector, affecting every stage from planning to deconstruction. There is a pressing need for a more rational, holistic and sustainable approach, which necessitates education, personal ethics, and a sense of responsibility. The United Nations report "Our Common Future" (1987) expanded the concept of sustainability beyond environmental aspects to include economic and social dimensions, influencing new generations of construction guidelines and codes.

Despite increased awareness, radical changes are still needed. The urgency of this shift is underscored by the projected 20% increase in the human population by 2050, necessitating substantial investments in infrastructure and housing, particularly in developing countries. This presents a unique opportunity to adopt a new paradigm in construction that focuses on sustainability and ethical responsibility.

One of the primary indicators of environmental impact is the emission of equivalent CO_2 (CO_{2eq}), which measures the global warming potential of all greenhouse gases produced by an activity throughout the whole life of a structure. As a rough estimation, the construction and manufacturing industries are responsible for approximately 30% of these emissions, with the concrete industry alone accounting for about 8%.

Efforts have been made within the construction material manufacturing sectors to reduce their environmental impact. However, concrete and steel have faced criticism for its perceived incompatibility with sustainable practices (refer to The Guardian article "Concrete: the most destructive material on Earth"). This criticism often overlooks scientific assessments showing that efficient structures can have similar CO_{2eq} footprints regardless of the materials used [1]. It is essential for experts to objectively evaluate these claims and guide society toward more sustainable construction practices.

The new version of fib Model Code 2020 places sustainability at its core. Introducing sustainability concepts to designers through codes and specialized literature aims to increase awareness on several fronts: minimizing material consumption, using appropriate materials and construction processes considering local conditions, and creating resilient, adaptable, and durable structures.

Decisions made during the early stages of planning and conceptual design significantly influence the sustainability of construction projects (Figure 1). Early, informed choices can lead to more efficient construction, maintenance, refurbishment, and eventual dismantling or recycling.

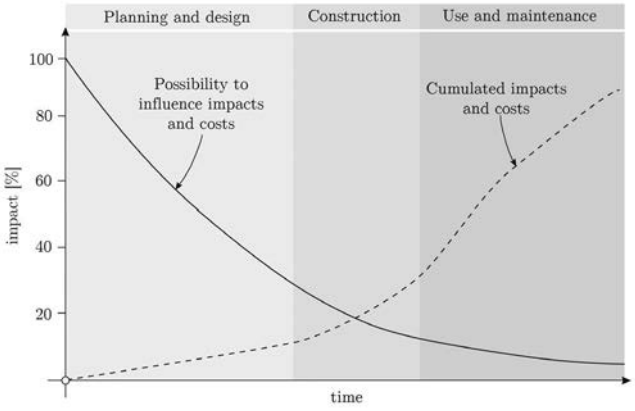

Figure 1. Influence of decisions made during the life cycle versus impacts and costs (qualitative impact of design decisions). European and North American average. Plot reproduced from [1], inspired from [2].

Life cycle energy of a building includes both operational energy (used for heating, cooling, hot water, ventilation, and lighting) and embodied energy (required for material supply, production, transportation, construction, and disassembly). The latter is more related to the work of structural designers because it is strongly influenced by the conceptual design of the structure.

The percentage of operational and embodied energy over the total life cycle energy varies depending on the type of construction and its use. As described by De Wolf et al. [3], buildings have a limited operational lifetime, which results in a significant percentage of embodied carbon contributing to the total environmental impact of the building. Many stadia built in the Middle East have not been used intensively, making embodied carbon the dominant factor in their total life cycle impact. Consequently, the role of structural designers is very important in these buildings. For example, according to De Wolf et al. [3], the material quantity and, therefore, the embodied carbon per seat in the Beijing stadium (3500

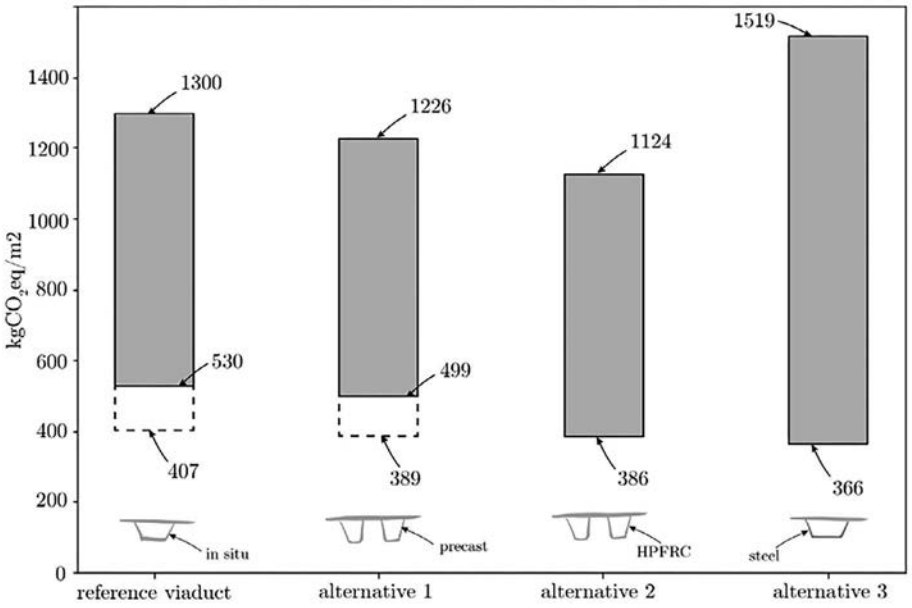

Figure 2. Comparison of CO_{2eq} associated with product and construction stages (A) for the reference viaduct and three alternatives [1].

kg CO_{2eq}/seat) is approximately ten times higher than in the London Olympic Stadium (350 kg CO_{2eq}/seat).

To demonstrate how critical decisions in conceptual design can lead to more sustainable construction practices, Figure 3 illustrates the results of an Integrated Life Cycle Assessment covering stages from A1 to A5 (cradle-to-practical construction) for the Molvizar viaduct (Spain), which serves as the reference case study (for instance, in bridges, nearly 100% of the energy is embodied, being the operational carbon almost negligible). The Molvizar viaduct is a nine-span curved prestressed box girder structure, with a total length of 432.50 m and typical spans of 51.50 m. Its deck consists of two prestressed concrete boxes, each 12.0 m wide and 2.75 m high, constructed using a moveable scaffolding system.

Two scenarios for embodied carbon coefficients (ECC, expressed as kg CO_{2eq}/kg of material) were analyzed: using either the highest or lowest factors for each material to estimate a range of emissions. The deck accounts for 50% of emissions on average, foundations (piles and pile caps) for 30%, and the rest coming from abutments and piers. To explore alternative structural typologies, the following options were considered:

- Alternative 1: Precast U-shaped beams with a reinforced concrete slab.
- Alternative 2: Precast UHPRC U-shaped beams (0.157 min ECC, 0.253 max ECC) with a reinforced concrete slab, based on [4], [5], [6].
- Alternative 3: Steel-concrete box composite deck.

The dimensions were adjusted based on the original viaduct. Alternatives 2 and 3 show higher potential for reducing emissions. In regions allowing slag cement for post-tensioned elements, emissions for the reference viaduct and all alternatives are similar in the minimum scenario (ranging from 366 to 407 kg CO_{2eq}/m², as shown by dashed lines in Figure 2). Alternative 2 demonstrates the best performance with average ECC values, indicating that high-performance materials can reduce emissions by decreasing material quantities. Alternative 3 performs comparably to concrete options with low steel emission values, but higher emissions if using standard steel. Significant differences arise between maximum and minimum ECC values, placing responsibility on designers to select materials that minimize emissions. Availability of low-emission materials, such as slag cement and scrap steel, significantly influences the optimal solution. The choice between full concrete and composite solutions depends on local industry capabilities, aligning with the need for project-specific evaluations based on location and sustainability indicators. Additionally, while the focus was on greenhouse emissions, other sustainability indicators, such as economic and social factors, must be considered. HPFRC-based alternatives have similar or lower costs compared to standard concrete, benefiting from lower transportation and crane costs. Prefabricated solutions across all alternatives enhance worker safety. The impact on local industries, either concrete or steel, and the long-term benefits of innovative materials like HPFRC, are also crucial. Environmental impacts, such as land disturbance from crane use, vary based on site conditions, further emphasizing the importance of location in determining the optimal solution.

The previous example is used also to contextualize the possible impact of structural engineers. A potential embodied carbon reduction of 20% in this case study would lead to save around 1300 tons of CO_{2eq} (calculation based on a total deck area of 5200 m²) which is equivalent to the emissions generated by 1300 Rome-to-New York one-way flights.

However, focusing solely on CO_2 emissions for assessing sustainability overlooks many critical aspects that significantly impact the sustainability of a structure, particularly in bridge engineering. These factors include the precise lo-

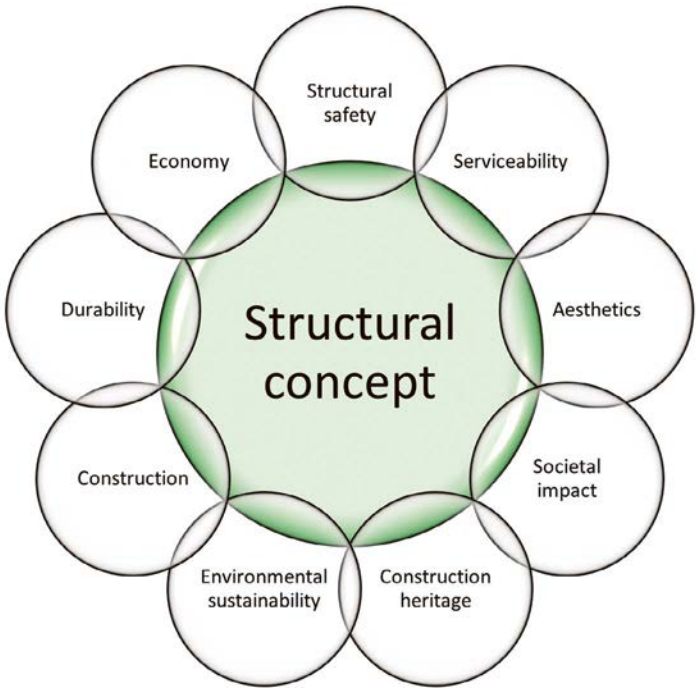

Figure 3. Overview of the criteria to be considered for a sound structural concept (image taken from slides of the Bridge Design Lectures – Prof. Kaufmann at ETHZ – freely available at https://concrete.ethz.ch).

cation, span lengths, structural type, vertical and horizontal clearances, accessibility, and width (with consideration for potential future widening). All these elements are crucial for ensuring functionality, economic efficiency, and both short- and long-term social impacts. Engineers and clients are not always fully aware of the long-term consequences their decisions may have on current and future generations. Therefore, understanding sustainability on a larger scale should take precedence over secondary concerns, such as the materials to be used [7]. For instance, the new Tamina Canyon Bridge in Bad Ragaz is a structural engineering marvel, yet it has a width of only 9.5 meters. One might question how the costs would change if the bridge's width were increased to 12 meters. Given that the construction process can account for 70-80% of a bridge's cost, increasing the width to accommodate future traffic demands would likely have a minimal impact on the overall cost.

The following section addresses the definition of the conceptual design of structure as a holistic approach that goes beyond the traditional approach.

2. ON THE CONCEPTUAL DESIGN OF STRUCTURES

The previous section has shown that the role (and responsibility) of structural designers is huge, and the most important and effective decisions are made during the conceptual design stage. Conceptual design is the creative process of combining different aspects to develop a holistic solution for a specific engineering problem. It is an iterative process guided by knowledge, intuition, experience and, if possible, creativity.

Conceptual design of structures is a cross-disciplinary activity that involve different individual disciplines such as solid mechanics, structural analysis, construction materials, building techniques, etc… [8], as well as the capacity to establish relations among them.

A sound conceptual design is not the result of a sudden moment of inspiration. On the contrary, it is the fruit of a serious, systematic and ambitious work in the search for the most adequate solution to a given engineering problem. Commonly to other creative fields (e.g. architecture, literature, culinary arts, painting, etc), successful processes are context-dependent, experience-based and principle-driven.

Figure 3 illustrates a proposed set of criteria to be considered for generating a sound structural concept. The involved disciplines clearly go beyond the pure technical ones mentioned before. In fact, they extend far beyond the classical structural considerations of safety, serviceability, construction, and economy. Structural engineers may not be experts in every domain, but their broad understanding allows them to integrate diverse perspectives and make informed decisions. Effective communication with specialists enables the team to navigate complex design challenges, ensuring that the final solution is well-rounded and robust.

A holistic approach ideally aimed to maximize all criteria simultaneously is impractical because many of these criteria are inherently contradictory. For example, a concrete mix based on CEM III/C has only one-third the environmental impact of CEM I. However, it also costs 10% more and has lower durability against carbonation compared to conventional concrete.

Evaluating all these criteria using a purely mathematical approach is inconsistent. There are multiple viable solutions, and it is the responsibility of the design team to choose the most appropriate one, prioritizing certain criteria over others.

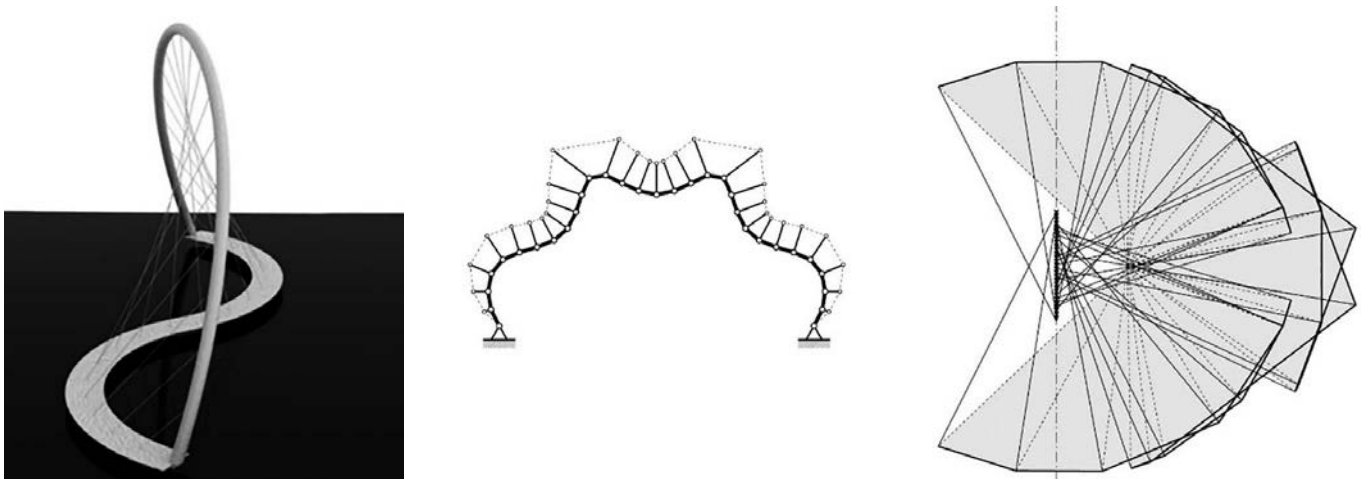

a) b)

Figure 4. Application of the equilibrium concept to spatial arch bridge supporting a curved deck (a) and free-form post-tensioned curved shapes (b).

3. ESSENTIAL INGREDIENTS FOR SOUND CONCEPTUAL DESIGN

According to the author, the essential ingredients for a sound Conceptual Design of a structure are creativity, experience and knowledge.

Regarding the first ingredient, creativity, often overlooked, it is insightful to recall Jörg Schlaich's words from the preface of the first international congress on the conceptual design of structures (IASS Symposium 1996): "The overall quality of many structures today leaves much to be desired. The rapid technological progress does not reflect adequately in their variety, beauty and sensitivity. Too often, structural engineers neglect the creative conceptual design phase by repeating standard designs and not sufficiently contributing with [their] own ideas to the fruitful collaboration with architects. Engineers thus often waste the chance to create building culture". Today, 28 years later, the situation has not changed.

The author does not have a clear idea of why this happens, but maybe is a mix of 3 different factors.

- Collaboration: engineers might not be sufficiently involved in the early conceptual phases where creative ideas are generated, leading to designs that lack aesthetic and innovative qualities.
- Education: Engineering education often emphasizes technical skills and problem-solving within established paradigms, sometimes at the expense of fostering creativity and innovation.
- Standards: Building standards restrict innovative design. Applying prescriptive regulations with novel designs can be complex and time-consuming,
- Incentives: There is a lack of economic incentives for engineers to pursue creative designs, in fact, rewards in the industry are often based on construction cost rather than innovation and creativity.

The author questions whether meeting minimum budgets is a cause for lack of creativity, noting that in the past, engineers like Maillart and Nervi demonstrated that their immensely creative designs were, at that time, the most cost-effective solutions. As reported by Kessler [9] in the tender for the Salginatobel bridge, the proposal by the contractor Prader & Cie. (built on the design of Maillart) was based on a lump sum of CHF 135000, 40% less expensive than the average cost of the other quotes. This demonstrate that at least the economic pillar of the sustainability has been always present in high quality engineering.

Experience can be considered on two levels: personal experience and knowledge of history.

Personal experience is vital as knowledge from past projects informs decisions, helps avoid mistakes, and allows for proactive issue identification and resolution. It enables designers to recognize best practices, anticipate potential problems, and take a holistic view of projects, which leads to more well-rounded designs.

Knowledge of History is equally important. Learning from past successes and failures leads to better-informed decisions and inspires innovation. For instance, knowing how ancient builders created impressive structures with limited technology can inspire sustainable, low-tech solutions today; examples in this line include the undulating brick walls by Eladio Dieste in the Church at Atlantida (Uruguay) or the water deposit by Eduardo Torroja in Fedala (Morocco). As Hugo Corres states, "When I think I have invented something, it is because I should read again Razón y Ser (the famous book by Eduardo Torroja) [10]," emphasizing that many concepts have already been invented and simply need to be studied and interiorized.

The third essential ingredient is knowledge. As mentioned before, a strong grasp of various disciplines and the ability to interrelate them are crucial. However, the most vital aspect remains a deep understanding of simple, yet powerful concepts associated to structural engineering. Several practical examples illustrate this point.

It is well-known that curved structures are characterized by the critical relationship between their geometry and structural performance. Selecting an appropriate shape

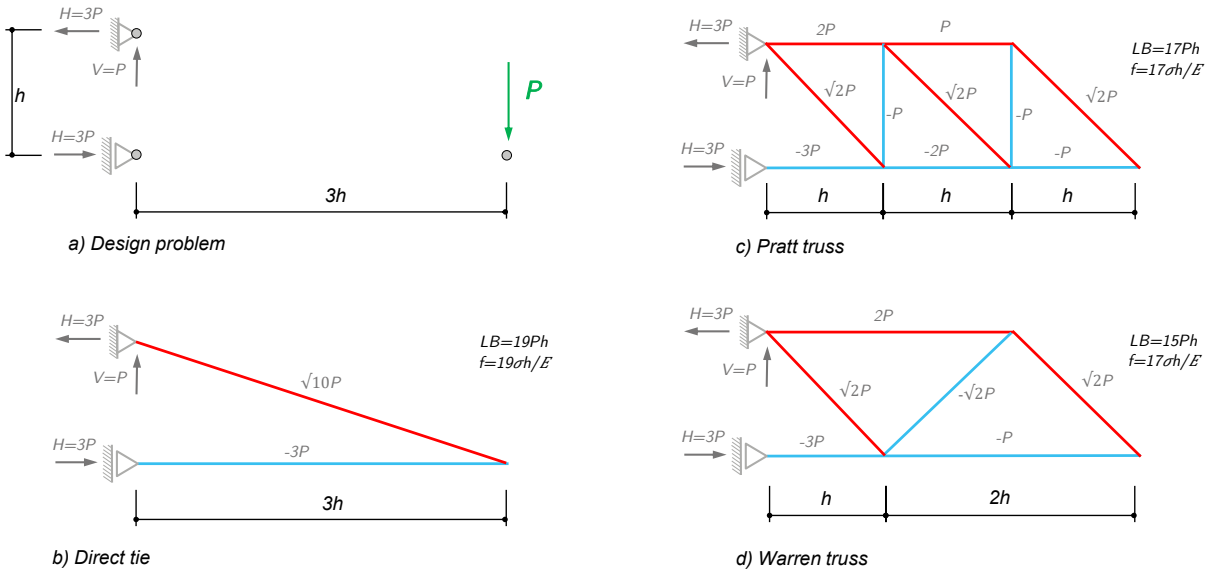

Figure 5. Application of Maxwell's Theorem on load paths. Image of the author reproduced from [14].

in the early-stage design of such structures is important for achieving material-efficiency. The definition of the funicular or antifunicular shape (i.e. a bending-free geometry under a specific set of loads) is well-know problem from the past and it has been well-documented in the literature (Huerta 2008). However, a profound understanding of this concept can lead to the development of spatial arch bridges supporting a curved deck [11], as shown in Figure 4a. The result represents an innovative answer to demands on functionality, structural optimization and aesthetics for curved decks, popular in urban contexts. Then, the implementation of this simple yet powerful concept in a parametric and interactive environment allows for the rapid exploration of numerous structural solutions in real time, providing great versatility to the designer during the initial design stages.

Another example of the power of the funicularity concept is achieving axial-only behavior in geometries that deviate from the ideal bending-free shape [12], [13]. This is accomplished by adding forces through an external post-tensioning system, with the layout defined using graphic statics. This method is particularly useful when non-structural design criteria, such as usability, architectural needs, or aesthetics, prevent the selection of purely bending-free shapes. Figure 4b illustrates the application of this methodology to an arbitrary shape. The example, featuring varying degrees of curvature, demonstrates the versatility of the methodology. Specifically, the left figure indicates the arbitrary shape with the applied post-tensioning system, while the right figure shows the corresponding force equilibrium at each node which ensure the pure bending-free behaviour.

A third example is the application of Maxwell's Theorem on load paths, originating from Maxwell's 1864 paper and revisited by Baker [14]. Maxwell's Theorem essentially states that the sum of a structure's tension load paths minus the sum of the compression load paths is equal to a value related to the applied external forces (including reactions). Although the definition of a structural system involves many other criteria, the example shown in Figure 5 (reproduced from [14]) shows its application to a truss for selecting a material-efficient location of the structural elements. Starting with a cantilever configuration (a), three different solutions (b-d) are presented. For each truss layout, the total load path is calculated by summing the products of the tension member forces and their corresponding lengths and the compression member forces and their corresponding lengths. Additionally, the deflection is shown, assuming the structure has equal stresses in tension and compression. From solutions b) to d), the length of the truss elements is reduced along with the deflections. In summary, by altering the truss layout, it is possible to increase the volume of material, resulting in a stiffer structure.

4. RETROSPECTIVE PERSPECTIVE VIEW: THE LEGACY OF EDUARDO TORROJA AND THE COURSE "TIPOLOGÍA ESTRUCTURAL"

3.1. Historical evolution

Although the importance of Conceptual Design of Structures has been emphasized repeatedly in previous sections, it is not typically included in university curricula. However, in the 1953-54 academic year, Eduardo Torroja introduced a course titled "Tipología Estructural" at the Civil Engineering School of the Universidad Politécnica de Madrid. Initially, this course was offered to fourth-year students and was conducted once a week.

Starting in the 1955-56 academic year, the frequency of lectures increased to four per week. During this period, the course syllabus included the following topics:

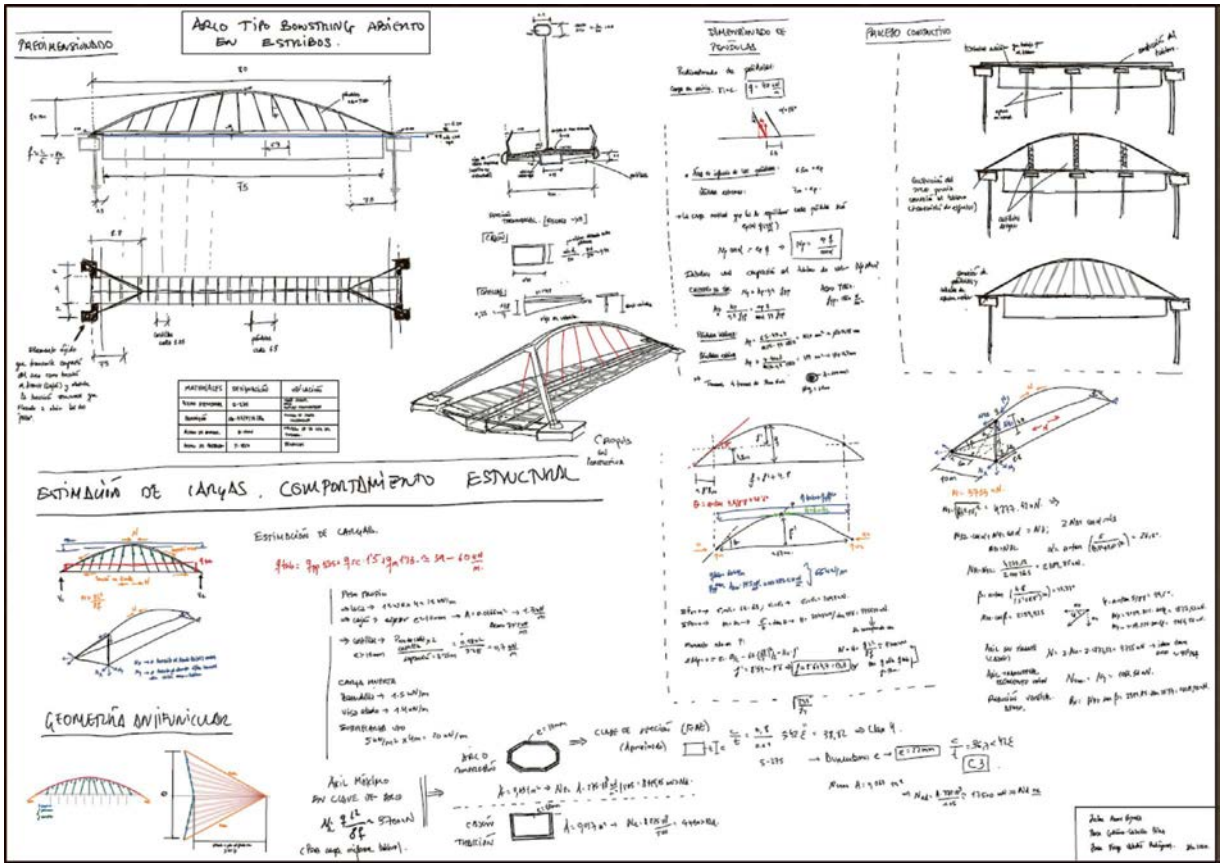

Figure 6. Example of intermediate submission with first design concept and hand calculations for an arch footbridge.

1. General approach to the topic.
2. Basic influence of the tensional phenomenon.
3. Materials: masonry, wood and steel, reinforced and prestressed concrete.
4. The basic elements: column and wall, arch, vault and dome, beam and shell, composite beam.
5. The functional groups of the construction: stories and building, bridges and aqueducts.
6. The static-resistant functionalism.
7. The construction process and its influence on the structural typology.
8. Aesthetic expression. Comments about lines and surfaces.
9. Origin of the structural diagram. The calculation. The project and its organization.

During the academic year 1958-59, Jose Calavera (honorary president of INTEMAC and former full professor at the Universidad Politécnica de Madrid) attended the course of Tipología Estructural and he reminisced on his experience as a student in a recent book [4]: "in fourth year Prof. Torroja taught Tipología Estructural', his favourite subject. In each class, he would lecture for 20 minutes and then call a student to the blackboard. The class was broken down into three-student teams, each of which was to draft a provisional design. The students were free to choose their partners as well as the subject of the design. When a student representing a team stood up in front of the class to explain their preliminary design, Prof. Torroja allowed no calculating, but asked continually about the depth and width of the members and the structural system".

In 1957, the first edition of Torroja's book "Razón y ser de los tipos estructurales" was published [10]. The book's content closely mirrored the course syllabus. Eduardo Torroja passed away in 1961, and Juan Batanero took over the course from 1961-62 until 1983-84, making slight changes to the syllabus. Jose Antonio Torroja, Eduardo's son, taught the course from 1984-85 until 2002-03. Since then, Hugo Corres has been the primary instructor, with support from the author since the 2012-13 academic year.

The following section is addressed to describe the current organization of the course.

3.2. Today

"Tipología Estructural" is an unconventional course where each instructor brings a unique approach to teaching. Due to its complexity, effective teaching of Conceptual Design relies heavily on lived experiences. Currently, "Tipología Estructural" is a mandatory course for all the students enrolled in the Master of Civil Engineering program; this introduces new challenges as it must engage students who may not primarily be interested in structural engineering. However, this challenge also presents an opportunity. Viewing engineering as a creative profession, the principles of conceptual design can be applied across various fields, including hydraulic works, ports, and linear infrastructure.

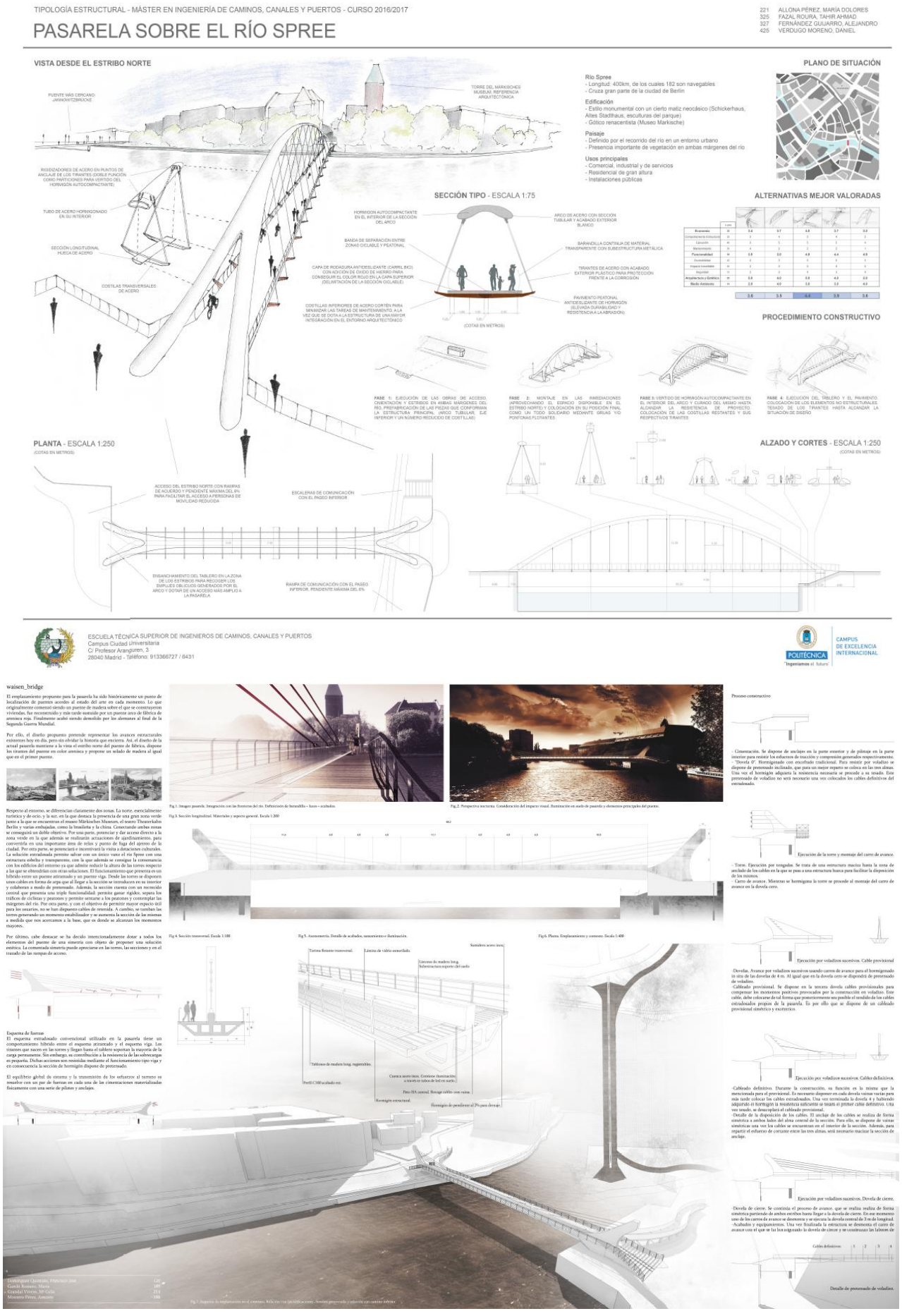

Figure 7. Examples of final submission.

The knowledge acquired in this course can be applied to various structural typologies such as bridges, buildings, residential towers, wind towers, cooling towers, water deposits, etc… For each typology, the course provides:

- Typical dimensions, geometrical ratio and material quantities.
- An overview of applications.
- Dimensioning of main elements.
- Analysis of specific details.
- Considerations about aesthetics and durability.

The course is structured as a project-based learning experience, where students gain hands-on skill in designing structural systems. By the end of the course, students should be able to:

- Define the main structural design parameters and identify constraints and boundary conditions.
- Visualise force flows and explain the fundamental behaviour of different structural typologies.
- Identify the relationships between structural form, internal forces and building.
- Analyse existing structures using appropriate terminology (in both English and Spanish) and objective arguments
- Dimension predominant elements of different structural typologies by hand.
- Have an awareness of material properties and their design potential and limits.
- Critically question structural design concepts of historical and contemporary references.
- Design an appropriate structural system for a given design challenge, considering a wide range of structural typologies.
- Design structures creatively and generate structural forms beyond known typologies.

Lectures are supplemented by flipped classrooms and invited speakers. To foster the interdisciplinary nature of the course, several speakers from various backgrounds have been invited in recent years: Taba Rasti and Pablo Urango on architecture, Fernando Porras on urbanism, Sandro Rocci on roads design, Luis Miguel Viartola on construction processes, Cristina Iglesias on sculptures, and Peter Tanner, José Romo, Borja Herraiz and Carles-Hug Bitlloch on structural design.

Students are tasked with developing a preliminary design for a structural solution to a given problem, which varies each year. There is an intermediate submission where students define the most relevant design criteria, develop several design alternatives, and finally select the proposal to be developed further. Figure 6 illustrates an example of intermediate submission with the first design concept and hand calculations for an arch footbridge.

The final submission consists of an A1-format poster with oral defence describing the develop project. Two examples of these posters are illustrated in Figure 7.

6. FINAL REMARKS

Structural designers have a huge responsibility in promoting sustainability within the construction industry. The integration of the sustainability framework into structural design requires ethical responsibility, comprehensive knowledge, and a holistic approach, encompassing environmental, economic, and social dimensions. This change must begin at the Conceptual Design stage, as early decisions profoundly impact the sustainability of the entire project.

The essential ingredients for a sound Conceptual Design of a structure are creativity, experience and knowledge. A deep understanding of fundamental structural concepts is crucial for innovation. Concepts like funicularity and Maxwell's Theorem are simple and powerful and should be perfectly know by every structural designer.

Education plays a vital role in this transformation. Eduardo Torroja was a pioneer in teaching Conceptual Design at academic level, integrating diverse knowledge areas and hands-on design experience. His visionary course, which continues today, uses a project-based learning to foster creativity and practical problem-solving skills, preparing students to tackle structural design challenges in the framework of the sustainability.

To conclude this paper, the author recalls an insightful statement by Hugo Corres "Problems should not be solved. They should be avoided." A sound conceptual design of a structure is an essential step in this direction.

References

[1] B. Regúlez, D. M. V. Faria, L. Todisco, M. Fernández Ruiz, and H. Corres, "Sustainability in construction: The urgent need for a new ethics," Structural Concrete, 2022, doi: 10.1002/SUCO.202200406.

[2] N. Kohler and S. Moffatt, "Life-cycle analysis of the built environment. ," in NEP Industry and Environment , Nairobi, Kenya, 2003, pp. 17–21.

[3] C. De Wolf, J. Hogroian, and J. Ochsendorf, "Comparing material quantities and embodied carbon in stadia," in Proceedings of IASS Annual Symposia, IASS 2014 Brasilia, International Association for Shell and Spatial Structures (IASS), 2014, pp. 1–8.

[4] R. Ruiz, L. Todisco, and H. Corres, "Application of high-performance fibre reinforced concrete to precast girders for road bridges: Conceptual considerations and numerical analyses," Structural Concrete, vol. 24, no. 4, pp. 4645–4659, Aug. 2023, doi: 10.1002/suco.202200907.

[5] R. Ruiz, V. Chozas-Ligero, L. Todisco, J. D. Jimenez-Vicaria, and H. Corres, "Experimental characterization of a cost-competitive tailor-made HPFRC mix design for wide application in precast girder of roadway bridges," Structural Concrete, vol. 25, no. 2, pp. 935–955, Apr. 2024, doi: 10.1002/suco.202300550.

[6] R. Ruiz, M. Fernández Ruiz, L. Todisco, and H. Corres, "Shear resistance of prestressed HPFRC beams without stirrups: A mechanical analysis of shear-transfer actions based on detailed experimental measurements," Eng Struct, vol. 306, p. 117711, May 2024, doi: 10.1016/j.engstruct.2024.117711.

[7] J. Romo, "Conceptual Design of Bridges and Sustainability," in IABSE Symposium 2019 Guimarães: Towards a Resilient Built Environment - Risk and Asset Management, Guimaraes: IABSE, Mar. 2019.

[8] A. Mari and J. A. Torroja, "Education of structural engineers in conceptual design: the Spanish experience," in Proceedings of Conceptual Design of Structures, Stuttgart: IASS, 1996.

[9] A. Kessler, Salginatobelbrücke. Buchdruckerei, Schiers, 2011.

[10] E. Torroja, Razón y ser de los tipos estructurales. Madrid: Instituto de la Construcción y del Cemento, 1957.

[11] L. Todisco, H. Corres, A. Pérez, A. Addante, and J. Cañada, "Conceptual design of spatial arch footbridges supporting curved decks," Structures, vol. 33, pp. 1207–1215, Oct. 2021, doi: 10.1016/J.ISTRUC.2021.05.003.

[12] J. Cañada Pérez-Sala and L. Todisco, "Conceptual design of externally posttensioned curved structures for live loads," Structural Concrete, vol. 21, no. 6, pp. 2220–2236, Dec. 2020, doi: 10.1002/SUCO.201900536.

[13] L. Todisco, H. C. Peiretti, and C. Mueller, "Funicularity through external posttensioning: Design philosophy and computational tool," Journal of Structural Engineering (United States), vol. 142, no. 2, 2016, doi: 10.1061/(ASCE)ST.1943-541X.0001416.

[14] W. F. Baker, L. L. Beghini, A. Mazurek, J. Carrion, and A. Beghini, "Structural innovation: Combining classic theories with new technologies," Engineering Journal, vol. 52, no. 3, pp. 203–217, 2015, [Online]. Available: http://www.scopus.com/inward/record.url?eid=2-s2.0-84934279219&partnerID=40&md5=bf0e488ee136d217f958d1a69fcda091

Disponible en **www.hormigonyacero.com**
https://doi.org/10.33586/hya.2026.4146

Harmony between Concrete and Reinforcement: From Ferrocemento to 3D Concrete Printing and Cementitious Composites

Armonía entre el hormigón y la armadura: del ferrocemento a la impresión 3D de hormigón y los compuestos cementicios

György L. Balázs[a,*]

[a] *Prof., Honorary President of fib. Budapest University of Technology and Economics. Faculty of Civil Eng., Dept. of Construction Materials and Technologies.*

Recibido el 29 de agosto de 2025; revisado el 15 de octubre de 2025, aceptado el 19 de febrero de 2026

ABSTRACT

One of the key elements for the performance of reinforced concrete structures is the interaction of concrete and reinforcement. Introductory examples are mentioned for the successful use of reinforced concrete.

Recent developments with 3D concrete printing established two questions concerning the potential use of reinforcements: i) a practical example is presented for 3D concrete printed shell element with tensile chords of FRP reinforcements; ii) interlaminar shear is solved with 3-dimensional reinforcing elements (STAREX). The 3-dimensional reinforcing elements improves the performance of the whole element.

FRP reinforcements are used in increasing amount to avoid electrolytic corrosion of the reinforcement. A new reinforcement is: Carbon fibres in cementitious matrix = CFCM, which does not include polymers as matrix, but a cementitious matrix is used to improve cooperation both the carbon fibres and concrete. The cementitious matrix reduces sensitivity for high temperatures. With carbon fibres in cementitious matrix reinforcement, the reinforced concrete elements can be produced with no or little cover.

This article presents conceptual and technological advances toward the integration of innovative reinforcing materials and technologies in concrete structures.

KEYWORDS: 3D concrete printing, interlaminar shear, 3-dimensional reinforcing elements, Carbon fibres in cementitious matrix reinforcement, no cover.

RESUMEN

Uno de los aspectos clave en el desempeño de las estructuras de hormigón es la interacción entre el hormigón y la armadura. En este artículo se mencionan algunos ejemplos introductorios del uso exitoso del hormigón armado.

Los desarrollos recientes en el hormigón impreso en 3D ponen de manifiesto dos cuestiones relacionadas con el uso de las armaduras:

i) se presentan ejemplos prácticos de láminas de hormigón impreso con cordones de tracción basados en armaduras de FRP;

ii) el esfuerzo cortante entre capas se resuelve mediante un armado tridimensional (STAREX). El armado tridimensional mejora el desempeño de todo el elemento estructural.

Las armaduras de FRP se utilizan cada vez más para evitar la corrosión electroquímica del acero de refuerzo. Un nuevo tipo de armadura consiste en fibras de carbono en matriz cementicia (CFCM), que no utiliza polímeros en la matriz, sino una matriz a base de cemento para mejorar la acción conjunta entre las fibras de carbono y el hormigón. La ma-

triz cementicia reduce además la sensibilidad a las altas temperaturas. Con fibras de carbono en matriz cementicia, los elementos de hormigón armado pueden producirse con un recubrimiento reducido o incluso nulo.

Este artículo presenta avances conceptuales y tecnológicos orientados a la integración de materiales y tecnologías de refuerzo innovadores en estructuras de hormigón.

PALABRAS CLAVE: hormigón impreso en 3D, cortante entre capas, elementos de armado 3D, fibras de carbono en matriz cementicia, recubrimiento nulo.

* Persona de contacto / *Corresponding author*:
Correo-e / *e-mail*: balazs.gyorgy@emk.bme.hu (György L. Balázs)

How to cite this article: Balázs, G. (2026). Harmony of Concrete and Reinforcement. *Hormigón y Acero*. 77(308):207-213 https://doi.org/10.33586/hya.2026.4146

Harmony of concrete and reinforcement

a) Conventional concrete:

Reinforced concrete	Prestressed concrete

b) Innovative concretes for the future:

Digital manufacturing	STAREX reinforcing elements	CFCM reinforcement =
3D concrete printing with or without reinforcement	3-dimensional reinforcement for general use	Carbon fibres in cementitious matrix reinforcement

Figure 1. Conceptual timeline for conventional and novel concretes

1. INTRODUCTION

Engineering intuition is strongly required for the harmony of materials to choose structural materials like concrete, steel, timber, glass, and FRP, and their combination in composite structures to define the most reasonable one or the most economic one to the given load history or to the given geometry.

Structural design requires a detailed understanding of both the material and the structural behaviours. An additional requirement is to incorporate the new structure into the existing environment as structures like bridges, buildings, halls, or reservoirs, etc.

Reinforced concrete is a composite structural material that has a continuous development considering its constituent materials as well as its technology to fulfil overall requirements of: safety, serviceability, constructability, economics, aesthetics, and nowadays sustainability.

The present paper is a vision how the novel materials and technological developments can provide the basis for scientific innovations for reinforced concrete [1] [2] and improving conceptual future designs [3].

There was already a harmony of concrete and reinforcement from the beginning of applications which resulted many patents and applications worldwide. Nevertheless, concrete became to most frequently used construction material. There have already been publications to advise the successful use of reinforced concrete [4] [5].

Recent novelties in concrete and reinforcement are discussed in the following Chapters Innovative concretes for the future including (i) digital manufacturing in 3D concrete printing, (ii) a new reinforcing element for general use called STAREX and (iii) a new type of non-metallic reinforcement of carbon fibres in cementitious matrix in addition to the presentation of the Palazzo dello Sport as a reference for successful use of reinforced concrete in a bit modified way in the fifties (Figure 1).

2. DESIGNING WITH REINFORCED CONCRETE

A beautiful example for harmonic use of reinforced concrete and the structural system is the *Palazzo dello Sport by Pier Luigi Nervi* is (Figure 2). He developed the reinforced concrete type for thin concrete elements like the cover of the dome, which is called in Italian *ferrocemento*. It included a small size of aggregate with a small diameter or reinforcement. This concept of material is important even today.

3. DESIGNING 3D PRINTED CONCRETE

The 3D concrete printing is a disruptive technology without using any formwork. It is also often distinguished as an additive technology indicating how the material is proceeded. This is very productive technology whenever the material composition is available supplied continuously.

The 3D concrete printing (often abbreviated as 3D CP) process is controlled by the fresh properties of the concrete. Specifically, the mix, which should have sufficient green strength, must be capable of flowing through a distribution system and then be deposited in layers onto a build substrate without experiencing significant damage while also supporting the weight of subsequent layers.

Formwork in concrete construction constitutes a high percentage of the structure cost [6], often generates substantial waste, and imposes limitations on geometric freedom. Complex geometries may escalate costs and impede construction speed. In addition to that, nearly every stage of the construction process demands significant energy and results in substantial greenhouse gas emissions [7].

Zhang et al. [8] outline various applications of 3D CP, including buildings, bridges, and structures printed with simulated lunar regolith.

Bhattacherjee et al. [9] examined the sustainability of Supplementary Cementitious Materials (SCMs) for 3DCP, using carbon footprint and embodied energy as metrics. Their findings indicate that concretes incorporating fly ash, slags as SCMs, and geopolymer concrete exhibit lower carbon footprints and embodied energy compared to conventional Portland cement-based concretes.

Freedom of design in 3D printed concrete structural elements is often emphasized. It is a very particular way of designing elements. The designer should draw a continuous line, how the printing head finally does it. The whole con-

Figure 2. Palazzo dello Sport, main hall and foyer Roma, Italy (Photo GL. Balázs).

struction – or segments of it – must be able to be followed by the method of line drawing.

Figure 3 indicates the 1st arch bridge in Hungary produced in 3D concrete printing. The specialities of this printing are the different structural elements, i.e. compressed arch, compressed columns and the horizontal deck in final position.

Figure 3. Arch bridge produced in 3D concrete printing (Lab. of Construction Materials and Technologies, BME, Budapest) (Photo GL Balázs).

4. REINFORCEMENT FOR 3D CONCRETE PRINTING

4.1. 3D concrete printing of a cylindrical shell element

The conceptual design in 3D concrete printing is of particular importance. An example is presented in Figure 4 for a structural element, a shell with constant curvature. The details of the shell element such as actual shape and curvature of the shell, support length, incorporation of tensile element in the anchorage zone are decided during the design printing. It is imperative to acknowledge the pivotal role that effective conceptual design plays in the realm of engineering structures [3] [10] [11].

Parameters, like printing speed, nose shape, nose diameter must be also decided before printing.

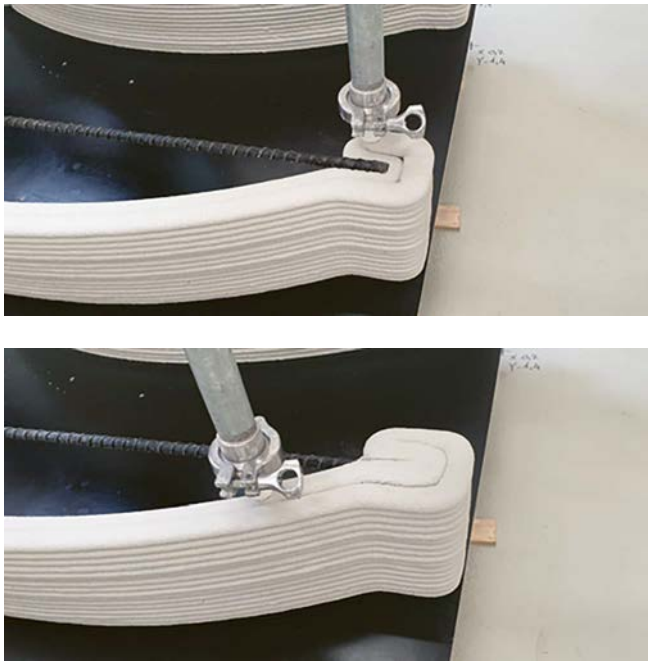

Figure 4. Anchorage details of 3D concrete printed shell element including tensile FRP reinforcement during the 3D concrete printing process (Lab. of Construction Materials and Technologies, BME, Budapest) (Photo GL Balázs).

As illustrated in Figure 4, the utilisation of FRP (Fibre Reinforced Plastic) reinforcement as tensile reinforcement is evident. The following presentation will provide a detailed overview of the process of applying tensile FRP reinforcement. Bond stresses must be analysed in order to conduct an anchorage analysis.

The incorporation of FRP reinforcement into 3D concrete printed cylindrical shell element is presented in Fib. 5.

Figure 5. The incorporation of FRP reinforcement into 3D concrete printed cylindrical shell element (Lab. of Construction Materials and Technologies, BME, Budapest) (Photo GL Balázs).

4.2. Interlaminar shear in 3D concrete printing

In the context of 3D concrete printing, a layered technique, interlaminar shear is of particular significance. It is evident

that the utilisation of short polymeric fibres, which are incorporated into the concrete mixture prior to printing, may not serve as a viable solution for the interlaminar shear of a beam or wall element.

A new solution is developed in Figure 6 to improve interlaminar shear capacity of printed concrete layers. The new solution includes distribution of 3-dimensional STAREX reinforcing elements within the printed layers. (The international patent known as STAREX was granted to Csongor Czintos.)

In this way performance of the whole wall or element in 3D concrete printing is improved [12].

Figure 6. Increase of interlaminar shear in 3D printed concrete by STAREX elements (Lab. of Construction Materials and Technologies, BME, Budapest) (Photo GL Balázs).

The STAREX reinforcing elements can be produced in different sizes for different applications (Figure 7). The overhanging hooks, the diameter of wire and even the material are parameters of the production STAREX reinforcing elements.

Figure 7. STAREX reinforcing elements of different sizes (Lab. of Construction Materials and Technologies, BME, Budapest) (Photo GL Balázs).

The potentials of STAREX reinforcing elements for structural applications are mentioned in [13].

5. CARBON FIBRES IN CEMENTITIOUS MATRIX

Carbon fibres in cementitious matrix reinforcement = CFCM reinforcement is a new patent that reduces the temperature sensitivity of FRP reinforcement (CFCM is an international patent).

Contrary to FRP reinforcement, the embedding matrix of the fibres is changed to cement-based matrix. In this way the reinforcement has a contact to the concrete by cement (not polymer) binder.

The CFCM reinforcement can be produced in any shape or cross-section, and it has been demonstrated that it provides a strong bond between the reinforcement, which is cement-bound, and the concrete [14]. As demonstrated in Figure 8, the utilisation of CFCM reinforcement serves to illustrate the spatial shell, thereby signifying the capacity for formability.

Figure 8. Spherical shell model in CFCM reinforcement [14].

Another example in Figure 9 is shown indicating an easy preparation of helical stirrup reinforcement.

Figure 9. Helical CFCM reinforcement.

Whenever the CFCM reinforcement is bonded to concrete the bond layer is extraordinary since the concrete has binder as cement and in the same way the reinforcement has binder as cement (Figure 10).

Figure 10. Bond layer of an embedded CFCM reinforcement opened after failure of the element – is still entirely connected to the concrete Lab. of Construction Materials and Technologies, BME, Budapest) [14] (Photo GL Balázs).

a) Beam with no concrete cover

b) Material properties of carbon fibres (ZOLTEK TORAY Group):

tensile strength:	f_{fib} = 4 137 N/mm²
modulus of elasticity:	E_{fib} = 242 000 N/mm²
ultimate elongation:	ε_{fib} = 1.5 %
diameter of single fibres:	7.2 x 10^{-6} m
number of fibres in 1 cable: :	50 000

Design concrete strength of I girder:

compressive strength: 80 N/mm²

c) Test arrangement (dimensions in mm

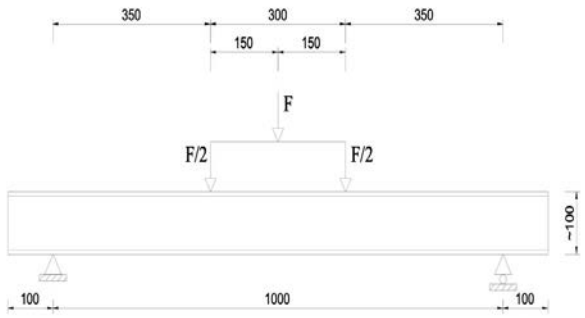

d) Load – midspan deflection diagram of beam with 24 x 50 000 carbon fibres

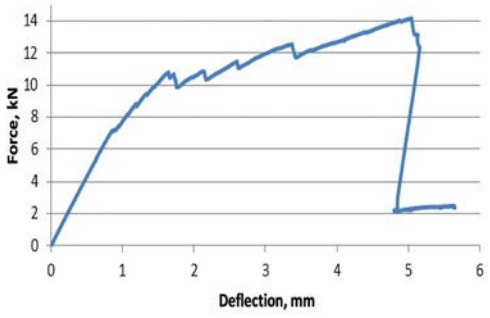

Figure 11. A concept with no cover of CFCM reinforcement in beam test, (Lab. of Construction Materials and Technologies, BME, Budapest) [14].

Since the CFCM reinforcement is in fresh form within several hours and insensitive for corrosion. there is real chance to a new definition of concrete cover with zero or a small value. Figure 11 indicates beams with zero concrete cover tested in 4-point bending (Figure 11.c). Material properties for the CFCM reinforcement as well as for concrete are given in Figure11.b. The force - deflection diagram indicates bilinear behaviour until failure (Figure 11.d).

6. CONCLUSIONS

The harmonious integration of concrete and reinforcement led to the global adoption of reinforced concrete across all continents. The requirements for safety, serviceability, constructability, economy, aesthetics and sustainability thus provide a stimulus for new ideas in development and innovation. In this work three disruptive inventions are presented and discussed with applications: 3D concrete printing, a new 3-dimentsional reinforcing element and the reinforcement that has carbon fibres in cementitious matrix.

a. *The 3D concrete printing* is a disruptive technology that does not use any formwork. It is also often distinguished as an additive technology, indicating how the material is processed. This is a very productive technology whenever the material composition is available and supplied continuously. Freedom of design in 3D printed concrete structural elements is often emphasized. The integration of reinforcement within three-dimensional concrete-printed elements presents certain technological challenges, which must be addressed to ensure the successful incorporation of the reinforcement. Two solutions were discussed to overcome these difficulties. An example was shown for printing of a *shell element* where FRP bars were inserted during printing as tensile reinforcement of the shell (see Figure 4 and 5).

b. As demonstrated by another example, the *overall stability of printed concrete layers* can be enhanced through the incorporation of three-dimensional reinforcing elements, which function as interlaminar shear reinforcement. (see Figure 6 and 7).

c. The most compatible reinforcement for concrete is provided by a new development, since carbon fibres are embedded into the cement matrix (rather than into a polymer). The cementitious matrix of reinforcement enables improved fire resistance and corrosion resistance. Since the carbon fibres are embedded into the cement matrix, the reinforcement is called carbon fibres in cementitious matrix reinforcement and abbreviated as CFCM. An ex-

ample is shown for helical CFCM reinforcement (see Figure 8). Since the electrolytic corrosion is entirely excluded and the temperature sensitivity of the reinforcement is improved, there is a possibility of reducing the concrete cover on the elements by employing CFCM reinforcements, provided that other factors do not necessitate a substantial cover (see Figure 11).

Acknowledgements:

This article is dedicated to my dear friends and colleagues Antonio Marí and Hugo Corres, on the occasion of their retirement and as a tribute to their academic and professional career in concrete structures.

The author acknowledges the support of the Hungarian Research Grant KFI_016-1-2017-0271 "Development of fibre reinforced cementitious composite reinforcements based on Csurgai's patent for application in concrete products".

The herein presented new reinforcing element of 3-dimensional form is the patent of Csongor Czintos (Patent Nr.: HU2017/050041). His help is gratefully acknowledged.

The CFCM reinforcement was prepared by the patent of Ferenc Csurgai "Production procedure and machinery to produce cables from single fibres by embedment in a matrix and its application to concrete-composites". PCT/HU2017/050010 int. (11 April 2016), final patent: P1700140 (dated 7 April 2017).

References:

[1] Marí, A., Bairán, J., Cladera, A., Oller, E., Ribas, C. (2014), "Shear-flexural strength mechanical model for the design and assessment of reinforced concrete beams", J. *Structure and Infrastructure Engineering: Maintenance, Management, Life-Cycle Design and Performance*, Taylor and Francis, http://dx.doi.org/10.1080/15732479.2014.964735

[2] Cladera, A, Marí, A., Ribas, C., Bairán, J., Oller, E. (2015), "Predicting the shear–flexural strength of slender reinforced concrete T and I shaped beams", J. *Engineering Stuctures*, Vol. 101 pp. 386-398., Elsevier, http://dx.doi.org/10.1016/j.engstruct.2015.07.025

[3] Corres, H., Todisco, L., Fivet, C. (Eds.) (2019), "Conceptual Design of Structures 2019", Madrid, September 26-28, 2019, Proceedings

[4] Ritter, W. (1899), *Construction method of Hennebique (Die Bauweise Hennebique)*, *Schweizerische Bauzeitung*, February 1899, pp. 41-61.

[5] Mörsch, E. (1908), *Reinforced concrete – Theory and application (Der Eisenbetonbau – Seine Theorie und Anwendung)*, Verlag von Konrad Wittwer, Stuttgart, pp. 146-215.

[6] Nematollahi, B., Xia, M., J. Sanjayan, J. (2017), "Current Progress of 3D Concrete Printing Technologies," in Proceedings of the 34th International Symposium on Automation and Robotics in Construction (ISARC), Jul. 2017, pp. 260–267, 10.22260/ISARC2017/0035

[7] Yan, H., Shen, Q., Fan, L.C.H., Wang, Y., Zhang, L. (2010), "Greenhouse gas emissions in building construction: A case study of One Peking in Hong Kong", Build. Environ. 45 (4) (2010), pp. 949–955, https://doi.org/10.1016/J.BUILDENV.2009.09.014.

[8] Zhang,J., Wang, J., Dong, S., Yu, X., Han, B, (2019) "A review of the current progress and application of 3D printed concrete", Compos. A Appl. Sci. Manuf. 125/2019, 105533, https://doi.org/10.1016/j.compositesa.2019.105533.

[9] Bhattacherjee, S. et al. (2021), "Sustainable materials for 3D concrete printing", Cem. Concr. Compos. Vol. 122, No. June (2021), 104156, https://doi.org/10.1016/j.cemconcomp.2021.104156.

[10] Fivet, C, D'Acunto, P., Fernandez Ruiz, M., Ohlbrock, P. O. (Eds.), "Conceptual Design of Structures 2021", Attisholz Areal, Switzerland, September 16-18, 2021, Proceedings

[11] Thajeel, M. M., Alimrani, N. S. and Balázs, G.L. (2022), "3D Concrete Printing Structural and Non-Structural Solutions," J. *Concrete Structures*, Vol. 23, pp. 47-53. www.fib.bme.hu/folyoirat/cs/cs2022/cs2022_7.pdf

[12] Balázs, G.L., Czintos, Cs., Pfeffermann, O., Sólyom, S. (2025), "New reinforcing element for automated production of reinforced concrete", Proceedings of Symp. Conceptual Design Rio de Janiero

[13] Balázs, G.L. (2025), "Future reinforcement for concrete", Proceedings of the *fib* Symposium 2025, June 16 to 18, 2025, Antibes, France, pp. 167-1773.

[14] Balázs, G.L., Csurgai, F. Sólyom, S. (2022), "Bond of CFCM", Proceedings (Eds. Hoffmann, J, and Plizzari, G.), "Bond Anchorage Detailing", 5th In Conf. Bond in Concrete 2022, Stuttgart, 25-27 July 2022, IWB Stuttgart University, pp. 945-954.

imesAPI
Servicios · Movilidad

REHABILITACIÓN DE PUENTES

- PUENTES METÁLICOS
- PASARELAS PEATONALES
- PUENTES DE FÁBRICA
- PUENTES HISTÓRICOS
- PUENTES DE HORMIGÓN
- HIDRODEMOLICIÓN
- GATEOS

PUENTES METÁLICOS

PUENTES DE FÁBRICA

PUENTES DE HORMIGÓN

Gateos y cambios de apoyos

imesAPI
Servicios · Movilidad

cobra IS VINCI

Avenida Ramón y Cajal, 107 · 28043 MADRID
Tel. 91 744 39 00 · Fax 91 744 39 01

AENOR Gestión Energética UNE-EN ISO 50001 · AENOR Gestión Ambiental UNE-EN ISO 14001 · AENOR Empresa Registrada UNE-EN ISO 9001 · AENOR Gestión I+D+i UNE 166002 · Cerne Seguridad y Salud ISO 45001 · International Certifications OHSAS 18001

www.imesapi.es

Disponible en **www.hormigonyacero.com**
https://doi.org/10.33586/hya.2025.4104

Montaje con dovelas en puentes atirantados

Segmental Assembly Method in Cable-Stayed Bridges

Conchita Lucas Serrano[a]

[a] *Ingeniera de Caminos, Canales y Puertos. Jefa del Departamento de Infraestructuras de Transporte. Dirección Técnica. DRAGADOS, SA.*

Recibido el 30 de septiembre de 2024; revisado el 10 de noviembre de 2024, aceptado el 5 de diciembre de 2024

RESUMEN

El montaje por dovelas es muy habitual en la construcción de puentes atirantados ejecutados con el procedimiento de avance en voladizo. Sin embargo, la definición de la dovela tipo es una cuestión delicada, pues implica la toma de una serie de decisiones que tienen una gran repercusión en la construcción. Asimismo, es muy importante prestar atención a la definición del carro de izado de dovelas, específicamente a cómo se apoya en el tablero ya construido y de dónde debe coger las dovelas a izar. Estas dos cuestiones determinan como serán las deformadas transversales de los labios a unir, el frente del tablero y la dovela que se iza, y puede transformar el acople de dovelas en una tarea más del ciclo o en un verdadero quebradero de cabeza.

Se expone en el artículo cómo se abordaron estas cuestiones en varios puentes atirantados construidos por Dragados en los últimos años, donde se realizó un montaje con dovelas: el Puente de la Constitución de 1812 sobre la bahía de Cádiz, el Queensferry Crossing en Reino Unido, el Nuevo Puente de Champlain en Canadá y la ampliación del Puente de Rande en Vigo.

PALABRAS CLAVE: Puente atirantado, dovela, avance en voladizo, carro de izado.

ABSTRACT

The segmental assembly method is very common in the construction of cable-stayed bridges built using the cantilever method. However, defining the typical segment is a delicate matter that involves making a series of decisions with significant implications for the construction process. Additionally, it is crucial to pay attention to the design of the lifting gantry, specifically how it is supported on the already-built deck and where it picks up the segments to be lifted. These two factors determine the transverse deflecfions of the joints to be connected, the deck front, and the segment being lifted. As a result, the segment assembly can either be as straightforward as any other task or turn into a real headache.

This paper explains how these issues were addressed in several cable-stayed bridges built by Dragados in recent years, where the segmental assembly method was used: 1812 Constitution Bridge over Cádiz Bay (Spain), Queensferry Crossing in the UK, the New Champlain Bridge in Canada and the expansion of the Rande Bridge in Vigo (Spain).

KEYWORDS: Cable-stayed bridge, segment, balanced cantilever, segment lifter.

* Persona de contacto / *Corresponding author*:
Correo-e / *e-mail*: clucass@dragados.com (Conchita Lucas)

Cómo citar este artículo: Lucas, C. (2026). Izado de dovelas en puentes atirantados. *Hormigón y Acero*. 77(308):215-233. https://doi.org/10.33586/hya.2025.4104

1.
INTRODUCCIÓN

En los últimos años hemos construido en Dragados una serie de grandes puentes atirantados, lo que nos ha permitido adquirir una experiencia muy valiosa y aplicar en cada uno de los proyectos todas las lecciones aprendidas en los anteriores.

La elección del procedimiento constructivo es siempre importante a la hora de afrontar la ejecución de un puente, pero lo es aún más cuando se trata de estructuras de gran envergadura. Con mucha frecuencia en grandes puentes es la fase constructiva la que gobierna el dimensionamiento, por lo que todas las decisiones que se tomen a ese respecto son cruciales. Pero no sólo es relevante la elección del proceso constructivo general, sino también la determinación de cuál será la unidad básica de construcción y cómo se procederá a su colocación. Es decir, la definición de la dovela y su instalación.

Este artículo se va a centrar en la construcción de varios puentes atirantados con tablero de sección cajón mixto, ejecutados por avance en voladizo y montados con dovelas, pero focalizándose en esta unidad básica de la construcción que es la dovela y su sistema de izado. En concreto nos referiremos al Puente de la Constitución de 1812 sobre la bahía de Cádiz (España), al Queensferry Crossing (Reino Unido), a la ampliación del puente de Rande (España) y al nuevo puente de Champlain sobre el río San Lorenzo (Canadá). En estos dos últimos Dragados contó durante su construcción con el apoyo del Profesor Corres Peirefti y su equipo de Fhecor, que prestaron una ayuda inestimable.

2.
PRIMERAS DECISIONES

Desde el punto de vista longitudinal, el procedimiento típico de construcción de puentes atirantados es el avance en voladizo; ya sea voladizo simple, cuando se construye primero el vano de retenida apoyado en el suelo (sobre cimbra, puntales, torres de apeo, etc.) para, a continuación, abordar el vano principal con avance en voladizo; o el *balanced cantilever*, cuando se va avanzando en voladizo desde la torre hacia los dos lados (vano principal y vano de retenida) de forma equilibrada. En la gran mayoría de los casos, la fase constructiva es la más desfavorable en la vida del puente, pues el tablero está sometido a acciones muy importantes y se encuentra en una situación mucho más precaria (un gran voladizo) que durante la fase de servicio, en la que el tablero descansa ya en todas las pilas y tiene todos los tirantes instalados. Es por ello, que desde el punto de vista económico y también constructivo es más recomendable, si se puede, recurrir al voladizo simple una vez se han construido los vanos de retenida, que a un *balanced cantilever* donde la seguridad estructural está mucho más comprometida y el dimensionamiento de la estructura (cimentación y torre) gobernado por el proceso constructivo.

Transversalmente la decisión que hay tomar es si se montan dovelas, una porción de tablero de sección completa previamente fabricada en taller, o se van colocando en altura los diferentes elementos metálicos que forman la sección transversal; lo que en inglés se denomina "stick build".

Es habitual en los puentes con sección cajón adoptar el sistema de dovelas, mientras que cuando se trata de secciones abiertas la opción de *stick build* resulta más interesante. Ambos sistemas tienen ventajas e inconvenientes, pero podríamos resumirlos aquí diciendo que las dovelas reducen los trabajos de soldadura o atornillado en altura, muy penosos en climas adversos, y exigen un control de fabricación muy estricto que da lugar a una estructura de gran calidad. Su principal desventaja es que la carga en la punta del voladizo es tan grande (peso del carro + peso dovela), que la hipótesis de izado suele dimensionar la estructura final. Por su parte, el método de *stick build* exige mucho trabajo en altura para ir ensamblando las piezas de la sección, lo que en el otro método se hace en taller, pero la carga en punta durante el izado es menor y las correcciones geométricas durante la construcción, inevitables, son más fáciles de implementar.

3.
DEFINICIÓN DE LA DOVELA TIPO

Como ya se ha dicho, una dovela es una porción de tablero que se fabrica previamente en taller y se iza para ser colocada en su posición final. Sin embargo, el concepto dovela admite algunas variantes. Longitudinalmente es habitual definir la longitud de la dovela de un puente atirantado igual a la distancia entre tirantes. Esto fue así en el caso del Queensferry Crossing (separación de tirantes y dovelas de 16,20 m), en la ampliación del Puente de Rande (separación de tirantes y dovelas de 21,06 m) y en el nuevo puente de Champlain (separación de tirantes y dovelas 12,60 m). Sin embargo, en el Puente de la Constitución de 1812 sobre la bahía de Cádiz para reducir el plazo de ejecución, se tomó la decisión de fabricar dovelas del doble de la longitud estándar, de forma que llevaran dos parejas de tirantes: 20 m de dovela cuando los tirantes estaban dispuestos cada 10 m. Esto supuso, sin duda, un gran reto, pues las demandas durante la fase constructiva aumentaban de forma considerable, pero se consiguió el objetivo buscado de reducir a la mitad el número de uniones en obra.

La dovela también admite variaciones transversales, pues se puede izar con o sin la losa de hormigón colocada, y eliminando o no los voladizos laterales. En los casos que se están exponiendo se subió la dovela del ancho completo en todos ellos (es lo habitual), pero respecto a la losa de hormigón, las decisiones fueron diferentes, muy condicionadas por el lugar donde cada uno de los puentes está ubicado. La decisión es trascendente, pues incluir o no la losa de hormigón condiciona totalmente el medio de izado (la carga se multiplica por 2 o por 3) y tiene un impacto en el dimensionamiento de la estructura permanente, pero el ciclo constructivo en altura se reduce y se minimizan las operaciones sobre el tablero, más sujetas a problemas e imprevistos. Subir la dovela con la losa de hormigón reduce el ciclo de forma significativa por dos razones:

1. La primera y más obvia, porque la losa de hormigón ya está colocada y sólo hay que hormigonar en altura la junta transversal con la dovela anterior.
2. La segunda es que se reducen las fases de tesado de los tirantes. Cuando se sube la dovela exclusivamente metálica hay que instalar los tirantes con muy poca carga para no generar

flexiones excesivas en la dovela metálica que, sin la losa de hormigón, tiene una cabeza superior muy reducida, ni aumentar significativamente las tensiones residuales en la sección metálica. Después, cuando se termina la losa superior, se hace un retesado de los tirantes para compensar esa nueva carga. Por el contrario, si la dovela se iza ya con la losa superior de hormigón ejecutada, tras la unión de la estructura metálica, se hormigona la junta y los tirantes se instalan con una carga superior, evitando una fase de tesado adicional.

El impacto de subir la dovela con la losa de hormigón ya ejecutada y tesar los tirantes en una única fase se debe al hecho de que el peso de la nueva dovela (con la losa) y el tesado de los tirantes tendría que ser resistido por la sección metálica de la junta entre dovelas y aparecerían ahí unas tensiones residuales (*locked in stresses*). En el otro caso, si se iza la dovela metálica y se da un primer tesado pequeño, esas tensiones residuales que aparecen en la sección metálica son más pequeñas y el segundo tesado, que es el de mayor entidad, entraría ya sobre la sección mixta una vez que se ha hormigonado toda la losa.

En los puentes que estamos usando de ejemplo, baste decir que, en los dos situados en clima frío, Queensferry Crossing y Champlain, las dovelas se izaron con la losa de hormigón (en Champlain no el 100% de la losa, pero sí la mayor parte), mientras que, en los dos españoles, Rande y Cádiz, la losa se colocó a posteriori.

Una vez decidida la geometría de la dovela, longitudinal y transversalmente, hay que tomar otras decisiones importantes: cómo se iza y cómo se ensambla. Cómo izar la dovela no sólo se refiere a qué medio usar; también hay que decidir, de qué puntos se coge la dovela, y dónde se apoya el elemento de izado. Estas decisiones tienen un impacto tremendo en la construcción del puente, pues una decisión equivocada puede llevar a sobredimensionar la estructura de forma importante y a complicar la construcción considerablemente por la dificultad de ensamblaje. Y es que uno de los problemas recurrentes en la construcción de puentes construidos por dovelas es el acople entre el frente del tablero ya construido y la dovela que se iza, pues ambas secciones que sobre el papel son idénticas, pueden tener deformaciones transversales diferentes cuando van a unirse.

4. MEDIOS PARA EL IZADO: CARROS DE IZADO DE DOVELAS

Los medios de izado de dovelas más habituales son los carros de izado, las grúas y las derricks. No vamos a entrar a discutir en este artículo las ventajas e inconvenientes de cada uno de estos tres medios de izado, pero sí podemos decir que en los cuatro puentes que se están usando como ejemplo se optó por emplear un carro de izado de dovelas: un medio diseñado específicamente para cada caso, que se adaptó a la geometría y necesidades de cada puente con una potente capacidad de izado.

Las grúas son poco habituales en el izado de dovelas pues el gran peso de éstas exige un contrapeso para funcionar que va en contra de la economía de pesos sobre el tablero. Las derricks tienen más tradición en Norteamérica, se anclan en el tablero por lo que no requieren contrapeso y se emplean para izar cargas en el entorno de las 150 t. Sin embargo, me atrevería a decir que su uso empieza a decaer pues no pueden competir con las modernas grúas hidráulicas, que cada vez son más seguras y están más automatizadas.

Si nos centramos en los carros de izado de dovelas, por ser los más habituales en grandes puentes, hay que decir, en primer lugar, que el diseño de estos elementos debe hacerse con el máximo esmero. Primero para que respondan a la perfección a las necesidades concretas de la obra, cumpliendo los estándares de seguridad requeridos. Segundo, para ajustar al máximo su peso y tercero, para definir un sistema de apoyo sobre el tablero ya construido de forma que no se requieran grandes refuerzos, ni se produzcan grandes deformaciones en el frente.

Estos elementos tienen un peso considerable, por lo que en muchos casos el peso del carro más la dovela que iza constituyen la carga dimensionante del puente. Piénsese que, en el momento del izado, el puente está en una situación estructural más precaria que en cualquier momento de su vida útil (voladizo de gran dimensión frente a la estructura terminada) y sometido a unas cargas en la punta como no va a volver a tener: el peso del medio de izado, más el peso de la dovela multiplicado por el coeficiente de impacto para considerar la eventual caída de la pieza durante el izado. A esto hay que sumarle el viento de maniobra, que hay que tratar de que sea el mayor posible, compatible con la seguridad de los trabajadores, para no condicionar la construcción y que se reduzca en exceso el número de días útiles de trabajo (cuando el viento es superior al de maniobra). A esta situación tan desfavorable hay que añadir, además, las sobrecargas de construcción, que no son en absoluto despreciables, pues hay que considerar el acopio de materiales (bobinas de cables, ferralla, etc.) y la circulación de maquinaria más o menos ligera sobre el tablero.

Pero no sólo hay que prestar atención al peso del medio a izar, sino también a cómo y dónde se apoya este elemento en el tablero ya construido y cómo se trasmiten estas grandes cargas a los tirantes, que son los elementos portantes. La idea es que la trasmisión sea lo más directa posible para minimizar los refuerzos necesarios y reducir al máximo las flexiones transversales y locales; de esa forma se conseguirá no deformar en exceso la sección de la punta del voladizo donde va a ensamblarse la siguiente dovela.

Es fundamental, en este sentido, la coordinación adecuada entre el diseño de la estructura permanente y el de los medios auxiliares, pues habitualmente están a cargo de equipos diferentes y es imprescindible una visión de conjunto que tenga en cuenta todas la implicaciones.

5. SUSTENTACIÓN DE LA DOVELA

La otra cuestión a estudiar es cómo se iza la nueva dovela. Y este cómo se iza, no se refiere sólo a cuántos gatos de izado y qué tipo emplear, sino de dónde se coge la dovela (puntos de cogida), si se usa balancín o no, etc. Hay que tratar de izar la dovela minimizando la deformación transversal. O, mejor dicho, tratando de que la deformación transversal durante el izado sea similar a la deformación que tendrá una vez colocada. Esto significa que los puntos de izado deben ser muy

Figura 1. Planta con los accesos a la ciudad de Cádiz.

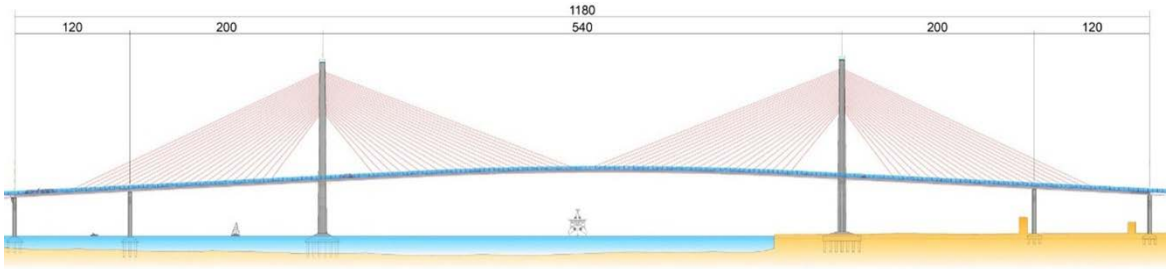

Figura 2. Distribución de luces del tramo atirantado. Puente de la Constitución de 1812.

similares a la sustentación que supondrán los tirantes una vez esté colocada en su posición final.

Por otra parte, como ya se ha dicho, lo ideal es izar la dovela con todos los elementos (losa de hormigón, conductos de servicio, barreras, etc.) para minimizar los trabajos posteriores sobre el tablero. Pero habitualmente hay que buscar un equilibrio entre este planteamiento de máximos y evitar sobredimensionar el tablero notablemente en la fase constructiva, pues izar la dovela con la losa de hormigón implica un peso muy importante, que requerirá un medio de izado más potente que pesará más, lo que conduce irremediablemente a un sobredimensionamiento del tablero en fase constructiva.

Si las deformadas transversales de la dovela que se iza y la sección del extremo del voladizo, donde está apoyado el elemento de izado, son muy parecidas, el acople será sencillo, lo que redundará en el ciclo. Pero si estas deformadas son muy distintas, será necesario realizar una serie de tareas previas al acople, encaminadas a igualar las deformadas transversales, que consumirán un tiempo precioso y requerirán del diseño de unos medios auxiliares específicos.

Los dos parámetros, por tanto, que influyen en la mayor o menor facilidad en el acople de dovelas son dos: el peso del carro de izado y su apoyo en el extremo del tablero ya construido, y los puntos de los que se iza la dovela en combinación con la distribución de su peso.

Veamos a continuación cómo se ha abordado este problema en los últimos puentes atirantados con tablero mixto construidos por Dragados en los últimos 10 años. Se presentarán cronológicamente.

6. PUENTE DE LA CONSTITUCIÓN DE 1812 SOBRE LA BAHÍA DE CÁDIZ

El primer puente donde este problema se nos presentó con claridad fue el de la bahía de Cádiz, el Puente de la Constitución de 1812.

Esta magnífica estructura diseñada por Javier Manterola constituye el tercer acceso a la ciudad de Cádiz, junto con el puente levadizo de Carranza, construido también por Dragados en 1969 y la carretera que discurre sobre el istmo [1].

Tiene una longitud de total de 3.093 m y está formado por dos viaductos de aproximación, uno desde Cádiz y el otro desde Puerto Real, un tramo desmontable y el puente atirantado, que cruza la bahía sobre el canal de navegación [1].

El tramo atirantado tiene una longitud total de 1.180 m con un vano central de 540 m de luz, que es el mayor de España y el tercero de Europa.

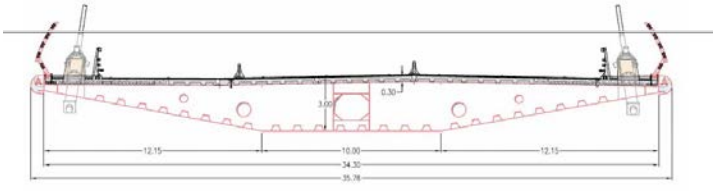

Figura 3. Sección transversal del tramo atirantado. Puente de la Constitución de 1812.

El tablero es mixto, con un ancho de 34,3 m y una sección cajón trapezoidal de 3,0 m de canto constante, lo que implica una extraordinaria esbeltez de L/180. Destaca también en este puente la gran luz de los vanos de retenida, 200 m, que reducen la eficacia del sistema de atirantamiento (el punto donde se anclan los tirantes de retenida es muy flexible) y complicó considerablemente la construcción por avance en voladizo [2].

El sistema de atirantamiento de este puente consiste en dos planos de tirantes situados en los extremos de la sección con una separación longitudinal de 10 m. El tablero, por tanto, flecta transversalmente colgado de sus extremos. En las secciones de tirantes (y en las intermedias, cada 5 m) hay diafragmas transversales que se encargan de llevar la carga del tablero hacia los tirantes.

6.1. Configuración de la dovela tipo del Puente de Cádiz

Como ya se ha comentado más arriba, para reducir el número de soldaduras en altura y acelerar la construcción, se decidió que las dovelas tipo tuvieran una longitud de 20 m, el doble de la distancia entre tirantes, y el ancho completo, 34,3 m.

La losa superior del tablero estaba formada por piezas prefabricadas de canto completo que se apoyaban en los diafragmas transversales del tablero. Como las losas no podían izarse con la dovela porque el peso total habría sido excesivo, se diseñó el carro de izado para que, con la ayuda de un balancín especial, pudiera subir el paquete de losas una vez estuviera la dovela metálica colocada. Este segundo izado, más ligero, se producía con una excentricidad tremenda (~25 m), pues el carro tenía que "salvar" la nueva dovela mientras se apoyaba en la anterior. Una vez arriba, era también el carro el encargado de colocar cada una de losas prefabricadas en su posición final [3].

Además, para tener capacidad de regulación en las tres dimensiones del espacio, se dotó al carro de izado de 4 unidades de izado hidráulicas de 500 t de capacidad que podían moverse longitudinal y transversalmente al eje del puente.

Para acelerar el ciclo, las primeras dovelas se izaron con una franja lateral de hormigón para, una vez terminada la soldadura de la sección metálica, hormigonar las juntas transversales correspondientes a las franjas laterales y proceder a la instalación y tesado de los tirantes delanteros (recuérdese que estas dovelas, por su longitud, llevaban dos parejas de tirantes).

Figura 5. Izado de dovela tipo. Puente de la Constitución de 1812.

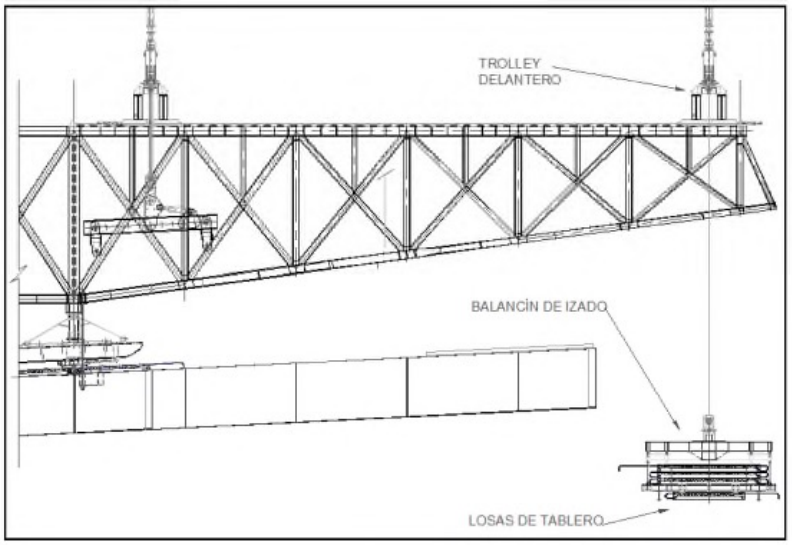

Figura 4. Izado del paquete de losas prefabricadas con el carro de izado. Puente de la Constitución de 1812.

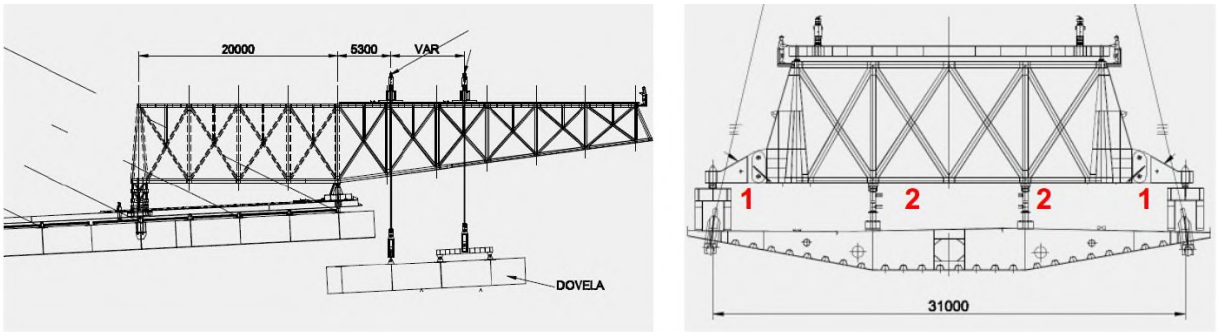

Figura 6. Sistema de apoyo del carro de izado. Puente de la Constitución de 1812.

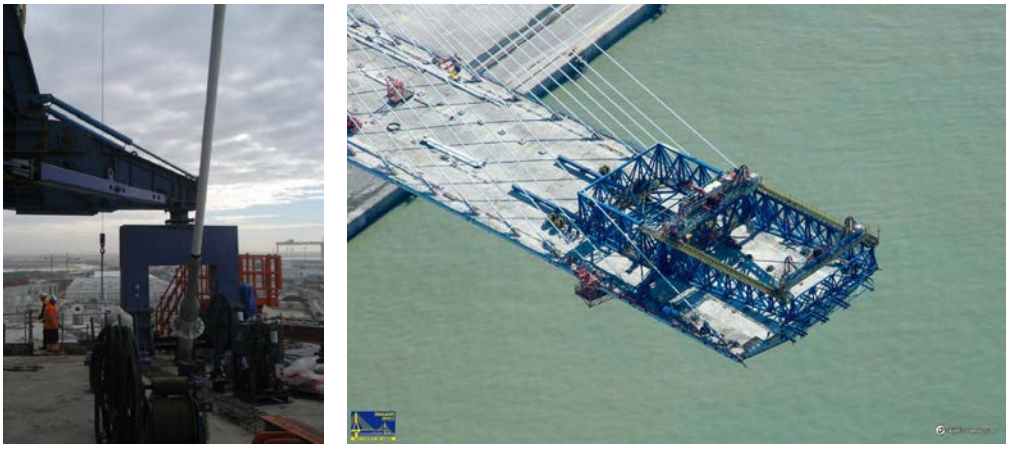

Figura 7. Carro de izado de dovelas apoyado en tirantes. Puente de la Constitución de 1812.

Llegó un momento en la construcción en que el momento de desequilibrio que se generaba en la torre en cada izado de dovela hizo necesario eliminar esas franjas laterales de hormigón para reducir peso. En esos casos, se hormigonaban esas franjas laterales de hormigón en cuanto la dovela estaba soldada, para instalar los tirantes cuanto antes, sin esperar a colocar todas las losas.

Como consecuencia de todo lo anterior, el carro de izado de dovelas se diseñó para izar una carga de hasta 400 t, lo que dio lugar a un peso de carro de casi 500 t [3].

6.2. Carro de izado de dovelas usado en el Puente de Cádiz

Con la idea de que este carro tan pesado no deformara excesivamente el tablero ya construido, y en especial la sección del frente de avance donde se iba a acoplar la siguiente dovela, se dotó al sistema de un doble sistema de apoyo: uno para el movimiento del carro, y otro para el momento del izado. El carro de izado dovelas se desplazaba sobre unos railes apoyados en los diafragmas transversales del puente y situados en el centro de la sección transversal (puntos 2 en la figura 6). Pero a la hora de izar una dovela, se diseñó el carro para que desplegara unas "patas" que hacían que se apoyara en los bordes de la sección transversal, donde estaban los anclajes de los tirantes, de forma que la carga importante (peso del carro + peso dovela) se trasmitiera lo más directamente posible a los tirantes (Puntos 1 en la figura 6).

De esta forma, se evitaba deformar excesivamente el frente de avance durante el izado de las dovelas; cosa que se conseguía sólo parcialmente, pues la carga trasmitida al puente, muy importante, estaba situada a sólo 3,5 m de la sección de unión en dirección longitudinal.

Se hizo un estudio de detalle con diversos modelos de Elementos Finitos que nos permitieron, por un lado, estudiar el comportamiento del tablero con el peso del carro durante el izado, y por otro, cuantificarla deformación transversal de la dovela izada [4].

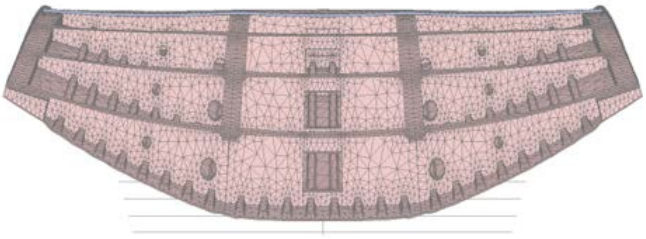

Figura 8. Deformada del frente de avance. Puente de la Constitución de 1812.

6.3. Izado de dovelas en el Puente de Cádiz

La otra variable que influye en el ensamblaje es la deformación de la dovela que se iza. Como ya se ha dicho, hay que tratar de izarla de forma que la deformada transversal sea lo más parecida a la que tiene el tablero con la sustentación definitiva(colgada de los tirantes). En este caso, por tanto, se debería haber subido la dovela sustentada por sus bordes, copiando el sistema de sustentación del tablero con los tirantes. Sin embargo, esto

no fue posible. La dovela no resistía su peso propio flectando con 34 m de luz (el ancho completo) y sin la colaboración de la losa superior de hormigón que proporcionara la necesaria resistencia a compresión frente a momentos positivos. Así que los puntos de izado tuvieron que acercarse (17 m en vez de 34 m), de forma que la dovela fuera capaz de resistir su peso propio solo con estructura metálica, pues la losa superior de hormigón se colocaba en una fase posterior.

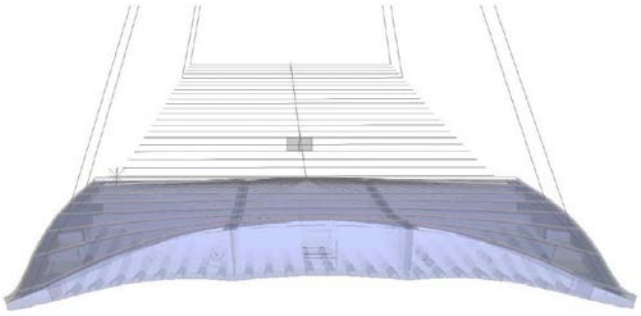

Figura 9. Deformada de la dovela izada. Puente de la Constitución de 1812.

La consecuencia de esta diferente sustentación fue que las deformadas transversales de la sección del frente de avance y la de la dovela que se izaba no eran iguales. La dovela que se izaba tenía una deformada convexa, con puntos de sustentación separados 17 m, mientras que, en el frente de avance del tablero, donde el carro de izado estaba apoyado, la deformada era cóncava, pues flectaba entre los puntos de anclaje de los tirantes separados 34 m [4].

Pero había otra componente más local que nos mostró el MEF que también es interesante comentar. Y es que, en los quiebros de la sección transversal del frente de avance, justo en el extremo del voladizo, se producían unas distorsiones que complicarían el acople.

Para reducir estas distorsiones locales se tomaron una serie de medidas "pasivas" consistentes en rigidizar algo más la sección de unión situada en el frente de avance.

Para compatibilizar las deformadas transversales de las dos secciones a unir, se previeron también una serie de medidas "activas" a base de gatos por si en el momento del acople era preciso deformar, forzar, la dovela que se estaba izando, pero finalmente esto no fue necesario, pues las medidas "pasivas" fueron suficientes para permitir el acople [4].

7. QUEENSFERRY CROSSING

El siguiente puente atirantado al que nos enfrentamos, y cuya construcción fue casi en paralelo al de Cádiz, fue el tercer puente sobre la ría Forth, el denominado "Queensferry Crossing".

La necesidad de esta nueva estructura surgió cuando se detectó que los cables portantes del puente colgante para tráfico carretero, el *Forth Road*, construido en 1964 presentaban problemas serios de corrosión. El Gobierno Escocés decidió entonces hacer un nuevo puente para tráfico rodado, el Queensferry Crossing, con el objetivo de reemplazar al existente. La instalación de un sofisticado sistema de deshumidificación en los cables afectados frenó drásticamente el problema de corrosión en el *Forth Road*, de forma que el puente colgante no fue finalmente demolido, sino destinado exclusivamente al tráfico de autobuses, bicicletas y peatones.

El nuevo Queensferry crossing es un puente de 2.637,5 m de longitud, formado por dos viaductos de aproximación, norte y sur, y un tramo central atirantado de 2.020,35 m, con dos vanos principales de 650 m de luz. El sistema de atirantamiento está formado por dos planos paralelos de tirantes, formados por cordones paralelos, situados en la parte central de la sección [5].

Figura 10. Vista de los tres puentes del estuario del Forth. Queensferry Crossing.

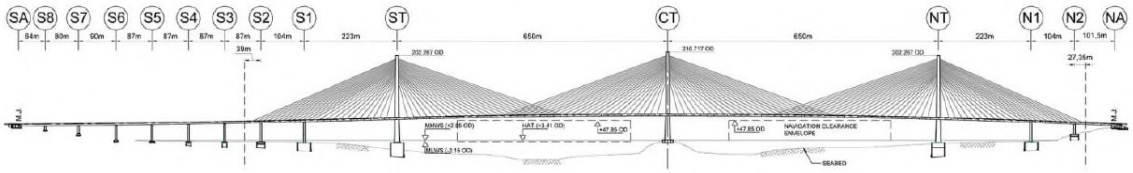

Figura 11. Distribución de luces. Queensferry Crossing.

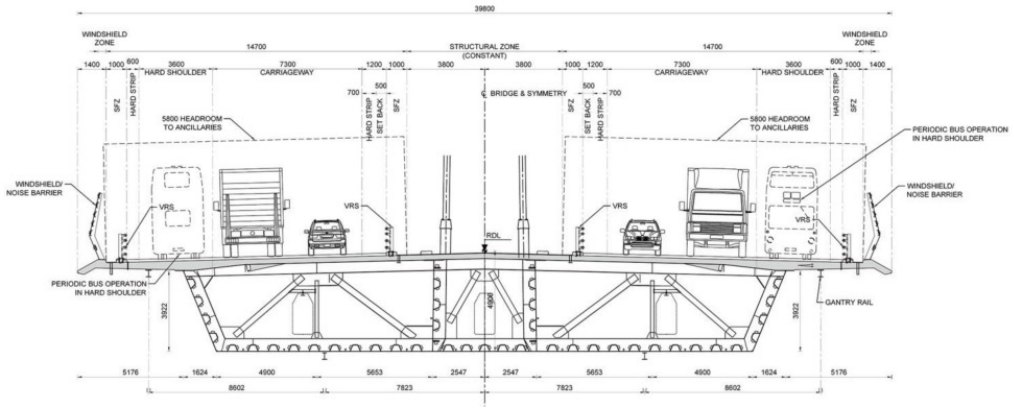

Figura 12. Sección transversal del tramo atirantado. Queensferry Crossing.

El tablero es mixto de 4,9 m de canto y 39,8 m de ancho, con una sección transversal tricelular (4 almas) en la que los tirantes se anclan en las dos almas centrales. La losa superior de hormigón está pretensada transversalmente para evitar la fisuración y la pérdida de rigidez a torsión asociada.

El puente Queensferry Crossing presenta, además, la característica única (primera vez que se emplea este sistema) de que los 9 tirantes más largos se solapan en el centro de los dos vanos principales. Este es un sistema muy elegante y efecfivo de dotar a la torre central de la suficiente rigidez para que el atirantamiento sea eficaz, sin tener la torre conectada a un vano más rígido como pasa en la mayor parte de puentes atirantados.

En el momento de redacción de este artículo (2024) el tramo atirantado ostenta tres récords: puente atirantado de tres torres con mayor luz del mundo, tablero mixto también con la mayor luz del mundo y construcción con doble voladizo (balanced canfilever) más largo jamás ejecutado.

Es importante destacar que por su configuración longitudinal el tercer puente de la ría del Forth tiene una cierta flexibilidad, pero transversalmente es muy rígido. La sección transversal apenas se deforma.

7.1. Configuración de la dovela tipo del Queensferry Crossing

En este caso, las dimensiones de la dovela fueron las estándares: longitud igual a la distancia entre tirantes, 16,20 m, y ancho completo, 39,80 m.

Para reducir al máximo la duración del ciclo de montaje se decidió hormigonar a pie de obra la losa de hormigón completa e izar una dovela de 720 t de peso, reduciendo los trabajos en altura dentro del ciclo a la unión de la estructura metálica, el hormigonado de las juntas y la instalación de tirantes [6].

Este peso tan considerable de la dovela, unido a la construcción en "balanced cantilever", obligó a instalar un sistema independiente de tirantes provisionales entre la cimentación de las torres y el tablero para resistir la eventual caída una dovela durante el avance en voladizo, que es una de las hipótesis a considerar en el dimensionamiento de un puente atirantado.

7.2. Carro de izado de dovelas usado en el Queensferry Crossing

Con los dos planos de tirantes colocados en el centro de la sección, este caso es completamente diferente al del Puente de Cádiz que se ha expuesto antes. Pero, aunque estructuralmente el funcionamiento sea muy distinto, la filosofía que se siguió al diseñar el carro de izado de dovelas fue la misma: apoyar el carro de dovelas en la sección transversal de forma que la transmisión de la carga (peso propio del carro + dovela) a los elementos portantes, que son los tirantes, fuera lo más directa posible. En este caso, como los tirantes están en el centro de la sección, el carro se apoyó en el centro de la sección también. Para que no hubiera interferencias, los carriles sobre los que deslizaba el carro estaban colocados más centrados, entre los dos planos de tirantes, pero las patas sobre las que se apoyaba el carro cuando tenía que izar una dovela, coincidían exactamente con la posición de las almas longitudinales de la sección transversal. Los tirantes, por su parte estaban ligeramente desplazados en transversal respecto a estas almas para evitar interferencias, pero la transmisión de cargas era muy directa.

El carro de izado que se diseñó para construir el Queensferry Crossing era, por tanto, mucho más sencillo, compacto y ligero que el de Cádiz. Tenía sólo dos unidades de izado y no ocupaba demasiado espacio en el tablero, sino que estaba circunscrito a la parte central, lo cual era muy positivo para todos los trabajos que habían de realizarse en altura. Por lo tanto,

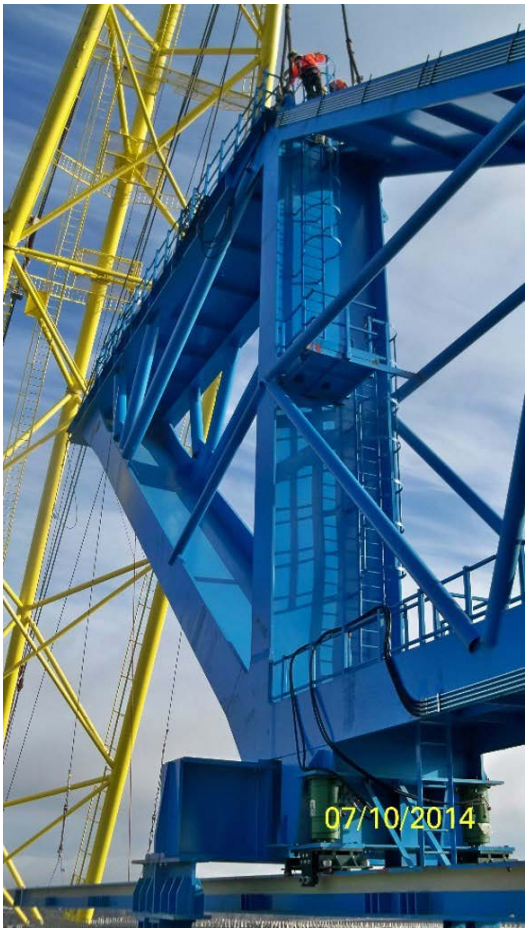

Figura 13. Carro izado dovelas. Queensferry Crossing.

la deformación del frente de avance debido a las cargas del propio carro y de la dovela a izar, era muy pequeña porque la transmisión de cargas a los elementos portantes era directa [7].

Prueba de esta eficacia es que el carro de izado empleado en el Queensferry Crossing, que tenía que izar dovelas de 720 t, sólo pesaba 250 t [7]. Mientras la situación en el Puente de Cádiz era bien distinta; para izar dovelas de 400 t se empleó un carro que pesaba 500 t [3].

7.3. Izado de dovelas en Queensferry Crossing

La otra cuestión relevante para el acople es la elección de los puntos de izado de dovela de forma que la deformación de ésta sea compatible con la que tiene el frente de avance. Esto también se resolvió de forma muy eficaz en el Queensferry Crossing.

Dado que el sistema de sustentación del puente (tirantes) estaba situado en el centro de la sección, se replicó esta disposición de elementos portantes en la dovela que se izaba. Para ello, los puntos de izado de la nueva dovela se colocaron exactamente sobre las almas interiores, muy próximas al punto donde se anclan los tirantes y, por otra parte, donde estaba apoyado el carro de izado de dovelas.

De esta forma, la deformación transversal de la dovela que se izaba era muy parecida a la que tenía la sección del frente de avance, y el acople se hacía sin mayores problemas.

El problema en el izado de dovelas del Queensferry Crossing podría haber venido de la reducidísima rigidez a torsión tanto del tablero en voladizo con los cables situados en el centro, como de la dovela que se izaba con la cogida situada también en el centro. Para evitarlo, fue preciso limitar el viento transversal


Figura 14. Carro izando una dovela del tramo atirantado. Queensferry Crossing.

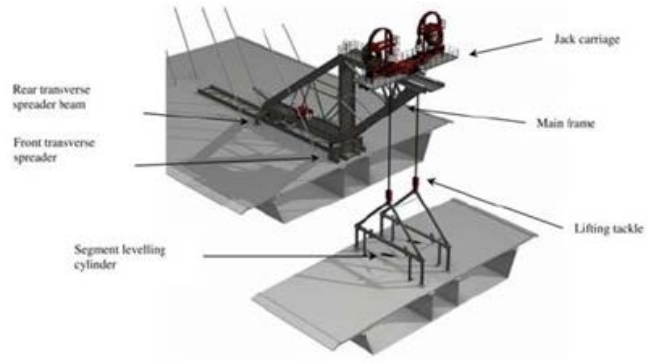

Figura 15. Croquis del izado de una dovela del tramo atirantado. *Queensferry Crossing*.

Figura 16. Izado de una dovela del tramo atirantado. *Queensferry Crossing*.

Figura 17. Puente de Rande ampliado.

admisible para el izado y comprobar que ese viento introducía en la dovela y/o en el tablero un giro de eje longitudinal compatible con la capacidad y tolerancias del carro de izado [6, 7].

8. AMPLIACIÓN DEL PUENTE DE RANDE

La siguiente actuación que se va a exponer no es un puente nuevo, sino la ampliación de uno existente, lo cual implica una complejidad aún mayor.

El puente de Rande original, situado en la Autopista del Atlántico AP-9 sobre la ría de Vigo, tenía un tablero puramente metálico con una longitud total de 695 m y un vano principal de 400 m de luz. Este puente se inauguró en 1981, y en ese momento fue un hito en la ingeniería de puentes española, pues fue el puente de mayor luz de España y segundo atirantado del mundo (por detrás del puente de Saint-Nazaire, 404 m de luz, en Francia), hasta que en 1984 se inauguró el Puente atirantado de Barrios de Luna, con una luz de 440 m.

En el año 2006 se vio la necesidad aumentar su capacidad, pues el tráfico que soportaba era ya muy superior al previsto, y se decidió ampliar el puente disponiendo un carril adicional por sentido de circulación. Es decir, un pequeño tablero a cada lado del existente. Para sostener estos nuevos tableros fue necesario instalar nuevos tirantes, pues no se conocía el estado tensional de los existentes, ni tampoco su estado de conservación; así que se dispusieron sendos haces de tirantes, que obligaron, lógicamente, a ampliar las torres para alojar los nuevos anclajes.

Figura 18. Vista inferior del tablero original durante la construcción de la ampliación.

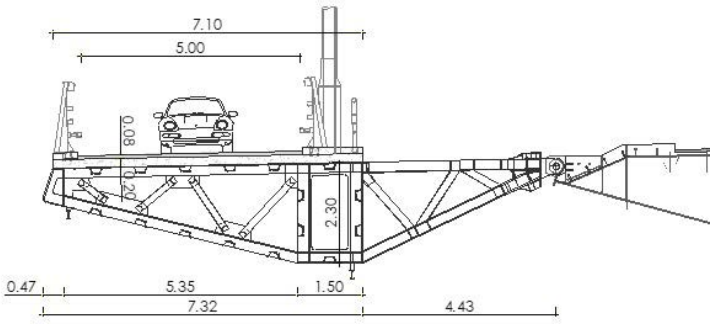

Figura 19. Sección transversal de la ampliación del Puente de Rande.

Figura 20. Dovela izándose en la ampliación del Puente de Rande.

Figura 21. Dovela de la ampliación del tablero durante el izado. Puente de Rande ampliado.

Uno de los mayores condicionantes de esta la obra fue que todos los trabajos de la ampliación debían realizarse sin cortar el tráfico en el tablero existente.

La sección transversal de los nuevos tableros está formada por un cajón mixto trapecial que se conecta al tablero existente mediante unas celosías verticales, articuladas en su extremo. Los nuevos tirantes se anclan en una viga longitudinal en la parte interior del cajón [8].

8.1. Configuración de la dovela tipo de la ampliación del Puente de Rande

Los nuevos cables que sustentaban la ampliación del tablero estaban separados 21 m, así que ésa fue la longitud que se adoptó para la dovela tipo. Como es habitual, el ancho era el completo e incluía las celosías de conexión con el tablero existente; dos celosías en cada dovela.

La parte metálica de esta dovela de 21 m pesaba 90 t y la losa de hormigón correspondiente a esta longitud otras 90 t. Las decisiones en la construcción de la ampliación del Puente de Rande no sólo estaban condicionados por la resistencia y proceso constructivo de las nuevas calzadas, sino, obviamente, por la resistencia del tablero existente, pues ambas estructuras están conectadas [9]. El peso a izar, por tanto, estaba condicionado no sólo por la capacidad portante de la pequeña sección transversal que constituía la ampliación del tablero, sino por la reserva resistente de la estructura metálica original. Por esa razón se optó por reducir al máximo el peso a izar subiendo las piezas sin la losa de hormigón.

8.2. Carro de izado de dovelas usado en la ampliación del Puente de Rande

Para izar estas dovelas sin sobrecargar excesivamente la estructura existente, ni cortar el tráfico, pues era una exigencia del contrato mantener en todo momento el servicio, se renunció rápidamente a la idea de colocar el carro de izado sobre el tablero existente, que a priori parecía una idea muy atractiva. Además, la gran flexibilidad de los nuevos tableros hacía inviable colocar el carro de izado en la punta del voladizo, pues las grandes cargas en punta (peso carro + dovela a izar) habrían producido unos movimientos y giros de eje longitudinal muy elevados, incompatibles con un izado vertical. Para resolver este problema se ideó un sistema muy novedoso. Consistía en emplear dos carros de izado, en vez de uno como es habitual. Uno colgado del tablero existente (por debajo), y el otro colocado sobre la ampliación que se iba construyendo. De esta forma, tanto el peso de los medios de elevación, como el de las

Figura 22. Carro de izado trasero empleado en la ampliación del Puente de Rande.

Figura 23. Sistema de apoyo doble del carro trasero. Ampliación del Puente de Rande.

dovelas que se iban izando, se repartía entre los dos tableros, el antiguo, y el nuevo. Los giros en la dovela del frente eran compatibles con la regulación hidráulica de las patas del carro y, así, los gatos de izado podían estar apoyados en un plano horizontal, como se precisaba para el buen funcionamiento. Por otra parte, el tablero existente no se sobrecargaba en exceso, ni se afectaba al tráfico y, además, podía emplearse para todas las tareas de rehabilitación que debían llevarse a cabo en la estructura metálica existente [10].

Para el problema que nos ocupa (ensamblaje de dovelas), el carro de izado de dovelas que tenía repercusión en la deformación del frente de avance era el carro trasero, el que se apoyaba en la nueva estructura. Éste era un medio muy sencillo y ligero, pues tenía que hacer frente sólo al 50% del peso de la dovela, con muy poco brazo, y disponía de una única unidad de izado, pues la otra cogida de la dovela se hacía desde el carro delantero. Su peso total era de sólo 40 t. Se desplazaba sobre unos raíles apoyados en los diafragmas transversales de la sección, y durante el izado, los apoyos situados a ambos lados del raíl permitían que se trasmitiera toda la carga casi directamente al tirante (ver Figuras 23 y 24). En este caso, las cargas del carro y dovela eran tan pequeñas (40 + 45 t), y la sección de la ampliación tan estrecha, que la deformación transversal del frente de la dovela era irrelevante.

8.3. Izado y acople de dovelas en la ampliación del Puente de Rande

Las dovelas de la ampliación eran piezas muy estrechas, de 21 m de longitud y 11,75 m de ancho. Aprovechando la existencia de dos carros (trasero en la nueva ampliación y delantero en el tablero existente), las dovelas se izaron de sus extremos, por lo que la flexión longitudinal era la dominante.

El problema que se planteó durante la construcción no fue tanto de deformaciones como en los casos anteriores, sino de movimientos: en concreto del giro de eje longitudinal al puente. Por el funcionamiento estructural conjunto del tablero central más las ampliaciones ideado por MC-2 [11], el peso de los tableros nuevos, cuyo centro de gravedad está por fuera de los nuevos tirantes, genera un momento torsor

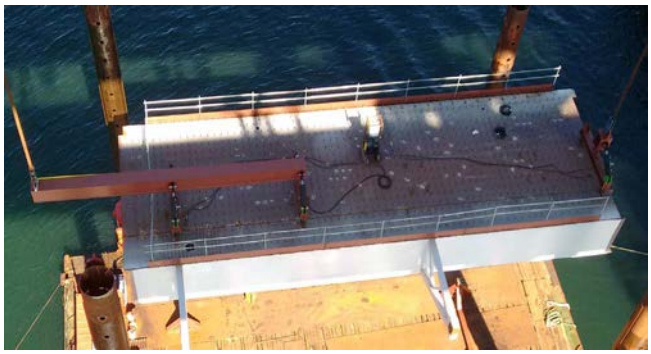

Figura 24. Balancín de regulación en la cogida delantera de la dovela. Ampliación del Puente de Rande.

que se transmite mediante un par de fuerzas situadas en los nuevos tirantes y en la rótula de conexión con el tablero existente. Este momento torsor produce un giro de eje longitudinal que había que compatibilizar con la posición de la nueva dovela a izar y con la conexión entre tableros (celosías rotuladas), teniendo en cuenta que al final del ciclo de montaje los tres tableros (central y laterales) debían quedar a la misma cota (teniendo en cuenta las pendientes transversales del conjunto). Fue preciso, por tanto, introducir en la fabricación y el montaje unos contragiros y contraflechas que permitieran lograr al final de la construcción una geometría correcta. Adicionalmente, en cada nuevo ciclo era necesario ajustar las pendientes longitudinal y transversal de la dovela en función de la geometría real de cada ciclo. La cota del extremo de la nueva dovela se corregía con las unidades de izado de los carros en longitudinal y con el balancín de regulación, que tenía unos gatos, en transversal [10].

9. NUEVO PUENTE SAMUEL DE CHAMPLAIN EN MONTREAL, CANADÁ

El último de los ejemplos que se exponen en el artículo es el Nuevo Puente Samuel de Champlain sobre el río San Lorenzo,

Figura 25. Nuevo Puente Samuel de Champlain. ©Thomas Heinser.

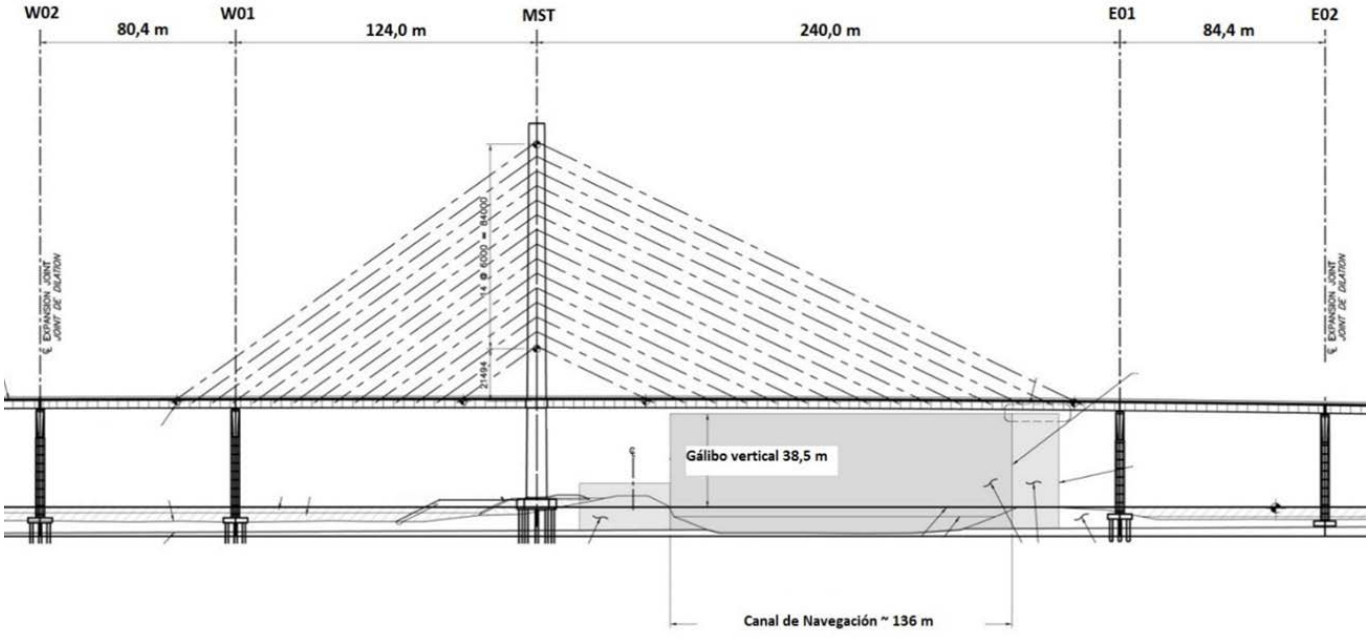

Figura 26. Distribución de luces del tramo atirantado. Puente de Champlain.

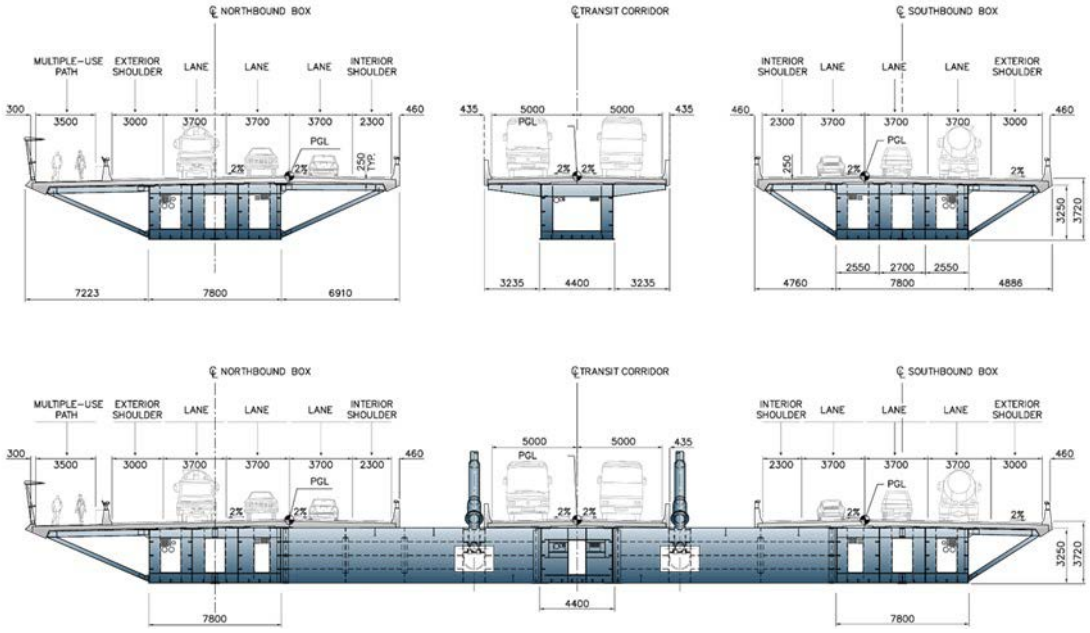

Figura 27. Sección transversal del tramo atirantado. Puente de Champlain.

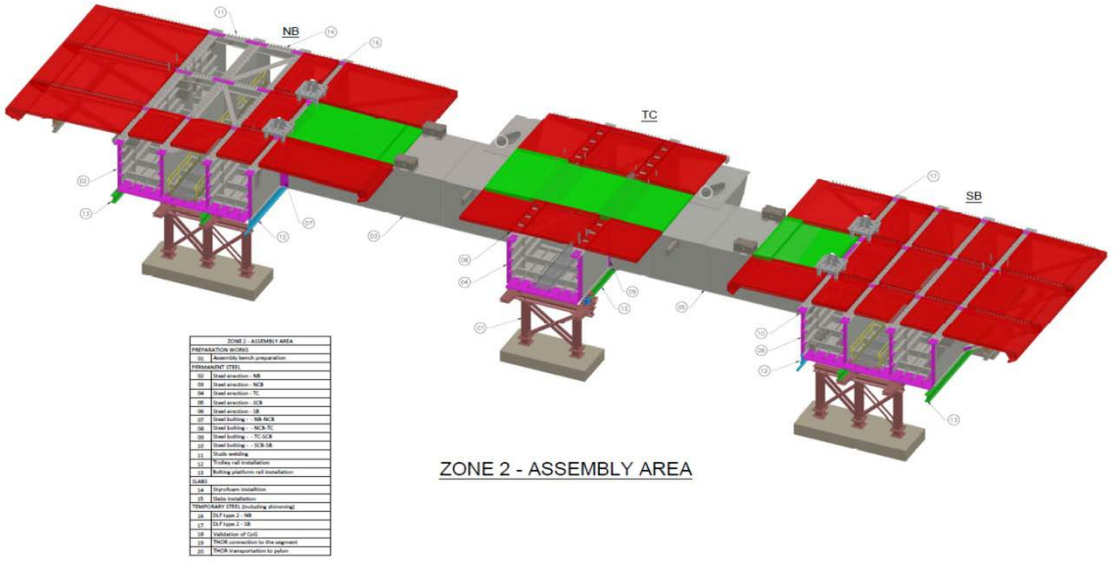

Figura 28. Configuración de la dovela tipo. Puente de Champlain.

en Montreal (Canadá). Se trata de una estructura de 3.335 m de longitud y 60 m de anchura construida para sustituir al puente de Champlain original, de 1962, que presentaba importantes deterioros debidos a problemas de durabilidad y obligaron a plantear su reemplazo por un puente nuevo.

La estructura está formada por tres tramos: los viaductos de aproximación Oeste y Este, de 2.044 m y 761 m respectivamente, y el tramo atirantado con una longitud total de 528,8 m y un vano central de 240 m de luz.

La sección transversal está compuesta por tres tableros de tipo cajón mixto. Uno para la calzada norte, otro para la sur y un tercero situado en el centro para alojar el metro ligero. Los tres tableros están unidos por vigas transversales coincidentes con la posición de los tirantes [12].

9.1. Configuración de la dovela tipo del Puente de Champlain

Las dovelas del tramo atirantado se definieron según el criterio habitual: ancho completo y longitud igual a la distancia entre tirantes. Esto condujo a izar unas piezas de 12,6 m de longitud y 60 m de ancho. Sin embargo, como el tablero está formado por tres corredores sólo conectados entre sí por vigas transversales en las secciones con tirantes, la geometría de la dovela resultante era muy compleja y poco habitual.

Figura 29. Vista de ½ dovela tipo. Puente de Champlain.

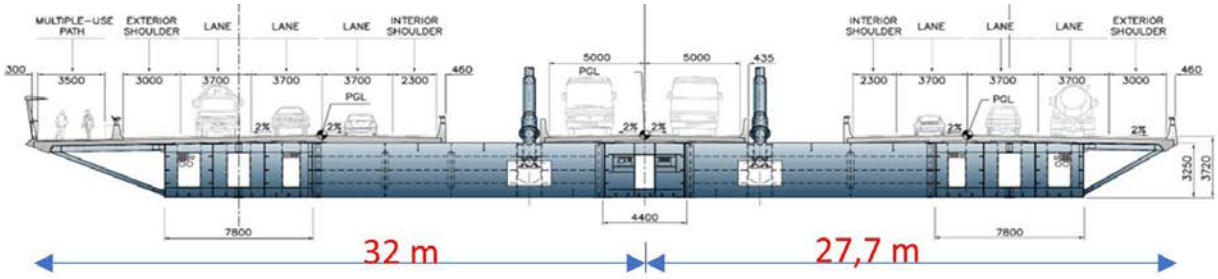

Figura 30. Dovela asimétrica. Puente de Champlain.

Respecto a las losas de hormigón, se decidió que subieran con la dovela, pues dado el clima canadiense era imprescindible minimizar los trabajos en altura y los hormigonados in situ. la mayor parte de las losas prefabricadas de hormigón, de canto completo, se colocaban sobre la dovela metálica previamente a su izado.

También era preciso incluir en la dovela unos contrapesos de hormigón en el interior del corredor sur, para equilibrar la dovela transversalmente, pues el corredor norte era mucho más ancho.

Con todos estos condicionantes, la dovela alcanzó un peso de 830 t.

9.2. Carro de izado de dovelas del puente de Champlain

El sistema de izado de dovelas en el Puente de Champlain fue muy complejo debido a la limitación de no invadir en ningún momento de la construcción el canal de navegación que discurría bajo el vano central. El denominado "Seaway" es la principal vía de comunicación entre el océano Atlántico y los Grandes lagos de Norteamérica, por lo que no se podía afectar de ningún modo. Este condicionante impidió el izado convencional de dovelas, en el que éstas se sitúan bajo la sombra del tablero y el medio de elevación realiza un izado vertical.

Las dovelas debían izarse hasta la cota inferior del tablero en las inmediaciones de la torre con unas unidades de izado (Movable lifting beam) y allí, con un carrito (trolley system) que circulaba por debajo del tablero, se transportaban hasta el frente de avance. El carro de dovelas (Dynamic lifting frame), colocado en la punta del voladizo, procedía a tomar la dovela y colocarla en su posición definitiva [12]. Vamos a centrarnos en este último, pues era el encargado de suspender la dovela para su acople. Aunque los tirantes del puente estaban colocados en el centro de la sección, junto al corredor central, y lo ideal habría sido trasmitir la carga del izado directamente a los elementos portantes (los tirantes), esto no fue posible por dos razones:

1. En primer lugar, los tirantes no estaban anclados a los cajones longitudinales que formaban el tablero, sino a las vigas

Figura 31. Vista del Seaway durante el avance en voladizo. Puente de Champlain.

Figura 32. Vista frontal del tablero con el carro de izado de dovelas. Puente de Champlain.

transversales, por lo que la carga del carro tenía que llevarse de los cajones longitudinales, que son los elementos resistentes con continuidad longitudinal, a las vigas transversales donde están los tirantes.

2. El corredor central, que es el que está más cerca de los tirantes, no podía hacer frente a esa carga tan enorme (carro 740 t + dovela 830 t = 1570 t), por lo que el carro de izado de dovelas se diseñó para repartir su carga, más la de la dovela a izar, entre los tres tableros.

Así pues, el carro se apoyó en los 3 cajones que formaban el tablero, lo que dio lugar a un medio auxiliar bastante complejo y pesado.

Respecto a los puntos de cogida de las dovelas y, de nuevo, para no sobrecargar el corredor central, que era el más débil (sólo dos almas, frente a las cuatro de los laterales), los puntos de izado de las dovelas se colocaron con una separación en transversal de 20 m (los tirantes están separados 12 m), de forma que la carga trasmitida a cada uno de los corredores se repartiera adecuadamente.

La sección frontal del tablero ya construido, sobre la que se apoyaba el carro, sufría una deformación transversal muy considerable pues estaba suspendida de los tirantes, separados 12 m, así que quedaban voladizos a cada lado de 26 y 21,7 m respectivamente. Los cajones norte y sur, por tanto, sufrían un descenso muy superior al cajón central, que se encontraba muy cerca de los tirantes.

Desde el punto de vista del ensamblaje de dovelas, el puente de Champlain fue el más complicado de todos los que se exponen en este artículo. Fundamentalmente porque su geometría era muy compleja y obedecía más a criterios estéticos y arquitectónicos que a una razón de ser estructural. El diseño era una exigencia del cliente, y TYLin hizo un trabajo magnífico consiguiendo que todo acabara funcionando. Las dificultades eran varias, pero las más importantes fueron:

- Un tablero tremendamente ancho, 60 m, que inevitablemente tendría deformaciones transversales importantes.
- Un puente formado por tres tableros semi-independientes, sólo conectados por vigas transversales en las secciones con tirantes, cada 12,6 m.

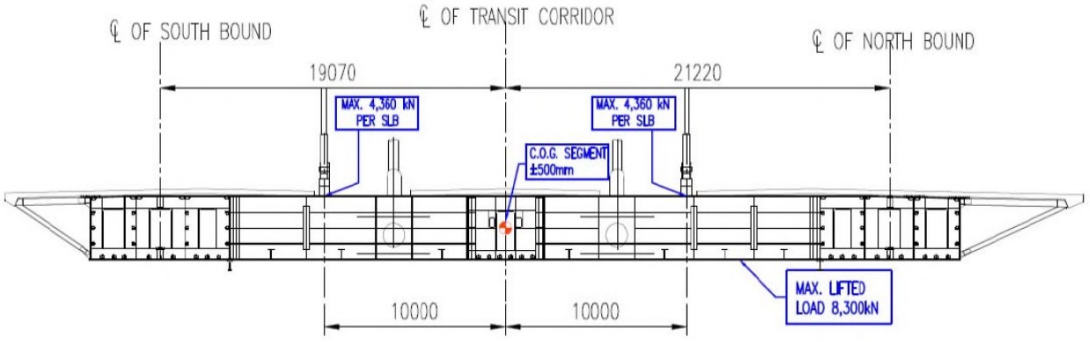

Figura 33. Disposición de puntos de cogida en la dovela. Puente de Champlain.

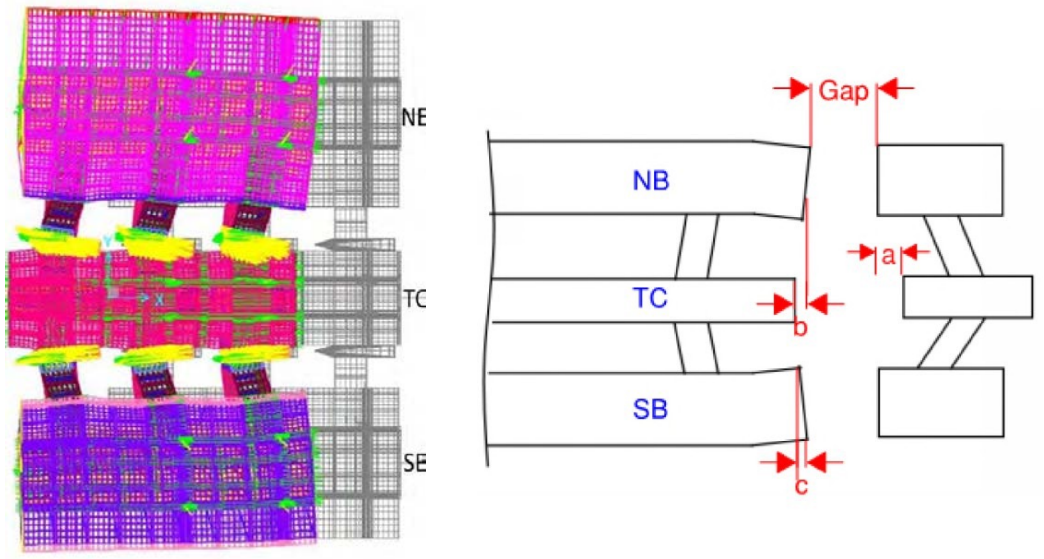

Figura 34. Planta del puente donde se aprecia la diferente deformación longitudinal de los corredores. Puente de Champlain.

- Una sección transversal con diez almas. Lo que implicaba que para ensamblar una dovela con la precedente había que alinear diez planos, cuatro almas de cada uno de los corredores laterales, más dos del cajón central.
- Unas dovelas pesadísimas, 830 t, pues además de las importantes dimensiones, para minimizar los trabajos en altura, muy complicados con el gélido clima de Montreal, se izaban con las losas ya colocadas.
- Un carro de izado de dovelas necesariamente pesado (740 t) y complejo, pues debía subir piezas muy pesadas y apoyarse en los tres tableros semi-independientes que forman la sección transversal.
- Tirantes colocados en el centro de la sección en dos planos separados 12 m, lo que dejaba voladizos de casi 26 y 21,7 m a cada lado (Figura 30).
- Estructura muy rígida, pues se trataba de una sección mixta formada por tres cajones con una esbeltez reducida (L/67).

Además, los tirantes no estaban anclados en el tablero o elemento longitudinal, sino en las vigas transversales que no tenían ninguna continuidad longitudinal. Esto producía una deformación en planta que dificultaba aún más el ensamblaje, pues al estar los tirantes más próximos al corredor central, la deformación longitudinal era mayor en éste que en los laterales. En la Figura 34 puede verse como el corredor central, situado muy cerca de los tirantes, recibe más axil y, por lo tanto, se deforma más longitudinalmente que los corredores norte y sur, más alejados en planta del punto de aplicación de la carga de los tirantes.

La dovela que se izaba, por su parte, con los puntos de apoyo (cogidas) separados 20 m y con un menor peso, pues no estaban colocadas todas las losas de hormigón, tenía una deformación claramente inferior. Esta diferencia de deformaciones planteó un problema complejo, pues la sección transversal era muy rígida y no era sencillo igualar estas deformaciones para proceder al atornillado de las 10 almas [13]. Por ello fue necesario diseñar unos sistemas de corrección bastante potentes que consistían en un conjunto de gatos y barras que permitían alinear los cajones laterales, una vez el central estaba unido, y comenzar el atornillado.

En la figura 36 se muestran las deformadas transversales de las secciones a unir. Los puntos representan cada una de las 10 almas a unir (cuatro por cada uno de los corredores laterales y dos en el corredor central). En la figura se aprecia, por un lado, en rojo, la deformación transversal del extremo dorsal de la dovela que se iza (MS5), y por otro, en azul, la deformada de la sección frontal de la dovela previa (MS4), que constituye el borde del tablero construido. Al alinearse

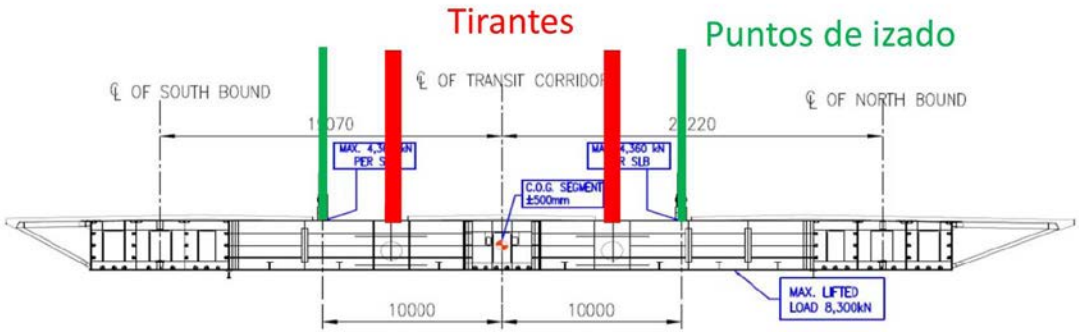

Figura 35. Disposición de cogidas en la dovela. Puente de Champlain.

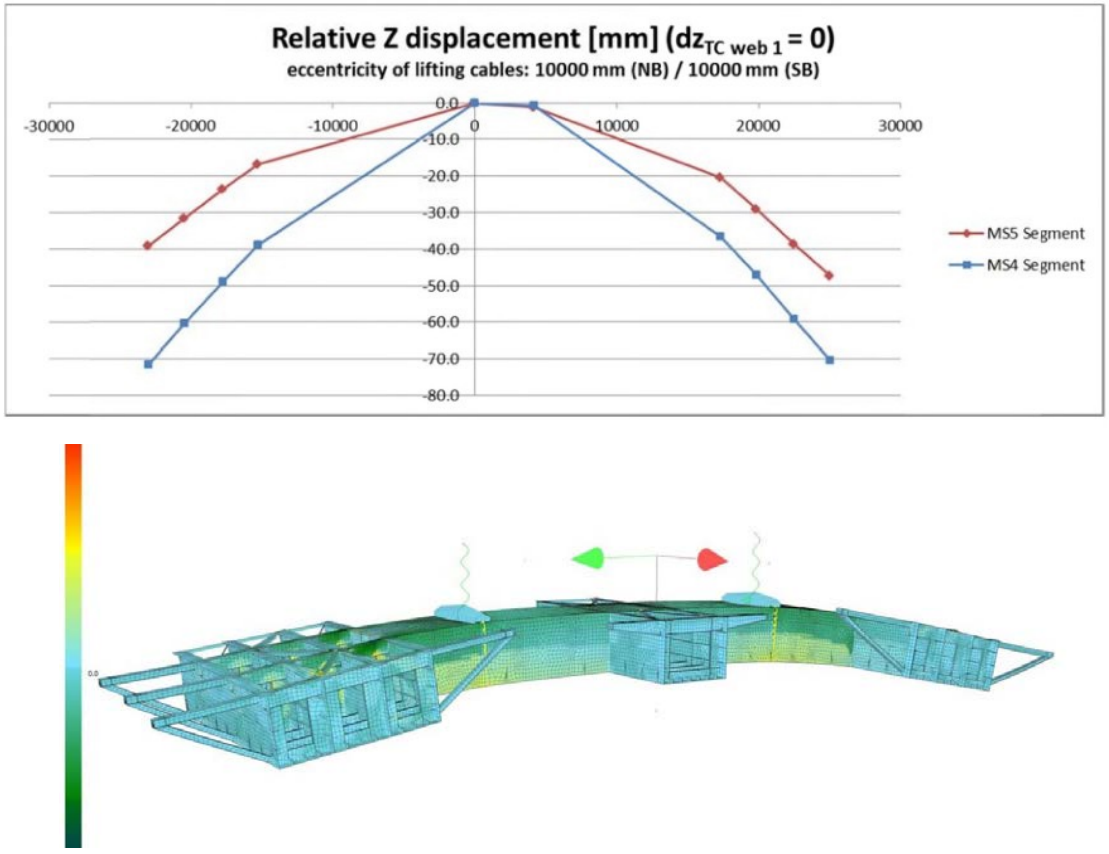

Figura 36. Deformada transversal de dovela y frente de avance. Puente de Champlain.

las dos almas del corredor central queda patente la diferencia entre las deformadas transversales, y la dificultad de proceder con la unión atornillada.

10. CONCLUSIONES

Es evidente durante el diseño de un puente atirantado pensar en las etapas constructivas, pero lo que se quiere poner de manifiesto en este artículo es que es fundamental pensar bien la configuración de las dovelas y cómo se van a izar antes de comenzar la construcción. Los cuatro ejemplos mostrados representan distintas opciones, pero las conclusiones son claras:

- Valorar en el programa (duración del ciclo tipo) y en el coste la posibilidad de subir las dovelas con la losa de hormigón colocada.
- Diseñar un carro de dovelas que deforme poco el tablero construido, donde se apoya.
- Tratar de transmitir las cargas de izado a los tirantes de la manera más directa posible.
- Pensar en las cogidas de las dovelas para tratar de que la deformación transversal se parezca lo más posible a la del frente de avance con el carro de izado encima.

En la siguiente tabla se resumen los parámetros más importantes de los ejemplos mostrados:

TABLA 1.
Resumen de las características relevantes para el izado de dovelas

	DEFINICIÓN DOVELA					*DEFINICIÓN CARRO DE IZADO*			
	Sep. long. tirantes	Longitud dovela	Ancho dovela	Izado con losas	Peso dovela	Sep. Transv. cogidas	Sep. Transv. tirantes	Apoyo carro en transv.	Peso carro
Puente de Cádiz	10 m	20 m	34,3 m	NO	400 t	17 m	31	Avance 10 m Izado	34 m 500 t
Queensferry Crossing	16,2 m	16,2 m	39,8 m	SÍ	720 t	5,0 m	4,0/6,0 m (3)	Avance 2,3 m Izado 5,0 m	247 t
Ampliación Puente Rande	21 m	21 m	7,3 m	NO	90 t	(2)	(2)	(2)	40 t
Puente de Champlain	12,6 m	12,6 m	60 m	SÍ	830 t	20 m	12,6	(1)	740 t

(1) El carro de Champlain se apoya en los tres corredores, por lo que este dato no tiene sentido.
(2) En la ampliación del puente de Rande sólo hay una cogida en transversal debido al ancho tan reducido de los tableros laterales.
(3) Como los cables de Queensferry Crossing se cruzan, los que parten de la torre central están separados 4 m y los que parten de las laterales están a 6,0 m.

Referencias

[1] Lucas, C., Peset, L., Martínez, A., Manterola, J. et. al. (2016). *Número Monográfico dedicado al Puente de la Constitucion de 1812 sobre la Bahía de CÁdiz*. Hormigón y Acero. Vol 67, Núm 278-276.

[2] Lucas, C., Peset, L., de los Ríos, J., Morejón, J.M. (2014). *La construcción del tramo atirantado del Puente sobre la bahía de Cádiz*. VI Congreso Internacional de Estructuras de ACHE. Madrid.

[3] Castro, J. L., De los Ríos, J., Arroyo, J., Salamanca, J. L. (2016). *Medios auxiliares empleados en la construcción del tramo atirantado del Puente de la Constitución de 1812 sobre la bahía de Cádiz*. Hormigón y Acero, vol. 67, número 278-279.

[4] Lucas, C., De los Ríos, J.; Martínez, J.L., Farkas, G. (2011). *Corrección de la deformación de las seciones en el izado de las dovelas del Puente Bahía de Cádiz*. Congreso internacional de Estructuras de ACHE, Barcelona.

[5] Martin, J., Curran P., Tarquis, F., Walser, P., Hamm, S. (2017). *El Puente Queensferry Crossing. Desarrollo del diseño ganador*. VII Congreso Internacional de Estructuras de ACHE. La Coruña.

[6] Vázquez, A., Raynor, D., Romberg, M., Walser, P., Tarquis, F. (2017). *Métodos constructivos en el tramo atirantado del nuevo Queensferry Crossing*. VII Congreso Internacional de Estructuras de ACHE. La Coruña.

[7] Vázquez, A., Raynor, D., Romberg, M., Walser, P., Tarquis, F. (2017). *Temporary works for the Cable Stayed Deck in the Queensferrt Crossing*. VII Congreso Internacional de Estructuras de ACHE. La Coruña.

[8] Bernardo, H., Tarquis, F., Lucas, C., Viartola, L. V., (2019). *Rande Bridge Widening: a 400-m-span Cable-stayed Bridge Expansion*. Practice Periodical on Structural Design and Construction. ASCE, ISSN 1084 - 0680

[9] Corres, H., De Cabo, J., Sánchez, J. Arroyo, J. (2020). *Ampliación del Puente de Rande. Diseño del Proceso Constructivo*. VIII Congreso Internacional de Estructuras de ACHE. Santander.

[10] Bernardo, H., Consuegra, J. J., Tarquis, F., Lucas, C., Otero, F. (2022). *Ampliación del puente de Rande. Proceso de montaje del nuevo tablero*. Hormigón y Acero, vol. 73, número 298, p. 25-34.

[11] Domínguez, P., Fernández, A., Serrano, A., (2018). *Ampliación del Puente de Rande*. Revista de la Asociación Española de la Carretera, número 238.

[12] Lorente, G. Lucas, C., Conesa, J. L., Caracena, A. et al. (2020). *Construcción del tramo atirantado del Nuevo Puente de Champlain sobre el río San Lorenzo en Montreal (Canadá)*. VIII Congreso Internacional de Estructuras de ACHE. Santander.

[13] Corres, H., Milián, J., Abel, A., Lucas, C. et al. (2020). *Nuevo Puente Champlain sobre el río Sa Lorenzo en Montreal. Diseño de las estructuras auxiliares para la construcción del puente atirantado*. VIII Congreso Internacional de Estructuras de ACHE. Santander.

DRAGADOS

Puente del Puerto de Corpus Christi
(Harbor Bridge) Texas, Estados Unidos

Ampliación del puente de Rande
Pontevedra, España

Puente de la Constitución de 1812
Cádiz, España

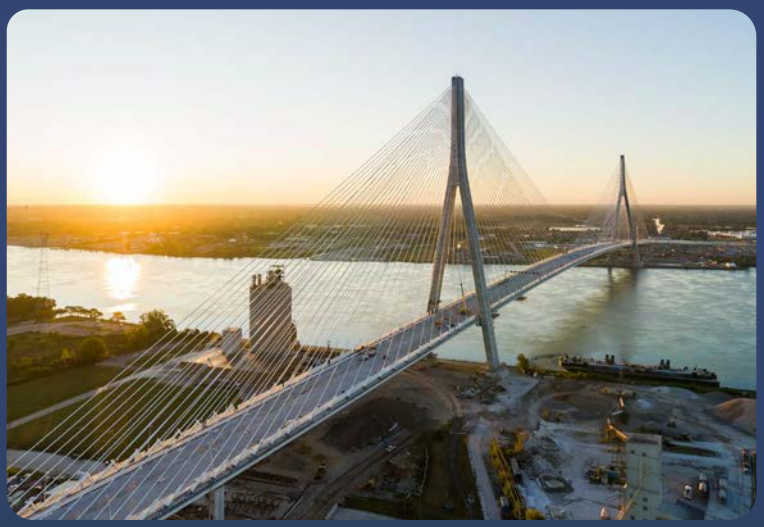

Puente Internacional Gordie Howe
Ontario, Canadá - Michigan, Estados Unidos

Queensferry Crossing
Edimburgo, Escocia

Puente de Champlain
Montreal, Canadá

Construyendo un **LEGADO**
Creando un **FUTURO** mejor

Disponible en **www.hormigonyacero.com**
https://doi.org/10.33586/hya.2026.4163

Lecciones aprendidas del diagnóstico y desmontaje del paso superior Joaquín Costa – Francisco Silvela, Madrid

Experience Achieved After Diagnosis and Dismantling of the Overpass Joaquín Costa - Francisco Silvela. Madrid.

Julio Sánchez Delgado[a,*], **Fco. Javier León González**[b]

[a] *Ingeniero de Caminos, Canales y Puertos. FHECOR. Codirector técnico.*

[b] *Dr. Ingeniero de Caminos, Canales y Puertos. FHECOR. Codirector técnico.*

Recibido el 19 de noviembre de 2025; revisado el 1 de diciembre de 2025, aceptado el 25 de febrero de 2026

RESUMEN

Construido en 1969, este viaducto de hormigón pretensado venía manifestando algunos problemas hasta que, en febrero de 2020, se detectó una grieta asociada a la rotura de un tendón. Eso exigió acometer un proceso de diagnosis para una adecuada evaluación estructural del tablero. Tras constatarse que cerca del 10% de los tendones presentaba alguna deficiencia relacionada con la inyección y con principios de corrosión, y que la resistencia característica del hormigón, con un diagnóstico inequívoco de fuerte ataque árido-álcali, apenas llegaba al 50% de la del proyecto –con un nivel de seguridad inadmisible e insalvable–, se recomendó al Ayuntamiento de Madrid el cierre y el desmontaje de la estructura. El soporte de la ETSICCP-UPM y nuestra perseverancia permitieron completar dos campañas paralelas de reconocimiento *post-mortem* de gran valor para confirmar el diagnóstico. Este artículo expone las lecciones aprendidas por los autores durante las fases de diagnosis, de diseño de la demolición y de asistencia técnica durante la ejecución.

PALABRAS CLAVE: corrosión bajo tensión, fragilidad, ataque árido-álcali, pretensado 'excesivo'.

ABSTRACT

Built in 1969, this prestressed concrete viaduct had been exhibiting various signs of distress until, in February 2020, a crack associated with the rupture of a tendon was detected. This required the implementation of diagnosis to enable an adequate structural assessment of the deck. After confirming that approximately 10% of the tendons exhibited deficiencies related to grouting and early-stage corrosion, and that the characteristic compressive strength of the concrete – with an unequivocal diagnosis of severe alkali–aggregate reaction (AAR) – barely reached 50% of the design value, resulting in an unacceptable and irrecoverable level of structural safety, the Madrid City Council was advised to proceed with the closure and dismantling of the structure. The support from the Engineering School of Madrid (ETSICCP-UPM) and our perseverance made it possible to complete two parallel post-mortem investigation campaigns of great value in confirming the diagnosis. This article presents the lessons learned by the authors during the diagnosis phase, the demolition design stage, and the technical assistance provided throughout execution.

KEYWORDS: stress-corrosion, brittle failure, alkali-aggregate attack, 'excess' of prestressing.

* Persona de contacto / *Corresponding author*:
Correo-e / *e-mail*: jsd@fhecor.es (Julio Sánchez Delgado)

Cómo citar este artículo: Sánchez, J, & León, J. (2026). Lecciones aprendidas del diagnóstico y desmontaje del paso superior Joaquín Costa – Francisco Silvela, Madrid. *Hormigón y Acero*. 77(308):235-257. https://doi.org/10.33586/hya.2026.4163

Figura 1. Puente José León de Carranza, inaugurado en 1969.

Figura 2. Palacio de los Deportes de La Coruña, inaugurado en 1970.[1]

1. EL PROYECTISTA Y LA OBRA

José Antonio López Jamar fue un gran ingeniero de INTECSA cuya obra ha sido insuficientemente reconocida. Como muchos de su generación, educados en la estela de los grandes profesores e ingenieros estructurales que ejercían brillantemente la profesión e impartían docencia de gran calidad en la Escuela de Ingenieros de Caminos, Canales y Puertos de Madrid, López Jamar redactó proyectos y supervisó obras muy variadas en el ámbito de los edificios, los puentes y otras construcciones. Cabe citar, por ejemplo, el puente José León de Carranza (Cádiz) (figura 1) y el espléndido Palacio de los Deportes de La Coruña [12] (figura 2). En 1968 proyectó el viaducto urbano que es objeto de este artículo, en aquel contexto en el que proliferaban por todo el país los pasos superiores urbanos como mejor sistema para asegurar la fluidez del tránsito de vehículos y que, además, venían a ser expresiones de modernidad. El autor del proyecto publicó un artículo en *Hormigón y Acero* [13] en el que, con prosa escueta, describe las características esenciales de la obra. El presente artículo viene precedido de dos referencias recientes [3, 14] a propósito del diagnóstico (primavera de 2020) y del inevitable desmontaje (verano de 2020) de este viaducto del que ahora queda la memoria. La historia de su final depara lecciones que deseamos presentar.

2. DESCRIPCIÓN DE LA ESTRUCTURA

El viaducto, proyectado en 1968 e inaugurado en 1970, enlazaba las calles de Joaquín Costa y Francisco Silvela, sobre la glorieta de López de Hoyos, así como la primera con la calle de Príncipe de Vergara mediante con un ramal de descenso hasta ésta (figuras 3 y 4).

1 Ver https://www.fgpatinaxe.gal/el-palacio-de-los-deportes-de-riazor-una-pista-con-sabor-a-hockey-sobre-patines/ y https://arquitecturayempresa.es/noticia/arquitectura-olvidada-se-cumplen-50-anos-del-palacio-de-deportes-de-la-coruna

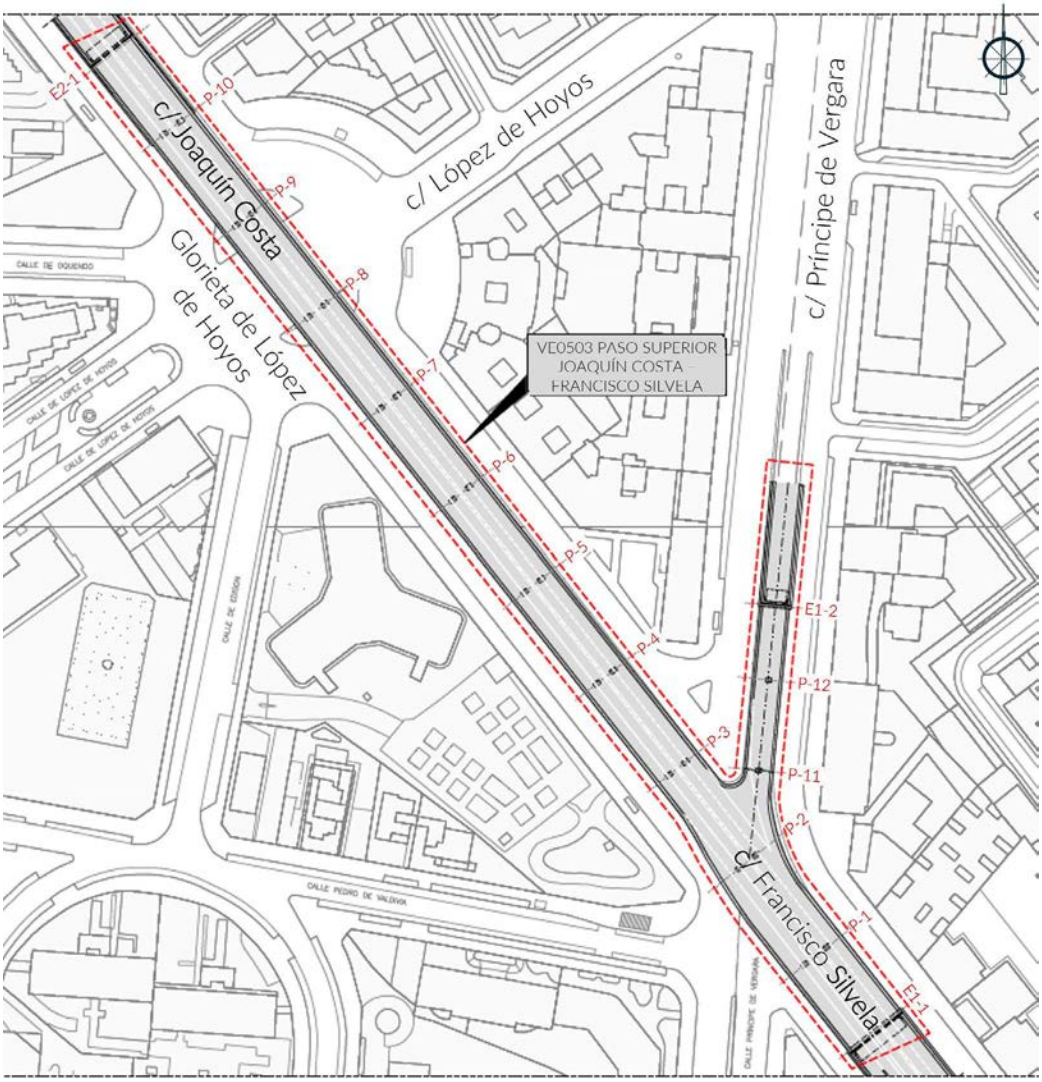

Figura 3. Ubicación (adaptada a partir de [3]) de la estructura, cuya planta se marca en rojo

Constaba de un tronco principal de 460 m de longitud incluyendo estribos y muros laterales, siendo la longitud de tablero de 359 m, distribuida en 9 vanos de 33.8 m de luz y vanos extremos de 27.6 m. El ramal de salida hacia la calle Príncipe de Vergara tenía 122 m de longitud, incluyendo estribos y muros laterales, correspondiendo 69 m al tablero, con 3 vanos de luces 22-22-25 m, el último de los cuales era el vano de conexión con el tronco principal. La superficie total de los tableros era de unos 6400 m². Las juntas de dilatación se localizaban en los tres estribos (E1-1, E1-2 y E2-1, figura 3) y la junta a media madera entre el ramal y el tronco a la altura de la pila 11. Salvo en la P-2 (conectada al tablero), los aparatos de apoyo eran de neopreno zunchado.

El tablero era una losa de hormigón pretensado, aligerada en casi toda su extensión. El tronco principal tenía, en 9 de sus 11 vanos, una sección transversal compuesta por dos núcleos en forma de artesa conectados entre sí por una faja central de losa, teniendo cada núcleo dos aligeramientos rectangulares con esquinas achaflanadas. El ancho era de 19.25 m en el vano 1 (junto al estribo de la calle Francisco Silvela) y 15 m en los vanos 4 a 11 (hasta el estribo de la calle Joaquín Costa). El canto máximo de la sección en el tronco principal era de 1.20 m, constante a lo

Figura 4. Perspectiva del tronco principal del viaducto, 13 de marzo de 2020 (foto de los autores).

largo de toda la longitud, que se reducía hacia los bordes laterales por el bombeo transversal (figura 5).

En los vanos 2 y 3 del tronco principal, en los que se materializaba la conexión con el ramal de la calle Príncipe

de Vergara, la anchura de tablero era variable entre 19.25 m y 15 m, las artesas eran macizas y la faja central entre artesas tenía un canto mayor que en el resto del tablero. La sección transversal del ramal de la calle Príncipe de Vergara constaba de un único núcleo con forma de viga artesa con dos aligeramientos, canto de 1.1 m en el eje, ancho de 8.5 m y voladizos de 2.75 m.

La considerable esbeltez (L/h = 28.15) de los vanos del tramo principal venía motivada por la necesidad de acotar la rasante y asegurar gálibos suficientes. Para eso fue preciso dotar a la estructura de una notable cuantía de armadura de pretensado: 37 kg/m² de acero de tensión última f_{pu}=170 kg/mm² (figura 6). Para comparar este valor con la práctica actual, se puede hacer una equivalencia con acero f_{pu}=1860 MPa, lo que supone una cuantía corregida de 33.3 kg/m², viniendo a ser un 33% mayor que las cuantías habituales hoy día (25 kg/m²) [5]. La cuantía de armadura pasiva (figura 7) ascendió a 49 kg/m²

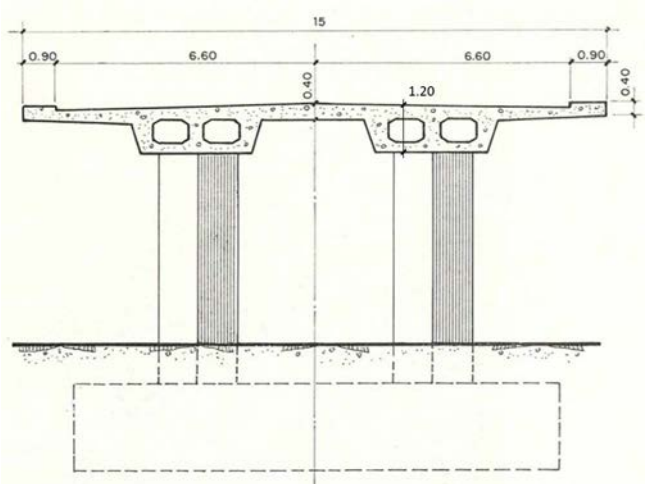

Figura 5. Sección transversal tipo, tomada de [13].

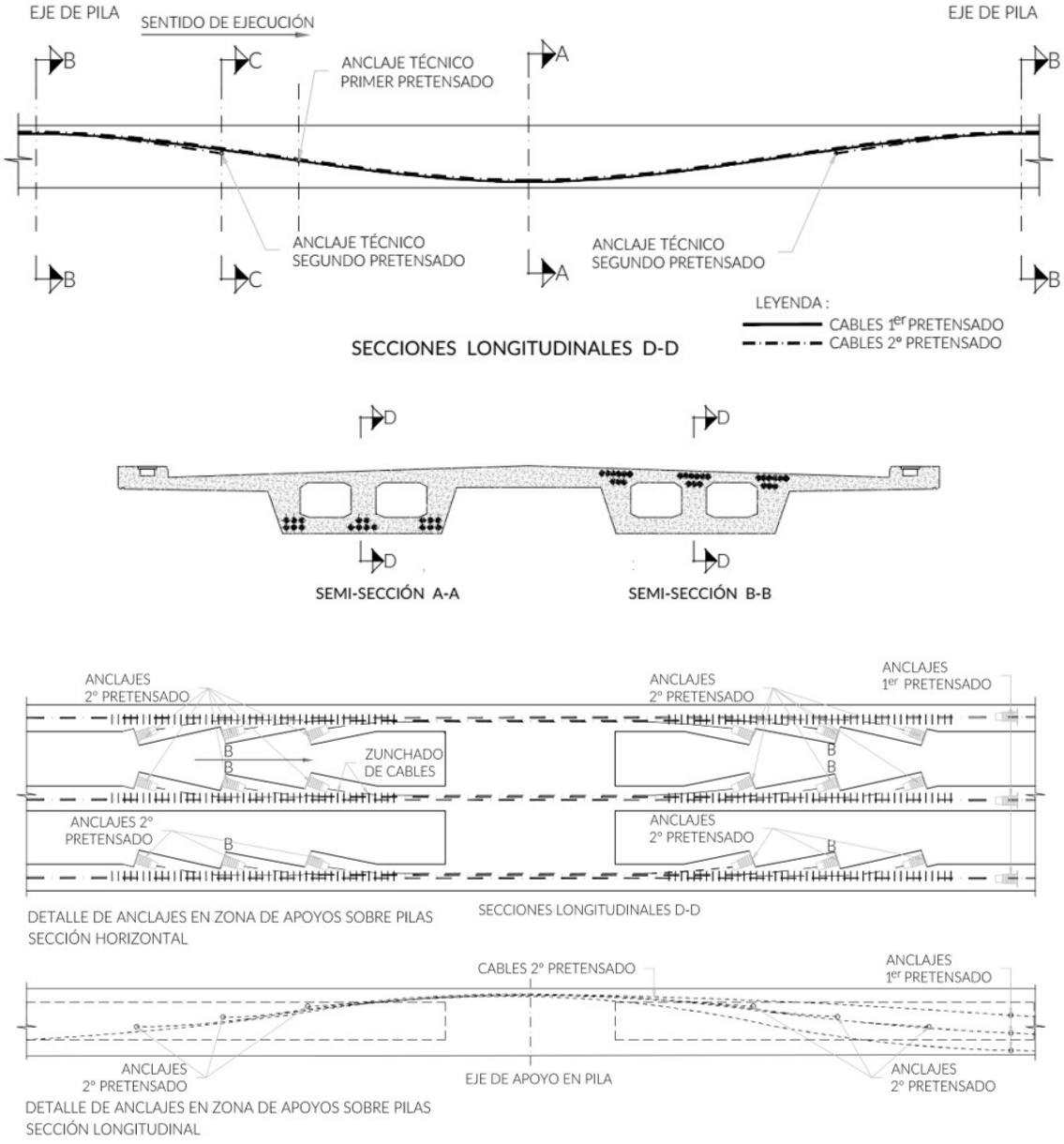

Figura 6. Disposición del pretensado (tomado y adaptado de [13]).

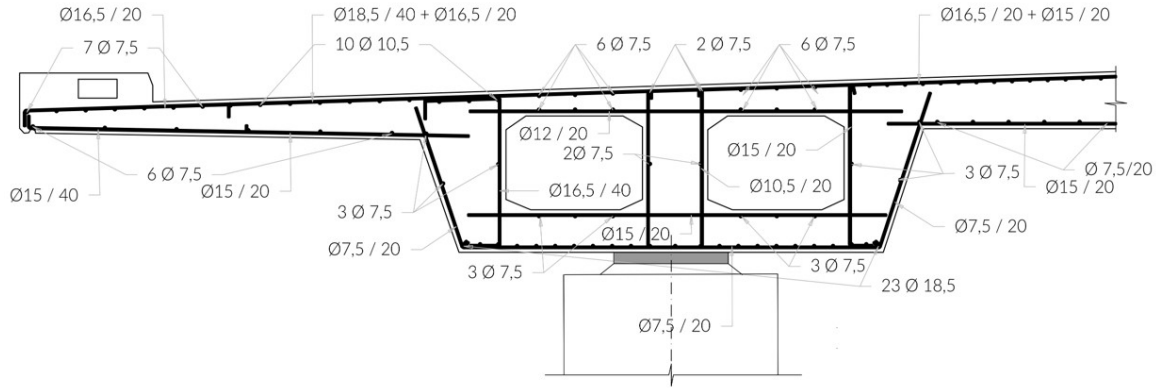

Figura 7. Armadura pasiva, a partir de los planos conservados en el Ayuntamiento de Madrid (57-237-1, Inv. 865).

Figura 8. Sección de una de las dovelas cortadas, en el proceso de desmontaje, en las proximidades de un apoyo. La altura de los alvéolos es de apenas 0.55 m (el canto total de la sección, constante, es de 1.20 m, con una esbeltez de L/28.15) (foto de los autores).

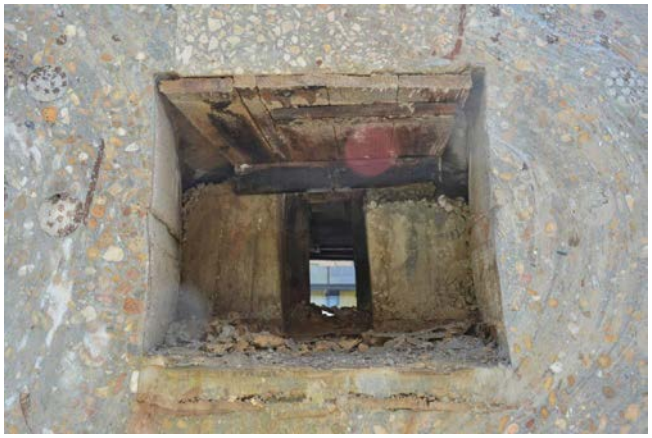

Figura 9. Cajetines de pretensado en uno de los alvéolos de una de las dovelas cortadas en el proceso de desmontaje (foto de los autores.)

Figura 10. Prueba de carga del viaducto, 13 de mayo de 1970.

de acero de límite elástico f_y =4200 kg/cm², que equivale a 40.4 kg/m² de acero B500, es decir menos de la mitad de los valores habituales hoy día (100 kg/m²). Globalmente, la cuantía total ponderada de acero de armar (multiplicando por tres la cuantía de acero de pretensar) se situaría en los 141 kg/m² (f_y = 500 MPa) frente a los aproximadamente 175 kg m² de un puente actual.

En ausencia de reglamentación española propia para hormigón pretensado —la primera Instrucción española de hormigón pretensado llegaría en 1977 [4]—, López Jamar hizo uso de reglamentos franceses y dejó constancia del análisis estructural en listados de ordenador, como consta en el archivo del Ayuntamiento de Madrid (57-237-1, Inv. 865).

La construcción, muy meritoria por el reducido canto de las piezas (figuras 5, 8 y 9), fue rápida —tan sólo 8 meses— inaugurándose la obra en 1970 (figura 10). Debe destacarse que la esbeltez de 1/28.15 y la disposición de anclajes intermedios en el interior de los aligeramientos debió suponer un reto constructivo importante. El propio autor explica en [13] que *El tablero se ha construido hormigonando in situ, por el sistema de avance por tramos completos —entre puntos de inflexión de tramos sucesivos—, empleando cimbras tubulares*.

3.
DAÑOS Y DETERIOROS OBSERVADOS INICIALMENTE

La estructura venía manifestando movimientos desmesurados de la junta más alejada del punto fijo (E2-1, figura 3), situada en el lado de Joaquín Costa, y unas misteriosas fisuras longitudinales en las losas de fondo y en las almas (figuras 11 y 12), prácticamente sistemáticas, que permanecieron inexplicablemente sin diagnóstico, con un tratamiento meramente paliativo (pintura y sellado).

A comienzos de febrero de 2020, en coincidencia con las labores de mantenimiento que llevaba a cabo DRAGADOS en el contexto de un contrato de conservación ordinaria y especializada, se detectó la muy rápida evolución, en cuestión de pocos días, de una de las fisuras longitudinales detectadas en los paramentos laterales y en la losa inferior. De la fisura se pasó a una grieta de abertura superior al centímetro, tal y como se advierte en la figura 13, situada aproximadamente a 0.60 de la luz de vano 6 en su lado sur. El 12 de febrero de 2020, FHECOR participó en la inspección de la estructura y solicitó practicar una calicata en la zona de la grieta observada. Se detectó, en efecto, en el lado oeste del vano 6 (entre P-5 y P-6), cerca del centro del vano, un tendón sin lechada protectora y roto, con fractura reciente (figuras 14 y 15).

Como es sabido, la rotura completa de un tendón, tras la rotura sucesiva de sus cordones, supone mecánicamente la aparición de una fuerza igual y contraria a la existente inmediatamente antes de la rotura. Esa fuerza de reacción provoca súbitamente en el elemento "tendón", especialmente si no está rodeado de la lechada de inyección (figura 15), una fuerza de compresión sobre un elemento tan esbelto que produce un efecto látigo (transversal) cuyo resultado se tradujo en la conversión de una de las fisuras longitudinales en una grieta. La ya referida escasez de cuantía de armadura pasiva transversal explica que el prisma de hormigón no pudiera resistir esa acción perpendicular al eje del tablero: las tracciones transversales inducidas por el efecto látigo no estaban equilibradas por una cuantía de armadura transversal que no exigía la reglamentación de la época[2].

2 La EP-77 [4] no llegaría hasta 8 años después de redactarse el proyecto. Por tanto, no está el cosido por efecto látigo entre las acciones de proyecto, ni siquiera implícitamente.

Figura 11. Fisuras longitudinales (foto del informe de inspección principal de INES Ingenieros Consultores, 2012, referido en [8]).

Figura 12. Fisuras longitudinales selladas en losa de fondo (foto de los autores, marzo de 2020).

Figura 13. Grieta en vano 6 (suroeste de la estructura). Foto de los autores, 12 de febrero de 2020.

Figura 14. Tendón roto, sin lechada, detectado tras practicar una calicata en la zona de la figura 13. Foto de los autores.

Figura 15. Tendón sin lechada en lado oeste del vano 6 (entre P-5 y P-6), en la calicata en la zona de la figura 13. Foto de los autores, 12.02.2020.

4.
TRAS LA PISTA DE LA CORROSIÓN

Dada la trascendencia de lo observado, el mismo día en que se detectó la referida rotura de tendón se acometió la realización de una calicata adicional en la zona de tablero ubicada sobre la pila 6, también en el lado suroeste (ver figura 3). Se trataba de averiguar si, además de en la zona baja afectada del vano 6 (figuras 13, 14 y 15), también se habría producido un déficit de inyección en la parte alta, asociada quizás a la inexistencia de puntos de purga en esa zona.

En la figura 16 se muestra el estado de las vainas y de los tubos de purga encontrados, y en la figura 17 se puede apreciar el estado de los alambres de los cordones de uno de los tendones sobre pila 6, con lechada y síntomas de incipiente corrosión (parte derecha).

Es oportuno recordar que el hecho de que el puente se construyera en 1969 no es razón suficiente para sospechar que fuera mayor la probabilidad de encontrar defectos ocultos achacables a tecnologías aún desconocidas o insuficientemente probadas. El proyecto, ya se ha dicho, contó con el apoyo de cálculos con ordenador, la cimbra fue modular y moderna, el hormigón de proyecto era de f_{ck} = 40 MPa y las técnicas de pretensado (aquí CCL, hoy VSL) estaban ya a punto. En 1969, recuérdese, el ser humano conquistó la Luna y DRAGADOS construyó este viaducto de manera muy eficiente. Los autores hemos encontrado tendones rotos, déficits de inyección y otros vicios ocultos en obras mucho más próximas en el tiempo.

Lo observado llevó a la recomendación, trasladada al Ayuntamiento de Madrid el mismo 12 de febrero de 2020, de que se restringiera el paso de vehículos, admitiéndolo sólo en los carriles centrales. Con el fin de evaluar el alcance de los déficits observados en el pretensado, se practicaron otras calicatas, a partir de un programa sistemático orientado al efecto, encontrándose otros tendones con ausencia o déficit de inyección de lechada (como en la figura 15), lo que representaba aproximadamente el 10% del total de tendones. Cabe añadir que la detección, en catas puntuales, de huecos de inyección y principios de corrosión en ese 10% de tendones, es un claro indicio, aunque no se encontraron más alambres rotos, de riego de rotura próxima en el tiempo o en otro lugar no inspeccionado.

De forma inmediata, ese mismo día 12 de febrero, se entregaron en el Laboratorio de Ciencia de Materiales de la Escuela de Ingenieros de Caminos, Canales y Puertos de Madrid unas muestras de los cordones de la zona de rotura detectada en citado vano 6 (figura 18).

Los resultados de las determinaciones realizadas sobre las muestras de los alambres fueron muy reveladores [6]. La figura 19 muestra la rotura dúctil del alambre central de uno de los cordones (típicamente formados por un alambre central y 6 perimetrales). En esa misma figura se aprecia también que no hay pérdidas tan significativas de sección por corrosión en dicho alambre central, a diferencia de lo que se observa en los alambres perimetrales.

En la figura 20 se compara el estado de daño interno del alambre central con el de uno de los periféricos [6]. En el alambre periférico se advierte nítidamente una discontinuidad que refleja, en definitiva, una corrosión bajo tensión, con rotura frágil en la forma típica de pico de flauta. Desde el punto de vista estructural, la figura 21 es de un gran interés. El efecto mecánico

Figura 16. Vainas y tubos de purga sobre pila 6. Armadura pasiva estirada en frío, típica de la época (foto de los autores, 12.02.2020).

Figura 17. Calicata sobre pila 6. Foto de los autores, 12.02.2020.

Figura 18. Muestras de los cordones rotos, en la zona de rotura (derecha) y en una zona menos dañada (foto del Laboratorio de Ciencia de Materiales).

que tiene la corrosión bajo tensión es el de la fragilización del acero. En efecto, en muestras mecanizadas hasta eliminar la corrosión de alambres corroídos (hasta eliminar las micro-entallas exteriores) el comportamiento es dúctil, típico del acero sano. Sin embargo, las muestras ensayadas del acero sin mecanizar (llevan incorporadas las microentallas) revelan que, manteniéndose el límite elástico, el comportamiento es frágil al alcanzarse el límite elástico.

Los alambres periféricos, pues, sin lechada a su alrededor, alcanzaron la rotura frágilmente, pasando la carga a los alambres restantes, rompiéndose sucesivamente los restantes periféricos, frágiles y con menor sección que el alambre central que, en mejor estado de conservación, habría roto dúctilmente (figura 19), sí, pero ya sin capacidad portante suficiente pues el área resistente se había reducido, en el cordón roto, a la séptima parte aproximadamente.

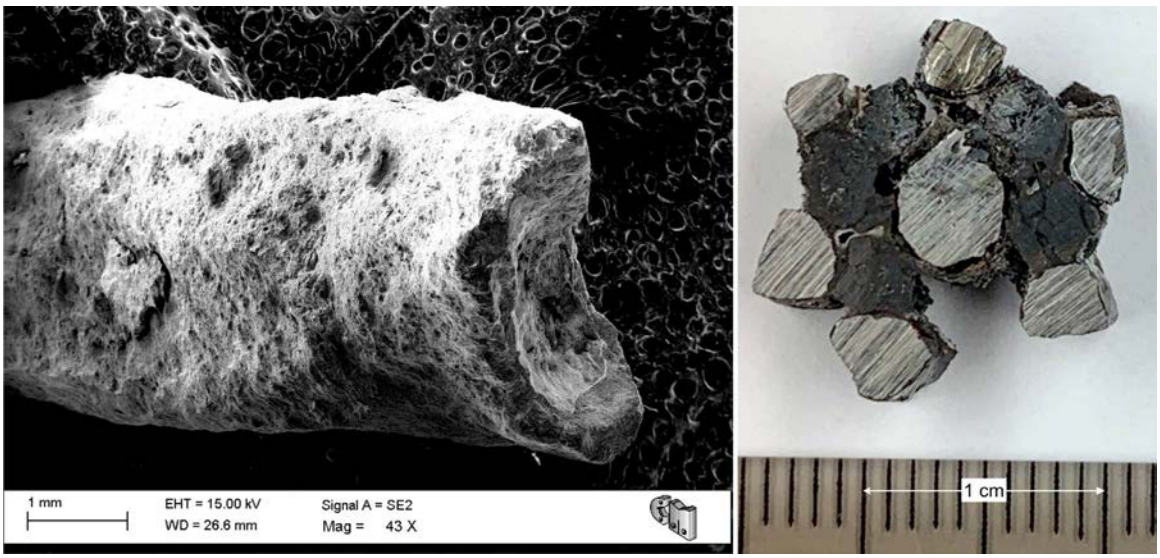

Figura 19. Rotura dúctil de un alambre central [6].

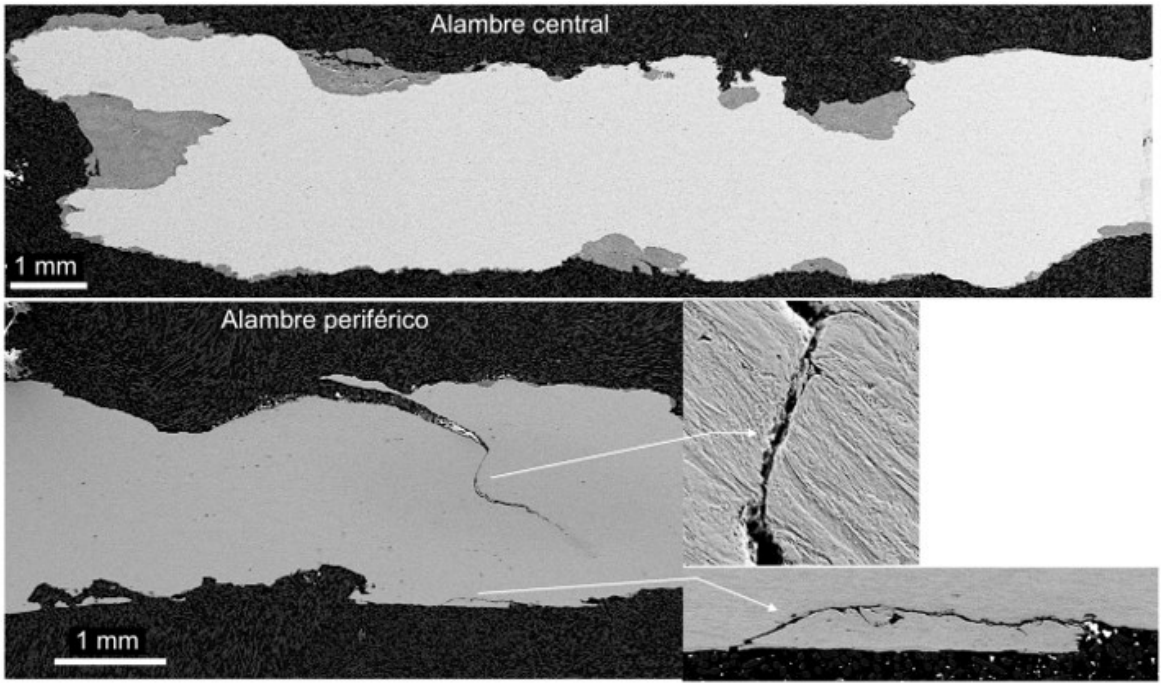

Figura 20. Comparativa de los estados de daño interno entre alambre central y uno periférico del cordón 1 [6].

Las consecuencias de este comportamiento de la armadura alertaron al equipo interviniente acerca de los riesgos asociados a una rotura seccional frágil en flexión al ser también frágil el comportamiento de la armadura activa, protagonista de la capacidad resistente de las piezas, especialmente en las zonas de vano.

En la parte superior de la figura 22 se representa, en abscisas, la carga total q uniformemente repartida que vendría a dar una ley de esfuerzos parecida a la envolvente de proyecto, al menos en centro de vano (y su vecindad) y en apoyos para las cargas permanentes y sobrecargas, creciendo de manera afín (es una hipótesis simplificada en este razonamiento) desde el valor nulo hasta el valor de agotamiento estructural, pasando por su valor nominal. En ordenadas se representan los momentos flectores en esas secciones de referencia M_v, M_{a1} y M_{a2} (vano y apoyos) para cada valor de la carga q recién descrita, de forma que, en general, la condición de equilibrio viene expresada por

$$\frac{qL^2}{8} = M_v + \frac{M_{a1} + M_{a2}}{2} \qquad (1)$$

Para valores moderados de las acciones, los momentos flectores en los apoyos y en los vanos (tramos iniciales de las curvas roja y verde) se parecerán mucho a la predicción de comportamiento elástico y lineal de las secciones porque también elásticos y lineales son los materiales y, con pretensado suficiente, no hay fisuración. De hecho, con los criterios de la época del viaducto, el pretensado "en clase 1" aseguraba que no se producían tracciones en el hormigón para las situaciones pésimas de carga nominal (de servicio). En esos ejes, las leyes lineales

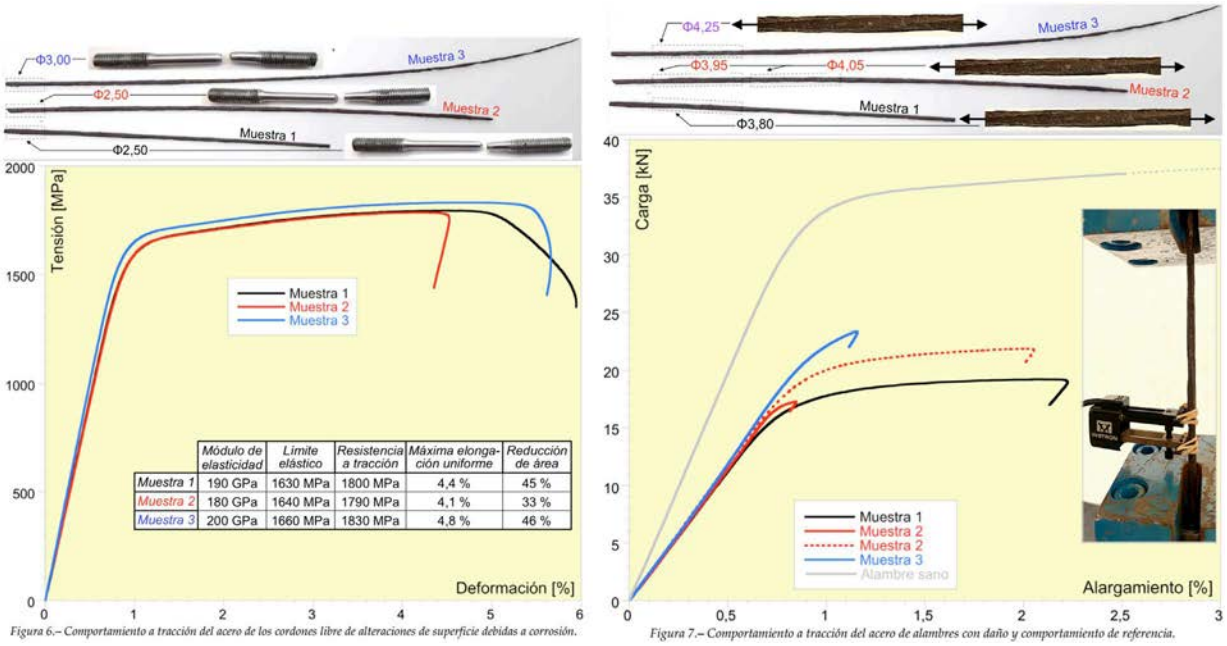

	Módulo de elasticidad	Límite elástico	Resistencia a tracción	Máxima elongación uniforme	Reducción de área
Muestra 1	190 GPa	1630 MPa	1800 MPa	4,4 %	45 %
Muestra 2	180 GPa	1640 MPa	1790 MPa	4,1 %	33 %
Muestra 3	200 GPa	1660 MPa	1830 MPa	4,8 %	46 %

Figura 6.– Comportamiento a tracción del acero de los cordones libre de alteraciones de superficie debidas a corrosión.

Figura 7.– Comportamiento a tracción del acero de alambres con daño y comportamiento de referencia.

Figura 21. Diagramas tensión-deformación y carga-alargamiento de muestras mecanizadas y muestras sin mecanizar, correspondientes a cordones ensayados. Los alambres no mecanizados son frágiles [6]. En la figura izquierda se muestran los resultados de alambres sin alteraciones de superficie por corrosión. En la figura derecha, la muestra 1 es de un alambre central no dañado; las muestras 2 se corresponden con alambre dañado exteriormente y no mecanizado (trazo continuo) y mecanizado hasta eliminar la corona exterior (trazo de puntos), respectivamente. Finalmente, la muestra 3 se corresponde con un alambre periférico.

tienen pendientes $L^2/12$ (apoyos) y $L^2/24$ (centro de vano) mientras el comportamiento sea lineal. La línea azul más alta, de trazos, expresa la condición de equilibrio global, de pendiente $L^2/8$. Si, por ejemplo, se fisurasen las secciones de vano, perdiendo rigidez, necesariamente crecerán los momentos en las regiones de apoyo porque ha de satisfacerse el equilibrio global. Consiguientemente, en esa hipótesis, la carga q_1 para la que se alcanza en los apoyos el valor de plastificación, muy parecido a $M_{a\,Rd}$ como se ha representado aquí, es menor que la que se obtendría en el irreal caso de que los materiales se comportasen siempre elástica y linealmente y el hormigón no se fisurase (hipótesis falsa, pero es la que se utiliza diariamente en el proyecto de estructuras de hormigón y parece sancionada como suficientemente segura … si hay ductilidad).

Si, en efecto, las secciones de apoyo son dúctiles —con la ductilidad que dan los aceros sanos— se configura una rótula plástica en la zona de apoyos, manteniéndose constante el valor $M_{a\,Rd}$ para incrementos sucesivos de q mientras que, a cambio, se acelera el crecimiento de los momentos en centro de vano, con pendiente $L^2/8$, en virtud del requisito de satisfacer el equilibrio global. Son las trayectorias de trazo discontinuo que se han dibujado en la figura 22, parte superior. Normalmente, si hay ductilidad suficiente, las secciones de apoyo mantienen vigente el momento $M_{a\,Rd}$ para valores crecientes de la carga q hasta que en el centro de vano se alcanza el momento de agotamiento $M_{v\,Rd}$. Configuradas así tres rótulas (en apoyos y en centro de vano), se habrá alcanzado el agotamiento de la pieza al movilizarse un mecanismo cinemático de rotura. La carga de agotamiento q'_{Rd} será parecida a la de proyecto o mayor. Es oportuno recordar de nuevo que las leyes elásticas, utilizadas en el proyecto cotidiano, son sólo criterios para dimensionar, pero no predicciones del comportamiento real, evidentemente no lineal en cuanto aparecen la fisuración o los materiales abandonan sus respectivas zonas de comportamiento asimilable al elástico y lineal.

Sin embargo, si la armadura (toda la armadura) de negativos ya no es dúctil sino completamente frágil (figura 21), el colapso se produce para el valor de carga q_1, menor que q_{Rd} como se deduce, si se fue estricto en el dimensionamiento, al entrar en la expresión (1) con un momento $M_v < M_{v\,Rd}$, dado que el momento en vano ha de crecer súbitamente para intentar restablecer el equilibrio, alcanzándose inmediatamente, para ese mismo valor q_1, la rotura en el vano y, por consiguiente, en la estructura.

Naturalmente, cabe plantear otros escenarios, como que se fisuren antes las zonas de apoyo, perdiéndose rigidez en esas zonas, como se muestra en la parte inferior de la figura 22, lógicamente con otros criterios de dimensionamiento (por eso no coinciden los valores de $M_{v\,Rd}$ y $M_{a\,Rd}$ en los diagramas de la parte superior y de la parte inferior). Se llega a conclusiones semejantes a las expuestas para el caso del diagrama superior de la figura 22.

En definitiva, si la evolución de esfuerzos se aparta de la previsión ideal de proyecto de comportamiento elástico y lineal —por fisuración o por cualquier otra variación de la ley real de rigideces E_cI_h con relación a la teórica— y, además, el comportamiento de las secciones (diagrama momento-curvatura) es elasto-frágil por serlo la armadura, es grande la probabilidad de que la seguridad estructural se vea gravemente comprometida. No fue el caso de este viaducto porque la pérdida de ductilidad (y de sección) no fue generalizada ni simultánea en todos los tendones de vano ni en todos los tendones de las zonas de apoyo, situación que, aunque cierta, está fuera de control. También ayuda el que, al proyectarse con envolventes de esfuerzos, se produce un efecto de sobre-armado de las piezas cuando se comparan

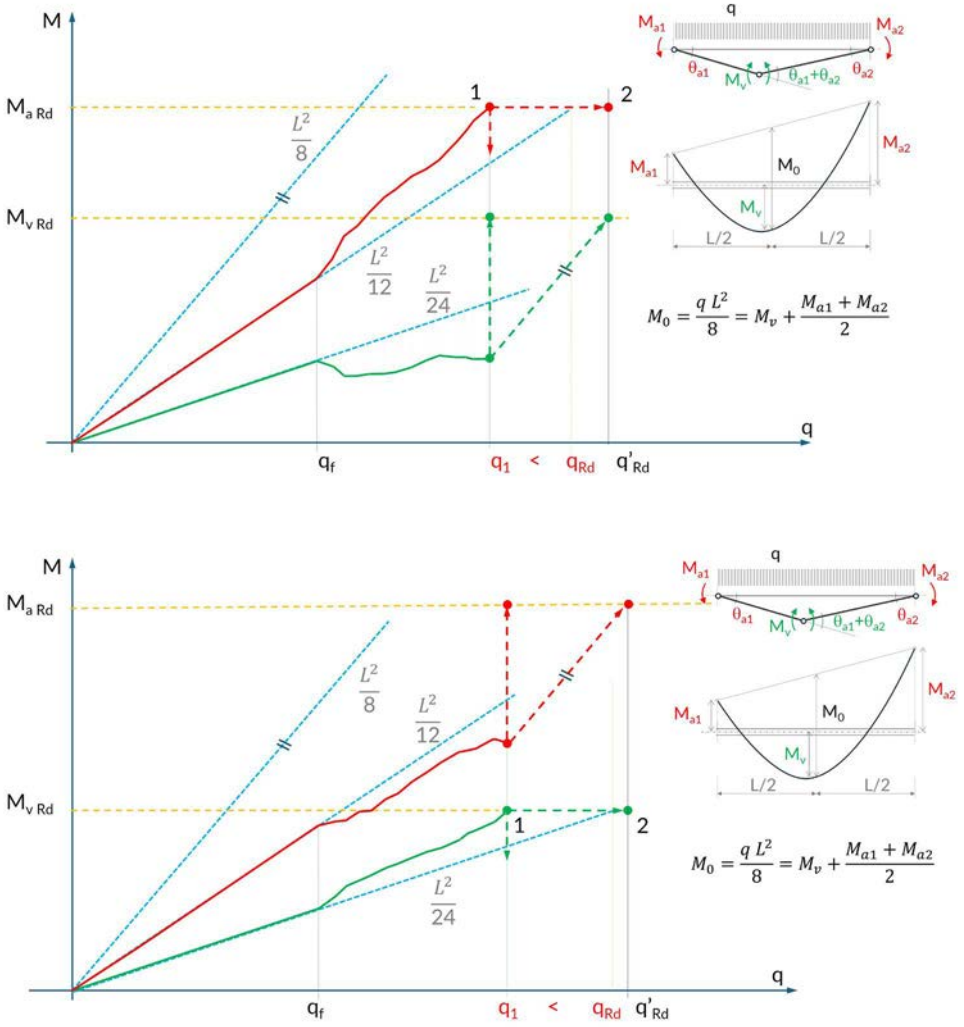

Figura 22. Arriba, esquema explicativo (a partir de [2]) de la influencia que tiene la pérdida de ductilidad seccional en el comportamiento estructural general si se fisura antes la zona de vano que la de apoyo. Abajo, situación equivalente en la hipótesis de que fisuran antes las zonas de apoyo. Figuras de los autores.

con las leyes reales (no envolventes). Esto último hace verdad (ver [2] entre otras referencias) que la ductilidad es condición necesaria pero no suficiente para garantizar la seguridad, siendo el citado sobre-armado un factor coadyuvante para dar por buena la praxis de proyecto.

En este contexto argumental, antes de conocer los resultados de los ensayos sobre el hormigón acerca de la reactividad árido-álcali, se mantuvo la recomendación de mantener sin tráfico dos de los cuatro carriles. Cabe añadir que, producido el cese de actividad como consecuencia de la pandemia de Covid-19, la repercusión práctica de esa medida en el tráfico fue insignificante.

5. TRAS LA PISTA DEL HORMIGÓN

La campaña de inspección especial —en pleno confinamiento por el tristemente famoso coronavirus— permitió sacar conclusiones aún más alarmantes que las deducidas tras los resultados del acero de pretensado. Se extrajeron 23 testigos de diferentes elementos del tablero [10], losa superior y cajón, dando un valor de la resistencia característica estimada, con los criterios al uso, de $f_{ck,est}$ = 18.37 MPa, el 47% de la resistencia característica especificada en proyecto, 40 MPa —un valor que no era extraordinario en 1969 y que venía impuesto, según el autor del proyecto, para materializar el pretensado exigido por la notable esbeltez del tablero—. Añádase que como resistencia media se obtuvo f_{cm} = 29.15 MPa. El valor del módulo de deformación longitudinal E_{cm} resultó ser de 15.8 GPa, equivalente apenas al 51% del de proyecto, estimado en unos 30 GPa.

La observación de los testigos extraídos (algunos de ellos en coincidencia con las fisuras detectadas, con el fin de medir su profundidad) y de las calicatas practicadas incorporaba, además, otros elementos interesantes para la reflexión. La figura 23 presenta, a título de ejemplo, áridos partidos en la misma alineación, pero no así la pasta de mortero o, al menos, no en términos comparables a los de las roturas de los áridos.

Observamos que la alineación de las roturas de los áridos era longitudinal, es decir, coincidente con la de la acción lon-

Figura 23. Fisuras longitudinales en testigos resultado de las perforaciones verticales *a posteriori* para el enhebrado del hilo de diamante durante el proceso de demolición. Foto cortesía del Laboratorio de Química de la Escuela de Ingenieros de Caminos, C. y P. de Madrid, no incluida en [11].

gitudinal del pretensado (muy fuerte en este tablero) y de las tensiones normales debidas a las restantes acciones. Aunque no es objeto de este artículo[3] entrar en la etiología de ese efecto, una posible causa, en nuestra opinión, tendría que ver con el efecto recíproco de áridos y pasta, semejante al que se produce en las obras de sillería o de ladrillo, en las que las piezas más rígidas (los sillares o los ladrillos) han de funcionar a tracción transversal para confinar al mortero, más deformable y menos resistente. La pérdida de adherencia árido-álcali como consecuencia del ataque árido-pasta completaría la explicación del fenómeno al verse sometidos los áridos a una especie de ensayo brasileño, cargados en los extremos y no confinados transversalmente por la presencia del gel en la interfaz, configurándose las roturas sistemáticamente alineadas en la dirección de las compresiones predominantes. La cuestión, que hemos visto después en otras situaciones, merece ser objeto de investigación pormenorizada.

3 En la referencia [7] se hace un interesante estudio de la reacción árido-álcali, fenómeno que aún no se comprende completamente. En el estudio se presentan los resultados de una campaña para conocer su cinética y las consecuencias estructurales. Se señala que el parámetro mecánico que mejor refleja dicho ataque es el módulo de deformación longitudinal, y no tanto la resistencia a compresión, cuyos resultados pueden enmascarar el alcance real del fenómeno. Las referencias [1] y [15] son también muy recomendables. Con relación a la orientación de las fisuras, la referencia [16] aporta un dato adicional interesante, relacionado con la influencia de la reactividad diferencial entre árido grueso (grava) y árido fino (arena). Si el primero es más reactivo que el segundo, es previsible la fisuración de los áridos; si sucede lo contrario, es más probable que se fisure el mortero entre áridos gruesos.

En esa valoración de la resistencia característica hay que tener en cuenta que la dirección del ensayo es ortogonal, sensiblemente, a los planos de fractura previa observada en los áridos. Cabe pensar, pues, a tenor de lo expuesto, que la resistencia no es una propiedad isótropa, sino anisótropa y probablemente tal resistencia sea menor en sentido longitudinal que en el sentido transversal ensayado, efecto que no se ha tenido en cuenta porque no hay manera de valorarlo.

El informe del Instituto Torroja [9] no entra en el análisis del origen de las fisuras de los áridos antes de hacerse los ensayos, aspecto que puede ser de gran importancia. Cabe añadir, con relación a los áridos, que podría tratarse de cuarcitas o de cuarzo-arenitas, con sílices reactivas (SiO_2 no cristalino, sino tendiendo a la fase amorfa), probablemente provenientes de la cuenca del Jarama en su parte alta, donde se da este tipo de áridos. Éstos, además, habrían visto iniciada su meteorización en la corteza exterior (figura 24).

Figura 24. Áridos partidos y meteorizados en coincidencia con una fisura longitudinal (foto de los autores).

Se pudo comprobar también, tras revisar el estado de los altares de pila y los aparatos de apoyo, que el punto fijo del tablero estaría situado en la conexión de P-2 con el tablero, en la bifurcación con el ramal de Príncipe de Vergara. La pila 10 habría sido testigo de un desplazamiento del tablero del orden de 10 cm. En la pila 9, se midieron 9 cm (figura 25).

Figura 25. Corrimiento acumulado en la pila 9 (foto de los autores).

Una valoración aproximada del incremento de deformación longitudinal desde el final de la construcción, debido a las deformaciones de retracción y fluencia, daría lugar, en el estribo del lado de Joaquín Costa (punto de problemas sistemáticos a

Figura 26. Correcta alineación de la estructura, sin flechas apreciables, o incluso aún con contraflecha. Fotos de los autores 12.02.2020.

lo largo de la vida útil del viaducto), a un corrimiento teórico acumulado de entre 14 y 17 cm. En esa estimación se tuvo en cuenta, simplificadamente, la variación del módulo de deformación. Tras deducir los efectos debidos al proceso constructivo (el punto fijo durante la construcción, hasta llegar a la P-12, fue precisamente el estribo sobre Joaquín Costa), de unos 8 a 10 meses, los resultados teóricos se compadecen suficientemente bien con la realidad observada. En todo caso, la magnitud del corrimiento está más directamente vinculada al valor del pretensado, que se confirmaría como muy alto y semejante al consignado en los planos del proyecto de ejecución.

Estos resultados hicieron pensar en un potencial ataque árido-álcali que, como es sabido, se manifiesta en términos mecánicos con una reducción tanto de la capacidad resistente como de la rigidez con relación a los valores iniciales de hormigón sano. Los autores de este artículo tenían experiencias previas de este tipo de ataques, en los que es habitual que las deformaciones a flexión de los tableros sean apreciables, incluso muy considerables. En efecto, como es bien sabido,

$$flecha = k\,\frac{qL^4}{EI} \qquad (2)$$

siendo q la carga uniforme aplicada, L la luz y EI la rigidez (k es un coeficiente que depende de las condiciones de vinculación). Es decir, si E_c se había dividido por dos, a igualdad de todo lo demás, la flecha se habría duplicado. Pero ¿por qué, a diferencia de otras situaciones vividas, aquí no se apreciaba flecha, como se comprobó el mismo 12 de febrero de 2020 (figura 26)? La respuesta está implícita en la propia expresión (2) y en la consideración de que q es la carga total neta, suma del peso propio y de las cargas muertas —también de una parte de las sobrecargas, pero los valores reales de éstas son pequeños con relación a los valores nominales, tratándose además de un viaducto urbano, con poca frecuencia de vehículos pesados—, y también de las fuerzas equivalentes de pretensado, tan importantes aquí, como era habitual en aquellos años y hasta entrada la década de 1990, de pretensado total, lo que significaba, en la práctica, $q_{neta} \approx 0$. Así, la expresión (2) da valor nulo de la flecha sean cualesquiera que sean los demás parámetros. Obsérvese que, con aquel criterio de proyecto, las curvaturas de las secciones son nulas (o muy pequeñas) y, por tanto, nulas también las flechas diferidas.

Evidentemente, el razonamiento anterior no colisiona con los aludidos, importantes y sistemáticos incrementos de la abertura de la junta del estribo del lado Joaquín Costa, el más alejado del punto fijo, en el cruce con Príncipe de Vergara.

Aún hay algo más. El mismo día 12 de febrero de 2020 —muy fecundo, como habrá deducido el lector que haya llegado hasta aquí— se realizó una perforación coincidente con uno de los alvéolos en la misma zona en que se había producido la rotura del tendón. Al punto (figura 27) salió una gran cantidad de agua, toda la acumulada en el interior de los alvéolos (figuras 5, 8 y 9), durando un día entero el proceso de drenaje forzado. Es oportuno recordar que el hormigón de la losa superior no es impermeable, lo que, unido quizás a una deficiente impermeabilización de origen y a problemas del sistema de drenaje de la plataforma, propició la acumulación de agua en los alvéolos a lo largo de los cincuenta años transcurridos.

Figura 27. Drenaje del alvéolo contiguo al tendón roto en vano 6. Foto de los autores, 12.02.2020.

El agua no era limpia y tenía un color parecido al de los refrescos de cola. Se pidió opinión al Laboratorio de Química de la Escuela de Ingenieros de Caminos, C. y P. de la UPM, que emitió un informe [11] que concluía que *La composición y carac-*

terísticas químico-físicas de la disolución pueden haber tenido una contribución significativa al proceso de corrosión de la armadura. La elevada conductividad de la disolución y la presencia de bicarbonatos pueden haber acelerado dicho proceso. / Las concentraciones encontradas, tanto de ion magnesio como de ion potasio, podrían indicar una contribución del árido a la presencia de dichos iones en disolución. Los feldespatos o los áridos dolomíticos pueden generar estos iones al disolverse.

Como es sabido, es buena práctica asegurar el drenaje de los alvéolos e incluir la operación de vigilancia en el plan de mantenimiento: el agua supone una importante carga permanente adicional, no prevista en proyecto, afecta a la durabilidad de las armaduras porque convierte con más facilidad al hormigón en electrolito y es catalizadora imprescindible en los procesos de ataque árido-álcali. De poco vale impermeabilizar *a posteriori* en una actuación coincidente, por ejemplo, con una reposición del firme, si el agua está dentro y no se drena.

La figura 28 evidencia un caso, muy repetido durante la fase de diagnóstico y aún más en la de autopsia, de ataque árido-álcali. Con el fin de confirmar las sospechas, se enviaron al Instituto Eduardo Torroja unos testigos para conocer dictamen acerca del ataque árido-álcali. Recibido este informe [9] el 29 de junio de 2020, que confirmaba sin lugar a duda el ataque, sistemático aunque no uniforme, se cerró el informe con el análisis estructural de valoración del nivel de seguridad de la estructura, que se trata en el apartado siguiente.

Figura 28. Probeta con aureolas de gel en la interfaz árido-pasta. Foto cortesía del Laboratorio de Química de la Escuela de Ingenieros de Caminos, C. y P. de Madrid, no incluida en [11].

6. EFECTOS ESTRUCTURALES DEL HORMIGÓN CARACTERIZADO Y DEL PRETENSADO

En paralelo con los trabajos de campo y de laboratorio, el equipo de FHECOR desarrolló un análisis estructural completo con la finalidad de valorar de la manera más fidedignamente posible el comportamiento estructural del viaducto a la luz de los datos disponibles. El objetivo era estimar razonablemente el nivel de seguridad tras el diagnóstico, confirmando las consecuencias estructurales de lo analizado en los materiales y en la observación de campo. Para ello se elaboró un modelo sobre el software SOFiSTiK[4] (figura 29), capaz de tener en cuenta las no linealidades correspondientes, si bien no todas se consideraron hasta sus últimas consecuencias, como la fluencia no lineal en la que, sin duda alguna, había entrado el hormigón, al superar las tensiones permanentes del hormigón el umbral aproximado de 0.45 f_{ck}, límite más o menos convencional a partir del cual no puede ignorarse que las deformaciones diferidas de fluencia crecen más que proporcionalmente con relación a las tensiones. El análisis realizado comprendía las comprobaciones en ELS y en ELU.

Figura 29. Modelo SOFiSTiK utilizado para la totalidad de la estructura.

En el contexto del estudio en ELS, la comprobación de tensiones en vacío se hizo teniendo en cuenta la resistencia del hormigón especificada en los planos de proyecto (f_{ck} = 40 MPa), ya que tal situación de vacío se produjo en el puente tras el tesado, al inicio de su vida útil, momento en el que aún no se había producido el deterioro del hormigón por ataque árido-álcali. Se observa que, entonces, se debieron producir tensiones de compresión de hasta 25 MPa, un 63% de la resistencia del hormigón (f_{ck} = 40 MPa), lo cual sobrepasa el valor máximo recomendado hoy del 60% bajo la combinación característica (EN 1992-1-1, 7.2 (2)), pero esta tensión está, sin embargo, en el límite de lo aceptable según el criterio de las antiguas normativas (EP-77, p. ej.), que limitaban la tensión a 0.625 f_{ck} = 25 MPa, valor muy semejante, en todo caso. Lo más destacable es que las tracciones resultantes en la fibra inferior de la sección de apoyos resultaban ser muy altas debido a la gran cantidad de pretensado que existe sobre pilas y, de ser ciertas, habrían dado lugar a una fisuración importante de la cara inferior del tablero en las proximidades de las pilas. Tales potenciales fisuras no se observaron en ninguna de las inspecciones realizadas, lo que llevó a pensar que el pretensado que aparece en los planos pudiera no haber sido el finalmente ejecutado. También cabía imaginar que las sucesivas reparaciones y pinturas aplicadas podrían haber camuflado este efecto, aunque los autores creemos más bien que tales fisuras no se habrían producido al tener el trazado del pretensado en las secciones de apoyo una cota menor y actuar concomitantemente un pretensado de elevada magnitud. Así, las calicatas realizadas confirmaron que las vainas se encontraron a 0.26 m por debajo de la cara superior de la losa, bajo pavimento, con un recubrimiento ma-

4 Programa SOFiSTiK 2018 15.1.3, de SOFiSTK AG

yor que el consignado en planos, por lo que, a menor diferencia de cotas entre puntos bajos y altos del pretensado, menores son las fuerzas de desvío y, consiguientemente, menor el momento debido al pretensado. No es menos cierto que la magnitud del pretensado se habría visto reducida si se tiene en cuenta el acortamiento del tablero como consecuencia tanto de los efectos diferidos clásicos (retracción y fluencia), magnificados como consecuencia del ataque árido-álcali.

La comprobación en servicio bajo la combinación frecuente (bajo la combinación característica los resultados son algo peores) dio lugar a los siguientes resultados: En la fibra superior sobre pila se producían compresiones de hasta 20.6 MPa, superiores a la resistencia característica deducida para el hormigón (f_{ck} = 18.37 MPa) obtenida de los ensayos realizados. En la fibra inferior se darían tracciones de hasta 4.2 MPa, aproximadamente el doble de la resistencia a tracción correspondiente al hormigón real (f_{ctm} = 2.1 MPa). De ser cierta esta tensión, se habrían producido fisuras en cara inferior de los cajones en las proximidades de las pilas que, como ya se ha comentado, no se apreciaron en las inspecciones realizadas. En todo caso, debido al elevado nivel de pretensado, no se producía descompresión del hormigón alrededor de los tendones.

La comprobación en ELU en flexo-compresión hizo uso del concepto de "eficiencia", que se puede expresar de forma simplificada como

$$Eficiencia = \frac{N_{Ed}}{N_{Rd}} + \left(\frac{M_{y\,Ed}}{M_{y\,Rd}}\right)^{\alpha} + \left(\frac{M_{z\,Ed}}{M_{z\,Rd}}\right)^{\beta} \qquad (3)$$

quedando del lado de la seguridad los resultados menores que la unidad. En la expresión (3) N_{Ed} y N_{Rd} representan, respectivamente, el axil solicitante mayorado y el axil resistente minorado; M_{Ed} y M_{Rd} representan los momentos, en y y en z, solicitantes mayorados y resistentes minorados, respectivamente. El pésimo resultado en centro del vano 6 (figura 30), representativo, fue de 1.04, valor ligeramente superior al aceptable, pero en la sección sobre apoyos esa ratio resultó ser de 1.48, valor manifiestamente inaceptable para las características deducidas del hormigón y los valores de proyecto de la fuerza de pretensado, aun con el 15% de pérdidas.

La comprobación frente a cortante y torsión, interactuantes, puso de manifiesto que el cortante está muy condicionado por el pretensado, con los picos más altos en aquellas secciones en las que el trazado del pretensado tiene pendiente máxima, a 1/5 de la luz del vano aproximadamente. Nos llamó la atención el hecho de que la envolvente de esfuerzos cortantes en servicio resultara mayor, en valor absoluto en algunas secciones, que la envolvente mayorada (ELU). Esta es una consecuencia curiosa del extraordinario valor de la fuerza de pretensado, que entra con coeficiente de ponderación unidad en ambas envolventes, mientras que el cortante debido al resto de acciones sí se mayora en ELU y no en servicio, y no llega a compensar el cortante debido al pretensado.

Ahorramos al lector el detalle de los criterios de análisis y reparto del cortante y del momento torsor entre las diferentes almas, resultando unos valores de la ratio V_{Rd}/V_{Ed} extraordinariamente deficientes, lo que está motivado por el agotamiento de la biela comprimida del hormigón. Asimismo, debe tenerse en cuenta la muy reducida cuantía de armadura pasiva transversal, resultado típico de los criterios de la época, que tanta relevancia otorgaban al papel del pretensado. Así, teniendo en cuenta incluso dos inclinaciones distintas para las bielas comprimidas de hormigón (cot θ = 2.5 según EC-2 y cot θ = 2 según EHE-08), con f_{ck} =18.37 MPa (valor deducido en la campaña de inspección especial) resultaba V_{Rd}/V_{Ed} = 0.08 con EC-2 en ELU. Sin embargo, se obtenía la ratio V_{Rd}/V_{Ed} = 1.09 en ELS si se considera para la resistencia del hormigón el valor medio f_{cm}=29.15 MPa.

La sección crítica resultó ser la coincidente con el punto de inflexión del pretensado, es decir, fuera de la zona maciza-da sobre apoyos, que revelaba agotamiento de la biela comprimida del hormigón con f_{ck}=18.37 MPa y por agotamiento de la armadura pasiva si se consideraba, también en ELU, el valor f_{cm}=29.15 MPa.

Se concluyó que el nivel de seguridad era nominalmente insuficiente e inasumible la incertidumbre. Teniendo en cuenta que no era viable, por ineficaz, un refuerzo sobre un material que está ya agotado se elevó al Ayuntamiento de Madrid informe final en el que se recomendaba, ya se ha dicho, el cierre y el desmontaje del viaducto.

Figura 30. Resumen de resultados en apoyo y en centro de vano 10 en ELU. Análisis seccional con FAGUS.[5]

5 Programa FAGUS 8, de CUBUS AG.

Figura 31. Ejemplo de desmontaje de paso superior urbano: el paso superior de Cuatro Caminos (Madrid).

7. EL PLANTEAMIENTO DEL PROCEDIMIENTO DE DESMONTAJE

Con carácter de emergencia, la demolición del paso fue ordenada por el Ayuntamiento de Madrid y ejecutada, durante el verano de 2020, por la empresa constructora DRAGADOS. En este apartado se recogen algunos aspectos relevantes del proyecto de demolición redactado por FHECOR, remitiendo al lector a la referencia [3] para los detalles de la ejecución.

7.1. Ideas rectoras

Teniendo en cuenta la naturaleza urbana del paso y la proximidad de la estructura a las edificaciones circundantes, la demolición del tablero se planteó como un desmontaje con grúa, para lo cual fue preciso apear y trocear previamente dicho tablero.

Este procedimiento de desmontaje de tableros de puente, que ya había sido empleado en la demolición (figura 31) del paso superior de Cuatro Caminos en la ciudad de Madrid en 2003 (en cuyo proyecto participó FHECOR), debía adaptarse ahora a las particularidades del paso superior de Joaquín Costa - Francisco Silvela. En este sentido, cabe recordar que el problema estructural de este paso era la pérdida progresiva de resistencia del hormigón del tablero, junto con un exceso de pretensado en relación con la carga permanente soportada. Por ello, las ideas rectoras que se establecieron para su demolición fueron la siguientes:

1. Antes del troceado de un vano, teniendo en cuenta la configuración del pretensado y la baja cuantía de la armadura pasiva, había de asegurarse que tanto ese vano como los dos adyacentes estaban cimbrados.
2. Previamente al corte, no debía retirarse la carga muerta del tablero, ya que ello se traducía en un aumento del nivel de compresiones de las zonas más comprometidas y en un incremento del riesgo de rotura frágil por estallido del hormigón comprimido.
3. Por la misma razón, no debía procederse al corte de los voladizos hasta haber realizado cortes transversales en las artesas que redujesen el nivel de compresiones producidas por el pretensado.
4. Como se ha indicado, las zonas con más pretensado se situaban en el entorno de las pilas, donde llegaban a cruzarse tres familias de pretensado. Por ello, para reducir el nivel de pretensado, los primeros cortes transversales de las artesas debían realizarse en dichas zonas.
5. Para compaginar la entrada en carga progresiva de la cimbra y la reducción previa del nivel de compresiones en las zonas más comprometidas, se planteó, con carácter preliminar, practicar cuatro cortes transversales en las artesas de cada vano por este orden: dos centrales a tercios de la luz y dos extremos a 1.90 m del eje de las pilas. La operación de troceado de cada vano se iniciaría por los cortes centrales y se completaría con los cortes extremos, en ambos casos sin cortar los voladizos.
6. Los cortes del tablero se debían realizar con hilo de diamante, cabiendo la posibilidad de utilizar corte con disco para espesores inferiores a 50 cm.
7. Una vez realizados los cuatro cortes transversales de las artesas, indicados en el punto precedente, el tablero ya se

habría apoyado en la cimbra y podía procederse al troceado completo del tablero siguiendo la secuencia que se establecería en un proceso de desmontaje específico para cada vano.

8. Dada la baja cuantía de armadura longitudinal de los voladizos, si se preveía la retirada individualizada de los mismos, debía preverse la disposición elementos auxiliares, asociados al "eslingado" que evitasen su rotura prematura durante la carga sobre camión.
9. Para la retirada de los soportes (pilas y estribos) y los muros de los accesos, se podían emplear métodos convencionales de demolición: mandíbulas y martillos hidráulicos.
10. Se debía proceder al desmontaje del ramal de Príncipe de Vergara previamente a la demolición del entronque en pantalón con el vano 2 puesto que, en la junta a media madera de la pila 11, el ramal apoyaba sobre el vano 2.
11. Aunque el puente se encontraba con unos niveles de seguridad que estaban significativamente por debajo de los valores contemplados en la reglamentación vigente, como se indica en el apartado 6, mantenía aún cierta reserva de seguridad en estado de carga permanente, lo que posibilitaba el montaje de la cimbra de apeo. En cualquier caso, se debía establecer un protocolo de montaje seguro de los castilletes de apeo desde los soportes (las pilas y estribos) hacia el centro de vano, de forma que, en caso de incidente, la cimbra previamente montada amortiguase la eventual caída del tablero y formase, junto con los soportes, un espacio de protección para el personal de montaje.

7.2. Cimbra de apeo

Se planteó un cimbra de apeo de seguridad que se dispuso exclusivamente bajo la planta de las artesas del tablero, salvo en los casos en los que se previese desmontar individualmente los voladizos laterales, en cuyo caso también se previeron torres de apeo bajo los mismos. La disposición de los castilletes permitió realizar los cortes del tablero.

Esta cimbra presentaba las siguientes singularidades:

- Paso de peatones en el vano 6, formado dos pasadizos de dos metros entre castilletes de cimbra.
- Vano 9, situado en la glorieta de López de Hoyos, sobre el tramo en falso túnel somero del túnel de María de Molina. Por ello se planteó un sistema de puenteo del túnel, con vigas metálicas apoyadas sobre zapatas extremas, sobre las que se dispusieron los castilletes de cimbra.
- En los vanos 2 y 3, de sección artesa maciza y faja central de canto varible, se dispuso la cimbra tanto bajo artesas como bajo la faja central y, cuando fue necesario, también bajo voladizo.
- En tramo abocinado del ramal, que formaba parte del pantalón, la cimbra tuvo que ser cuajada, cimbrando bajo los voladizos y bajo el núcleo central.
- La cimbra del ramal de Príncipe de Vergara también dispondría de castilletes bajo los voladizos laterales, ya que estaba previsto independizarlos del núcleo central.

La cimbra se diseñó como de clase B1 según la norma UNE-EN12812:2004 y, por tanto, siguiendo los Eurocódigos Estructurales y sus Anexos nacionales de aplicación. Por otra parte, a diferencia del diseño habitual de una cimbra convencional, en el que se considera que ésta funciona como arriostrada horizontalmente en cabeza por la estructura soporte del encofrado, en este caso debía prestarse una especial atención a la estabilidad de los castilletes de cimbra, pues el troceado del tablero indivualizaba su comportamiento estructural (figura 32).

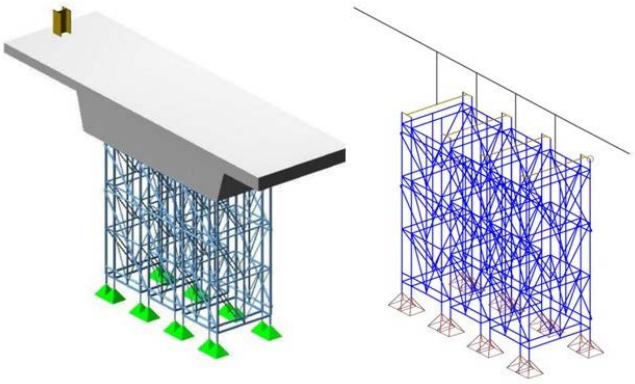

Figura 32. Modelo realizado para validar la estabilidad de un castillete de cimbra con el software de CUBUS AG.[6]

Las cargas consideradas en el diseño de la cimbra fueron:

- Peso propio de la cimbra.
- Cargas gravitatorias del tablero a soportar durante la demolición, recogidas en el apartado 4.1.
- Sobrecarga de ejecución de 1.50 kN/m².
- Acción del viento (según UNE-EN 1991-1-4 +AN):
  - Velocidad básica de referencia de 26 m/s.
  - Entorno urbano IV.
  - Período de retorno para el viento T= 5 años (según EN 1991-1-6 para tiempo de ejecución entre 4 y 90 días).
  - Superficie expuesta tranversal del tablero de 1.45+1.20 = 2.65 m²/m.
- Presión del viento de operación: 0.20 kN/m, correspondiente a una velocidad de ráfaga de 65 km/h, coherente con la velocidad máxima de operación con grúa.
- Acciones horizontales:
  - Mínima del 2% de la carga soportada. EN 1991-1-6 Acciones durante la ejecución solicita su determinación sin establecer un valor concreto. El valor adoptado se corresponde con el 1% de tolerancia de verticalidad, más 1% de inclinaciones no previstas durante la puesta en carga de la cimbra durante el corte del tablero.
  - Pendiente longitudinal del tablero (a considerar sólo en el caso de que el sistema de apoyo no garantice que las cargas trasmitidas sean verticales):
    - Vano 1: 6%.
    - Vano 2: 3%.
    - Vano 3: 2.75%.
    - Vanos 4 a 8: lineal de 2.75% a 1.25%.
    - Vanos 9 a 11: 1.25%.
    - Ramal: 6.75%.
    - Entronque 3.50%.
  - Acción accidental de impacto de carga del 2% de la carga soportada (a considerar sólo con las operaciones de grúa). EN 1991-1-6 remite a EN 1991-3 para las

6 Programas STATIK 8 y AVENA 8, de CUBUS AG.

Figura 33. Cimbra cuajada instalada por ULMA. Vista desde pila P4 a estribo E2-1.

acciones accidentales relacionadas con el tiro con grúa. El valor establecido se corresponde con un error de 10 cm en la posición del centro de gravedad de la pieza adyacente y la cogida de la misma con una altura de eslinga de 5.0 m, por lo que accidentalmente se podría trasmitir una carga horizontal a la pieza soportada.

Por otra parte, en relación con las condiciones de apoyo de la cimbra en una zona urbana (figura 33) con multitud de servicios, se establecieron los siguientes criterios:

- La tensión máxima trasmitida por los durmientes de la cimbra debía ser tal que, a nivel de explanada, se situase en el entorno de 150 kPa y, a nivel de superficie, no superasen los 600 kPa, presión de inflado de los neumáticos de los vehículos pesados.
- Debía analizarse la estabilidad de las galerías de servicio y de arquetas enterradas, estableciendo losas armadas de puenteo en caso necesario.
- Alternativamente, para las arquetas de pequeñas dimensiones, se podría proceder al relleno de las mismas con material granular para que soportasen las cargas actuando a modo de caja de arena.

7.3. *Troceado del tablero*

Para establecer el troceado del tablero se realizó inicialmente una cubicación de éste a partir de los planos disponibles. La geometría del tablero, reflejada en los planos, se contrastó con la obtenida de los perfiles levantados topográficamente por la constructora. Además, en las cubicaciones, se consideraron 7 cm de pavimento bituminoso y 3 cm de sobreespesor de hormigón, así como una incertidumbre global en la estimación de las cargas del 10%. Así, a partir de las estimaciones de pesos, se pudieron elaborar planos esquemáticos con la distribución de la carga (figura 34), que sirvieron de base para definir la configuración de la cimbra y el troceado del tablero (figura 35).

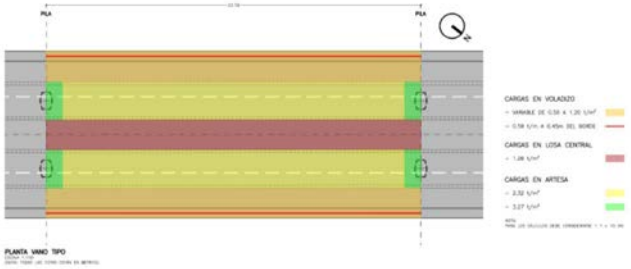

Figura 34. Esquema de cargas en el vano tipo del tronco.

Para llevar a cabo este troceado del tablero se utilizaron varios de equipos de corte con hilo de diamante como los que aparecen en la figura 36.

Por otra parte, para el transporte de las piezas cortadas, el constructor optó por el empleo de camiones plataforma con una capacidad de 70 t. Asimismo, por criterios de movilidad de estos equipos de transporte, se estableció, con carácter general, la anchura óptima de las piezas a cortar en 3.0 m. Atendiendo a

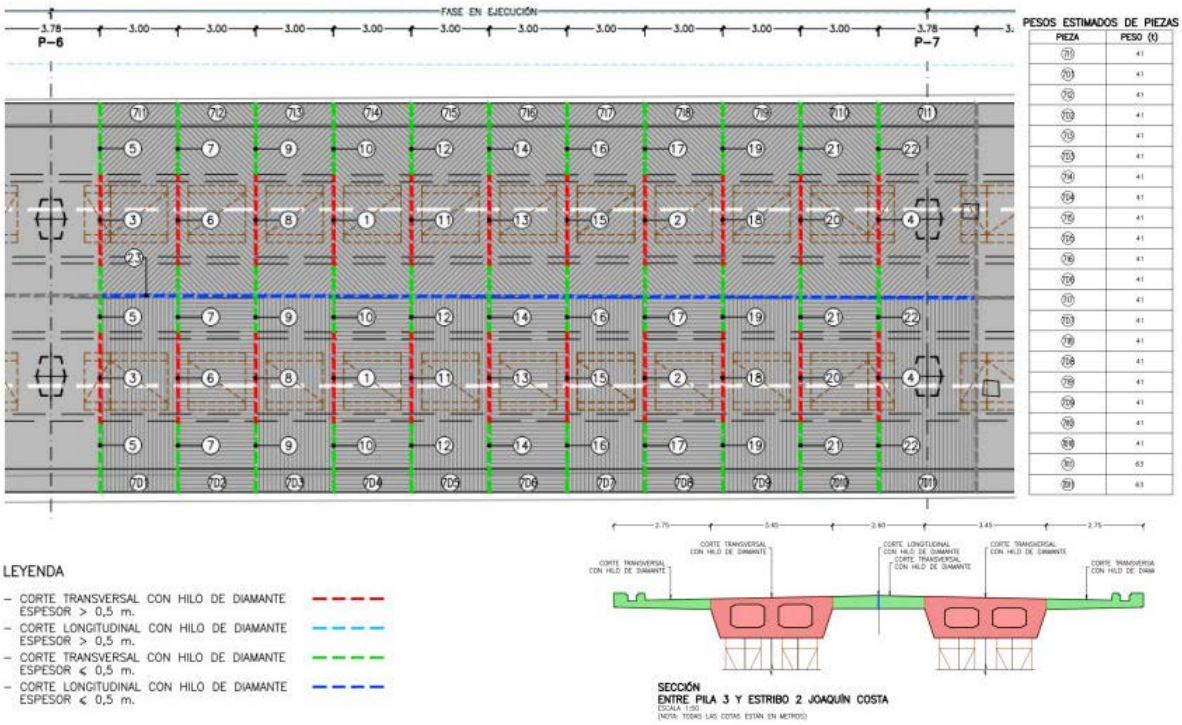

Figura 35. Esquema del proceso de corte de un vano tipo.

Figura 36. Equipos de corte con hilo de diamante.

lo anterior, a la estimación de tiempos y a las ideas rectoras del proceso, se establecieron planos, como el de la figura 35, incluyendo la secuencia de corte, el tipo de corte a emplear y el peso estimado de cada pieza. A partir de estos planos, teniendo en cuenta los radios máximos de las grúas a emplear, la constructora pudo establecer la secuencia de desmontaje de cada vano [3].

7.4. Manipulación de cargas

Para el izado con grúa de las piezas cortadas se pueden utilizar balancines superiores y perfiles de puenteo inferiores que, conectados mediante eslingas verticales alojadas en taladros realizados previamente, permiten elevar las piezas como se indica en el croquis de la izquierda de la figura 37. Pero la presencia de la cimbra dificulta enormemente la disposición de los prefiles inferiores y las operaciones de conexiones entre elementos.

Otra posibilidad era disponer sistemas de "estrobaje" (mediante esligas y cadenas) que abrazasen a la pieza a manipular, como en el croquis de la derecha de la figura 37. Con esta configuración deben tenerse especialmente en cuenta las limitaciones de carga debidas a los quiebros del estrobo, así como

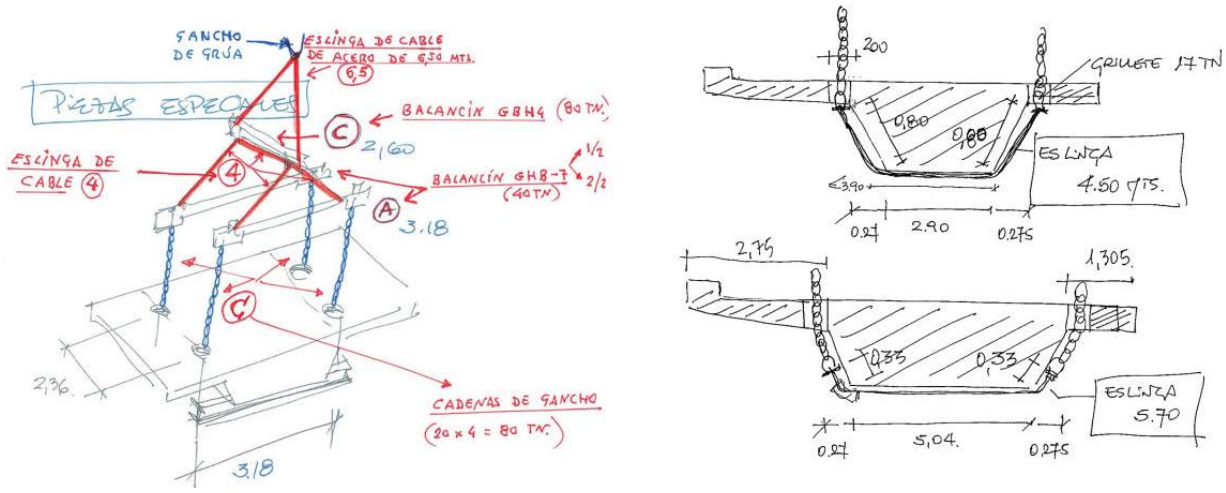

Figura 37. Opciones de "estrobaje" de las piezas cortadas (croquis de alternativas propuestas por el equipo constructor).

Figura 38. Sistemas de izado de piezas empleados: con balancines inferiores (izda.) y con eslinga de abrazo inferior (dcha.).

la disposición de cantoneras que lo protejan de roces y cargas muy concentradas (véanse las Notas Técnicas de Prevención NTP 841, 842, 866 y 862 de Instituto de Seguridad e Higiene en el Trabajo). Además, se deben respetar en todo momento los criterios establecidos en la declaración de prestaciones del fabricante del estrobo.

Inicialmente se empleó la solución con balancines inferiores, pero las dificultades que, para su colocación, suponía la presencia de las torres de apeo, llevó a adoptar finalmente la solución con eslinga de abrazo (figura 38), como se había utilizado en el desmontaje del viaducto de la M-40 sobre la carretera de Colmenar [17].

Por último, debe prestarse atención a la estiba de la carga sobre el camión plataforma atendiendo a lo indicado en el Anejo III del RD 563/2017, que hace referencia a varias normas europeas (figura 39) relativas a los dispositivos para la sujeción de la carga en vehículos de carretera (figura 40).

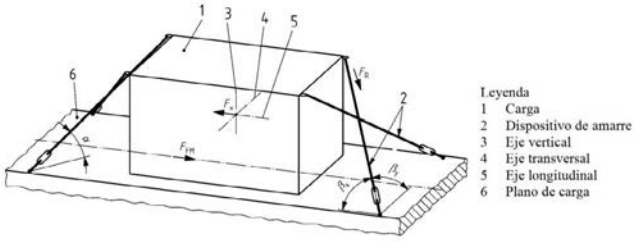

Figura 39. Ejemplo de estiba con amarre en diagonal tomado de la UN EN 12915-1

7.5. Secuencia global de desmontaje

La secuencia global de desmontaje fue planificada por DRAGADOS [3] atendiendo a la disponibilidad de espacio para las operaciones con grúas y a las vías de salida de las plataformas de carga. Así se inició el desmontaje por el ramal de Príncipe de Vergara, desde la junta a media madera en pila P11 hacia el estribo E1-2. Posteriormente se desmontó el vano 4, lo que permitió tener dos frentes de desmontaje: hacia el estribo E1-1 y hacia pilas crecientes. También se abrió un nuevo frente con la retirada del vano 9 sobre la glorieta de López de Hoyos, bajo la que pasa el túnel de María de Molina que limitaba la circulación de las grúas, de forma que se pudieron compaginar los desmontajes desde P4 a P8 y de P9 a E2-1. Posteriormente

Figura 40. Transporte de pieza del tablero sobre plataforma.

se procedió a la retirada de los fustes de pilas, previo corte con hilo de diamante por su base. Finalmente se demolieron los estribos y los muros de los accesos con técnicas convencionales.

7.6. Destino de los materiales retirados

Los materiales procedentes del desmontaje fueron trasladados a una planta de valorización y reciclaje de residuos de construcción y demolición. Además, gracias a la generosidad de IMESAPI se pudo acometer una labor de autopsia, que incluyó la toma de muestras y su traslado a los laboratorios de Química y Ciencia de Materiales de la Escuela de Ingenieros de Caminos, Canales y Puertos de la UPM.

8. CONCLUSIONES. LECCIONES APRENDIDAS

Con relación al diagnóstico:

a) Las fisuras longitudinales no siempre son inocuas, ni han de estar unívocamente asociadas a ataque químico. Su origen probable podría situarse en las primeras edades, por gradiente térmico —hormigón de $f_{ck,esp}$= 40 MPa, con mucho cemento CEM I (o el equivalente en 1969) y gran calor de hidratación— más el gradiente de contenido de humedad (retracción diferencial), dando lugar a tensiones de tracción ubicadas en la periferia y orientadas en sentido longitudinal merced al elevado valor del pretensado. Posteriormente, la aportación de agua habría propiciado el ataque árido-álcali con las consecuencias que se han expuesto, agravadas por el elevado valor de la fuerza de pretensado, excesiva en relación con la resistencia real final del hormigón.
b) No podemos dejar de recordar la obviedad de que el diagnóstico —especialmente complejo en esta estructura— es imprescindible y que el técnico responsable de la evaluación de una estructura existente no debe descansar hasta dar con la explicación de lo que sucede ante sus ojos. Ignorar los problemas —nos referimos a las fisuras longitudinales que venían apareciendo persistentemente— so pretexto de que los síntomas no se corresponden con lo habitual no es bueno, como afirmaba Ortega y Gasset[7].
c) En sintonía con lo anterior, debe evitarse pintar una estructura que exhibe fisuras si el diagnóstico no es claro. Al inspector se le recomienda desconfiar de lo pintado y sellado.
d) Es muy recomendable drenar los alvéolos o aligeramientos, analizando su contenido. Cada vez son más frecuen-

7 *Toda realidad ignorada prepara su venganza*. José Ortega y Gasset. Párrafos finales del "Epílogo para ingleses" de su "Rebelión de las masas" (1927-1930).

Figura 41. Desmontaje de vano 4.

tes —porque ha ido transcurriendo el tiempo y se revelan ahora problemas congénitos— los ataques químicos (árido-álcali y etringita).

e) Debe tenerse especial cuidado con los puentes pretensados en clase I —típicos del periodo 1950-1990, aproximadamente— porque un comportamiento deformacional aparentemente correcto puede encubrir deficiencias de módulo de deformación pues la q_{neta} puede ser próxima a cero (merced a las fuerzas de desvío). Además, no pueden descartarse déficits de inyección en vainas y, por tanto, fenómenos de corrosión en aceros que, hasta 1970 aproximadamente, tenían una especial sensibilidad frente a la corrosión y corrosión bajo tensión.

f) La fragilización por corrosión bajo tensión rebaja drásticamente las posibilidades de redistribución de esfuerzos, lo que afecta al nivel de seguridad global, siendo muy difícil su cuantificación.

g) La reducción de la resistencia del hormigón afecta a la seguridad en flexo-compresión y, sobre todo, a cortante y torsión. Cabe añadir que, para el ingeniero que trata con construcciones existentes, el hormigón se caracteriza con algo más que $f_{ck}(t)$. Debe profundizarse en el conocimiento del comportamiento a nivel "meso".

h) Como ya se indicó en [18], a propósito del valor de las autopsias y de este paso superior, *el gran riesgo que corría la estructura era precisamente que agotase por compresión (flexo-compresión y cortante), debida fundamentalmente al pretensado. Sucedía algo que tiene mucho de paradójico: la rotura por corrosión de un cierto número de tendones de pretensado, unida al acortamiento y, consiguientemente, a unas considerables pérdidas diferidas de pretensado había tenido un efecto beneficioso. Los autores de esta ponencia jamás habrían pensado que llegarían a hacer una afirmación tan rara. La propuesta de desmontaje que planteamos incluía una campaña de autopsia que, en honor a la verdad, no contó con apoyo decidido. La actitud de los laboratorios de la ETSICCP-UPM y nuestra perseverancia permitieron completar dos campañas paralelas de reconocimiento* postmortem *de gran valor. Cinco meses después de concluir el desmantelamiento, se celebró en el Colegio de Ingenieros de Caminos un acto de presentación de lo sucedido, auspiciado también por el Ayuntamiento*.

Con respecto a la planificación de las tareas de desmontaje de viaductos urbanos:

a) El desmontaje es el método de demolición más adecuado en zonas urbanas, donde prima el minimizar las afecciones por ruido y polvo, frente a otras soluciones con explosivos o con equipos mecánicos de mandíbulas y martillos hidráulicos que disgregan las piezas *in situ*.

b) En zonas urbanas hay un gran número de servicios e instalaciones que se pueden ver afectadas por las obras. Tener una información precisa de su ubicación y de los

criterios de diseño de los elementos subterráneos facilita la toma de decisiones.

c) En los casos en los que las estructuras presenten deterioros significativos no se puede determinar con fiabilidad su capacidad resistente y, por tanto, no se puede contar con su contribución resistente a la hora de plantear el proceso de desmontaje. Así, debe plantearse el apeo previo del tablero para evitar el riesgo de rotura en cadena, de forma que, cuando se vaya a cortar un vano, debe estar apeado no sólo éste sino también los dos adyacentes. Para una mayor seguridad durante las operaciones de montaje de la cimbra, éste debe hacerse desde los soportes hacia el centro de los vanos.
d) El diseño convencional de los apeos y cimbras en obra nueva cuenta con la estabilidad horizontal que ofrece el encofrado que soportan. Pero cuando se diseñe una cimbra como apeo en la demolición de un tablero, deben revisarse los criterios de estabilidad de la cimbra frente a fuerzas horizontales (incluyendo posibles acciones accidentales durante el corte y la carga de las piezas), pues los castilletes de cimbra no van a contar con el arriostramiento horizontal del tablero cuando éste sea troceado.
e) En tableros pretensados con pérdida progresiva de la resistencia del hormigón, debe plantearse una secuencia de corte del tablero que reduzca progresivamente la compresión producida por el pretensado sin reducir la sección resistente y sin reducir la carga muerta del tablero, evitando incrementos locales de la tasa de compresión del hormigón.
f) El corte con hilo con diamante es una técnica muy versátil y poco ruidosa que agiliza los procesos de desmontaje, pero hay que prever cómo canalizar y recoger los lodos que genera este proceso.
g) La estimación de pesos a desmontar debe cubrir las incertidumbres sobre el relleno de los aligeramientos y los sobreespesores de hormigón.
h) El estrobado de las piezas durante el desmontaje debe tener presente las condiciones de seguridad de eslingas, cables y cadenas en las zonas donde se produzcan quiebros en su trazado.
i) El transporte de piezas por carretera está regulado por lo que se denomina la "ley de la estiba", que en realidad es el RD 563/2017 y una serie normas UNE-EN relativas a los dispositivos de sujeción y fijación de la carga.
j) No es raro que los conductos de canalizaciones de instalaciones en el tablero sean de fibrocemento, lo que implica protocolos muy estrictos de desmontaje.

Agradecimientos

Los autores agradecen al Ayuntamiento de Madrid la confianza depositada en DRAGADOS y en FHECOR para la realización del trabajo de referencia. Extendemos nuestro agradecimiento a los laboratorios de Ciencia de Materiales y de Química de Materiales de la Escuela de Ingenieros de Caminos, Canales y Puertos de la UPM las facilidades y la profesionalidad en los trabajos de diagnóstico. De manera especial, agradecen los autores a Francisco J. Martín Carrasco, director entonces de la Escuela, por el apoyo brindado para la autopsia durante el desmontaje, así como a Miguel Ángel Delgado Núñez (IMESAPI) por la desinteresada ayuda prestada para la extracción de testigos y otras muestras en la aludida autopsia. Gracias especiales al equipo de DRAGADOS que confió en nosotros tanto en la fase previa de diagnóstico como de asistencia técnica durante el desmontaje y campaña de confirmación del diagnóstico.

De una manera muy especial queremos dedicar este texto a Hugo Corres, gracias a quien hemos tenido la oportunidad, a lo largo de nuestra vida profesional, de participar en tantos proyectos de gran interés. De forma particular agradece a Hugo el segundo de los autores el haberlo incorporado y apoyado en la aventura docente en la Escuela, muy singularmente —a los efectos de este artículo—, en el ámbito de la Ingeniería de Conservación, disciplina que ha adquirido, en muy poco tiempo, carta de naturaleza. ¡Muchas gracias!

Referencias

[1] British Cement Association (BCA) (1992). The diagnosis of alkali-silica reaction. Report of a working party.

[2] Calavera, J., Corres, H., Fernández, J., León, J. (1993). Bending moment distribution for designing reinforced and prestressed beam-block floors. CEB Bulletin d'Information, nº 218. Ductility – reinforcement.

[3] Cobo Rodríguez, C., Álvarez Andrés, J.J., Sánchez Delgado, J., Martín Galán, A., León González, F.J., Lucas Serrano, C. (2025). Desmontaje del Puente Joaquín Costa - Francisco Silvela (Madrid). Ponencia presentada en el IX Congreso de ACHE. Granada.

[4] Comisión Permanente del Hormión (1977). EP-77. Instrucción para el proyecto y la ejecución de obras de hormigón pretensado. Decreto 1408/1977 de 18 de febrero. BOE 149 de 23 de junio de 1977.

[5] DGC. Dirección General de Carreteras (2000). Obras de paso de nueva construcción. Conceptos Generales. Ministerio de Fomento. ISBN 84-498-0474-04.

[6] Departamento de Ciencia de Materiales, Escuela de Ingenieros de Caminos, Canales y Puertos (2020). Ensayos y análisis de daño mecánico y fractográfico del acero de pretensado del paso elevado VE0503. Documento no publicado.

[7] Esposito, R., Anac, C., Hendriks, M. A. N., & Copuroglu, O. (2016). Influence of the alkali-silica reaction on the mechanical degradation of concrete. Journal of Materials in Civil Engineering, 28(6), 04016007-1-04016007-13. https://doi.org/10.1061/(ASCE)MT.1943-5533.0001486.

[8] INES Ingenieros Consultores (2015). Proyecto de Acondicionamiento de cuatro estructuras en Madrid (VE0403 Eduardo Dato – Juan Bravo; PE0501 Pasarela J. Vasconcelos – Gral. Aranda; VI0502 Joaquín Costa – Rep. Argentina; VE0503 Joaquín Costa – Fco. Silvela). Documento no publicado.

[9] Instituto de Ciencias de la Construcción Eduardo Torroja (2020). Identificación de los posibles productos indicativos de desarrollo de reacciones expansivas en el hormigón de una estructura sobre la glorieta de López de Hoyos. Documento no publicado.

[10] INTEMAC (2020). Informe de los ensayos efectuados sobre 23 testigos de hormigón extraídos en el tablero del puente entre la c/ Joaquín Costa y la c/ Francisco Silvela en Madrid. Documento no publicado.

[11] Laboratorio de Química de Materiales, Escuela de Ingenieros de Caminos, Canales y Puertos (2020). Informe preliminar sobre las muestras de hormigón y líquido recogido de la estructura sobre la glorieta de López de Hoyos. Documento no publicado.

[12] López Jamar, J. A. (1973); Cubierta del pabellón municipal de deportes, en La Coruña. Hormigón y Acero, 24(107), pp. 331-334. Recuperado a partir de https://www.hormigonyacero.com/index.php/ache/article/view/1363.

[13] López Jamar, J.A., Gimeno Fungairiño, A. (1971). Paso elevado Francisco Silvela- Joaquín Costa, Hormigón y Acero. 22 (100): 43–48.

[14] Martín Galán, A, Sánchez Delgado, J., León González, F. J., Cobo Rodríguez, C., Álvarez Andrés, J. J., Lucas Serrano, C. (2025). Diagnosis del paso superior Joaquín Costa – Francisco Silvela. Ponencia presentada en el IX Congreso de ACHE. Granada.

[15] Martín-Caro Álamo, J.A., Martínez Martínez, J.L., Arias Hofman, G. (2021). Los problemas árido álcali o la necesidad de anticiparse a un proceso irreversible en los puentes, Hormigón y Acero, 72(294-295), 219-232, https://doi.org/10.33586/hya.2021.3069.

[16] Menéndez Méndez, E. (2010) Análisis del hormigón en estructuras afectadas por reacción árido-álcali, ataque por sulfatos y ciclos de hielo-deshielo. Instituto Español del Cemento y sus aplicaciones (IECA).

[17] Rodado, J., & Otero, F. (2025). Replacement of the Deck and Rehabilitation of the Viaduct at the Link Between M-40 and M-607 in Madrid (Spain). Hormigón y Acero. 76(306):7-16. https://doi.org/10.33586/hya.2024.3090.

[18] Sánchez Delgado, J., León González, J. (2023). Las autopsias como fuente de aprendizaje y valoración del patrimonio. I Congreso Internacional del Patrimonio de la Obra Pública y de la Ingeniería Civil. Toledo, 2023.

cubus
ENGINEERING SOFTWARE

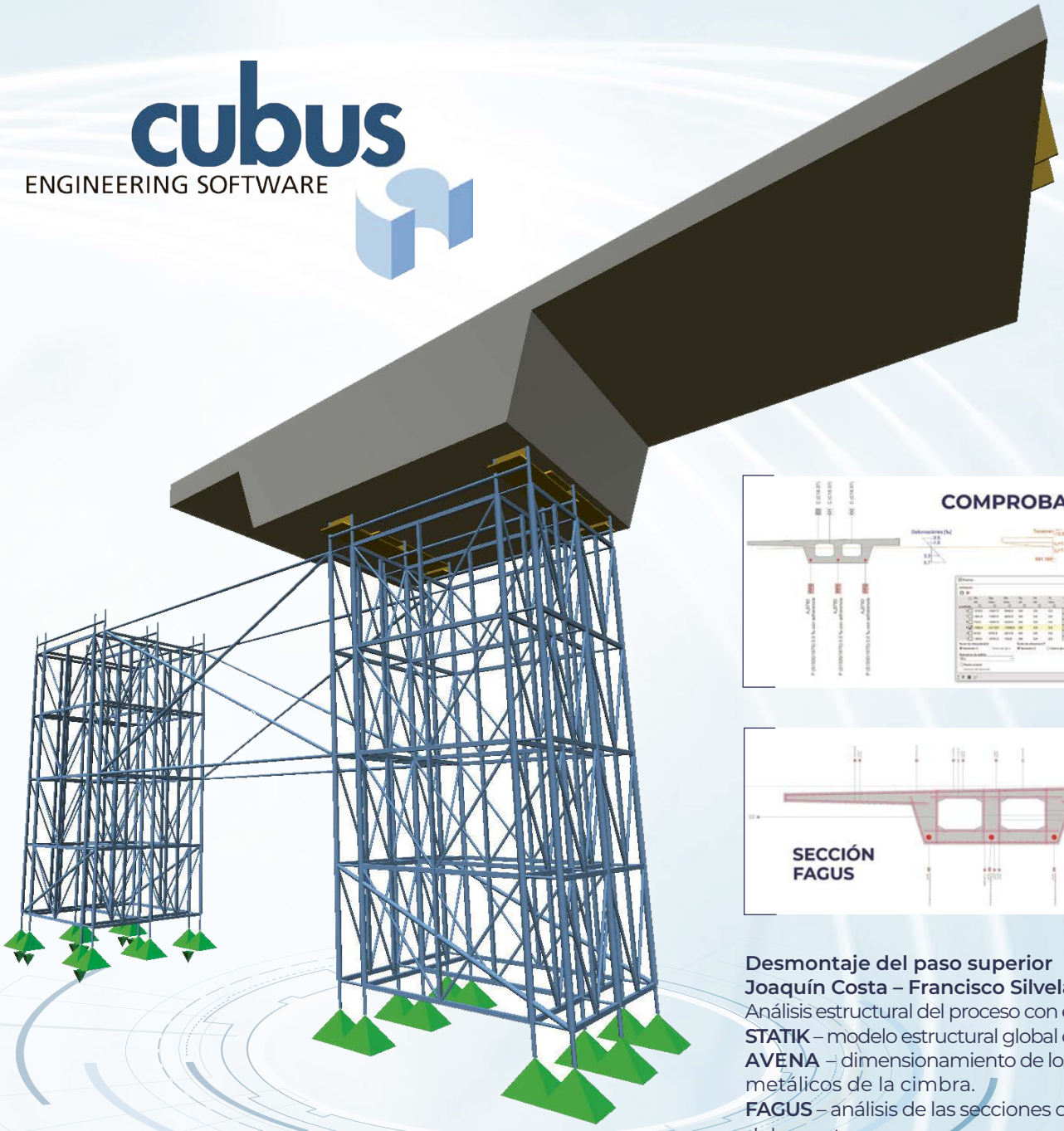

Desmontaje del paso superior Joaquín Costa – Francisco Silvela (Madrid).
Análisis estructural del proceso con el apoyo de:
STATIK – modelo estructural global de la cimbra.
AVENA – dimensionamiento de los elementos metálicos de la cimbra.
FAGUS – análisis de las secciones de hormigón del puente.

El cálculo estructural no es solo diseño: también es diagnóstico y decisión

Desde el proyecto hasta la inspección y evaluación, el software de CUBUS acompaña al ingeniero en cada etapa del análisis estructural.

https://cubus-software.es

cubus
software españa sl

info@cubus-software.es

Disponible en **www.hormigonyacero.com**
https://doi.org/10.33586/hya.2025.4102

Engineering Between History and Future

La ingeniería entre la historia y el futuro

Tullia Iori[a]

[a] *Rome Tor Vergata University, Roma, Italia*

Recibido el 7 de mayo de 2024; revisado el 10 de noviembre de 2024, aceptado el 5 de marzo de 2025

ABSTRACT

My students often ask me: "Tell me, prof, what is the use of history of civil engineering?", revisiting the question that opens Marc Bloch's famous book "The Historian's Craft". For some time now, I have been responding to their provocation (I teach civil engineering history) by telling 3 short stories: the stories of three engineers who lived in the nineteenth century, in the twentieth century and in the first century of the new millennium.

The first is the story of Charles, born in 1810 in France and a graduate of the École Polytechnique. Charles tells in first person all the transformations he saw in the world of structural engineering in the nineteenth century: materials, construction techniques, and calculation theory developed so rapidly that we went form the 40-meter span cast-iron Coalbrookdale arch bridge to the 500-meter span Gerber truss Firth of Forth bridge.

The story of Giulio, born in 1900 in Rome and graduated in engineering, is similar. He tells us too of the many technical changes linked to reinforced concrete in Italy and around the world, embedded in the political and social history of the twentieth century. In particular, he tells how a great difficulty such as the fascist autarkic propaganda triggered the most interesting experiments of post-war Italy. In particular, he recalls how reinforced concrete, just born in the early 20th century, underwent two genetic mutations in few decades: thin vaults and prestressing, so useful during reconstruction after World War II.

Neo Jane, born in Botswana in 2000, tells the last story. She predicts the story of structures in the 21st century. In particular, how everything changed in her university years, after the covid-19 pandemic. And how new rare earths materials applied in bridges, new transportation paradigms, new theories have led to very fast transformations in structures.

The three fictional stories should serve to clarify to my students what is the point of studying and researching history in structural engineering.

KEYWORDS: Teaching, future, design, history, construction history, engineering history.

RESUMEN

Mis alumnos me preguntan a menudo: "Dígame, profesora, ¿para qué sirve la historia de la ingeniería civil?", retomando la pregunta que abre el famoso libro de Marc Bloch "El oficio de historiador". Desde hace algún tiempo, respondo a su provocación (enseño historia de la ingeniería civil) contando 3 pequeñas historias: las de tres ingenieros que vivieron en el siglo XIX, en el siglo XX y en el primer siglo del nuevo milenio.

La primera es la historia de Charles, nacido en 1810 en Francia y licenciado por la École Polytechnique. Charles relata en primera persona todas las transformaciones que presenció en el mundo de la ingeniería estructural en el siglo XIX: los materiales, las técnicas de construcción y la teoría del cálculo evolucionaron tan rápidamente que pasamos del puente de arco de Coalbrookdale, de hierro fundido y 40 metros de luz, al puente Firth of Forth, de cerchas Gerber y 500 metros de luz.

La historia de Giulio, nacido en 1900 en Roma y licenciado en ingeniería, es similar. También nos habla de los numerosos cambios técnicos relacionados con el hormigón armado en Italia y en todo el mundo, inmersos en la historia política y social del siglo XX. En particular, relata cómo una gran dificultad, como la propaganda autárquica fascista, desencadenó los experimentos más interesantes de la Italia de posguerra. En particular, recuerda cómo el hormigón armado, recién nacido a principios

del siglo XX, experimentó dos mutaciones genéticas en pocas décadas: las bóvedas delgadas y el pretensado, tan útil durante la reconstrucción tras la Segunda Guerra Mundial.

Neo Jane, nacida en Botsuana en 2000, cuenta la última historia. Predice la historia de las estructuras en el siglo XXI. En concreto, cómo cambió todo en sus años universitarios, tras la pandemia del covid-19. Y cómo los nuevos materiales de tierras raras aplicados en puentes, los nuevos paradigmas del transporte y las nuevas teorías han provocado transformaciones muy rápidas en las estructuras.

Las tres historias ficticias deberían servir para aclarar a mis alumnos qué sentido tiene estudiar e investigar la historia en ingeniería estructural.

PALABRAS CLAVE: enseñanza, futuro, diseño, historia, historia de la construcción, historia de la ingeniería.

* Persona de contacto / *Corresponding author*:
Correo-e / *e-mail*: tullia@tulliaiori.com (Tullia Iori)

How to cite this article: Iori, T. (2026). Engineering between History and Future. *Hormigón y Acero*. 77(308):259-265. https://doi.org/10.33586/hya.2025.4102

1. INTRODUCTION

Predicting the future of technological development can only be conjecture: but change is certain and waiting for us.

Do we train students in change at the university? Generally, we explain what we know and train generically to solve problems (that's what engineers do: solve problems). However, we are aware that our students, in the future, will face other problems, different from those for which we offer them solutions. But we do not go into the classroom and say: we have no idea what you will be handling, and what you will really need to know. We have no idea of the material, the theory, the tools that you will be dealing with, but we are sure that they will be different from what we are explaining to you.

How can we be so sure that everything will change? Even without a crystal ball or specific courses in futurology: banally, it is history that predicts the future.

To demonstrate this, I offer three short stories, stories of engineers who did not really exist: they are fictional but feasible stories; three fictional engineers who lived in the nineteenth century, in the twentieth century and in the first century of the new millennium. I accepted one of the most popular lines in futurology research, predictive history, with constant speed, no acceleration and no technological singularity.

2. CHARLES' TALE

2.1. The first story is about Charles.

According to his diary: "I was born in 1810, in France. My family was rich and in 1830 I attended the École Polytechnique, the best engineering school in the world at that time. My mathematical analysis professor was Augustin-Louis Cauchy and Claude-Louis Navier taught Mechanics. At that time, teaching bridge construction meant teaching masonry bridge construction. The textbook was decades old, full of Ancient Roman bridges examples. Around 1820, Marc Seguin invented wire suspension bridges. In 1826, Navier tried to build one suspended bridge over the Seine but he failed. What an embarrassment for the École!

I wasn't interested in suspended bridges – they seemed to me medieval, like drawbridges. Instead, I preferred to design bridges for railways, the new superfast way of connecting places. I admired George and Robert Stephenson, who completed the first railway between Liverpool and Manchester in 1830. As soon as I graduated, I moved to England to join my uncle. Stephenson hired me and I managed many construction sites. Then, in 1846, he involved me in the design team for the Britannia Bridge, a continuous wrought-iron beam 140 m span. What I had studied at the École was not enough. To understand the behaviour of the continuous beam, we tested a scale model, and it worked fine. Then, a few years after the inauguration, a classmate of mine, Benoît Clapeyron, demonstrated the "three moment theorem". After him came many scholars devoted to understanding statically indeterminate structures – the big calculation dilemma of that period – and they fixed it: they just added a condition – the minimum work – and everything was solved. The solution to the big question was in plain sight, but only Maxwell understood it in 1856! In the meantime, I decided to move back to France. For a few years, I designed compressed-air foundations for bridges, a new technique for bridge foundations in deep water. I designed the metal caissons, but I never went down into the caisson: the workers were sick after returning to the surface and many of them died. A few years later, a doctor figured out why workers were getting sick and how to prevent it – the compressed air technique spread throughout the world and completely transformed methods of building bridges. Then, I met Gustave Eiffel. He was 34 when he founded his company and he hired me: I had a lot of experience in construction and he needed someone older to manage his team. He hired young engineers from Switzerland. They studied with Carl Culmann in Zurich, at the best

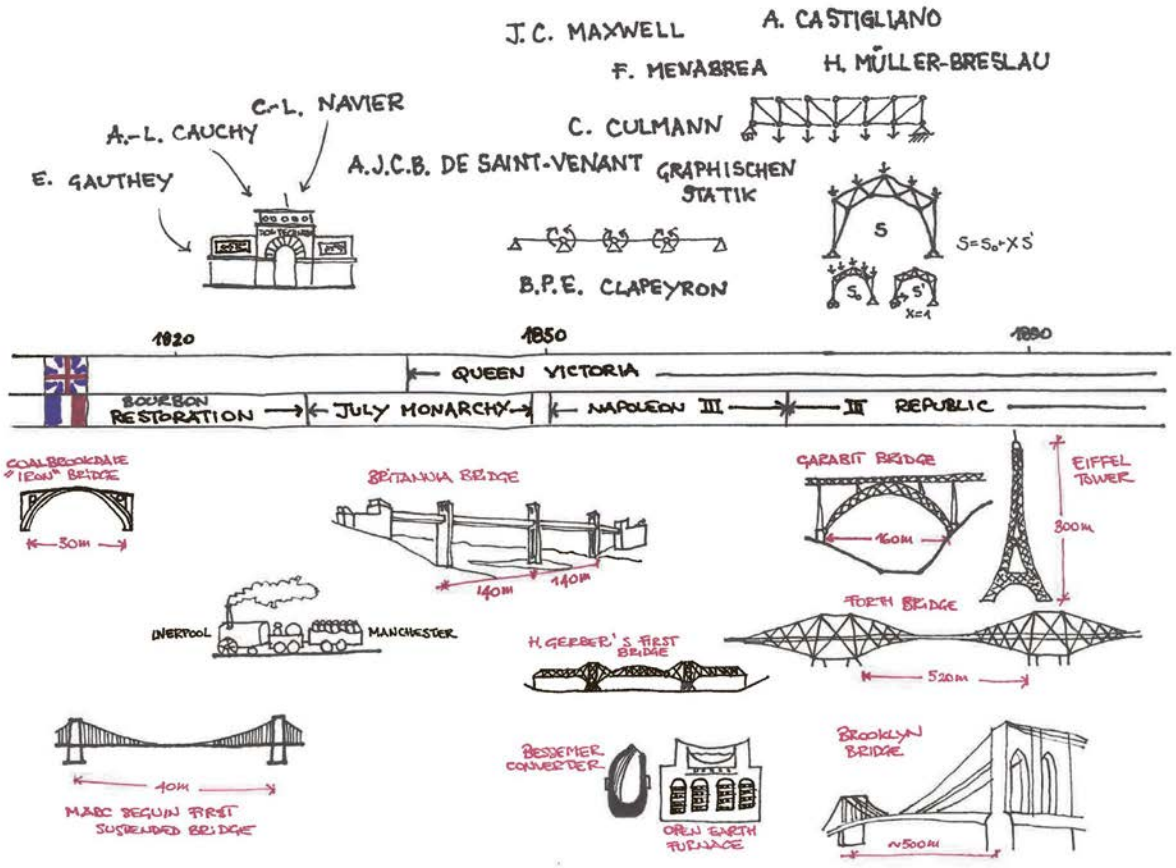

Figure 1. Concept map of Structural engineering in the 19th century.

university in the world at that time. They calculated faster than us, using a new technique: graphical statics. I understood nothing about the theory behind it, but the application was easy. Our company was the only one in France using this new method of calculation: Eiffel won all the bids. I managed the construction site of the Maria Pia bridge in Porto (1877), a gigantic arch spanning 160 m. Meanwhile, new things were happening: in 1867 a German engineer, Heinrich Gerber, invented a new kind of beam bridge, the cantilever beam, named the Gerber beam in his honour. There was more to come: we started to use steel, the new material, produced with the Bessemer converter and the open-earth process. But Eiffel didn't trust steel: he said, "wrought iron was the perfect material for bridges". In 1883 I received a telegram from the United States (my first telegram, just invented!) from Emily Warren, the wife of Washington Roebling, who I met in France visiting a compressed air foundation site. She invited me to the inauguration of a suspension bridge spanning almost 500 m in New York, the Brooklyn bridge: the piers were neo-medieval, but it looked nothing like a drawbridge. I was wrong when I was young! When I retired, Gustave asked a last favour of me: to manage the construction site of a tower in Paris for the 1889 Expo: we changed the skyline of Paris! What a pity that the tower had to be demolished. The following year, we went to the inauguration of another stunning bridge: in Edinburgh, on the Firth of Forth: 520 meters of span. A steel bridge: looking at the bridge, Eiffel realized that he had underestimated that powerful material. Heinrich Gerber was there too, with us: he couldn't believe his eyes. His simple invention transformed into such a huge bridge! Every now and then, I think of Navier's classes. Before his time, technological progress went very slowly. New things took decades, centuries to mature. Navier figured that the world would always go at the same speed. What an error! In our century, we knew of completely new, amazing materials, revolutionary ways of performing calculations, big, global new challenges like the railway. In the nineteenth century, the history of engineering changed completely". (Figure 1).

3. GIULIO'S TALE

The second story is about Giulio, an engineer of the 20th century. Again, according to his diary: "I was born in 1900 in Italy, in Rome. When I was 10 years old, my father took me to see the construction site of the Risorgimento Bridge, over the Tiber. The company used a new material: reinforced concrete. Every now and then, on the banks of the river, I would see a gentleman in a white raincoat, who spoke French: his name was François Hennebique. He decided to design the bridge, with its 100-meter span, without following the rules of his patent. Thanks to him and the revolutionary bridge in Rome, reinforced concrete became a free material: no more royalties! After the bridge was inaugurated, no one believed

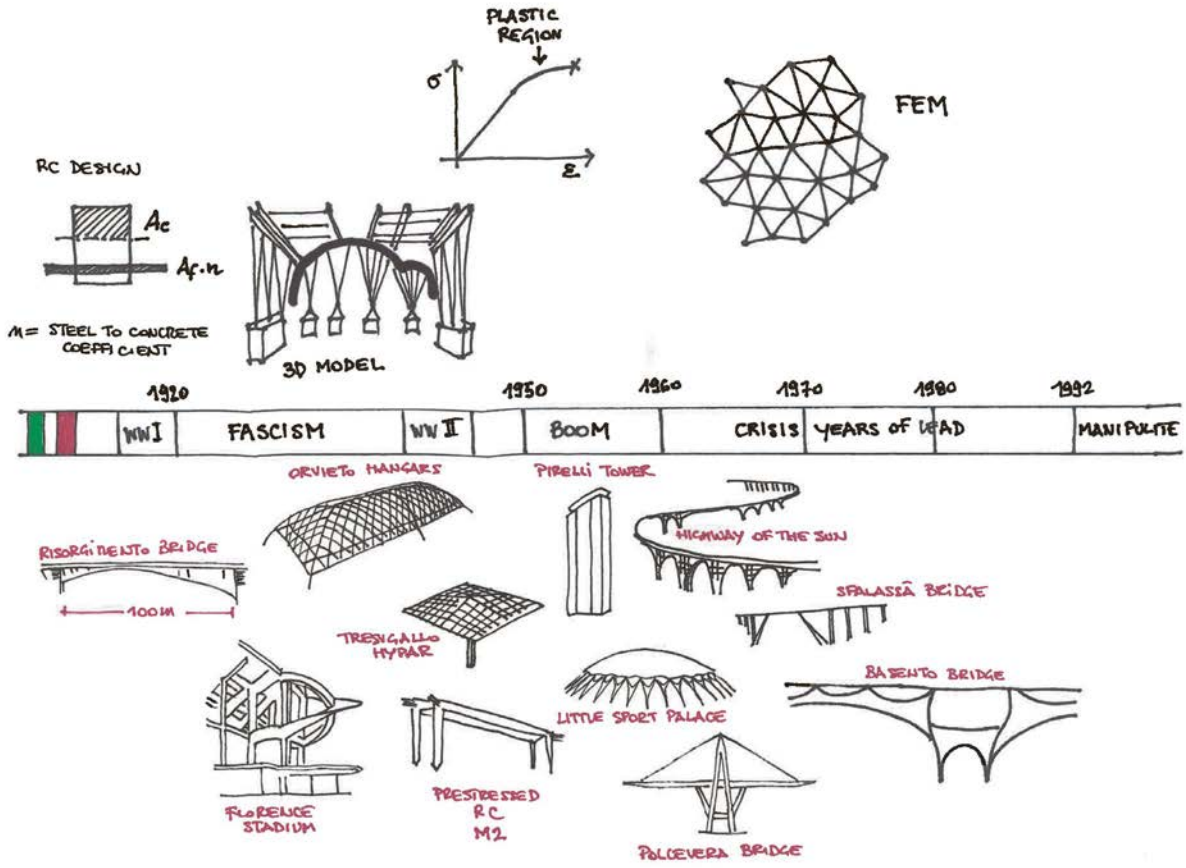

Figure 2. Concept map of Structural engineering in the 20th century in Italy.

that it would remain standing. Hennebique calculated it, refusing to use elasticity theory. A German engineer checked the calculations of the bridge and demonstrated that the bridge should collapse. But the bridge did not collapse. I still walk on it each Sunday! I fell in love with that stubborn reinforced concrete: concrete and steel together, joined in a marriage. Each material takes the load it can bear best. It was so easy to think of this kind of mixed solution, but nobody did it before Monier and Hennebique. I graduated in engineering in Turin, in 1924. We studied mostly masonry and steel construction; reinforced concrete was given very little space in the books. But at my university the teacher was Camillo Guidi, a fan of reinforced concrete.

I was hired by Pier Luigi Nervi's construction company: he founded his first company when he was 30 years old. He asked me to supervise the construction of a stadium in Florence. It was a success! Nervi never smiled: there was nothing to smile about, in those years in Italy. Mussolini had taken power: dictatorship and fascism. Mussolini did not like reinforced concrete: he preferred the materials used by the ancient Romans, marble and bricks. In 1935, Mussolini invaded Ethiopia and the League of Nations imposed sanctions against Italy. Nobody sold us steel anymore. We could no longer find steel rebar on the market. In 1936, Mussolini said that to build with reinforced concrete was forbidden. The fascists said we had to build with stone and brick, as the Romans had always done. Fortunately, Nervi didn't listen to them. He obtained some work from the Air Force: hangars to protect aircraft. We could use reinforced concrete but we had to save steel. He invented a new way to build structures: he divided them into many pieces and our workers prepared them on the ground. Then they would put the pieces on a scaffold and connect the pieces with cast-in-place concrete: a jigsaw puzzle. Nervi got help from a professor at the Milan Polytechnic, Arturo Danusso, who made a scale model for him to understand the behaviour of the structure without mathematical calculation. Nervi also invented a new material, ferroconcrete, to build thin curved slabs. Then, in July, 1943 Fascism fell in Italy. In September, after the armistice, Rome was occupied by the Nazis. Nervi closed the Company for a year. He did not want to collaborate with the Nazis. He took the slabs home and spent time checking how they performed under the weather. After the war, putting the two inventions together, Nervi built his masterpieces: 100 m diameter domes using ferroconcrete and structural prefabrication. He became the most famous engineer in the world: the fascists forbidden him to use his favourite material and, without complaint, he invented a new successful way of building.

In the meantime, I escaped to Switzerland. I was Jewish and I couldn't stay in Italy. In Switzerland I met Gustavo Colonnetti, he was my professor at the Turin Polytechnic. He also had to escape, because he was an anti-fascist militant. In Vevey, he organized a university camp where young exiled people could study and I helped him. Colonnetti taught everyone a technique he learned in France: prestressed concrete. It

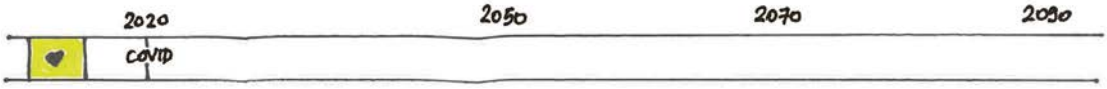

Figure 3. Concept map of the possible history of structural engineering in the 21st century.

seemed like an ingenious invention. Prestressing concrete with steel cables lends the concrete tensile strength. Again, it was so easy to think about this kind of coaction, but nobody could do it before Eugène Freyssinet. In the university camp, I met Silvano Zorzi. When the war ended, I went to work with him. We designed dozens of prestressed concrete bridges together. In the meantime, the private car became popular. Italy built hundreds of kilometres of highways. In 1964, when the Highway of the Sun was opened, Italian engineers were a benchmark for the world. They did everything with concrete: skyscrapers, dams, highways, domes, even cable-stayed bridges like the Morandi bridge in Genoa: no other material could compete in our country. So much for the fascists!

Later, things changed in Italy: the economic boom ended, workers began to strike, and students began to protest. When workers began to cost too much, Zorzi invented machines to build beautiful bridges using fewer workers: self-launching formworks, "little by little" automatic systems.

I retired when a visionary engineer, Sergio Musmeci, built a fantastic bridge in southern Italy, in Potenza, using a soap bubble as a model.

Musmeci tried to use finite elements methods (FEM), a method of calculation that four guys had invented in the United States in 1956, but he needed an automatic calculator. "Calculators will come soon" Musmeci said "and then everything will change. I can't wait!". He unluckily died young, and he didn't see the advent of computers. Every now and then, I thought about professors of my era: how much more of them I have seen! Everything changed in the 20th century: new materials, new ways of building, new calculation methods, and new social challenges. My teachers knew that everything would change: they had learned the lessons of the 19th century, but now the pace of change was much faster. The most important thing they taught me by their example is not to be afraid of crises. Crises are incredible opportunities for change, for growth. This is true on a personal level, too: after the persecutions, the war, and the exile, a second life began for me. Crises propose new problems, and new problems need new solutions. (Figure 2).

4.
NEO JANE'S TALE

We have walked the timeline of the nineteenth century; then that of the twentieth century; now it is the turn of the 21st century. This is the history of Neo Jane, a female engineer. According to her diary: "I was born in 2000, in Botswana. While I was attending university, the Covid-19 pandemic arrived. During the curfew, from my home, thanks to the internet, I could attend university courses all over the world: a big opportunity amid the tragedy. I took my PhD in Singapore. In the meantime, in the second half of the 20s, the world witnessed the birth of the United States of Africa. The peaceful revolution started from South Africa and from my rich Botswana. Africa did what the United States of America and Italy had done in the 19th century, and Europe in the 20th century (after a very bloody war). Africa was saturated with "rare earths", the lanthanide series of chemical elements, the new oil. Due to strong investments, Cape Town's university became the most important engineering university in the world. In its laboratories, a new construction material was invented: starting with a rare metal, dysprosium, number 66 in the periodic table, and reinforcing it with Thulium, another lanthanide with the atomic number 69. The combined material was stronger than steel and more beautiful than silver and titanium: thuliumed dysprosium, the material of the century.

After graduation, I was hired by a company investing in modern, high-speed transportation system across Africa: it was kind of a guided road. We would design the plan and then the robots would assemble it on their own: the beams were all the same, so the robots were never wrong. And above all, they didn't get hurt (zero accidents at work) and there were no strikes.

Then, with thuliumed dysprosium, we designed and built a bridge over the Strait of Gibraltar spanning 13 kilometres to connect Africa to Europe. (We did a little test before: the bridge over the Strait of Messina, in Italy, 3 kilometres span, a big dream for that backward country.)

Then, in the middle of the century, a new calculation theory for structures arrived: trying to understand the behaviour of rare-earths metal structures, scientists finally understood that elasticity does not exist, it is only an apparent effect of a more complex theory. Everything became much clearer, just as it did when Einstein explained that Newton's gravity force was only an apparent force due to curvature of space-time. The new theory was under everyone's eyes, but only Sharbat, an Afghan professor, understood it in 2056 (56, what a special year: in 1856 the Maxwell paper, in 1956 the FEM paper, and now the Sharbat paper). She was in exile, in Africa, after the return of the Taliban dictatorship to Afghanistan: she was expelled from the university, like the Jews during fascism. A second life began for her in Cape Town. And then….". (Figure 3).

5.
CONCLUSIONS

What is the moral of my tales? Don't be afraid of innovations, new materials, new systems of calculations, new technologies,

and new challenges. Even if you don't accept these turnarounds, they will still come. Don't be afraid of crises: crises are always an opportunity for innovation. Be an engineer of your time. Always look around you. And do it quickly, because everything is faster now.

Let's study history! To make new things, you have to know everything already happened in your world. History is a tool to imagine the future!

Learn the path that your predecessors took. Put yourself in their path and continue their journey. You are leading a very large group, standing behind you, watching you and supporting you: Navier, Stephenson, Eiffel, Hennebique, Nervi, Musmeci… and many other engineers are near you along the way and can help you, like Hugo Corres, a master of structures. Join him in the history of structural engineering!

Disponible en **www.hormigonyacero.com**
https://doi.org/10.33586/hya.2026.4179

La colaboración entre arquitectos e ingenieros: Una experiencia personal

Architect–Engineer Collaboration: A Personal Experience

Carlos Rubio Carvajal[a]

[a] *Arquitecto. RUBIO ARQUITECTURA.*

Recibido el 15 de mayo de 2024; revisado el 8 de septiembre de 2025, aceptado el 12 de febrero de 2026

RESUMEN

La colaboración entre arquitectos e ingenieros, debido a la complementariedad de sus conocimientos, es fundamental en el campo de la arquitectura y la construcción

La relación personal entre ambas profesiones juega un papel determinante en la colaboración y el éxito de proyectos y obras. Esta conexión va más allá del papel de cada uno. Implica una comprensión profunda de los requisitos y necesidades del proyecto para que pueda ser desarrollado en un ambiente creativo, propicio para la innovación y resolución de problemas.

Mi larga relación con Hugo Corres nos ha permitido llevar a buen término todos los proyectos que hemos compartido. El último en el que estamos trabajando, el Salón de Reinos, dejará grabada nuestra amistad en un edificio de indudable valor histórico.

PALABRAS CLAVE: colaboración arquitectura ingeniería, Salón de Reinos, Hugo Corres.

ABSTRACT

Collaboration between architects and engineers, due to the complementary nature of their expertise, is essential in the field of architecture and construction.

The personal relationship between both professions plays a decisive role in collaboration and in the success of projects and works. This connection goes beyond the formal roles of each discipline; it involves a deep understanding of the project's requirements and needs, allowing it to be developed in a creative environment conducive to innovation and problem solving.

My long-standing professional relationship with Hugo Corres has enabled us to successfully complete all the projects we have worked on together. The most recent one, the Salón de Reinos, on which we are currently working, will leave our friendship embedded in a building of undeniable historical value.

KEYWORDS: architect–engineer collaboration, Salón de Reinos, Hugo Corres.

* Persona de contacto / *Corresponding author*:
Correo-e / *e-mail*: crc@rubioarquitectura.com (Carlos Rubio Carvajal)

Cómo citar este artículo: Rubio, C. (2026). La colaboración entre arquitectos e ingenieros. Una experiencia personal. *Hormigón y Acero*. 77(308):265-272. https://doi.org/10.33586/hya.2026.4179

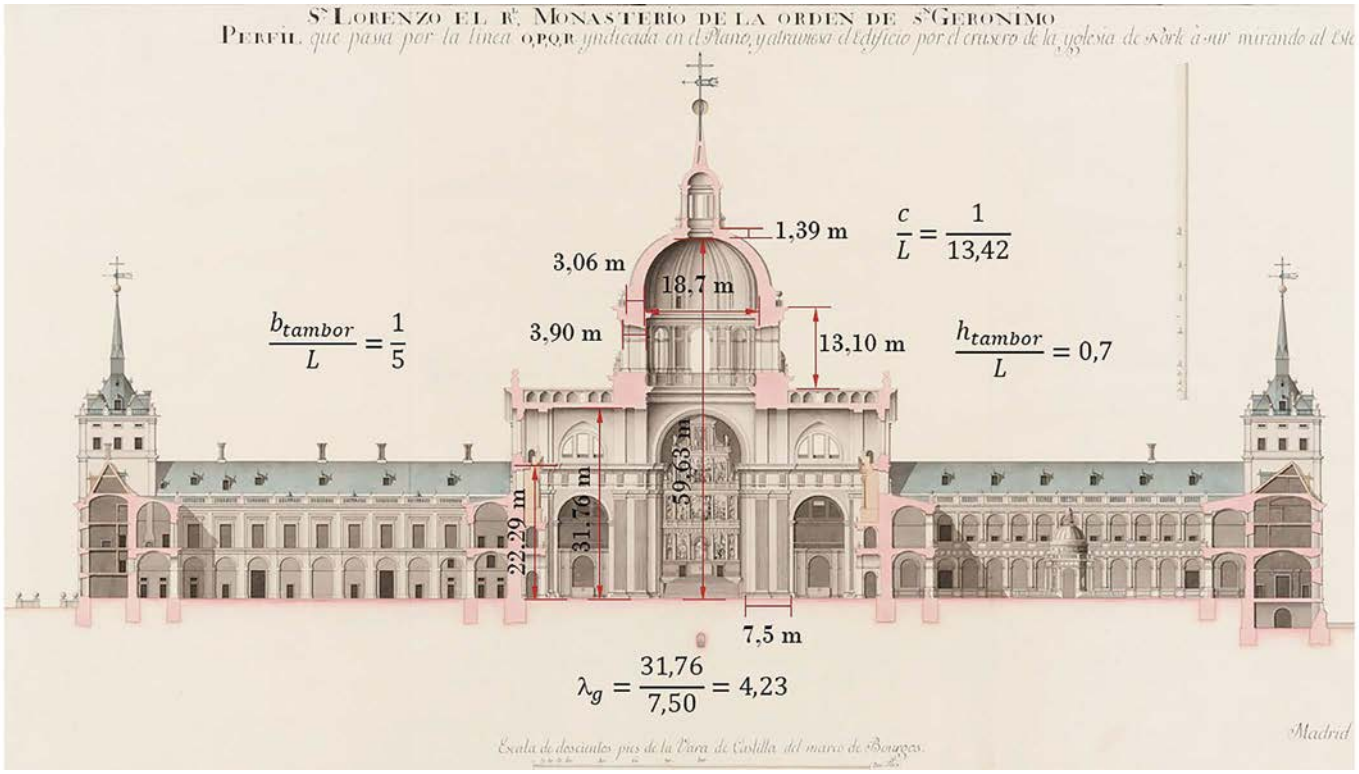

Figura 1. Sección transversal norte-sur del monasterio de El Escorial.

1. INTRODUCCIÓN

Muchos han sido los proyectos y los momentos compartidos a lo largo de estos años con mi amigo Hugo Corres.

Hugo, al cumplir 70 años, se despide de la vida académica, y pone fin a una etapa que no es más que el comienzo de otra nueva. Culmina su actividad docente activa ligada a la Escuela Técnica Superior de Ingenieros de Caminos, Canales y Puertos de la Universidad Politécnica de Madrid. Una larga y exitosa etapa que comienza en 1980 como profesor adjunto al Departamento de Física y Física de Materiales, que continua como profesor titular de Universidad en la Unidad Docente de Hormigón Armado y Pretensado y que culmina como Catedrático de Universidad de la Unidad Docente de Hormigón Estructural en el Departamento de Mecánica de Medios Continuos y Teoría de Estructuras. Muchos años impartiendo conocimiento y formando futuros ingenieros.

El ciclo vital del profesor, catedrático y docente llega a su fin, mientras que el del ingeniero y amigo sigue activo y con gran vitalidad.

La rehabilitación del Salón de Reinos y su incorporación al Museo del Prado es el proyecto que ahora nos ocupa y nos une. El Salón de Reinos antiguo Museo del Ejército, ahora un edificio exento en el barrio de los Jerónimos es solo una pequeña parte del inmenso y desaparecido Palacio del Buen Retiro construido en el siglo XVII.

El Salón de Reinos y la figura de Hugo Corres en su nueva situación profesional me hacen pensar en el ciclo vital de las cosas. En este caso de los edificios y los profesionales. Unos y otros, edificios y profesionales, disfrutan de un ciclo vital o vida útil, que sólo en los casos más notables se prolonga y renace encontrando un nuevo uso o una nueva actividad poniendo en valor sus mejores cualidades arquitectónicas y espaciales, o personales y profesionales.

Del mismo modo que los edificios son capaces de prolongar su ciclo vital, los profesionales y profesores, al finalizar su carrera académica pueden dedicar los mejores años de su vida, con plena dedicación, a disfrutar de la profesión que aman.

Igualmente es posible reflexionar sobre la relación entre la Arquitectura y la Ingeniería. Sobre la historia común de dos profesiones que juntas han construido el valiosísimo Patrimonio Histórico que nos rodea.

2. ARQUITECTURA VS INGENIERÍA

El oficio de construir existe desde el origen de los tiempos. Los humanos necesitamos vivir juntos y disponer de espacios confortables y seguros para convivir. Los responsables de organizar y ordenar esos primeros espacios de convivencia ya fueron los primeros arquitectos, al tiempo que los primeros ingenieros.

La arquitectura y la ingeniería comparten una larguísima historia de siglos en común. Cuando en el siglo XV, Filippo Brunelleschi diseña y construye la cúpula de la Catedral de Florencia es tanto arquitecto como ingeniero. Levanta la primera cúpula que se construye sin cimbra, progresando en espiral desde el tambor hasta la linterna. Una cúpula de doble "cáscara" construida con ladrillo, y no con sillares de piedra, para aligerar su peso propio.

Figura 2. Vista de las operaciones de erección de la primera columna en un pórtico de la catedral de San Isaac en San Petersburgo. Colaboración del ingeniero Augustin de Betancourt con el arquitecto Auguste de Montferrand [1].

Igualmente, en la Basílica y cúpula de San Pedro en Roma, Miguel Ángel Buonarotti, es tan arquitecto como ingeniero. O Juan de Herrera, cuando da continuidad a la "Traza Universal" de Juan Bautista de Toledo en el Monasterio de San Lorenzo de El Escorial lo hace como arquitecto mientras que, como ingeniero, resuelve los esfuerzos de la cúpula y la bóveda de la Basílica o diseña puentes como el de Segovia sobre el río Manzanares en Madrid.

Tras las guerras napoleónicas y la aparición de una sociedad industrial con una nueva organización académica, todo ello unido al poco interés de los arquitectos por las nuevas tecnologías, se produce el desdoblamiento definitivo de la figura, hasta entonces única, del "arquitecto–constructor", en arquitecto o ingeniero, consumando una ruptura que ya no volverá a recomponerse.

En España, Agustín de Betancourt, militar e ingeniero fundó en 1802 el Cuerpo y la Escuela de Ingenieros de Caminos y Canales con el fin de evitar errores técnicos y económicos en la ejecución de las obras públicas de reconstrucción tras la Guerra de la Independencia, pues según él, los arquitectos no estaban interesados en el rigor técnico ni económico de las obras. "...en las Academias llamadas de Bellas Artes sólo se enseña el ornato de la Arquitectura...".

Agustín de Betancourt aunque estudió en la Real Academia de Bellas Artes de San Fernando nunca ejerció como arquitecto. Sus especiales dotes para el dibujo le abrieron las puertas para expresar su talento como ingeniero, haciendo brillantes aportaciones a la ingeniería de minas, mecánica, aeronáutica y naval. [4].

Con la Revolución Industrial aparecen nuevas tecnologías domésticas que invaden rápidamente los hogares con nuevos y diversos artefactos. Una invasión provocada por una industria emergente surgida de la colaboración de empresarios e ingenieros y en la que los arquitectos prefirieron no participar [5].

Entre los inventos domésticos de aquellos años destaca la llegada a principios del siglo XIX del alumbrado de gas, que originó una auténtica revolución, tanto en las ciudades como en la vida doméstica. Como consecuencia de la mejor iluminación de los interiores aumentó el confort en las viviendas y la lectura nocturna, lo que provocó un notable incremento de la alfabetización y, a nivel urbano una mayor seguridad nocturna en las calles.

Pero la luz de gas exigía una mayor ventilación y, al instalarse en el interior de las viviendas, hizo necesario atender al nuevo y "engorroso" requerimiento de la aireación. Requerimiento al que la mayoría de los arquitectos, siempre más preocupados en prolongar sus discusiones bizantinas sobre los estilos históricos. no prestaron la debida atención. En ese mundo en transformación, se llegó a decir que "sólo la arquitectura y los arquitectos se han quedado inmóviles, cubiertos por el polvo de los siglos" [6].

Esta falta de interés de la mayoría de los arquitectos decimonónicos por las nuevas tecnologías señaló la línea divisoria entre arquitectos e ingenieros. A los arquitectos de la época les seguía interesando más la estética y la búsqueda de la belleza, dejando los conceptos del confort y la comodidad en segundo término. Los arquitectos se sentían incómodos con la aparición de los nuevos artefactos y muy preocupados por la mecanización, cada vez mayor, de su "arte". Las nuevas instalaciones representaban una injerencia, a veces insoportable para una profesión que se creía destinada a las más altas metas.

Figura 3. Urbanización de Madrid Rio. Un puente entre ingeniería, arte y arquitectura [9].

La arquitectura y las nuevas tecnologías se fueron distanciando sin darse cuenta de que, al mismo tiempo, lo estaban haciendo de una sociedad cada vez más interesada en las nuevas tecnologías. Se produjo, como dice Sigfried Giedion en su libro Espacio Tiempo y Arquitectura, la ruptura entre arte, por un lado, y ciencia y técnica por otro, lo que dejó la construcción y las grandes obras del momento en el lado de los ingenieros. El ingeniero apareció ante la sociedad como el conocedor de las nuevas técnicas, al tiempo que la arquitectura perdía el ritmo de las transformaciones históricas en curso.

Es con la llegada del siglo XX y la irrupción del Movimiento Moderno, cuando los objetivos de la arquitectura y los arquitectos cambian, evolucionando hacia una mayor conciencia social desde la que proponer nuevas ideas encaminadas a solucionar problemas y reconciliarse con la sociedad.

Esta realidad social fue, muy posiblemente, la que hizo que aquellos arquitectos decimonónicos abandonaran sus debates endogámicos y centraran su actividad en atender las necesidades de la sociedad de su tiempo, ahora sí, en compañía de los ingenieros. Un modo de trabajar que ha llegado a nuestros días. Arquitectura e ingeniería son profesiones diferentes pero complementarias con un tronco común; el arte de construir.

La colaboración entre arquitectos e ingenieros hoy es fundamental en el campo de la arquitectura y la construcción, debido a la complementariedad de sus conocimientos. Mientras que los arquitectos se centran más en el diseño estético y funcional de los edificios, los ingenieros aportan conocimientos técnicos especializados para garantizar la viabilidad estructural y constructiva.

3. REHABILITACIÓN DEL SALÓN DE REINOS

En mi actividad profesional como arquitecto, en compañía de Fhecor, y de la mano de Hugo Corres, he compartido y desarrollado proyectos de muy distinta índole: concursos de edificación, viviendas y oficinas, pasarelas y puentes peatonales en Madrid Río [8], ecoductos para el Bosque Metropolitano, rehabilitaciones como la del Edificio Metrópolis [10] o el Salón de Reinos [1], proyectos algunos realizados y otros que nunca pasaron del papel a la realidad.

De entre todas las colaboraciones es necesario destacar la Rehabilitación del Salón de Reinos actualmente en marcha, que con toda seguridad no será la última en la que trabajemos juntos. Un proyecto consecuencia del desarrollo de la propuesta que resultó ganadora del Concurso Internacional convocado por el Museo del Prado en 2016 y que tuvimos el privilegio de elaborar junto con Norman Foster. Colaborar con Norman Foster, el primer arquitecto global de la historia de la arquitectura que ha proyectado y construido en todos continentes y en todas las escalas y tamaños. El arquitecto más conocido y reconocido mundialmente, trabajar con él y su oficina de Madrid, requería llamar al mejor y más completo ingeniero que conozco, mi amigo Hugo.

Nuestro proyecto consiste en rehabilitar un edificio del siglo XVII, declarado BIC (Bien de Interés Cultural) en la categoría de Monumento. Un edificio que ya hace unos años agotó su ciclo vital como Museo del Ejército, y que ahora se prepara para volver a la vida con un nuevo uso y completar junto con los edificios de Villanueva, Jerónimos y Casón, el llamado "Campus del Prado".

El Salón de Reinos es sólo una pequeña parte, pero la más importante del desaparecido Palacio del Buen Retiro, palacio de fiestas y residencia de descanso de Felipe IV; proyectado por Alonso Carbonel y construido en la década de 1630, el este de Madrid, por sugerencia del Conde-Duque de Olivares.

El Salón de Reinos, sala principal del antiguo palacio, recibe su nombre por tener pintados en la bóveda de su sala principal veinticuatro escudos de distintos reinos de la corona española, bóveda que ha llegado intacta hasta nuestros días.

Si el exterior del nuevo Palacio resultaba relativamente modesto, excepto en sus dimensiones, no ocurría lo mismo con el interior donde no se escatimaron medios para decorarlo y vestirlo, en especial el Salón de Reinos, proyectado inicialmente como un palco real desde donde el rey y su familia pudieran contemplar las fiestas y espectáculos de la Plaza Sur o Principal. En 1634 se trazó un programa decorativo para

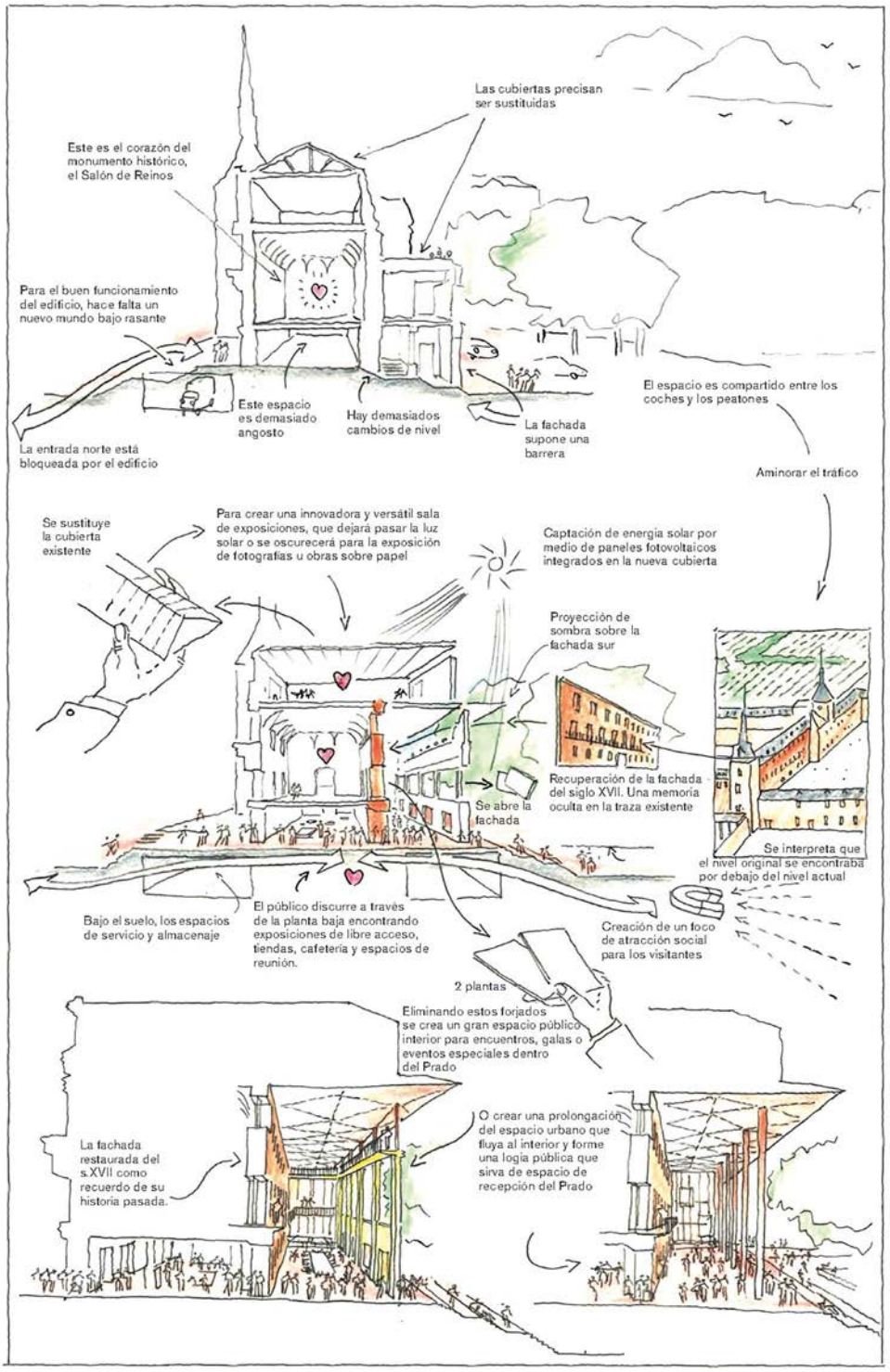

Figura 4. Salón de Reinos, ideas rectoras de la propuesta de rehabilitación. Solución ganadora del concurso internacional convocado por el Museo Nacional del Prado (2016) [1].

embellecer el Salón, encargándose una serie de pinturas de medio y gran formato que hoy forman parte destacada de la colección permanente del Museo del Prado.

Doce cuadros de batallas, de distintos autores, alusivos a las victorias militares de los comienzos del reinado de Felipe IV, estaban dispuestos a lo largo de los muros norte y sur, por debajo de la balconada que rodeaba la estancia. Sobre las ventanas, cuadros, de menor tamaño, pintados por Zurbarán, con escenas de los trabajos de Hércules y en los testeros cinco retratos ecuestres: al oeste, Felipe III y Margarita de Austria y al este, Felipe IV, Isabel de Borbón y el heredero Baltasar Carlos, todos ellos pintados por Velázquez.

En 1701, con la llegada al trono de España de la Casa de Borbón en la figura de Felipe V, el edificio cayó en desuso y todo hacía pensar que su ciclo vital había llegado a su fin, pero el incendio del viejo Alcázar en la Nochebuena de 1734

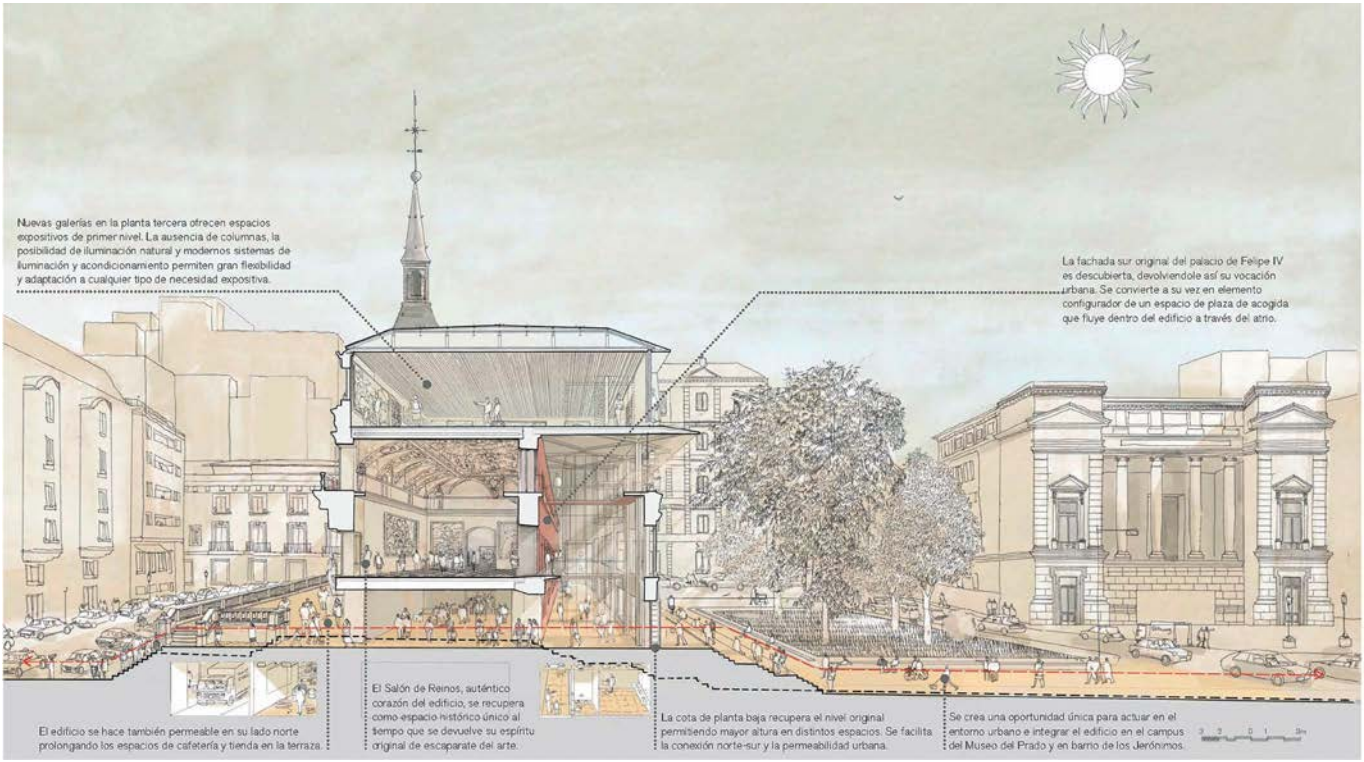

Figura 5. Sección transversal de la Rehabilitación del Salón de Reinos. [1].

prolongó su vida como palacio real otros treinta años hasta que el nuevo palacio de Oriente estuvo terminado.

En 1792 Agustín de Betancourt instaló en el Palacio del Buen Retiro, junto al Salón de Reinos, el Real Gabinete de Máquinas, una institución pionera en la divulgación técnica de la ingeniería. Allí se instalaron y exhibieron modelos de ingeniería, prototipos, máquinas y planos que Betancourt había reunido en sus viajes por Europa. Con el progresivo deterioro del conjunto del buen Retiro El Gabinete perdió su función original y muchas de sus piezas pasaron al Museo de Ciencias Naturales y mas tarde al actual Museo de Ciencia y Tecnología.

Con la invasión francesa en 1808, las tropas napoleónicas ocuparon el deshabitado Palacio del Buen Retiro como cuartel general que quedó en gran parte destruido con la entrada del ejército anglo-español en 1812. En 1868 se ordenó la demolición del Palacio a excepción de la iglesia de San Jerónimo, el Casón y el Salón de Reinos, piezas que se incorporaron como edificios exentos al nuevo barrio de Los Jerónimos con sus jardines convertidos en parque público. Posteriormente, el edificio pasó a ser, primero, sede del Museo de Artillería y después Museo del Ejército siendo objeto de sucesivas transformaciones y ampliaciones. Así, la vieja ruina renació como museo, que, al concluir su ciclo vital en 2005 por el traslado del Museo del Ejercito a Toledo, está a la espera de volver a renacer, esta vez, de la mano del Museo del Prado para albergar parte de su colección.

Para arquitectos e ingenieros intervenir en el patrimonio es una responsabilidad que, durante muchos años, dado el rechazo hacia la historia y la indiferencia de gran parte de los arquitectos hacia la actividad restauradora, quedó en manos de un reducido número de especialistas.

Desde hace años se ha venido desarrollando una creciente sensibilidad en la valoración y consideración de la historia, sus monumentos, y el patrimonio construido, siendo hoy en día, la intervención en el patrimonio, el centro de la actividad de la mayoría de los arquitectos e ingenieros, lo que ha requerido una especialización en el estudio de las técnicas constructivas del pasado.

Esta mayor valoración de la historia y sus edificios ha conllevado una mayor estima por la arquitectura y la ciudad, y por consiguiente una mayor preocupación por mantener, conservar y usar su legado histórico.

El monumento ya no es entendido solo como un testimonio artístico aislado, sino como un documento histórico que debe ser comprendido en relación con sus acontecimientos, su entorno y sus circunstancias.

Son muchos los textos que analizan las diferentes formas de abordar la intervención en el patrimonio arquitectónico, los criterios que se pueden y deben aplicar y las tendencias y teorías que han existido. Todos señalan la necesidad de actuar desde el máximo respeto y conocimiento del edificio sobre el que se va a intervenir.

Un edificio histórico pocas veces permanece intocado manteniendo íntegro su estilo arquitectónico original. Lo normal es que, a lo largo del tiempo, con mayor o menor fortuna, haya sufrido transformaciones, reformas, adiciones, demoliciones y cambios de uso.

Los edificios, al igual que las personas, nacen viven y envejecen, y viviendo, se transforman y cambian. El cambio es consustancial con la vida. Los años dejan huella. Un edificio antiguo es un documento vivo sobre el que cada generación ha dejado su impronta.

El Salón de Reinos no es una excepción, a lo largo de casi cuatro siglos, distintas manos han intervenido y dejado en él su huella, todas ellas fieles testimonios de su tiempo. Testi-

Figura 6. Escalinata y fachada principal del Salón de Reinos.
Solución ganadora del concurso internacional convocado por el Museo Nacional del Prado (2016) [1].

monios todos diferentes pero todos auténticos. Los sucesivos acontecimientos acaecidos en el Salón de Reinos han acabado conformando un edificio de indudable valor e interés histórico, artístico y arquitectónico. Lo que fue parte de un extenso palacio, es hoy un edificio exento convertido en un valioso documento en el que estudiar las diferentes etapas de su vida y analizar todas las capas que la historia y el tiempo han ido depositado en sus fábricas.

Hoy nos corresponde, a arquitectos, ingenieros y arqueólogos, interpretar con el máximo respeto, qué de todas esas páginas del pasado deben conservarse, cuáles pueden borrarse y cuáles pueden añadirse para que, con un nuevo uso, el edificio pueda gozar de una nueva y larga vida.

Junto con Hugo y Fhecor, Foster+Partners, Úrculo Ingenieros, Esdicain, Proskene, TEA Arqueólogos, los técnicos del Museo del Prado y la UTE Sacyr Empty, intentamos desde Rubio Arquitectura entender conjuntamente un edificio que no deja de sorprendernos y que solo con el compromiso de todos y el trabajo diario podremos afrontar los retos que, a diario, van surgiendo en la obra.

4. CONCLUSIONES

La relación entre arquitecto e ingeniero se basa en la comunicación abierta, el respeto mutuo y la comprensión de los objetivos del proyecto. En el caso del Salón de Reinos y en otros muchos, ambas profesiones colaboran desde las etapas iniciales del diseño hasta la finalización de la construcción, trabajando en equipo para superar obstáculos encontrando soluciones técnicas y creativas.

La colaboración es esencial para el éxito de cualquier proyecto. La combinación de conocimientos y habilidades garantiza que los edificios no solo sean visualmente atractivos, sino también seguros, funcionales, eficientes y respetuosos con el medio ambiente.

De la puesta en común de ideas y soluciones está surgiendo un edificio que dejará nuestra amistad plasmada en él y que recordaremos siempre que lo visitemos y veamos el nuevo SALÓN DE REINOS recuperado con sus cuadros, tal como lo vieron Felipe IV, Olivares y Velázquez.

Agradecimientos

Gracias Hugo por tu compromiso, dedicación y talento puesto al servicio de este gran proyecto.

Referencias

[1] Foster + Partners L.T.D. y Rubio Arquitectura S.L.P. *Traza Oculta.Salón de Reinos. Museo del Prado*. https://www.museodelprado.es/museo/salon-de-reinos (31/01/2026)

[2] Pedro Perret (1587-1589). *Estampas de la Fábrica de San Lorenzo el Real de El Escorial*. Patrimonio Nacional. Real Biblioteca Digital https://rbdigital.realbiblioteca.es/s/realbiblioteca/item/15569 (31/01/2026)

[3] Auguste de Montferrand (1845) *Église cathédrale de Saint Isaac: description architeturale, pittoresque et historique de ce monument*, San Petersburgo, Bibliothèque de l'Institut National d'Histoire de l'Art, collections Jacques Doucet

[4] Daniel Crespo, Adrián Fernandez (2024). BNE Catálogo de la exposición Agustin de Betancourt (1758 – 1824). Fundador de la Escuela de Caminos y Canales. Ingeniero Cosmopolita. https://hdl.handle.net/20.500.14352/112256 (31/01/2026)

[5] Carlos Rubio (2015). *Arquitectura-Ingeniería*. Revista de Obras Públicas. ISSN 0034-8619, Nº. 3564, 2015, págs. 73-76

[6] Rybczynski, W. (1989). *La casa: Historia de una idea* (F. Santos Fontenla, Trad.). Ed.Nerea.(Obra original publicada en 1986)

[7] Sigfried Giedion (2009). *Espacio, tiempo y arquitectura. Origen y desarrollo de una nueva tradición* (Traducción de Jorge Sánchez). Reverté (Obra original publicada en 1940)

[8] Manuel Arnáiz... et al. (2011) *MADRID RÍO, un proyecto de transformación urbana*. Editorial Turner

[9] Hugo Corres, José Romo, Julio Sánchez, Cristina Sanz (2011). Pasarelas Cáscara del Matadero y del Invernadero sobre el río Manzanares en Madrid. *Revista de Obras Públicas*. ISSN 0034-8619, Nº. 3520, 2011, págs. 39-50

[10] Roberto Duque, Fernando Bravo, Eduardo Romero, Daniel Bianchi (2025). Remodelación del Edificio Metrópolis en Madrid. Revista *Hormigón y Acero*. Volumen 76 Especial IX Congreso ACHE, Junio 2025 (pag 452). https://doi.org/10.33586/hya.2025.GRANADA. Editorial Cinter

Nota: Referencias y figuras incorporadas por el editor

Disponible en **www.hormigonyacero.com**
https://doi.org/10.33586/hya.2025.4129

Prefabricación de puentes en España. Un viaje fascinante

Precast Concrete Bridges in Spain. A Fascinating Journey.

Jesús Montaner Fragüet [a]

[a] *Ingeniero de Caminos, Canales y Puertos; Presidente de ALVIPRE.*

Recibido el 12 de mayo de 2025; revisado el 23 de junio de 2025, aceptado el 15 de septiembre de 2025

RESUMEN

En este artículo se da una visión de la evolución de la prefabricación de puentes en España, desde sus inicios en los años 60 hasta la actualidad. Se muestra el camino recorrido a medida que los medios de transporte y elevación permitían la ejecución de elementos de mayores dimensiones y peso, hasta que fue necesario buscar soluciones con continuidad por las limitaciones de transporte, abriendo la posibilidad de adaptar las soluciones prefabricadas a geometrías y tipologías estructurales que a priori no estarían dentro de su ámbito de aplicación. En esta posibilidad de aplicar elementos prefabricados a tableros continuos, jugó un importante papel Antonio Marí Bernat, quien logró dar un soporte técnico a las nuevas soluciones que se proponían, en un momento en que el cálculo mediante la técnica de los elementos finitos comenzaba a desarrollarse.

PALABRAS CLAVE: puentes prefabricados, continuidad, vigas curvas y de canto variable.

ABSTRACT

This article provides an overview of the evolution of bridge prefabrication in Spain, from its beginnings in the 1960s to the present day. It traces the progress made as transportation and lifting equipment enabled the execution of larger and heavier elements, until it became necessary to seek continuous solutions due to transport limitations. This opened the possibility of adapting prefabricated solutions to geometries and structural typologies that, at first glance, would not fall within their usual scope of application. In enabling the use of prefabricated elements in continuous decks, Antonio Marí Bernat played a key role, providing technical support for the new proposed solutions at a time when finite element analysis techniques were beginning to be developed.

KEYWORDS: prefabricated bridges, continuity, curved beams, and variable-depth beams.

* Persona de contacto / *Corresponding author*:
Correo-e / *e-mail*: fosan@alvipre.es (Jesús Montaner)

Cómo citar este artículo: Montaner, J. (2026). Prefabricación de puentes en España. Un viaje fascinante. Hormigón y Acero. 77(308):273-285. https://doi.org/10.33586/hya.2025.4129

1. INICIO DE LA PREFABRICACIÓN EN ESPAÑA

Se puede afirmar con rotundidad que la prefabricación de puentes en España es líder a nivel mundial por la cantidad de soluciones construidas, la novedad de muchas de ellas y las posibilidades de futuro que se abren, facilitando la construcción de cualquier tipología de puente de hormigón usando elementos prefabricados. Puede constatarse y así lo hemos hecho en distintas conferencias en países como Inglaterra, China, EEUU, Perú, Chile, Georgia, etc.

El desarrollo de estas tecnologías es como un gran viaje a lo largo del tiempo en los últimos 60 años.

Yo me subí a este tren en el año 1973, cuando tras acabar mis estudios en la ETS de Ingenieros de Caminos de Madrid (no había otra entonces) en 1970, con 21 años y tras dos años como investigador en el Laboratorio de Estructuras de dicha Escuela de Caminos bajo la dirección de mi buen amigo, DEP,

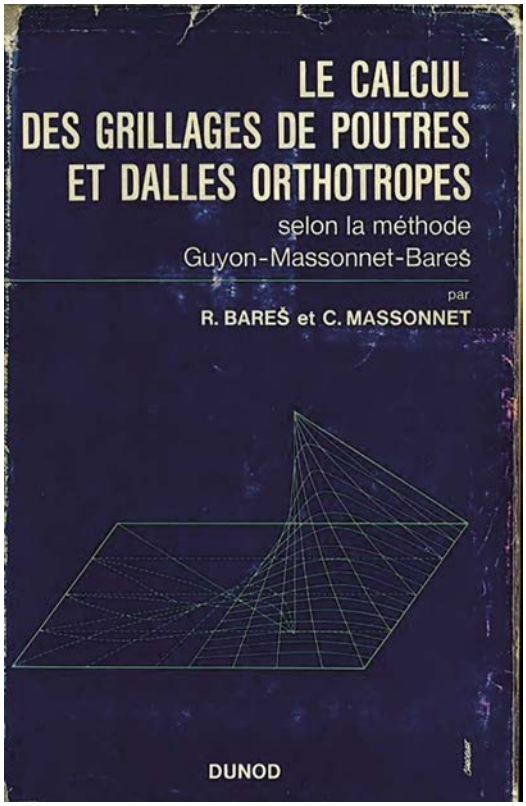

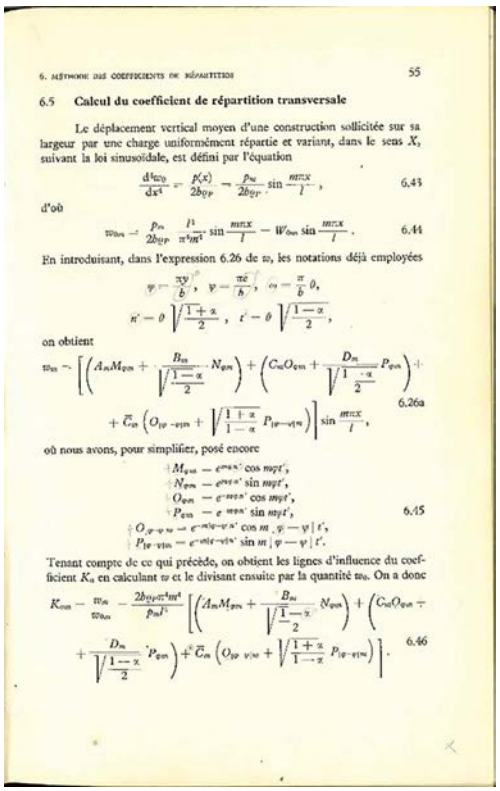

6. MÉTHODE DES COEFFICIENTS DE RÉPARTITION 55

6.5 **Calcul du coefficient de répartition transversale**

Le déplacement vertical moyen d'une construction sollicitée sur sa largeur par une charge uniformément répartie et variant, dans le sens X, suivant la loi sinusoïdale, est défini par l'équation

$$\frac{d^4w_0}{dx^4} = \frac{p(x)}{2b_0\rho} = \frac{p_m}{2b_0\rho}\sin\frac{m\pi x}{l}, \qquad 6.43$$

d'où

$$w_{0m} = \frac{p_m}{2b_0\rho}\frac{l^4}{\pi^4 m^4}\sin\frac{m\pi x}{l} = W_{0m}\sin\frac{m\pi x}{l}. \qquad 6.44$$

En introduisant, dans l'expression 6.26 de w, les notations déjà employées

$$\varphi = \frac{ay}{b}, \quad \psi = \frac{\pi c}{b}, \quad \alpha = \frac{\pi}{b}\theta,$$
$$n' = \theta\sqrt{\frac{1+\alpha}{2}}, \quad t' = \theta\sqrt{\frac{1-\alpha}{2}},$$

on obtient

$$w_m = \left[\left(A_m M_{\varphi m} + \frac{B_m}{\sqrt{\frac{1-\alpha}{2}}}N_{\varphi m}\right) + \left(C_m O_{\varphi m} + \frac{D_m}{\sqrt{\frac{1-\alpha}{2}}}P_{\varphi m}\right) + \right.$$
$$\left. + \overline{C}_m\left(O_{|\varphi-\psi|m} + \sqrt{\frac{1+\alpha}{1-\alpha}}P_{|\varphi-\psi|m}\right)\right]\sin\frac{m\pi x}{l}, \qquad 6.26a$$

où nous avons, pour simplifier, posé encore

$$\left.\begin{aligned} M_{\varphi m} &= e^{m\varphi n'}\cos m\varphi t', \\ N_{\varphi m} &= e^{m\varphi n'}\sin m\varphi t', \\ O_{\varphi m} &= e^{-m\varphi n'}\cos m\varphi t', \\ P_{\varphi m} &= e^{-m\varphi n'}\sin m\varphi t', \\ O_{|\varphi-\psi|m} &= e^{-m|\varphi-\psi|n'}\cos m\,|\varphi-\psi|\,t', \\ P_{|\varphi-\psi|m} &= e^{-m|\varphi-\psi|n'}\sin m\,|\varphi-\psi|\,t'. \end{aligned}\right\} \qquad 6.45$$

Tenant compte de ce qui précède, on obtient les lignes d'influence du coefficient K_m en calculant w et le divisant ensuite par la quantité w_0. On a donc

$$K_m = \frac{w_m}{w_{0m}} = \frac{2b_0\rho\pi^4 m^4}{p_m l^4}\left[\left(A_m M_{\varphi m} + \frac{B_m}{\sqrt{\frac{1-\alpha}{2}}}N_{\varphi m}\right) + \left(C_m O_{\varphi m} + \right.\right.$$
$$\left.\left. + \frac{D_m}{\sqrt{\frac{1-\alpha}{2}}}P_{\varphi m}\right) + \overline{C}_m\left(O_{|\varphi-\psi|m} + \sqrt{\frac{1+\alpha}{1-\alpha}}P_{|\varphi-\psi|m}\right)\right]. \qquad 6.46$$

Figura 1. Portada de "LE CALCUL DES GRILLAGES DE POUTRES ET DALLES ORTHOTROPES" y apartado de cálculo de coeficientes de reparto transversal en tableros de vigas y losa según el método de Guyon-Massonnet-Bares [1].

Juan Antonio Torroja, entré a formar parte del departamento técnico de una empresa de prefabricados que acababa de aparecer, ALVISA, que era continuación de otra anterior, IASA (Industrias Albajar S.A.).

Realmente el viaje había comenzado a finales de los años 50, cuando la necesidad de construir una gran cantidad de viviendas hizo aparecer la fabricación de viguetas pretensadas para la construcción de forjados de edificación, ya que eran mucho más baratas y versátiles que las dobles T metálicas que habían empezado a usarse. Estas viguetas con cantos de 18, 20, 25 y hasta 30 cm se usaron hasta la aparición de los forjados reticulares en los años 90. Fábricas de viguetas pretensadas había varias en cada provincia, pero solo 3 empresas dieron el salto a realizar vigas de mayor canto hasta 1.00 m y 1.20 m, para usarlas en la construcción de puentes. Esas empresas eran PACADAR, CADE e IASA.

2. DESARROLLO DE LA PREFABRICACIÓN ESTANDARIZADA DE IASA

Hay que tener muy presente que, en esa época, la red de carreteras española tenía muy poco que ver con la actual y que los elementos de transporte estaban empezando a desarrollarse. Al final de los años 60 habían aparecido los primeros tráileres articulados con plataforma de 12.00 m y una grúa de 15 o 20 toneladas de capacidad de elevación era una máquina excepcional.

En I.A.S.A. había empezado su labor profesional, recién acabada su carrera a mediados de los 60, un ingeniero llamado Juan José Arenas de Pablo natural de Huesca. IASA tenía la sede social en Huesca y, por supuesto, en aquellos años no existía ningún tipo de ordenador ni nada que se le pareciese, como ejemplo, la topografía se resolvía con las tablas de logaritmos, que hoy en día serían como un hacha de sílex comparadas con las herramientas actuales. En el cálculo de los puentes, donde la dificultad estaba en cómo se repartían transversalmente las cargas puntuales prescritas por la Instrucción vigente entre las distintas vigas del tablero (hay que pensar por un momento como se podría hacer esto hoy en día sin ningún tipo de ayuda informática), había un sistema que asimilaba el tablero a una losa ortótropa. Los ingenieros franceses Guyon y Massonet habían desarrollado un método para asimilar el tablero a una losa con rigideces longitudinal y transversal distintas y, con unas fórmulas (Figura 1) que hoy nos parecerían chino, se podía llegar a obtener el coeficiente de excentricidad que nos permitía obtener el esfuerzo a soportar por cada uno de los nervios longitudinales del tablero.

Un ingeniero llamado Rowe había trabajado con esas fórmulas y desarrollado unos gráficos que permitían llegar a ese reparto [2]. Hay que tener en cuenta que en esa época no existían las fotocopiadoras, por lo que este libro, "el famoso Rowe", se convirtió en la Biblia de todos los calculistas de puentes de la época. Como muestra de ello, en la figura 2, se puede ver las portadas de la citada publicación y del catálogo de la colección de vigas que Juan José Arenas había desarrollado para IASA, donde se aprecia con toda claridad la influencia del mencionado texto.

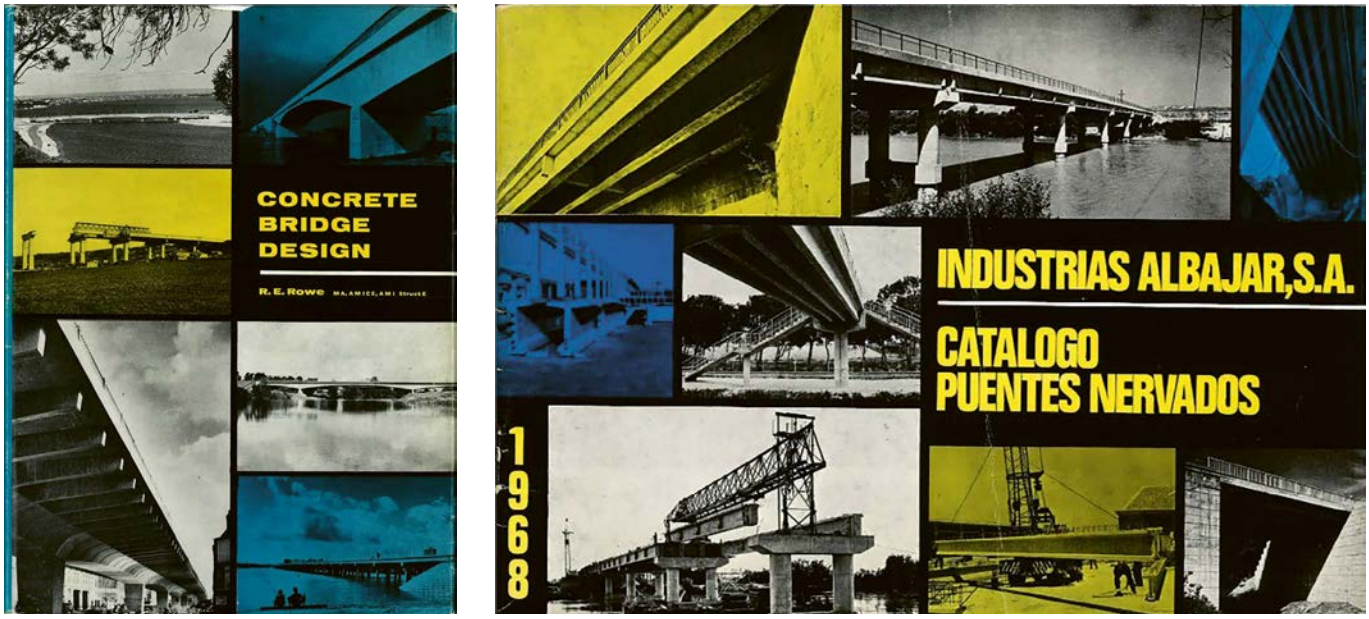

Figura 2. Portada de "CONCRETE BRIDGE DESIGN" [2] y portada del catálogo de vigas doble T de I.A.S.A [5].

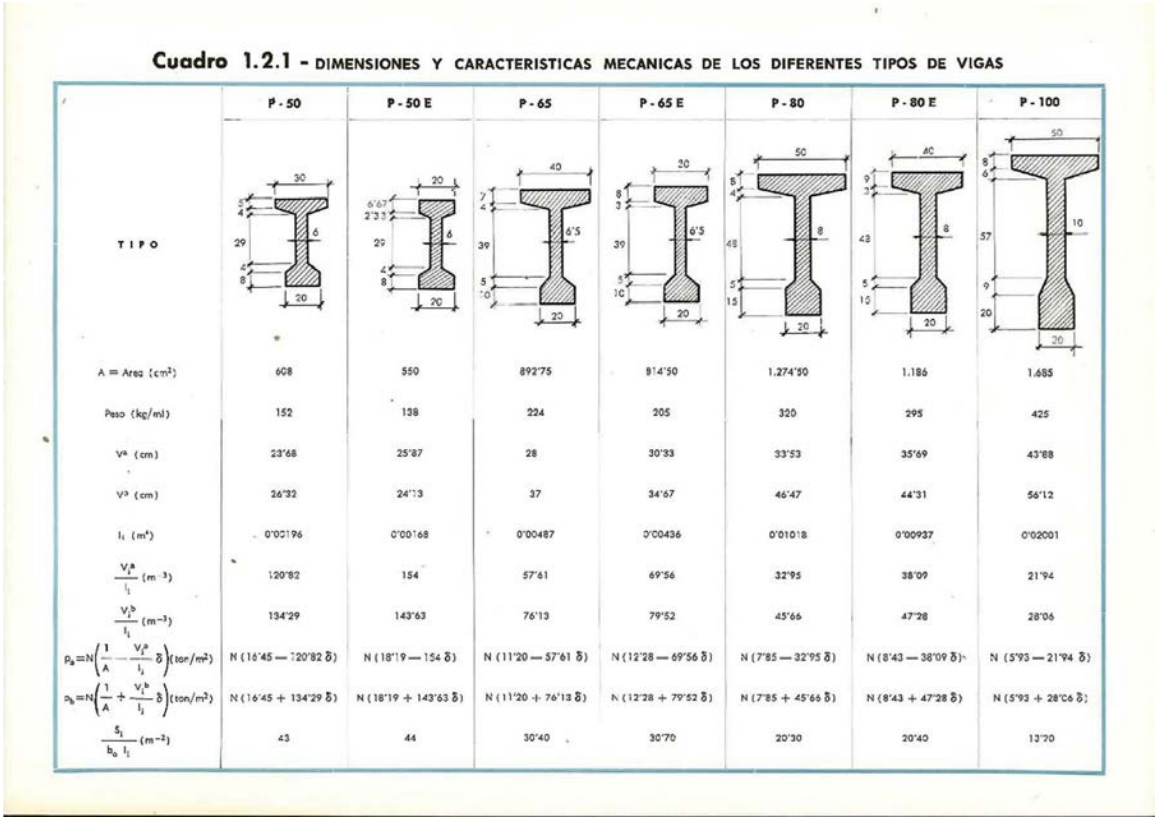

Cuadro 1.2.1 - DIMENSIONES Y CARACTERISTICAS MECANICAS DE LOS DIFERENTES TIPOS DE VIGAS

TIPO	P - 50	P - 50 E	P - 65	P - 65 E	P - 80	P - 80 E	P - 100
A = Area (cm²)	608	550	892'75	914'50	1.274'50	1.186	1.685
Peso (kg/ml)	152	138	224	205	320	295	425
V^a (cm)	23'68	25'87	28	30'33	33'53	35'69	43'88
V^b (cm)	26'32	24'13	37	34'67	46'47	44'31	56'12
I_i (m⁴)	0'00196	0'00168	0'00487	0'00436	0'01018	0'00937	0'02001
$\frac{V_i^a}{I_i}$ (m⁻³)	120'82	154	57'61	69'56	32'95	38'09	21'94
$\frac{V_i^b}{I_i}$ (m⁻³)	134'29	143'63	76'13	79'52	45'66	47'28	28'06
$\sigma_a = N\left(\frac{1}{A} - \frac{V_i^a}{I_i}\delta\right)$ (ton/m²)	N (16'45 — 120'82 δ)	N (18'19 — 154 δ)	N (11'20 — 57'61 δ)	N (12'28 — 69'56 δ)	N (7'85 — 32'95 δ)	N (8'43 — 38'09 δ)	N (5'93 — 21'94 δ)
$\sigma_b = N\left(\frac{1}{A} + \frac{V_i^b}{I_i}\delta\right)$ (ton/m²)	N (16'45 + 134'29 δ)	N (18'19 + 143'63 δ)	N (11'20 + 76'13 δ)	N (12'28 + 79'52 δ)	N (7'85 + 45'66 δ)	N (8'43 + 47'28 δ)	N (5'93 + 28'06 δ)
$\frac{S_i}{b_o I_i}$ (m⁻²)	43	44	30'40	30'70	20'30	20'40	13'70

Figura 3. Características de las secciones del catálogo de vigas doble T de I.A.S.A. [5].

En esa colección de vigas del año 1968 (ver figura 3), puede apreciarse que, para la viga de la mayor sección (P-100), con un peso de 425 kg/ml, y la luz máxima a la que se llegaba, en el entorno de los 22 metros, se obtenía un peso total de 9500 kg, valor ajustado a la capacidad de la maquinaria de elevación de la época. El Ingeniero Arenas dejó la empresa IASA en 1969, continuando su carrera como proyectista de puentes de reconocido prestigio, como hoy todos sabemos.

3. ALVISA Y LAS GRANDES ESTRUCTURAS PREFABRICADAS

El escenario de la prefabricación evolucionaba muy deprisa y, en el año 1973, los medios de transporte permitían ya pesos mayores. Comenzaban a aparecer los transportes tipo DOLLY, en los que la tractora se independizaba de las ruedas traseras

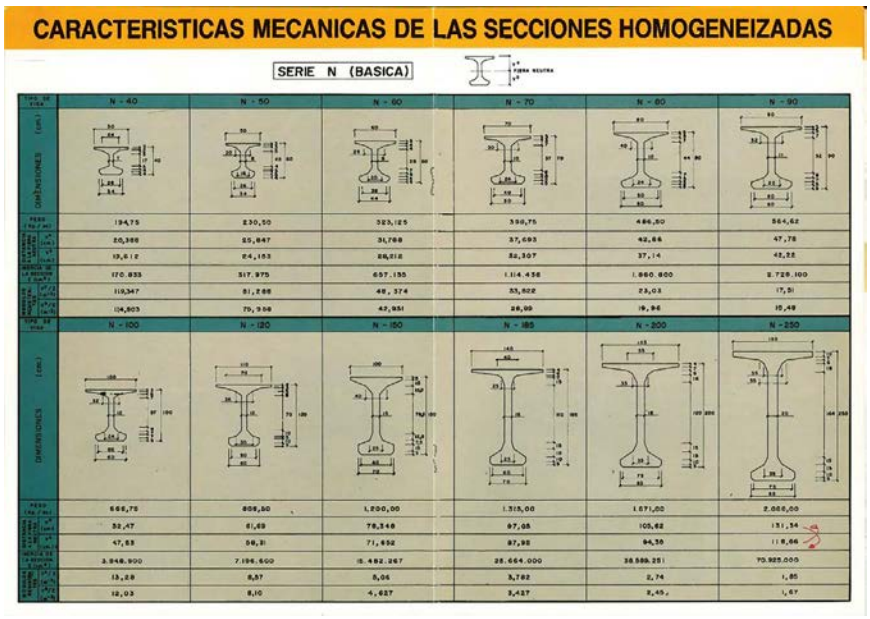

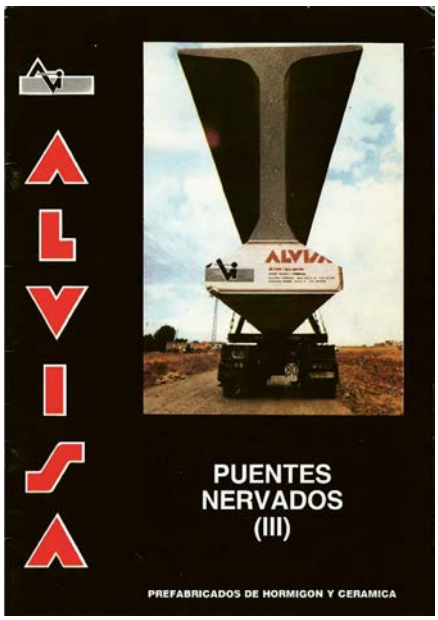

Figura 4. Portada y características de las secciones del catálogo de vigas doble T de ALVISA [6].

Figura 5. Imágenes del puente sobre el río Alcanadre (Huesca), 1989: vista inferior acabado, colocación de vigas del vano centra y paso del transporte de las vigas por el puente existente sobre el río Alcanadre.

Figura 6. Imágenes de la duplicación del puente sobre el río Alcanadre (Huesca): vista inferior durante el montaje con lanzavigas, vista inferior y vista general acabado.

haciendo la viga de chasis entre ambas, con lo que el problema de la longitud de la viga pasaba al trazado de la carretera y no al transporte. Asimismo, iban apareciendo grúas de 50, 100 y hasta 150 t de capacidad de elevación, con lo que el trabajo durante unos años fue el ir aumentando la longitud y el peso de las vigas (ver figura 4, catálogo de ALVISA, empresa que sucedió a IASA). A mediados de los años 70 aparecieron en España las vigas artesas que, posteriormente, al menos con 8 o 9 años de diferencia, surgirían en EE. UU.

El viaje fue discurriendo y se fueron fabricando vigas de 30, 35, 40, 45 metros de longitud, hasta que en el año 1988 llegamos a un puente que considero muy importante y estación fundamental en el viaje. Es el puente sobre el río Alcanadre en la CN-240 en la provincia de Huesca (figura 5), del que teníamos que desarrollar el proyecto completo del mismo. Diseñamos un puente de 225 metros de longitud total, con 5 vanos de 36/51/51/51/36 metros, eliminando las juntas sobre pilas con el sistema de rótulas de continuidad que ALVISA venía usando habitualmente y que luego recogería la Norma Española. Las pilas laterales tenían una altura sobre 17 y 25 m, mientras las dos pilas centrales eran de aproximadamente 50 m de altura. El puente estaba en zona sísmica. El diseño de las pilas con forma piramidal presentaba la dificultad de abordar su cálculo para los esfuerzos de segundo orden con flexión esviada, siendo su sección rectangular hueca y variable en altura. Mi buen amigo Antonio Marí Bernad (Toni) con el que me unía una relación muy cercana, casi familiar, estaba trabajando en el tema de discretizar y compatibilizar deformaciones en secciones de hormigón armado. Mediante un análisis paso a paso, conseguimos encajar perfectamente las 4 pilas. A parte del tema de cálculo, el puente presentaba un problema de montaje muy importante, pero ALVISA había tomado la decisión de adquirir maquinaria pesada no existente en España para apostar firmemente por la prefabricación de grandes elementos, su Gerente, el ingeniero José Emilio Jimeno, había convencido a los propietarios de seguir por ese camino. Así que este montaje se realizó en 1989 con dos grúas LIEBHER, una de 400 t con 50 m de pluma y otra que era la mayor grúa que fabricaba LIEBHER en esa época, una máquina que era la nº6 de las fabricadas, estando las primeras 5 unidades trabajando en Puertos de Europa para la descarga de barcos. La grúa Nº6, nunca trabajó en ningún puerto y fue utilizada por ALVISA en

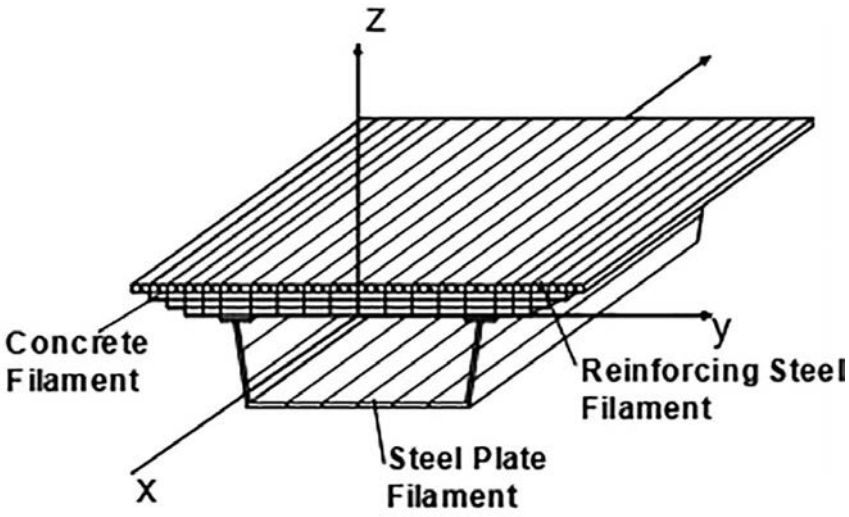

Figura 7. Esquema de filamentos utilizados por el programa CONS en la discretización de un elemento [3].

el montaje de una gran cantidad de estructuras prefabricadas durante los años siguientes. Era una máquina con posibilidad de trabajar con pluma hidráulica de 60m, o con pluma de celosía de hasta 120 m de longitud. Una auténtica maravilla que aumentaba las posibilidades de la prefabricación hasta límites impensables hasta entonces.

El puente con sus 9 vigas centrales (3 por vano) de 51 m de longitud y 150 t de peso fue récord de España en tramos isostáticos. Veinticuatro años después y al convertirse la CN-240 en autovía, se duplicó el puente repitiéndolo exactamente, pero entonces ya habían aparecido los lanzavigas con capacidad de movimiento de 200 t diseñados por ALVISA y su montaje se hizo de forma mucho más sencilla (Figura 6).

Construido este puente, llegamos a la conclusión de que la carrera por vigas más largas y más pesadas había llegado a su fin y había que pensar en otra filosofía. Lo que en el argot de fábrica se decía, "había que empalmar las vigas" o lo que es lo mismo, había que pasar a los puentes hiperestáticos.

4. LA CONSTRUCCIÓN PREFABRICADA EVOLUTIVA

Estamos en el año 1991-1992 y PACADAR construía en Gerona un puente sobre el río Oñar, con continuidad basada en la tecnología de moda en aquel entonces del pretensado exterior. La verdad es que a mí esta tecnología nunca me gustó como sistema constructivo (admito que puedo estar equivocado), si bien es muy adecuada para reparaciones o refuerzos de puentes, ya que su coste resulta muy elevado y su conservación muy costosa. Nosotros fuimos por otro camino (y el tiempo nos ha dado la razón) y planteamos un sistema conceptualmente más sencillo: "¿Por qué no atornillamos las vigas entre sí?" que diría un castizo y a ello nos pusimos. La unión, muy sencilla, consiste en dejar separadas las vigas, con sus extremos muy rugosos, lo suficiente para rellenar esta junta con un material autonivelante y de muy baja retracción. Posteriormente se comprime esta junta superior e inferiormente con barras y/o tendones para asegurar la ausencia de tracciones en dicha sección. El concepto era claro y fácil, pero había un gran problema: ¿cómo se comportarían estos elementos unidos a lo largo del tiempo? Dos hormigones muy distintos, cada uno con sus características mecánicas y reológicas diferentes, a los que vamos a obligar a trabajar unidos a lo largo del tiempo, intercambiando tensiones entre ellos y sus armaduras. El reto era grande y no existía ningún programa de cálculo (hoy en día sí los hay) que lo pudiera abordar.

La solución era Toni y las nuevas ideas que había traído de su estancia en la U.C de Berkeley, para desarrollar los cálculos de estructuras con elementos finitos en ordenadores. Estaba desarrollando un programa llamado CONS [3] donde se discretizaban las secciones en multitud de filamentos de hormigón y/o acero (figura 7). A cada filamento se le asignaban sus características reológicas propias y al establecer la compatibilidad de deformaciones entre los filamentos adyacentes, además de incluir la variable del tiempo en un análisis paso a paso, se podía observar cómo se intercambiaban las tensiones los distintos filamentos a lo largo del tiempo. Los resultados eran espectaculares y confirmaban plenamente la validez del sistema, pero tanto Toni como yo, estuvimos de acuerdo que, como investigadores, había que verlo en la realidad y contrastar los resultados del CONS con un ensayo en modelo real, ya que el paso era lo suficientemente importante para invertir en ello.

Construimos en la fábrica un puente a escala 1/2 con dos vanos (figura 8), uno armado y otro postesado, con una conexión mediante barras pretensadas y colocamos alrededor de 100 puntos de medida de tensiones y deformaciones tanto en el hormigón como en el acero activo, pasivo y barras de empalme, así como células de carga en los apoyos para el control de reacciones. El puente, así construido y monitorizado, lo instalamos en el laboratorio de la ETS de Ingenieros de Caminos de Barcelona [4]. Allí estuvo durante casi dos años sometido a todo tipo de ensayos, realizándose sobre él varias tesis doctorales y sirvió para confirmar que el CONS funcionaba perfectamente (figura 9).

Figura 8. Imágenes del ensayo en el laboratorio de la Universidad Politécnica de Barcelona.

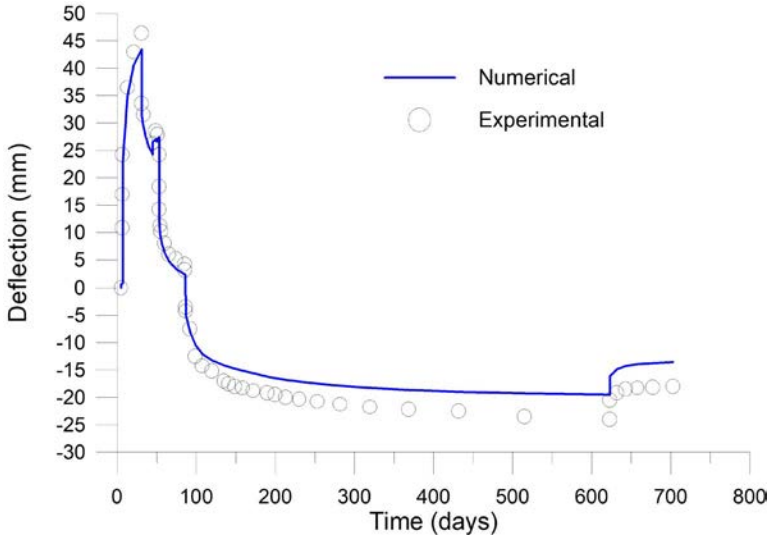

Figura 9. Gráfica comparativa de las deformaciones a lo largo del tiempo entre los resultados del ensayo y los obtenidos con el programa CONS [4].

Figura 10. Paso superior prefabricado continuo en la Autovía A-10.

Figura 11. Construcción del Puente de Las Pilas sobre el río Cinca (Huesca).

Figura 12. Imágenes de puentes curvos con soluciones prefabricadas.

Los primeros puentes de vigas prefabricadas con este sistema de continuidad estructural se construyeron entre 1992 y 1993 en Navarra en la Autovía A-10 o de "La Barranca" (figura 10). En 1996 se alcanzaron luces de 60.00 m en el Puente de Las Pilas sobre el río Cinca en Huesca (figura 11), mientras las primeras estructuras resueltas de esta forma para alta velocidad ferroviaria fue en la Línea de Alta Velocidad Madrid – Barcelona en 2001.

Habíamos abierto la puerta de la prefabricación a un nuevo mundo. El viaje atravesaba una gran frontera. A partir de allí las tipologías fueron apareciendo, luces de 60, 70 y hasta 90 m fueron alcanzables, puentes curvos, puentes con pilas en V, puentes con trazados complicados, puentes con vigas adosadas para secciones de gran anchura, puentes con jabalcones, puentes con placas realzadas para conseguir cantos de hasta 4.50 m, etc (figuras 12, 13, 14 y 15).

ALVISA desapareció, pero ALVIPRE recogió el testigo y nuevos ingenieros se subieron al tren para realizar nuevos hitos, como la muy reciente "cubierta singular" de la nueva estación intermodal de la Sagrera en Barcelona. Esta estructura sobre las líneas de AVE, consta de 8 cúpulas troncopiramidales de aprox. 1800 m² cada una, que soportan un parque público arbolado con voladizos de hasta 17m de longitud. En este caso, las vigas principales sirven como pasillos de evacuación de la es-

Figura 13. Imágenes de puentes arcos o aporticados con soluciones prefabricadas.

Figura 14. Imágenes de puentes de pilas en V prefabricadas y con jabalcones.

tación, con una dimensión interior libre de 6.40 m por 2.40 m, con lo que las vigas tienen unas dimensiones exteriores de 8.50 m de ancho por 3.40 m de canto. Dichas vigas forman una retícula que sustenta el entramado de costillas transversales sobre las que se disponen inferiormente unas placas de hormigón, a modo de falso techo con un diseño disipador acústico, y superiormente las prelosas de encofrado perdido colaborante, sobre las que se ejecuta la losa superior de 40 cm de espesor, en la que va dispuesto todo el postesado necesario de la cubierta.

Al tener que funcionar las vigas como pasillos de evacuación, es necesario disponer en el fondo de las vigas y en la losa superior, una gran cantidad de grandes huecos para escaleras y ascensores que dificultan sobremanera el cálculo de la retícula (figuras 16, 17, 18 y 19).

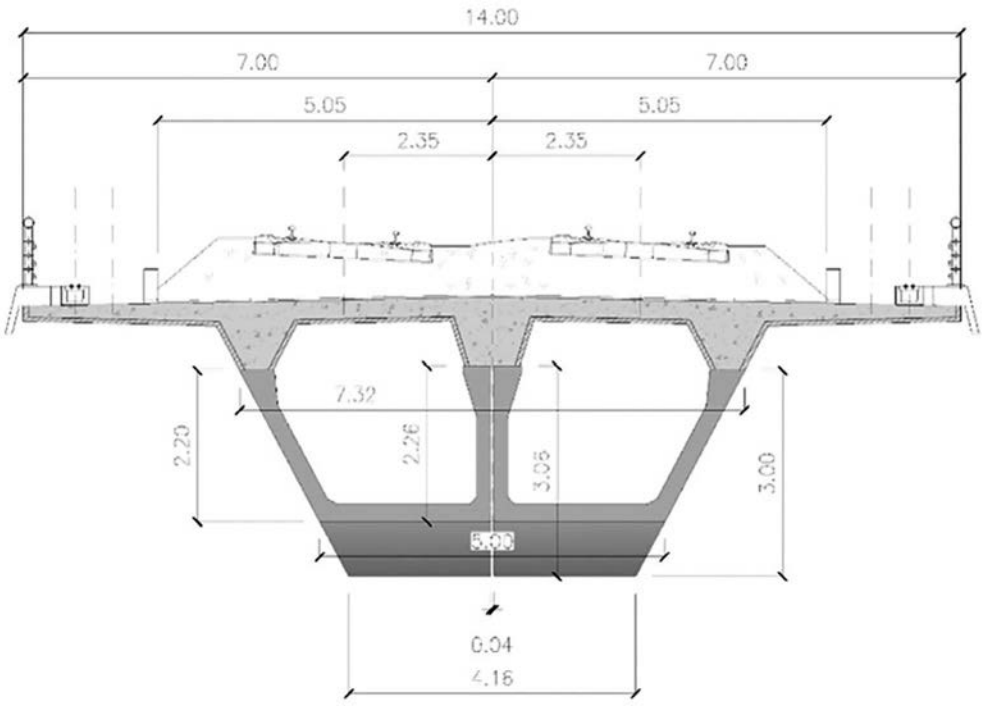

Figura 15. Imagen de puente para línea AVE con vigas adosadas y placa realzada, vano central 60 m.

Figura 16. Vista aérea durante la construcción de la parte singular de la cubierta de la nueva estación intermodal de la Sagrera.

Figura 17. Imágenes de la colocación de semivigas para la construcción del entramado principal de cajones.

La prefabricación de estas grandes vigas "no transportables en sección completa" se ha diseñado la solución de dos vigas en L que unidas por su labio inferior forman una viga U. Esta solución de vigas en L, junto con la que hemos denominado "placa nervada realzada", abre la posibilidad a la construcción prefabricada en taller de poder realizar vigas con anchos del entorno de los 8 m y cantos totales (viga más losa) de alrededor de 8-9m (figura 20), o lo que es lo mismo, el prefabricado puede acceder, con los lanzavigas correspondientes, a soluciones para las grandes luces, pudiendo competir perfectamente con bastantes ventajas constructivas sobre el método actual de voladizos sucesivos.

5
CONCLUSIONES Y FUTURO

Las crecientes dificultades para conseguir mano de obra cualificada para trabajar en obras in situ, la posibilidad de obtener en fábrica mejor control sobre los materiales y ejecución de las piezas, la posibilidad de uso de materiales específicos en hormigones de altas prestaciones, la independencia de la climatología en el desarrollo de la obra y con ello, el acortamiento significativo de los plazos de construcción, el uso de lanzavigas específicos que facilitan la independencia del terreno en las labores de construcción y menor afección a las actividades o vías

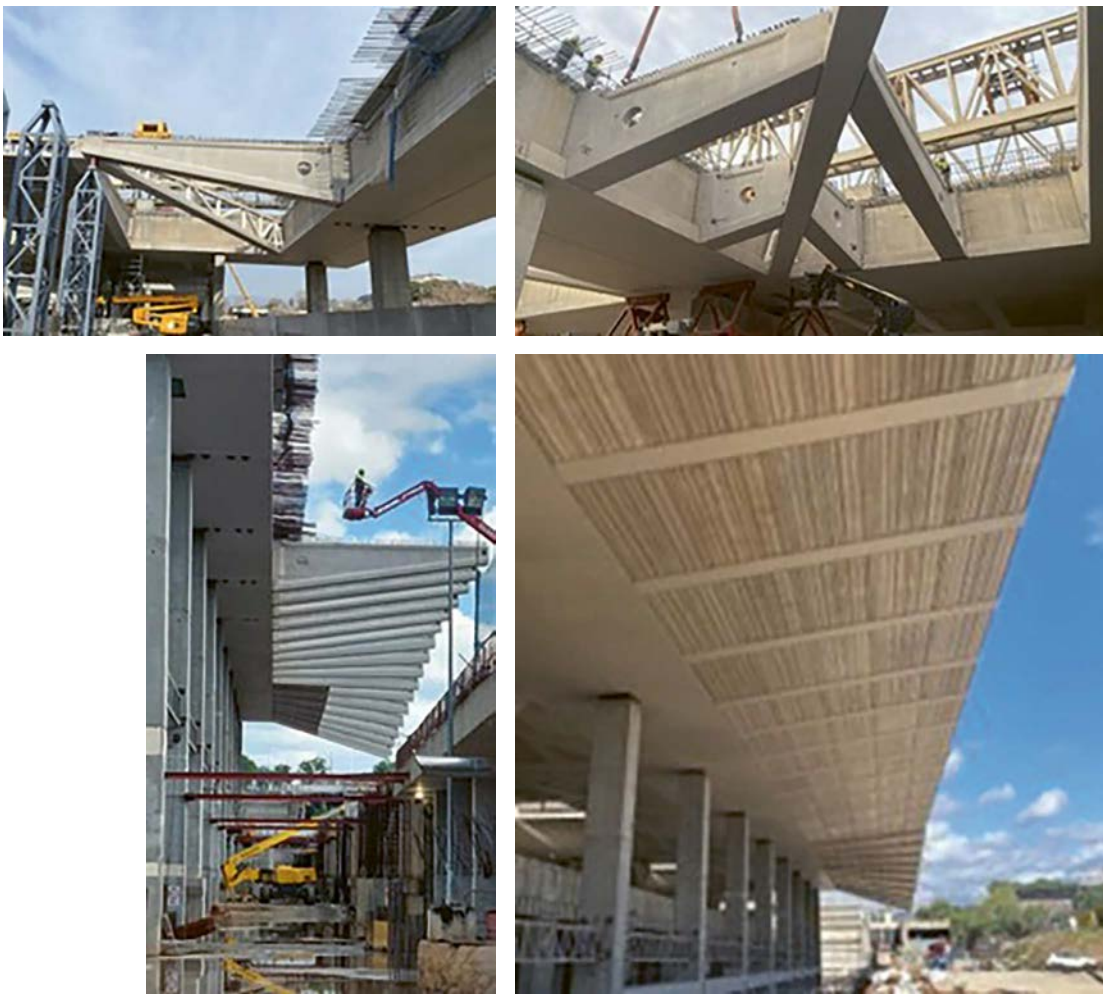

Figura 18. Imágenes durante la construcción de las cúpulas troncopiramidales y voladizos laterales.

Figura 19. Imagen inferior de una cúpula completada.

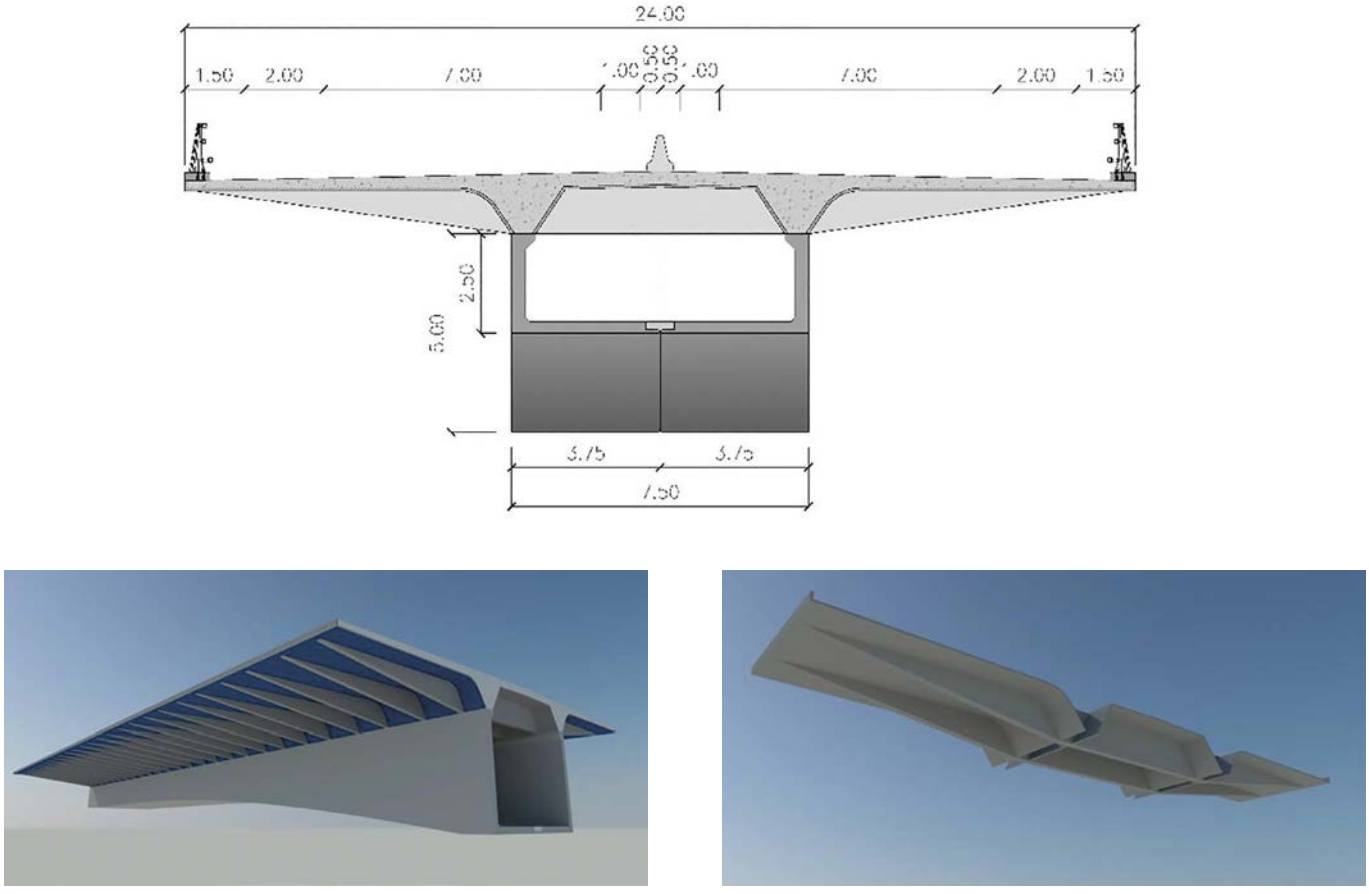

Figura 20. Propuesta de sección transversal con elementos prefabricados para puentes de grandes luces.

inferiores, la posibilidad de dar solución a cualquier tipo de trazado, condiciones geométricas del tablero y luces entre apoyos, la disminución muy significativa de los riesgos laborales, etc, etc, son factores que hacen que, a nuestro juicio, el uso de la prefabricación en la construcción de puentes de hormigón sea el sistema constructivo del futuro, como se viene demostrando con el uso cada vez más frecuente de estos sistemas en la actualidad. El viaje continúa, pero Toni, estoy convencido de que sin tu ayuda no hubiera sido posible. ¡Gracias Toni!

Referencias

[1] R. Bares et C. Massonnet., Le calcul des grillages de poutres et dalles orthotropes. . Dunod , 1966.

[2] Roy Edward Rowe, Concrete_Bridge_Design. 1962.

[3] Antonio. Marí, "Numerical simulation of the segmental construction of three dimensional concrete frames," Eng Struct, vol. 22, pp. 585–596, 2000.

[4] A. R. Mari and J. Montaner, "Continuous precast concrete girder and slab bridge decks," Proceedings of the Institution of Civil Engineers: Structures and Buildings, vol. 140, no. 3, 2000, doi: 10.1680/stbu.2000.140.3.195.

[5] J.J. Arenas, J. E. Jimeno y J. L. Lleyda, "Catalogo puentes nervados," Industrias Albajar, S.A. (I.A.S.A). 1968.

[6] J. Montaner y J. L. Lleyda, "Puentes nervados (III)," ALVI, S.A. 1984.

ACHE

MONOGRAFÍAS

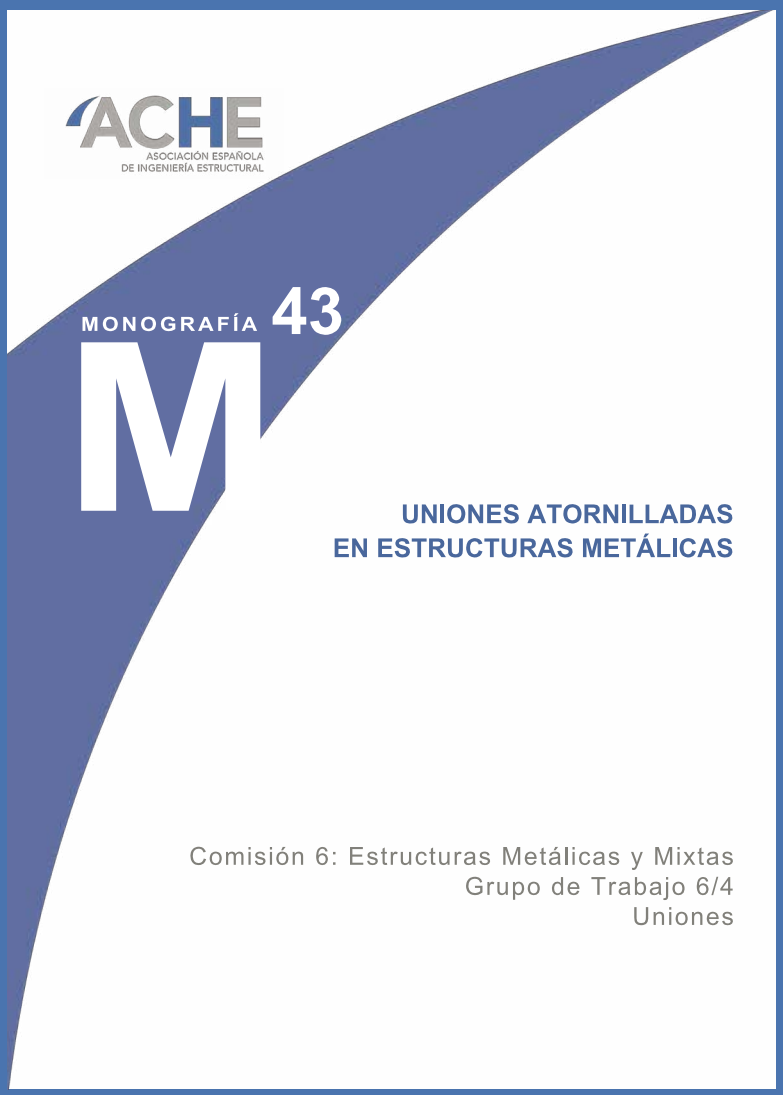

SECRETARÍA DE ACHE
Tel.: 91 336 66 98
www.e-ache.com

Disponible en **www.hormigonyacero.com**
https://doi.org/10.33586/hya.2025.4143

El hormigón pretensado en la construcción de puentes en Italia. Primeros pasos vacilantes y afirmación de la tecnología

Prestressed Concrete in Italian Bridge. Hesitant Beginnings and the Consolidation of the Technology.

Antonio Recupero[a]

[a] *Università degli Studi di Messina.*

Recibido el 21 de agosto de 2025; revisado el 29 de septiembre de 2025, aceptado el 9 de noviembre de 2025

RESUMEN

Este artículo analiza la génesis, la evolución y la afirmación del hormigón pretensado en la construcción de puentes en Italia, en el marco de un proceso internacional iniciado en Europa y Norteamérica a comienzos del siglo XX. A partir de las intuiciones pioneras de Eugène Freyssinet y de los aportes teóricos de Gustavo Colonnetti, se reconstruye el tránsito desde las primeras experimentaciones hasta la plena consolidación de la tecnología en la posguerra. El estudio se centra en el papel decisivo de ingenieros como Riccardo Morandi y Silvano Zorzi, cuyas obras ejemplifican tanto la dimensión artesanal y visionaria del pretensado como su progresiva industrialización. La narrativa pone de relieve cómo la innovación técnica se entrelaza con las biografías de sus protagonistas y con el contexto histórico de la reconstrucción italiana, transformando cada puente en un símbolo de audacia e ingenio. Finalmente, se subraya la vigencia del hormigón pretensado como técnica estructural consolidada, pero en constante evolución, capaz aún de abrir nuevas fronteras en la ingeniería contemporánea.

PALABRAS CLAVE: Hormigón pretensado, Puentes en Italia, Eugène Freyssinet, Gustavo Colonnetti, Riccardo Morandi, Silvano Zorzi, Reconstrucción de posguerra, Historia de la ingeniería estructural.

ABSTRACT

This article examines the origins, evolution, and consolidation of prestressed concrete in bridge construction in Italy, within the broader international development that began in Europe and North America in the early 20th century. Building on the pioneering insights of Eugène Freyssinet and the theoretical contributions of Gustavo Colonnetti, it traces the path from the first experimental applications to the full establishment of the technology in the postwar years. The study highlights the decisive role of engineers such as Riccardo Morandi and Silvano Zorzi, whose works exemplify both the artisanal and visionary dimension of prestressing and its progressive industrialization. The narrative underscores how technical innovation became intertwined with the lives of its protagonists and with the historical context of Italy's reconstruction, turning each bridge into a symbol of audacity and ingenuity. Finally, it emphasizes the continued relevance of prestressed concrete as a consolidated yet constantly evolving structural technique, still capable of opening new frontiers in contemporary engineering.

KEYWORDS: Prestressed concrete; bridges in Italy; Eugène Freyssinet; Gustavo Colonnetti; Riccardo Morandi; Silvano Zorzi; post-war reconstruction; history of structural engineering.

* Persona de contacto / *Corresponding author*:
Correo-e / *e-mail*: antonino.recupero@unime.it (Antonino Recupero)

Cómo citar este artículo: Recupero, A. (2026). El hormigón pretensado en la construcción de puentes en Italia. *Hormigón y Acero*. 77(308):287-302. https://doi.org/10.33586/hya.2025.4143

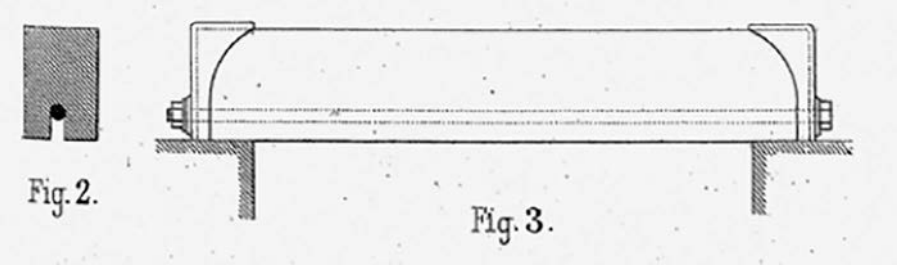

Figura 1. Viga de hormigón postensado diseñada por François Chaudy (1894). (Reproducida de [1]).

1. INTRODUCCIÓN

Cuando me fue propuesto contribuir con un artículo técnico para un número especial en homenaje a la trayectoria de dos grandes Amigos y Maestros, decidí no hablar de mí ni de aquello que yo sé hacer, sino más bien de las cosas que hacen grande nuestro oficio.

Narrar la génesis y la evolución de las construcciones en hormigón pretensado, tanto en el mundo como en Italia, constituye una empresa capaz de intimidar incluso al estudioso más experto. No en vano, tras haber elegido este tema hace ya más de un año, me encontré a menudo frente a la página en blanco con la sensación de enfrentarme a una síntesis tan ambiciosa como inevitablemente parcial. Cada intento de delinear sus contornos me pareció incompleto, como si la complejidad de la materia se escapara de cualquier delimitación precisa.

La tecnología del pretensado no hunde sus raíces exclusivamente en Italia: su origen es compartido, disputado entre experiencias europeas y norteamericanas, en un camino hecho de intuiciones, experimentos, fracasos y conquistas. Algunos estudiosos, que anteriormente se han acercado a este fascinante tema, sitúan el nacimiento de la precompresión en una intuición primitiva: la tensión preliminar como forma arcaica de solicitación de los artefactos [1]. Sus primeras aplicaciones podrían reconocerse quizá en estructuras simples, como tiendas o cobertizos temporales, donde ya se comprendía la necesidad de aplicar una fuerza previa para garantizar estabilidad y forma.

En aquella época, por supuesto, los fenómenos reológicos vinculados a las pérdidas de tensión en el tiempo eran del todo desconocidos. Sin embargo, empíricamente debía de intuirse que las estructuras sometidas a tracción exigían un pretensado periódico para mantener su eficiencia. Miles de años más tarde, un nuevo ejemplo de precompresión apareció con el nacimiento de la navegación a vela: el mástil principal de una embarcación, probablemente egipcia, se estabilizaba mediante obenques pretensados, dando origen a una estructura rudimentaria —pero eficaz— de hormigón pretensado en potencia.

Al término de esta larga fase arcaica emergen ejemplos más articulados, como los arcos de fábrica atados con elementos de madera (como en la Mezquita de Kairuán, siglo IX) o con tirantes metálicos (como en la Catedral de Parma, siglo XII). Estas técnicas, convertidas en clásicas durante el Renacimiento italiano, no utilizaban en sentido estricto la precompresión, o lo hacían de modo muy limitado, pero influyeron profundamente en el imaginario técnico de los pioneros de la precompresión moderna, desde Whipple [2] hasta Freyssinet [3], quienes a menudo se refirieron a ellas en sus escritos y proyectos.

Podría prolongarse largamente este viaje por la historia de las presolicitaciones: quizá no bastaría un volumen entero para analizar las numerosas patentes que, ya en el siglo XIX, comenzaron a abordar el tema de manera más sistemática. Entre ellas, una de las más significativas fue presentada en 1894 por François Chaudy, ingeniero francés que marcó la transición hacia la segunda fase de la historia del hormigón pretensado. Chaudy fue el primer europeo en proponer y comprender un sistema eficaz de precompresión —en la forma de postensado— aplicado a una viga de hormigón ya endurecida.

Su propuesta consistía en hormigonar una viga con una acanaladura longitudinal en su parte inferior. En ella se disponía una barra tensada contra tapones de hierro fundido en los extremos, generando un momento negativo uniforme a lo largo de todo el vano de la viga (Fig. 1). Chaudy intuía que este sistema podía extenderse también a otros materiales frágiles a tracción, como la fundición. Sus ideas fueron publicadas en el *Bulletin* de la Société des Ingénieurs Civils de París [4], entonces el principal órgano científico de la ingeniería francesa, precedidas por otra contribución dedicada al cálculo de placas delgadas.

2. A LOS ORÍGENES DE UNA REVOLUCIÓN: LOS PRIMEROS PASOS DEL PRETENSADO MODERNO

Entre 1903 y 1904, poco más de una década después de la publicación del artículo pionero de François Chaudy, un joven estudiante de ingeniería civil comenzaba a interrogarse sobre el potencial de la precompresión: su nombre era Eugène Freyssinet (1879–1962) (Fig. 3), destinado a convertirse en uno de los más grandes innovadores de la ingeniería estructural del siglo XX.

En aquellos años, Freyssinet asistía a las clases del profesor Charles Rabut (1852–1925), figura de primer orden en el panorama técnico francés y considerado entre los primeros en haber enseñado de manera sistemática el uso del hormigón armado desde 1896. Fue precisamente durante esas lecciones, dedicadas por un lado al comportamiento del hormigón armado y por otro al estudio minucioso de las deformaciones espontáneas o inducidas en las estructuras, donde Freyssinet

Figura 2. el puente de tres articulaciones de Praireal-sur-Besbre (1907). (Reproducida de [7]).

tuvo sus primeras intuiciones. Más tarde él mismo recordaría que la idea de la precompresión se le había ocurrido en aquel contexto, entre 1903 y 1904 [5],[6].

Uno de los primeros momentos de revelación tuvo lugar durante una visita a la obra de la ménsula de la Rue de Rome, junto a la estación de Saint-Lazare, donde observó aplicaciones prácticas de aquellas "deformaciones provocadas" de las que hablaba Rabut. El hecho de que su profesor dedicara parte del curso al estudio de los efectos de las deformaciones inducidas demuestra hasta qué punto el ambiente cultural era fértil para el desarrollo de ideas nuevas y radicales: conceptos como la deformación controlada, la presolicitación y la precompresión aún no estaban sistematizados, pero ya serpenteaban en el pensamiento técnico más avanzado.

Tras graduarse en 1905, Freyssinet no abandonó aquella intuición. Al contrario, la cultivó con tenacidad, buscando pronto ponerla en práctica. Entre 1906 y 1908 intentó dos aplicaciones experimentales de su idea de la deformación inducida como medio para mejorar la eficiencia estructural. Uno de estos intentos se reveló particularmente prometedor: en 1907 construyó el puente de tres articulaciones de Praireal-sur-Besbre (Fig. 2), con una luz de 26 metros, en el cual empleó técnicas de deformación controlada para facilitar el desencofrado.

Si bien el sistema no estaba aun formalmente definido como "precompresión", en aquella estructura pueden leerse ya, en filigrana, los principios fundamentales que habrían de revolucionar la manera de concebir las obras de hormigón armado.

3. EL ESTUDIO SISTEMÁTICO DE LA FLUENCIA: 1905–1937

En el primer cuarto del siglo XX, mientras en Estados Unidos el interés por los fenómenos reológicos del hormigón se iba consolidando —con figuras como Franklin R. McMillan [9] profesor en la Universidad de Minnesota, quien ya en los primeros años de la década de 1910 emprendió estudios pioneros que proseguiría hasta los años cincuenta—, en Francia ningún académico se había aventurado todavía a abordar de manera sistemática el fenómeno de la fluencia del hormigón. Una vez más, fue Eugène Freyssinet quien vino a llenar ese vacío, con el pragmatismo del ingeniero y la intuición del pionero.

Figura 3. Un joven Eugène Freyssinet. (Reproducida de [8]).

En 1911, durante la construcción del puente de Le Veurdre, Freyssinet se enfrentó a los efectos tangibles de la fluencia del hormigón. Desde aquel momento reconoció en este fenómeno el principal obstáculo para la utilización sistemática del hormigón pretensado. La ocasión para enfrentarlo científicamente llegó en 1922, cuando se le encomendó la realización de una obra ambiciosa: el puente de Plougastel, en Bretaña (Fig. 4). Con sus tres arcos de 186 metros cada uno, representaba un récord mundial y planteaba desafíos estructurales nunca antes afrontados.

Entre 1926 y 1929, Freyssinet llevó a cabo en esta estructura una serie de ensayos sistemáticos destinados a medir y comprender los efectos a largo plazo de las deformaciones viscosas. En arcos de semejante magnitud, las compresiones eran significativas, y el fenómeno se manifestaba en acorta-

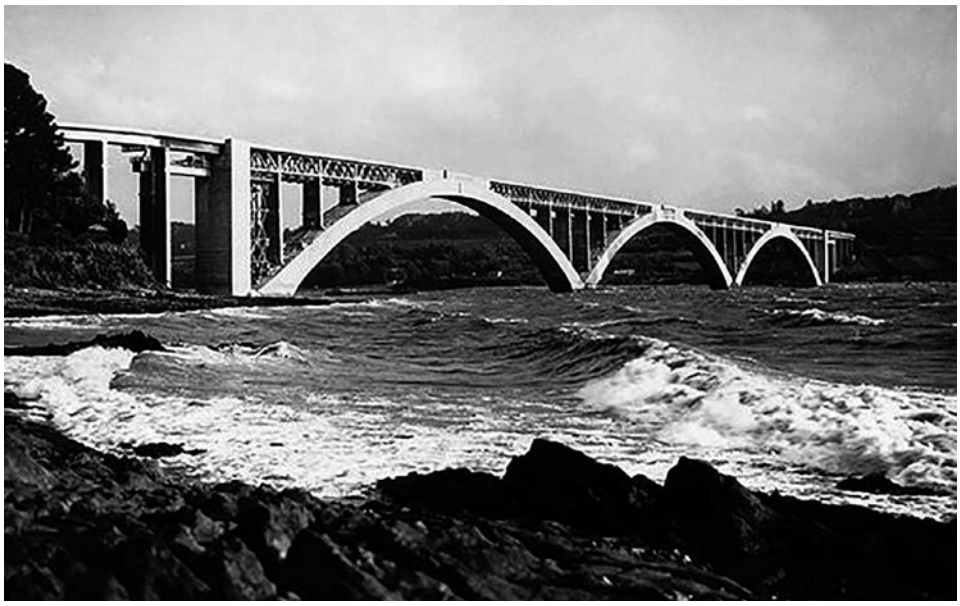

Figura 4. El puente de Plougastel, en Bretaña (Reproducida de [10]).

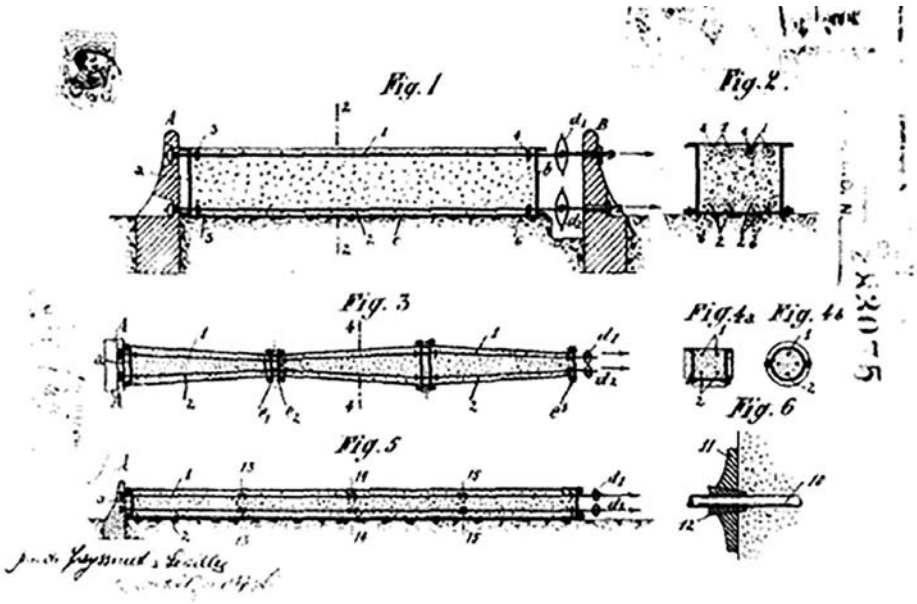

Figura 5. Sistema de precompresión para elementos de hormigón prefabricado, diseñado por E. Freyssinet y J. Seailles. (Reproducida de [13]).

mientos notables. Algunos resultados fueron publicados en 1930 [11], pero la versión íntegra de sus reflexiones sobre el tema no vería la luz hasta después de su muerte, en 1966 [12]. Ya entonces, sin embargo, su conocimiento de la viscosidad se contaba entre los más avanzados del mundo. Y, aun así, con su habitual lucidez, Freyssinet no dudaba en declarar cuánto quedaba todavía por comprender.

Entretanto, el trabajo en el frente tecnológico avanzaba. En octubre de 1928, junto a su colaborador Jean Seailles, Freyssinet obtuvo una patente destinada a marcar un hito: un sistema de hormigón pretensado mediante alambres tesados (Fig. 5).

Esta patente abarca todas las posibilidades de la tecnología de pretensado: (1) muestra lo que podrían ser modernos bloques de anclaje; (2), (4a) y (4b) las diferentes secciones transversales; (3) y (5) muestran las vistas en planta y sección; finalmente, (6) muestra el sistema de anclaje de el alambre.

Aunque la idea no era del todo nueva —otros, especialmente en Alemania, ya habían explorado la posibilidad de incorporar elementos pretesos en el hormigón prefabricado (entre ellos Doehring, Mandl, Lund, Zisseler, Siegwart, Mezzetti, Wettstein y Hoyer)—, su propuesta se distinguía al menos por dos aspectos cruciales [14].

En primer lugar, Freyssinet y Seailles sabían con exactitud dónde colocar la armadura para lograr un equilibrio óptimo de las solicitaciones. En segundo lugar, habían comprendido y cuantificado las pérdidas asociadas a la viscosidad y a la retracción, integrándolas en el proyecto de manera sistemáti-

Figura 6. Bloques de anclaje en la Estación Marítima de Le Havre, solución de rehabilitación de Freyssinet (1934). (Reproducida de [7]).

ca y ofreciendo soluciones concretas. Su patente —ampliada en 1930— era sorprendentemente detallada, con recomendaciones que anticipaban muchos principios de la moderna concepción estructural:

- empleo de hormigones de alta calidad y alambres de acero de altísima resistencia;
- sistemas diferenciados para la puesta en tensión;
- configuraciones poligonales de las armaduras;
- posibilidad de prefabricar elementos múltiples en serie sobre una misma bancada de pretensado;
- reducción o eliminación de la armadura a cortante, gracias a la precompresión.

Pero fue en 1933 cuando el destino del pretensado conoció una aceleración decisiva. En ese año, la estación marítima de Le Havre, recién terminada, comenzó a sufrir asientos del terreno excesivos. Convertido en un asunto de Estado, el proyecto parecía destinado al fracaso, hasta que Freyssinet fue llamado para intentar una intervención de rescate. Se trataba de una apuesta tanto técnica como personal, que él afrontó con audacia y determinación.

Aplicó la precompresión a gran escala: pilotes prefabricados compuestos por segmentos unidos mediante fuerzas de compresión, cabezales precomprimidos en las cimentaciones, cada elemento concebido para colaborar en la estabilización del conjunto. El resultado fue un éxito. La estación fue salvada, y toda Francia —junto con una parte significativa del mundo técnico europeo— fue testigo de ello. Era la consagración definitiva del hormigón pretensado como tecnología fiable e innovadora (Fig. 6).

En los años siguientes, entre 1935 y 1939, Freyssinet trabajó en Oued-Fodda, en Argelia (Fig. 7), donde construyó la primera presa del mundo en hormigón pretensado y uno de los primeros puentes con vigas prefabricadas con armaduras pretesas. Era el inicio de una nueva era para la ingeniería estructural.

4. LA PATENTE QUE LO CAMBIÓ TODO: EL NACIMIENTO DEL SISTEMA MODERNO DE POSTENSADO

En agosto de 1939, en vísperas de la Segunda Guerra Mundial, Eugène Freyssinet depositó la que pasaría a la historia como su patente más icónica y resolutiva: el sistema completo para el postensado del hormigón armado (Fig. 8). Con esta invención no solo consolidó décadas de experimentación, sino que definió de manera sistemática los componentes fundamentales de una tecnología destinada a revolucionar la ingeniería estructural del siglo XX.

El sistema patentado integraba, en un conjunto coherente y funcional, todos los elementos necesarios para hacer operativa la técnica del postensado:

- un dispositivo de anclaje capaz de transmitir eficazmente los esfuerzos al hormigón,
- un conducto para guiar los cables a través del elemento estructural,
- un gato hidráulico para aplicar la tensión de manera controlada,
- y finalmente un cable compuesto por alambres paralelos, en contraste con los cordones trenzados que serían adoptados en épocas posteriores.

En aquella época también era más fácil utilizar cables con alambres paralelos para insertarlos en los conductos.

Esta innovación representaba la síntesis de años de observaciones, fracasos, perfeccionamientos técnicos y reflexiones

Figura 7. Viga prefabricada de 19 metros de luz del puente sobre el río Oued-Fodda, Argelia, 1936. (Reproducida de [7]).

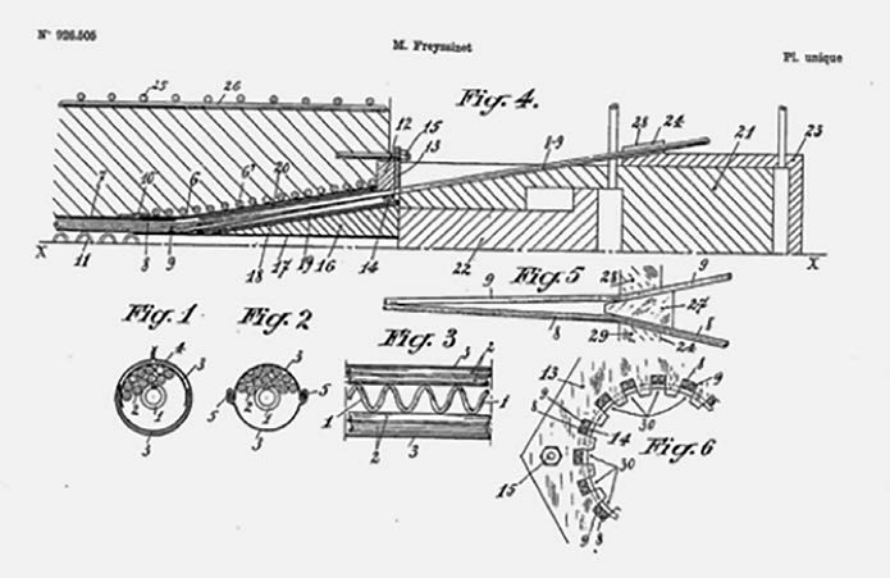

Figura 8. El primer sistema moderno de postensado con anclaje, diseñado por E. Freyssinet. Incluye: anclaje, cuña para bloquear los alambres, cable, vaina y gato hidráulico. (Reproducida de [1]).

teóricas. Con ella, Freyssinet hizo posible una aplicación industrial y confiable de la precompresión, liberándola de las incertidumbres empíricas que todavía aquejaban a muchos de sus predecesores. El hormigón postensado, tal como lo conocemos hoy, encontraba en esta patente su verdadera formalización.

En pleno conflicto mundial, en 1941, Eugène Freyssinet inició la construcción del puente de Luzancy, sobre el río Marne (Fig. 9), una obra que sería completada en 1945, al término de la guerra [15]. La estructura consistía en un pórtico prefabricado de 55 metros de luz, caracterizado por pilas-estribos triangulares y por una esbeltez estructural extraordinaria para la época. Aunque técnicamente se trataba de un pórtico, el puente presentaba problemáticas asimilables a las de una viga continua, ya que las células triangulares que lo componían eran de dimensiones reducidas y estaban sometidas a deformaciones e inestabilidades propias de elementos alargados.

La configuración utilizada en Luzancy fue retomada por Freyssinet en la posguerra para la reconstrucción de cinco puentes destruidos, también sobre el Marne, terminados en 1951. Entre ellos, el más célebre es, sin duda, el puente de Esbly, aunque todos compartían el mismo esquema estático y constructivo, con luces de hasta 74 metros. En estas obras, el ingeniero francés aplicó íntegramente su sistema de precompresión, poniendo en práctica lo desarrollado en las décadas anteriores y consolidando tanto la fiabilidad como la repetibilidad de la tecnología.

Estos puentes, realizados en un contexto de gran necesidad reconstructiva, representaron la primera demostración a gran escala de la eficacia y la versatilidad del hormigón armado pretensado. No solo marcaron un punto de inflexión en la técnica constructiva europea, sino también el reconocimiento definitivo del sistema Freyssinet como una de las herramientas ingenieriles más innovadoras e influyentes del siglo XX [3],[7],[11],[12], [15].

5. EL PAPEL DE GUSTAVO COLONNETTI EN EL DESARROLLO DEL PRETENSADO EN ITALIA

En febrero de 1939, mientras en Italia rige la fase más rígida de la política autárquica, Gustavo Colonnetti, desde las páginas de la revista *Il Cemento Armato*, intenta persuadir a técnicos, científicos y políticos italianos de que "*la economía de hierro no debe buscarse en absurdos regresos a formas constructivas decididamente y definitivamente superadas – ni en la adopción de no menos absurdos sucedáneos – sino persiguiendo serenamente, con todos los medios y recursos de la ciencia y de la experiencia, el diseño de una técnica más avanzada*" [13], [16].

En las palabras del entonces más célebre – y más incómodo – científico italiano en el campo de la construcción, se lee la condena de las imposiciones reaccionarias del régimen que favorecen un retorno a las tradicionales fábricas portantes y a las autárquicas cubiertas abovedadas. Una condena análoga se dirige al mismo tiempo a las paralelas experimentaciones visionarias que buscan sustituir la armadura de acero del hormigón armado con varillas de madera o de bambú, descuidando culposamente la exigua magnitud del módulo elástico de estos sucedáneos; experimentaciones – estas últimas – alentadas por los industriales del cemento, en la búsqueda de soluciones rápidas para afrontar la crisis derivada de la prohibición del empleo del hormigón armado en la edificación civil.

La técnica más avanzada a la que se refiere Colonnetti estaba ya en experimentación desde hacía algunos años en Europa, de la mano de Eugène Freyssinet en Francia y de Wayss & Freytag y Dywidag en Alemania: se trata del llamado "hormigón armado pretensado".

¿Por qué Colonnetti se siente tan fascinado por la precompresión, hasta el punto de considerarla la solución a los problemas económicos del mundo de la construcción? Pueden identificarse al menos dos razones.

Figura 9. Puente de Luzancy sobre el Marne. Luz de 55 metros. 1945. (Reproducida de [7]).

La primera es que el científico italiano, coincidiendo respectivamente con Eugène Freyssinet, Eduardo Torroja y Ove Arup, siempre había considerado el hormigón armado un material "absurdo", "extraño" y "difícil". Los dos elementos que lo componen tienen características de resistencia prácticamente opuestas, y la fuerza de su unión reside precisamente en esta total diversidad: uno absorbe las solicitaciones que el otro no es capaz de soportar. Pero la paradoja consiste en que la fiabilidad estática del hormigón armado se basa en la garantía de adherencia entre hierro y hormigón: adherencia que queda gravemente comprometida por la incapacidad del hormigón de resistir a tracción y, por tanto, de acompañar las deformaciones del acero. Las inevitables fisuras del hormigón en la zona traccionada habían suscitado dudas ya a principios de siglo, durante la fase pionera de la experimentación del hormigón armado. Ni siquiera la difusión, a finales de los años treinta, de cementos especiales de alta resistencia proporcionaba una solución al problema, porque las prestaciones de los conglomerados mejoraban solo en términos de resistencia a compresión, mientras no crecía en la misma proporción la resistencia a tracción. También la posibilidad de empleo de aceros de alta resistencia, que permitiría un notable ahorro de material, se ponía en entredicho precisamente por la débil resistencia a tracción de los hormigones y por su tendencia a fisurarse en cuanto se les imponían deformaciones de tracción más allá de un cierto límite.

Con la técnica de la presolicitación, en cambio – resulta claro para Colonnetti, así como para sus colegas europeos, que las relaciones recíprocas entre hormigón y hierro quedan completamente revolucionadas: la armadura ya no se utiliza para soportar una parte de los esfuerzos debidos a las solicitaciones externas, sino para crear en el hormigón estados de tensión preventivos de signo contrario a los que producirán dichas solicitaciones. La colaboración entre los dos materiales se ha transformado en una coacción: el acero precomprime al hormigón, el cual se hace capaz de resistir también a los esfuerzos de tracción gracias al benéfico mecanismo de la superposición de los efectos. Este juego de roles resuelve la paradoja de las fisuras en la zona traccionada y readmite sin vacilación el uso de aceros de alta resistencia, destinados a ser solicitados a elevadísimos esfuerzos de tracción, y de cementos especiales, llamados a resistir solo a solicitaciones de compresión. En el hormigón pretensado por la armadura tesada, el hormigón y el acero son solicitados de manera conforme a sus características de resistencia y se aprovechan al máximo: la técnica permite, por tanto, una concreta economía de material [17].

El segundo motivo por el que Colonnetti (Fig. 10) impulsa la precompresión es que la nueva técnica llega a sanar una herida abierta en el flanco de la ciencia de las construcciones. Colonnetti se expresa con gran claridad en relación con el valor de la teoría del hormigón armado formulada por Edmond Coignet y Napoléon de Tédesco más de cuarenta años antes, en 1894, y aún en uso en 1939: simplemente considera que aquellos métodos de cálculo eran «*carentes, absolutamente carentes de cualquier valor científico. Y ello no solo en el sentido de que, basados en hipótesis injustificadas e injustificables, conducen a conclusiones que la experiencia desmiente notoriamente, sino también en el sentido de que, al ser esas hipótesis entre sí incompatibles y contradictorias, a la teoría que de ellas se deriva no puede reconocérsele siquiera el carácter de una construcción lógica capaz de sostenerse a la luz de la crítica más elemental*» [18]. Quienes habían introducido aquellos cálculos en la normativa y en el uso no se hacían ilusiones sobre su valor; solo posteriormente el procedimiento había asumido un carácter definitivo, autorizando a aplicar a ciegas los métodos simples y conocidos de la teoría de la elasticidad.

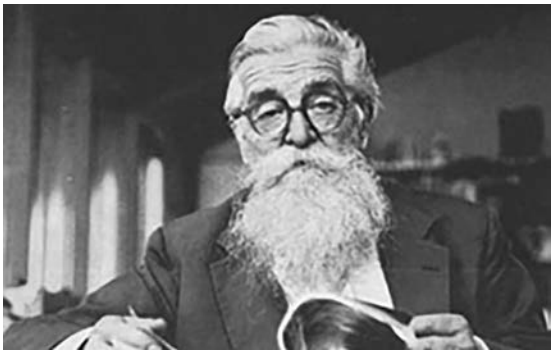

Figura 10. Gustavo Colonnetti. (Reproducida de [19]).

Colonnetti era un competente teórico: a partir de 1917, jovencísimo catedrático en Pisa se había ocupado de la definición del estado de equilibrio de un cuerpo en presencia de deformaciones no compatibles –definido por él como estado de coacción–; en 1924 había formulado un teorema de mínimo del trabajo de deformación, que aún lleva su nombre: una generalización del teorema de Menabrea en presencia de coacciones elásticas. Desde 1937 se dedicaba a reorganizar el corpus de la teoría matemática del sólido elástico, adaptándola a un sólido no perfectamente elástico, sino más bien elastoplástico, hipótesis más próxima al comportamiento del hormigón armado.

Sin entrar en el detalle de sus intuiciones, es cierto que en 1939 Colonnetti era muy consciente de cuánto los estados de coacción artificial podían mejorar el comportamiento estático de las construcciones y, paralelamente, de cuánto los métodos de cálculo "clásicos" del hormigón armado debían ser urgentemente sustituidos por una teoría rigurosa y científica.

En septiembre de 1939, Colonnetti elabora y publica un método de cálculo para las vigas con armaduras previamente tesadas, aplicación directa de su elegante teoría de las coacciones elásticas [20]. En esta nueva configuración las hipótesis de la teoría elástica resultan científicamente aplicables: la acción de compresión del acero sobre el hormigón, de hecho, catapulta el eje neutro fuera de la sección de hormigón, que resulta entonces toda reactiva, enteramente comprimida, además de homogénea, no estando ya llamada la armadura a resistir a las cargas externas. El comportamiento del material puede, por tanto, describirse perfectamente sin recurrir a improbables procedimientos de homogeneización del acero al hormigón o al empleo de coeficientes de valores ficticios y sin significado físico alguno.

La técnica de la precompresión del hormigón le permite, por una parte, promover la prohibición definitiva de aquel arbitrario método de cálculo y, por otra, dar respuesta y aplicación directa a sus valiosos estudios juveniles. La semilla sembrada no tarda en dar frutos y en Italia los jóvenes ingenieros comienzan a ensayar en las experimentaciones.

6.
LOS PRIMEROS ENSAYOS SOBRE ELEMENTOS DE HORMIGÓN PRETENSADO EN ITALIA

Los ingleses utilizan el término *serendipity*, que me permito traducir como *serendipia*, para indicar un hallazgo interesante o valioso que no se estaba buscando. Sin duda, de esta cualidad estaban dotados los dos jóvenes ingenieros Pietro Noli y Giuseppe Marioni cuando, habiendo conocido por los textos fundamentales de Eugène Freyssinet la existencia de la precompresión, se propusieron experimentar sus efectos en un forjado de viguetas y bovedillas [21].

Estamos en 1942, la Segunda Guerra Mundial está ya en pleno desarrollo y ciertamente no abundan los medios técnicos para realizar semejantes ensayos. Esto no desanima a los dos jóvenes ingenieros, que consiguen montar un rudimentario banco de pruebas con medios de fortuna. Las armaduras de precompresión están constituidas por cuerdas de piano que, en aquel tiempo, representaban la única fuente comercial de acero de altísima resistencia. Por ello, el acero para pretensado aún hoy en ocasiones se denomina *acero armónico*.

Sin embargo, para la validación de los primeros resultados experimentales obtenidos con medios precarios, es necesaria la realización de pruebas más detalladas bajo la supervisión de laboratorios oficiales. Los primeros prototipos de viguetas pretensadas enviados al Politécnico de Milán producen, inesperadamente, un resultado negativo, aunque no desde el punto de vista experimental, ya que las viguetas ni siquiera fueron probadas, sino desde el de las relaciones públicas. El hecho es que el joven asistente al que se le había sometido la cuestión de las viguetas pretensadas en vista de la experimentación, al no haber comprendido de inmediato que las viguetas estaban ya realizadas y listas para ensayarse, desaconsejó su ejecución sosteniendo que la precompresión de un elemento esbelto provocaría su inestabilidad. La equivocación no favoreció las relaciones posteriores entre los inventores y algunos importantes docentes del Politécnico de Milán, que desde entonces y durante más de una década miraron con sospecha y desconfianza, e incluso obstaculizaron, la tecnología del pretensado, calificándola de algo antinatural o de "un procedimiento que transformaba la estructura en un queso gruyer."

Las primeras pruebas de carácter oficial se realizan, como puede imaginarse en medio de grandes dificultades, en Zúrich en 1944. A raíz del interés de Colonnetti, las pruebas se llevan a cabo en el laboratorio dirigido por el Prof. Roš, bajo el control del entonces joven ingeniero Franco Levi. Tanto Colonnetti como Levi eran en aquel tiempo, como se verá más adelante, refugiados en Suiza y se encontraban en Lausana.

7.
COLONNETTI Y LA ESCUELA DE LAUSANA

En 1943 Colonnetti, ya rector del Politécnico de Turín y conocido por su firme antifascismo, se ve obligado al exilio en Suiza para escapar de la persecución fascista. En Lausana obtiene un puesto en la École des Ingénieurs de la Universidad de Lausana, convirtiéndose en su dirigente y docente.

Su principal obra es la concepción y organización de una suerte de "***universidad italiana en el exilio***": funda y dirige el *Campo Universitario Italiano* de Lausana (además de otros campus análogos en ciudades suizas como Friburgo, Ginebra, Neuchâtel, Huttwil y Mürren), destinados a estudiantes militares internados y refugiados.

El Campo de Lausana se inaugura oficialmente el 26 de enero de 1944, con Colonnetti al frente de la iniciativa. Participan en él más de doscientos estudiantes y entre los docentes figuran intelectuales de relieve como Gino Fano, Luigi Einaudi, Amintore Fanfani, Concetto Marchesi y otros.

Entre sus asistentes se recuerdan Franco Levi y Aldo Favini, y entre sus alumnos Silvano Zorzi, todos ellos posteriormente protagonistas de la afirmación de la técnica del pretensado en la posguerra, gracias a las enseñanzas de Colonnetti en el período suizo. En efecto, Colonnetti en aquel tiempo no escatimó lecciones, no solo sobre los fundamentos teóricos del pretensado, sino también sobre los aspectos prácticos de la nueva tecnología.

Finalmente, tras la liberación, regresa a Italia en diciembre de 1944, transportado en un vuelo militar a Roma gracias a una precisa solicitud del gobierno provisional italiano, y se convierte en Presidente del *Consiglio Nazionale delle Ricerche* (*CNR*).

8. DESARROLLO DEL HORMIGÓN ARMADO PRETENSADO EN ITALIA EN LA INMEDIATA POSGUERRA

Un hecho resulta emblemático para la historia de Italia. En la noche entre el 3 y el 4 de agosto de 1944, las tropas alemanas en retirada ponen en marcha la Operación *Feuerzauber* ("Hechizo de fuego"), destruyendo todos los puentes sobre el Arno en Florencia, con excepción del Ponte Vecchio. Las explosiones comienzan a las 22:00 del 3 de agosto y se suceden durante toda la noche. El primero en ser demolido es el Ponte alle Grazie; a medianoche vuela el Ponte Santa Trinita y, posteriormente, caen el Ponte alla Carraia, el Ponte San Niccolò y el Ponte alla Vittoria. Finalmente, son demolidas las construcciones situadas en los accesos al Ponte Vecchio, lo que hace que el paso resulte inutilizable, aunque el puente en sí permanezca en pie.

El Ponte Vecchio se libra de la destrucción, lo que alimenta de inmediato mitos y leyendas. Algunos sostienen que hubo una orden directa de Hitler, quien habría querido salvar el puente por su belleza y valor artístico; otros afirman que intervino el cónsul alemán Gerhard Wolf, siempre comprometido con la salvaguardia del patrimonio artístico florentino. Una versión alternativa, aparecida solo en los últimos años, sugiere que algunos orfebres locales sabotearon las minas cortando los cables; se cuenta el testimonio de un ayudante de los orfebres, un tal Burgasso, considerado por los alemanes un insensato, que habría retirado los explosivos durante la colocación.

En cualquier caso, aunque permaneciera en pie, el Ponte Vecchio quedó inutilizado a causa de las demoliciones de las viviendas circundantes y de las fortificaciones de primera línea construidas por los alemanes en la orilla opuesta. El Arno se convirtió en un obstáculo físico y psicológico para la ciudadanía y para las tropas aliadas, dividiendo la ciudad en dos. Solo en las horas posteriores a la liberación, los Aliados construyeron puentes Bailey provisionales (por ejemplo, en las inmediaciones del Ponte Santa Trinita) para restablecer las conexiones.

Florencia no fue un caso aislado: al final de la Segunda Guerra Mundial, la red de infraestructuras italiana se hallaba reducida a escombros. Más de 10.000 puentes carreteros y ferroviarios habían sido destruidos por los bombardeos o volados durante las retiradas; las grandes arterias de comunicación estaban interrumpidas, los firmes deteriorados, las estaciones y los puertos inutilizables. En muchas zonas del país se recurría a pasos provisionales de madera o a puentes Bailey suministrados por los Aliados, pero la circulación de mercancías y personas seguía siendo lenta y precaria. La reconstrucción requería soluciones rápidas, resistentes y económicas en el uso de materiales: en este contexto, el hormigón armado pretensado, aún poco conocido en Italia, se impuso como tecnología innovadora, abriendo el camino a una nueva etapa de la ingeniería estructural.

Colonnetti no pierde tiempo: en calidad de presidente del CNR, el 1 de julio de 1945 instituye en el Politécnico de Turín un "*Centro de Estudio sobre los Estados de Coacción Elástica*", confiando su dirección operativa a su discípulo predilecto, Franco Levi. Es el momento de pasar de la teoría a la reconstrucción concreta del país. No se trata de un simple laboratorio: el Centro, por encargo del Ministerio de Obras Públicas, tiene la misión estratégica de examinar, aprobar y orientar todos los proyectos italianos de estructuras de hormigón armado pretensado.

Las actividades del Centro se desarrollan en un clima de gran dinamismo: la reconstrucción de posguerra demanda puentes, viaductos e infraestructuras modernas, y el hormigón armado pretensado se presenta como la tecnología ideal, ligera, duradera y económica en el uso del acero. En sus dos primeros años de vida, el Centro publica más de cuarenta artículos científicos —veinte de ellos firmados o editados por Levi—, perfecciona métodos de cálculo y procedimientos de prueba. En 1946 organiza la primera conferencia nacional sobre el hormigón armado en la posguerra, acompañada de espectaculares ensayos de laboratorio sobre una viga pretensada de doce metros y un forjado [22], [23], [24].

Dos años después de la creación del Centro, la época estaba madura y, bajo el impulso del propio Colonnetti, Italia legisla por primera vez sobre la técnica del pretensado: el 20 de diciembre de 1947 se promulga el Decreto del Capo Provvisorio dello Stato (DCPS) n. 1516 - *Norme per la esecuzione e l'impiego delle strutture di cemento armato precompresse*. Publicado en la *Gazzetta Ufficiale*, Serie General n.° 8 del 12-01-1948, en su artículo 2 establece: «Todos aquellos, incluidos los organismos y oficinas estatales, que en el territorio de la República Italiana pretendan ejecutar estructuras pretensadas, independientemente de las demás disposiciones del Real Decreto de 16 de noviembre de 1939, n.° 2229, están obligados a someter los cálculos y procedimientos constructivos a la previa revisión del Consejo Superior de Obras Públicas, que otorgará la eventual aprobación».

La promulgación del Decreto Ministerial de 1947, que regula el uso del pretensado en Italia, convierte al Centro en paso obligado para los proyectistas: centenares de esquemas estructurales pasan bajo la lupa de Levi y sus colaboradores, entre ellos Giorgio Macchi y Piero Marro, quienes detectan errores, sugieren mejoras y transforman cada proyecto en una lección técnica. Paralelamente, el Centro se convierte en semillero de innovación: aquí, en 1959, nace el sistema de anclaje Tecnicavi, patentado por Macchi y Levi, destinado a un gran éxito internacional.

Entre 1945 y 1955, el Centro acompaña la construcción de obras emblemáticas de la reconstrucción italiana, como los viaductos de la ***Autostrada del Sole***, y contribuye a la creación de una auténtica escuela italiana del pretensado. Cuando la actividad se cierra, en 1961, deja como herencia un patrimonio de conocimientos, métodos y proyectistas que marcará durante décadas la ingeniería estructural del país.

En 1955, en un contexto de creciente difusión del pretensado y de ampliación de la red nacional de infraestructuras, la función de aprobación pasa al Consejo Superior de Obras Públicas, que instituye una Comisión especial para el hormigón armado pretensado. De ella forman parte tres de los mayores expertos en la materia: Franco Levi, garante de la con-

tinuidad científica con la experiencia turinesa; Carlo Cestelli Guidi, prestigioso profesor de Técnica de las Construcciones en La Sapienza y referente para la codificación normativa; y Giuseppe Rinaldi, ingeniero y docente, autor de uno de los primeros manuales italianos sobre hormigón armado pretensado, que aporta a la comisión su competencia técnica y su experiencia en la formalización de las reglas para el cálculo, el diseño y el ensayo de las estructuras pretensadas. Este paso marca la transición de una gestión fuertemente centralizada en el ámbito universitario a un control institucional de alcance nacional, acompañando la fase de máxima expansión del hormigón armado pretensado en la Italia de posguerra.

En ese período aparecen los primeros textos sobre el tema en la literatura técnica italiana, y los proyectistas comienzan a considerar una tecnología que sale de los laboratorios de investigación [25], [26], [27]. De hecho, con la promulgación del DCPS n.º 1516/1947, el hormigón pretensado puede ser empleado en la construcción de obras; además, dicho decreto, debido al procedimiento de aprobación, permite una trazabilidad completa de las intervenciones realizadas en el territorio nacional.

Sería tarea ardua reconstruir el desarrollo a través de cada una de las obras, puesto que, a partir de la promulgación del decreto, estas comienzan a multiplicarse sin tregua, como brotes que florecen en cada estación.

Por ello, con la certeza de que una narración centrada en las obras resultaría imposible, se ha optado por contar la historia no a través de las construcciones, sino de sus proyectistas; porque detrás de cada creación, sobre todo cuando se trata de una obra primera, siempre hay un hombre —con sus dudas, sus inquietudes y, sobre todo, su coraje. Sí, el coraje de transformar lo que había sido experimentado en el laboratorio en una realidad concreta; de pasar del objeto de estudio de los investigadores a una estructura viva, tangible, funcional y segura.

En 1949 nace la Asociación Nacional Italiana del Hormigón Armado Pretensado (ANICAP). Las primeras aplicaciones se sitúan entre ese mismo año y los primeros años cincuenta, y cuentan con la participación de proyectistas ya consagrados —como Morandi, Rinaldi y Cestelli Guidi— junto a técnicos de empresa, como Carlo Pradella de SACAIM, y jovencísimos profesionales, entre los cuales Silvano Zorzi.

Todavía no existe una norma técnica de referencia: a colmar ese vacío es el ingeniero Levi, que asume la responsabilidad de validar, aprobar y ensayar los proyectos.

El primer viaducto en hormigón armado pretensado lleva la firma de Carlo Pradella, ingeniero véneto que, aunque no se había formado oficialmente en la escuela de Lausana, mantenía estrechas relaciones con Zorzi. Se trata del viaducto de Vallesella sobre el Piave (1949) (Fig. 11), realizado en el marco de las obras para la planta hidroeléctrica Piave–Boite–Maè: un tablero en hormigón armado pretensado con vigas apoyadas sobre pilas formadas por celosías de hormigón armado, con un total de siete vanos de 24 metros.

La elección del pretensado por parte de SACAIM responde a una voluntad precisa: adoptar sin vacilaciones una tecnología nueva y prometedora. Para esta obra, Pradella opta por la patente Freyssinet. Los alambres de acero armónico se recubren de betún y luego de papel; una técnica constructiva que nunca más se repetiría en Italia.

Figura 11 - Viaducto de Vallesella sobre el Piave (1949) (Reproducida de [28]).

En el congreso de ANICAP de 1954, en la memoria de Marletta, se lee: «*Las primeras autorizaciones ministeriales para puentes en hormigón armado pretensado se remontan a mayo de 1949; desde entonces se han aprobado 72 proyectos, muchos de ellos ya realizados y en servicio, mientras que otros se encuentran en fase de ejecución o de proyecto*» [29].

La difusión comienza a ser sorprendentemente rápida: ya a finales de 1961 se cuentan cerca de quinientos puentes y viaductos ejecutados o en vías de finalización. En el solo tramo Milán–Florencia de la Autostrada del Sole se realizan hasta treinta y seis obras en hormigón armado pretensado, con un desarrollo total de 7.5 kilómetros.

En la fase inicial de desarrollo, el empleo del pretensado en Italia se orienta principalmente hacia esquemas estructurales isostáticos, menos sensibles a los estados de coacción inducidos artificialmente por los cables tensados. Esto no impide, sin embargo, alcanzar luces y configuraciones geométricas significativamente superiores a las realizables con el hormigón armado ordinario.

El primer ejemplo nacional de puente en hormigón armado pretensado es, como se ha dicho, el viaducto proyectado por Carlo Pradella, al que sigue poco después el puente sobre el torrente Samoggia, en las cercanías de Bolonia, realizado por Giuseppe Rinaldi entre octubre de 1949 y enero de 1950. Este último, constituido por un único vano de 26 metros, está formado por dovelas prefabricadas solidarizadas mediante cables postensados y dispositivos de pretensado Magnel: una viga simplemente apoyada, sobria y esencial, pero destinada a abrir el camino a nuevas experimentaciones.

9. RICCARDO MORANDI, EL PROYECTISTA VISIONARIO

Pocos meses después, en Canneto, cerca de Empoli (Fig. 12), se completa el puente sobre el río Elsa, diseñado por Riccardo Morandi y construido por la empresa Fratelli Giovannetti [30]. Con sus 40 metros de luz, la estructura se distingue por la claridad y la modernidad del esquema: cuatro vigas longitu-

Figura 12- R. Morandi, puente sobre el Elsa en Canneto, cerca de Empoli, 1950 (ACS, Morandi). (Amablemente proporcionada por el Eng. E. Codacci Pisanelli).

dinales en doble T prefabricadas, unidas por siete diafragmas y perfectamente armados a cortante. Los cables de pretensado, compuestos por 16 alambres de acero de 5 mm, discurren siguiendo trazados parabólicos en el interior del alma de las vigas y encuentran anclaje en un sistema inédito: la primera patente de Morandi, íntegramente en acero y capaz de permitir el retesado. Se trata de una alternativa audaz a las cuñas perdidas típicas de los sistemas Freyssinet y Magnel.

Con esta obra Morandi hace su entrada en el sector de los puentes de hormigón pretensado. No es un debutante: ya desde 1948 elabora soluciones originales de tesado que, a lo largo de su carrera, se transformarían en seis variantes sucesivas (M1…M6). Innovador incansable y espíritu abierto a la experimentación, aborda con decisión todos los principales tipos estructurales de su tiempo, transformándolos en ocasiones para inventar.

En 1952, el puente de Giunture sobre el río Liri, en la provincia de Frosinone, marca una de sus primeras afirmaciones. Con una luz teórica de 61.60 metros, se presenta como un conjunto de tres pórticos paralelos, con pilas moldeadas empotradas en la base y sin apoyos intermedios: una solución que se adapta bien al carácter impetuoso del río, refractario a pilas en el cauce. El tablero, íntegramente pretensado, es una precisa composición de tres vigas cajón de dos metros de altura y unos siete de ancho, ensambladas en obra a partir de dovelas prefabricadas. Los diafragmas y la losa, en cambio, son de hormigón armado ordinario.

Un año más tarde, para la empresa Ferrocemento, Morandi concibe en Sicilia un tablero reticular, compuesto por cinco vigas cajón y siete diafragmas, también prefabricados y pretensados en obra sobre los ríos Agrò y Fiumidinisi (Fig. 13).

Casi de forma consecutiva, en Benevento, tomó forma el puente San Nicola: un vano central de 80 metros, dos laterales de 20, y una idea más evolucionada respecto al puente de Giunture. Aquí el tablero, formado por cuatro cajones longitudinales empotrados en las pilas, renuncia a servirse de estas últimas para equilibrar las solicitaciones. Los cables de pretensado, libres, se prolongan más allá, extendiéndose a lo

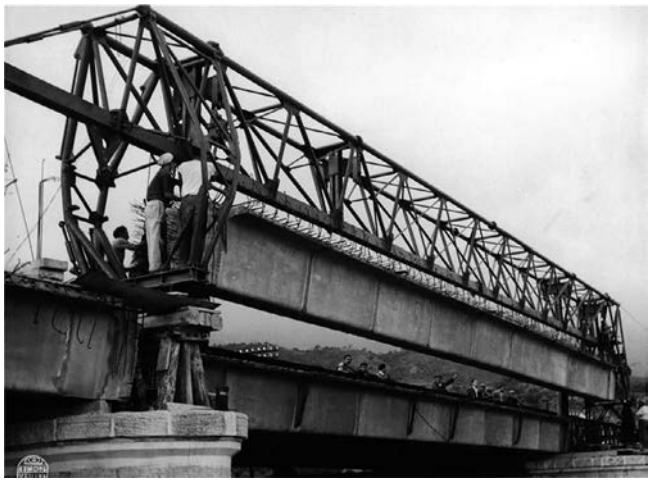

Figura 13 - Vigas cajón para los tableros de los viaductos Agrò y Fiumidinisi. (Reproducida de [31]).

largo de los voladizos laterales hasta superar los taludes: un preludio al concepto de viga balanceada que Morandi perfeccionaría en los años siguientes.

En torno a 1960, la visión estructural de Morandi alcanza plena coherencia y originalidad. Convencido de que el pretensado debía emplearse con la máxima eficiencia, intuye que la reducción de las solicitaciones de flexión no requiere pórticos complejos, sino que puede lograrse equilibrando los momentos positivos del vano con momentos negativos generados en el paso sobre las pilas.

De esta intuición nace la viga balanceada con tirantes inferiores: un voladizo simétrico dispuesto sobre dos pilas inclinadas, cuyas extremidades se hallan conectadas a la base mediante elementos de tracción. La posibilidad de variar tanto la inclinación de las pilas como el pretensado de los tirantes ofrece una libertad proyectual inédita, adaptable a contextos diversos. Morandi recupera así un principio antiguo y lo transforma en un instrumento moderno y versátil, capaz de generar soluciones hasta entonces inimaginables.

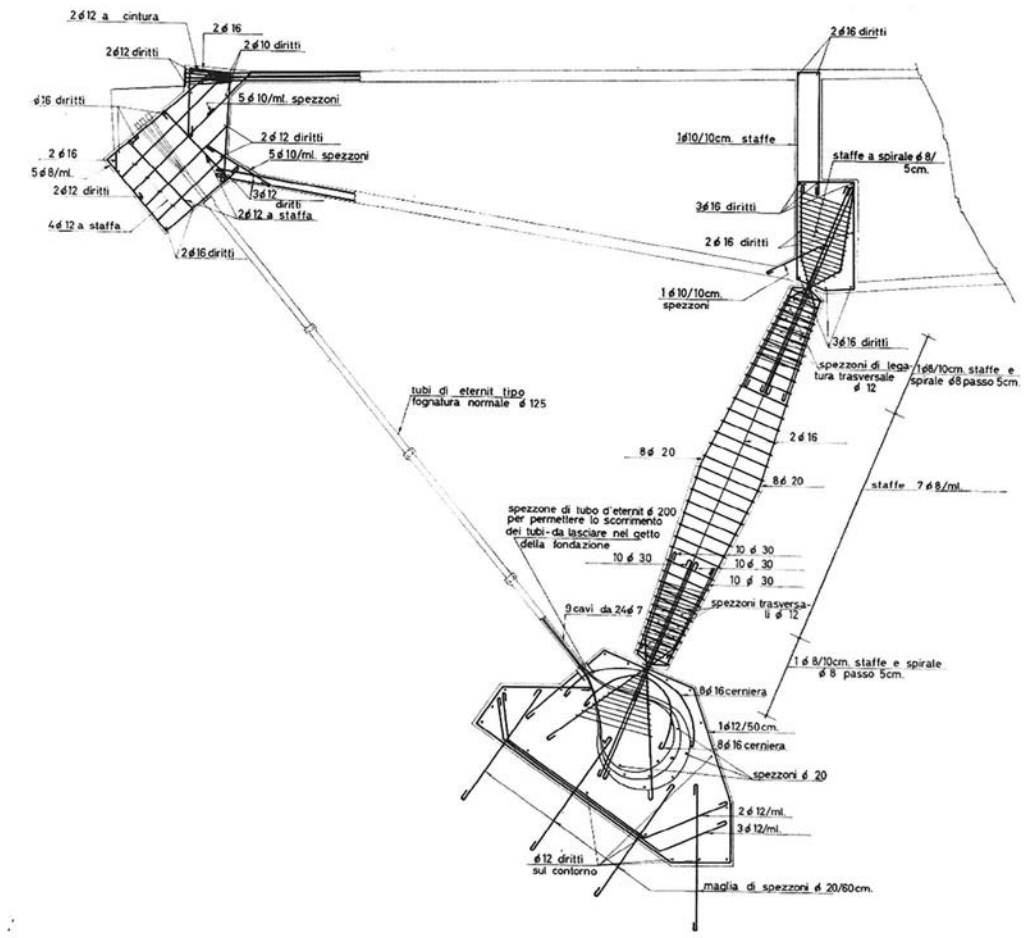

Figura 14 - Sistema equilibrado del puente Cerami. (Reproducida de [32]).

El primer ejemplo de esta tipología es el puente sobre el Cerami en Gagliano Castelferrato (Enna) [32] (Fig. 14), proyectado para la empresa Ferrocemento en 1953-54: un vano central de 58.80 metros, dos tramos laterales de 8.50, y tres cajones centrales que, al acercarse a las pilas, se funden con una contralosa.

Algunos años más tarde, entre 1958 y 1959, el mismo principio reaparece en el paso superior de la Via Olimpica en Roma: una viga única, con extremidades en voladizo bloqueadas por tirantes y apoyada sobre nueve caballetes distantes dos metros entre sí. Longitud total: 55.40 metros; luz central: 38.60. Conceptualmente afín fue el puente de Sulmona (1960-62), que une el centro histórico con el nuevo barrio de Piana della Potenza: similar en el esquema, pero de mayores proporciones y con detalles constructivos más refinados.

Morandi amaba explorar posibilidades, perseguir tipologías óptimas para cada puente, como un artesano que nunca se contenta con replicar una obra ya realizada. Ya en 1960 había construido un patrimonio suficiente para garantizarle un lugar en los manuales de ingeniería. Sin embargo, la tipología que más que ninguna otra se identificará con su nombre está aún por llegar: el puente atirantado de hormigón pretensado [32].

La idea nace casi por casualidad; en Venezuela, llamado por la empresa *Precomprimido* de los hermanos Giovannetti, Morandi se enfrenta al desafío de un puente de gran luz. Él, el "Señor de los arcos", que sabía doblegarlos a su diseño para superar obstáculos imposibles, debe cambiar de tipología. Allí, en la inmensa extensión del Lago de Maracaibo, el arco no encuentra ni espacio ni armonía. Entonces su mente se abre a una nueva invención: el puente atirantado homogenizado.

La viga atirantada se convierte así en su nuevo alfabeto. En hormigón pretensado puede asumir dos formas: anclada al terreno mediante una estructura de contrapeso, o bien con tirantes autoanclados al tablero. En todo caso, Morandi deseaba que los tirantes estuviesen envueltos en vainas de hormigón pretensado por dos buenas razones: garantizar la estanqueidad protege las armaduras y, además, los tirantes de hormigón pretensado confieren a la estructura una rigidez adicional en servicio. Lamentablemente en el Viaducto del Lago Maracaibo (Fig. 15), por razones contingentes, y solo allí, tendrá que renunciar a ello.

Al final, de esta elección nace una serie de obras convertidas en leyenda: el Viaducto General Rafael Urdaneta en Maracaibo - Venezuela (1962), el Viaducto Polcevera en Génova (1967), el Viaducto della Ansa del Tevere en Roma (1967), el Puente del Wadi al-Kuf en Libia (1967-71), el Viaducto del Pumarejo en Colombia (1970-74) y el Viaducto del Carpineto en Italia (1977). Junto a estas estructuras principales merecen mención los viaductos de acceso, tanto en Maracaibo como en el valle del Polcevera, con sus pilas en pórtico espacial, esbeltas y casi invisibles, concebidas para dar mayor relieve a la esencialidad de las estructuras atirantadas.

Figura 15 - Viaducto General Rafael Urdaneta en Maracaibo - Venezuela (1962) (Reproducida de [33]).

Solo tres de estos puentes se encuentran en Italia, pero todos ellos pertenecen a un mismo hilo conceptual, desarrollado con creciente coherencia y refinamiento. Con el Carpineto, Morandi alcanza la perfección de los detalles constructivos, justo en el momento en que el mundo comienza a abandonar los tirantes de hormigón pretensado en busca de nuevos caminos. Y, por desgracia, el 14 de agosto de 2018, el pilar 9 del viaducto Polcevera colapsa, víctima del descuido humano y de la ausencia de mantenimiento. La obra de Morandi fue reemplazada en 2020, pero permanece en la memoria como un capítulo irrepetible de la historia de la ingeniería.

10. SILVANO ZORZI, EL PROYECTISTA PROLÍFICO

Pero entre los artífices de la reconstrucción de la posguerra no puede ciertamente olvidarse a Silvano Zorzi, véneto de nacimiento, pero hijo de aquella escuela fundada por Colonnetti, exiliado en Lausana junto a él. En 1939 Zorzi se inscribe en la facultad de ingeniería de su ciudad natal, Padua, pero con el estallido de la guerra es llamado al servicio militar y se ve obligado a abandonar los estudios. El armisticio del 8 de septiembre de 1943 lo sorprende bajo las armas, en el Norte: con tal de no colaborar con la República de Saló y no arriesgar la deportación a Alemania, huye a Suiza. Apenas terminada la guerra, recién graduado, es inmediatamente contratado en el Centro de Estudios sobre los Estados de Coacción Alástica de Colonnetti. Pero Zorzi no es un investigador de laboratorio y, en cuanto puede, se dedica al diseño de puentes. La experiencia suiza lo había marcado para siempre: el hormigón armado pretensado y el diseño permanecerán como los elementos clave de su modo de concebir las estructuras; de la compresión previa del hormigón hace una auténtica fe y en Italia logra dominarla como pocos.

Aún no treintañero, se enfrenta al diseño del puente de servicio con tablero inclinado para la central hidroeléctrica del Mucone (1950) (Fig. 16), con una luz de la parte pretensada de 37.50 m (pendiente 38.6%). Poco después abre un estudio de ingeniería con su propio nombre, con sede en Milán, que en 1961 se convertirá en IN.CO., Ingegneri Consulenti [34].

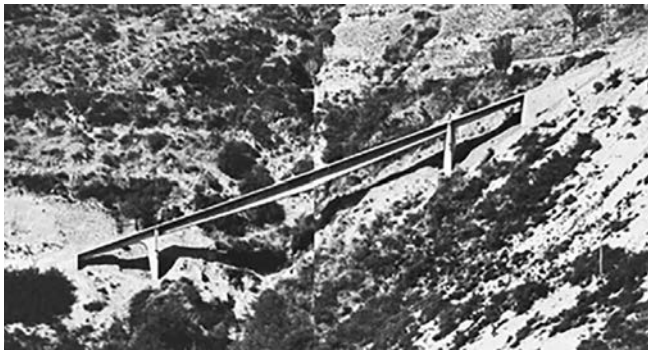

Figura 16 - Puente del Mucone (1950) (Reproducida de [35]).

Para la empresa Rizzani, sobre el Po – Autostrada del Sole en Mortizza, cerca de Piacenza, Zorzi proyecta en 1956 un viaducto compuesto por dieciséis vanos. Los tableros, simplemente apoyados entre los pilares, se distinguían por una luz notable de 60.80 m, una anchura de 18.50 m y un canto de 3.20 m. La longitud total del viaducto era de 1.176.00 m.

Es la época de la construcción de la Autostrada del Sole: las empresas compiten por contratar a los mejores proyectistas, y Silvano Zorzi junto con Giorgio Macchi son llamados por Astaldi S.p.A. para dos proyectos particulares: el viaducto sobre el Arno en Incisa y el viaducto sobre el Arno en Levane. Giorgio Macchi, discípulo de Franco Levi, había trabajado con él en la experimentación sobre elementos en hormigón pretensado. En los años siguientes fundará la escuela de estructuras de la Universidad de Pavía, contribuyendo de manera determinante al rescate de la catedral de la misma ciudad.

Figura 17 - Viaducto de Incisa (1962-1963) (Reproducida de [36]).

Figura 18 - Viaducto de Levane (1962-1963) (Reproducida de [34]).

El viaducto de Incisa (1962-1963) (Fig. 17), concebido por ambos, es audaz: un arco central–portal de 104 m de luz en hormigón armado que permite el apoyo continuo de los tableros de acceso en hormigón pretensado, de modo que estos últimos tuvieran luces, en suma, ordinarias de 36.00 m. El viaducto fue duplicado con la misma tipología para la pista gemela adyacente.

El viaducto de Levane (1962-1963) (Fig. 18) presenta una propuesta original: un arco de 136.00 m de luz, cuya forma reproduce el antifunicular de las cargas, acoge los pilares y, por tanto, los tableros en hormigón pretensado de 36 m de luz. En este caso, las dos pistas se alojan en una única estructura. El tablero alcanza aquí una anchura de 24 m. En ambos casos los arcos se hormigonaron sobre cimbras metálicas realizadas con tubos ensamblados mediante uniones tipo *Innocenti* (una invención enteramente italiana).

Posteriormente, la empresa Rizzani S.p.A. vuelve a llamar a Zorzi para otro desafío. En Pinzano, la Administración Provincial de Udine había decidido atravesar el río Tagliamento (Fig. 19) para sustituir un anterior puente pionero con tres arcos de hormigón armado, inaugurado en 1906 y destruido por una riada en 1966. Allí Zorzi proyecta un puente de luz única (1968-1969), de 163 metros: se trata de un pórtico de tres articulaciones, en hormigón armado pretensado, construido en voladizo desde las orillas, tras inmovilizar provisionalmente las articulaciones con profundos anclajes fijados en la roca: dovela tras dovela, las dos ménsulas llegan a encontrarse en la clave sin deformarse, gracias al efecto de la precompresión

Figura 19 - Puente de Pinzano (1968-1969) (Reproducida de [37]).

provisional. El canto en la clave del tablero es de 2.50 m y en los arranques de 7.00 m. La proporción es perfecta; como corresponde a la historia del lugar, escenario de una épica batalla durante la Primera Guerra Mundial, el puente resulta monumental: la luz gigantesca y la gran altura sobre el agua lo aíslan de la escala humana, pero al mismo tiempo aparece como una huella sutil, casi mágica, en el paisaje encantado de aguas cristalinas, fondo rosado y verde dolomítico.

11.
LA CRISIS Y EL EPÍLOGO DE LA FASE PIONERA

Luego llega la crisis energética de 1973. El estallido de la guerra del Yom Kippur y el embargo petrolero decretado por la OPEP provocan un brusco aumento de los precios y ponen fin al ciclo de crecimiento que había acompañado a Occidente en los años cincuenta y sesenta. La industria, obligada por primera vez a enfrentarse al ahorro energético, reduce sus ambiciones y la contratación pública sus inversiones.

También la ingeniería italiana entra en una crisis irreversible. A mediados de los años setenta se hace cada vez más difícil ganar licitaciones proponiendo soluciones innovadoras. Los comitentes, atentos únicamente a la contención de costes, reducen las grandes luces, abandonan pórticos y arcos, y hacen desaparecer las imponentes cimbras. Se impone un nuevo modelo de viaducto, ya difundido en Europa: filas de pilares delgados y próximos que sostienen vigas rectilíneas suspendidas en el cielo.

Zorzi, al principio reticente, trata no obstante de adaptarse: racionaliza la obra, la industrializa, pero sin renunciar al hormigonado in situ. Así logra dejar igualmente obras maestras, aun en una época en que la epopeya artesanal de los grandes viaductos en hormigón pretensado estaba a punto de concluir. La tecnología del pretensado ya se había afianzado, pero ahora como producto en serie: el espacio para los proyectistas de autor se reducía cada vez más, y el testigo pasaba a otros, con filosofías diferentes. Pero, eso ya es otro capítulo.

12.
DOS ALMAS FRENTE A FRENTE

Aunque ambos fueron protagonistas de la afirmación del hormigón armado pretensado en Italia, Morandi y Zorzi no fueron coetáneos: casi veinte años los separaban, y eran hijos de épocas distintas.

Morandi es el artesano puro, que concibe cada puente como una obra única, irrepetible, casi una escultura en equilibrio entre técnica y arte. Zorzi, por el contrario, se convierte en el proyectista industrial: sobre todo en la segunda parte de su carrera, trabaja con un método y un rigor próximos a los del diseñador, produciendo obras repetibles, pero siempre originales y nunca banales.

Morandi adapta el artefacto a la medida del territorio; Zorzi perfecciona un producto industrial, replicable varias veces, pero cuidado con una atención maniática a la calidad. Dos trayectorias distintas que, juntas, marcaron un capítulo irrepetible de la ingeniería italiana, parte integrante de aquel "Made in Italy" capaz de conjugar invención, forma y técnica.

13.
CONCLUSIONES

Narrar la historia es siempre una empresa ardua. Ya se trate del arte, de la política o de la cultura, toda narración corre el riesgo de ofrecer una visión parcial, marcada por la perspectiva y la sensibilidad de quien escribe. Con mayor razón, cuando la historia se refiere a las técnicas constructivas, el relato se vuelve complejo: un territorio sembrado de intuiciones, de inventos y de propuestas que se multiplican como sendas divergentes en un bosque.

Quien escribe es consciente de que no puede restituir una verdad absoluta, sino tan solo una trama subjetiva, atravesada también por la pasión y la admiración hacia aquellos que se atrevieron a explorar lo desconocido. Fue precisamente en los primeros años de la aventura del hormigón pretensado en Italia donde tomó forma esa red de hombres e ideas. Ingenieros

y proyectistas que, con valentía, depositaron sobre la mesa no solo su saber técnico, sino también su alma y su entusiasmo. Eran tiempos de experimentación, de audacia y de temores: como en todo viaje hacia lo inédito, no todos lograron avanzar, pero los más arriesgados quedaron en la memoria, esculpidos en la historia como faros que iluminan la ruta.

Así, casi inevitablemente, todo relato técnico acaba convirtiéndose en un relato humano, tejido con nombres, rostros y desafíos. Porque son siempre las figuras de quienes osan las que mantienen viva la memoria de una tecnología.

Hoy, tras décadas de experiencia, el pretensado es ya un conocimiento consolidado. Sin embargo, su historia no se cierra: la búsqueda de nuevas soluciones continúa, y la frontera de la innovación sigue abierta. En Italia, como en el resto del mundo, la construcción permanece como un espacio de desafío, donde la tradición dialoga con el futuro y cada puente, cada estructura, lleva consigo el eco de aquel primer y valiente paso hacia lo desconocido.

Referencias

[1] M. Sanabra-Loewe, J. Capellà-Llovera, The four ages of early prestressed concrete structures, PCI Journal 59 (2014) 93–121. https://doi.org/10.15554/pcij.09012014.93.121.

[2] S. Whipple, Bridge. US Patent 2064, issued April 24, 1841, 1841.

[3] Association Eugène Freyssinet, Eugène Freyssinet : a revolution in the art of construction, Presses de l'école nationale des ponts et chaussées, 2004.

[4] F. Chaudy, Sur le Calcul des Plaques Élastiques Minces et le Rôle de Tirants Dans les Poutres en Ciment Armées, Mémoires et Compte Rendus Des Travaux de La Société de Ingénieurs Civils de France - Paris 2ème Semestre (1894) 545–550.

[5] D.P. Billington, Historical Perspective on Prestressed Concrete, PCI Journal (2004). https://doi.org/10.15554/pcij49.1-07.

[6] P. Jartoux, The Work of Eugène Freyssinet: The Most Significant Bridges of his Career, Docomomo Journal (2011) 30–41. https://doi.org/10.52200/45.A.VFKHFTLE.

[7] D. Fernández-Ordóñez Hernández, Eugène Freyssinet. I was born a builder, in: Proceedings of 28th Dresden Bridge Construction Symposium – Design, Construction, Maintenance and Upgrading of Bridges - 12/13 March, Dresden, 2018.

[8] https://heritage.ecoledesponts.fr/enpc/fr/content/trouver-un-ingenieur-des-ponts-la-liste-des-ingenieurs-freyssinet-eugene, (n.d.).

[9] F.R. McMillan, Shrinkage and Time Effects in Reinforced Concrete, Minneapolis, MN: University of Minnesota, 1915.

[10] https://www.ce.jhu.edu/perspectives/protected/ids/Index.php?location=Plougastel%20Bridge, (n.d.).

[11] E. Freyssinet, Études sur les Déformations Lentes des Ciments ou Retraits., in: Premier Congrès International Du Béton et Du Béton Armé , La Technique des Travaux, Liège, Belgium, 1930: pp. 520–532.

[12] E. Freyssinet, Relations Entre les déformations et la Constitution des Ciments et des Matériaux de Structure Colloïdale (Résultats de Recherché Faites par Eugène Freyssinet entre 1926 et 1929), Travaux 376 (Numéro Spécial – Un Demi-Siècle de Technique Française de La Précontrainte Tome II (1966) 921–936.

[13] T. Iori, Prime sperimentazioni sul Cemento Armato Precompresso in Italia, in: Curare Il Moderno, I Modi Della Tecnologia, a cura di P. G. Bardelli, E. Filippi, Emilia Garda, 2002.

[14] E. Freyssinet, J. Seailles, Procédé de fabrication de pièces en béton armé. French Patent 680547, filed October 2, 1928, and issued May 1, 1930, 1928.

[15] J.A. Fernández Ordóñez, Eugène Freyssinet, Éd. du Linteau, 2012.

[16] G. Colonnetti, Teoria e calcolo delle travi con armature preventivamente tese, Pontificia Accademia Scientiarum - Acta IV (1939).

[17] T. Iori, Prestressed Concrete: First Developments in Italy , in: Proceedings of the First International Congress on Construction History, Madrid, Spain: Reverte, 2003: pp. 1167–1176.

[18] G. Colonnetti, Calcolare meglio, Il Cemento Armato 4 (1938) 61.

[19] https://atlas.landscapefor.eu/category/parco-urbano/poi/15901-parco-colonnetti/13327-gustavo-colonnetti/, (n.d.).

[20] G. Colonnetti, Problemi nuovi e nuovi orientamenti, Il Cemento Armato 2 (1939) 22.

[21] A. Marioni, L'invenzione delle strutture parzialmente precompresse: Un contributo tutto italiano all'evoluzione della precompressione , in: Giornate AICAP '99 - Torino, 4-6 Novembre, 1999.

[22] F. Levi, Calcolo delle strutture composte di elementi in stato di coazione e di calcestruzzo allo stato naturale non deformato, Pontificia Accademia Delle Scienze, Acta (1943).

[23] F. Levi, Le Béton armé précontraint, Bulletin Du Centre d'Etudes Du Batiment, Losanna (1944).

[24] F. Levi, Esperienze su travi parzialmente precompresse, , Rivista "Il Cemento" (1945).

[25] C. Cestelli Guidi, Il conglomerato precompresso – Teoria, esperienze ed applicazioni , 1947.

[26] F. Levi, G. Pizzetti, Fluage, Plasticitè, Precontrainte, 1951.

[27] G. Rinaldi, Il Cemento Armato Precompresso e sua codificazione, 1962.

[28] https://murimuseodiffuso.it/it/viadotto-sul-fiume-piave-0, (n.d.).

[29] A.N.I.C.A.P., Associazione Nazionale Italiana del Cemento Armato Precompresso. Giornate del Cemento Armato Precompresso del 1954. Edizioni del giornale del Genio Civile. , 1956.

[30] R. Morandi, Strutture di calcestruzzo armato e di calcestruzzo precompresso , Libreria Dedalo Editrice – Roma, 1954.

[31] Proverbio Edoardo, Recupero Antonino, Quality and durability of bridges in Italy, in: Proceeding of Construction Expert Workshop: XVI Scientific and Technical Conference., Kielce - Cedzyna, 2020: pp. 177–195.

[32] G. Boaga, Riccardo Morandi – Serie di Architettura, Zanichelli Editore Bologna, 1984.

[33] https://i.pinimg.com/736x/e7/04/5d/e7045df-96273896661348595ce309cc1--ponti-the-bridge.jpg , (n.d.).

[34] T. Iori, G. Capurso, Silvano Zorzi, designer strutturale, Archi 5 (2019).

[35] https://inco-eng.com/wp-content/uploads/2021/03/Libro-ROSSO-storico.pdf, (n.d.).

[36] https://www.webuildgroup.com/_next/image/?url=https%3A%2F%2Fadmin.webuildgroup.com%2Fsites%2Fdefault%2Ffiles%2F2025-01%2FAutostrada_del_Sole_A1-Italia-Webuild_WBL414516.jpg&w=1920&q=75, (n.d.).

[37] https://andarpervalli.it/wp-content/uploads/2021/02/3-ponte-pinzano1-scaled.jpg , (n.d.).

ÚLTIMOS NÚMEROS PUBLICADOS

ISSN: 0439-5689

HORMIGÓN y ACERO

REVISTA CUATRIMESTRAL DE ACHE ASOCIACIÓN ESPAÑOLA DE INGENIERÍA ESTRUCTURAL

Septiembre - Diciembre 2024 I Volumen 75 - Número 304

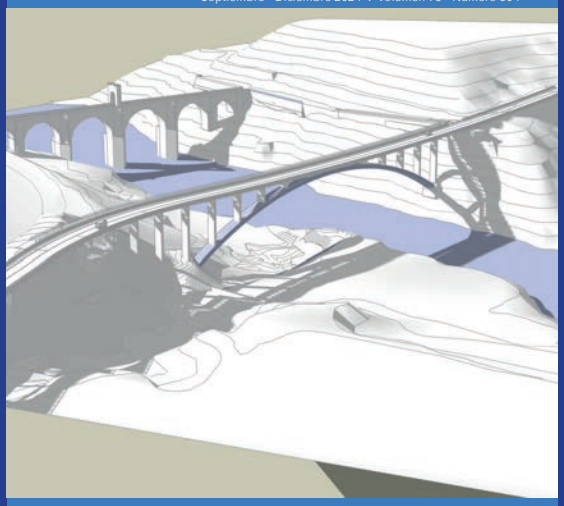

www.hormigonyacero.com

ISSN: 0439-5689

HORMIGÓN y ACERO

REVISTA CUATRIMESTRAL DE ACHE ASOCIACIÓN ESPAÑOLA DE INGENIERÍA ESTRUCTURAL

Enero - Abril 2025 I Volumen 76 - Número 305

www.hormigonyacero.com

ISSN: 0439-5689

HORMIGÓN y ACERO

REVISTA CUATRIMESTRAL DE ACHE ASOCIACIÓN ESPAÑOLA DE INGENIERÍA ESTRUCTURAL

Mayo - Agosto 2025 I Volumen 76 - Número 306

www.hormigonyacero.com

ISSN: 0439-5689

HORMIGÓN y ACERO

REVISTA CUATRIMESTRAL DE ACHE ASOCIACIÓN ESPAÑOLA DE INGENIERÍA ESTRUCTURAL

Septiembre - diciembre 2025 I Volumen 76 - Número 307

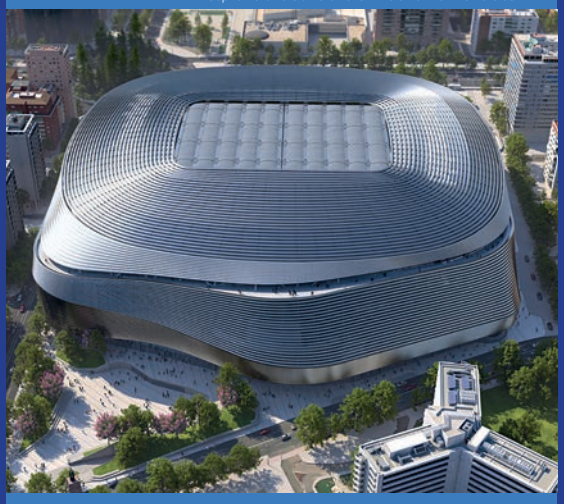

www.hormigonyacero.com

ACHE

Base de datos de artículos publicados en números:

www.hormigonyacero.com

CONSTRUCCIÓN SOSTENIBLE

40 años construyendo confianza

- Desde 1986, AENOR lidera la certificación en el sector de la construcción.
- Más de **2.000 empresas** y **100.000 productos certificados** en más de **60 países**.
- AENOR acompaña a empresas en procesos de internacionalización y adaptación a nuevas realidades.

Compromiso con la Sostenibilidad

- AENOR impulsa la certificación de valores ESG (ambientales, sociales y de gobernanza).
- Ofrece soluciones específicas para cada agente de la cadena de valor de la construcción.

EDIFICIO SOSTENIBLE

Certificación que evalúa el desempeño medioambiental del edificio y la utilización de materiales sostenibles según criterios Ambientales, Sociales y de Gobernanza, en línea con los requerimientos de la marca AENOR N Sostenible.

AENOR
EDIFICIO SOSTENIBLE

Uso de materiales sostenibles

Los productos con marca **AENOR N Sostenible** evalúan hasta 20 indicadores ESG que incluyen aspectos:

- **Ambientales:** Energía, Agua, Emisiones, Sustancias peligrosas.
- **Sociales**: Empleo, Seguridad y Salud, Igualdad, Impacto en la comunidad local.
- **Gobernanza:** Transparencia, Ética empresarial, Cumplimiento normativo, Gestión de riesgos.

40 años
transformación y confianza
AENOR